

**IMPROVING THE ABSORPTION OF LEVODOPA EMPLOYING A
MULTI-CROSSLINKED ORAL NANOCOMPOSITE-CHARGED TABLET
PLATFORM**

NDIDI CHINYELU NGWULUKA

A thesis submitted to the Faculty of Health Sciences, University of the Witwatersrand,
in fulfillment of the requirements for the degree of
Doctor of Philosophy



Supervisors:

Professor Viness Pillay
University of the Witwatersrand, Department of Pharmacy and Pharmacology,
Johannesburg, South Africa

Professor Girish Modi
University of the Witwatersrand, Department of Neurosciences, Division of Neurology,
Johannesburg, South Africa

Dr. Dinesh Naidoo
University of the Witwatersrand, Department of Neurosciences, Division of Neurosurgery,
Johannesburg, South Africa

2012

DECLARATION

I, Nndi Chinyelu Ngwuluka declare that this thesis is my own work. It has been submitted for the degree of Doctor of Philosophy in the Faculty of Health Sciences at the University of the Witwatersrand, Parktown, Johannesburg, South Africa. It has not been submitted before for any degree or examination at this or any other University.



.....

Signed this 19th day of September, 2012.

RESEARCH PUBLICATIONS

1. Levodopa delivery systems: Advancements in delivery of the gold standard. Ndidi C. Ngwuluka, Viness Pillay, Girish Modi, Dinesh Naidoo, Yahya E. Choonara and Lisa C. du Toit. *Expert Opinion on Drug Delivery*, 7(2): 203-224, 2010.
2. Fabrication, modeling and characterization of multi-crosslinked Eudragit E100/Eudragit E100 polymer blended nanoparticles for oral drug delivery. Ndidi C. Ngwuluka, Viness Pillay, Girish Modi, Dinesh Naidoo, Yahya E. Choonara and Lisa C. du Toit. *International Journal of Molecular Sciences*, 12, 6194-6225, 2011.
3. Rheological characterization and modeling of the synthesis of interpolyelectrolyte complex of methacrylate copolymer and sodium carboxymethylcellulose. Ndidi C. Ngwuluka, Yahya E. Choonara, Lisa C. du Toit, Pradeep Kumar, Valence M.K. Ndesendo and Viness Pillay. *Journal of Polymer Science*, under review, 2011.
4. Synthesis, modeling and characterization of a novel pH-responsive interpolyelectrolyte complex hydrogel. Ndidi C. Ngwuluka, Yahya E. Choonara, Lisa C. du Toit, Pradeep Kumar, Valence M.K. Ndesendo, Riaz Khan and Viness Pillay. *International Journal of Pharmaceutics*, under review, 2011.
5. The influence of addition of a polysaccharide on the physicochemical characteristics of an interpolyelectrolyte complex. Ndidi C. Ngwuluka, Yahya E. Choonara, Lisa C. du Toit, Pradeep Kumar, Valence M.K. Ndesendo and Viness Pillay. *AAPS PharmSciTech*, under review, 2011.
6. A triple-mechanism gastroretentive drug delivery system, Ndidi C. Ngwuluka, Yahya E. Choonara, Lisa C. du Toit, Valence M.K. Ndesendo, Pradeep Kumar and Viness Pillay. *International Journal of Pharmaceutics*, under review, 2011.
7. Physicochemical/physicomechanical characterization and *in vivo* studies of optimized interpolymeric blend/nano-enabled three-mechanism gastroretentive levodopa-loaded delivery systems. Ndidi C. Ngwuluka, Yahya E. Choonara, Lisa C. du Toit, Pradeep Kumar and Viness Pillay. *AAPS PharmSciTech*, under review, 2011.

(Appendix A)

RESEARCH PRESENTATIONS

1. Enhancing the drug delivery properties of a carbohydrate polymer employing lyophilization. N. Ngwuluka, V. Pillay, G. Modi, D. Naidoo, Y. Choonara and L. du Toit: Oral presentation at the School of Therapeutic Sciences research day, University of Witwatersrand, South Africa, August, 12, 2009.
2. Characterization of prolamine-based polymeric nanocomposites. N.C. Ngwuluka, V. Pillay, G. Modi, Y.E. Choonara, L.C. du Toit and D. Naidoo: Poster presentation at the British Pharmaceutical Conference, Manchester, United Kingdom, September, 6 – 9, 2009.
3. Comparative textural and drug release profiling of a native polymer and its lyophilized form. N.C. Ngwuluka, V. Pillay, G. Modi, Y.E. Choonara, L.C. du Toit and D. Naidoo: Oral presentation at 2nd postgraduate cross faculty symposium, University of Witwatersrand, South Africa, October, 19 – 22, 2009.
4. Synthesis and characterization of a novel hydrogel formulation for oral drug delivery. N.C. Ngwuluka, V. Pillay, G. Modi, Y.E. Choonara, L.C. du Toit and D. Naidoo: Poster presentation at American Association of Pharmaceutical Scientists, Los Angeles Convention Center, Los Angeles, USA, November, 8 -12, 2009.
5. Computational modeling and drug release characteristics of a pH-responsive interpolyelectrolyte complex. N.C. Ngwuluka, V. Pillay, G. Modi, D. Naidoo, Y.E. Choonara, L.C. du Toit, R. Khan and P. Kumar: Poster presentation at American Association of Pharmaceutical Scientists, New Orleans Ernest N. Morial Convention Center, New Orleans, Louisiana, USA, November, 13 – 18, 2010.
6. Physicochemical characterization of nanoparticles prepared from a basic ester of poly (acrylic) acid for sustained levodopa delivery, N.C. Ngwuluka, V. Pillay, G. Modi, D. Naidoo, Y.E. Choonara, and L.C. du Toit: Poster presentation at American Association of Pharmaceutical Scientists, New Orleans Ernest N. Morial Convention Center, New Orleans, Louisiana, USA, November, 13 – 18, 2010.
7. A triple-mechanism gastroretentive system for zero-order delivery of levodopa. Ndidi C. Ngwuluka, Viness Pillay, Girish Modi, Dinesh Naidoo, Yahya E. Choonara and Lisa C. du Toit: Poster presentation at Controlled Release Society meeting, National Harbor, Maryland, USA, July, 30th - 3rd August 2011.

(Appendix B)

PATENT FILED

An oral multi-crosslinked nanocomposite charged pharmaceutical dosage form. Inventors: Ngwuluka Ndidi, Viness Pillay, Yahya E. Choonara and Lisa C. du Toit. The patent has been filed with South Africa Patents and Trade Mark Office, 2010. South African Application (2010/03741 – provisional – green gazette SA – published July 30, 2010).

ABSTRACT

The time- and cost-consuming drug discovery process necessitated the current research trend of improving the absorption and bioavailability of existing drugs especially where drugs such as levodopa (L-dopa) remain the gold standard of treatment in Parkinson's disease (PD). One effective approach of improving absorption and bioavailability is to prolong the residence time of the drug delivery system at the absorption site of the drug. Various mechanisms of gastroretention have been employed for the delivery of Narrow Absorption Window drugs including L-dopa. However, despite the various formulations currently available, delivery of L-dopa is still fraught with low exposure time at the absorption site which leads to poor absorption and bioavailability as well as erratic plasma concentrations. Hence, the development of an oral drug delivery system that may improve the absorption and subsequent bioavailability of L-dopa with constant therapeutic plasma concentrations will provide a momentous advancement in the treatment of PD. Consequently, the aim of this study was to develop and characterize a Gastroretentive Drug Delivery System (GDDS) and a multi-crosslinked nano-enabled tablet matrix to improve the oral absorption and subsequent bioavailability of existing commercially available L-dopa/carbidopa and L-dopa/benserazide preparations such as Sinemet CR[®] and Madopar[®] HBS. In this research, the process of developing an oral nano-composite tablet matrix for the delivery of L-dopa commenced with the synthesis of a novel polymer by complexation and culminated in the testing of the drug delivery systems in the Large White pig model. An interpolyelectrolyte complex (IPEC) was synthesized by interacting methacrylate copolymer and carboxymethylcellulose. The IPEC was delineated by employing techniques such as Fourier Transform Infra-Red (FTIR) spectroscopy, thermal analysis, mechanical strength analysis, swellability and *in vitro* drug release studies. Based on the results generated, a natural polymer, locust bean was added to further enhance the drug delivery properties of the IPEC such as drug release. The interpolymeric blend produced was employed to develop a triple-mechanism (GDDS). This was characterized by determining the density, gastroadhesive properties, swellability and the physicomachanical strength. The system was optimized and further explicated by scanning electron microscopy, pore size and surface area analysis as well as magnetic resonance imaging. Nanoparticles were fabricated by multi-crosslinking technology and characterized by techniques such as particle size and zeta potential analysis, molecular mechanics computation, microscopy and *in vitro* drug release. The GDDS and the nano-enabled tablet matrices were characterized *in vitro*; administered to pigs and compared to conventional dosage forms. An interpolymeric blend with improved drug delivery properties in comparison to the native polymers was successfully developed and its application in the development of a GDDS led to a device with superior mechanical integrity, high density, swellable and gastroadhesive with extended gastric residence time and the ability to release L-dopa over 24 hours at a controlled and constant rate exhibiting zero order release kinetics. The nanoparticles were spherical hollow capsules with high drug entrapment efficiency of 85%. The comparative study with the conventional dosage forms indicated that the GDDS has the potential to improve the absorption and bioavailability of existing formulations. The *in vivo* studies which included x-ray imaging of tablet matrix and cytotoxicity testing, confirmed the GDDS gastroretentive ability with low toxicity and the pharmacokinetic data elucidated the liberation of L-dopa from the GDDS and nano-enabled tablet matrices, its absorption, distribution, metabolism and excretion. The GDDS was proven to be congruous for the delivery of L-dopa in the management of PD.

ACKNOWLEDGEMENTS

The journey to the top is never a smooth ride; for there are mirages, potholes, hills and valleys. However, it becomes bearable with the help of people within and without the vehicle. Indeed, I could not have come to this point of submission of my thesis without the help of colleagues, family and friends.

I would like to thank my supervisor, Prof Viness Pillay for accepting me on board his research team. Although it was not a smooth course, I have learnt a lot as a team member. I remember what he said the first day I met him. "You came at the right time; when the labs have been equipped to world class standards". Learning how to use the equipment and analyzing data obtained is indeed added value. Gracias! Dhanyavad!! Shukriya!!!

Thanks to Dr. Yahya Choonara and Ms. Lisa Du Toit for your constructive criticisms of the papers for publication and abstracts for conferences amongst other valuable assistance despite your busy schedules.

I have met you on uncountable occasions Prof Danckwerts for assistance such as signing of documents and you have always put whatever you were doing aside to attend to me. Baie Dankie!

I am privileged to have such a father like my Dad who has been so supportive. He never forgot his weekly check up on me; not just to find out how I am doing but also to enquire about my research progress. In fact, in one of those calls, he told me he was also one of the researchers. Yes, Dad, your weekly check up spurred me to work so that I can have something to tell you each week. Daalu!

My sister, Ngozi and her husband Zuby have been immensely supportive both morally and financially. How can I forget that the laptop I used for the research was made possible by you? Thank you so much.

I would like to acknowledge other fellow team members: Adeleke Oluwatoyin, Bawa Priya, Cooppan Shivaan, Dawood Yusuf, Dott Clare, Fasinu Pius, Frank Derusha, Govender Thiresen, Harilall Sheri-Lee, Hazle Deanne, Hibbins Angus, Kgesa Teboho, Khan Zaheeda, Kumar Pradeep, Manyikana Martina, Mashingaidze Felix, Masina Nonhlanhla, Moodley Kovanya, Mufamadi Maluta, Ndesendo Valence, Ngoepe Mpho, Reddy Deshika, Rubina Shaikh, Sibeko Bongani, Tsong Tsai, Wadee Ameena, and the list goes on. You guys are one of a kind. Indeed, teaching and learning from each other have been phenomenal.

My gratitude also goes to the support staff of the Dept of Pharmacy and Pharmacology. A shout of 'viva' to Mr. Sello Ramarumo, Ms. Nompumelelo Damane, Mrs. Lehlohonolo Chandu, Mrs. Olgar Kunene, Mr. Bafana Themba and Mr. Kleinbooi Mohlabi for always going out of their way to ensure my needs were met.

What can I say to the staff of the Central Animal Services – Dr. Leith Meyer, Sr. Mary-Ann Costello, Mr. Patrick Selahle, Ms. Lorraine Setimo, Sr. Amelia Rammekwa, Mr. Nico Douths, Mr. Kwandakwethu Ndaba and Ms. Keshnee Chetty? Your co-operation and commitment to the animal studies are highly appreciated.

Mr. Jimoh Sikiru, my transmission electron microscopy consultant! Thank you for sacrificing your time on a number of occasions to help me out.

I would also like to thank my ultra performance liquid chromatography (UPLC) consultants – Ms. Ildi Fenyvesi, Ms. Yolande Rautenbach, and Dr. Nelson Ocheke. Nelson I will not forget the night you stayed awake on the phone telling me what to do.

Mrs. Tracy Ferrao, you are a gem, a life-saver and a great chemical analyst. Thanks for your sacrifice. I really can't thank you enough.

The first warning of the difficulty of a PhD came from a colleague and friend, Prof. Dugga, who said, "No matter what happens, hang in there and complete your program". Thanks for those words. They kept pushing me even when I wanted to give up.

I want to appreciate my siblings, Chudi, Dubem, Ijeoma, Ada and Emeka for enduring my absence while encouraging this pursuit. And thanks to my dear aunts, Mrs. Comfort Ubosi and Mrs. Chiebo Egbuna for their support and prayers. My Uncle, Dr. Egbuna who encouraged me to go to South Africa.

Thanks to some members of staff of the University of Jos, Nigeria – Prof. Patrick Olorunfemi, Mrs. Patricia Odumosu and Dr. Nep Elijah for your encouragement and support.

I appreciate UNESCO and L'Oréal Corporate Foundation for L'Oréal/UNESCO regional fellowship for women in science awarded to me in my third year. Indeed it was a breather to the financial stress.

I would also like to acknowledge my friends and support group, Ola Olaleye, Alice Magombo, Yemisi Onimode, Modupe Ogunrombi, Rosie Mcneil, Vovo Bangani, Kutemba Kapanji, Udeme Ekrikpo, Daisi Alabi, Olu Odumosu, Pamela Owie, Ada Ukariwe, Cally Arikaiwe, Okeke Uzodinma, my pastor, Dotun Reju, my uncle and his wife, Mr. and Mrs. IK Ngwuluka and Mr. Julius Khosa who would forfeit his sleep to pick me up from school at early hours of the morning.

Ultimately, to the greatest Scientist, Father God; I owe you my life.

DEDICATION

To my mother, Alice Nkechi Ngwuluka who left a legacy for me.

And

To every dreamer – for if you can think of it, then you are loaded with the potential to make it happen amidst all the trials and tribulations on the way.

TABLE OF CONTENTS

CHAPTER ONE *INTRODUCTION*

1.1. Background of this study	1
1.2. Rationale and motivation for this study	5
1.3. Aim and objectives of this study	7
1.4. Overview of this thesis	9
1.5. Concluding remarks	11

CHAPTER TWO
***A LITERATURE REVIEW OF LEVODOPA DELIVERY SYSTEMS: ADVANCEMENTS IN
THE DELIVERY OF THE GOLD STANDARD***

2.1. Introduction	12
2.2. Immediate release oral drug delivery systems for the administration of levodopa	15
2.3. Conventional controlled release formulations for levodopa administration	18
2.4. Administration of levodopa as a liquid formulation	19
2.5. Dispersible tablets for delivery of levodopa	20
2.6. Oral disintegrating levodopa tablets	20
2.7. Dual-release formulations for the delivery of levodopa	23
2.8. Delivery of levodopa by infusions	26
2.9. Biodegradable microspheres as a drug delivery system for levodopa	27
2.10. Gastroretentive dosage forms as drug delivery systems for levodopa	28
2.10.1. Single-unit sustained floating systems for delivery of levodopa	29
2.10.2. Multiple-unit sustained release floating dosage forms for delivery of levodopa	30
2.11. Long term implantable levodopa controlled release matrix	32
2.12. Pulmonary delivery of levodopa	33
2.13. Nasal delivery systems for levodopa	33
2.14. Transdermal delivery systems for levodopa	34
2.15. Prodrugs as a delivery vehicle for levodopa	35
2.16. Delivery of levodopa via the rectal route	37
2.17. Expert opinion on the progress made to date in delivery of the gold standard	38
2.18. Concluding remarks	42

CHAPTER THREE
**RHEOLOGICAL CHARACTERIZATION OF THE SYNTHESIS OF AN
INTERPOLYELECTROLYTE COMPLEX OF METHACRYLATE COPOLYMER AND
SODIUM CARBOXYMETHYLCELLULOSE**

3.1. Introduction	43
3.2. Experimental section	44
3.2.1 Materials	44
3.2.2. Equipment	44
3.2.3. Methodology	44
3.2.3.1. Synthesis of interpolyelectrolyte complex (IPEC)	44
3.2.3.2. Rheological studies	45
3.2.3.2.1. <i>Basic viscosity</i>	45
3.2.3.2.2. <i>Yield stress test</i>	45
3.2.3.2.3. <i>Oscillatory stress sweep</i>	45
3.2.3.2.4. <i>Oscillatory frequency sweep</i>	45
3.2.3.2.5. <i>Creep and recovery test</i>	46
3.2.3.2.6. <i>Temperature ramp</i>	46
3.2.3.3. Static lattice atomistic simulations	46
3.3. Results and discussion	47
3.3.1. Basic viscosity	47
3.3.2. Yield stress analysis	51
3.3.3. Oscillation stress sweep	54
3.3.4. Oscillation frequency sweep	60
3.3.5. Creep and recovery test	63
3.3.6. Temperature ramp	65
3.3.7. Molecular mechanics assisted model building and energy refinement	67
3.3.7.1. <i>Molecular mechanics energy relationship</i>	67
3.3.7.2. <i>Elucidation of step by step synthesis of IPEC</i>	69
3.3.7.3. <i>Effect of normality of acetic acid on reactional profile of IPEC</i>	70
3.4. Concluding remarks	72

CHAPER FOUR
PHYSICOCHEMICAL/ PHYSICOMECHANICAL CHARACTERIZATION OF A NOVEL
INTERPOLYELECTROLYTE COMPLEX FOR DRUG DELIVERY

4.1. Introduction	74
4.2. Experimental section	76
4.2.1. Materials	76
4.2.2. Synthesis of the interpolyelectrolyte complex (IPEC)	76
4.2.3. Microscopical analysis of IPEC	76
4.2.4. Structural elucidation of IPEC	77
4.2.5. Evaluation of the polymeric thermal behavior of IPEC	77
4.2.6. Direct compression of IPEC into matrices	77
4.2.7. Evaluation of the physicomechanical strength of the matrices	77
4.2.8. Degree of swelling of the directly compressed matrices	78
4.2.9. <i>In vitro</i> drug release studies	78
4.3. Results and discussion	79
4.3.1. Microscopical analysis of IPEC	79
4.3.2. Structural elucidation of IPEC	80
4.3.3. Analysis of the polymeric thermal behavior of IPEC	83
4.3.4. Direct compression of IPEC into matrices	88
4.3.5. Physicomechanical strength of the IPEC matrices	88
4.3.6. The degree of swelling of IPEC matrices	90
4.3.7. <i>In vitro</i> drug release studies	94
4.4. Concluding remarks	96

CHAPTER FIVE
THE INFLUENCE OF ADDITION OF A POLYSACCHARIDE ON THE
PHYSICOCHEMICAL CHARACTERISTICS OF THE INTERPOLYELECTROLYTE
COMPLEX

5.1. Introduction	97
5.2. Experimental section	98
5.2.1. Materials	98
5.2.2. Synthesis of interpolyelectrolyte complex	98
5.2.3. Formation of interpolymeric blend	98
5.2.4. Structural elucidation of IPEC and interpolymeric blend	98
5.2.5. Evaluation of the polymeric thermal behavior of IPEC and interpoly- meric blend	98
5.2.6. Direct compression of IPEC and interpolymeric blend	98
5.2.7. Swellability and erosion studies of directly compressed matrices	99
5.2.8. <i>In vitro</i> drug release studies and data analysis	99
5.2.9. Molecular modeling simulations	99
5.2.9.1. <i>Static lattice atomistic simulations</i>	99
5.2.9.2. <i>Molecular dynamics simulation</i>	100
5.3. Results and discussion	100
5.3.1. Synthesis of IPEC and formation of interpolymeric blend (IPB)	100
5.3.2. Structural analysis of IPEC and IPB	100
5.3.3. Polymeric thermal analysis of IPEC and IPB	102
5.3.4. Direct compression of drug loaded IPEC and IPB	107
5.3.5. Swellability and erosion studies of IPEC and IPB	107
5.3.6. <i>In vitro</i> drug release studies and analyses of IPEC and IPB matrices	111
5.3.7. Molecular modeling simulations	119
5.3.7.1. <i>Elucidation of stabilization of IPEC using atomistic simulations</i>	119
5.3.7.2. <i>Elucidation of stabilization of IPEC using dynamics simulations</i>	122
5.3.7.3. <i>Molecular mechanics energy relationship analysis</i>	124
5.3.7.4. <i>3D-computational modeling for polymer-polymer complexes</i>	124
5.4. Concluding remarks	129

CHAPTER SIX

APPLICATION OF INTERPOLYMERIC BLEND IN FORMULATION OF A TRIPLE-MECHANISM GASTRORETENTIVE DRUG DELIVERY SYSTEM

6.1. Introduction	130
6.2. Experimental section	133
6.2.1. Materials	133
6.2.2. Synthesis of interpolymeric blend	133
6.2.3. Structural elucidation of the interpolymeric blend	133
6.2.4. Direct compression of the interpolymeric blend into matrices	133
6.2.5. Determination of the densities of matrices	134
6.2.6. Evaluation of the physicochemical strength of the matrices	134
6.2.7. Gastroadhesivity testing of the matrices	134
6.2.8. Degree of swelling of the matrices	135
6.2.9. <i>In vitro</i> drug release studies and data analysis	135
6.2.10. Static lattice atomistic simulations	135
6.3. Results and discussion	136
6.3.1. Synthesis of interpolymeric blend	136
6.3.2. Structural elucidation of the interpolymeric blend	136
6.3.3. Direct compression of the interpolymeric blend into matrices	138
6.3.4. Densities of the matrices	138
6.3.5. Physicochemical strength analyses of the matrices	139
6.3.6. Gastroadhesivity testing of the matrices	141
6.3.7. Degree of swelling of the matrices	143
6.3.8. <i>In vitro</i> drug release studies and mathematical analysis	145
6.3.9. Prediction of mucoadhesive potential of the GDDS	150
6.4. Concluding remarks	153

CHAPTER SEVEN
EMPLOYING DESIGN OF EXPERIMENTS AND DESIRABILITY FUNCTION FOR
OPTIMIZATION OF A GASTRORETENTIVE DRUG DELIVERY SYSTEM

7.1. Introduction	154
7.2. Experimental section	155
7.2.1. Materials	155
7.2.2. Generated composition of variables	155
7.2.3. Synthesis of the interpolymeric blend	156
7.2.4. Direct compression of the interpolymeric blend into matrices	156
7.2.5. Determination of the densities of matrices	156
7.2.6. Gastroadhesivity testing of the matrices	157
7.2.7. Swellability testing of matrices	157
7.2.8. <i>In vitro</i> drug release studies	157
7.3. Results and discussion	158
7.3.1. Observations for the generated experimental design	158
7.3.2. Analysis of the response surface design	164
7.3.2.1. <i>Estimated regression coefficients and standard error of fits</i>	164
7.3.2.2. <i>Pearson product moment correlation coefficient</i>	165
7.3.2.3. <i>Residual plots</i>	166
7.3.2.4. <i>Surface plots</i>	168
7.3.2.5. <i>Application of desirability function for optimization</i>	170
7.4. Concluding remarks	170

CHAPTER EIGHT
FABRICATION AND CHARACTERIZATION OF MULTI-CROSSLINKED
POLYMER-LIPID NANOPARTICLES

8.1. Introduction	172
8.2. Experimental section	174
8.2.1. Materials	174
8.2.2. Nanofabrication of polymer-lipid nanoparticles	174
8.2.3. Determination of pH and absorbance changes during fabrication	174
8.2.4. Computational modeling of the fabrication of multi-crosslinked nanoparticles	175
8.2.5. Size and surface charge analyses of the <i>iPoly-X-Lipo</i> nanoparticles	175
8.2.6. Structural elucidation of the <i>iPoly-X-Lipo</i> nanoparticles	175
8.2.7. Microscopical analysis of the levodopa-loaded <i>iPoly-X-Lipo</i> nanoparticles	175
8.2.8. Determination of drug loading and drug entrapment efficiency of <i>iPoly-X-Lipo</i> nanoparticles	176
8.2.9. Direct compression of the <i>iPoly-X-Lipo</i> nanoparticles	176
8.2.9.1. <i>Direct compression of the iPoly-X-Lipo nanoparticles</i>	176
8.2.9.2. <i>Incorporation of iPoly-X-Lipo into IPB</i>	176
8.2.10. <i>In vitro</i> drug release studies	177
8.2.10.1. <i>Drug release studies of nanosuspension employing dialysis technique</i>	177
8.2.10.2. <i>Drug release studies of the compressed matrices</i>	177
8.2.11. Magnetic resonance imaging of mechanical behavior	177
8.2.12. Static lattice atomistic simulations	178
8.3. Results and discussion	179
8.3.1. Modeling, changes in pH and absorbances of <i>iPoly-X-Lipo</i> nanoparticles during fabrication	179
8.3.2. Size and surface charge analyses of <i>iPoly-X-Lipo</i> nanoparticles	186
8.3.3. Structural elucidation of the <i>iPoly-X-Lipo</i> nanoparticles	186
8.3.4. Surface morphology of the <i>iPoly-X-Lipo</i> nanoparticles	189
8.3.5. Drug loading efficiency of <i>iPoly-X-Lipo</i> nanoparticles	190
8.3.6. Direct compression of <i>iPoly-X-Lipo</i> nanoparticles into tablet matrices	190
8.3.7. <i>In vitro</i> drug release studies	191
8.3.8. Improvement in mechanical strength afforded by polymeric nanoparticles	195
8.3.9. Molecular mechanics assisted model building and energy refinements	196
8.3.9.1. <i>Molecular mechanics energy relationship analysis</i>	196
8.3.9.2. <i>Energy-minimizations involving crosslinked-polymer morphologies</i>	197
8.4. Concluding remarks	202

CHAPTER NINE
**CHARACTERIZATION OF OPTIMIZED GASTRORETENTIVE LEVODOPA-LOADED
MULTI-CROSSLINKED NANOCOMPOSITE TABLET PLATFORM**

9.1. Introduction	204
9.2. Experimental section	205
9.2.1. Materials	205
9.2.2. Fabrication of <i>iPoly-X-Lipo</i> nanoparticles	205
9.2.3. Synthesis of interpolymeric blend	206
9.2.4. Structural elucidation of the interpolymeric blend and nanoparticles	206
9.2.5. Evaluation of thermal behavior of interpolymeric blend	206
9.2.6. Direct compression of the interpolymeric blend and formation of <i>PXLNET</i>	207
9.2.7. Determination of the densities of matrices	207
9.2.8. Gastroadhesivity testing of the matrices	207
9.2.9. Physicomechanical characteristics and swellability of IPB and <i>PXLNET</i> matrices	208
9.2.10. Surface morphological analysis of IPB Matrices	208
9.2.11. Surface area and porosity analyses of IPB matrices	208
9.2.12. Comparative <i>in vitro</i> drug release studies and analytical method	209
9.2.13. Elucidation of release mechanisms	210
9.2.14. Magnetic resonance imaging of IPB matrices	210
9.2.15. Stability of levodopa/benserazide/carbidopa in nanoparticles and matrices	210
9.3. Results and discussion	210
9.3.1. Fabrication of <i>iPoly-X-Lipo</i> nanoparticles	210
9.3.2. Synthesis of interpolymeric blend	210
9.3.3. Structural elucidation of the interpolymeric blend and nanoparticles	211
9.3.4. Analysis of thermal behavior of interpolymeric blend	212
9.3.5. Density of IPB and <i>PXLNET</i> matrices	215
9.3.6. Gastroadhesivity of IPB and <i>PXLNET</i> matrices	216
9.3.7. Physicomechanical characteristics and swellability of IPB and <i>PXLNET</i> matrices	217
9.3.8. Surface morphological analysis of IPB matrices	219
9.3.9. Surface area and porosity analyses	220
9.3.10. Comparative <i>in vitro</i> drug release studies	223
9.3.11. Magnetic resonance imaging	232
9.3.12. Stability of IPB, drugs-loaded nanoparticles and <i>PXLNET</i>	236
9.4. Concluding remarks	237

CHAPTER TEN
**IN VIVO INVESTIGATION AND ANALYSIS OF THE OPTIMIZED INTERPOLYMERIC
BLEND/NANO-ENABLED THREE-MECHANISM GASTRORETENTIVE LEVODOPA
DELIVERY SYSTEMS**

10.1. Introduction	239
10.2. Experimental section	240
10.2.1. Materials	240
10.2.2. Methodology	240
10.2.2.1. <i>In vivo animal ethics clearance</i>	240
10.2.2.2. <i>Arrival of pigs and habituation</i>	240
10.2.2.3. <i>Venous catheterization of the pigs for blood sampling</i>	241
10.2.2.4. <i>Flushing and bleeding</i>	243
10.2.2.5. <i>Gastric dosing and blood sampling of the pigs</i>	243
10.2.2.6. <i>Cerebrospinal fluid collection</i>	245
10.2.2.7. <i>Urine collection</i>	246
10.2.2.8. <i>In vivo measurement of the GDDS and PXLNET residence time in Large White pig model</i>	247
10.2.2.9. <i>Histopathological evaluation</i>	248
10.2.2.10. <i>Cytotoxicity testing</i>	248
10.2.2.11. <i>Ultra performance liquid chromatography for analysis of plasma samples</i>	249
10.2.2.12. <i>Pharmacokinetic modeling and analysis</i>	251
10.3. Results and discussion	251
10.3.1. <i>In vivo measurement of the GDDS and PXLNET residence time in Large White pig model</i>	251
10.3.2. <i>Histopathological findings</i>	254
10.3.3. <i>Cytotoxicity testing</i>	255
10.3.4. <i>UPLC/MS/MS method validation</i>	256
10.3.5. <i>Pharmacokinetic data and analysis</i>	257
10.3.6. <i>In vitro-in vivo correlation of dissolution and pharmacokinetic parameters</i>	263
10.4. Concluding remarks	264

CHAPTER ELEVEN
CONCLUSIONS AND RECOMMENDATIONS

11.1. Conclusions	266
11.2. Recommendations	267
REFERENCES	268
APPENDICES	312
Appendix A: Research publications	312
Appendix B: Research presentations	314
Appendix C: ADSC scans	321
Appendix D: Animal ethics approval	324
Appendix E: UPLC chromatograms	325

LIST OF FIGURES

- Figure 1.1:** Theoretical profile of zero order release.
- Figure 1.2:** A schematic depicting the mechanism of free-drug and *iPoly-X-Lipo* nanoparticle release from the *PXLNET*.
- Figure 2.1:** Schematics showing the a) Mechanism of action of L-dopa, the 'gold standard' in the brain (Adapted from Somani, 2008) and b) Synthesis and catabolism of dopamine - L-dopa and dopamine are precursors to norepinephrine, which in turn could be further metabolized to epinephrine (not shown). Catechol-O-methyltransferase (COMT) catalyzes the 3-O-methylation of L-dopa (not shown) as well as dopamine (and other catechols). Monoamine oxidase (MAO) deaminates and oxidizes the monoamines, dopamine, norepinephrine, epinephrine, and serotonin (only the dopamine pathway is shown) (Adapted from Fahn, 2008).
- Figure 2.2:** a) Summary of the study results on Stalevo[®] in patients experiencing 'off' periods and b) Assessment of efficacy of Stalevo[®] (Data extracted from Koller et al., 2005).
- Figure 2.3:** Preferences of patients undergoing treatment with L-dopa/carbidopa ODT and conventional tablets (Data extracted from Nausieda et al., 2005).
- Figure 2.4:** Mean L-dopa plasma concentration–time curves of the DRF (closed symbols) and the SRF (open symbols) following a) single-dose administration on day 1; b) multiple-dose administration on day 7 (n=18) (Source: Gasser et al., 1998) and c) an ideal controlled release profile.
- Figure 2.5:** In vitro release profiles of L-dopa from microspheres depicting a scanning electron micrograph of the L-dopa-loaded microspheres (inset) (Source: Arica et al., 2005).
- Figure 2.6:** a) A picture of the gastroretentive dosage form (GRDF) drawn out of the dog stomach 15 min postadministration - the GRDF has unfolded almost completely to its original size and; b) Effect of the mode of L-dopa administration on the plasma concentrations in beagle dogs (n=6) for CR-GRDF C in comparison to the two control modes of administration (oral solution and CR-particles) (Source: Klausner et al. 2003).
- Figure 2.7:** Rate of release modified by presence or absence of impermeable membrane for a) uncoated polymer matrix; b) one side uncoated and; c) an opening (pore)/coated (Adapted from: Sabel et al., 1990).
- Figure 2.8:** Transdermal apparatus for delivery of alkyl-esters of L-dopa (Adapted from: Kushnir and Heldman, 2004).
- Figure 2.9:** Overview of the pros and cons of the gamut of L-dopa delivery systems.
- Figure 3.1:** a) Viscosity as a function of shear rate for native polymers and IPEC at the first stage (sampling point I) of synthesis; b) Viscosity as a function of shear rate for native polymers and IPEC at the end stage (sampling point IV) of

synthesis and; c) Viscosity as a function of shear rate for IPEC at the 4 sampling points of the synthesis using 0.1N acetic acid.

Figure 3.2: a) Yield stress rheogram for native polymers and IPEC at the first stage of synthesis; b) Yield stress rheogram for native polymers and IPEC at the end stage of synthesis and c) Yield stress rheogram for IPEC at the 4 sampling points of synthesis using 0.1N acetic acid.

Figure 3.3.1: a) Elastic modulus as a function of shear stress for the native polymers and IPEC at 1st stage of synthesis at frequency of 0.1Hz; b) Elastic modulus as a function of shear stress for the native polymers and IPEC at end stage of synthesis at frequency of 0.1Hz and; c) Elastic modulus as a function of shear stress for IPEC 0.1N at the 4 sampling points of synthesis of synthesis at frequency of 0.1Hz.

Figure 3.3.2: a) Elastic modulus as a function of shear stress for the native polymers and IPEC at initial stage of synthesis at frequency of 1Hz; b) Elastic modulus as a function of shear stress for the native polymers and IPEC at end stage of synthesis at frequency of 1Hz and; c) Elastic modulus as a function of shear stress for IPEC 0.1N at the 4 sampling points of synthesis at frequency of 1 Hz.

Figure 3.3.3: a) Elastic modulus as a function of shear stress for the native polymers and IPEC at 1st stage of synthesis at frequency of 10 Hz; b) Elastic modulus as a function of shear stress for the native polymers and IPEC at end stage of synthesis at frequency of 10 Hz and; c) Elastic modulus as a function of shear stress for IPEC 0.1N at the 4 sampling points of synthesis at frequency of 10 Hz.

Figure 3.4: a) Elastic and viscous modulus as a function of angular frequency for NaCMC and IPEC at 1st stage of synthesis; b) Elastic and viscous modulus as a function of angular frequency for NaCMC and IPEC at end stage of synthesis and; c) Elastic and viscous modulus as a function of angular frequency for IPEC 0.1N at the 4 sampling points of synthesis.

Figure 3.5: a) Creep recovery rheogram for NaCMC and IPEC at 1st stage of synthesis; b) Creep recovery rheogram for NaCMC and IPEC at end stage of synthesis and; c) Creep recovery rheogram for IPEC 0.1N at the 4 sampling points of synthesis.

Figure 3.6: a) Elastic modulus as a function of temperature for NaCMC and IPEC at 1st stage of synthesis; b) Elastic modulus as a function of temperature for NaCMC and IPEC at the end stage of synthesis and; c) Elastic modulus as a function of temperature for IPEC 0.1N at the 4 sampling points of synthesis.

Figure 3.7: Visualization of geometrical preferences of the NaCMC-E100 (IPEC) complex a) First stage: initial mixing of two polymers; b) Second stage: after 1 hour; c) Third stage: breaking point; and d) Fourth stage: final product after molecular mechanics simulations.

Figure 3.8: Visualization of geometrical preferences of IPEC molecule presence of a) No acetic acid molecules; b) 2 acetic acid molecules; c) 4 acetic acid molecules; and d) 8 acetic acid molecules after molecular simulation in a solvated system consisting of water molecules.

- Figure 4.1:** Digital microscopic images of interpolyelectrolyte complex: a) IPEC at the ratio of 0.5:1; b) Viscous portion of IPEC; c) Diluted dispersion of IPEC; d) IPEC in 0.8N acetic acid; e) The shredded nature of the IPEC and; f) IPEC in 0.4N acetic acid.
- Figure 4.2:** a) FTIR spectra of native polymers - methacrylate copolymer and NaCMC as well as IPEC; b) FTIR spectra of IPEC before and after lyophilization; c) Spectra of IPEC synthesized with different normalities of acetic acid and; d) Comparative spectra of the physical mixture (methacrylate copolymer and NaCMC) and IPEC.
- Figure 4.3:** a) Differential scanning calorimetry thermogram of methacrylate copolymer (E100); b) Differential scanning calorimetry of native polymers – methacrylate copolymer and NaCMC; c) Differential scanning calorimetry of IPEC synthesized at different normalities of acetic acid; d) Non-reversing, total and reversing heat flows derived from ADSC scans for EC 0.1 N: i) temperature range -10 – 130°C and; ii) 130 – 250°C; e) Non-reversing, total and reversing heat flows derived from ADSC scans for methacrylate copolymer: i) temperature range -10 – 130°C and; ii) 130 – 250°C and; f) Non-reversing, total and reversing heat flows derived from ADSC scans for NaCMC: i) temperature range -10 – 130°C and; ii) 130 – 250°C.
- Figure 4.4:** A typical Force-Distance and Force-Time profiles of the interpolymeric blends for determining: a) matrix hardness and deformation energy and; b) Matrix resilience.
- Figure 4.5:** a) Matrix hardness and energy absorbed profiles of the native polymers and IPEC synthesized in 0.1 to 1.0N acetic acid and; b) Matrix resilience profile of the native polymers and IPEC synthesized in 0.1 to 1.0N acetic acid.
- Figure 4.6:** a) Comparative degree of swelling of the IPEC and NaCMC in an aqueous environment (0.1N HCl) over 24 hours; b) IPEC hydrogel retained its shape and the unhydrated inner core is an indication of further swellability: 1) IPEC hydrogel before swelling; 2) IPEC hydrogel after swelling. NaCMC lost its shape and was fully hydrated: 3) NaCMC before swelling and; 4) NaCMC after swelling and; c) Comparative degree of swelling for IPEC at different normalities of acetic acid.
- Figure 4.7:** a) Drug release profiles from the native polymers and the novel IPEC; b) Drug release profiles of IPECs of different normalities of acetic acid in buffer pH 1.5; c) Drug release profiles of IPECs of different normalities of acetic acid in buffer pH 4.5.
- Figure 5.1:** a) FTIR spectra of native polymers – locust bean, methacrylate copolymer and NaCMC; IPEC and IPB and; b) Comparative spectra of interpolyelectrolyte complex and interpolymeric blend.
- Figure 5.2:** a) Differential scanning calorimetric (DSC) curves of native polymers – methacrylate copolymer, NaCMC and locust bean; b) DSC curves of IPEC synthesized at different normalities of acetic acid; c) DSC curves of interpolymeric blend synthesized with different normalities of acetic acid; d) Non-reversing, total and reversing heat flows derived from modulated DSC curves for: i) EC 0.4 N and; ii) ELC 0.4N at temperature range -10-130°C; e)

Non-reversing, total and reversing heat flows derived from modulated DSC curves for: i) EC 0.4 N and; ii) ELC 0.4N at temperature range 130-250°C; f) Non-reversing, total and reversing heat flows derived from modulated DSC curves for NaCMC: i) temperature range -10 – 130°C and; ii) 130 – 250°C; g) Non-reversing, total and reversing heat flows derived from modulated DSC curves for methacrylate copolymer: i) temperature range -10 – 130°C and; ii) 130 – 250°C and; h) Non-reversing, total and reversing heat flows derived from modulated DSC curves for locust bean: i) temperature range -10 – 130°C and; ii) 130 – 250°C

Figure 5.3: a) The degree of swelling profiles of interpolyelectrolyte complex matrices in pH 1.5; b) The degree of swelling profiles of interpolymeric blend matrices in pH 1.5; c) The degree of swelling and erosion profiles of interpolyelectrolyte complex matrices in pH 4.5 and; d) The degree of swelling and erosion profiles of interpolymeric blend matrices in pH 4.5.

Figure 5.4: Digital images of swollen matrices in pH 1.5 after 24 hours a) IPEC matrix and; b) IPB matrix.

Figure 5.5: a) Drug release profiles of IPEC formulations in pH 1.5; b) Drug release profiles of IPB formulations in pH 1.5; c) Drug release profiles of IPEC formulations in pH 4.5 and; d) Drug release profiles of IPB blend formulations in pH 4.5.

Figure 5.6: Visualization of geometrical preferences of a) CMC-E100 and; b) magnified view of CMC-E100 along with H-bond lengths after molecular simulation in vacuum. Color codes: C (cyan), O (red), N (blue) and H (white).

Figure 5.7: Kinetic energy (EKIN), potential energy (EPOT), total energy (ETOT) (kcal/mol), and temperature (Kelvin) varying with the time of a) CMC; b) E100 and; c) IPEC.

Figure 5.8: Visualization of geometrical preference of a) CMC in complexation with E100; b) CMC in complexation with LBG; and c) E100 in complexation with LBG, after molecular mechanics simulations.

Figure 5.9: Visualization of geometrical preference of a) CMC-E100-LBG tripolymeric complex; and b) Connolly molecular electrostatic potential surfaces in translucent display mode showcasing the matrix compactness, after molecular mechanics simulations.

Figure 6.1: FTIR spectra for the interpolymeric blends a) Native polymers-locust bean, methacrylate copolymer and NaCMC; b) Formulations F1, F2 and F3 and; c) FTIR spectra for Formulation F1 in varying normalities of acetic acid

Figure 6.2: Typical force-distance and force-time profiles of the interpolymeric blends for determining: a) matrix hardness and deformation energy and; b) Matrix resilience.

Figure 6.3: Typical gastroadhesive Force-Distance profile of the IPB.

Figure 6.4: Gastroadhesive profiling of Formulation F1 in different normalities of acetic acid employing applied force of 1N.

- Figure 6.5:** Gastroadhesive profiling of Formulations F1, F2, and F3 employing applied force of 1N.
- Figure 6.6:** Gastroadhesive profiling for Formulation F1 in different normalities of acetic acid employing applied force of 0.5N.
- Figure 6.7:** Epithelial adhesive profiling of Formulation F1 in different normalities of acetic acid employing applied force of 0.5N.
- Figure 6.8:** Degree of swelling (%) for Formulation E₃ in varying normality of acetic acid.
- Figure 6.9:** Drug release profiles for Formulations F1, F2 and F3 employing 0.1N HCl as dissolution medium.
- Figure 6.10:** Drug release profiles for Formulation F1 in different normalities of acetic acid employing 0.1N HCl as dissolution medium.
- Figure 6.11:** Drug release profiles for Formulation F1 in different normalities of acetic acid employing buffer pH 1.5 (standard buffer KCl/HCl) as dissolution medium.
- Figure 6.12:** Drug release profiles for Formulation F1 in different normalities of acetic acid employing buffer pH 4.5 (0.025M KH₂PO₄/H₂PO₄) as dissolution medium.
- Figure 6.13:** Digital images of E3 matrices in different pH media: a) matrix before and after *in vitro* drug release study in pH 1.5 and; b) matrix before and after *in vitro* drug release study in pH 4.5.
- Figure 6.14:** Visualization of energy minimized geometrical preference of a) pullulan; b) glycosylated oromucopptide; and c) pullulan in complexation with mucin, after molecular mechanics simulations.
- Figure 7.1:** Drug release profiles of formulations F1 to F7.
- Figure 7.2:** Drug release profiles of formulations F8 to F14.
- Figure 7.3:** Drug release profiles of formulations F15 to F21.
- Figure 7.4:** Drug release profiles of formulations F22 to F27.
- Figure 7.5:** a) Residual plots for density; b) Residual plots for dissolution; c) Residual plots for bioadhesion and; d) Residual plots for swelling.
- Figure 7.6:** Surface plots of a) Bioadhesion versus locust bean and IPEC; b) Swelling versus solvent and temperature; c) Density versus temperature and solvent and; d) Dissolution versus temperature and IPEC.
- Figure 7.7:** Output of optimization by desirability function showing the values for independent variables and predicted values for the responses.
- Figure 8.1:** The molecular surface, topology and spaces of the polymers–chitosan and methacrylate copolymer for incoming ligands.
- Figure 8.2:** a) Space-fill/matrix occupation diagram showing maximum occupancy in unit area for chitosan and; b) space-fill/matrix occupation diagram showing maximum occupancy in unit area for methacrylate copolymer.

- Figure 8.3:** a) Space-fill/matrix occupation diagram showing maximum occupancy of methacrylate copolymer and chitosan before mixing or fusion in unit area for equal number of molecular weighted polymers (Both methacrylate copolymer and Chitosan - approx mol weight ~12K amu) and; b) fused polymeric matrix containing methacrylate copolymer and Chitosan (it may or may not have L-Dopa, lecithin, TPP or solvent - almost all filled in the space between chain).
- Figure 8.4:** Tree branching pattern: a) Octree representation; b) Two-dimensional depiction and; c) Three-dimensional representation.
- Figure 8.5:** Nodal space fillings: a) Two-dimensional and; b) Three-dimensional representation.
- Figure 8.6:** a) Two-dimensional depiction of cone-array formations and; b) Particle development, crowding and thinning of the density (space versus number of particles).
- Figure 8.7:** Frontal view of mixed triangle formations of nanoparticles: a) Two-dimensional slice representation and; b) Three-dimensional slice representation.
- Figure 8.8:** Linear pattern of nanoparticle formation: a) Progenesis and initial propagation; b) More lines of propagation and; c) Two-dimensional model of the matrix containing nanoparticles on the lines.
- Figure 8.9:** Two-dimensional chaotic pattern of nanoparticle formation.
- Figure 8.10:** mixed patterns of nanoparticle formation based on randomizations: a) two-dimensional slice of a single progenitor random patterning; b) three-dimensional model of single embedded progenitor in a chaotic-random mix state and; c) three-dimensional model of the multiple progenitors in a chaotic-random mix state based on turbulence in the medium.
- Figure 8.11:** FTIR spectra of: a) the various components employed for fabrication of nanoparticles as well as the fabricated L-dopa-loaded nanoparticles and; b) L-dopa-loaded nanoparticles; c) Methacrylate copolymer nanoparticles and methacrylate copolymer/chitosan nanoparticles and; d) L-dopa- and L-dopa/benserazide-loaded nanoparticles.
- Figure 8.12:** Digital images of: a) methacrylate copolymer/chitosan crosslinked with lecithin alone and; b) mult-crosslinked methacrylate copolymer nanoparticles (mag x 32).
- Figure 8.13:** Transmission electrom microscopic images of L-dopa-loaded methacrylate copolymer/chitosan *iPoly-X-Lipo* nanoparticles: a) magnification x 20000 and; b) magnification x 8000.
- Figure 8.14:** Scanning electron microscopic images of L-dopa-loaded methacrylate copolymer/chitosan *iPoly-X-Lipo* nanoparticles: a) magnification x 15000 and; b) magnification x 5500.
- Figure 8.15:** a) Drug release profiles of L-dopa-loaded nanoparticles employing dialysis technique in pH 1.5 buffer and; b) drug release profiles of L-dopa-loaded nanoparticles employing dialysis technique in pH 4.5 buffer.

- Figure 8.16:** a) Drug release profiles of L-dopa-loaded nanoparticles incorporated into an interpolymeric blend in pH 1.5 buffer and; b) drug release profiles of L-dopa-loaded nanoparticles incorporated into an interpolymeric blend in pH 4.5 buffer.
- Figure 8.17:** a) Comparative drug release profiles of the different formulations of levodopa-loaded methacrylate copolymer nanoparticles (B18) in pH 1.5 and; b) comparative drug release profiles of the different formulations of levodopa-loaded methacrylate copolymer/chitosan nanoparticles (B19) in pH 1.5.
- Figure 8.18:** Magnetic resonance images of the mechanical behavioral changes of matrices in different pHs: a) nanoparticles incorporated into interpolymeric blend at pH 1.5; b) interpolymeric blend matrix without nanoparticles at pH 4.5 and; c) nanoparticles incorporated into interpolymeric blend at pH 4.5 at 0, 3, 6, 9 and 12 hours.
- Figure 8.19:** Visualization of geometrical preference of phospholipid residues in complexation with: a) Chitosan and; b) methacrylate copolymer (Eudragit E100) after molecular mechanics simulations. The atoms forming the hydrogen bonds are emphasized by dotted lines after recomputing the H bonds after energy minimizations.
- Figure 8.20:** Visualization of geometrical preference of chitosan and eudragit in complexation with Phospholipid residues (PR) after molecular mechanics simulations: a) E100-PR-CHT molecular complex in full geometry; b) Connolly molecular electrostatic potential surfaces in transparent display mode showcasing the nanoparticulate system and; c) A typical conformation showcasing the bridging of E100 and CHT by phospholipid residue.
- Figure 8.21:** Visualization of geometrical preferences of TPP (stick rendering) in complexation with CHT (tube rendering) after molecular mechanics simulations.
- Figure 9.1:** Infrared spectra of a) interpolymeric blend and; b) L-dopa-loaded *iPoly-X-Lipo* nanoparticles.
- Figure 9.2:** a) Thermograms of sodium carboxymethylcellulose at temperature ranges: i) 0 to 450°C and; ii) -10 to 270°C; b) Thermogram of locust bean at temperature ranges: i) 0 to 450°C and; ii) -10 to 270°C; c) Thermogram of optimized interpolymeric blend at temperature ranges: i) 0 to 450°C and; ii) -10 to 270°C and; d) Temperature modulated thermogram of optimized interpolymeric blend at temperatures: i) -10 to 130°C and; ii) 130 to 250°C.
- Figure 9.3:** Gastro-adhesive profiling for the interpolymeric blend and PXLNET employing an applied force 0.5 N.
- Figure 9.4:** Textural profiling of IPB matrices at different time intervals (2nd, 4th, 6th and 8th hours).
- Figure 9.5:** Surface morphology of the directly compressed IPB matrices a) Mag x 173; b) Mag x 10,178 showing the granules of the matrix components and crystals of levodopa and; c) Surface morphology of hydrated and lyophilized IPB matrices showing the pores left after sublimation of water molecules during lyophilization (Mag x 168).

- Figure 9.6:** Linear Isothermic plot – Nitrogen adsorption (+ - red) and desorption (o – wine red) isotherms of interpolymeric blend.
- Figure 9.7:** a) Pore size distribution with respect to cumulative pore area and; b) Pore size distribution with respect to cumulative pore volume.
- Figure 9.8:** a) Drug release profiles of: i) IPB matrices and; ii) *PXLNET* matrices with benserazide as the DOPA decarboxylase inhibitor; b) Drug release profiles of: i) IPB matrices and; ii) *PXLNET* matrices with carbidopa as the DOPA decarboxylase inhibitor; c) Drug release profiles of: i) Madopar[®] IR and; ii) Madopar[®] HBS; d) Drug release profiles of: i) Sinemet[®] IR and; ii) Sinemet[®] CR; e) Comparative drug release profiles of levodopa from IPB matrices and Madopar[®] HBS capsules and f) Comparative drug release profiles of levodopa from IPB matrices, Madopar[®] HBS capsules and Sinemet[®] CR.
- Figure 9.9:** a) MRI images of interpolymeric blend tablet matrices: 1) at pH 1.5 and; 2) at pH 4.5; b) Area analysis of MRI images as a function of time: i) the area of the dry core over time; ii) the hydrated and gelled area of the matrix over time at pH 1.5 and; iii) increase in absorbance over time which is indicative of rate of drug release over time at pH 1.5 and; c) Area analysis of MRI images as a function of time: i) the area of the dry core over time; ii) the hydrated and gelled area of the matrix over time at pH 1.5 and; iii) increase in absorbance over time which is indicative of rate of drug release over time at pH 1.5.
- Figure 9.10:** a) L-dopa-loaded nanoparticles changes to black color and; b) carbidopa-loaded nanoparticles change to yellow in the presence of moisture.
- Figure 10.1:** Images depicting habituation procedures.
- Figure 10.2:** Surgical procedures for insertion of catheter into the jugular vein.
- Figure 10.3:** The daily flushing procedures to keep the catheter open and prevent infection.
- Figure 10.4:** Gastric dosing procedure for oral administration.
- Figure 10.5:** Flow diagram detailing *in vivo* animal studies for drug delivery system six (DDS).
- Figure 10.6:** The process of withdrawing cerebrospinal fluid from a pig.
- Figure 10.7:** Process of bladder catheterization and urine sampling.
- Figure 10.8:** Images of a pig as it is prepared for X-ray imaging.
- Figure 10.9:** schematic diagram of a 96-wells plate depicting the arrangement of the samples, no-cell background and cells only.
- Figure 10.10:** Radiographic images of a) GDDS with the pig in the anterior-posterior position b) GDDS with the pig in the lateral position and; c) *PXLNET* with the pig in the anterior-posterior position.
- Figure 10.11:** a) Images from dosed pig's stomach showing i) Mild lymphocytic aggregate in lamina propria interstitium and; ii) Lymphoid follicle in deep lamina propria and sub-mucosal edema and; b) Images from control tissue: i) Moderate lymphoplasmacytic interstitial lamina propria infiltration - higher magnification

(x20). ii) Moderate lymphoplasmacytic interstitial lamina propria infiltration - Lower magnification (x10) iii) Mild lymphoplasmacytic interstitial aggregated in the lamina propria.

Figure 10.12: Microscopical images of CaCo 2 adhesion cells.

Figure 10.13: Mean methyldopa plasma concentration after administration of a) Madopar[®] HBS capsules; b) *PXLNET* matrices and; c) IPB matrices.

Figure 10.14: A typical mean dopamine plasma concentration observed for all formulations.

Figure 10.15: Comparative L-dopa pharmacokinetic curve of Madopar[®] HBS capsules, *PXLNET* and IPB matrices after single dose administration.

Figure 10.16: Predicted L-Dopa plasma concentrations from 0.24 to 8 hours.

Figure 10.17: Linear regression multiple-level C IVIVC correlation models for a) Madopar[®] HBS capsules; b) *PXLNET* matrices and; c) IPB matrices.

LIST OF TABLES

- Table 2.1:** Comparative pharmacokinetic parameters of levodopa analysis obtained from Dual release formulation (DRF) and controlled release formulation (CRF) (data extracted from Gasser, 1998).
- Table 3.1:** Yield values of native polymers and IPEC at the sampling stages during synthesis.
- Table 3.2:** Computational differential energy attributes calculated for the simulated IPEC system in a molecular mechanics' force field setup performed using HyperChem™ 8.0.8.
- Table 4.1:** The parameter settings for the textural analysis of the matrices.
- Table 5.1:** The degree of erosion (at the 8th hour) in pH 4.5 by gravimetric method.
- Table 5.2:** Dissolution Efficiencies of IPEC and IPB.
- Table 5.3:** Mathematical modeling of drug release profiles of IPEC and IPB.
- Table 5.4:** Computational molecular attributes calculated for the simulated IPEC system in a molecular mechanics' force field setup performed using HyperChem™ 8.0.8.
- Table 5.5:** Energy attributes calculated for the simulated IPEC system in a molecular dynamics setup performed using HyperChem™ 8.0.8.
- Table 5.6:** Computational differential energy attributes calculated for the simulated IPEC/LBG system in a molecular mechanics' force field setup performed using HyperChem™ 8.0.8.
- Table 6.1:** Compositions of the polymers utilized for generation of interpolymeric blends.
- Table 6.2:** Composition of a directly compressed matrix.
- Table 6.3:** The parameter settings for the gastroadhesivity test of the matrices.
- Table 6.4:** Densities of the IPB formulations.
- Table 6.5:** Texture profiling analysis of IPB formulations.
- Table 6.6:** Degree of swelling of IPB matrices.
- Table 6.7:** Mathematical modeling of drug release profiles of IPB formulations.
- Table 6.8:** Calculated molecular attributes of the complexes involving pullulan, mucopeptide analogue and pullulan-mucopeptide analogue.
- Table 7.1:** The experimental variables employed in generating the formulation compositions.
- Table 7.2:** The formulation compositions generated by Box-Behnken design.

- Table 7.3:** Composition of a directly compressed matrix employing BBD generated IPB.
- Table 7.4:** Density data chart for twenty-seven formulations.
- Table 7.5:** Force of adhesion and work of adhesion data for the experimentally derived formulations.
- Tablet 7.6:** Data depicting rigidity and deformation energy for unhydrated and hydrated matrices.
- Table 7.7:** A cumulative data indicating the generated independent variables and the experimental values of dependent variables.
- Table 7.8:** Standard error of fits for the 27 formulations with respect to the responses.
- Table 7.9:** P-values for lack-of-fit with respect to responses.
- Table 7.10:** Correlations between the variables employed in the response surface design.
- Table 8.1:** Components and the respective quantities employed for nanoparticles formation.
- Table 8.2:** Image acquisition parameters applied during magnetic resonance imaging using MARAN-i.
- Table 8.3:** Comparative pH changes during nano-fabrication.
- Table 8.4:** Changes in absorbances during nano-fabrication.
- Table 9.1:** Composition of L-dopa-loaded *iPoly-X-Lipo* nanoparticles.
- Table 9.2:** Optimized values for independent variables and predicted values for dependent variables.
- Table 9.3:** Composition of a directly compressed matrix employing optimized IPB.
- Table 9.4:** Degassing parameters for evacuation and heating phases
- Table 9.5:** Parameter settings for analysis conditions
- Table 9.6:** Density results for interpolymeric blend and nano-enabled tablet matrices.
- Table 9.7:** a) Textural data of unhydrated interpolymeric blend and PXLNET matrices and; b) Swellability result for IPB and PXLNET matrices employing textural analyzer.
- Table 9.8:** A summary of surface area and pore analyses of IPB matrices.
- Table 9.9:** a) Comparative release kinetics and dissolution efficiencies of the various drug devices and; b) Outcomes of Higuchi and Korsmeyer-Peppas modeling.
- Table 9.10:** Similarity factor f_2 .

- Table 10.1:** Multiple reaction monitoring parameters.
- Table 10.2:** Cytotoxicity step-wise data of *PXLNET* and IPB.
- Table 10.3:** Mean cerebrospinal fluid concentration after oral administration of Madopar[®] HBS capsules, *PXLNET* and IPB matrices.
- Table 10.4:** Mean urine concentration after oral administration of Madopar[®] HBS capsules, *PXLNET* and IPB matrices.
- Table 10.5:** L-dopa non-compartmental pharmacokinetic parameters following oral administration of Madopar[®] HBS capsules, *PXLNET* and IPB matrices.

LIST OF EQUATIONS

Equation 3.1: Molecular mechanics energy relationship (MMER) model for potential energy factor in various molecular complexes.

Equation 3.2: The total potential energy deviation of IPEC system.

Equation 3.3: The global energy relationship for NaCMC derived after assisted model building and energy refinements.

Equation 3.4: The global energy relationship for methacrylate copolymer derived after assisted model building and energy refinements.

Equation 3.5: The global energy relationship for IPEC at onset of synthesis derived after assisted model building and energy refinements.

Equation 3.6: The global energy relationship for IPEC one hour into synthesis derived after assisted model building and energy refinements.

Equation 3.7: The global energy relationship for IPEC at breaking point derived after assisted model building and energy refinements.

Equation 3.8: The global energy relationship for IPEC at the end of synthesis derived after assisted model building and energy refinements.

Equation 3.9: The global energy relationship for IPEC and solvent derived after assisted model building and energy refinements.

Equation 3.10: The global energy relationship for the various complexes derived after assisted model building and energy refinements for IPEC and 0.2N acetic acid.

Equation 3.11: The global energy relationship for IPEC and 0.4N acetic acid derived after assisted model building and energy refinements.

Equations 3.12: The global energy relationship for IPEC and 0.8N acetic acid derived after assisted model building and energy refinements.

Equation 4.1: The degree of swelling.

Equation 5.1: Dissolution efficiency.

Equation 5.2: Trapezoidal method for calculating the numerator of Equation 5.1.

Equation 5.3: The zero-order model.

Equation 5.4: The First-order model.

Equation 5.5: Higuchi equation.

Equation 5.6: Korsmeyer-Peppas equation.

Equation 5.7: Logarithm of Korsmeyer-Peppas equation.

Equation 5.8:The global energy relationship for NaCMC derived after assisted model building and energy refinements.

Equation 5.9:The global energy relationship for methacrylate copolymer derived after assisted model building and refinements.

Equation 5.10:The global energy relationship for locust bean derived after assisted model building and refinements.

Equation 5.11:The global energy relationship for IPEC derived after assisted model building and refinements.

Equation 5.12:The global energy relationship for NaCMC-locust bean derived after assisted model building and refinements.

Equation 5.13:The global energy relationship for methacrylate copolymer-locust bean derived after assisted model building and refinements.

Equation 5.14:The global energy relationship for NaCMC-methacrylate copolymer-locust bean derived after assisted model building and refinements.

Equation 5.15: The total potential energy deviation.

Equation 6.1:The global energy relationship for pullulan derived after assisted model building and energy refinements.

Equation 6.2:The global energy relationship for mucopeptide analogue derived after assisted model building and energy refinements.

Equation 6.3:The global energy relationship for pullulan – mucopeptide analogue derived after assisted model building and energy refinements.

Equation 8.1: The percentage drug loading.

Equation 8.2: Drug entrapment efficiency.

Equation 8.3:Molecular mechanics energy relationship (MMER) model for steric energy factor in various molecular complexes.

Equation 8.4: MMER model for steric energy factor for chitosan.

Equation 8.5: MMER model for steric energy factor for phospholipid residues.

Equation 8.6: MMER model for steric energy factor for chitosan – phospholipid residues.

Equation 8.7: MMER model for steric energy factor for methacrylate copolymer.

Equation 8.8:MMER model for steric energy factor for methacrylate copolymer – phospholipid residues.

Equation 8.9:MMER model for steric energy factor for methacrylate copolymer – phospholipid residues – chitosan.

Equation 8.10: MMER model for steric energy factor for tripolyphosphate.

Equation 8.11: MMER model for steric energy factor for chitosan – tripolyphosphate.

Equation 9.1: Similarity factor f_2 .

CHAPTER ONE

INTRODUCTION

1.1. BACKGROUND OF THIS STUDY

One of the most prevalent movement disorders of old age is Parkinson's Disease (PD) (Dick, 2006). PD has a peak age onset of 65 years although younger onset in individuals of less than 40 years and rare juvenile forms may occur (Dick, 2006). In the United Kingdom, approximately 30-40 patients are diagnosed daily with PD (Taylor and Counsell, 2006). In the United States approximately, one million people are affected costing the economy an estimated \$28 billion (Bogdanov et al., 2008). It is envisaged that as people age and life expectancy increases, the number of individuals living with PD will increase substantially. PD is the second most common neurodegenerative disorder after Alzheimer Disease (Schapira, 2006). The cause of PD is not known but the discovery of several pathogenic mechanisms and etiologies have led to the belief that PD is not a single entity but rather several forms of a debilitating disease (Tintner and Jankovic, 2002). Evidence suggests that the determinants of PD are both genetic and environmentally related with a family history of PD also earmarked as a potential risk factor (Dick, 2006; Schapira, 2006; Dick et al., 2007).

Several drugs are currently used for the treatment of PD. These include levodopa (L-dopa), selegiline, amantadine, bromocriptine and catechol-O-methyltransferase (COMT) inhibitors such as entacapone (Singh et al., 2007). L-dopa remains the gold standard for the initial treatment of PD that provides superior symptomatic control in the early stages of PD (Olanow, 2004). However, although L-dopa is soluble, the absorption after oral administration and its bioavailability are significantly reduced by extensive metabolism of L-dopa principally through decarboxylation, O-methylation, transamination and oxidation in the gastrointestinal tract (GIT) and liver (Muzzi et al., 2008). After oral administration, the gastric region has a limited capacity to absorb L-dopa due to the presence of degradative enzymes such as aromatic amino acid decarboxylase that metabolize L-dopa to dopamine (DA), homovanillic acid and dihydroxyphenylacetic acid (Muzzi et al., 2008). Hence, more than 95% of L-dopa is metabolized in the GIT, liver and plasma while only 1% of the ingested dose penetrates into the central nervous system (CNS) for the treatment of PD (Jankovic, 2002). Absorption of L-dopa occurs mainly in the duodenum by a saturable facilitated transport mechanism specific to aromatic and branched amino acids (Muzzi et al., 2008). Based on the poor absorption and bioavailability of L-dopa, attempts have been made to improve oral formulations by increasing the dose of L-dopa and adding a decarboxylase inhibitor such as carbidopa to reduce the associated side-effects of peripherally converted L-dopa to DA

(Zhang et al., 2001). However, this approach significantly increased the associated side-effects due to larger doses that need to be administered with carbidopa (Jankovic, 2002).

Concomitant administration of L-dopa with carbidopa (Sinemet[®], Merck and Co., Inc. Whitehouse Station, NJ, USA) regulates the plasma concentrations of DA thereby reducing the side-effects caused by the peripheral conversion of L-dopa to DA. This affords lower doses of L-dopa to be used effectively for the treatment of PD (Sagar and Smyth, 2000). Another decarboxylase inhibitor, benserazide, has also been used in combination with L-dopa (Madopar[®], Hoffmann-La Roche Ltd, Basel, Switzerland). Combination products such as Sinemet[®] and Madopar[®] reduce the peripheral conversion of L-dopa to DA and consequently the associated side-effects. However, they do not reduce the dyskinesias and motor fluctuations prevalent with long-term use of L-dopa (Olanow, 2004). Furthermore, Sinemet[®] and Madopar[®] immediate release formulations produce erratic plasma levels of L-dopa that are dependent on the biological half-life of L-dopa, the frequency of dosing and the release rate of L-dopa leading to side-effects (Sagar and Smyth, 2000). In an attempt to improve the erratic plasma levels of L-dopa, controlled release formulations of L-dopa/carbidopa and L-dopa/benserazide combinations (Sinemet[®] CR and Madopar[®] HBS) were developed. These formulations comprise polymeric delivery systems that offer temporal relief from side-effects and reduced dosing compared to immediate release formulations (Hurtig, 1997). Erratic plasma levels of L-dopa were found to be reduced with Sinemet[®] CR and Madopar[®] HBS. However, these formulations still display poor absorption and bioavailabilities requiring the dose of L-dopa to be increased (Piccini et al., 2000). The absolute bioavailability of L-dopa from Sinemet[®] CR is approximately 44% (FDA – CDER, 2000). This culminates to approximately 56% of L-dopa lost through poor GIT absorption, GIT and liver metabolism as well as the peripheral conversion of L-dopa to DA. Furthermore, the release of L-dopa/carbidopa from Sinemet[®] CR was investigated by Sagar and Smyth (2000) and was found to follow first-order release kinetics. In addition, the side-effects profile did not differ significantly from immediate release formulations of Sinemet[®] and Madopar[®] (Koller et al., 1999).

In order to further improve the therapy of PD, in November 2003, the US Food and Drug Administration (FDA) approved the product Stalevo[®] (Orion Pharma, Espoo, Finland) which is a combination of L-dopa, carbidopa and entacapone in a single formulation. Entacapone, a highly potent peripherally acting COMT inhibitor increases the bioavailability of L-dopa by reducing the peripheral conversion of L-dopa to 3-O-methyldopa and therefore enhances the clinical efficacy of both immediate and controlled release L-dopa/carbidopa formulations (Piccini et al., 2000). However, in a large prospective double-blind placebo-controlled trial, Stalevo[®] did not improve the dyskinesias and motor fluctuations due to the erratic plasma

levels of L-dopa (Olanow and Stocchi, 2004). Hauser reported that entacapone increases the dyskinesias and therefore the daily dose of L-dopa may be reduced (Hauser, 2004). Increased frequency of dosing to four times daily was suggested by Smith and co-workers to reduce the incidence of dyskinesias (Smith et al., 2004). However, this may generate patient non-compliance which in turn will not achieve the aim of the increased frequency of dosing.

Although L-dopa remains the most effective anti-parkinsonian agent that is eventually required by all PD patients, it does not provide an optimal clinical response due to inadequate modes of delivery, poor absorption, erratic plasma level fluctuations and subsequent CNS bioavailability. Consequently, in order to stabilize the erratic plasma fluctuations of L-dopa, an aqueous-based infusion of L-dopa/carbidopa (Duodopa[®], Solvay Healthcare Ltd., West End, Southampton, UK) was introduced (Nilsson et al., 2001). Duodopa[®] is administered through a continuous intra-duodenal infusion via a cumbersome portable pump. The infusion delivers L-dopa continuously to the duodenum and bypasses the gastric region (Nilsson et al., 2001). However, infusion therapies are impractical for patients, caregivers and physicians. In a seven year study, challenges such as change and repair of pumps, infections, minor discharges and change or adjustment of catheters by gastroscopy or X-ray guidance were encountered (Nilsson et al., 2001). Thus, although Duodopa[®] infusion therapy may enhance the absorption, achieve constant plasma concentrations and the bioavailability of L-dopa to the CNS, they are difficult to handle and leads to poor patient compliance.

Therefore, the development of more simplified treatment modalities employing an oral formulation (being the most convenient route of administration for chronic drug therapy) that may improve the absorption and subsequent bioavailability of L-dopa/carbidopa with constant therapeutic plasma concentrations will provide a significant advancement in the treatment of PD. Apart from co-administration with enzyme inhibitors or other bioavailability enhancers and increased doses, alternative approaches that have been employed to improve the absorption and bioavailability of various drugs include micronization (Thanos et al., 2003a) self-emulsification (Neslihan and Benita, 2004); solid dispersions (Leuner and Dressman, 2000); solubilization (Francis et al., 2003); bioadhesion (Thanos et al., 2003b) and more recently nanotechnology (Italia et al., 2007). Nanotechnology has led to the development of nanostructures for therapeutic purposes such as nanomicelles, nanoliposomes, nanocapsules, nanoemulsions, lipid nanoparticles, dendrimers and polymeric nanoparticles for targeted drug delivery (Sahoo and Labhasetwar, 2003; Yih and Al-Fandi, 2006).

Factors that affect the absorption and bioavailability of L-dopa are mainly enzymatic degradation in the GIT and liver, the GIT transit time and the competition of L-dopa with larger neutral amino acids for absorption and transport in the GIT and CNS respectively (Seeberger and Hauser, 2007). Polymeric nanoparticles are able to protect drug from degradation in the GIT; are able to bypass the liver thereby avoiding “first pass metabolism”; remain in the systemic circulation for longer periods; target the delivery of drugs to the CNS and are able to deliver drugs via the oral route (Soppimath et al., 2001; Nimesh et al., 2006; Italia et al., 2007). The oral absorption and subsequent bioavailability of L-dopa can be improved by the use of polymeric nanoparticles that are able to exploit specialized uptake mechanisms such as absorptive endocytosis and/or bioadhesivity due to carboxylic end-group exposure enhancing binding and penetration through the GIT mucosa (Langer and Peppas, 2003). Furthermore, particle size and zeta potential may influence the functionality and effectiveness of the nanoparticles in order to prolong the GIT transit time and protect the drug from premature degradation (Peppas, 2004). Various approaches have been used for synthesizing polymeric nanoparticles that are able to control drug release and include solvent evaporation, emulsification-diffusion, solvent-displacement, supercritical fluid technology, crosslinking, emulsion-polymerization and interfacial-polymerization (Soppimath et al., 2001; Pinto et al., 2006). Currently, a handful of oral nano-enabled drug delivery products are marketed which comprise nano-suspensions of sirolimus (Rapamune[®], Wyeth, Madison, NJ, USA), aprepitant (Emend[®], Merck and Co., Inc. Whitehouse Station, NJ, USA), fenofibrate (Tricor[®], Abott Labs, Illinois, USA) and megestrol acetate (Megace[®] ES, Par Pharmaceuticals, Woodcliff Lake, NJ, USA). Nanoparticulate tablet formulations include sirolimus (Rapamune[®], Wyeth, Madison, NJ, USA) and fenofibrate (Tricor[®], Abott Labs, Illinois, USA) formulated employing Elan[®] Pharmaceutical’s NanoCrystal[®] technology that reduces drug particles to nano-size to improve bioavailability (Van Eerdenbrugh et al., 2007).

However, to date, there is no nano-enabled formulation that specifically explores the enhancement in the oral absorption and subsequent bioavailability profiles of L-dopa/carbidopa and L-dopa/benserazide combinations. Although conventional polymeric nanoparticles have been used to improve the bioavailability of some drugs as mentioned above, they are not ideal since they are restricted by the homogenous design of the nanostructures that are purely dependant on the properties of the polymer incorporated and thus do not afford maximal flexibility in terms of GIT absorption and subsequent bioavailability. Therefore due to the poor absorption and subsequent bioavailability of L-dopa, this study developed an orally administered drug delivery system loaded with L-dopa/carbidopa composite ionic polymer-crosslinked-lipoid (*iPoly-X-Lipo*) (i.e. crosslinked ionic-rich composite polymer and lipid based nanoparticle matrices, *not of the liposome type*)

nanoparticles targeted for maximal duodenal absorption within the GIT as opposed to conventional polymeric nanoparticles. The *iPoly-X-Lipo* nanoparticles were envisaged to provide constant plasma levels of L-dopa/carbidopa via the poly-phase in order to reduce the inherent side-effects and subsequently improve the bioavailability of L-dopa via the inherent lipo-phase.

1.2. RATIONALE AND MOTIVATION FOR THIS STUDY

This study proposed to develop a multi-crosslinked *iPoly-X-Lipo* Nano-Enabled Tablet (*PXLNET*) platform comprising either L-dopa/carbidopa or L-dopa/benserazide loaded *iPoly-X-Lipo* nanoparticles embedded within directly compressible polymers as an oral tablet platform. The *PXLNET* was designed to improve the oral absorption of existing L-dopa/carbidopa and L-dopa/benserazide preparations such as Sinemet CR[®] and Madopar[®] HBS. Due to the Narrow Absorption Window of L-dopa, an oral gastroretentive drug delivery system may prolong the gastric transit time, thereby enhancing the extent of L-dopa-loaded *iPoly-X-Lipo* nanoparticles to be maximally absorbed through the duodenum. It was envisaged that the *PXLNET* would display pH and density dependence and gastroretentive behavior (within the gastric region) and allow for site-specific release of the *iPoly-X-Lipo* nanoparticles for duodenal absorption with zero-order kinetics. A graph depicting ideal constant plasma levels is shown in Figure 1.

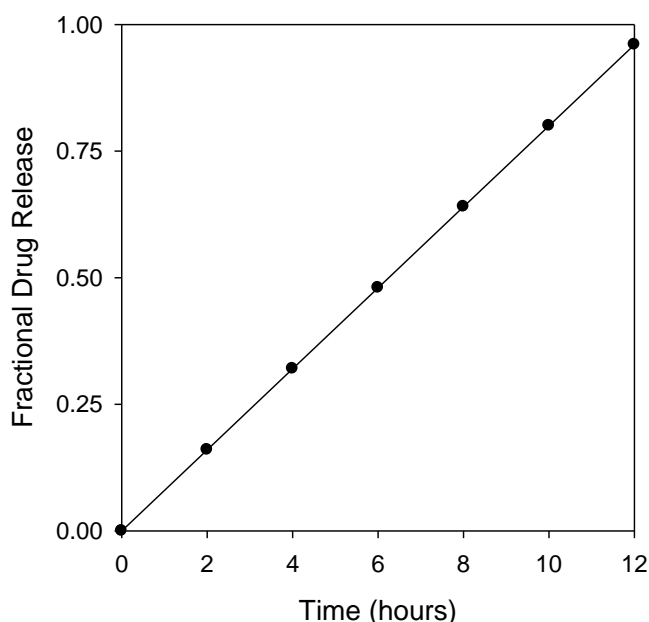


Figure 1.1: Theoretical profile of zero-order drug release.

The *PXLNET* was formulated to feature enhanced gastro-adhesion, superior mechanical strength and high density that would facilitate exodus of the *PXLNET* to the antrum of the stomach once hydrated. Novel multi-crosslinking technology employing chemical polymer-lipid interfacial mechanisms was used to synthesize the *iPoly-X-Lipo* nanoparticles and to further modify the physicochemical and physicomechanical properties of the nanostructures in order to achieve superior control over L-dopa/carbidopa release and the erosional dynamics of the *PXLNET*. The polymeric chains of the *PXLNET* platform will be rendered denser by introducing additional chemical bonds between the polymers, whereby the number of crosslinks would be proportional to the ability to hydrate and the density of the *PXLNET*.

Polymers suitable for incorporation into the poly-phase of the *iPoly-X-Lipo* nanoparticles comprised a natural polysaccharide (chitosan) and a polyacrylate (Eudragit® E100). To facilitate the enhanced duodenal absorption and eventual delivery of the *iPoly-X-Lipo* nanoparticles to the CNS, surfactant-based phospholipids were constituted as the Lipo-phase of the *iPoly-X-Lipo* nanoparticles. It was envisaged that the *iPoly-X-Lipo* nanoparticles would be able to protect L-dopa from peripheral conversion to DA thereby reducing the associated side-effects and allow more L-dopa to be available at the blood-brain barrier for entry into the CNS.

To further modify the release of L-dopa/carbidopa, *iPoly-X-Lipo* nanoparticles were incorporated into an interpolymeric blend of highly compressible pharmaceutical natural and synthetic polymers designed for oral drug delivery in order to maintain the stability of the *iPoly-X-Lipo* nanoparticles during compaction and compression processes ensuring that the performance of the nanoparticles for targeting to the duodenum and subsequent absorption. To ensure prolonged gastro-adhesion of the *PXLNET*, exopolysaccharides such as pullulan was incorporated into the *PXLNET* platform. Blending and interaction of the polymeric permutation would also enhance gastro-adhesion, control the erosional dynamics of the *PXLNET*, modulate the release of the L-dopa/carbidopa *iPoly-X-Lipo* nanoparticles and enhance the mechanical stability of the *PXLNET*.

The proposed triple gastroretentive mechanism achieved through gastro-adhesion, high density and swelling of the *PXLNET* would prolong the gastric residence time of the system within the antrum of the stomach thereby increasing the time available for the L-dopa/carbidopa *iPoly-X-Lipo* nanoparticles to be released and absorbed in the duodenum. Polymers such as the polysaccharides which are bioadhesive and able to swell at gastric pH was selected to design the *PXLNET* platform such that the system would swell, significantly increase in density, migrate to the antrum and thereafter gelate to facilitate gastro-adhesion to the antrum of the stomach (Figure 1.2). As the interpolymeric blend dissociates and

swells, L-dopa/benserazide or L-dopa/carbidopa would diffuse through the gelled *PXLNET* polymeric network and migrate toward the duodenum for maximal absorption into the systemic circulation. To further enhance the density of the *PXLNET*, modify the release of the *iPoly-X-Lipo* nanoparticles and to facilitate *in vivo* radio-labeled imaging of the *PXLNET*, radio-opaque barium sulphate was included in the formulation.

It was envisaged that the proposed *PXLNET* would improve the duodenal absorption and plasma levels of L-dopa/carbidopa throughout the delivery period. The computed pharmacokinetic duodenal absorption and cerebrospinal fluid (CSF) bioavailability attained with the *PXLNET* was compared with conventional oral formulations currently marketed such as Sinemet[®], Madopar[®], Sinemet[®] CR, Madopar[®] HBS. The proposed mechanism of drug-loaded *iPoly-X-Lipo* nanoparticles released from the *PXLNET* is conceptualized in Figure 1.2.

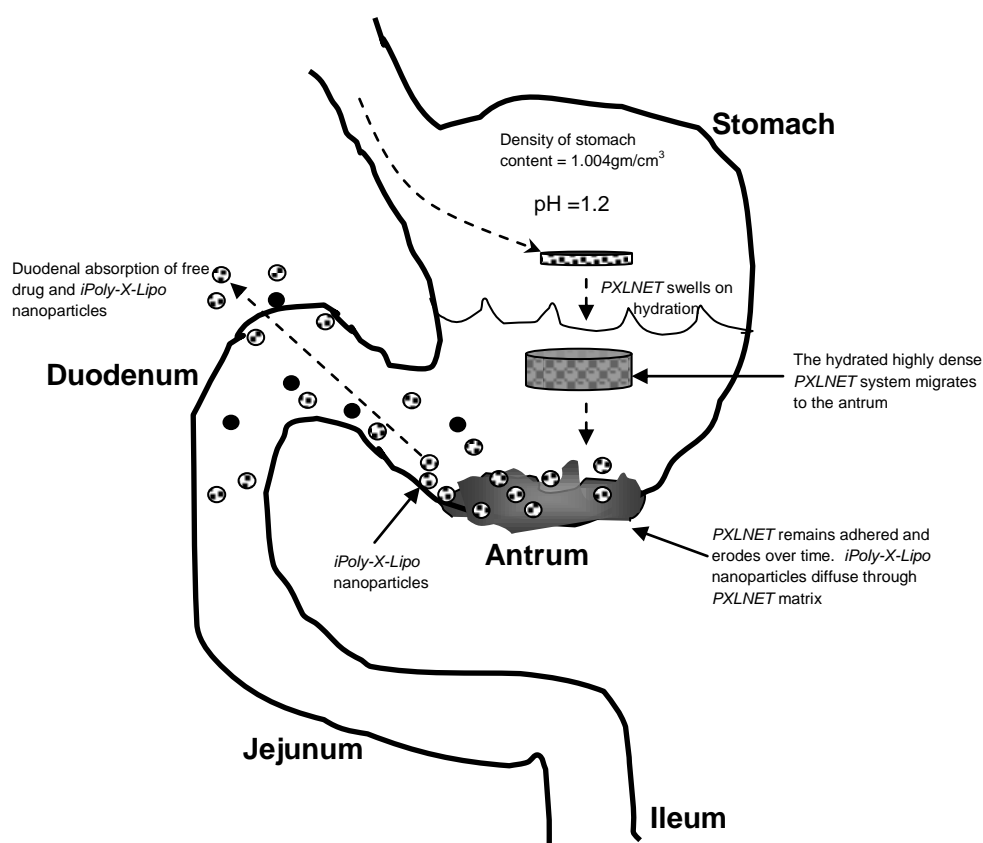


Figure 1.2: A schematic depicting the mechanism of free-drug and *iPoly-X-Lipo* nanoparticles release from the *PXLNET*.

1.3. AIM AND OBJECTIVES OF THIS STUDY

The study was undertaken to improve the absorption and bioavailability of L-dopa by synthesizing a polymeric blend and employing nanotechnology and pharmaceutical

technology to fabricate a triple mechanism gastroretentive *PXLNET* to deliver L-dopa at a constant and sustained rate over a prolonged period. The core objectives of this study were:

1. To explore methods such as chemical crosslinking in conjunction with solvent-evaporation and/or emulsification-diffusion for synthesizing the *iPoly-X-Lipo* nanoparticles.
2. To explore suitable surfactants, phospholipids or polysorbates for incorporation into the lipo-phase of the *iPoly-x-Lipo* nanoparticles.
3. To synthesize and characterize an interpolymeric blend (employing suitable polymers such as natural polysaccharides and polyacrylates) which will be employed in formulation of *PXLNET*.
4. To formulate the highly dense gastro-adhesive *PXLNET* using interpolymeric blend, exopolysaccharides such as pullulan and high dense substances such as barium sulphate. The technique envisaged at this stage would be direct compression of the interpolymeric blend with the L-dopa/carbidopa *iPoly-X-Lipo* nanoparticles to form the *PXLNET*.
5. To evaluate the physicochemical and physicomechanical properties of the interpolymeric blend and the *iPoly-X-Lipo* nanoparticles. This will include zeta and size analyses, surface morphological analyses, thermal behavior of *PXLNET* components, drug entrapment efficiency within the *iPoly-X-Lipo* nanoparticles, textural profiling of the solid interpolymeric blend and subsequent L-dopa/carbidopa release.
6. To assess the L-dopa/carbidopa release behavior from the *iPoly-X-Lipo* nanoparticles and *PXLNET* and compare the release kinetics to conventional formulations.
7. To perform *ex vivo* studies on gastric tissue to assess the extent of gastro-adhesion and veracity of the *PXLNET*.
8. To perform *in vivo* studies in a Large White pig model to assess the L-dopa/carbidopa release kinetics from the *PXLNET*. A statistical experimental design strategy such as Response Surface Methodology was employed in order to optimize the formulation variables in order to obtain a desired formulation for *in vivo* animal studies.

1.4. OVERVIEW OF THIS THESIS

Chapter 1 provides a concise background of Parkinson's disease, the current pharmacological therapies, their challenges and the rationale and motivation for this study. A triple-mechanism gastroretentive drug delivery system which will improve the bioavailability of L-dopa, providing a constant plasma delivery of the drug over a prolonged period was proposed and rationalized. The aim, objectives and technologies to be employed were also indicated in the later part of the chapter.

Chapter 2 is a literature review of the L-dopa loaded drug delivery systems developed over the past three decades. The L-dopa loaded delivery systems elaborated amongst others include immediate release formulations, liquid formulations, dispersible tablets, controlled release formulations, dual release formulations, microspheres, infusion and transdermal delivery systems. This review critically assessed the attempts directed at improving L-dopa absorption, bioavailability and maintenance of constant plasma concentrations, including the drug delivery technologies implicated.

Chapter 3 deals with the rheological characterization of an interpolyelectrolyte complex during and at the end of synthesis. The rheological properties of the interpolyelectrolyte complex were monitored and compared with the rheological properties of the individual polymers used in the formation of the interpolyelectrolyte complex. The rheological studies undertaken included basic viscosity, yield stress test, oscillatory stress sweep, oscillatory frequency sweep, creep and recovery and temperature ramp. It was found that the interpolyelectrolyte complex exhibited different rheological behaviors at different points during synthesis. In comparison to the individual polymers, the end product obtained after synthesis of the interpolyelectrolyte complex exhibited increased elastic modulus suggesting a solid-like behavior and having the potential for controlled release delivery of drugs.

Chapter 4 provides insights into the interactions between the polymers that made up the interpolyelectrolyte complex with the aid of computational modeling and also explores the drug delivery properties of the interpolyelectrolyte complex. The interpolyelectrolyte complex was loaded with L-dopa and directly compressed without excipients in order to assess its drug delivery abilities unaided. Physicomechanical and physicochemical characterizations were undertaken by digital microscopy, moisture content, Fourier Transform Infra-Red (FTIR) spectroscopy, thermal behavioral analysis, determination of mechanical strength, swellability and *in vitro* drug release studies. The interpolyelectrolyte complex as a drug carrier exhibited superior mechanical strength and controlled the release of L-dopa over 24 hours at a fairly constant rate.

Chapter 5 studies the influence of blending a natural polysaccharide with the interpolyelectrolyte complex. The drug delivery properties of the interpolyelectrolyte complex were compared to its blend with a natural polysaccharide. Most of the characterizations undertaken in chapter 4 were also carried out in this chapter. The presence of a natural polysaccharide decreased the excessive swelling of interpolyelectrolyte complex; eliminated bulk erosion while promoting surface erosion and exhibited zero order release kinetics.

Chapter 6 explores the use of the interpolymeric blend (IPB) between interpolyelectrolyte complex and the natural polysaccharide in the development of a gastroretentive drug delivery system. The development of the gastroretentive drug delivery system involved the incorporation of three mechanisms of gastroretention to enhance gastric residence time. The system was characterized by assessing its swellability, gastroadhesive properties and density amongst other properties. It was found that the system has the potential to be retained in the stomach and release L-dopa at a constant rate over a prolonged period and consequently may improve the absorption and bioavailability of L-dopa.

Chapter 7 undertakes the process of optimization of the gastroretentive drug delivery system. The process factors which influence the responses (such as bioadhesion, swelling and dissolution) were assessed as well as the impact of the interactions between the process factors. Box-Behnken design and desirability function were employed to generate the optimized gastroretentive drug delivery system. It was found that Box-Behnken design and desirability function were adequate in obtaining an optimized system. All the responses had the desirability of 1 which is ideal.

Chapter 8 involves the fabrication, modeling and characterization of L-dopa-loaded nanoparticles. The nanoparticles' characterization involved molecular mechanics computation, size and zeta potential determination, FTIR spectroscopy, digital microscopy, scanning and transmission electron microscopies, drug loading efficiency, drug entrapment efficiency and *in vitro* drug release studies. The nanoparticles were incorporated into the interpolymeric blend prepared in Chapter 5 for comparative *in vitro* drug release studies. Multi-crosslinking in fabrication of the nanoparticles was achieved, spherical capsules were obtained with high drug entrapment and controlled drug release over a prolonged period was achieved by incorporation of the nanoparticles into the interpolymeric blend. The computational modeling predicted the interaction mechanisms between the polymers and the crosslinking agents employed.

Chapter 9 provides further characterization of the optimized IPB gastroretentive drug delivery system and the *iPoly-X-Lipo* nano-enabled tablet matrices (*PXLNET*). The studies

undertaken included pore size and surface area analyses, surface morphological analysis of matrices, FTIR spectroscopy, thermal analysis of the interpolymeric blend, magnetic resonance imaging of the matrices and comparative *in vitro* drug release studies with conventional dosage forms. The gastroretentive drug delivery matrices were mesoporous, exhibited good mechanical strength, found to be pH responsive and had the best fit for zero order kinetics in comparison with the conventional dosage forms.

Chapter 10 provides the *ex-vivo* and *in vivo* studies in Large White pigs which included histopathology, cytotoxicity testing, assessment of gastroretention, comparative drug release studies with Madopar[®] HBS as well as pharmacokinetic analysis. The histopathology and cytotoxicity confirmed that the drug delivery systems were safe for consumption. X-rays analysis after 7 hours of drug administration showed the tablet matrix was still in the stomach proving its gastroretentive ability. The pharmacokinetic data provided insight into the liberation, absorption, distribution, metabolism and excretion of L-dopa from the gastroretentive drug delivery systems (GDDS) designed and developed in this study. There was strong *in vitro* and *in vivo* correlation which endorsed the proficiency of GDDS for delivery of L-dopa in management of Parkinson's disease.

Chapter 11 concludes the thesis by summarizing the suitability of the developed drug delivery system as a gastroretentive device for delivery of levodopa and provides recommendations for further studies.

1.5. CONCLUDING REMARKS

It is envisaged that the novel IPB GDDS and *PXLNET* with enhanced gastric residence time will provide an alternative to the commercially available drug delivery systems for PD by improving the absorption and plasma levels of L-dopa. It is envisaged that the combination of nanotechnology and pharmaceutical technology will provide a breakthrough towards better management of PD.

CHAPTER TWO

A LITERATURE REVIEW OF LEVODOPA DELIVERY SYSTEMS: ADVANCEMENTS IN THE DELIVERY OF THE GOLD STANDARD

2.1. INTRODUCTION

To date, the successful management and treatment of Parkinson's disease (PD) has remained elusive despite the disease being discovered many years ago. James Parkinson was the first to describe the disease in 1817 in his article entitled 'An Essay on the Shaking Palsy'. This was written after observing the symptoms by examining three patients and watching three on the streets of London (Parkinson, 2002). It was only later in the 19th century that Charcot named the disease 'maladie de Parkinson' or Parkinson's disease (PD) after adding to Parkinson's description of what he called 'non-tremulous forms of the disease' (Kempster et al., 2007). The commonality and severity of the debilitation of this disease makes it a significant concern (Veazey et al., 2005).

Anticholinergic drugs were the first drugs to be used in the symptomatic treatment of PD (Brocks, 1999; Schapira, 2005). The trigger for PD was not identified until 1919 when it was recognized that PD patients lose neuronal cells in the substantia nigra (Jankovic, 2008). Thirty eight years later, Carlsson and co-workers (Carlsson et al., 1957) identified dopamine as a neurotransmitter in the brain and suggested the effects of its deficiency in PD (Girault and Greengard, 2004; Thanvi and Lo, 2004; Björklund and Dunnett, 2007; Jankovic, 2008). In 1960, Ehringer and Hornykiewicz discovered that dopamine is depleted from the striatum of PD patients (Ehringer and Hornykiewicz, 1998; Périer et al., 2003; Gordon et al., 2007; Jankovic, 2008). The discovery of dopamine's inability to cross the blood brain barrier (BBB) (Birkmayer and Hornykiewicz, 1961; Collister and Albenski, 2005; Poldrigo, 2005; Tyler and Federoff, 2006; Kabanov and Gendelman, 2007; Sandoval and Witt, 2008), led to the trial studies of L-dopa, a dopamine precursor (Figure 2.1a), which was injected into PD patients for the first time in 1961 (Birkmayer and Hornykiewicz, 1961; Goetz, 2011).

A study conducted by Cortzias and his co-workers in 1967 utilizing high doses of L-dopa, emphasized its significance for symptomatic treatment of PD (Kordower and Goetz, 1999; Périer et al., 2003). However, the bioavailability and consequently the therapeutic efficacy were found to be significantly reduced by extensive metabolism of L-dopa, principally through decarboxylation, O-methylation, transamination, and oxidation (Figure 2.1b) (Fahn, 2008; Muzzi et al., 2008). The metabolic products of L-dopa (Figure 2.1b) were also observed to generate side effects such as nausea, vomiting and cardiac arrhythmias (i.e. dopamine) as well as inhibit further absorption of L-dopa in the gastro-intestinal tract (i.e. 3-O-methyldopa

which competes with L-dopa for the same transport system – saturable facilitated large neutral amino acid transport system) (GIT) (Okereke, 2002; Muzzi et al., 2008). In general, more than 95% of L-dopa is metabolized in the GIT, liver and plasma while only 1% of the ingested dose of L-dopa penetrates into the central nervous system (CNS) for the treatment of PD (Jankovic, 2002; Kostoff and Briggs, 2008; Muzzi, et al. 2008).

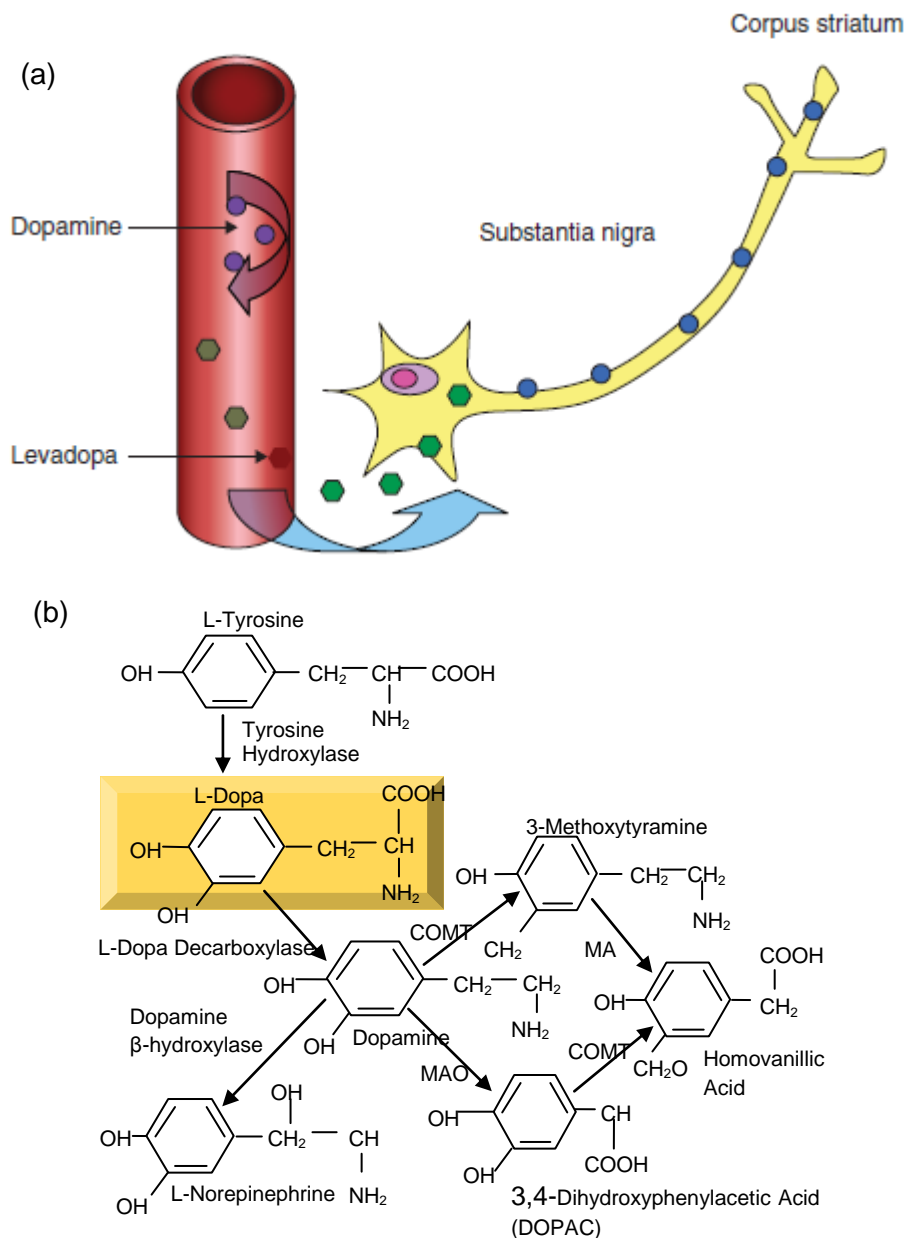


Figure 2.1: Schematics showing the **a)** Mechanism of action of L-dopa, the ‘gold standard’ in the brain (Adapted from Somani, 2008) and; **b)** Synthesis and catabolism of dopamine - L-dopa and dopamine are precursors to norepinephrine, which in turn could be further metabolized to epinephrine (not shown). Catechol-O-methyltransferase (COMT) catalyzes the 3-O-methylation of L-dopa (not shown) as well as dopamine (and other catechols). Monoamine oxidase (MAO) deaminates and oxidizes the monoamines, dopamine, norepinephrine, epinephrine, and serotonin (only the dopamine pathway is shown) (Adapted from Fahn, 2008).

It has been observed that L-dopa absorption is highly affected by irregular gastric emptying time, metabolism and competition with aromatic and branched chain amino acids for absorption and transport. Additionally, its half-life is relatively short (50mins) and a t_{max} is 1.4 hrs (Seeberger and Hauser, 2007). Due to poor bioavailability of L-dopa (33%), further attempts were made to improve the efficacy of oral formulations by increasing the dose of L-dopa and the frequency of dosing (Nutt et al., 2000; LeWitt and Nyholm, 2004). However, these did not reduce the side effects emanating from the extensive metabolism of L-dopa (Stocchi, 2003). The product formed by combining aromatic L-amino acid decarboxylase inhibitor with L-dopa was shown to reduce the side effects of L-dopa by either decreasing the metabolism or the dose (Thanvi and Lo, 2004). Decarboxylase inhibitors (which do not cross the BBB), can increase the plasma level and half life of L-dopa (from 50mins to 1.5hrs) and also enable a reduction in the L-dopa dose by 75% thereby allowing 10% of the ingested L-dopa to reach the CNS (Hsu and Han, 2006; Jankovic, 2008). Studies have shown that although PD is initiated by loss of dopaminergic nigral neurons, there are still sufficient neurons to maintain constant striatal dopamine concentrations and a continuous activation of the striatal dopamine receptors for normal or close to normal basal-ganglia function in the early stage of the disease (Pfeiffer, 2005; Olanow et al., 2006). The dopaminergic neurons convert the administered L-dopa to dopamine and can still store, release, reuptake, recycle or auto regulate large amounts of dopamine to maintain constant dopamine concentrations. Furthermore, it has been proposed that dopaminergic neurons are able to buffer the fluctuation of the plasma levels by masking the pulsatile stimulation of the striatal dopamine receptors (Olanow, 2004).

However, the pulsatile stimulation becomes magnified as the loss of dopaminergic neurons progresses because the buffering and auto-regulation capacity lessens, leading to motor complications such as dyskinesias and motor fluctuations (Olanow, 2004; Poewe, 2004; Pfeiffer, 2005; Olanow et al., 2006; Palhagen et al., 2006). The conversion of administered L-dopa then takes place at the non-dopaminergic sites such as glial cells, serotonergic neurons and non-aminergic interneurons (Melamed et al., 2000). These sites do not store dopamine, but rather convert L-dopa to dopamine and release it to the striatum (Figure 2.1a). Lack of storage capacity forces the striatal dopamine receptors to depend almost entirely on the peripheral availability of L-dopa which in turn is limited by its short half-life (Olanow, 2004). Hence constant striatal dopamine concentration and continuous activation of the striatal dopamine receptors are impaired and replaced by pulsatile stimulation determined by the pharmacokinetics of L-dopa leading to motor complications (dyskinesias and motor fluctuations) experienced by PD patients. Motor fluctuations consist of 'on' periods in which therapeutic response and good anti-parkinsonian effect are experienced, and 'off' periods

during which patients experience crippling Parkinsonism due to absence of or low L-dopa concentrations in the plasma (Olanow, 2004).

Despite all these drawbacks and the fact that there are several therapeutic agents for the management of PD, L-dopa still remains the gold standard and most effective agent for the initial treatment of PD (Olanow, 2004). Compared to other therapeutic agents, L-dopa is more effective, better tolerated, easier and quicker to titrate, and less expensive (Baron, 2005). This review considers the pros and cons of L-dopa drug delivery systems developed over the past three decades with a focused assessment of the attempts at improving absorption, subsequent bioavailability, and maintenance of constant plasma concentration of L-dopa, as well as the technological basis of the delivery systems, with ultimate elucidation of an informed critique of these systems. This critical analysis underlines the fact that neuropharmaceutics is at a precipice, and investigators need to be encouraged to take that leap to enable the generation of innovative delivery systems for the effective management of PD.

2.2. Immediate release oral drug delivery systems for the administration of L-dopa

The first immediate release drug delivery systems for L-dopa were tablets composed of L-dopa in combination with carbidopa (Sinemet[®], Merck & Co., Inc. Whitehouse Station, NJ, USA) (Koller et al., 1999). Carbidopa is a peripheral dopa decarboxylase (DDC) inhibitor. Administration of L-dopa with carbidopa controlled the concentration of dopamine at appropriate levels with reduced side-effects (Sagar and Smyth, 2000). This was proposedly achieved through the diminished conversion of L-dopa to dopamine in the peripheral tissues, which also permitted lower effective doses of L-dopa for the treatment of PD (Sagar and Smyth, 2000). Benserazide is another decarboxylase inhibitor that is used in combination with L-dopa as Madopar[®] (Madopar[®], F.Hoffmann-La Roche Ltd, Basel, Switzerland). These combinations, namely Sinemet[®] and Madopar[®], could reduce the peripheral metabolism of L-dopa and side effects such as nausea and vomiting but were ineffective in controlling dyskinesias and motor fluctuations associated with long term use of L-dopa (Olanow, 2004). Generally, Sinemet[®] and Madopar[®] produce fluctuations of L-dopa plasma levels which either exceed safe therapeutic concentrations or fall below the minimum effective concentrations (Sagar and Smyth, 2000). However, the plasma fluctuations do not only depend on L-dopa's biological half-life but also on frequency of administration and release rate from the drug delivery systems; the latter of which can be modulated (Sagar and Smyth, 2000).

Catechol-O-methyltransferase (COMT) inhibitors such as entacapone and tolcapone have been added to L-dopa/carbidopa to block the second metabolic pathway (O-methylation) – there is thus the possibility to associate tolcapone or entacapone as a unique formulation to the conventional L-dopa/ DDC inhibitors. An example of a triple combination of L-dopa, carbidopa and entacapone as a single tablet, Stalevo[®] (Orion Pharma, Espoo, Finland) was approved by the Food and Drug Administration (FDA) in 2003. Catechol-O-methyltransferase (COMT) inhibitors such as entacapone and tolcapone have been added to L-dopa/carbidopa to block the second metabolic pathway (O-methylation). Entacapone is a highly potent peripherally acting COMT inhibitor. It increases the bioavailability of L-dopa by reducing its peripheral conversion to 3-Methoxytyramine (Figure 2.1b) (Piccini et al., 2000). It also enhances the clinical efficacy of both standard and controlled release L-dopa/carbidopa. The main function of Stalevo[®] was to replace L-dopa/carbidopa in PD patients who experience ‘off’ periods (Koller et al., 2005). It has been demonstrated that entacapone increases the plasma level of L-dopa by 35% and the half-life from 1.5 to 2.4 hrs (Hsu and Han, 2006). However, it has also been observed that entacapone increases dopaminergic side-effects such as dyskinesias therefore necessitating L-dopa dose reduction (Hauser, 2004).

In preparing Stalevo[®], the conventional wet granulation method, which involves combining the active ingredients, retarded the release of carbidopa with decreased absorption and subsequent poor bioavailability. To increase the bioavailability of carbidopa from the solid composition, entacapone and L-dopa were granulated together, adding carbidopa separately in the form of granules before compression. Furthermore, microcrystalline cellulose, which is an excipient used mostly in L-dopa/carbidopa and entacapone formulations, was found to be incompatible due to poor stability on long term storage when the three active ingredients are combined (Kallioinen, et al., 2001).

Hauser performed a 39-week, randomized, double-blind, multicenter study for comparison of the efficacy, safety, and tolerability of L-dopa/carbidopa/entacapone (LCE, Stalevo[®]) with L-dopa/carbidopa (LC, Sinemet[®] IR) in patients with early PD (Hauser, 2004). Four hundred and twenty-three patients with early PD warranting L-dopa were randomly assigned to treatment with LCE 100/25/200 or LC 100/25 three times daily. The adjusted mean difference in total Unified Parkinson's Disease Rating Scale (UPDRS) Parts II and III between groups using the analysis of covariance model (pre-specified primary outcome measure) was 1.7 (standard error = 0.84) points favoring LCE. Significantly greater improvement with LCE compared with LC was also observed in UPDRS Part II scores. There was no significant difference in UPDRS Part III scores. Wearing-off was observed in 29 (13.9%) subjects in the LCE group and 43 (20.0%) in the LC group. Dyskinesia was observed in 5.3% subjects in the

LCE group and 7.4% in the LC group. Nausea and diarrhea were reported more frequently in the LCE group. LCE provided greater symptomatic benefit than LC and did not increase motor complications.

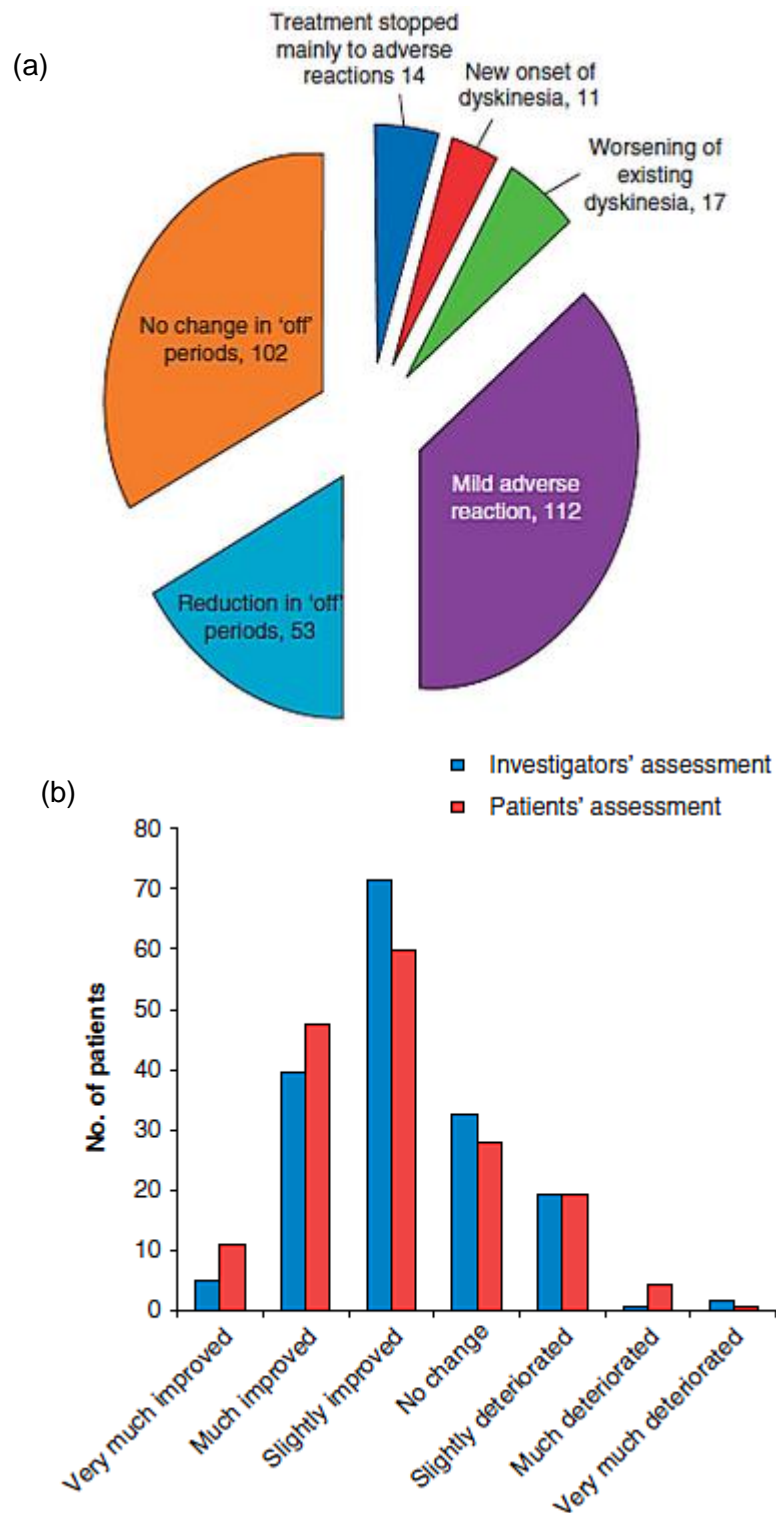


Figure 2.2: a) Summary of the study results on Stalevo® in patients experiencing 'off' periods and; b) Assessment of efficacy of Stalevo® (Data extracted from Koller et al., 2005).

Koller and co-workers (2005) were the first group of scientists to conduct a study on Stalevo[®] as a single tablet. They carried out a multicentered open-label single-arm 4-week study on 169 PD patients who experienced 'off' periods. The results of their study are illustrated in Figure 2.2 and indicated that the incidence of dyskinesias as a result of enhanced dopaminergic activity was ameliorated with a reduction in Stalevo[®] dose or return to baseline levels without a change of dose. Thus, Stalevo[®] could reduce 'off' periods principally by enhancing the pharmacokinetic profile of L-dopa (Koller et al., 2005). However, these observations were countered in a large prospective double-blind placebo-controlled trial; L-dopa/carbidopa/entacapone could not improve dyskinesias and motor fluctuations mainly due to its inability to provide constant therapeutic plasma concentrations (Olanow and Stocchi, 2004; Stocchi et al., 2008). Benefits were only seen in several quality of life measures. Smith and co-workers (2004) suggested that the frequency of dosing be increased to four times daily. They conducted their study in primates with the aim of providing continuous activation of the striatal dopamine receptors so as to reduce the incidence of dyskinesias (Smith et al., 2004). However, frequency of dosing could certainly instigate patient non-compliance, which in return will not achieve its aim.

2.3. Conventional controlled release formulations for L-dopa administration

Reducing the interval between L-dopa doses through the administration of controlled release formulations, was one of the approaches utilized to solve the 'wearing off' problem encountered with L-dopa (Barone, 2003). Thus, controlled release formulations (CRF) were developed with the intention of delivering L-dopa to the brain in such a manner that little or no fluctuations in L-dopa concentrations would occur. Unfortunately the intention was not fulfilled as patients still experienced motor complications as a result of plasma fluctuations (Barone, 2003). However, these formulations were established to be useful for patients experiencing sleep disturbances (Stocchi et al., 2004). Controlled release formulations are often associated with the problem of variable bioavailability and consequently unpredictable efficacy (Gasser et al., 1998). Peak plasma levels are reached approximately 2-4 hours after administration and peak concentration may be lower than those obtained with immediate release formulations (IRF). This may necessitate the patients to take an IRF in the morning and a CRF or combination an IRF and a CRF during the day in order to achieve a rapid onset of action (Gasser et al., 1998).

Advanced PD patients have been observed to be more sensitive to minor changes in plasma and brain L-dopa levels as the disease progresses due to more dependence on peripheral availability of L-dopa (Chen et al., 2008a). Therefore, IRFs may be preferred to CRFs in advanced PD patients, due to the fact that GI absorption can be irregular and unpredictable

with controlled-release formulations as a result of the gastrointestinal changes such as delayed gastric emptying and constipation that occur as the disease progresses (Chen et al., 2008). Furthermore, CRFs have no significant advantage over IRFs in 'time to onset' of motor fluctuations (Barone, 2003).

Sinemet[®] CR (L-dopa/carbidopa; Merck & Co., Inc. Whitehouse Station, NJ, USA) is a conventional CRF currently available on the market. Sinemet[®] CR is a sustained release polymer-based drug delivery system which releases L-dopa/carbidopa as it slowly erodes (Han et al., 2006). Principally, L-dopa, carbidopa and carrier agents such as hydroxypropylcellulose and polyvinylacetate-crotonic acid copolymer are blended and compressed into tablets. Koller et al. (1999) conducted a five year blinded randomized parallel study using a total of 618 patients in 36 centers worldwide to compare the effects of IRFs and CRFs. Their study showed that there was no significant difference between the IRF group and the CRF group. However, compared to the IRF, Sinemet[®] CR provided a slight but statistically significant improvement in the quality of life of the individuals evaluated. This might have been due to the less dramatic change to the 'off' effect with Sinemet[®] CR (Koller et al., 1999).

2.4. Administration of L-dopa as a liquid formulation

Liquid L-dopa formulations were introduced to facilitate rapid onset of action, even though their effects were observed to last for a very short period. Patients were observed to benefit from liquid L-dopa formulation within 5 minutes, with the duration of the effect persisting for 1-2 hours (Stacy, 2000). L-dopa liquid formulations are therefore given to reduce the delay in the 'on' effect which has been observed to be augmented by CRFs (Adler, 2002). Unlike conventional formulations, the pharmacokinetic profiles of liquid L-dopa formulations are not affected by the gastric emptying rate. Liquid formulations allow for a rapid gastric transit as the gastric emptying interval does not affect their absorption (Woitalla et al., 2006). Thus, L-dopa liquid formulations may allow more precise dose titration throughout the day and may therefore prove to be useful particularly in patients with prolonged gastric transit time, difficulties in swallowing, advanced motor fluctuations and also during the 'off' effect period (Verhagen, 2002; Calne and Kumar, 2003; Obering et al., 2006; Weintraub et al., 2008).

Woitalla and his team (2006) conducted a study which involved 50 PD patients that were randomly selected at various stages of the disease, fasted overnight and then given a single dose of dissolved L-dopa/benserazide formulation in 100mL of water. Blood samples were withdrawn at predetermined intervals between 0 and 180 minutes while the patients were scored on the Unified Parkinson's Disease Rating Scale (UPDRS) and Hoehn and Yahr

Scale. The results depicted that there was an increased plasma availability of L-dopa compared to the conventional formulations (Högl et al., 2001; Woitalla et al., 2006).

The conventional method for preparing liquid L-dopa involved the crushing of a tablet of L-dopa/carbidopa and then incorporating it into a fluid such as orange juice (Compton et al., 1999). However, Remenar and co-workers (2005) formulated stable compositions of liquid L-dopa/carbidopa in various forms such as dispersible tablets, dry powders and stable liquids. These allowed for the incorporation of an acid e.g. citric acid, metal chelator e.g. EDTA, sweetener e.g. aspartame or sugar or a preservative e.g. sodium benzoate. One of the liquid compositions was found to be stable for about one year with less than 5% degradation of carbidopa at 40°C.

It has been observed that although L-dopa liquid formulations may be independent of the gastric emptying rate, pulsatile delivery is often obtained instead of the desired constant delivery (Obering et al., 2006). Furthermore, liquid formulations are cumbersome as their therapeutic effects are short-lived thus requiring patients to take an hourly or bihourly dose, which makes them considerably prone to non-compliance. Thus, patients cannot rely entirely on liquid L-dopa because the frequent dosing does not consistently reduce motor fluctuations (Obering et al., 2006).

2.5. Dispersible tablets for delivery of L-dopa

Mathur and co-workers (2006) formulated dispersible tablets of L-dopa/carbidopa using wet granulation with the aim of achieving quick onset of action and accurate dosing as was the case with liquid L-dopa. The formulation comprised of L-dopa, carbidopa, filler and a coloring agent. The intragranular portion of a superdisintegrant such as croscarmellose sodium was granulated with a dispersion of a binder such as pregelatinized starch in a granulating fluid. The granules were blended with sweetener, flavoring agent, and the extragranular portion consisted of a superdisintegrant and a lubricant/glidant, which was then compressed into tablets. The tablet completely dispersed in water in 3 minutes or less to form a solution which presented as a non gritty suspension or slurry with smooth feeling to the patient (Mathur et al., 2006).

2.6. Oral disintegrating L-dopa tablets

To compensate for the reduced duration of clinical response experienced by immediate release drug delivery systems, oral disintegrating tablets were introduced in 2004 (Iyer et al., 2005). L-dopa oral disintegrating tablets (ODTs) enable the patient to take smaller and more frequent doses, which made it possible to tailor dosages to individual patient needs (Hsu and

Han, 2006). ODTs do not need to be administered with water, which makes it easy for the elderly patients that may have difficulty swallowing. ODTs dissolve quickly once placed on the tongue. The solubilized L-dopa/carbidopa is then swallowed with saliva (Chen et al., 2008a). ODTs permit reliable and rapid absorption of L-dopa. However, the absorption occurs in the proximal intestine (duodenum) in the same manner as the IRFs and its time-to-peak is not shortened significantly when compared to IRFs (Chen et al., 2008a). Thus, if a patient has a bowel malfunction such as paralytic ileus, ODTs are not superior to IRFs (Iyer et al., 2005). Clinically, ODTs are preferred for naive and late stage PD patients as well as patients maintained at low doses or patients requiring dose titration (Nausieda et al., 2005). The results obtained from a multicentered, open-label, sequential study that compared preferences for ODTs and conventional tablets in PD subjects, suggested that ODTs may be of value in certain patients with PD depending on their personal preferences, disease status and willingness to alter an aspect of their use of medication (Nausieda et al., 2005). The attributes of ODTs which influenced subjects' preference included accessibility to medication to treat 'off' times, ease of activities of daily living, reduced concern about swallowing, applicability for night time dosing, ease of compliance with the dosing schedule, and lowered self-consciousness regarding medication use (Nausieda et al., 2005). Parcopa[®] (Schwarz Pharma, Inc., Milwaukee, Wisconsin, USA), a commercially available ODT approved by FDA in 2004 was used in the study. It was manufactured based on RapiTab[™] technology which formulates drugs into ODTs that dissolve rapidly on the tongue. Results from the study are depicted in Figure 2.3.

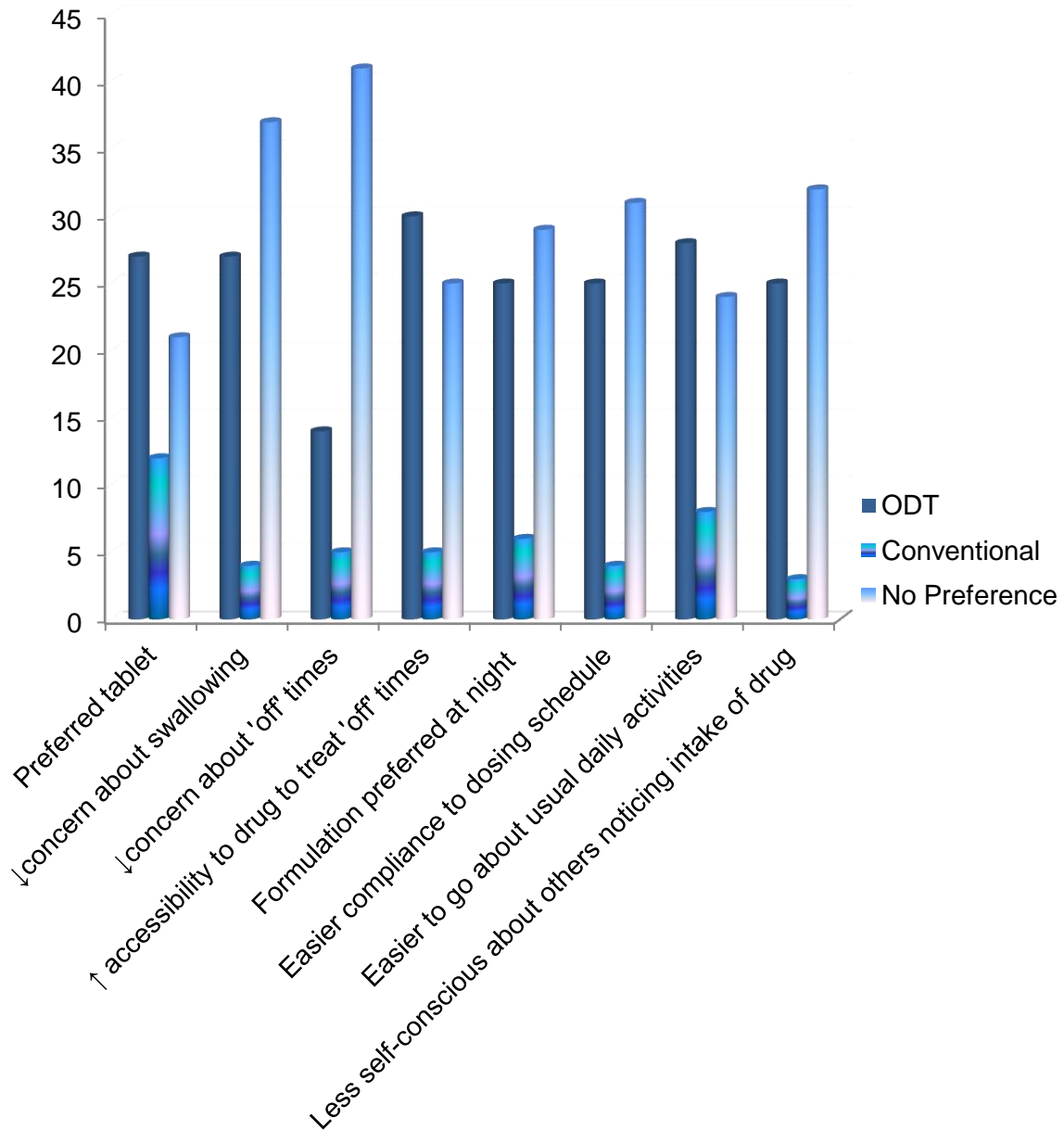


Figure 2.3: Preferences of patients undergoing treatment with L-dopa/carbidopa ODT and conventional tablets (Data extracted from Nausieda et al., 2005).

Hsu and Han (2006) prepared ODTs by wet granulation. The ingredients included a binder (which could also function as a disintegrant) and an intragranular disintegrant to disintegrate the granules; and intergranular disintegrant to disintegrate the tablet into granules. The ODT formulations contained a poorly water soluble filler such as microcrystalline cellulose to improve compressibility and avail rapid dispersion characteristics. The ODTs were found to disintegrate rapidly (60 seconds or less) in an *in vitro* disintegrating apparatus (Hsu and Han, 2006).

2.7. Dual-release formulations for the delivery of L-dopa

For the conventional controlled release delivery systems of L-dopa, the onset of action is normally about two hours which is then followed by a prolonged release over a period of 4-6 hours. To overcome the delayed action of these delivery systems, dual release formulations (DRFs) were introduced. A DRF is a two compartment delivery system comprising a sustained release inner core and an immediate release outer layer.

Cohen and co-workers (1998) developed a dual release tablet of L-dopa ethyl ester with the aim of achieving an initial burst effect of L-dopa for rapid onset of action followed by a sustained release period. L-dopa ethyl ester was incorporated into a uniform blend of hydroxypropylmethylcellulose, hydroxypropylcellulose and carboxylvinyl polymer in desired proportions with other excipients and compressed into a conventional tablet. However, *in vivo* results in healthy volunteers were the same as those obtained with Sinemet[®] CR because the terminal half-life was only 2 hours (Xiang et al., 2008).

Madopar[®] DR (SkyePharma, London, UK for F. Hoffmann-La Roche Ltd, Basel, Switzerland) is a dual release formulation containing L-dopa and benserazide currently available in Switzerland and was developed in the ratio of 4:1 of L-dopa/benserazide (Gasser et al., 1998). Madopar[®] DR combines the advantages of a rapid onset of efficacy as well as a sustained effect. This delivery system consists of an IRF layer, a barrier and controlled release layer which lead to early peak plasma levels at about 1 hour, followed by sustained plasma levels (Gasser et al., 1998).

An open-label, multiple-dose randomized two-way crossover clinical trial employing this dual formulation was carried out on 18 subjects (Gasser et al., 1998). The assessment was at day 1 after a single dose (200mg L-dopa and 50mg benserazide) and day 7 after a 5-day three times daily pre-treatment with 100mg L-dopa and 25mg benserazide in fasting state. Pharmacokinetic parameters such as bioavailability, accumulation and metabolism of L-dopa were determined. On day 1, the results showed that there was rapid absorption, marked peak plasma concentration and an apparent elimination half-life with DRF when compared to the slow release formulation (SRF), as shown in Table 2.1. The marked difference was still apparent on day 7. After multiple dosing for 7 days, there was accumulation of 3-O-methyldopa for these formulations. It was further observed that there was no difference in accumulation of 3-O-methyldopa but plasma fluctuation was higher on day 7 with the DRF. However, bioavailability after single and multiple doses of the DRF was 40% higher than that of the SRF (Gasser et al., 1998). Furthermore, the study was conducted on healthy patients and therefore its impact on motor complications and 'on and off' effects could not be ascertained. Additionally, from the results shown in Figures 2.4a and b it can be proposed

that a continuous delivery of L-dopa and stable plasma levels, which is envisaged to overcome the already existing problems, may not be obtainable. An ideal profile of a CRF with continuous drug delivery is schematically depicted in Figure 2.4c.

Table 2.1: Comparative pharmacokinetic parameters of L-dopa analysis obtained from dual release formulation (DRF) and controlled release formulation (CRF) (Data extracted from Gasser et al., 1998).

Formulation	Cmax ($\mu\text{g/ml}$)	Tmax (hr)	$T^{1/2}$ (hr)	AUC ₀₋₁₂ ($\mu\text{g} \times \text{h/ml}$)	Comments
DRF day 1	1.7	1.1	1.2	4.3	Rapid absorption – DRF achieved almost double the plasma concentration attained by CRF in about half the time it took CRF to attain its maximum concentration
DRF day 7	2.1	1.1	2.6	5.9	
CRF day 1	1.0	2.3	1.5	3.1	37.0% on the 1 st day and (34.3%) on the 7 th day
CRF day 7	1.1	2.0	1.9	4.2	

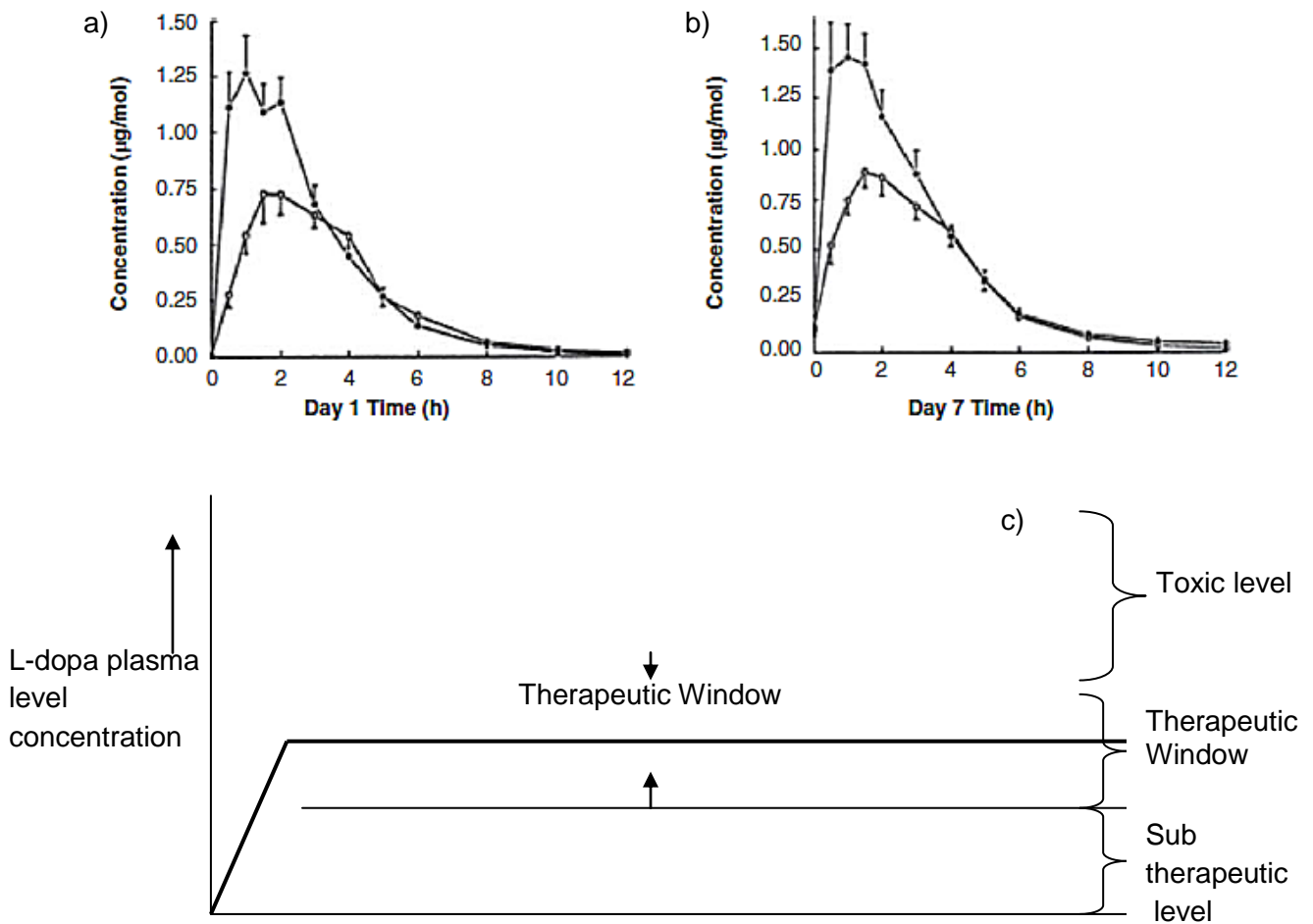


Figure 2.4: Mean L-dopa plasma concentration–time curves of the DRF (closed symbols) and the SRF (open symbols) following **a)** single-dose administration on day 1; **b)** multiple-dose administration on day 7 (n=18) (Source: Gasser et al., 1998) and; **c)** an ideal controlled release profile.

Rubin (2000) developed three methods of preparing L-dopa/carbidopa dual release delivery systems. In the first method, the components for the inner core and the outer layer were blended separately, and subsequently the compressed inner core tablet was overcoated with the compressed outer layer blend with a suitable coating press. In the second method, a bilayer tablet was formed whereby the sustained layer blend and the immediate release blend were compressed adjacent to each other (or separated by an additional excipient layer) using a suitable layered press. In the third method, the uncoated pellets of immediate release L-dopa/carbidopa and polymer coated pellets of sustained release L-dopa/carbidopa were included into an oral dosage form such as capsule or compressed as a tablet in the desired ratio of immediate and sustained release L-dopa/carbidopa. DRFs developed by Rubin showed that the L-dopa immediate release compartment provided a rapid onset of

anti-parkinsonian effect while the sustained release inner core, which was also loaded with L-dopa, prolonged the therapeutic effect (Rubin, 2000).

Descombes and co-workers (2001) conducted a single-dose, cross-over study on 16 PD patients utilizing a two-centre randomized double-dummy (one dual-release tablet of 200 mg L-dopa, plus 50 mg benserazide or two slow-release capsules of 100 mg L-dopa, plus 25 mg benserazide). The efficacy parameters were time for onset of action ('on' effect relative to time of drug intake), duration of 'on' effect, time switch to 'off' effect relative to time of drug intake and motor performance (reduction in United Parkinson's Disease Rating Scale [UPDRS] III baseline score). The severity of dyskinesia was assessed with the Dyskinesia Rating Scale - maximum score, 28 (Durif et al., 1997). Although the $t_{1/2}$ was similar for both DRF and SRF, the DRF had a significantly faster absorption, greater peak plasma concentration (by about 45%), and greater systemic bioavailability (about 20%) (Descombes et al., 2001). The mean onset of the 'on' effect was more rapid with the DRF (43 ± 31 minutes) than with the SRF (81 ± 39 minutes). 'On' effect duration showed a trend for longer response with the DRF than the SRF (114 ± 92 minutes vs. 80 ± 75 minutes) while the mean UPDRS baseline motor score was similar for both formulations (33.8 ± 10.6 vs 34.3 ± 11.6). However, maximum percentage reduction in UPDRS score was slightly more pronounced ($49 \pm 32\%$ vs. $37 \pm 34\%$) and occurred earlier (90 minutes versus 3 hours) with the DRF. The results also showed that the mean Dyskinesia Rating Scale severity score was similar for both formulations (2.8 ± 2.5 versus 2.7 ± 3.1) (Descombes et al., 2001).

2.8. Delivery of L-dopa by infusions

Infusions for the delivery of L-dopa were introduced with the intention of achieving constant plasma concentrations, which would in turn produce continuous dopaminergic stimulation of the dopamine receptors. An intravenous infusion of L-dopa was prepared by dissolving L-dopa in normal saline to a final concentration of 2mg/ml, while carbidopa was given orally about one hour before providing the infusion (Black et al., 2003). Based on previous studies on IV and enteral infusions of water solutions of L-dopa, which resulted in a reduction of fluctuations in L-dopa plasma concentrations and milder side effects (though impractical); a more practical long term intraduodenal infusion (Duodopa[®], Solvay Pharmaceuticals GmbH, Hannover, Germany) was developed as L-dopa/carbidopa enteral gel with a portable pump and intestinal tube (LeWitt and Nyholm, 2004; Nyholm et al., 2005a). Duodopa[®] is an aqueous suspension containing 20 mg/mL L-dopa and 5mg/mL carbidopa as active ingredients in 2.92% carmellose sodium (carboxymethylcellulose). Twenty-five advanced PD patients were enrolled in a study which compared the intraduodenal infusion as monotherapy with individual combinations of conventional pharmacotherapy. There was significantly

improved motor performance with the infusion in comparison to individual combinations of conventional therapy (Nyholm et al., 2005a). In another study, Nyholm and co-workers (2005b) stated that in addition to improvement of motor performance, a 24 hour intraduodenal infusion improved sleep in advanced PD patients without clinically relevant tolerance or side effects. Hence, patients were found to have had improved quality of life when placed on intraduodenal infusion (Mouradian, 2005; Nyholm et al., 2005a).

Thus far, L-dopa duodenal infusion has been found to produce continuous plasma concentrations of L-dopa, reduced dyskinesias and 'off time' in clinical studies (Antonini, 2007). In a study that involved seven patients, L-dopa/carbidopa infusion (5/20mg/mL) reduced daily motor fluctuations by 81% and dyskinesias by 70%. Most dyskinesias experienced by the patients were attributed to the bolus doses of L-dopa taken in the mornings since the pump was turned off at night and the dyskinesias reportedly had a short duration. The administration of L-dopa was controlled by a pump with an adjustable infusion rate allowing individual adaptation of the dose which varied from 40-120mg/h or more when required. Overall, the L-dopa continuous infusion significantly increased the quality of life of the investigated patients (Antonini, 2007).

2.9. Biodegradable microspheres as a drug delivery system for L-dopa

Microspheres are controlled drug delivery systems for various applications including hormone therapy, chemotherapy, cardiovascular diseases, neurological disorders, ocular drug delivery, and protein and vaccine deliveries (Benoit et al., 2000; Herrero-Vanrell and Refojo, 2001; Hickey et al., 2002; Vasir et al., 2003; Van Tomme et al., 2005; Bubeníková et al., 2008; Wei et al., 2009). Microspheres are known to modulate drug release and absorption characteristics (Vasir et al., 2003). It has been shown that with the use of microspheres as a drug delivery system for L-dopa, the dosage size, frequency of administration, systemic side effects and dose dumping decreased, while the drug could be released continuously (Hickey et al., 2002). This ultimately enhances patient compliance. Microspheres have been fabricated from a variety of biodegradable polymers which include gelatin, albumin, polyanhydrides, polyorthoesters, polyesters and polysaccharides (Brime et al., 2000; Herrero-Vanrell and Refojo, 2001; Arica et al., 2005).

The use of microspheres as drug delivery agents for L-dopa and carbidopa is another approach for improving the bioavailability and subsequent clinical response of L-dopa (Arica et al., 2005). Arica and co-workers (2005) prepared L-dopa and carbidopa microspheres by solvent-evaporation technique employing biodegradable polymers, namely poly (D, L-lactide) and poly (D, L-lactide-co-glycolide). Both *in vitro* and *in vivo* studies were performed. The *in*

in vitro results revealed that both L-dopa- and carbidopa-loaded microspheres exhibited sustained profiles over ten hours (as depicted in Figure 2.5) while the *in vivo* results portrayed a sustained slow release in each rat (Arıca et al., 2005). The *in vitro* controlled drug release from the microspheres was attributed to the diffusion of L-dopa or carbidopa through the pores or channels on and/or close to the surface of the microspheres while the *in vivo* results show that drug release was attributed to the degradation of the polymers. The microspheres were then stereotactically implanted into the brains of Parkinson-induced albino rats as an injectable dosage form. Reduced rotational behavior was observed indicating that L-dopa/carbidopa loaded microspheres exerted functional effects on the striatal dopamine receptors (Arıca et al., 2005). The bioavailability of L-dopa was improved because the L-dopa/carbidopa was released directly on the striatal dopamine receptors thereby reducing wide distribution of side effects (Arıca et al., 2005). However, the method is invasive and the improvement of motor complications can only be clearly evaluated in man.

In related studies, Arıca and co-workers (1998; 2005) fabricated L-dopa loaded chitosan microspheres using the emulsion-polymerization technique. They assessed the physicochemical characteristics of these microspheres with the intention of obtaining an optimal formulation for brain delivery of L-dopa. They observed that upon implanting these microspheres in the rats, the rotational behavior of rats reduced (Arıca et al., 1998; Arıca et al., 2005).

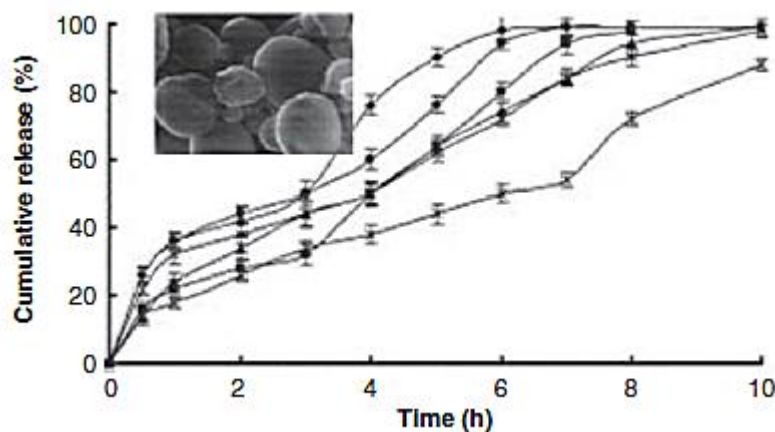


Figure 2.5: *In vitro* release profiles of L-dopa from microspheres depicting a scanning electron micrograph of the L-dopa-loaded microspheres (inset) (Source: Arıca et al., 2005).

2.10. Gastroretentive dosage forms as drug delivery systems for L-dopa

It has been observed that the extent of absorption for drugs with maximal absorption at the proximal intestine (duodenum) is limited by the conventional immediate release and controlled release formulations (Morrison et al., 1997; Hoffman et al. 2004; Streubel et al.,

2006). Once emptied from the stomach, the passage of these formulations through the upper region of the intestine is rapid, limiting the bioavailability of drugs such as L-dopa. Therefore, prolonging the residence time of drug delivery systems in the upper region of the intestine will enhance absorption and subsequent bioavailability of drugs with a narrow absorption window (Talukder and Fassihi, 2004; Streubel et al., 2006). Gastroretentive dosage forms (GDFs) are time-controlled oral drug delivery systems which can enable prolonged and continuous delivery of drugs to the upper region of the GIT (duodenum and jejunum), improve absorption of drugs with a narrow absorption window, minimize erratic plasma concentrations of drugs, reduce the frequency of dosing, and reduce the total administered dose and associated side effects, thereby optimizing the therapeutic efficacy which ultimately improves patient compliance (Hoffman et al., 2004; Talukder and Fassihi, 2004; Streubel et al., 2006). However, continuous and sustained delivery of drugs in the upper region of the GIT may enhance the metabolic activity of the metabolic enzymes in the intestine wall which will in turn reduce the bioavailability of drugs that have extensive metabolism (Klausner et al., 2003; Hoffman et al. 2004). Various approaches have been employed to increase gastroretention of drug delivery systems. These include swelling or unfolding to a size which will prevent passage of GDFs through the pyloric sphincter; bioadhesion; buoyancy of gastric fluids and delaying of gastric emptying by the addition of lipid excipients and high density delivery systems (Klausner et al., 2003; Hoffman et al., 2004; Talukder and Fassihi, 2004; Streubel et al., 2006).

2.10.1. Single-unit sustained floating systems for delivery of L-dopa

Hydrodynamically balanced systems are single-unit delivery systems designed and formulated to prolong gastric residence time thereby improving absorption. They are formulated to be less dense than gastric content to enable them float on the surface of gastric content. Madopar[®] HBS (L-dopa/benserazide; F.Hoffmann-La Roche Ltd, Basel, Switzerland) is a single-unit floating system currently available in the market. Madopar[®] HBS (hydrodynamically balanced system) is a floating delivery system that combines L-dopa and benserazide. The system was designed with the aim of prolonging the residence time of the drugs in the gastric region so as to enhance absorption (Erni and Held, 1987). The Madopar[®] HBS is formulated as capsules. On oral administration, the capsule dissolves in the gastric fluid forming a mucous body with a bulk density less than 1g/cm³. L-dopa/benserazide is then released as the system remains in the stomach for a prolonged period of time (Erni and Held, 1987). However, the gastric residence time of Madopar[®] HBS was observed not to be significantly prolonged, which may explain the similar pharmacokinetic profile it shares with Sinemet CR (Klausner et al., 2003).

2.10.2. Multiple-unit sustained release floating dosage forms for delivery of L-dopa

It has been shown that multiple-unit dosage forms such as pellets and minitablets are more advantageous when compared to single-unit dosage forms in that they have more reproducible gastric residence time (GRT), less inter-subject variability in absorption and dose-dumping and better dispersion through the GIT with less chance of localized mucosal damage (Singh and Kim, 2000; Goole et al., 2007). It has been postulated that the majority of the particles from floating multiple-unit dosage forms remain above stomach contents for an extended period of time (Waterman, 2007).

Klausner and co-workers (2003) developed a L-dopa-loaded unfolding multilayer delivery system which comprised an inner layer of polymer-drug matrix (ethylcellulose: L-dopa 1:1) framed with rigid polymeric strips (L-poly(lactic acid): ethylcellulose, 9:1); then covered on both sides with two layers comprising enzymatically hydrolyzed gelatin, methacrylic acid copolymer type B, glycerin and glutaraldehyde, at a ratio of 48:30:20:2. The exterior part of these layers was covered with a thin anti-adhesive layer of microcrystalline cellulose powder (Figure 2.6a). Three compositions of CR-GRDFs were employed in the study and they differed in the thickness of ethylcellulose-L-dopa membrane and in the amount of ethylcellulose-L-dopa incorporated: CR-GRDF A, 0.50 mm, 50 mg L-dopa; CR-GRDF B, 0.31 mm, 125 mg L-dopa; CR-GRDF C, 0.61 mm, 200 mg L-dopa. Subsequently, controlled release gastroretentive dosage forms (CR-GRDFs) were folded (6mm long folds) before insertion into gelatin capsules. *In vitro* analysis results indicated that the CR-GRDFs released L-dopa in a controlled manner (Klausner et al., 2003). CR-GRDF C was found to exert controlled release of L-dopa for more than 12 hours.

CR-GRDFs were administered to beagle dogs and the gastroscopy showed that it unfolded to its extended size 15 minutes after administration and maintained the extended size for at least 2 hours (Klausner et al., 2003). CR-GRDF A resulted in a low plasma concentration of L-dopa while CR-GRDF C resulted in an elevated plasma concentration for more than 10 hours. The enhanced metabolic activity at the intestinal wall may explain the low bioavailability of CR-GRDF A in comparison to the oral solution; hence the dose of L-dopa in CR-GRDF B was increased, but a high concentration of L-dopa was only obtained for a short period of time (Klausner et al., 2003). A further increase of L-dopa dose coupled with modification of the release kinetics in CR-GRDF C produced prolonged and sustained release of L-dopa, as visualized in Figure 2.6b compared to two control modes of administration (non-gastroretentive CR particles and an oral solution). Overall, the study showed that the unfolding CR-GRDF can achieve prolonged absorption and sustained blood levels for L-dopa (Klausner et al., 2003). It must be taken into account, however, that the dog

is a poor representative model for the human's gastrointestinal tract (Davis and Wilding, 2001; Paulson et al., 2001; Fotaki et al., 2005; Chen et al., 2008b); an indication that the results may not translate well in humans (Davis, 2005). Furthermore, the pylori of dogs are smaller than those of humans (Klausner et al., 2003) and therefore the gastric residence time for CR-GDRF in dogs may significantly differ from that of humans.

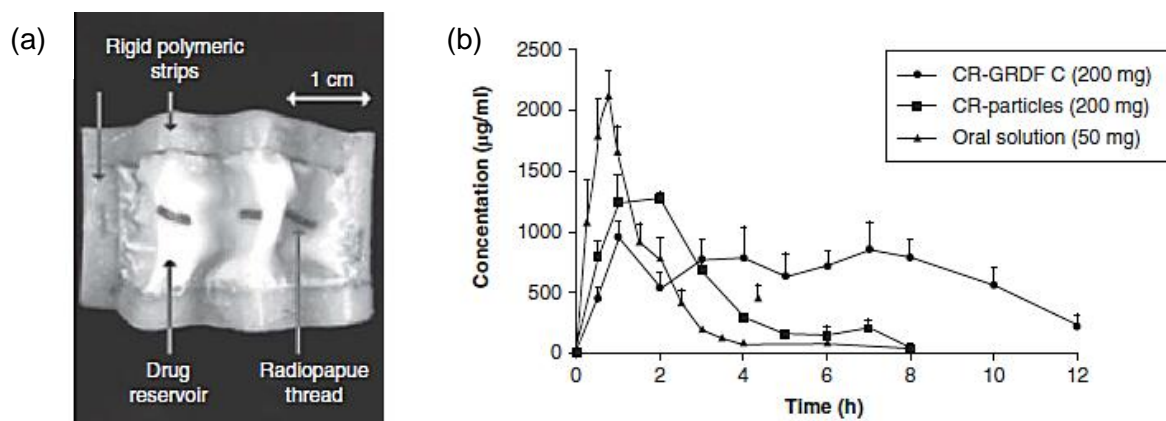


Figure 2.6: **a)** A picture of the gastroretentive dosage form (GRDF) drawn out of the dog stomach 15 min post-administration - the GRDF has unfolded almost completely to its original size and; **b)** Effect of the mode of L-dopa administration on the plasma concentrations in beagle dogs (n=6) for CRGRDF C in comparison to the two control modes of administration (oral solution and CR-particles). (Source: Klausner et al., 2003).

Goole and co-workers (2007) prepared L-dopa sustained release floating minitables by melt granulation and subsequent compression. Melt granulation exploits the melting or softening of a binder at a low melting point. The delivery system comprised of L-dopa, precirol ATO5 (glyceryl palmitostearate) as a meltable binder and drug release regulator, methocel K15M (HPMC) as swellable polymer, lactose and Compritol® 888 as hydrophilic and lipophilic diluents, respectively, while sodium bicarbonate and calcium carbonate were gas-generating agents. L-dopa and excipients were mixed in a laboratory scale high-shear mixer at regulated revolutions and a temperature of 60°C. The granules were cooled and then compressed into minitables by direct compression. The *in vitro* results for one of the formulations indicated that minitables floated after 12 minutes, remained buoyant for more than 13 hours and exhibited sustained release of L-dopa with no 'burst' effect for more than 8 hours (Goole et al., 2007).

In other studies, Goole and his team (2008a; 2008b) developed coated L-dopa multiple-unit sustained release floating minitables with the overall aim of improving the floatability of such delivery systems. The procedure involved preparing sustained release granulates by melt granulation, compressing them into minitables and then coating them with Eudragit® RL30D, a water insoluble acrylic polymer. The resultant minitables were found to be buoyant for

more than 13 hours and provided sustained release of L-dopa for more than 20 hours. However, *in vivo* study which was carried out in ten healthy humans depicted that the floating minitables exhibited floating on the surface of the gastric content for more than 4 hours. The floating minitables were comparable to a marketed product, Prolopa[®] HBS 125 with regards to AUC, T_{max} and C_{max} . The non-significant difference between formulations however was attributed to inter-subject variability and the small number of volunteers. In comparison to Prolopa and coated floating minitables, the uncoated floating minitables displayed a more evenly distributed plasma levels of levodopa while Prolopa had no floating lag time which was attributed to its low density (Goole et al., 2008c).

2.11. Long term implantable L-dopa controlled release matrix

Sabel and co-workers (1990) fabricated a long term controlled release matrix aimed at achieving continuous delivery of L-dopa with less or no plasma fluctuations, which in turn may eliminate the 'on and off' syndrome. The fabricated matrices were able to deliver L-dopa *in vitro* for more than 600 days, and for 225 days in rats following subcutaneous implantation. To prepare the matrices, ethylene vinyl acetate (EVA) copolymer was dissolved in methylene chloride at 37°C for 24 hours. L-dopa was then added to the liquid polymer and thoroughly mixed. The blend was cast into a frozen rectangular glass mould at -60°C with subsequent evaporation at -20°C under vacuum. To ensure linear release of L-dopa, the L-dopa loaded polymer matrices were coated with an impermeable barrier. Samples with a dimension of 15x30x2mm were cut out of the polymer matrix and were variably coated to identify a configuration that created preferred release kinetics. Three types of samples were obtained. The first one was the uncoated polymer matrix, the second one, coated polymer matrix on all sides except one face of the slab, while the third one was fully coated except for the presence of pore size diameters of 2, 4 and 6mm such that the incubation medium could gain access to the loaded core (Sabel et al., 1990) (Figure 2.7).

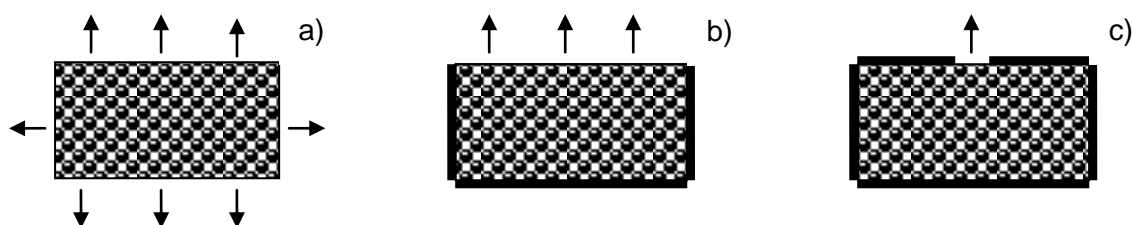


Figure 2.7: Rate of release modified by presence or absence of impermeable membrane for **a)** uncoated polymer matrix; **b)** one side uncoated and; **c)** an opening (pore)/coated (Adapted from Sabel et al., 1990).

The results revealed that the uncoated polymer matrix released L-dopa in all directions and for a short period of time. The one-side uncoated polymer matrix released L-dopa in one direction thereby producing more linear release kinetics, while the polymer matrix with a pore diameter uncoated had linear release kinetics as well as a prolonged delivery period. In both cases, there was an initial 'burst' effect from all formulations followed by a sustained release of L-dopa. The proposed mechanism of release was drug diffusion through the communicating channels and pores within the polymer matrix (Sabel et al., 1990).

In a test that was undertaken employing a rat model, the polymer matrix implants exhibited a continuous release of L-dopa, which assured stable elevated plasma concentrations for about a year (Sabel et al., 1990). However, there might be a need to determine the potential of this delivery system for future applicability by assessing its ability to achieve stable levels of L-dopa, thereby preventing the possibility of motor complications in human subjects.

2.12. Pulmonary delivery of L-dopa

Jackson and co-workers (2004) attempted to improve on the bioavailability of L-dopa by developing pulmonary formulations for L-dopa, which was anticipated to achieve a rapid onset of action and maintain the effective therapeutic level of L-dopa. The formulation comprised of an aqueous solution of L-dopa with either sugars, such as trehalose, and phospholipids, such as dipalmitoyl phosphatidylcholine (*DPPC*), with salt (NaCl) as an option, which was then mixed with an organic solvent such as ethanol, passed through an atomizer and spray-dried (Jackson et al., 2004). Particles containing more than 90% drug were delivered to the patient's pulmonary system (targeted at the alveoli or deep lung structures) utilizing either inhalation devices such as dry powder inhalers, metered dose inhalers or nebulizers. This pulmonary formulation was compared to an oral liquid formulation in PD-induced rat model. The pulmonary formulation furnished a rapid onset of action and elevation of plasma levels of L-dopa, while the oral liquid formulation produced a delayed onset of action and lower C_{max} (Bartus et al., 2004). Despite these promising results, pulmonary formulations have not yet been shown to provide continuous dopaminergic stimulation (Linazasoro, 2008).

2.13. Nasal delivery systems for L-dopa

Nasal route is explored for drug delivery due to its large surface area enhanced by the presence of microvilli that covers the epithelial cells which in turn are highly vascularized (Brime et al., 2000). Other important aspects are the facts that it is easily accessible and avoids first pass metabolism. Brime and team (2000) fabricated L-dopa loaded gelatin microspheres by the w/o emulsification solvent extraction technique for delivery via the

transnasal route. Bioadhesive properties of gelatin facilitated prolongation of the contact between the microspheres and the nasal mucosa thereby enhancing absorption. However, *in vivo* release studies were not performed. The *in vitro* release profiles exhibited a dual phase release for L-dopa, which was characterized by an initial burst release followed by a slow release phase (Brime et al., 2000).

Kim and co-workers (2009) compared three routes of administration for L-dopa; oral, intravenous and intranasal in a rat model. L-dopa without carbidopa given intranasally was rapidly absorbed achieving the same peak plasma concentration (C_{max} $0.55 \pm 0.14 \mu\text{g/mL}$) in 0.2 hours as that given orally (T_{max} , 1.0 ± 0.5 hour) and was rapidly eliminated ($t_{1/2}$, 0.23 ± 0.09 hours). However, incorporation of carbidopa shifted the time courses by decreasing the T_{max} to 0.1 ± 0.0 hours and increasing elimination half life to 0.31 ± 0.09 hours. The absolute bioavailabilities for the nasal and oral formulations with carbidopa were 45.4% and 17.7% respectively (Kim et al., 2009). The nasal drug delivery system is an immediate release system which would not provide constant and sustained delivery of L-dopa in order to provide continuous dopaminergic stimulation.

2.14. Transdermal delivery systems for L-dopa

Transdermal delivery of L-dopa has been envisaged to be an alternative route for delivery of L-dopa, which could overcome the adverse effects and complications encountered with the oral route (Babita et al., 2004; Babita and Tiwary, 2005). It is also more preferred than infusion and implantation because of its non-invasiveness and therefore enhanced patient adherence. It has been considered to be the optimum route for achieving constant plasma concentrations of L-dopa which therefore makes it possible to avoid akinesia and dyskinesia (Babita et al., 2004; Babita and Tiwary, 2005). The transdermal route is recommended for the administration of drugs in geriatric PD patients who tend to have dementia and dysphagia (Lindner et al., 1998; Babita and Tiwary, 2005). However, one of the major limitations encountered with the transdermal route is the permeability barrier properties of skin due to the presence of a series of lipid multilayers made of ceramides, cholesterol and fatty acids (Babita et al., 2004; Babita and Tiwary, 2005). Hence, the penetration of polar drugs such L-dopa through the skin is inhibited and so would require the disruption of the lipid layers. Thus far, organic solvents such as ethanol and methanol have been used as cutaneous absorption enhancers to improve the penetration of L-dopa through the skin (Lindner et al., 1998).

Linder and his team (1998) prepared a hydrogel of L-dopa using ethanol and methanol as absorption enhancers and assessed the transdermal L-dopa absorption *in vitro* and *in vivo* using a rat model. The *in vitro* profiles of L-dopa permeation indicated that ethanol and

methanol in combination enhanced the penetration of L-dopa through the skin while *in vivo* L-dopa concentration continued to rise until 180 minutes. The cutaneous permeation rate *in vitro* was 1375ng/cm²/min and 1236ng/cm²/min *in vivo*. It was postulated that the death of some rats after 240 minutes may have been due to the adverse effects generated by the elevated levels of the L-dopa metabolites. This is very likely considering the fact that carbidopa was not utilized in this study. With organic solvents it was observed that there was a rapid restoration of lipids resulting in normalization of the permeability barrier function (Lindner et al., 1998). For example, the organic solvents' inhibitory effect of triglyceride was found to have waned after 5 hours of treatment (Lindner et al., 1998). Babita and Tiwary (2005) prepared adhesive transdermal patches consisting of a lipid synthetic inhibitor-cerulenin, calcium chloride (optional in some patches), carbidopa (optional in some patches) and L-dopa which were applied to ethanol perturbed shaved skins of rats. The presence of cerulenin produced 60% inhibition of triglyceride synthesis within 2 hours of treatment and 20% of triglyceride synthesis remained inhibited after 48 hours. Application of cerulenin and calcium chloride produced a significantly enhanced inhibitory effect compared to cerulenin alone. On normal skin, the plasma concentration of L-dopa was negligible, but with carbidopa and cerulenin, effective plasma concentrations were attained in 3 hours and maintained up to 10 hours while further addition of calcium chloride increased the duration of activity to 24 hours with a higher C_{max} and lower T_{max}.

In another study, Babita and team (2004) employed three lipid synthesis inhibitors – atorvastatin, cerulenin and β-chloroalanine for inhibition of cholesterol, triglycerides and sphingosine (a precursor of ceramide) syntheses, respectively. The combination of the three lipid synthesis inhibitors reduced lag time to 1 hour compared to the individual applications (2, 4 and 6 hours) and maintained the effective plasma concentration of L-dopa for over 48 hours in the rat model (Babita et al., 2004). Thus far, transdermal studies seem to offer a non-invasive route for the delivery of L-dopa. However, studies in human subjects would be a necessity to assess if the dopaminergic stimulation is continuous and able to reduce motor complications.

2.15. Prodrugs as a delivery vehicle for L-dopa

In an attempt to improve the solubility and subsequent pharmacokinetic profile of L-dopa, prodrugs such as methyl, ethyl, isopropyl, butyl, cyclohexyl and 4-hydroxybutyl esters of L-dopa were developed (Fix et al., 1989; Bettini et al., 2002; Djaldetti et al., 2002). It has been suggested that L-dopa prodrugs are not absorbed through the neutral amino acids transport system as is the case with L-dopa but rather they are absorbed across the intestinal epithelium by active and/or passive transport (Fix et al., 1989; Xiang et al., 2008).

Esters and alkyl esters of L-dopa have been studied as solutions and tablets for transdermal, intranasal, subcutaneous, intramuscular and oral administration and also as microenemas for rectal application (Repta, 1987; Djaldetti and Melamed, 1996; Stocchi et al., 1996; Cohen et al., 1998; Kao et al., 2000; Djaldetti et al., 2002; Kushnir and Heldman, 2004; Parkinson Study Group, 2006). It was observed that the alkyl esters of L-dopa that were administered nasally in Sprague-Dawley rats exhibited rapid and complete absorption into the systemic circulation, while the butyl ester prodrug, specifically, did not result in significant formation of peripheral dopamine thereby enhancing the bioavailability to the CNS, which was comparable to an equivalent intravenous dose (Kao et al., 2000).

An oral controlled release system of L-dopa methyl ester and carbidopa was developed by Bettini and co-workers who designed a three layer matrix tablet with each layer possessing different release mechanisms (Bettini et al., 2002). The first layer was swellable, the second layer was erodible and the last layer was disintegrating. Each layer incorporated several components (polymers and other excipients such as hydroxypropylmethylcellulose, magnesium stearate, talc and polyvinylpyrrolidone) as well as L-dopa methyl ester. The three layer matrix was manufactured using a single punch machine. *In vitro* and *in vivo* studies showed that the drug release depended on the composition of the layers and their relative positions in the matrix (Bettini et al., 2002). The approach of including a swellable layer in the middle of the matrix can be exploited as a means of reducing morning 'on-off' fluctuations, while a disintegrating layer in the middle may be useful in preventing end of dose deterioration in the afternoon.

In 2004, Kushnir and Heldman formulated an apparatus for the transdermal delivery of alkyl esters of L-dopa. L-dopa was dissolved in a non-aqueous solvent which also contained a transdermal enhancer and a detergent (Kushnir and Heldman, 2004). The apparatus comprised of a storage compartment (compressible by mechanical pressure) containing a fluid for transdermal treatment of PD, a dermal patch connected to the storage compartment and a regulating valve to control flow of fluid from the storage compartment to the dermal patch as depicted in Figure 2.8. Results obtained from an *in vivo* study in two human volunteers indicated that an effective concentration of 200ng/mL was obtained.

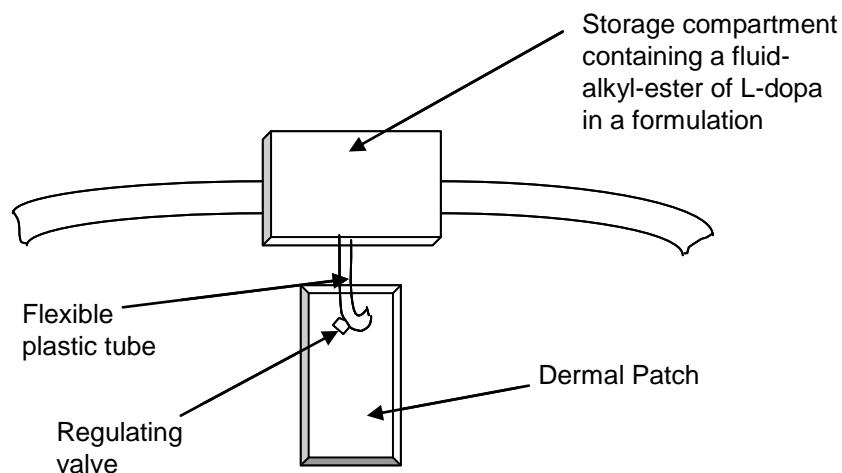


Figure 2.8: Transdermal apparatus for delivery of alkyl-esters of L-dopa (Adapted from Kushnir and Heldman, 2004).

Maleic- and fumaric-diamides of (O, O-diacetyl)-L-dopa-methylester loaded liposomes have also been developed and administered intraperitoneally in rats (Di Stefano et al., 2006). The prodrug had the ability to induce sustained delivery of dopamine in the striatal dialysate of the rat with respect to intraperitoneal administration of equimolar concentrations of L-dopa (Di Stefano et al., 2006).

Furthermore, it has been demonstrated that etilevodopa which is an ethyl ester of L-dopa, has greater gastric solubility compared to L-dopa (Seeberger and Hauser, 2007). It is rapidly hydrolyzed to L-dopa, and possesses a shortened time to maximum L-dopa concentration (Seeberger and Hauser, 2007). However, despite the aforementioned advantages, it has been noted that its clinical response is not superior to L-dopa. In a double-blind, randomized, comparative clinical trial which was undertaken in 44 sites using a total number of 327 patients for the assessment of etilevodopa's efficacy, safety and tolerability in PD patients with motor fluctuations, there was no improvement in the onset of drug benefit, response failure and 'off' periods compared to L-dopa (Parkinson Study Group, 2006). Dispersible tablets of etilevodopa/carbidopa also had no advantage in 'on and off' effects experienced by PD patients when compared with L-dopa/carbidopa tablets (Seeberger and Hauser, 2007).

2.16. Delivery of L-dopa via the rectal route

Thus far, L-dopa has been administered through the rectal route in the form of tablets, suppositories and insufflations of powdered tablets but its absorption into the systemic circulation of PD patients has not been adequate (Eisler et al., 1981; Iyer et al., 2005). This may possibly have been due to the alkalinity of rectal secretions, high bacterial content of the

rectum, or perhaps due to absence of neutral amino acids transport system. Contrary to that, rectal absorption of simple alkyl esters of L-dopa was found to be greater than that obtained with oral dosing in a study carried out in rats and dogs with the butyl ester prodrug, which exhibited bioavailabilities of 100% and 32% in rats and dogs, respectively (Fix et al., 1989).

2.17. Expert opinion on the progress made to date in delivering the gold standard

Much effort has been directed towards the management of PD but a large chasm is yet to be bridged in terms of ultimate efficacy, especially in advanced PD patients. Constant plasma levels of L-dopa and subsequent continuous dopaminergic stimulation is highly needed in PD patients. Although intraduodenal infusions have achieved constant plasma levels, its invasiveness limits its use in consideration of the fact that it is a chronic therapy. The transdermal route for L-dopa is promising but studies have to be undertaken in humans to assess its ability to produce continuous dopaminergic stimulation. Furthermore, the oral route is the most preferred route of administration for chronic therapy, thus an oral formulation that is able to achieve constant plasma concentration of L-dopa will be of significant advancement in the management of PD.

From these discussions, the described developments in L-dopa systems can be summarily compared in terms of their relevant pros and cons, as depicted in Figure 2.9.

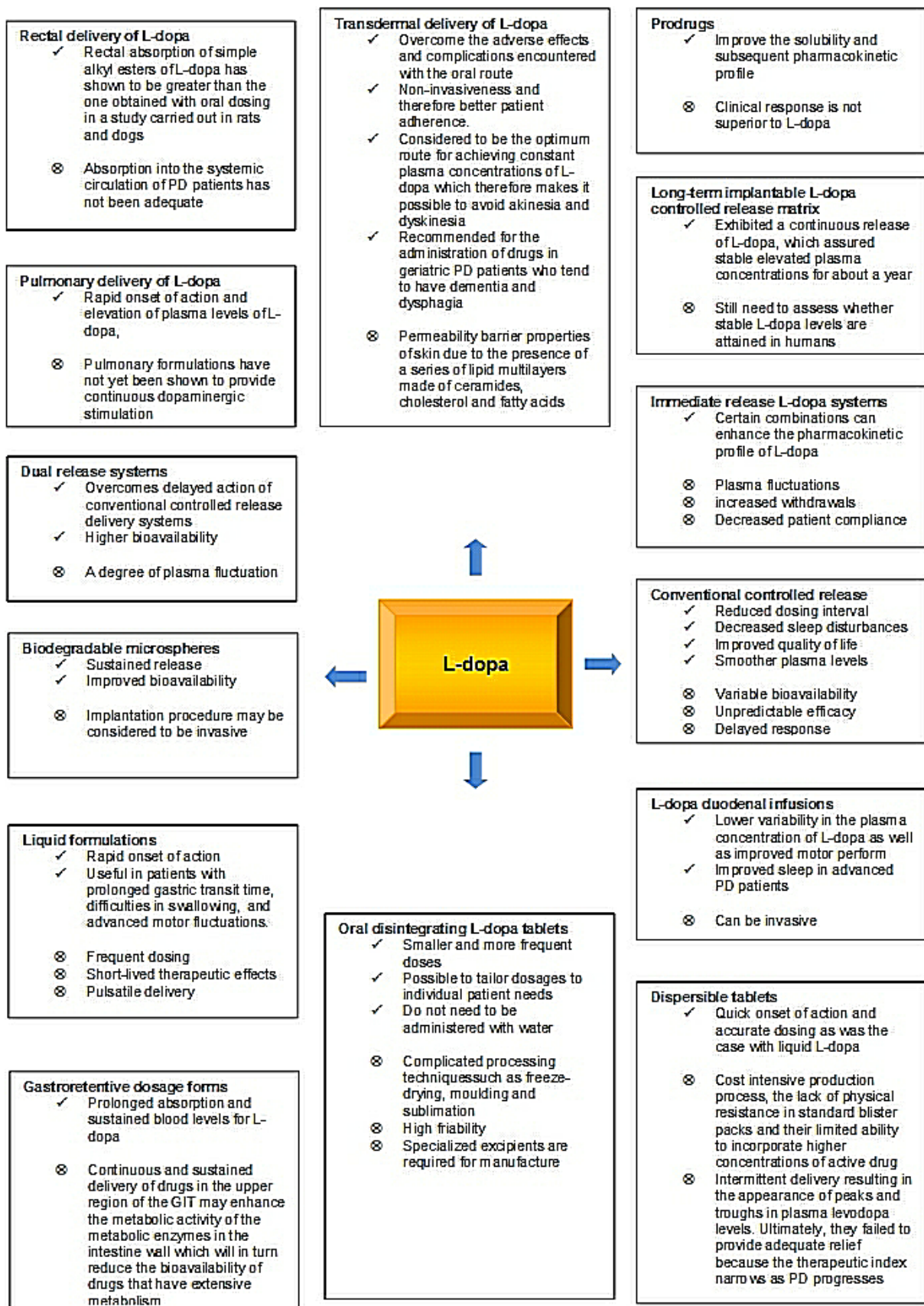


Figure 2.9: Overview of the pros and cons of L-dopa delivery systems (Extracted from Ngwuluka et al., 2010)

In considering the afore-described technologies, one of the sobering facts elicited when considering chronic suppressive maintenance therapy in neurodegenerative disorders such as PD is the often insurmountable presence of the BBB (Kreuter, 2005) and the considerable side effects of currently prescribed therapies (Mukai and Lipsitz, 2002). The vascular endothelial cells, choroid plexus and the arachnoid membrane act together to form the barrier between the blood and cerebrospinal fluid (CSF) for efficient restriction of agents from entering the brain (Lum et al., 1991). An understanding of the intricacy of the BBB is imperative for the design of techniques to manipulate the barrier for transport of therapeutic agents to the brain for PD management.

An authority in the field, Prof. William Pardridge (Brain Research Institute, UCLA, Los Angeles, CA, USA) wrote in *Drug Discovery Today* (2007): 'Considering the potential size of the global CNS pharmaceutical market, and considering that so few drugs cross the BBB, one would expect that the development of BBB drug delivery technologies would be a high priority in the pharmaceutical industry and in the academic sciences. In fact, there is not a single medium or large pharmaceutical company in the world today that has a BBB-drug-targeting technology program. Even if big pharma wanted to change this situation, there would be no staff to hire because there are so few BBB scientists being trained in academia. In the USA, there is not a single academic neuroscience program that has any emphasis on BBB drug targeting technology...'

Consequently, in conceptualizing and developing a targeted system for PD management, the obstacle presented by the BBB must be tackled. Enhancement of drug lipophilicity through chemical modification, or drug conjugation with a BBB-specific transport vector have been considered (Pardridge, 1999); however, these systems commonly implicate a 1:1 ratio of vector to drug, thus limiting their carrying capacity (Calvo et al., 2001). The carrying capacity could be vastly improved via incorporation of the drug into particulate systems such as liposomes or polymer nanoparticles. The design of antibody-coated liposomes (Huwyler et al., 1996) and mannosylated liposomes (Umezawa and Eto, 1988) has been attempted. Still, studies emanating from these approaches were not entirely convincing (Calvo et al., 2001). Discussed in this review were L-dopa methylester loaded liposomes formulated by Stefano et al. (Di Stefano et al., 2006). More concerted efforts are necessitated.

A forward-thinking approach needs to be exercised, rationally applying nanotechnology to achieve neuropharmaceutical innovations to enhance PD management. Nanotechnology encompasses engineered materials or devices with the smallest functional organization on the nanometer scale (1–100 nm), and may provide an avenue for the manipulation of complex biological systems such as the BBB with greater selectivity and responsiveness

than conventional pharmacological approaches. Nanotechnology has a potentially revolutionary impact on the basic understanding and therapeutic approaches of neuroscience, and thus, pertinently, PD. The power of nanotechnology must be channeled towards the development of nano-enabled drug delivery systems for the treatment of PD, exploiting the nanoscale structures of neural cells. Nano-enabled systems, such as polymeric nanoparticles are able to protect the drug from degradation in the GIT, bypassing the liver thereby avoiding first pass metabolism, consequently improving bioavailability. In addition, polymeric nanoparticles are able to remain in the systemic circulation for extended periods, and therefore would be able to target the delivery of L-dopa to the CNS more effectively (Soppimath et al., 2001; Nimesh et al., 2006; Italia et al., 2007).

Di Stefano and co-workers (2009) highlighted that a key challenge in PD therapy is the targeted and localized delivery, which will purportedly limit severe side effects, such as psychiatric disturbances and dyskinesia deriving from the distribution of L-dopa in healthy tissues. The concept of developing drug delivery systems able to target pharmacologically active molecules in close proximity to their site of action is receiving heightened attention. Pertinently applicable systems capable of interacting with biological systems at the molecular level with a high degree of specificity for the provision of neuroprotection, and enabling the delivery of drugs and small molecules across the BBB include liposomes, polymeric or lipidic micro- and nanoparticles, polymeric micelles, and dendrimers (Di Stefano et al., 2009). In fact, scientists recently developed dendrimers for investigation of their effect on the fibrillation of α -synuclein (Rekas et al., 2009). The dendrimers redirected α -synuclein to an amorphous aggregation pathway. It is these α -synuclein oligomers that are also believed to be the cytotoxic species associated with amyloidoses, and compounds such as dendrimers, that reduce the amount of prefibrillar oligomers by inducing amorphous aggregation may be an attractive alternative preventative approach for PD. Furthermore, the rapid action of the dendrimers on pre-formed fibrils holds an additional therapeutic advantage of removing physiologically-stable amyloid deposits already present in patients with PD (Rekas et al., 2009). The eventual impact of this research has yet to be fully realized through ensuing investigations.

To exploit the nanotechnological approach to its full potential, directed strategies are required to modify the bodily distribution of such entities (Calvo et al., 2001). Proposed properties that would be advantageous for targeted systems include: (a) prolonged circulation, thus drug loading and release can be adjusted fairly independently from fluid circulation; (b) tissue distribution, which will be largely lipid dose independent, such that therapeutic dose escalation produces increasing drug effects with minimal changes in pharmacokinetics; and

(c) the facilitation of the addition of ligands (targeted to PD biomarkers, for example) or other functionalities to the polymer surface layer through chemical modifications. This will serve to intelligize devised nanosystems through introduction of targeting capabilities.

In looking towards nanotechnology for answers, however, cognizance must be taken of the fact that the uniquely beneficial properties of engineered nanosized systems undoubtedly goes hand-in-hand with their equally unique health risks when used in medical applications and their environmental impact (Aitken et al., 2004; Nel et al., 2006). According to the Australian Department of Employment and Workplace Relations, a customer-focused organization (Australian Department of Employment and Workplace Relations, 2005), such nanosized systems, given the novelty and variety of products, are highly reactive and mobile within the human body. Furthermore there are currently no effective methods of monitoring the risks of nanoparticle exposure in patients or healthcare workers. The lack of knowledge regarding the manner in which nanoparticles interact with the biochemical pathways and processes of the human body is worrisome (Garber, 2007) and should spur scientists to have an implicit focus on nanoparticle toxicity, characterization and exposure pathways during delivery system development.

2.18. CONCLUDING REMARKS

Ultimately, the need for the effective delivery of existing agents, such as L-dopa, for the therapeutic management of PD is thus imperative and should be the focus of extensive research (Aubin et al., 1998; Bharath et al., 2002; Bridge et al., 2004; Brotchie et al., 2005; Mandel et al., 2005; Schrag and Jonathan, 2006). From a pharmaceutical viewpoint, the vast challenges presented by PD must be tackled if we are to take a step forward in its management.

CHAPTER THREE

RHEOLOGICAL CHARACTERIZATION AND MODELING OF THE SYNTHESIS OF AN INTERPOLYELECTROLYTE COMPLEX OF METHACRYLATE COPOLYMER AND SODIUM CARBOXYMETHYLCELLULOSE

3.1. INTRODUCTION

Rheological characterizations of polymer blends or modified polymers are undertaken to assess the influence of the components as well as the interactions that may have occurred. While the size, shape, concentration and mode of particle size distribution influence the rheological properties of the blend, the interactions within the system influence the properties of the continuous medium (Lipatov et al., 1982).

Rheology is frequently employed to characterize pharmaceutical formulations especially emulsions, ointments, colloids and gels. Furthermore, the rheological properties of a polymer determines its suitability and application in pharmaceutical industry in terms of dosage forms, route of administration, site of action and the desired rate of release. Rheology is a useful tool which provides indirect information on the structure and consistency which refers to yield value, viscosity and loss factor; and in turn influences sensory attributes and drug release (Pérez et al., 2004). Generally, rheological behaviors exhibited by polymer depend on the inter-chain interactions, crosslinking and entanglements; and relate to swelling, shrinking, erosion, degradation and diffusion of drugs (Bonferoni et al., 1995; Michailova et al., 1999; Lee et al., 2004; Ghosh et al., 2005; Weng et al., 2007; Santoveña et al., 2009). For polyelectrolyte such as sodium carboxymethylcellulose (NaCMC), the conformation and rheological behavior exhibited is influenced by its ionization grade which depends on the pH and ionic strength (Bonferoni et al., 1995).

An interpolyelectrolyte complex (IPEC) is formed by the blending of a cationic polyelectrolyte and an anionic polyelectrolyte at a stoichiometric ratio. IPECs are employed as modified polymers in drug delivery, actuators in biotechnology and flocculants in various environmental and industrial processes (Liu et al., 2001).

NaCMC is a soluble semi-synthetic derivative of cellulose. Rheological characterization of NaCMC has been undertaken by several researchers (Elliot and Ganz, 1974; Abdelrahim and Ramaswamy, 1995; Kulicke et al., 1996; Michailova et al., 1999; Edali et al., 2001; Yaşar et al., 2007; Benchabane and Bekkour, 2008). It is known to exhibit marked shear thinning flow pattern, visco-elastic properties and behaves as an entanglement polymer (Florjancic et al., 2002). It is employed as viscosity-enhancing agent in food, cosmetics and pharmaceutical industries.

Methacrylate copolymer (Eudragit[®] E100) is a cationic polymer with low viscosity (Mustafin et al., 2005) that is soluble in acid medium while it swells in higher pH.

This study was undertaken to elucidate the rheological changes that occur during the synthesis of IPEC of methacrylate copolymer and NaCMC; and compare the rheological properties of the individual polymers with those of the IPEC to provide insight on its potential as a drug carrier for controlled release. The rheological studies undertaken included basic viscosity, yield stress test, oscillatory stress sweep, oscillatory frequency sweep, temperature ramp; and creep and recovery test.

3.2. EXPERIMENTAL SECTION

3.2.1. Materials

Methacrylate copolymer (Eudragit[®] E100, Evonik Röhm GmbH & Co. KG, Darmstadt, Germany), sodium carboxymethylcellulose (NaCMC, Fluka Biochemika, Medium viscosity, Sigma-Aldrich Chemie GmbH, Buchs, Switzerland), acetic acid glacial (Rochelle Chemicals, Johannesburg, South Africa) and deionized water.

3.2.2. Equipment

A Haake MARS (Modular Advanced Rheometer System) rheometer (Thermo Electron Corporation, Karlsruhe, Germany) fitted with a cone and plate geometry with a diameter of 35mm and cone angle of 1° – sensor C35/1°Ti was employed. The measurements were undertaken in controlled stress mode in oscillation. Data were acquired with RheoWin PC Software, version 3.

3.2.3. Methodology

3.2.3.1. Synthesis of the interpolyelectrolyte complex

The methacrylate copolymer was milled and 0.84g dissolved in 50mL of 0.1, 0.4 and 0.8N acetic acid while solutions of 1.68g NaCMC were prepared by dissolving in 50mL deionized water. A transparent methacrylate copolymer solution was added into a transparent NaCMC solution and stirred under vigorous agitation at ambient temperature. Samples were withdrawn at intervals during synthesis for analyses of rheological properties at the following sampling points:

Sampling point I: 30secs of stirring after methacrylate copolymer solution was added to NaCMC solution.

Sampling point II: 1 hour later.

Sampling point III: At breaking point. Breaking point is regarded as the point during synthesis where the IPEC thickens in such a manner that magnetic stirring becomes a challenge; and at this point, interaction and blending are still non-homogenous but synthesis is on the verge of completion.

Sampling point IV: End of synthesis.

3.2.3.2. Rheological studies

The IPEC was loaded onto the rheometer plate using a spatula. All tests were undertaken at the different sampling points to monitor the rheological changes and how these changes relate to the interactions such as intermolecular and intramolecular bondings taking place at each sampling point. Other than temperature ramp, other studies were undertaken at 25°C.

3.2.3.2.1. Basic viscosity

To determine the degree of resistance to flow at each interval of sampling as stated in section 3.2.3.1; the samples were subjected to shear rate range of 0.00 – 200.00 1/s over 180 seconds.

3.2.3.2.2. Yield stress test

Yield stress is undertaken to obtain structural strength (yield value) of a system at rest beyond which it starts to flow. It was undertaken at the different sampling points to monitor the changes in yield stress from start to end of synthesis. It was also important to obtain the yield value for each sampling as it was employed in some of the other tests such as temperature ramp, frequency sweep; and creep and recovery test. Hence the yield stress test was undertaken within the shear stress range of 0.200 – 200Pa over 200 seconds.

3.2.3.2.3. Oscillatory stress sweep

One of the factors that influence the uptake of solvent and subsequent drug release from a polymeric matrix is the visco-elastic characteristics of the polymer utilized. Hence, oscillatory stress sweep was conducted over a shear stress of 0.100 – 70.00Pa at frequencies 0.1, 1 and 10 Hz to determine the visco-elastic region of IPEC.

3.2.3.2.4. Oscillatory frequency sweep

Oscillatory frequency sweep was utilized to determine the degree of elasticity and subsequent structural behavior of IPEC. The condition and consistency of the IPEC at each sampling point were assessed by undertaking frequency sweep from 50.00 – 0.05Hz (314.2 – 0.3142 rad/s). The shear stress for each sample is dependent on the yield value obtained from yield stress test.

3.2.3.2.5. Creep and recovery test

To assess the degree of deformation of IPEC on application of stress and its ability to recover, creep and recovery test was employed. The test is used to monitor the resultant strain on a material after stress is applied. Stress was applied for 60 seconds and allowed to recover over 180 seconds

3.2.3.2.6. Temperature ramp

The impact of temperature on IPEC structure during and after synthesis was monitored over a temperature range of 15 – 70°C. A solvent trap was used to cover the cone and plate to prevent evaporation and drying of samples during the tests. The frequency employed was the frequency at which the yield value was obtained.

3.2.3.3. Static lattice atomistic simulations (SLAS)

All modeling procedures and calculations were performed using the HyperChem™ 8.0.8 Molecular Modeling System (Hypercube Inc., Gainesville, Florida, USA) and ChemBio3D Ultra 11.0 (CambridgeSoft Corporation, Cambridge, UK) at the 4 sampling points – IPEC-I, IPEC-II, IPEC-III, IPEC-IV. SLAS was undertaken to provide insight into the interactions between methacrylate copolymer and NaCMC, mechanisms involved in the formation of IPEC as well as their energy properties. The methacrylate copolymer (E100) was drawn using ChemBio3D Ultra in its syndiotactic stereochemistry as a 3D model whereas the structure of CMC (4 saccharide units) was built from standard bond lengths and angles using sugar builder module on HyperChem™ 8.0.8. Structure of acetic acid was built up with natural bond angles as defined in the HyperChem™ software. The models were energy-minimized using a progressive-convergence-strategy where initially the MM+ (Molecular Mechanics plus) Force Field was used followed by energy-minimization using the Amber 3 (Assisted Model Building and Energy Refinements) Force Field. The conformer having the lowest energy was used to create the polymer-polymer and polymer-solvent complexes. A complex of one polymer molecule with another was assembled by disposing the molecules in a parallel way, and the same procedure of energy-minimization was repeated to generate the final models: CMC, E100 and CMC-E100. Full geometry optimization was carried out in vacuum employing the Polak–Ribiere conjugate gradient algorithm until an RMS gradient of 0.001kcal/mol was reached. For Molecular Mechanics calculations in vacuum, the force fields were utilized with a distance-dependent dielectric constant scaled by a factor of 1. The 1-4 scale factors used were electrostatic - 0.5 and van der Waals - 0.5 (Kumar et al., 2011).

To generate the final models in solvated system the MM simulations were performed for cubic periodic boxes with the polymer-polymer complex (IPEC) at the centre of the cubic box

and the remaining free space filled with water and acetic acid (AcA). The same procedure of energy-minimization was repeated to generate the solvated models except that the force fields were utilized with a distance-independent dielectric constant with no scaling. For simplification, IPEC, IPEC-AcA₂, IPEC-AcA₄, and IPEC-AcA₈ represented IPEC, IPEC in 0.2N acetic acid, IPEC in 0.4N acetic acid, and IPEC in 0.8N acetic acid, respectively. In addition, the force field options in the AMBER were extended to incorporate cutoffs to Inner and Outer options with the nearest-image periodic boundary conditions and the outer and inner cutoffs were to ensure that there were no discontinuities in the potential surface (Choonara et al., 2011).

3.3. RESULTS AND DISCUSSION

As normality of acetic acid increased, the solubility of methacrylate copolymer increased. Furthermore, as methacrylate copolymer was added to NaCMC gel, the viscosity of the gel increased initially with visibly white strands running through the gel. However, on vigorous agitation, the viscosity decreased with time and thereafter increased towards the breaking point before it assumed its final viscosity. This was clearly observed where 0.1N acetic acid was employed to dissolve methacrylate copolymer. The degree of reduction in viscosity is dependent on the degree of viscosity of NaCMC gel and the normality of acetic acid. As the normality of acetic acid increased from 0.1N to 1.0N, the viscosity of the end product decreased. At the stoichiometric ratio of 0.5 of methacrylate copolymer and 1.0 of NaCMC, there appeared to be complete polymer-polymer crosslinking or interaction as the end product was completely white (homogenous) and were like shreds which sedimented when the viscosity was low. It was envisaged the bonds within the NaCMC gel were broken faster at 0.8 and 1.0N of acetic acid to generate IPEC with methacrylate copolymer in less than an hour unlike that of 0.1N which took about three hours. These visible observations during synthesis prompted the rheological studies of IPEC.

The rheological properties of polymers employed for drug delivery can influence both *in vitro* and *in vivo* behaviors of a drug delivery system. The factors that determine the rheological outcome of the polymers include pH, temperature, polymer concentration, polymer modification, polymer combinations, ions and additives (Lee et al., 2009). Hence, the need to study the rheological behavior of IPEC since some of the factors such as polymer concentration, modification, combination and ions were involved in its synthesis and may influence its drug release kinetics.

3.3.1. Basic viscosity (η) of the native polymers and IPEC

Methacrylate copolymer, NaCMC and IPEC generated from the interaction of methacrylate copolymer and NaCMC exhibited non-newtonian flow pattern; for viscosity (η) decreased as

shear rate ($\dot{\gamma}$) increased. Methacrylate copolymer is a polymer of low viscosity as can be seen from its rheogram depicting it as having the lowest viscosity while NaCMC is widely employed as a viscosity-enhancing agent. The IPEC like NaCMC exhibited shear thinning behavior and so could be said to be pseudoplastic which is also an indication that the interaction between the polymers did not alter shear thinning properties of the NaCMC (Figures 3.1a-c). Increasing shear rate ($\dot{\gamma}$) forces the molecular chains to untangle which leads to molecular alignment making the molecules slip over each other with ease (Dapía et al., 2005; Nakason et al., 2012).

It is worthy to state that the same quantities of polymers were utilized for the rheological studies of the native polymers and IPEC. This means 1.68g was used to determine the rheological properties of NaCMC and same quantity was used for the synthesis of IPEC and its rheological assessments. Initially at the onset of synthesis, the viscosity of the blends at the different normalities of acetic acid, 0.1, 0.4 and 0.8N were less viscous than NaCMC (Figure 3.1a). However, at the end of synthesis, viscosity of IPEC increased compared to NaCMC but experienced more shear thinning than NaCMC with increased shear rate as depicted in Figure 3.1b. Decrease in viscosity with increased shear rate is attributed to the orientation or molecular deformation of the polymer network in the direction of the flow (Ghannam and Esmail, 1997). However, IPECs synthesized with 0.4N and 0.8N acetic acid at the end of synthesis behaved differently; for as shear rate increased, they exhibited shear thinning, shear thickening and then sharp shear thinning (Figure 3.1b). Perhaps, the order of untangling of molecular chains (molecular deformation) may have been interrupted or slowed down as shear rate increased and then resumed as shear rate further increased. Gradients were calculated for each rheogram to quantify the impact of shear rate on the viscosities of IPEC at different sampling points and normality of acetic acid in comparison to NaCMC. The gradients at the end of synthesis were in the order: NaCMC (0.1757) < IPEC with 0.4N acetic acid (0.3438) < IPEC with 0.1N acetic acid (0.4353) < IPEC 0.8N acetic acid (0.6554). Application of gradient confirmed that IPEC experienced more shear thinning than NaCMC for a higher gradient value indicated a steeper decrease in viscosity.

Figure 3.1c depicts viscosity versus shear rate for IPEC synthesized with 0.1N acetic acid at the 4 stages of sampling during synthesis. The lowest viscosity of less than 5000mPa.s was observed at the onset of synthesis and the highest viscosity of over 100000mPa.s was observed at the end of synthesis. The changes in viscosity can be attributed to the electrostatic interactions taking place within the two polymers (Rodríguez et al., 2001). The thickening or stiff behavior of IPEC at 1hr and breaking point could be due to the formation of entanglements of the polymer coils and increase in the intermolecular interactions

(Benchabane and Bekkour, 2008). In addition, shear thinning was more with IPEC 0.1N at 1hr and breaking point than at the end stage of synthesis which was confirmed by gradient values (0.5318 at 1hr, 0.4435 at breaking point and 0.4353 at the end). For one hour and breaking point, rheograms were only obtained for IPEC synthesized using 0.1N acetic acid (Figure 3.1c). The rate of synthesis is accelerated as the normality of acetic acid increased and so rheograms could not be obtained for 0.4N and 0.8N acetic acid at one hour and breaking point as the synthesis reached completion at one hour.

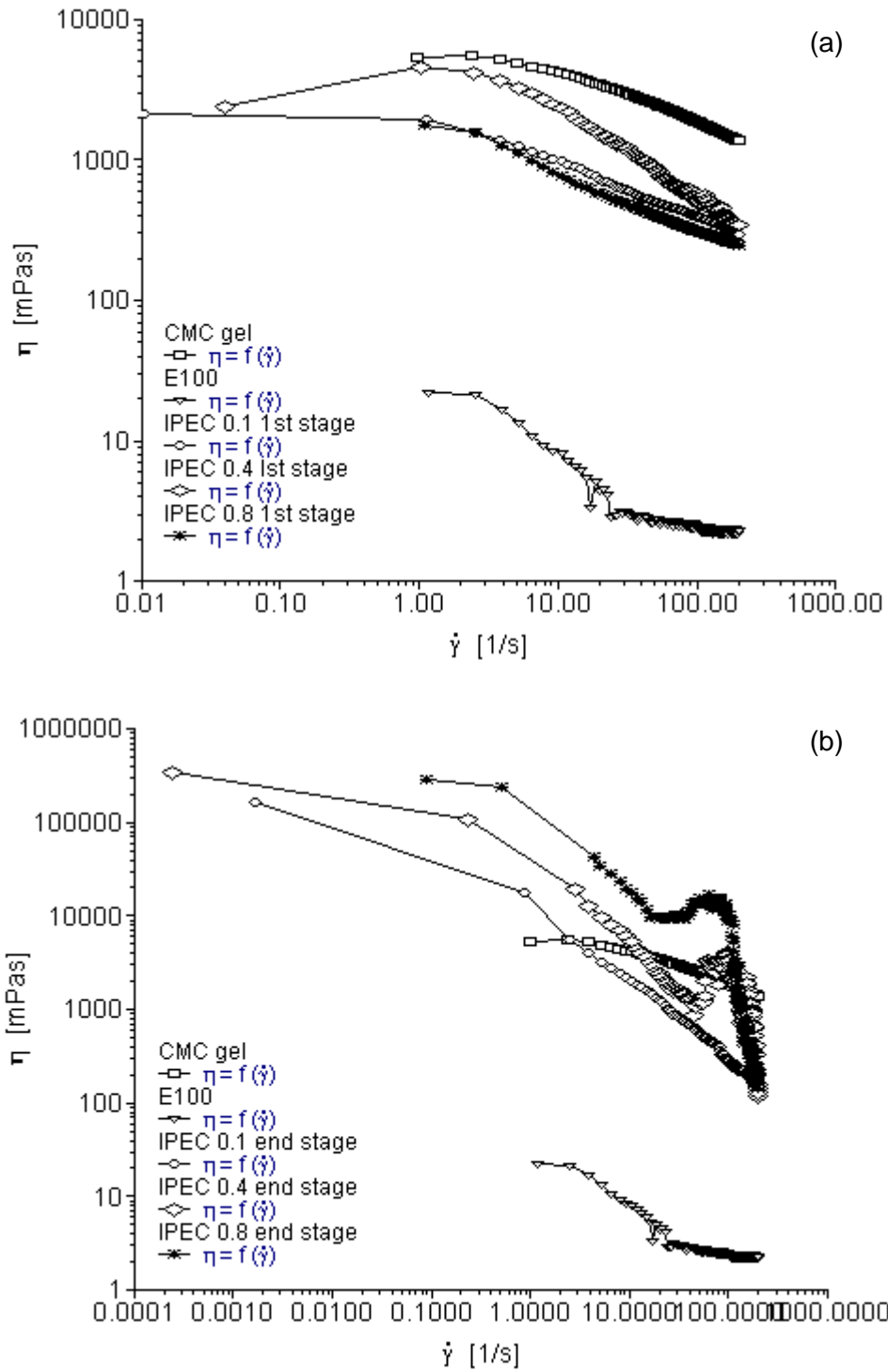


Figure 3.1: **a)** Viscosity as a function of shear rate for native polymers and IPEC at the first stage (sampling point I) of synthesis and; **b)** Viscosity as a function of shear rate for native polymers and IPEC at the end stage (sampling point IV) of synthesis.

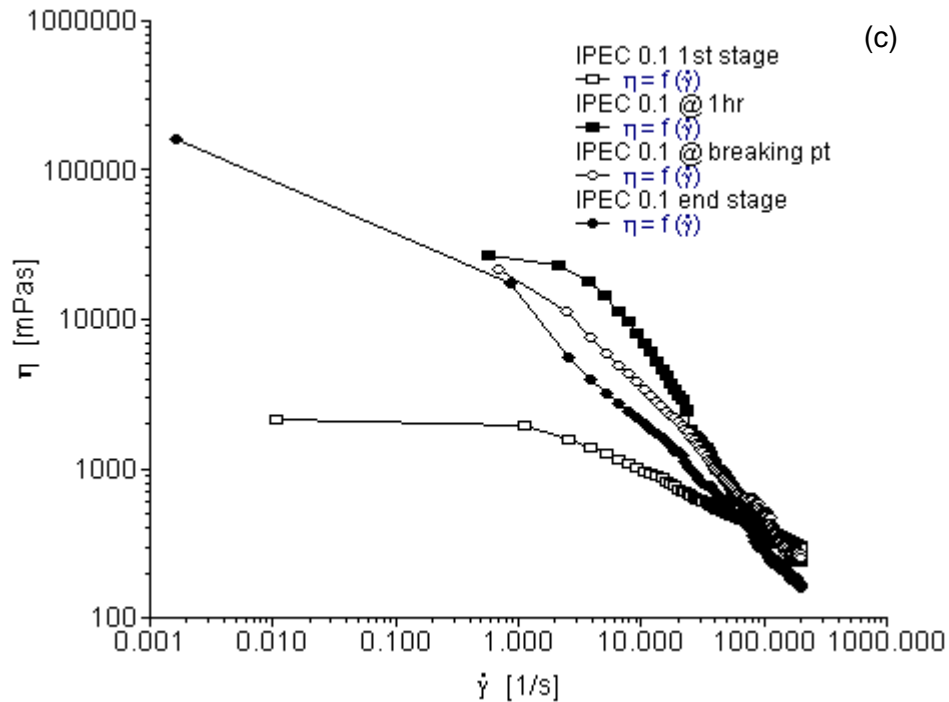


Figure 3.1c: Viscosity as a function of shear rate for IPEC at the 4 sampling points of the synthesis using 0.1N acetic acid.

3.3.2. Yield stress analysis

Yield stress is the point or stress above which a substance flows due to deformation of its internal structure. Below the yield value, a material is a solid exhibiting elasticity under small stresses and strains (Rudraraju and Wyandt, 2005) and above the yield value the material behaves as a liquid with plastic viscosity (Barnes and Walters, 1985). Although Barnes and Walters argues there is no real yield stress as fluids that flow in high stresses can also flow in small stresses (Barnes and Walters, 1985), the apparent yield stress is valuable. A material may generate apparent yield stress if studied in a shear stress versus shear rate region just above the large increase in viscosity (Barnes, 2000). Yield stress tests were undertaken to obtain the yield values of the native polymers and IPEC to provide insight on their yield strength as the IPEC would be employed in matrix formation. The shear (γ) versus shear stress (τ) rheograms was used to determine yield points for the native polymers and IPEC which are shown in Figures 3.2a-c while the apparent yield values calculated using the software RheoWin PC version 3 are given in Table 3.1.

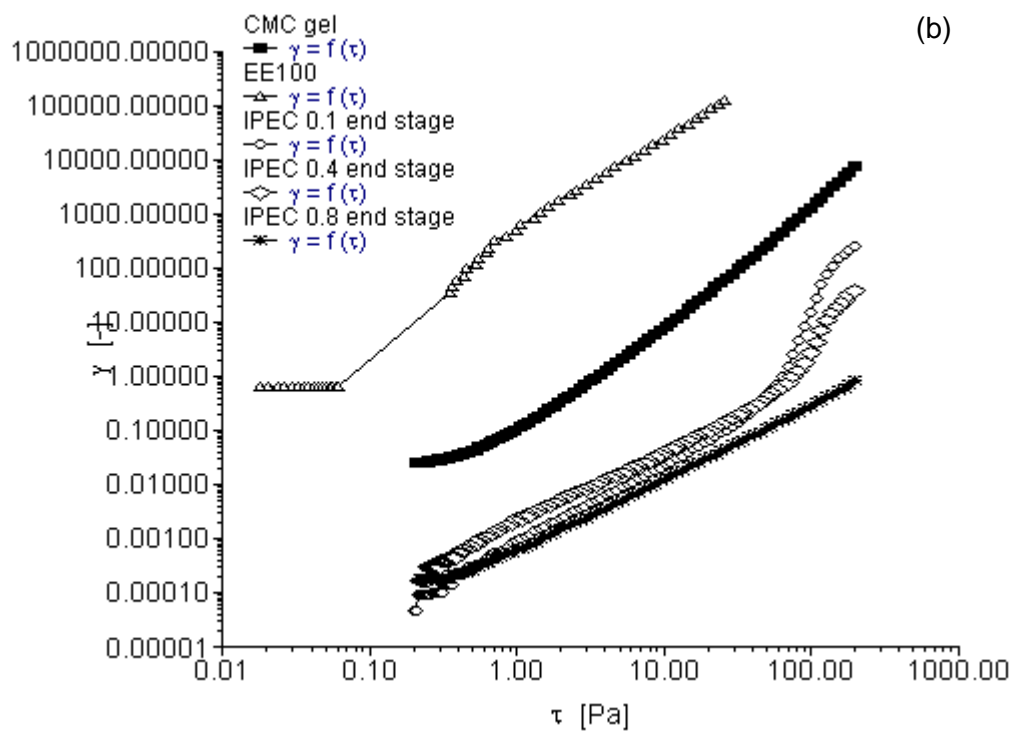
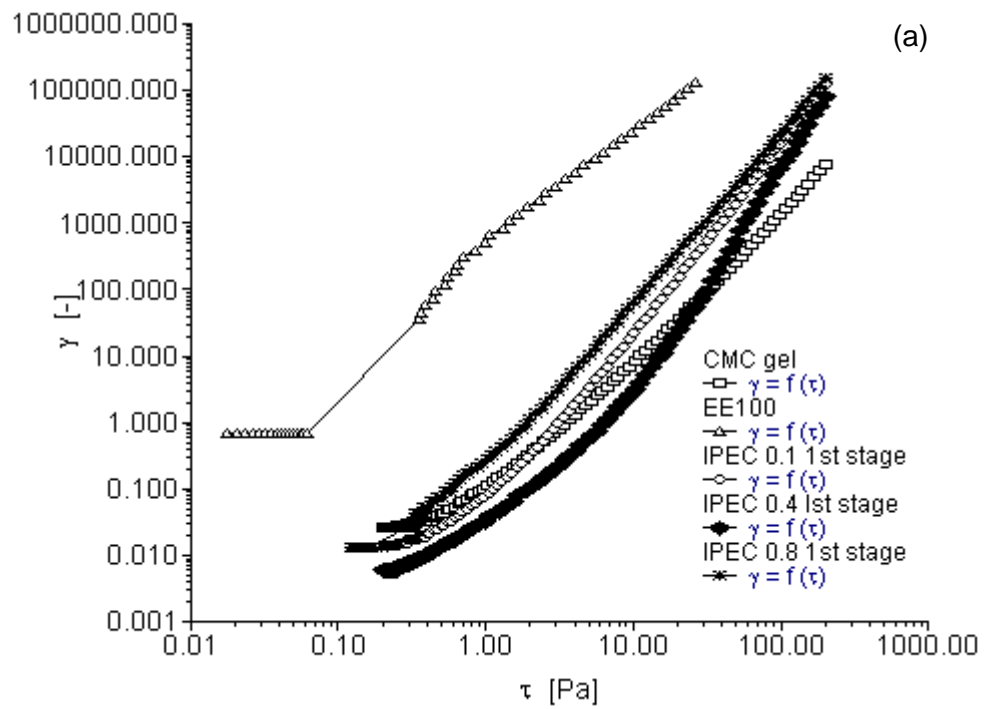


Figure 3.2: **a)** Yield stress rheogram for native polymers and IPEC at the first stage of synthesis and; **b)** Yield stress rheogram for native polymers and IPEC at the end stage of synthesis.

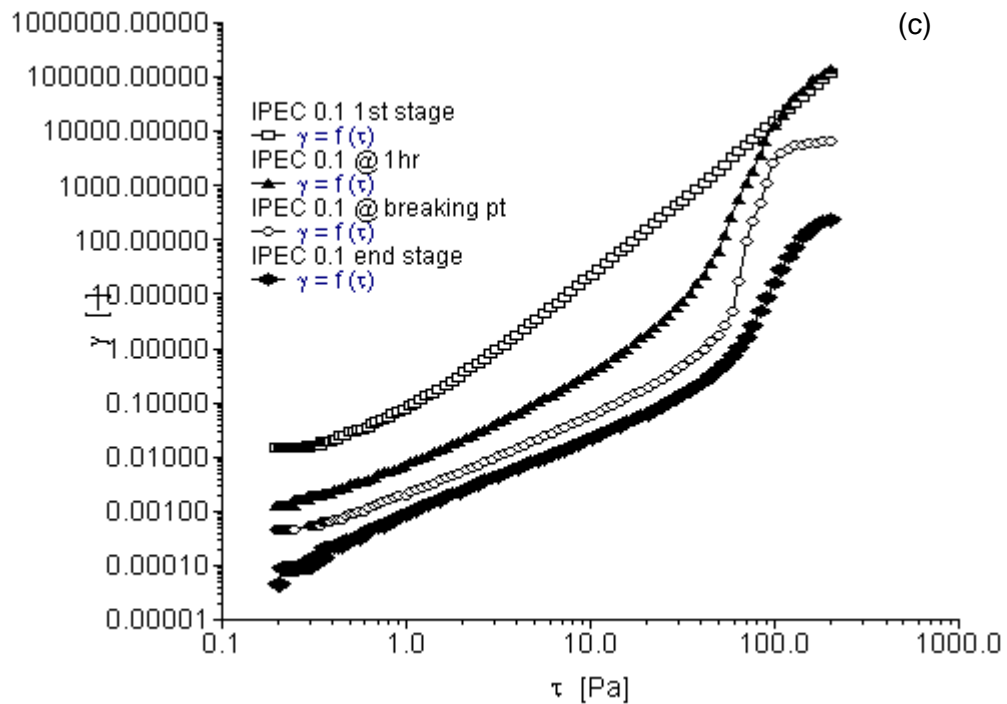


Figure 3.2c: Yield stress rheogram for IPEC at the 4 sampling points of synthesis using 0.1N acetic acid.

Table 3.1: Yield values of native polymers and IPEC at the sampling stages during synthesis.

Sample	Yield value (Pa)	Shear	Time (sec)
NaCMC	0.2911	0.02802	31.47
E100	0.07212	0.9648	32.17
IPEC ¹ 0.1N initial stage	0.2482	0.01442	31.22
IPEC 0.1N @ 1hr	0.2356	0.001318	30.98
IPEC 0.1N breaking pt	41.42	0.9988	72.35
IPEC 0.1 final stage	53.31	0.5160	83.77
IPEC 0.4N initial stage	0.2904	0.006955	31.13
IPEC 0.4N final stage	0.2311	0.0001735	30.67
IPEC 0.8 initial stage	0.1923	0.01345	30.66
IPEC 0.8N final stage	0.3329	0.0001819	31.03

¹ denotes Complex of Eudragit E100 and NaCMC

The yield stress which is an indication of internal strength of IPEC 0.1N increased from the initial stage of synthesis to its completion. In comparison to NaCMC, the yield value of IPEC 0.1N (Table 3.1) is significantly higher. An increase in yield value represents a strengthening of the three-dimensional network structure of the polymer (Lee et al., 2009). Crosslinking NaCMC with methacrylate copolymer enhanced its polymeric structure making it more elastic and thereby improving the mechanical strength of NaCMC. Therefore, it is envisaged that

matrices formed with IPEC will have improved physico-mechanical properties. It was observed that the yield values (resistance to flow) of IPEC synthesized with 0.4N and 0.8N acetic acid (at the end stage) were lower than that of IPEC synthesized with 0.1N acetic acid. Hence, the application of IPEC may determine the normality of acetic acid that will be employed for synthesis.

3.3.3. Oscillation stress sweep

Oscillation stress sweep is used to obtain the visco-elastic region of a material. The visco-elastic region will impact on the mechanical strength of IPEC which will in turn influence the drug release kinetics when used as a drug carrier. The visco-elastic region is frequency dependent and so stress sweep is performed over three frequencies in this study (0.1, 1 and 10Hz). The strength and subsequently the stability of a material correlate with its yield value. As the elastic modulus (G') begins to decrease, the material undergoes structural deformation. The stress at which the material begins to exhibit non-linear behavior is the yield stress. The increase in elastic modulus also relates to the degree of intermolecular crosslinking within the polymer network (Moura et al., 2007). Furthermore, degree of crosslinking correlates with the increase in yield stress and subsequently the extension of the visco-elastic region. Crosslinking increases the elastic modulus of a polymer thereby increasing its mechanical strength (Anseth et al., 1996). Storage or elastic modulus G' represents the elastic property of the polymer while loss modulus G'' represents the viscous properties.

Figures 3.3.1a-c depict elastic modulus G' as a function of shear stress at frequency 0.1Hz. It was apparent methacrylate polymer lacked elasticity and hence showed no evidence of a visco-elastic region. On addition of methacrylate copolymer into NaCMC, elastic modulus of IPEC was increased (Figure 3.3.1a-b). However, compared to NaCMC, IPEC visco-elastic region was not as extended. As shear stress increased, the resistance to deformation decreased. As the synthesis proceeded for one hour, the elastic modulus of IPEC 0.1N increased (Figure 3.3.1c) and continued increase was observed at breaking point with higher resistance to deformation. At the breaking point, there were large intermolecular forces enabling inter-chain crosslinking to occur between NaCMC and methacrylate copolymer which in turn caused increased resistance to deformation and the polymer complex behaved as a solid. It is envisaged that significant increase in elastic modulus at breaking point could be due to shear induced transformation of intramolecular chain associations to intermolecular chain associations (Xu et al., 2010). On completion of the associations, the elastic modulus was reduced and it is envisaged that this was due to little or no complexing ions left and on continued shear stress, the polymer succumbed to deformation. Contrary to the initial stage

of synthesis, the end stage indicated that the elastic modulus increased as normality increased.

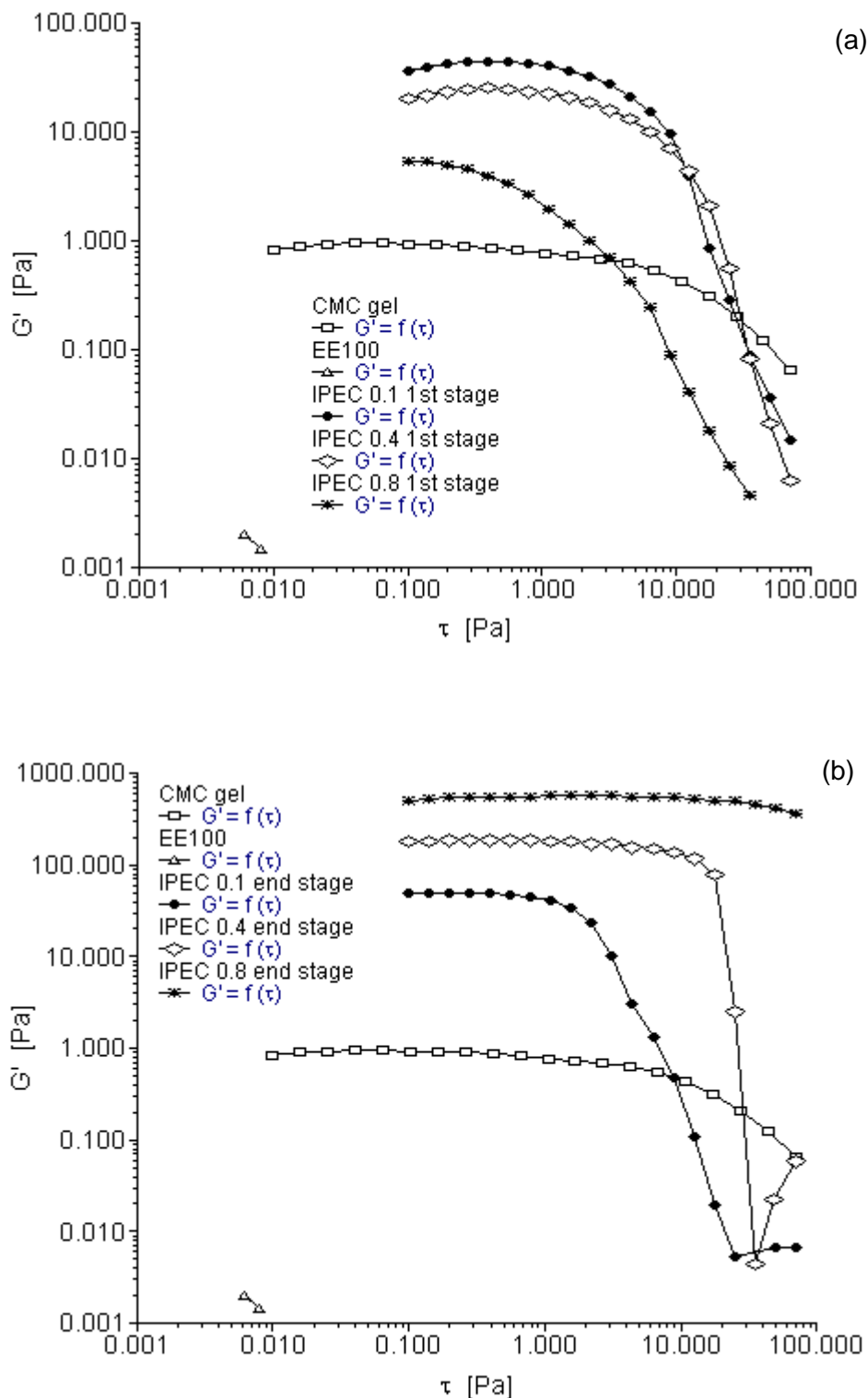


Figure 3.3.1: **a)** Elastic modulus as a function of shear stress for the native polymers and IPEC at 1st stage of synthesis at frequency of 0.1Hz and; **b)** Elastic modulus as a function of shear stress for the native polymers and IPEC at end stage of synthesis at frequency of 0.1Hz.

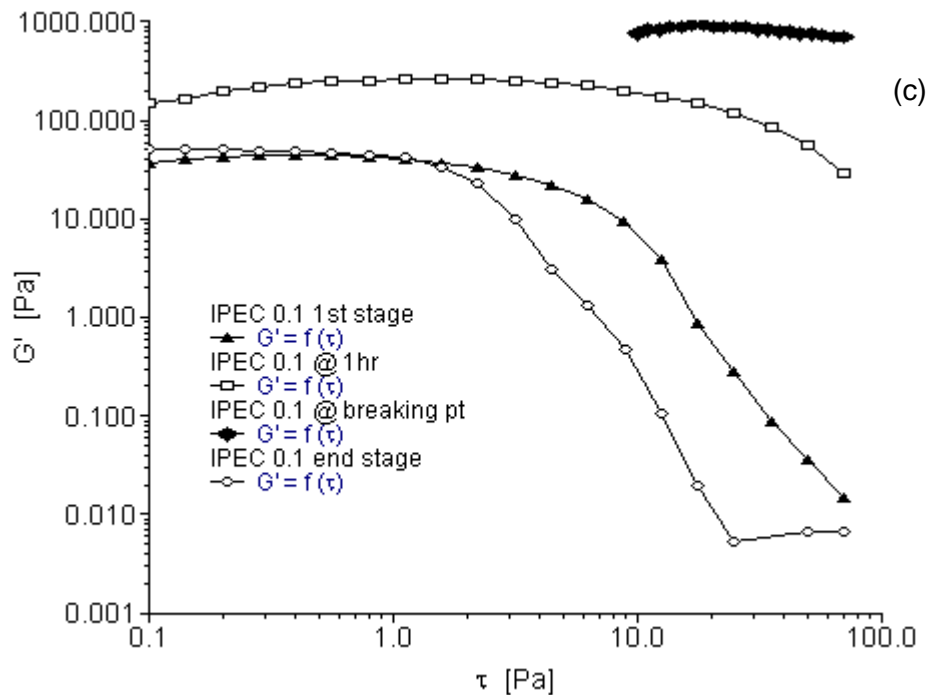


Figure 3.3.1c: Elastic modulus as a function of shear stress for IPEC 0.1N at the 4 sampling points of synthesis at frequency of 0.1Hz.

Figures 3.3.2a-c depict elastic modulus as a function of shear stress at frequency 1Hz while Figures 3.3.3a-c depict elastic modulus as a function of shear stress at frequency 10Hz. Generally, elastic modulus increased with increase in frequency. NaCMC's elastic modulus increased from 1Pa at frequency 0.1Hz to a little above 10Pa at frequency 1Hz and almost 100Pa at frequency 10Hz while the final product of IPEC 0.8N was well over 1000Pa at frequency 1 and 10Hz. The visco-elastic region was also found to be extended for IPEC as frequency increased. At the initial stage of synthesis, it seemed NaCMC was more resistant to deformation; however by one hour into synthesis, the increased strength of the internal structure of IPEC became evident indicating improved mechanical strength by crosslinking as IPEC required increased shear stress to deform and flow as a liquid. Furthermore, as normality of acetic acid employed increased, the shear stress required for deformation increased. From the visco-elastic regions the yield points were obtained and utilized in frequency sweep test for each sampling stage.

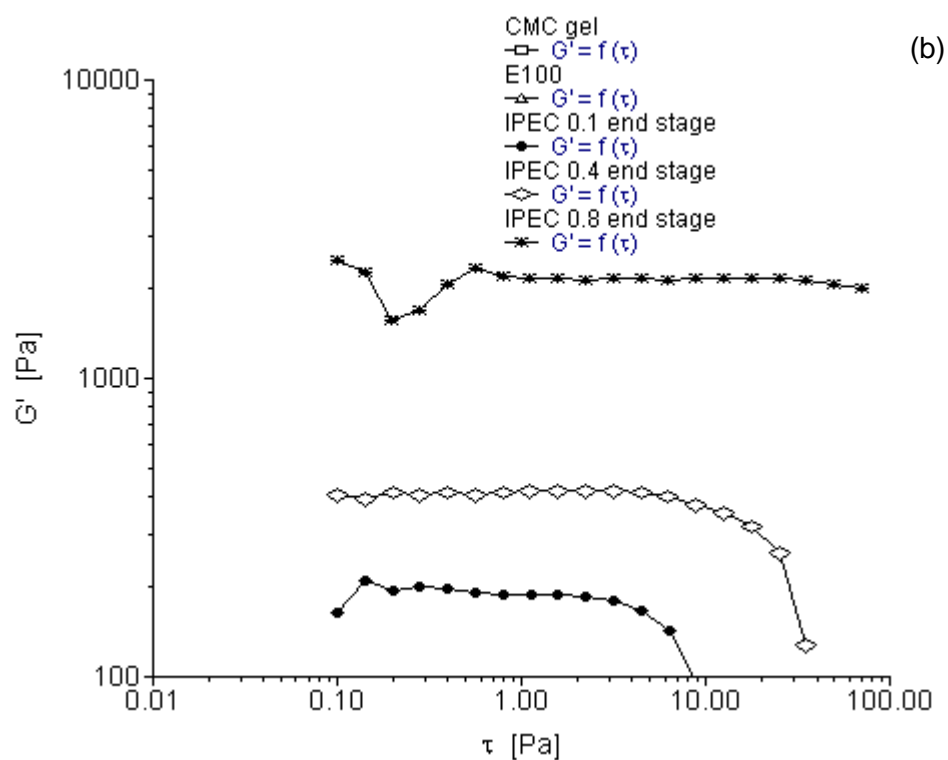
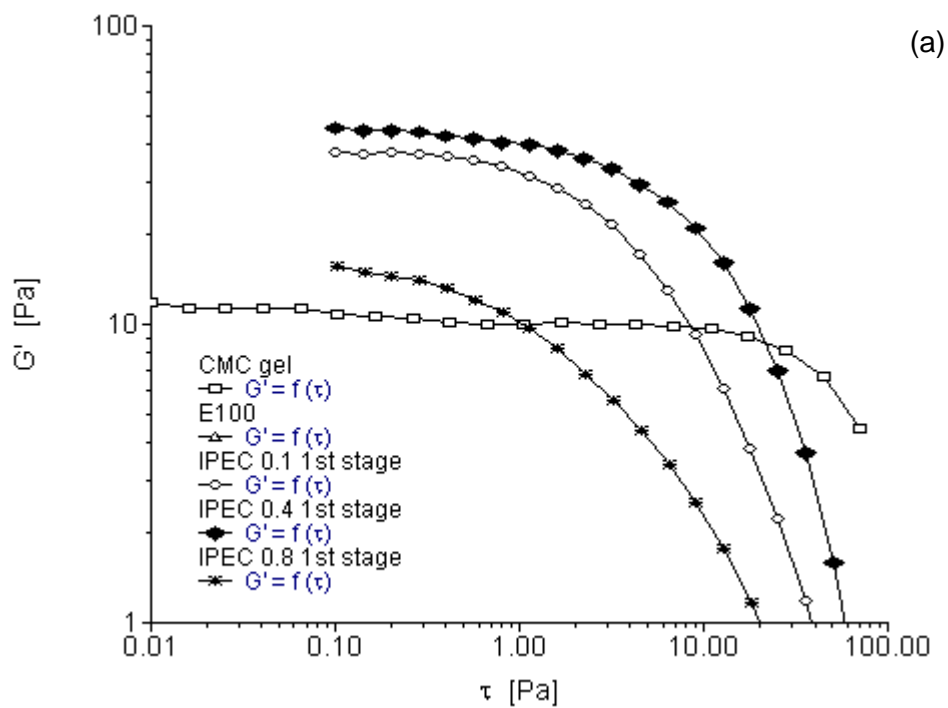


Figure 3.3.2: **a)** Elastic modulus as a function of shear stress for the native polymers and IPEC at initial stage of synthesis at frequency of 1Hz and; **b)** Elastic modulus as a function of shear stress for the native polymers and IPEC at end stage of synthesis at frequency of 1Hz.

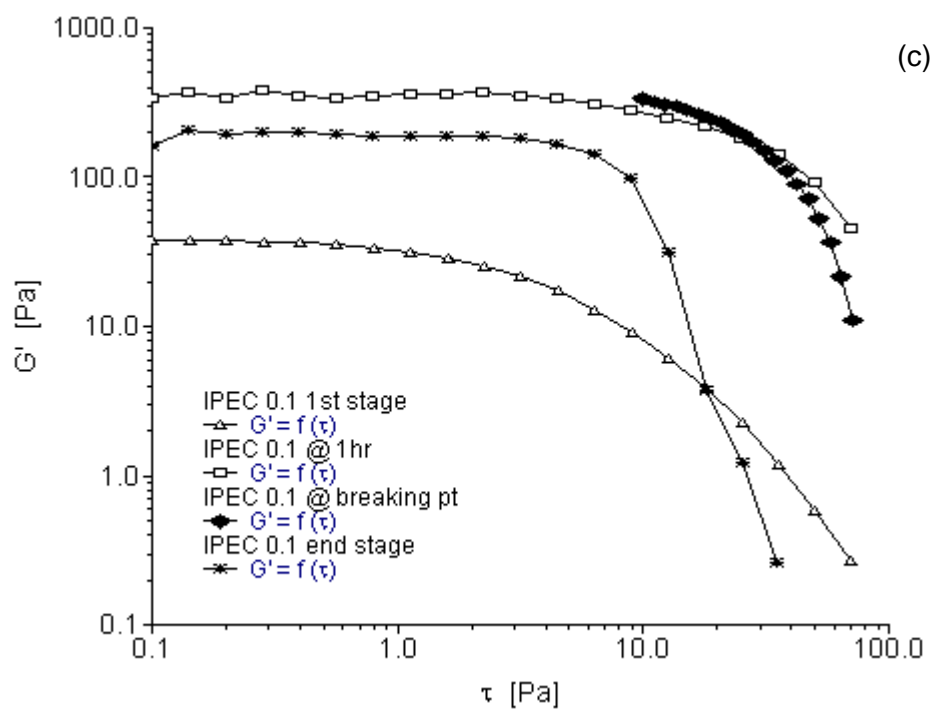


Figure 3.3.2c: Elastic modulus as a function of shear stress for IPEC 0.1N at the 4 sampling points of synthesis at frequency of 1Hz.

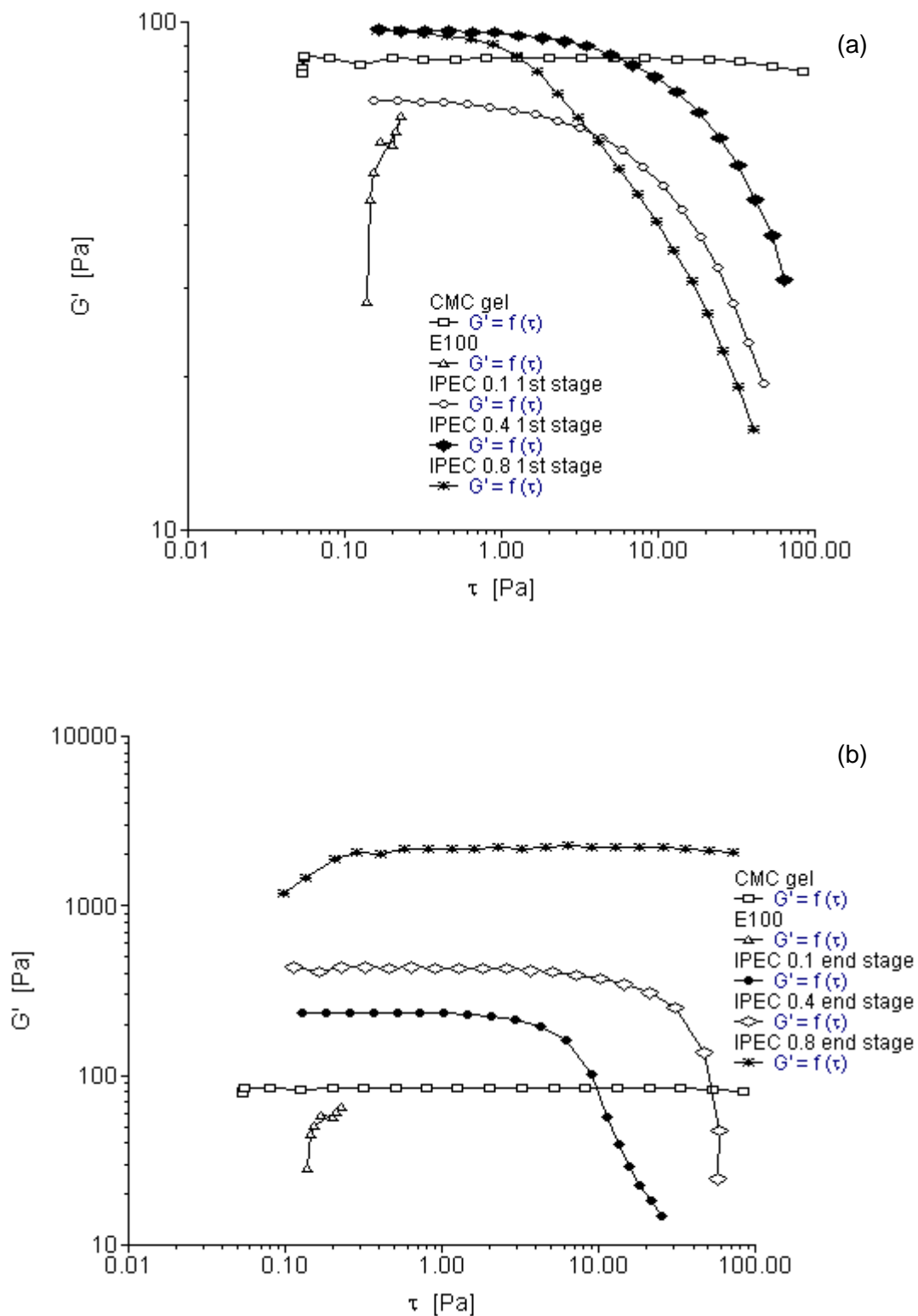


Figure 3.3.3: **a)** Elastic modulus as a function of shear stress for the native polymers and IPEC at 1st stage of synthesis at frequency of 10Hz and; **b)** Elastic modulus as a function of shear stress for the native polymers and IPEC at end stage of synthesis at frequency of 10Hz.

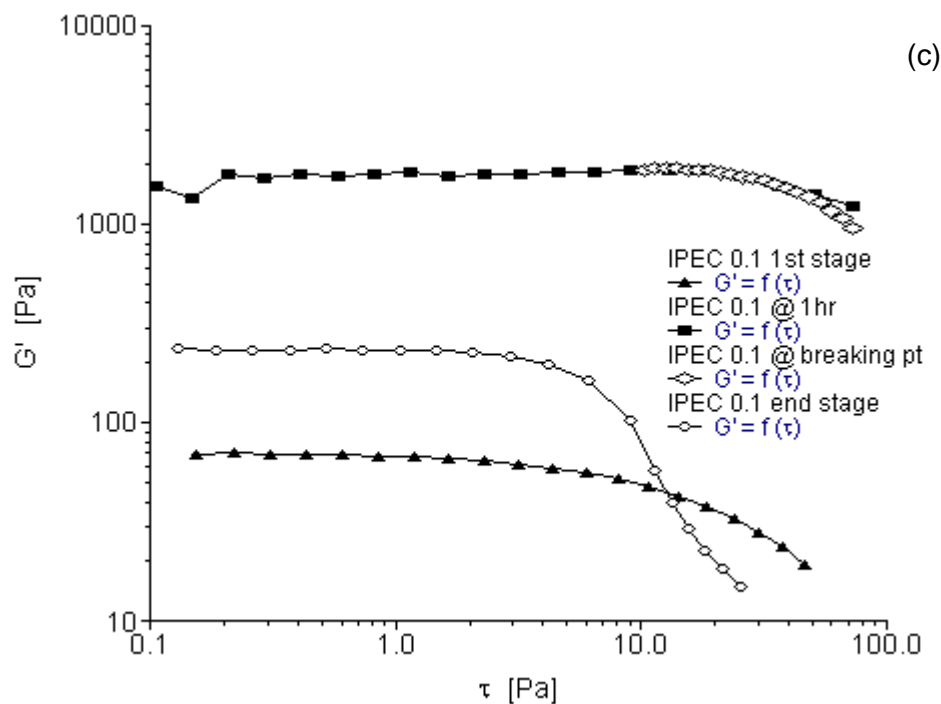


Figure 3.3.3c: Elastic modulus as a function of shear stress for IPEC 0.1N at the 4 sampling points of synthesis at frequency of 10Hz.

3.3.4. Oscillation frequency sweep

Frequency sweep is used to characterize materials in terms of their various structures. It can be used to determine if a material is a three-dimensional network, an entangled solution or a particle solution; in order words gel, paste or liquid.

The rheograms depicted in Figures 3.4a-c showed that elastic and loss moduli increased with increasing frequency (angular frequency – ω). However, for NaCMC, loss modulus was higher than elastic modulus until the frequency increased to about 500 rad/s; then a crossover took place and elastic modulus became slightly higher (Figure 3.4a-b). This is an indication that for most part of the test, NaCMC behaved as a viscous liquid.

On the contrary IPECs with the different normalities of acetic acid were elastic as the elastic moduli were higher than the loss moduli. Generally, IPEC exhibited a solid-like behavior. However, IPEC 0.1N at one hour into synthesis exhibited viscous behavior at low frequency and then there was a crossover and it became elastic as the frequency increased behaving as an entangled solution (Figure 3.4c). The final product of IPEC 0.1N behaved similarly. The elastic and loss moduli of IPEC 0.1N at breaking point rheogram merged at a lower frequency (below 10rad/s); however as the frequency began to increase towards 10 rad/s, elastic modulus was higher than loss modulus. At the beginning of the test it showed a visco-

elastic behavior and as the test continued and frequency increased it was elastic indicating and confirming its high resistance to deformation and subsequent high yield value.

The elastic and loss moduli for IPEC 0.4 and IPEC 0.8N were basically parallel; with elastic moduli higher than loss moduli which indicates that they behaved as three-dimensional network (Figure 3.4b). At lower normality of acetic acid, entangled solution was obtained while higher normality of acetic acid generated a gel – an improvement on NaCMC which behaved as a viscous liquid. Hence, IPEC has improved structural ability which suggests it may be used for formulation of matrix tablets and possibly hydrogel for controlled release.

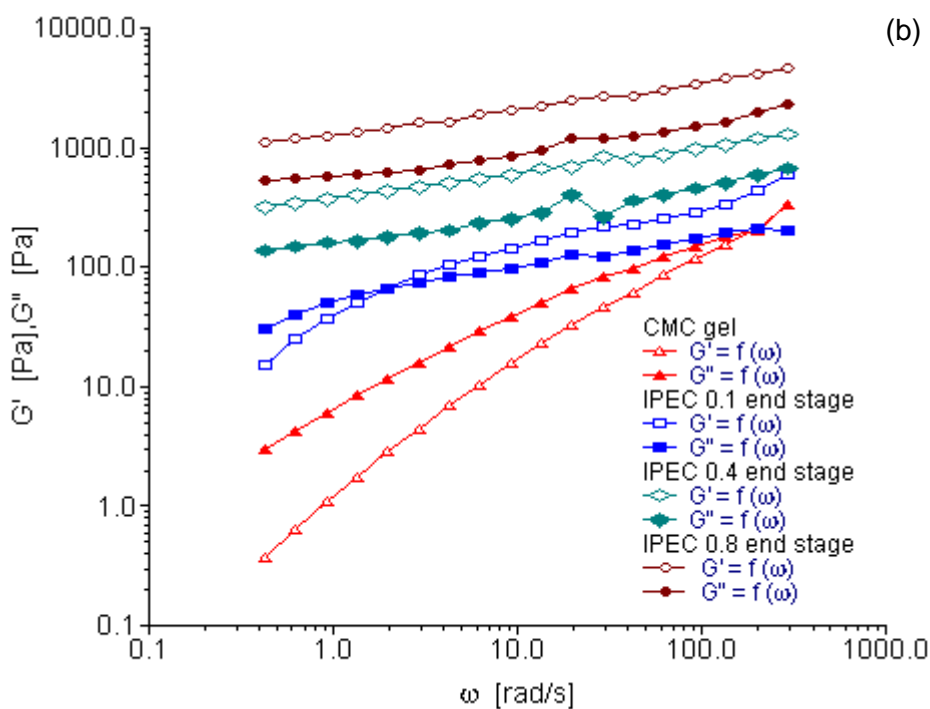
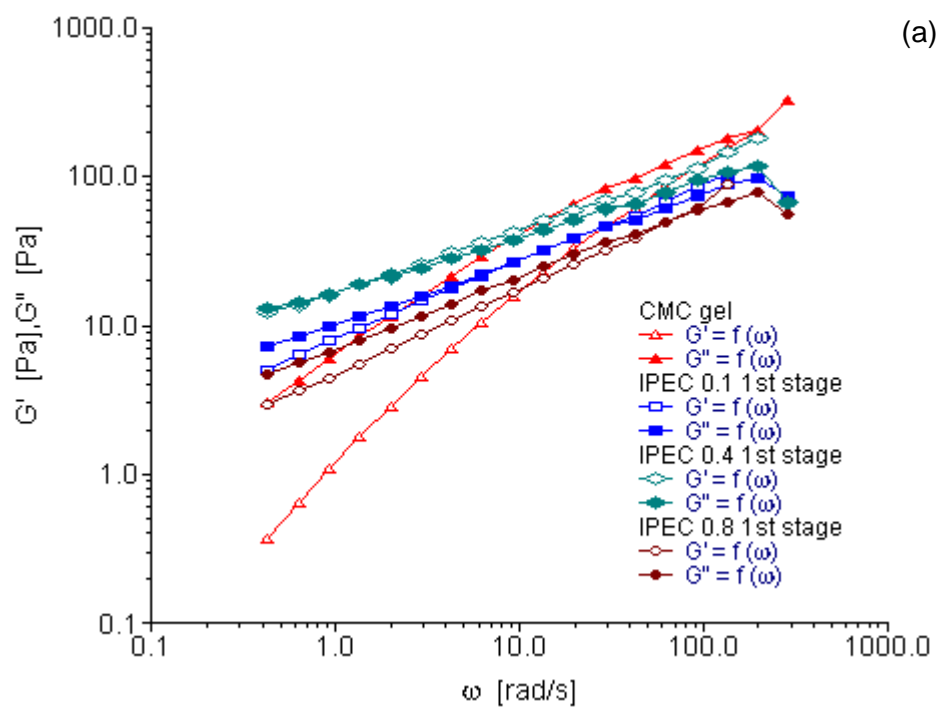


Figure 3.4: **a)** Elastic and viscous modulus as a function of angular frequency for NaCMC and IPEC at 1st stage of synthesis and; **b)** Elastic and viscous modulus as a function of angular frequency for NaCMC and IPEC at end stage of synthesis.

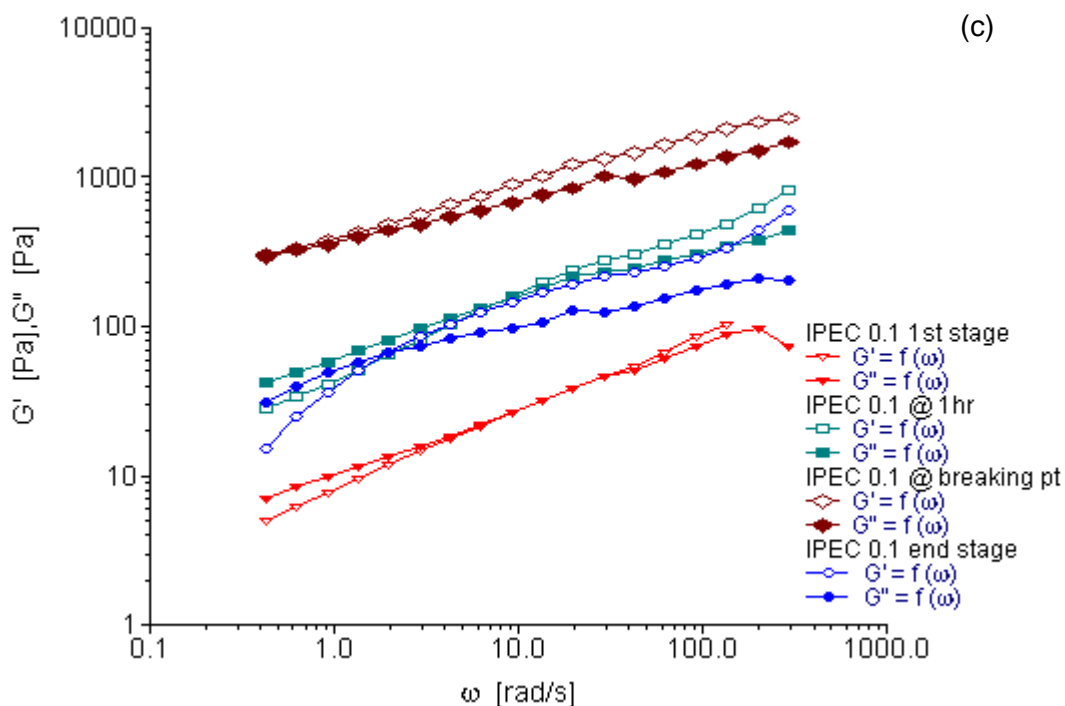


Figure 3.4c: Elastic and viscous modulus as a function of angular frequency for IPEC 0.1N at the 4 sampling points of synthesis.

3.3.5. Creep and recovery test

When stress is applied, a material is easily deformed if the material has higher compliance (J) (Bonferoni et al., 1995; Edali et al., 2001). Creep recovery test helps to assess the elasticity of a material – when stress applied is removed, the materials after deformation may recoil and attempt to restore back to its original shape. Furthermore, the level of deformation is dependent on the period of stress, the amount of stress/strain applied and temperature. High amount of creep strain during creep test will result in higher residual strain in recovery (Adalja and Otaigbe, 2002). A slow recovery indicates that the material stores residual stress (Edali et al., 2001). The rheograms show elastic deformation as well as elastic recovery within the applied stress. The rheograms are non-linear which is indicative of elastic recovery of NaCMC and IPEC as well as viscous behavior. From Figures 3.5a – b, it could be observed that within the stress applied, the native polymer, NaCMC and IPEC at the different normalities of acetic acid showed elastic deformation and when the stress was removed, they were able to recover. However, IPEC 0.1N at breaking point (Figure 3.5c) did not fully recover like the others showing the polymer was not as stable at that stage of synthesis. The rheograms of IPEC had lower compliance than NaCMC; an indication that it is not as easily deformed as NaCMC which suggests and confirms that polymer-polymer crosslinking may have enhanced its elasticity and mechanical strength. Comparison among IPECs showed that as normality of acetic acid increased, the compliance decreased; however the lower

normality (0.1N) has a more superior recovery which may suggest that the lower normality (0.1N) has slightly more ability to recoil and restore to original shape faster than the higher normalities (Figure 3.5b).

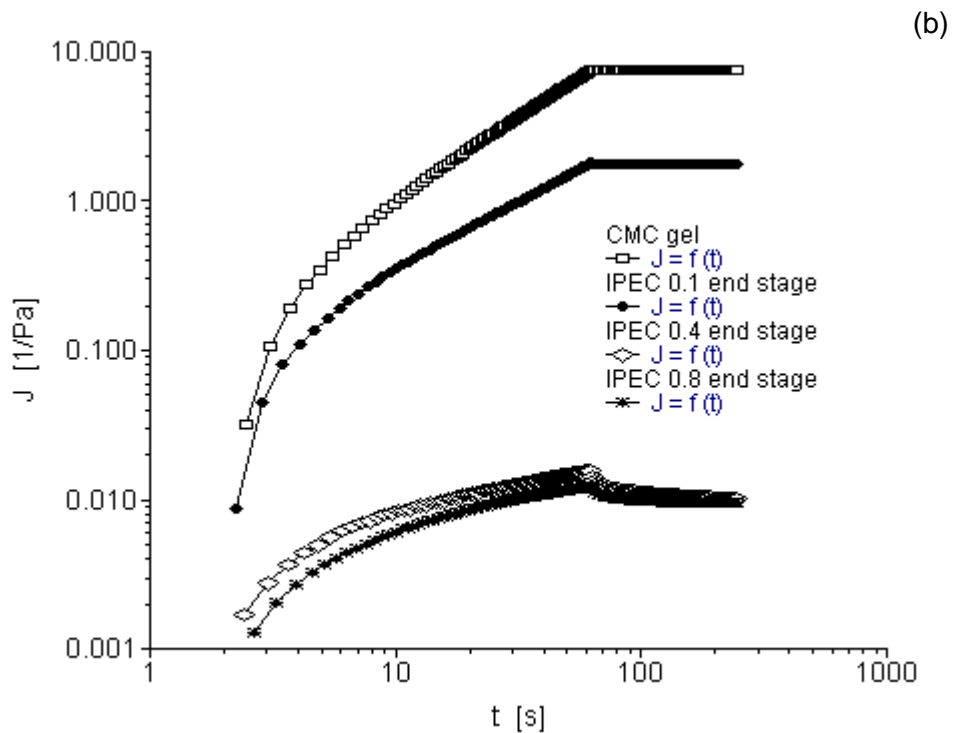
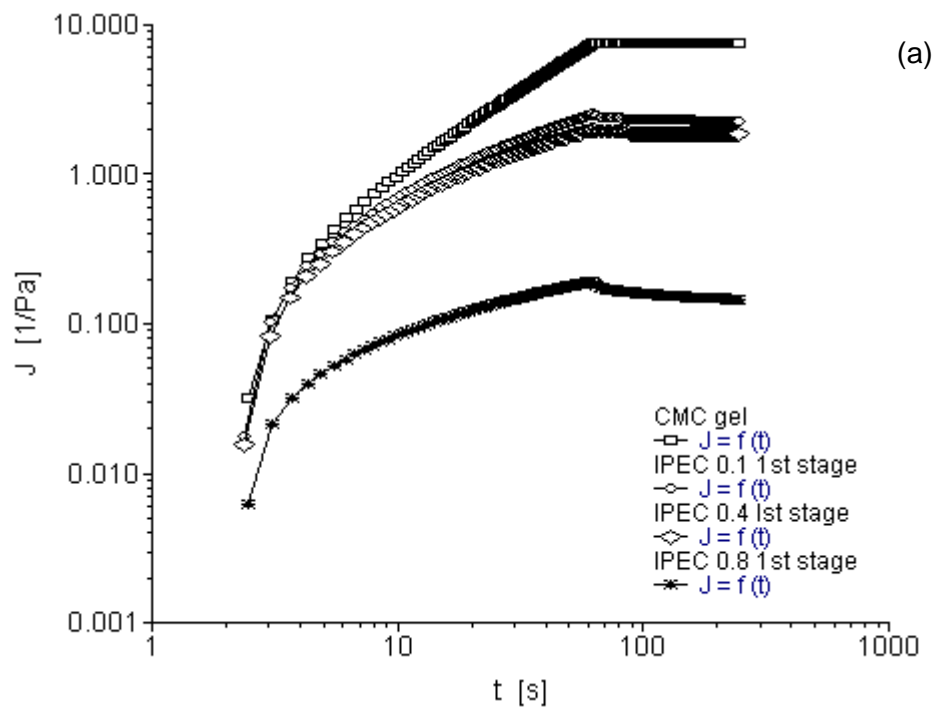


Figure 3.5: a) Creep recovery rheogram for NaCMC and IPEC at 1st stage of synthesis and; b) Creep recovery rheogram for NaCMC and IPEC at end stage of synthesis.

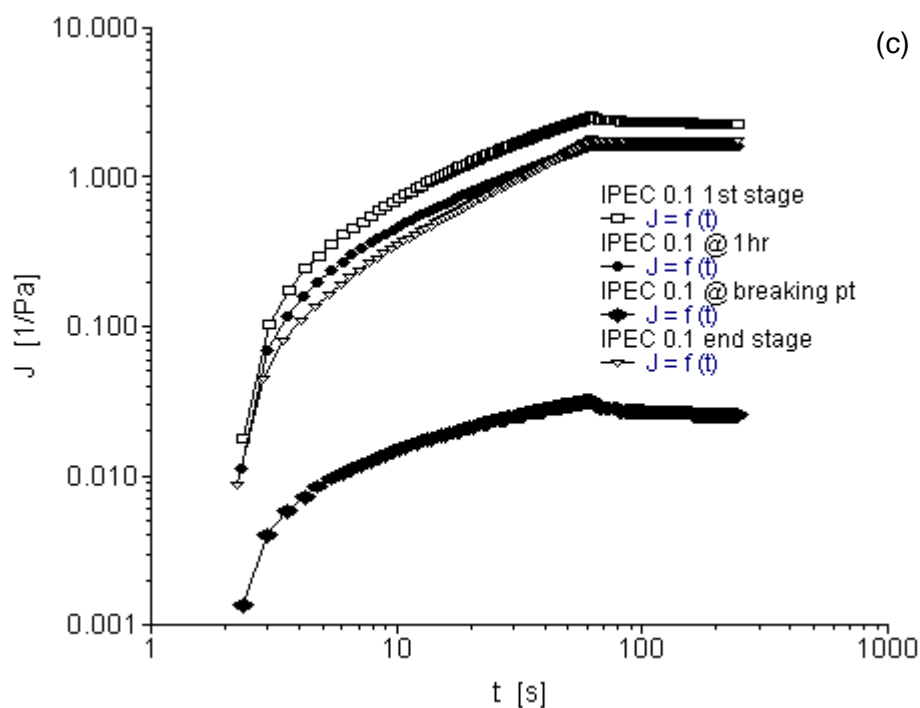


Figure 3.5c: Creep recovery rheogram for IPEC 0.1N at the 4 sampling points of synthesis.

3.3.6. Temperature ramp

Temperature ramp is used to observe the change in the properties of a polymer due to temperature. The stress or strain applied is within the visco-elastic region. Figures 3.6a-c depict rheograms of elastic modulus as a function of temperature. The elastic modulus of NaCMC decreased slightly with increase in temperature and then began to increase after 50°C. Initial increase in temperature increased slightly the fluidity of NaCMC which is confirmed by several studies (Lin and Ko, 1995; Bokias et al., 2001; Cancela et al., 2005; Yang and Zhu, 2007). Elastic moduli for IPEC 0.4N, IPEC 0.8N and IPEC 0.1N at one hour into synthesis appeared independent of temperature until about 60°C after which a slight increase of elastic modulus was observed. The elastic moduli of IPEC 0.1N at breaking point was clearly decreased by temperature. Attempt to increase temperature at breaking point may affect the intramolecular as well as intermolecular interactions causing them to separate instead of interact thereby increasing the fluidity of the polymer complex. However, the elastic modulus of the polymer complex at the end of synthesis was not affected significantly by temperature (Figure 3.6b). The slight effect of temperature on IPEC at the end of synthesis suggests it is not thermo-sensitive.

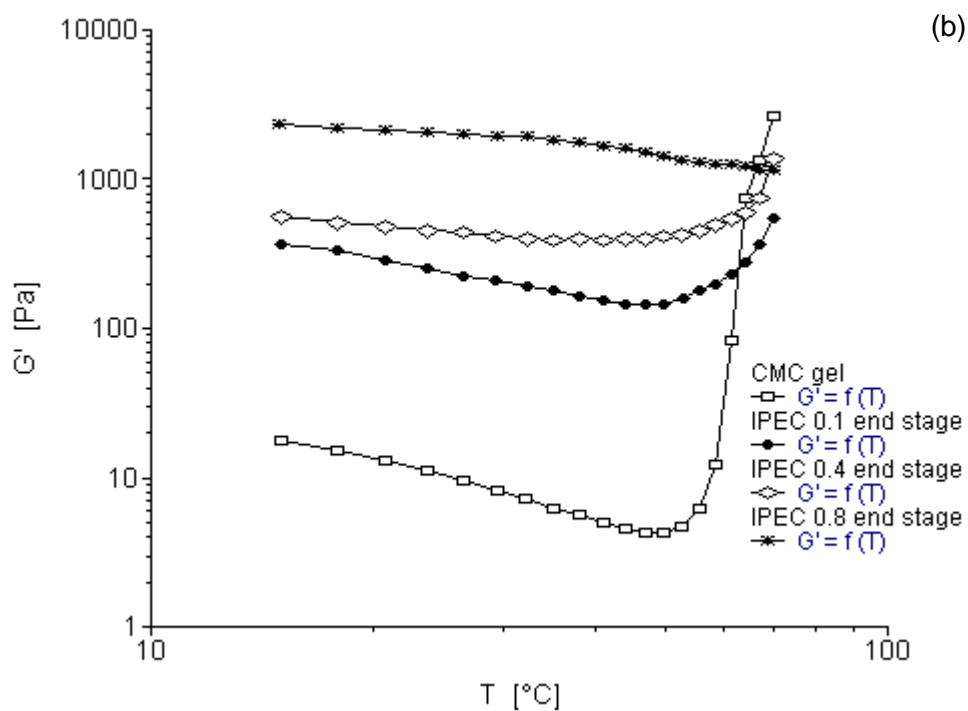
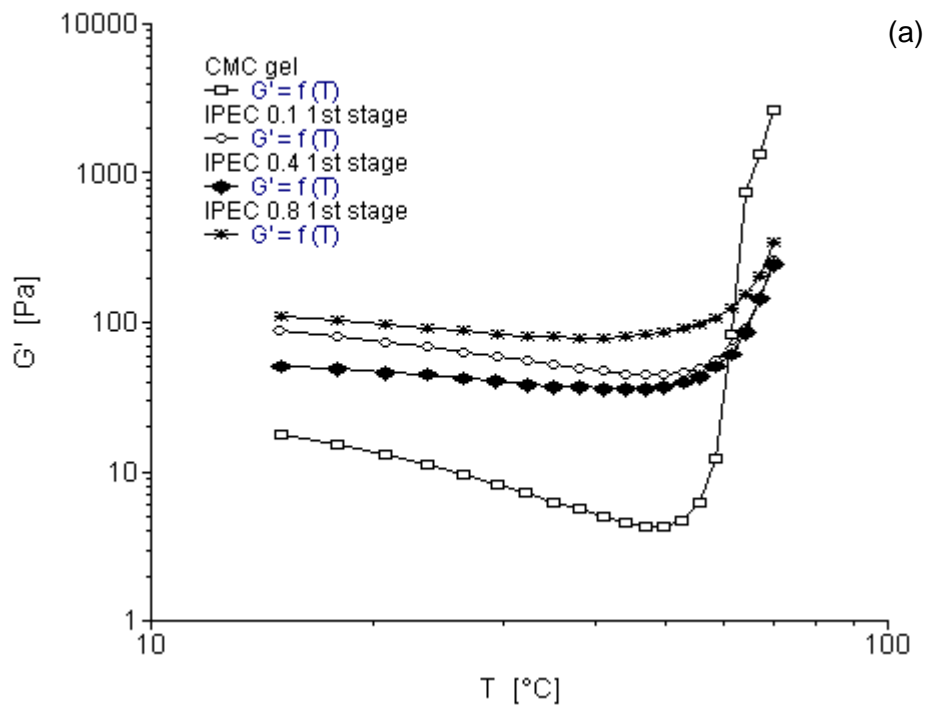


Figure 3.6: **a)** Elastic modulus as a function of temperature for NaCMC and IPEC at 1st stage of synthesis and; **b)** Elastic modulus as a function of temperature for NaCMC and IPEC at the end stage of synthesis.

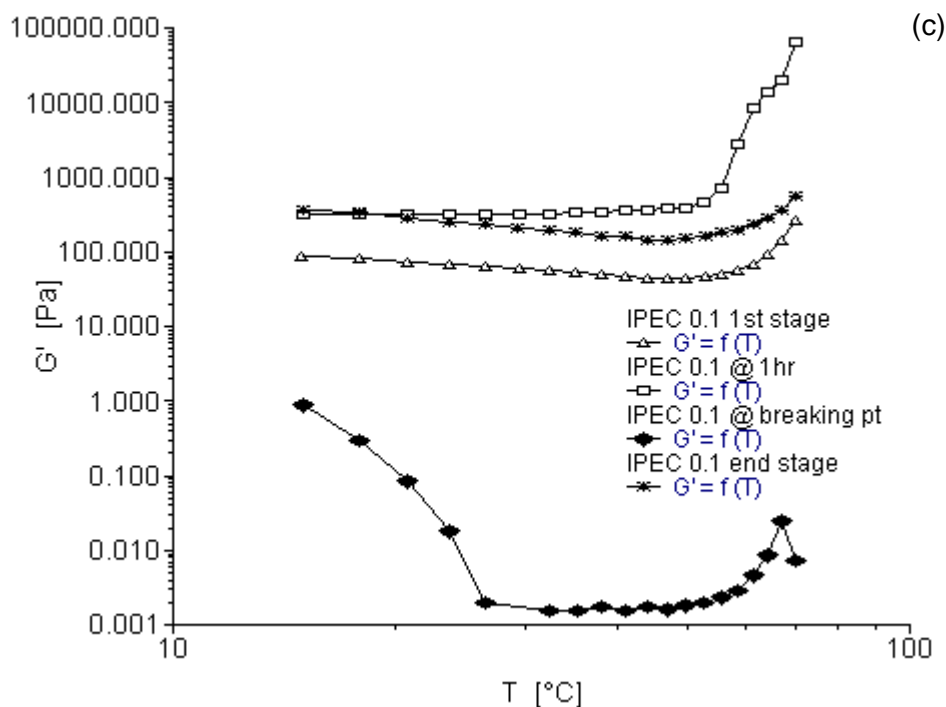


Figure 3.6c: Elastic modulus as a function of temperature for IPEC 0.1N at the 4 sampling points of synthesis.

3.3.7. Molecular mechanics assisted model building and energy refinements

A molecular mechanics conformational searching procedure was employed to acquire the data employed in the statistical mechanics analysis, and to obtain differential binding energies of a Polak–Ribiere algorithm and to potentially permit application to polymer composite assemblies. MM+ is a HyperChem™ modification and extension of Norman Allinger's Molecular Mechanics program MM2 (Warhurst et al., 2003) whereas AMBER, is a package of computer programs for applying molecular mechanics, normal mode analysis, molecular dynamics and free energy calculations to simulate the structural and energetic properties of molecules (Pearlman et al., 1995).

3.3.7.1. MMER analysis

Molecular mechanics energy relationship (MMER), a method for analytico-mathematical representation of potential energy surfaces, was used to provide information about the contributions of valence terms, non-covalent Coulombic terms, and non-covalent van der Waals interactions for solute partitioning from the bulk phase. The MMER model for potential energy factor in various molecular complexes can be written as:

$$E_{\text{molecule/complex}} = V_{\Sigma} = V_b + V_{\theta} + V_{\varphi} + V_{ij} + V_{hb} + V_{el} \dots (3.1)$$

where, V_{Σ} is related to total steric energy for an optimized structure, V_b corresponds to bond stretching contributions (reference values were assigned to all of a structure's bond lengths), V_{θ} denotes bond angle contributions (reference values were assigned to all of a structure's bond angles), V_{φ} represents torsional contribution arising from deviations from optimum dihedral angles, V_{ij} incorporates van der Waals interactions due to non-bonded inter-atomic distances, V_{hb} symbolizes hydrogen-bond energy function and V_{el} stands for electrostatic energy.

In addition, the total potential energy deviation, ΔE_{total} , was calculated as the difference between the total potential energy of the complex system and the sum of the potential energies of isolated individual molecules, as follows:

$$\Delta E_{Total(A/B)} = E_{Total(A/B)} - (E_{Total(A)} + E_{Total(B)}) \dots (3.2)$$

The molecular stability can then be estimated by comparing the total potential energies of the isolated and complexed systems. If the total potential energy of IPEC is smaller than the sum of the potential energies of isolated individual molecules (NaCMC and E100) in the same conformation, the IPEC is more stable and its formation is favoured (Yu et al., 2008). The monomer length for the polymer chain depicting molecular structures of the polymers were determined on the basis of equivalent grid surface area covered by the polymers so that the inherent stereo-electronic factors at the interaction site can be perfectly optimized. The set of low-energy conformers that were in equilibrium with each other was identified and portrayed as lowest energy conformational model.

In the present SLAS study, a set of three compounds were used to build the energy models for the polyelectrolytic systems. The synthesis and stability properties of the IPEC entities that vary in rate of formation were studied using this polymer/solvent system (IPEC/acetic acid). The global energy relationships for the various complexes derived after assisted model building and energy refinements are as follows:

$$E_{CMC} = -9.605 V_{\Sigma} = 3.024 V_b + 19.746 V_{\theta} + 32.574 V_{\varphi} + 8.459 V_{ij} - 1.759 V_{hb} - 71.649 V_{el} \dots (3.3)$$

$$E_{E100} = 100.577 V_{\Sigma} = 10.018 V_b + 45.058 V_{\theta} + 13.454 V_{\varphi} + 32.052 V_{ij} - 0.006 V_{hb} \dots (3.4)$$

$$E_{IPEC-I} = 90.972 V_{\Sigma} = 13.043 V_b + 64.804 V_{\theta} + 46.028 V_{\varphi} + 40.512 V_{ij} - 1.767 V_{hb} - 71.649 V_{el} \dots (3.5)$$

$$E_{IPEC-II} = 72.9 V_{\Sigma} = 13.13 V_b + 65.816 V_{\theta} + 46.161 V_{\varphi} + 21.409 V_{ij} - 2.509 V_{hb} - 71.108 V_{el} \dots (3.6)$$

$$E_{IPEC-III} = 69.543 V_{\Sigma} = 12.607 V_b + 66.001 V_{\theta} + 43.271 V_{\varphi} + 19.977 V_{ij} - 4.265 V_{hb} - 68.049 V_{el} \dots (3.7)$$

$$E_{IPEC-IV} = 66.219 V_{\Sigma} = 12.184 V_b + 63.708 V_{\theta} + 45.470 V_{\varphi} + 14.936 V_{ij} - 3.919 V_{hb} - 66.161 V_{el} \dots (3.8)$$

$$E_{IPEC-Sol} = -5426.791 V_{\Sigma} = 61.652 V_b + 115.959 V_{\theta} + 55.433 V_{\varphi} + 61.924 V_{ij} - 18.994 V_{hb} - 5702.76 V_{el} \dots (3.9)$$

$$E_{IPEC-AcA2} = -5501.659 V_{\Sigma} = 60.073 V_b + 119.566 V_{\theta} + 56.049 V_{\varphi} + 61.745 V_{ij} - 15.457 V_{hb} - 5791.63 V_{el} \dots (3.10)$$

$$E_{IPEC-AcA4} = -5520.468 V_{\Sigma} = 60.102 V_b + 119.615 V_{\theta} + 56.075 V_{\varphi} + 50.928 V_{ij} - 19.303 V_{hb} - 5787.89 V_{el} \dots (3.11)$$

$$E_{\text{IPEC-ACa8}} = -5539.437 V_{\Sigma} = 59.302 V_b + 118.963 V_{\theta} + 58.314 V_{\phi} + 34.261 V_{ij} - 25.67 V_{hb} - 5784.61 V_{el} \dots \quad (3.12)$$

3.3.7.2. Elucidation of step-by-step synthetic profile of IPEC

A novel technique was employed for modeling the sampling points of the synthesis of an IPEC using an Intermittent Snapshot Modeling Approach (ISMA). The snapshot was taken just after a major change in molecular conformation during energy minimization and energy values calculated by pausing the minimization process. The various energy equations generated using MMER for the step-by-step elucidation are represented by Equations 3.3-3.8 where $E_{\text{IPEC-I}}$, $E_{\text{IPEC-II}}$, $E_{\text{IPEC-III}}$, and $E_{\text{IPEC-IV}}$ correspond approximately to first (30secs after methacrylate copolymer solution was added into NaCMC solution), second (one hour later), third (at breaking point), and fourth (end of synthesis) stages, respectively.

Table 3.2: Computational differential energy attributes calculated for the simulated IPEC system in a molecular mechanics' force field setup performed using HyperChem™ 8.0.8 (Hypercube Inc., Gainesville, FL).

Name	$\Delta E_{\text{Total}}^1$	ΔE_{Bond}	ΔE_{Angle}	$\Delta E_{\text{Dihedral}}$	ΔE_{Vdw}	$\Delta E_{\text{H-bond}}$	ΔE_{Elec}
$E_{\text{IPEC-II}}$	-18.072	0.087	1.012	0.133	-19.103	-0.742	0.541
$E_{\text{IPEC-III}}$	-21.429	-0.436	1.197	-2.757	-20.535	-2.498	3.600
$E_{\text{IPEC-IV}}$	-24.753	-0.859	-1.096	-0.558	-25.576	-2.152	5.488

¹ ΔE calculated with in comparison to the energy values of first stage.

As evident from the energy equation (3.3-3.8) and Table 3.2, all the stages were accompanied by a significant decrease in total steric energy as compared to the respective previous stage with $E_{\text{IPEC-IV}}$ having the least energy. No particular trend was observed during the formation of different stages as the component energy minimizations varied around the spatial arrangements of the reacting functional groups. The bond energy and van der Waals forces underwent minimization as the reaction progressed. Alternatively, electrostatic interactions displayed upward energetic trajectory.

The difference in the visco-elastic behaviour at all the stages can be predicted from a close look at the geometrical conformations generated after Molecular Mechanics simulations. It is proposed that change in viscosity may be due to breaking and forming of intramolecular (NaCMC) and intermolecular (NaCMC-E100) bonds and interactions as shown in Figure 3.7 and as discussed below:

1. At initial stage (where the E100 was added to NaCMC) numerous intramolecular bonds in NaCMC were observed with no intermolecular bonding between E100-NaCMC (Figure 3.7a). This is confirmed by the initial formation of a gel phase by NaCMC in the reaction medium observed at the onset of synthesis.

2. At 1hr into synthesis, it was observed that NaCMC intramolecular bonds reduced in number and bond-length also decreased along with formation of an intermolecular bond with E100 depicting the first evidence of formation of an IPEC. This is corroborated experimentally by the increase in elastic modulus at one hour into synthesis (Figures 3.3.1c, 3.3.2c and 3.3.3c). The formation of intermolecular bonding enable crosslinking between E100 and NaCMC leading to increased elastic modulus.

3. At breaking point; again the intramolecular bond of NaCMC started rebuilding with a slight increase in the length of the intermolecular bonds. This supports observations during synthesis and rheological studies. A thickening of the reaction medium, increase in elastic modulus and shear stress occurred at this stage which was generated by the entanglements of NaCMC coils due to rebuilding of intramolecular bonds and then gradual increase in intermolecular bonds between E100 and NaCMC.

4. The formation of final product displayed a homogenous IPEC which was accompanied with the formation of numerous intra- and inter-molecular bonds depicting the formation of a well interconnected polymeric matrix. Additionally, the bond length also seemed to be playing a part as the average bond length decreased to $<2\text{\AA}$. The formation of numerous bonds yielded a polymeric matrix with increased resistance to flow as observed with increased yield values in comparison to the individual polymers.

3.3.7.3. Effect of normality of acetic acid on the reactional profile of IPEC

Experimentally, an increase in normality of acetic acid increased the rate of synthesis. An attempt was made to explicate the mechanisms by which this is achieved using Molecular Mechanics simulations in a solvated system.

As evident from Equations 3.9-3.12, we observed a specific trend during the simulations: higher the normality of the acid used, higher was the stability obtained (total energy decreases). This means that the reaction will go faster towards completion with an increase in normality. It was further confirmed by the fact that the rate of synthesis was accelerated as the normality of acetic acid increased and hence rheograms could not be obtained for 0.4N and 0.8N acetic acid at one hour and breaking point since the synthesis reached completion at one hour. Furthermore, interestingly, the end product remained almost the same as the bonding interaction remained almost the same as depicted by the bond, angle and dihedral energies (Figure 3.8; Equations 3.9-3.12). However, as the normality increased the electrostatic forces also increased giving rise to a trend of increased repulsion among the

constituent polymer molecules. This doesn't mean that the IPEC would break with time as it seems to remain intact because of the highly stabilized van der Waals forces and H-bonding.

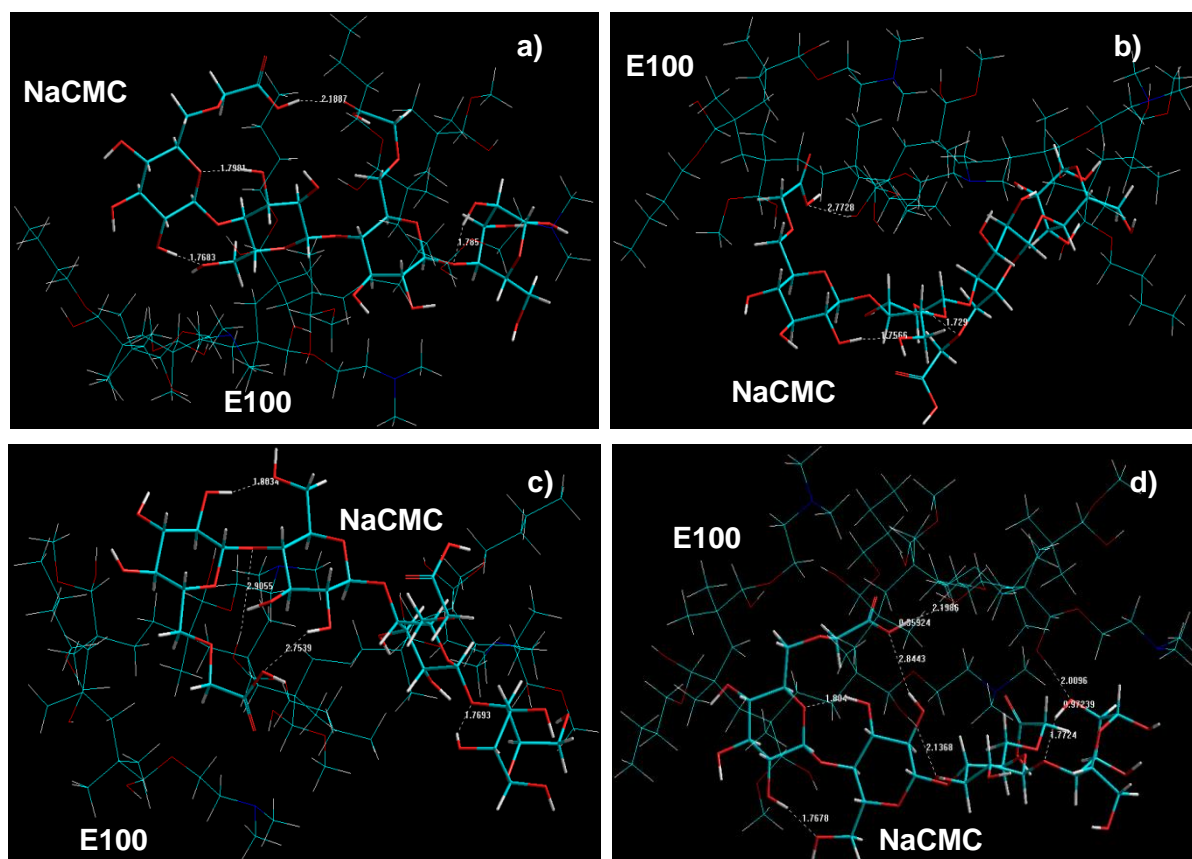


Figure 3.7: Visualization of geometrical preferences of the NaCMC-E100 (IPEC) complex **a)** First stage: initial mixing of two polymers; **b)** Second stage: after 1 hour; **c)** Third stage: breaking point and; **d)** Fourth stage: final product after Molecular Mechanics simulations. Color codes: C (cyan), O (red), N (blue) and H (white).

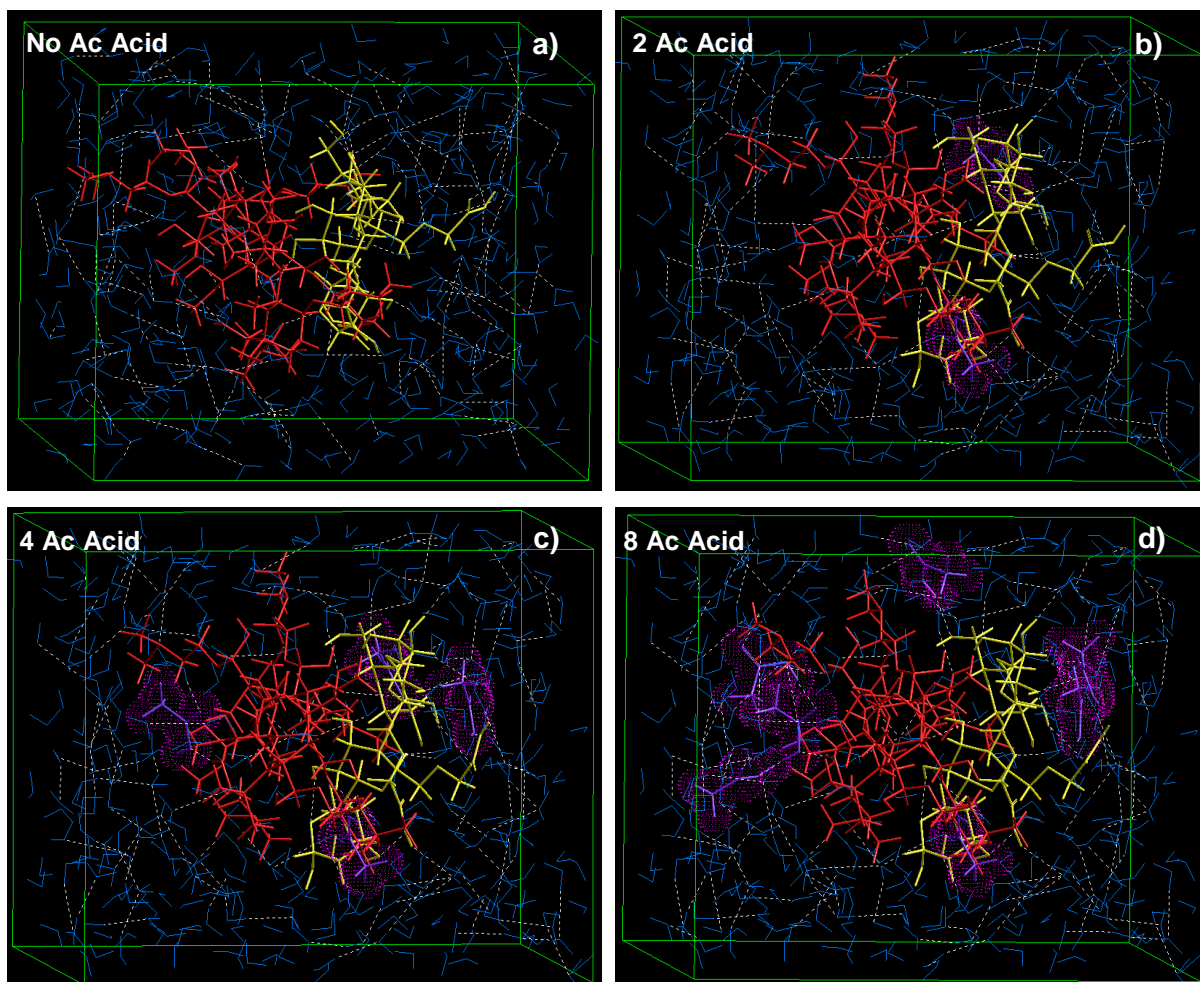


Figure 3.8: Visualization of geometrical preferences of IPEC molecule presence of **a)** No acetic acid molecules; **b)** 2 acetic acid molecules; **c)** 4 acetic acid molecules and; **d)** 8 acetic acid molecules after molecular simulation in a solvated system consisting of water molecules. Color codes for molecules: NaCMC (yellow), E100 (red), Acetic acid (purple), and water (blue).

3.4. CONCLUDING REMARKS

The rheological investigations have been employed to monitor the visco-elastic and mechanical changes that occurred during synthesis of the IPEC. The polymer-polymer crosslinking of methacrylate copolymer and NaCMC improved their rheological properties. This was proven by monitoring the different stages of synthesis which showed increased elastic modulus suggesting that the IPEC exhibited a solid-like behavior while NaCMC behaved like a viscous liquid. The tests undertaken in oscillation stress mode showed that a three-dimensional network was obtained from the complexation of a low viscous solution (methacrylate copolymer) and an entangled solution (NaCMC). The complex high yield and elastic behavior stipulates that IPEC formed will behave more like a solid with hard consistency and so may be employed in formation of matrices and possibly hydrogel for controlled release and not be used in spreadable pharmaceutical dosage forms such as

creams. The *in silico* findings perfectly corroborated with the experimental findings by elucidating the interactions between NaCMC and methacrylate copolymer (E100) at the sampling points of synthesis and how they influenced the rheological changes observed. Having elucidated that IPEC can be used for formation of matrices for controlled release; it will be employed in the next Chapter to formulate matrix tablets and characterized for possible delivery of L-dopa.

CHAPTER FOUR

PHYSICOCHEMICAL/PHYSICOMECHANICAL CHARACTERIZATION OF A NOVEL INTERPOLYELECTROLYTE COMPLEX FOR DRUG DELIVERY

4.1. INTRODUCTION

In Chapter three, rheological information of IPEC obtained provided insights on its potential as a drug carrier with enhanced mechanical strength and controlled release of drugs. Hence, considering the inference of improved mechanical strength, three-dimensional networking and gel-like behavior, this chapter aims at characterizing IPEC as a matrix tablet or hydrogel for oral drug delivery.

Polymeric materials such as hydrogels are able to retain high water content and still maintain their three-dimensional network. The hydrogel polymeric network retains the solvent in which it is immersed to form a swollen gel, which does not dissolve regardless of the solvent (Kim et al., 1992). The shortcomings of the traditional hydrogels include poor mechanical properties and slow or delayed response to stimuli (Kopeček, 2007). The fabrication of hydrogels into various delivery systems, which include discs, beads, films, slabs, micro- and nanogels has broadened the applications of hydrogels in drug delivery, tissue engineering and diagnostics (Hoare and Kohane, 2008). Hydrogels' applications include protection of drugs from hostile environments such as the presence of enzymes and low pH in the stomach; and also control of drug release by modifying the gel structure in response to environmental stimuli (Qiu and Park, 2001).

Hydrogels are crosslinked networks achieved by some crosslinking strategies which include physicochemical interactions (hydrophobic interactions, charge condensation, hydrogen bonding, stereocomplexation, or supramolecular chemistry), covalent crosslinking, small molecule crosslinking and polymer-polymer crosslinking (Qiu and Park, 2001; Hoare and Kohane, 2008). Hydrogels can be classified based on source (natural or synthetic polymers); type of network (homopolymer networks, copolymer networks, interpenetrating networks, or double networks); presence and nature of pores (homogeneous - optically transparent hydrogels, microporous and macroporous hydrogels); the nature of crosslinking (covalent or physical crosslinking); and degradability (Kopecek and Yang, 2007).

Polymer-polymer crosslinking or blending is the current trend in polymer technology whereby two or more polymers are combined to obtain new materials that have superior qualities from the native polymers. Compared to chemical synthesis, polymer blending reduces the cost in research and development of new monomers and polymers as well as cost of scale-up and commercialization. It is a well known simple and efficient way of developing new materials

with improved properties and is less time consuming (Vasile et al., 2004). The various types of polymer blends include elastomeric blends, engineering polymer blends, blends containing crystalline polymers, impact modified blends, liquid crystalline polymer blends, polyolefin blends, thermoset blends, emulsion blends, block copolymers, biodegradable blends, water soluble blends, natural polymer blends and interpolyelectrolyte complexes (Robeson, 2007).

Interpolyelectrolyte complexation produces hydrogels thereby providing alternative to the use of bio-incompatible crosslinkers for formation of hydrogels (Berger et al., 2004). Interpolyelectrolyte complexes are formed by the presence of interactions as elucidated in Chapter 3, Section 3.3.7 and are generated mainly in aqueous solvents (Pergushov et al., 2006; Lu et al., 2007; Lu et al., 2008). The complexation may be indicated by the presence of turbidity and/or precipitation which may also be followed by change in viscosity, pH, and conductivity (Nurkeeva et al., 2003). The interaction between polymers modifies the polymeric structure which generates a novel polymeric material having properties different from the native polymers (Mustafin et al., 2006). For drug delivery applications, the selection of the polyelectrolytes for complexation is based on some basic properties which include biocompatibility, swellability, stimuli responsiveness and physicochemical stability (Moustafine et al., 2006). Interpolyelectrolyte complexes (IPEC) have been employed to improve physicomachanical properties, fluid absorption, modify drug release profiles, prolonged drug delivery (Mitrevej et al., 2001; Yu et al., 2005; Foda et al., 2007; Abdelbary and Tadros, 2008), and in fabrication of nano- and microparticles (Buchhammer et al., 2003; Sajesh. and Sharma, 2006; Hameed and Guo, 2008).

Recently IPECs have been employed to develop novel materials with enhanced drug delivery properties (Tapia et al., 2004; Moustafine et al., 2008; Prado et al., 2008; Prado et al., 2009). However, despite the number of polymer blends available commercially, there is still need to improve on the existing native polymers for drug delivery and other applications.

Methacrylate copolymer (E100) is a pH-dependent cationic polymer with a dimethylaminoethyl ammonium group which is employed in taste masking since it is insoluble in saliva (pH 6.8-7.4) and soluble in gastric fluids (Shishu et al., 2007; Augsburg and Hoag, 2008). Its solubility in acids is up to pH 5.0 making it unsuitable for sustained release matrices as it does not retard the release of drugs (Ammar and Khalil, 1997; Anand et al., 2007). Other applications include film formation for transdermal and transmucosal drug delivery. Film coatings from methacrylate copolymer are soluble below pH 5.0 but swellable and permeable above pH 5.0 (Margetson et al., 2007).

Carboxymethylcellulose (NaCMC) is a carboxymethyl ether of cellulose with good water solubility, widely used due to its low cost, biodegradability and lack of toxicity. CMC evidently provides good performance in many applications; however, in hydrated form, it has poor physicochemical properties which thereby limit its applications in many other areas (Long et al., 2008). NaCMC hydrogel for instance, on swelling does not retain its three dimensional network. To its advantage though, NaCMC is an anionic polyelectrolyte and interacts to form complexes (Zhang and Huang, 2000; Esposito et al., 2005; Zhao et al., 2009a) which can be utilized to form new materials with improved properties such as matrix rigidity.

This phase of the study was undertaken to synthesize and characterize novel IPEC hydrogel to retard methacrylate copolymer's rapid drug release profile as well as exchange NaCMC's poor mechanical strength for superior physicochemical properties; and consequently achieve sustained and prolonged drug delivery.

4.2. EXPERIMENTAL SECTION

4.2.1. Materials

Methacrylate copolymer (Eudragit E100, Evonik Röhm GmbH & Co. KG, Darmstadt, Germany), sodium carboxymethylcellulose (NaCMC, Fluka Biochemika, Medium viscosity, Sigma-Aldrich Chemie GmbH, Buchs, Switzerland), 3-(3,4-dihydroxyphenyl)-L-alanine (L-dopa, Sigma-Aldrich, Steinheim, Germany), acetic acid glacial, hydrochloric acid (Rochelle Chemicals, Johannesburg, South Africa), potassium phosphate monobasic (KH_2PO_4) (Sigma-Aldrich, Steinheim, Germany), potassium chloride (KCl) (Saarchem, Krugersdorp, South Africa) and ortho-phosphoric acid (BDH Chemicals, Poole, England).

4.2.2. Synthesis of the interpolyelectrolyte complex

The methacrylate copolymer was milled; and 1.4g was dissolved in 50mL of 0.1, 0.2, 0.4, 0.6, 0.8 and 1.0N of acetic acid while solutions of 2.8g NaCMC were prepared by dissolving in 50mL deionized water. A transparent methacrylate copolymer solution was added into a transparent NaCMC solution and stirred under vigorous agitation for 1-3 hours depending on the normality of acetic acid employed. The IPEC was lyophilized for 48 hours and milled for utilization in formulation of direct compressible tablet matrices.

4.2.3. Microscopical analysis of interpolyelectrolyte complex

The surface morphology of the novel IPEC was examined microscopically. The digital microscopical images of the novel IPEC after synthesis were obtained using Olympus digital microscope - Olympus SZX-ILLD2-200 (Olympus Corporation, Tokyo, Japan).

4.2.4. Structural elucidation of interpolyelectrolyte complex

FTIR spectra were obtained for the native polymers and the novel IPEC using a PerkinElmer spectrometer (PerkinElmer Spectrum 100, Beaconsfield, United Kingdom) over a range of 4000-650 cm^{-1} to elucidate the structural modification of IPEC from the native polymers.

4.2.5. Evaluation of the polymeric thermal behavior of interpolyelectrolyte complex

To evaluate the thermal properties of IPEC in comparison with the native polymers, differential scanning calorimetry (DSC 1 STAR[®] system, Mettler Toledo, Schwerzenbach, Switzerland) was undertaken. The native polymers – methacrylate copolymer and NaCMC and IPEC in hermetically sealed aluminum pans with lids possessing pinholes were subjected to a heating gradient ranging from -10-270 $^{\circ}\text{C}$ at a rate of 5 $^{\circ}\text{C}$ per minute under a nitrogen atmosphere. While temperature alternating differential scanning calorimetry (ADSC) was undertaken at a heating gradient ranging from -10-130 $^{\circ}\text{C}$ and 130-250 $^{\circ}\text{C}$ with a heating rate of 1 $^{\circ}\text{C}$ and amplitude of 0.3 $^{\circ}\text{C}$ at a period of 0.8min and the raw curve deconvoluted into the different components with reducing factor 50. The samples of IPEC analyzed were based on the normalities of acetic acid in the range of 0.1-1.0N while mass of the samples were in the range of 10.3-10.8 mg for DSC and 5.0-5.5 mg for ADSC.

4.2.6. Direct compression of interpolyelectrolyte complex into matrices

A weighed quantity (100mg per matrix) of the model drug, 3-(3,4-dihydroxyphenyl)-L-alanine (L-dopa) was incorporated into a weighed quantity (500mg) of the IPEC powder and directly compressed using Carver Press (Model 3851-0, Carver Industries Inc., Wabash, IN, USA) with evacuable pellet die (Specac Ltd, Orpington, Kent, England) of 13mm at 3tonnes. Same quantity of drug was also incorporated into the native polymers separately. The matrices were utilized for physicomechanical analysis, swellability test and *in vitro* drug release studies.

4.2.7. Evaluation of the physicomechanical strength of the matrices

The physicomechanical strength of the matrices was determined by Force-Distance profiles using Texture Analyzer (TA.XT^{plus}, Stable Microsystems, Surrey, UK). The matrix hardness and deformation energy were performed with a 2mm flat-tipped steel probe while matrix resilience was carried out with a 36mm cylindrical probe fitted to the texture analyzer. The data was captured with Texture Exponent Software (Version 3.2). The parameter settings employed are as shown in Table 4.1. The physicomechanical strength of IPEC was compared with the native polymers.

Table 4.1: The parameter settings for the textural analysis of the matrices.

Parameters	Settings
Pre test speed	1 mm/sec
Test speed	0.5 mm/sec
Post test speed	1 mm/sec
Compression force ¹	40 N
Trigger type	Auto
Trigger force	0.5 N
Compression strain ²	25%

¹employed for matrix hardness and deformation energy; ²employed for matrix resilience

4.2.8. Degree of swelling of the directly compressed matrices

The swelling of the NaCMC and IPEC matrices was undertaken in 0.1N HCl. The matrices were placed in pre-weighed mesh baskets and weighed with the mesh baskets. The mesh baskets were submerged in 100mL of the medium (0.1N HCl) and placed in a shaker bath (Orbital Shaker incubator, LM-530, Laboratory & Scientific Equipment Co, Gauteng, South Africa) at 37°C. The mesh baskets were weighed at intervals of 1, 2, 3, 4, 5, 6, 8, 10, 12, and 24 hours for comparative study of IPEC and NaCMC and 0.5, 1, 2, 3, 4, 5, 6, 7, 8, 10, 12, 14, 16, 18, 20, 22, and 24 hours for IPEC using different normalities of acetic acid. The use of mesh baskets ensured the matrices were not handled during the test; as the mesh baskets were blotted dry and weighed at the stated time intervals. Increase in weight was determined gravimetrically and was carried out in triplicate. The degree of swelling was determined using Equation 4.1:

$$\text{Degree of swelling} = \frac{W_t - W_o}{W_o} \times 100$$

Equation 4.1

Where W_t is the weight of the matrix at time t , and W_o is the weight of matrix at time zero.

4.2.9. *In vitro* drug release studies

Drug release was assessed using USP apparatus II dissolution system (Erweka DT 700, Erweka GmbH, Heusenstamm, Germany). Temperature and stirring rate were at $37 \pm 0.5^\circ\text{C}$ and 50rpm respectively while the dissolution media were pH 1.5 and 4.5. Samples were withdrawn at intervals of 0.5, 1, 2, 3, 4, 5, 6, 8, 10, 12, and 24 hours for comparative study of IPEC, methacrylate copolymer and NaCMC and 0.5, 1, 2, 3, 4, 5, 6, 7, 8, 10, 12, 14, 16, 18, 20, 22, and 24 hours for IPEC using different normalities of acetic acid. The withdrawn samples were replaced with the same volume of fresh medium to maintain sink conditions,

and the quantity of L-dopa released was quantified using UV spectrophotometer (LAMBDA 25 UV/Vis spectrophotometer, PerkinElmer, Massachusetts, USA) at 280nm. The *in vitro* studies were undertaken in triplicate. The drug release profiles from the IPEC matrices were compared with those from the native polymers as well as with matrices based on IPEC synthesis in different normalities (0.1 – 1.0N) of acetic acid. Furthermore, the degree of variability of the drug release profiles was analyzed by statistical standard deviation as will be observed on the profiles.

4.3. RESULTS AND DISCUSSION

Elucidation of the synthesis of IPEC has been undertaken in Chapter 3, Section 3.3.7.

4.3.1. Microscopical analysis of interpolyelectrolyte complex

The digital microscopy (magnification - x32) of the interpolymeric blend ratio 0.5:1 of methacrylate copolymer and NaCMC respectively are as shown in Figure 4.1. Two transparent fluids (methacrylate copolymer and NaCMC) on interaction with each other generated a white composition which had a surface morphology different from the native polymers. At the stoichiometric ratio of 0.5:1 of Eudragit E 100 and NaCMC, the shreds appeared homogeneously white and irregularly shaped as shown from Figures 4.1a - f.

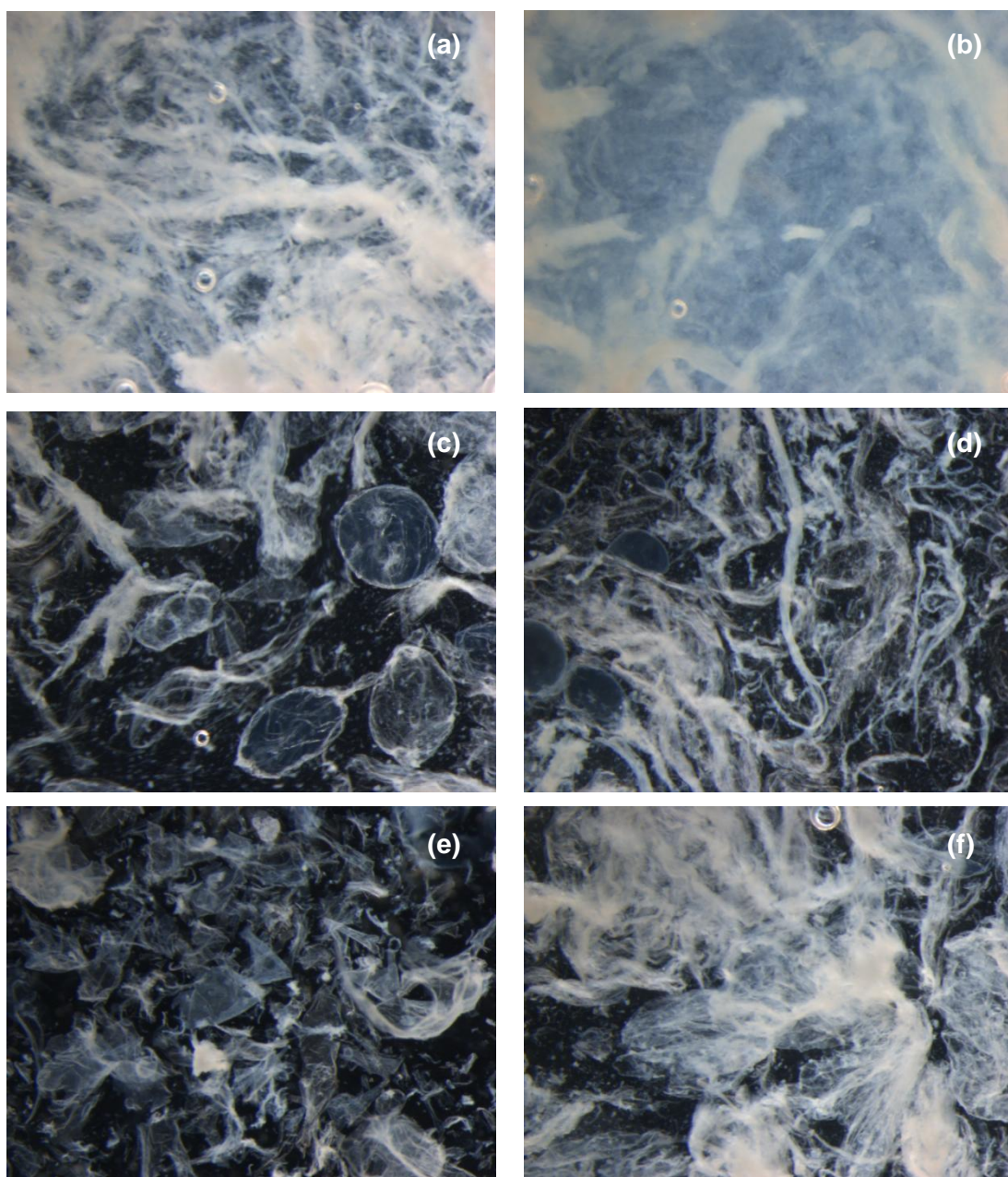


Figure 4.1: Digital microscopic images of interpolyelectrolyte complex: **a)** IPEC at the ratio of 0.5:1; **b)** Viscous portion of IPEC; **c)** Diluted dispersion of IPEC; **d)** IPEC in 0.8N acetic acid; **e)** The shredded nature of the IPEC and; **f)** IPEC in 0.4N acetic acid.

4.3.2. Structural elucidation of interpolyelectrolyte complex

It could be observed from Figure 4.2a that the spectrum of the IPEC differed from those of methacrylate copolymer and NaCMC. The FTIR spectra were obtained for IPEC directly after synthesis and after lyophilization (Figure 4.2b). The spectrum of IPEC after synthesis indicated the presence of aliphatic alcohol at ranges such as $3500-3100\text{cm}^{-1}$, $2850-2000\text{cm}^{-1}$, $1210-900\text{cm}^{-1}$ and $1510-1405\text{cm}^{-1}$ which may have been obtained by the reduction of aliphatic aldehyde in methacrylate copolymer at the ranges such as $4000-3125\text{cm}^{-1}$, $3000-$

2835 cm^{-1} , 2775-2690 cm^{-1} and 1745-1720 cm^{-1} . However, the aliphatic alcohols in IPEC after synthesis may have sublimated during lyophilization. There was no difference in the spectra obtained as the normality of acetic acid increased (Figure 4.2c) as the difference between the IPECs is the concentration of acetic acid. The comparison of the physical mixture (methacrylate copolymer and NaCMC) and IPEC showed that the physical mixture had the carbonyl group characteristic of methacrylate copolymer at 2768.75 cm^{-1} while IPEC did not; indicative the carbonyl group could have been involved in the interaction (Figure 4.2d). Furthermore, IPEC had a peak at 1052.25 cm^{-1} which was not distinct in the spectrum of the physical mixture. In addition, the peaks that are similar in the spectra did not absorb at the same frequencies.

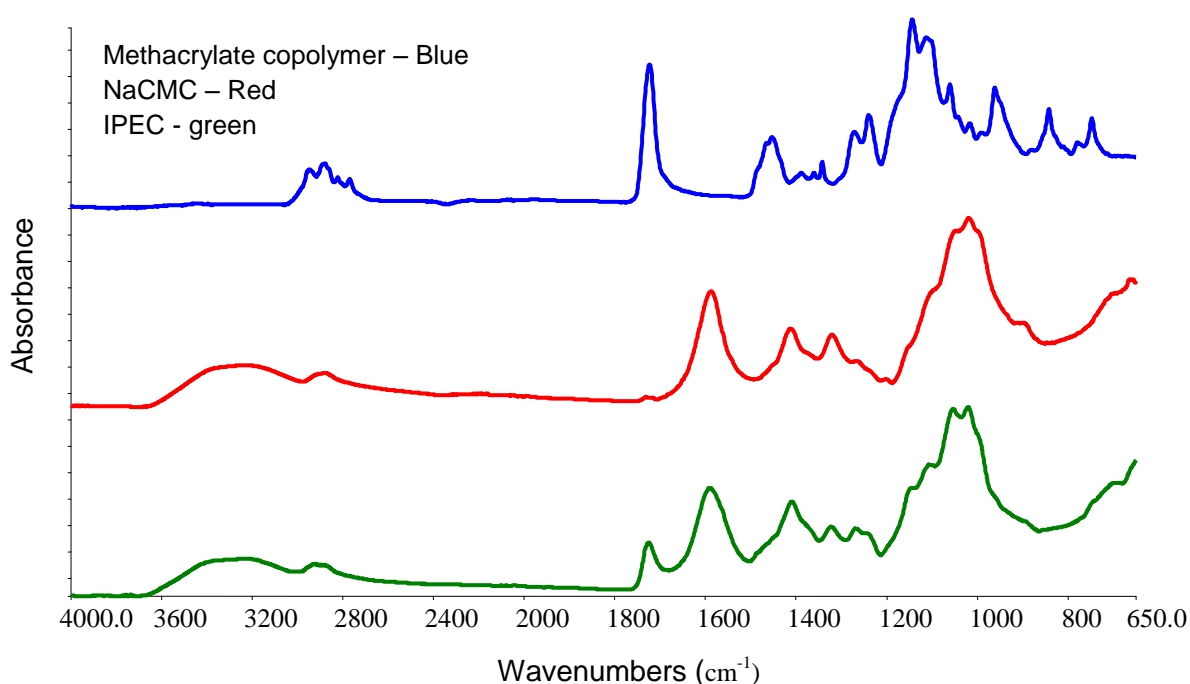


Figure 4.2a: FTIR spectra of native polymers - methacrylate copolymer and NaCMC as well as IPEC.

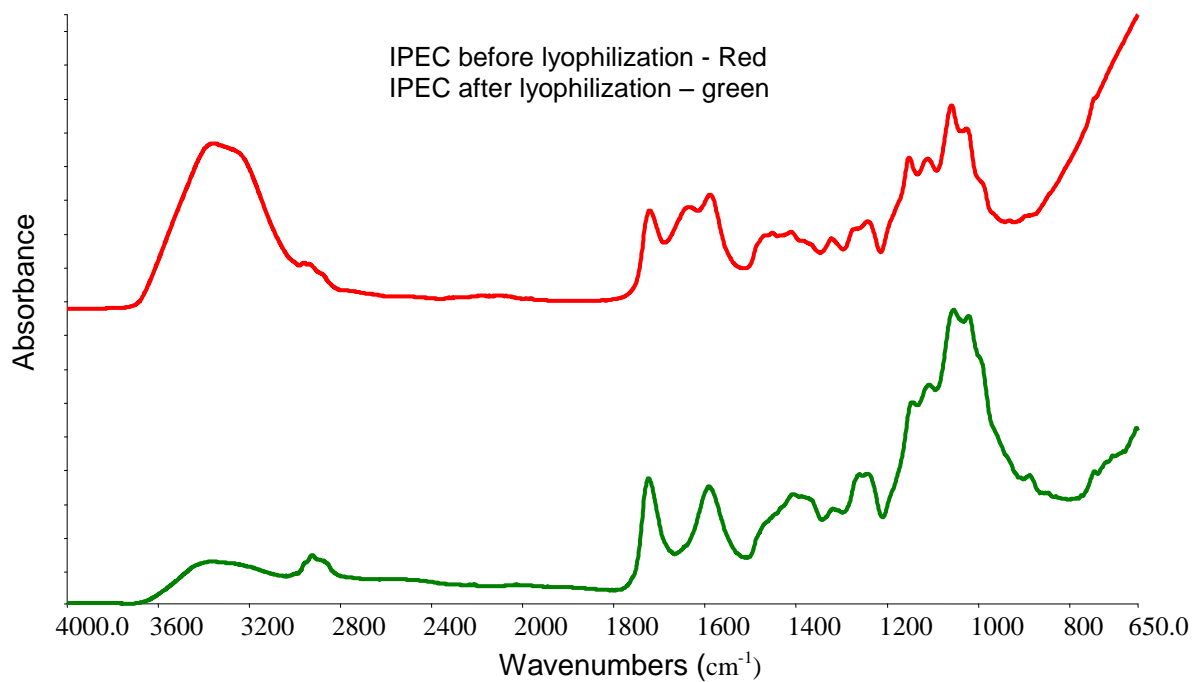


Figure 4.2b: FTIR spectra of IPEC before and after lyophilization.

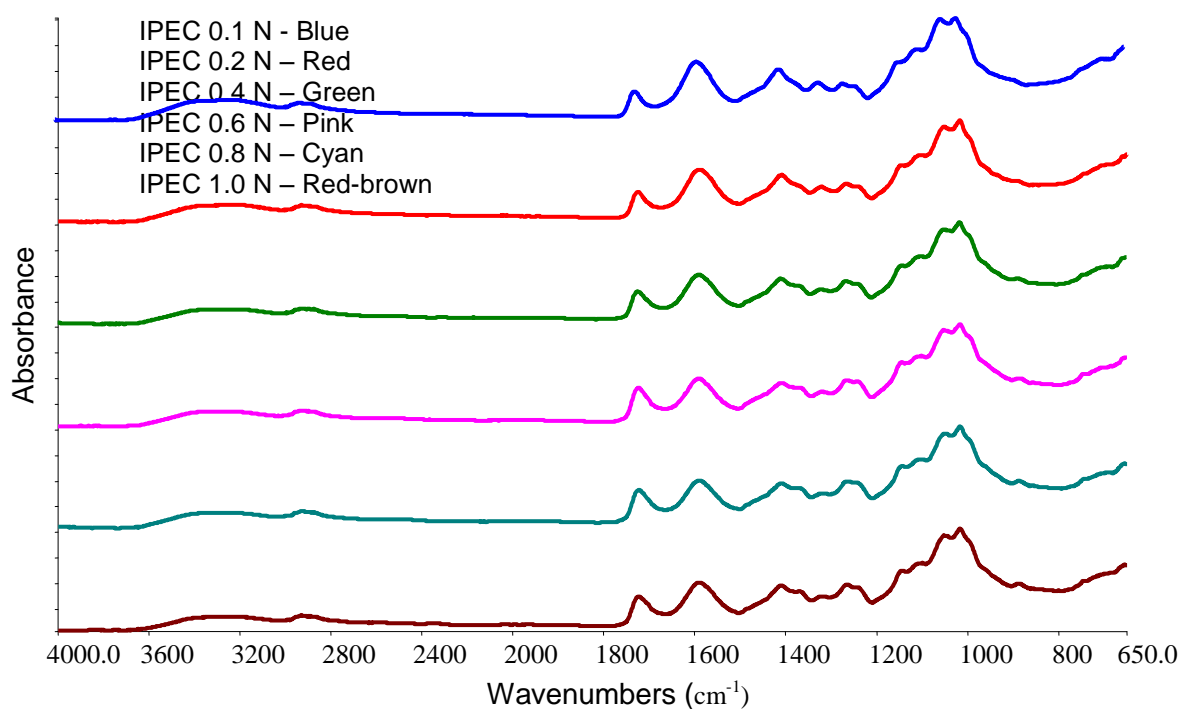


Figure 4.2c: Spectra of IPEC synthesized with different normalities of acetic acid.

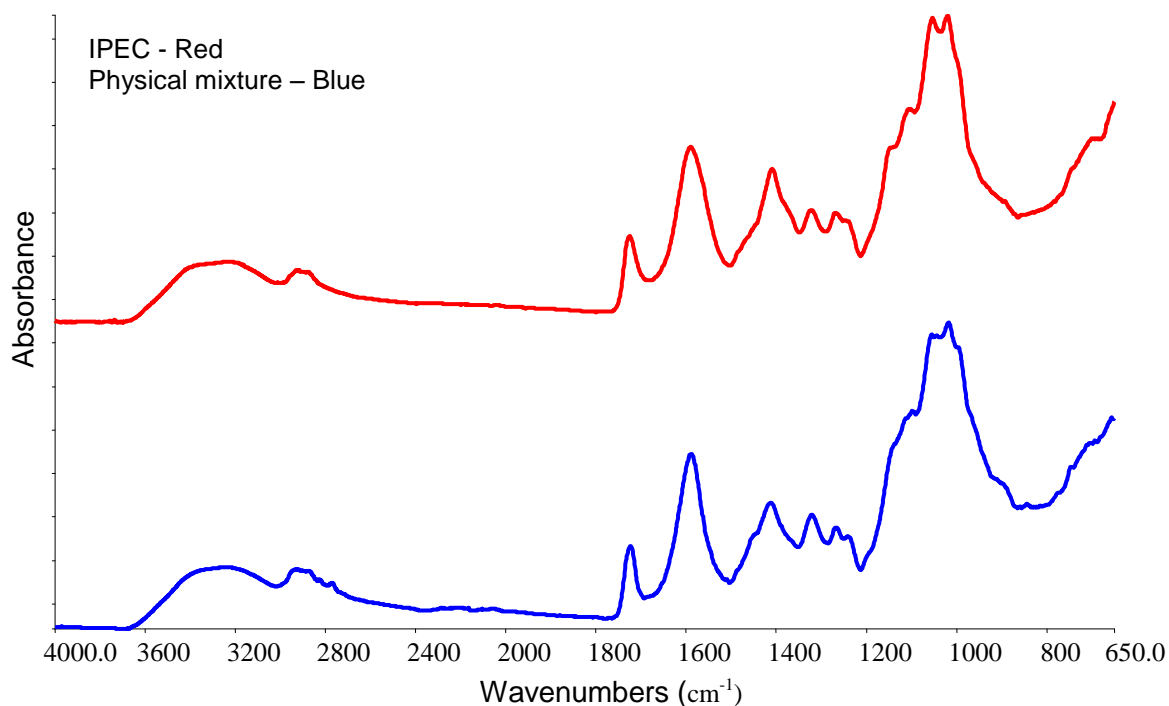


Figure 4.2d: Comparative spectra of the physical mixture (methacrylate copolymer and NaCMC) and IPEC.

4.3.3. Analysis of the polymeric thermal behavior of interpolyelectrolyte complex

DSC is employed to assess the thermal transitions/properties of a material and has found applications in several industries which include food, pharmaceutical and chemical industries. It provides qualitative and quantitative information of material transitions which involve endothermic, exothermic process or heat capacity changes and these are measured as a function of time and temperature (Verdonck et al., 1999). One of the challenges of DSC is the interpretation of heat flow when multiple overlapping processes occur over the same temperature range (Verdonck et al., 1999). For instance, a semi-crystalline polymer (e.g. polysaccharides) may have overlapping melting and recrystallization events.

From the DSC thermogram (Figure 4.3a) the melting point of methacrylate copolymer (crushed beads) is distinct at $\sim 58^{\circ}\text{C}$ and there was no indication of recrystallization after melting point but it was observed that decomposition occurred after 255°C . However, as a complex with NaCMC, the melting point is no longer distinct. NaCMC thermogram (Figure 4.3b) exhibited two endothermic curves before decomposition but as complex with methacrylate copolymer, three endothermic curves occurred before decomposition. The first broad endothermic peak occurred in NaCMC at $\sim 110^{\circ}\text{C}$ but as a complex with methacrylate copolymer, it occurred before 95°C . For instance, the endothermic peak occurred in IPEC 0.1N at $\sim 85^{\circ}\text{C}$ as shown in Figure 4.3c. This broad peak could be an overlapping of irreversible transitions which may include evaporation of moisture or melting or crystallization

as cooling and heating yielded a straight baseline line. The third concave curve initiated the decomposition process of the polymers. Figure 4.3c exhibits the thermograms of IPEC at different normalities of acetic acid and the difference observed amongst them was that their endotherms/first concave curves occurred at slightly different temperatures.

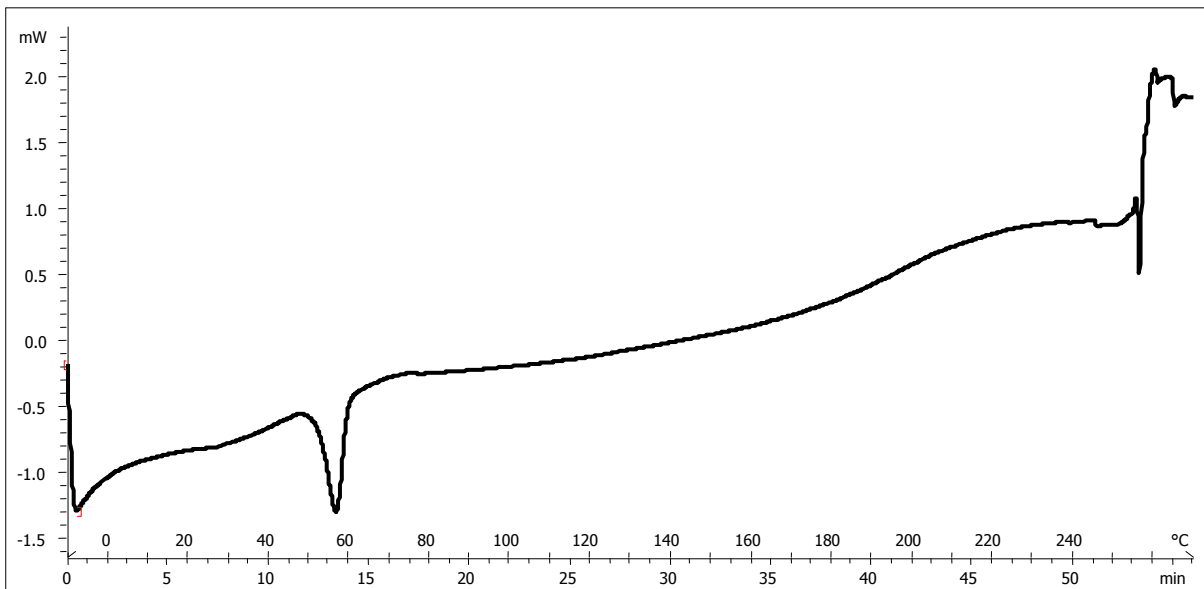


Figure 4.3a: Differential scanning calorimetry thermogram of methacrylate copolymer (E100).

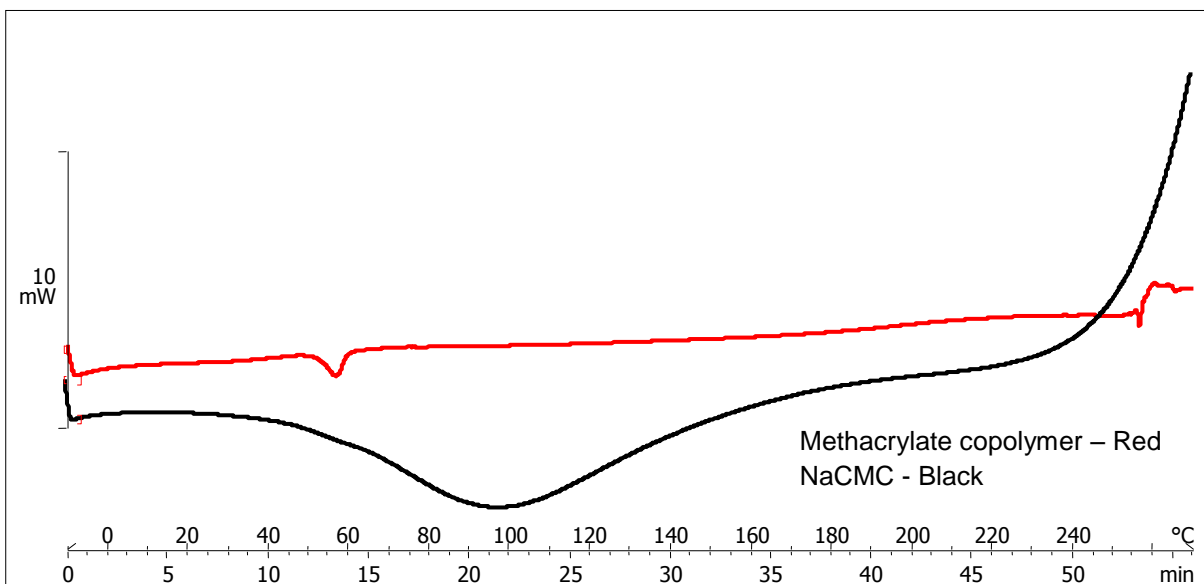


Figure 4.3b: Differential scanning calorimetry of native polymers – methacrylate copolymer and NaCMC.

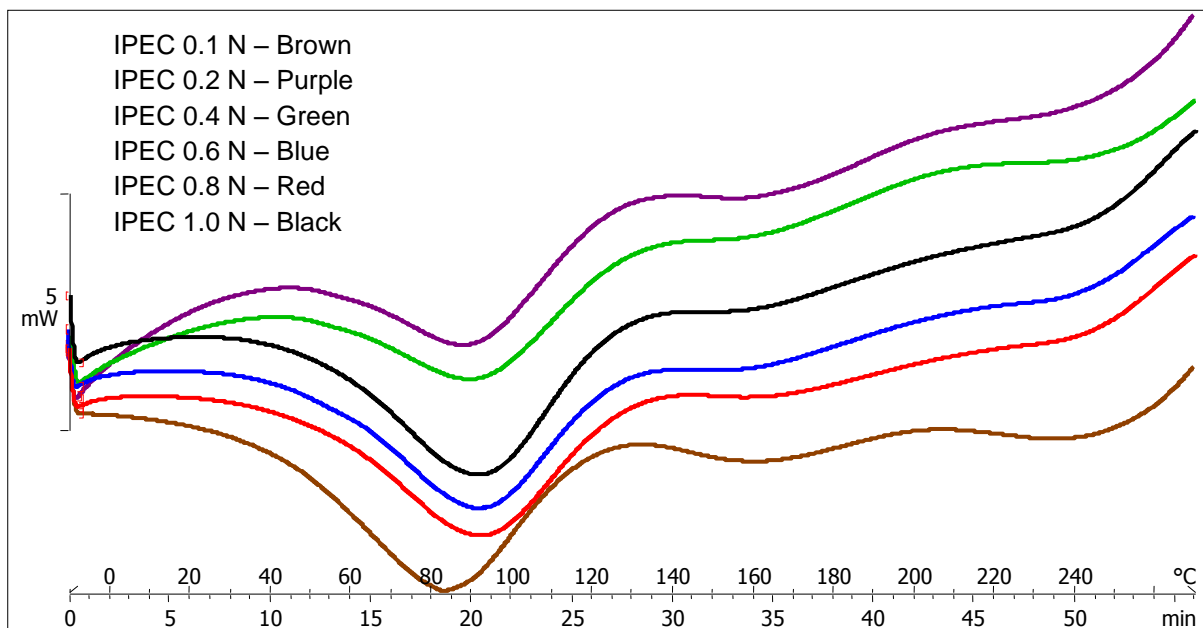


Figure 4.3c: Differential scanning calorimetry of IPEC synthesized at different normalities of acetic acid.

To further elucidate the thermal behavior of the native polymers and IPEC; and attempt to identify the different transitions occurring over the same temperature range, ADSC was undertaken. This involved temperature modulation superimposed over the DSC linear temperature ramp whereby the heating rate is no longer constant but varies in a periodic manner (Verdonck et al., 1999; Sauer et al., 2000). The resultant heat flow comprised two components; while one component is a function of the material's heat capacity C_p and rate of change in temperature, the other component is a function of absolute temperature and time (Verdonck et al., 1999). ADSC affords the analysis of the different polymer thermal transitions. After sample run, the thermogram is interpreted first by deconvolution of the raw curve into reversing heat flow, non-reversing heat flow, total heat flow, complex, in-phase and out-phase specific heat capacities, and phase angle. However, emphases are usually placed on reversing heat flow, non-reversing heat flow and total heat flow for interpretation of thermograms obtained. These components of ADSC separate the overlapping transitions for identification and quantification. While glass transition is detected in the reversing heat flow; evaporation, enthalpy relaxation, crystallization, decomposition and cure are identified in the non-reversing heat flow (Verdonck et al., 1999; Sauer et al., 2000). However, for crystal polymers, identification of melting is a challenge since the endotherms can occur in reversing and non-reversing heat flows (Okazaki and Wunderlich, 1997).

NaCMC is semi-crystalline and this nature is attributed to the inter-molecular and intra-molecular hydrogen bonding (Zhao et al., 2009b; Li et al., 2011) while methacrylate polymer (Eudragit® E100) is made as crystalline beads. These polymers contain crystallites of different degrees of perfection and therefore have different melting temperatures. Hence, a broad range of melting and crystallization temperatures were observed. Before the complete melting of a polymer, melting and crystallization are reversible to the fraction of a Kelvin (Okazaki and Wunderlich, 1997). However, once the polymer has melted completely, reversibility is lost due to lack of molecular nucleation (Ishikiryama and Wunderlich, 1997; Sauer, et al., 2000). The thermograms which depicted the heat flows as a function of time, as shown in Figures 4.3d - f revealed the thermal behaviors of IPEC and native polymers. The melting and crystallization at different temperatures are shown; the crystallization temperatures are shown in non-reversing heat flow mainly from the temperature range -10 to 130°C. Furthermore, crystallization was also observed with melting in the reversing heat flow in the range of -10 to 130°C. The recrystallization of the melted chains on existing crystals is made possible by the small modulation amplitude relative to the underlying heating rate. Polymer IPEC 0.1N in Figure 4.3d (i) may be exhibiting a unique thermogram in comparison to the native polymers and other IPECs at different normalities of acetic acid (Appendix C). It exhibited an endotherm in the non-reversing heat flow and an exotherm in the reversing heat flow below 0°C. The native polymer, NaCMC exhibited a combination of sinusoidal and meander-type of modulations while IPEC had only sinusoidal modulation which may confirm that IPEC is not a physical mixture. Rather it is a modified polymer with its own thermal behavior. At temperature range 130 – 250°C, sinusoidal modulation is observed for IPEC (EC 0.1N - 1.0N) which represent irreversible heat flow rates. It is envisaged that IPEC characteristic thermal behavior will modulate its rate of degradation/erosion and drug release from the tablet matrices formed with it which may be distinctly different from the behavior of NaCMC.

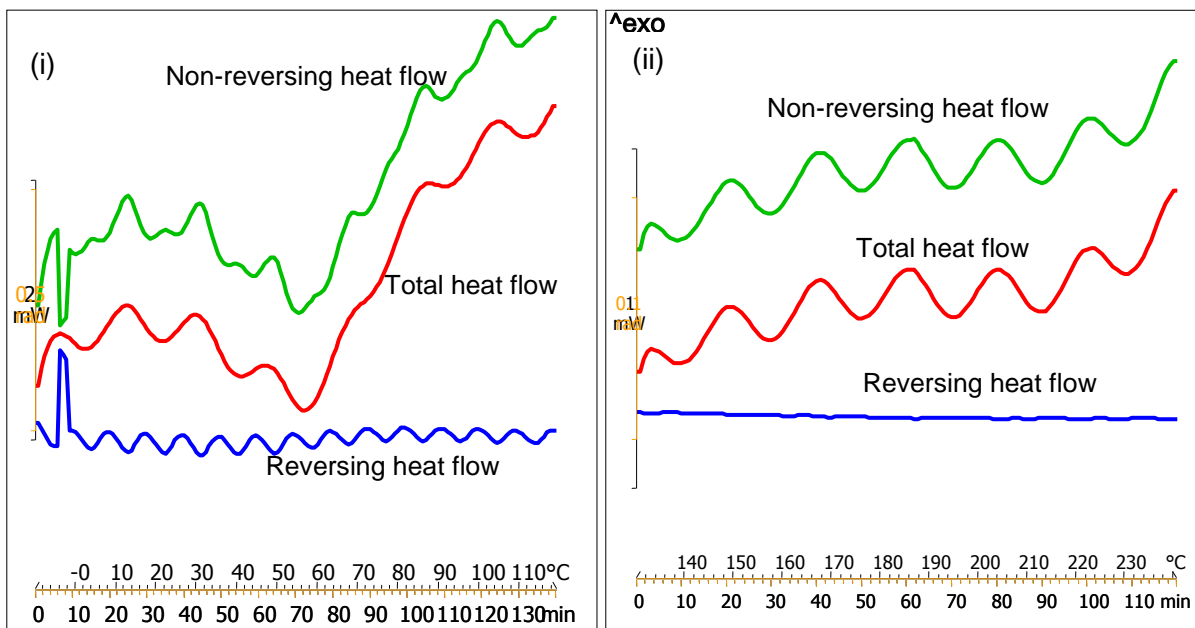


Figure 4.3d: Non-reversing, total and reversing heat flows derived from ADSC scans for IPEC 0.1N: **i)** temperature range -10 – 130°C and; **ii)** 130 – 250°C.

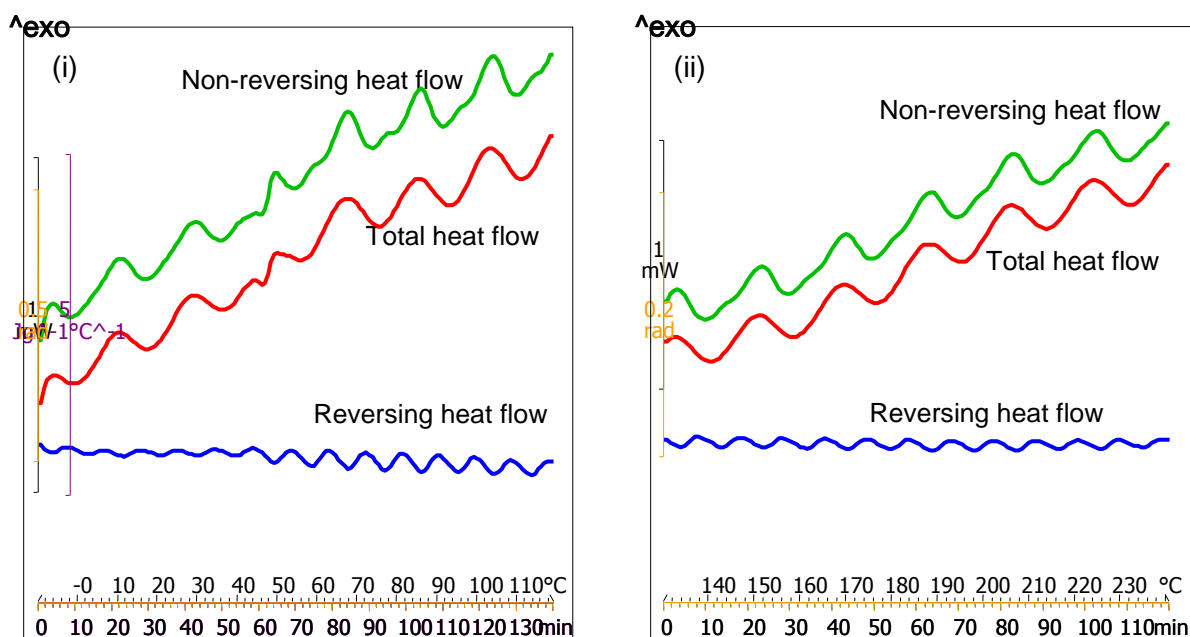


Figure 4.3e: Non-reversing, total and reversing heat flows derived from ADSC scans for methacrylate copolymer: **i)** temperature range -10 – 130°C and; **ii)** 130 – 250°C.

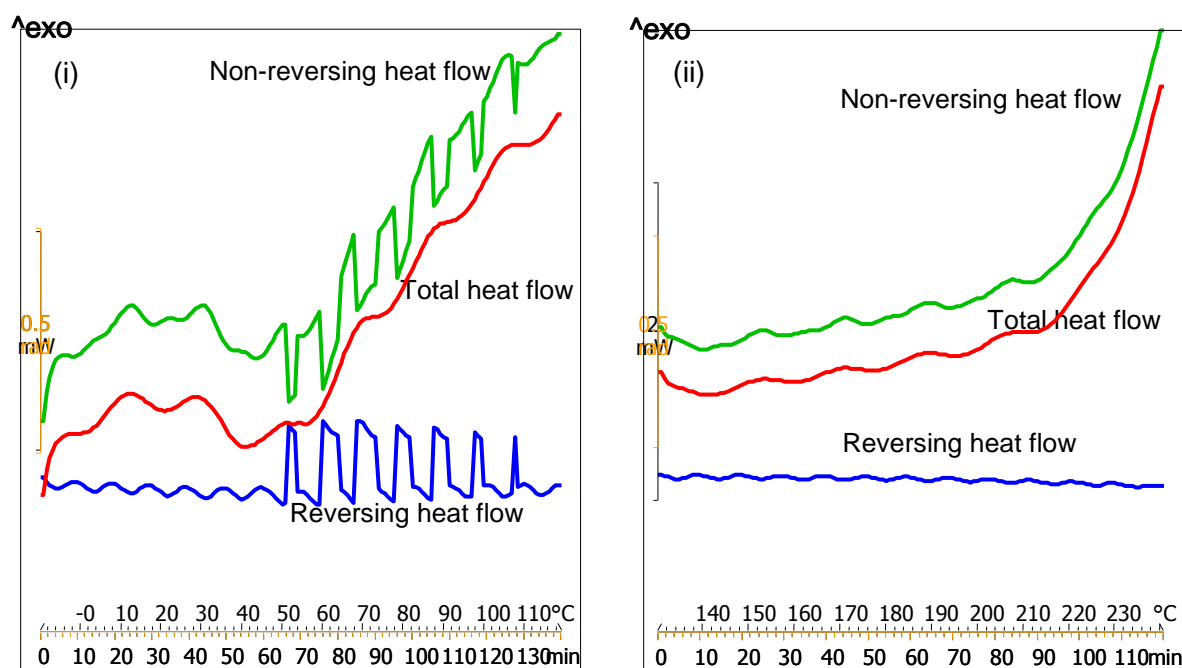


Figure 4.3f: Non-reversing, total and reversing heat flows derived from ADSC scans for NaCMC: **i)** temperature range -10 – 130°C and; **ii)** 130 – 250°C.

4.3.4. Direct compression of IPEC into matrices

The novel IPEC was directly compressible and did not require the presence of excipients to enhance compaction. Due to less excipients and steps of operation involved in direct compression, it is cost effective and suitable for drugs with stability problems such as L-dopa. Furthermore, direct compression is regarded as the tableting method of choice for thermolabile and moisture sensitive drugs (Jivraj et al., 2000). IPEC exhibited excellent compactibility with no evidence of capping or lamination and was compatible with L-dopa, the model drug.

4.3.5. Physicomechanical strength of IPEC matrices

Matrix hardness is the force in order to deform IPEC matrices in the presence of an external pressure while the deformation energy is the energy required to withstand the forces within the matrices. The harder the tablet, the more the deformation energy required to distort the matrix. Analysis of the physicomechanical strength is employed to indicate the stability of the matrices, their ability to withstand compressional pressure and the degree of capability to return to their original dimension after applied stresses. Matrix hardness and resilience denote the degree of density as well as porosity of a matrix thereby affecting the drug release from the matrix by influencing the rate of penetration of the dissolution medium into the matrix (Nur and Zhang, 2000)

A harder and more resilient matrix indicated more compactness and less voids and hence the matrix is not likely to collapse in the presence of an applied stress. The degree of porosity in the tablet determines the amount of energy absorbed for its deformation. The hardness of a tablet is also influenced by the inherent properties of the polymer employed in the formulation of the matrix. The different formulations had superior matrix hardness ranging from 19.152 - 27.590N/mm; the deformation energy ranging from 0.013 - 0.034Nm while the matrix resilience was from 42.08 - 46%. The difference in the composition of the matrices in formulations IPEC 0.1N - IPEC 1.0N is based on the varying normality of acetic acid from 0.1 - 1.0N. A typical Force-Distance and Force-Time profiles obtained are shown in Figure 4.4 while Figure 4.5a is a graphical representation of matrix hardness and energy absorbed and Figure 4.5b shows matrix resilience of the native polymers and IPEC at different normalities of acetic acid. As observed from the graph, IPEC had improved matrix resilience in comparison to NaCMC.

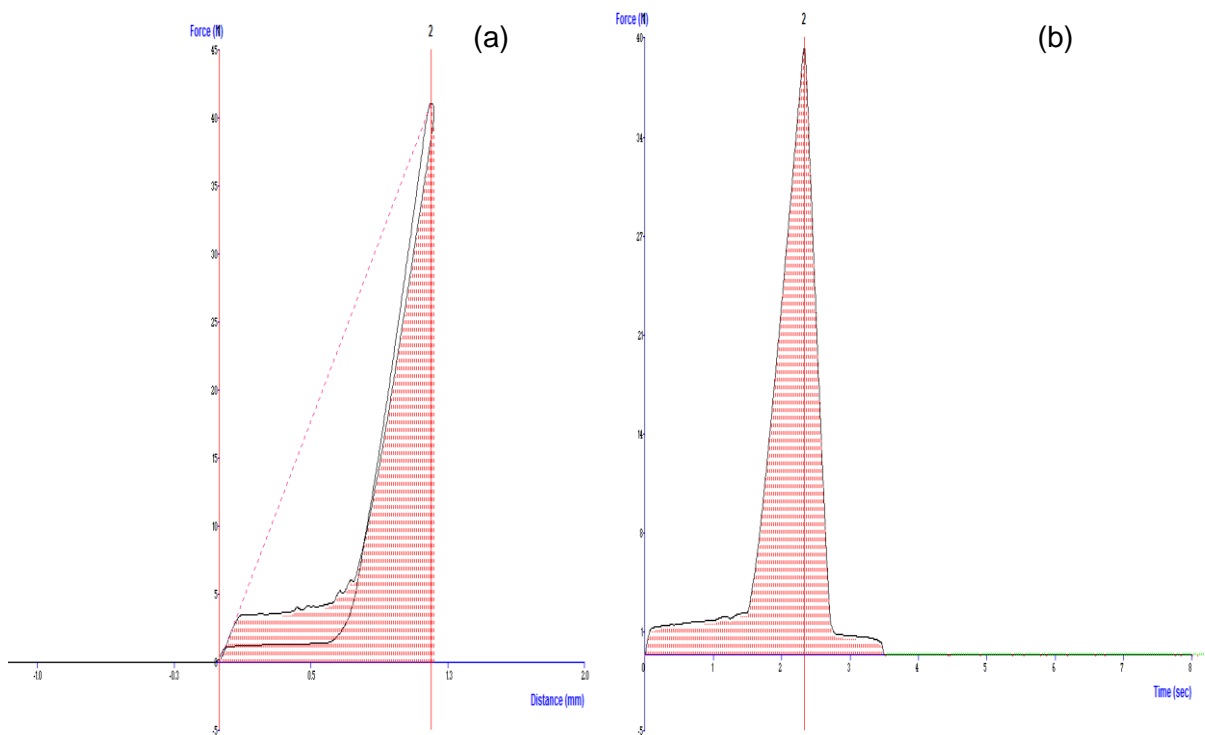


Figure 4.4: A typical Force-Distance and Force-Time profiles of the interpolymeric blends for determining: **a)** Matrix hardness and Deformation energy and; **b)** Matrix resilience.

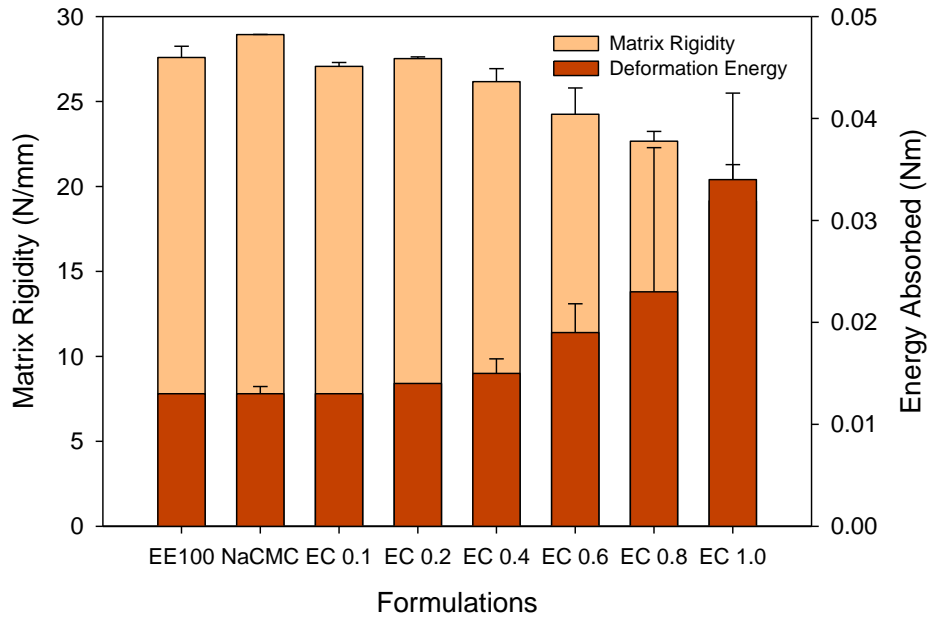


Figure 4.5a: Matrix rigidity and energy absorbed profiles of the native polymers and IPEC synthesized in 0.1 to 1.0N acetic acid.

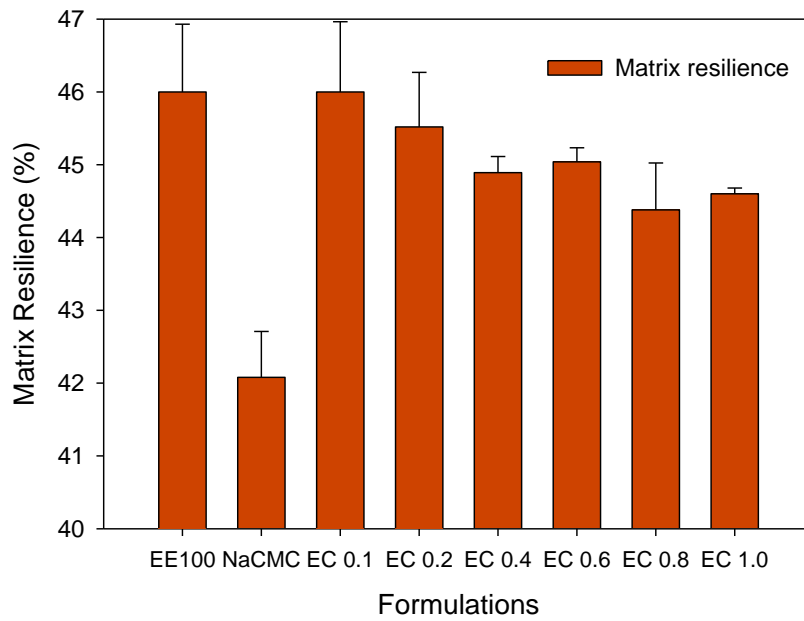


Figure 4.5b: Matrix resilience profile of the native polymers and IPEC synthesized in 0.1 to 1.0N acetic acid.

4.3.6. The degree of swelling of IPEC

The overall drug release rate from a polymeric system is a function of structural features of the network, process of hydration, swelling and degradation of the polymer(s) (O'Brien et al., 2009). IPEC matrices retained their three-dimensional network and behaved as hydrogel

matrices in 0.1N HCl. As water or in this case HCl is absorbed by the matrix, the loaded drug is dissolved and diffused out through the pores. The diffusion rate is dependent on the degree of swelling of IPEC which then determines the quantity of drug released with time. The swelling is affected by the polymer-solvent interaction, presence of drug and degree of crosslinking (Kim et al., 1992). Increase in crosslinking density would lower the degree of equilibrium swelling thereby reducing water content and subsequent diffusion of drug from the matrix (Wise, 1995).

The degree of swelling over 24 hours by IPEC as shown in Figure 4.6a indicated a possible drug release with zero-order kinetics especially between the 2nd and the 12th hours. Hence, should a drug be incorporated into IPEC hydrogel, zero order kinetic release of the drug is envisaged. The novel IPEC was compared to only one of the native polymers, NaCMC as methacrylate copolymer dissolves in 0.1N HCl without visible swelling. The IPEC hydrogel when compared with NaCMC had a higher degree of swelling at 24th hour of 465%, near zero order pattern of swelling, retained its shape as shown in Figure 4.6b. Shown by the fact that the inner core was not hydrated, it is envisaged swelling may continue after 24 hours whereas NaCMC had lost its shape and was fully hydrated. Figure 4.6c depicts the degree of swelling profiles for IPEC at different normalities of acetic acid. The degree of swelling was found to be highest when the normality of acetic acid was 0.1N. The trend observed was that as the normality of acetic acid increased, degree of swelling decreased. Perhaps increase in normality of acetic acid increases the degree of crosslinking which in turn may decrease the degree of swelling.

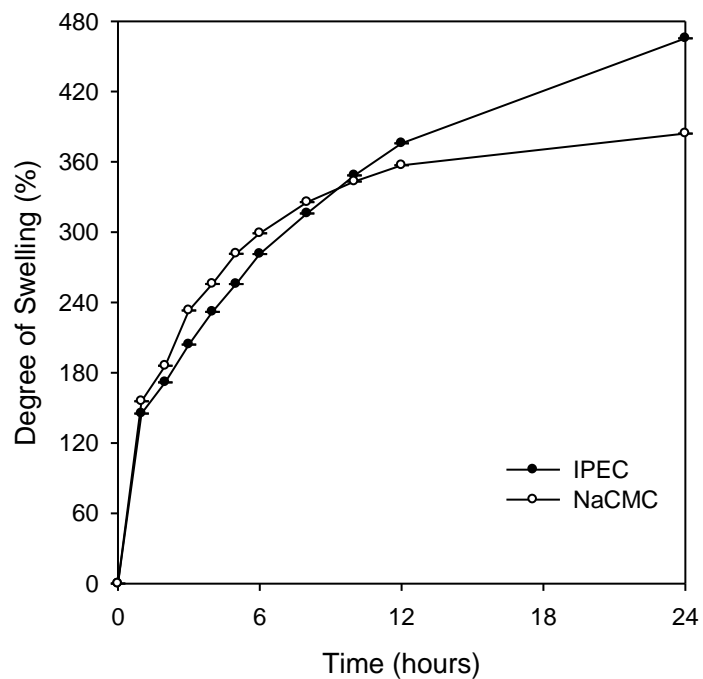


Figure 4.6a: Comparative degree of swelling of the IPEC and NaCMC in an aqueous environment (0.1N HCl) over 24 hours.

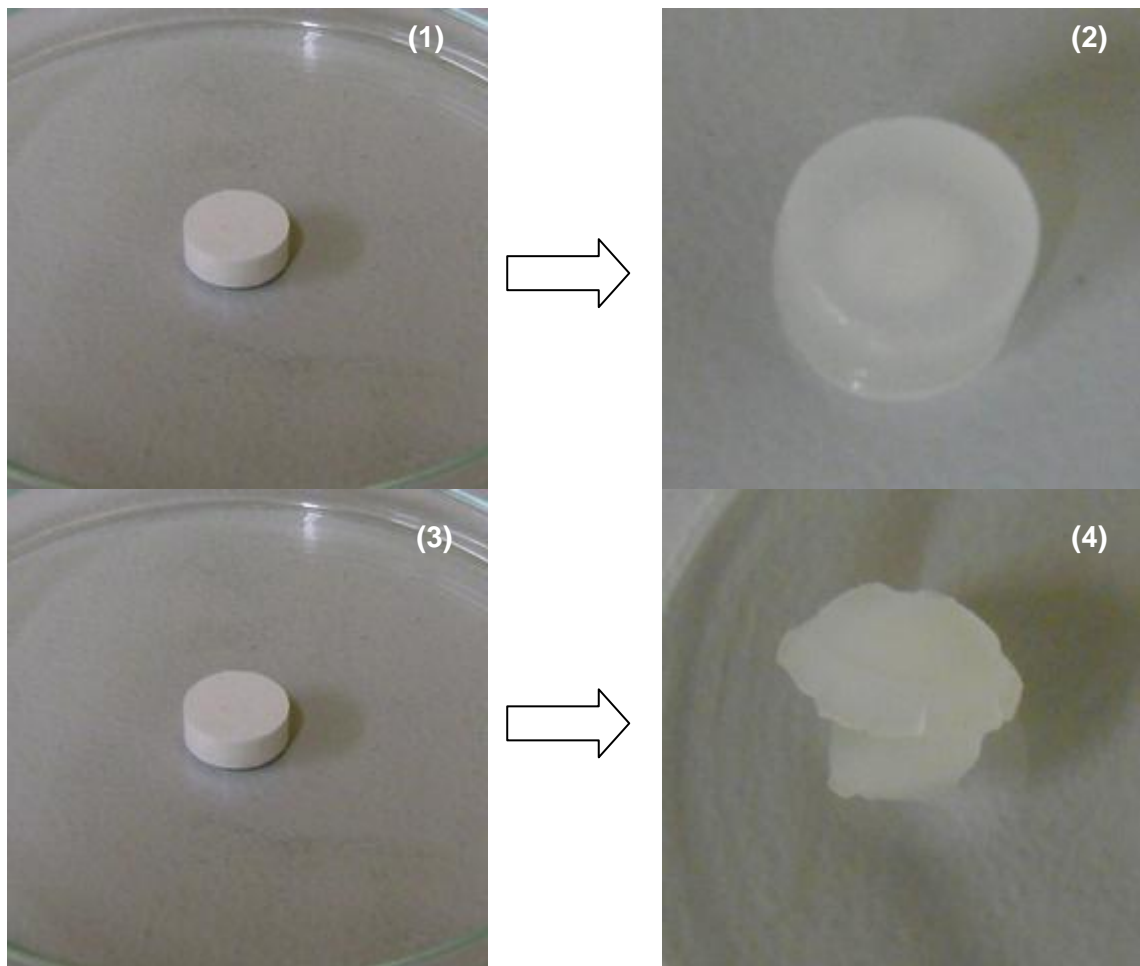


Figure 4.6b: IPEC hydrogel retained its shape and the unhydrated inner core is an indication of further swellability: **1)** IPEC hydrogel before swelling; **2)** IPEC hydrogel after swelling. NaCMC lost its shape and was fully hydrated: **3)** NaCMC before swelling and; **4)** NaCMC after swelling.

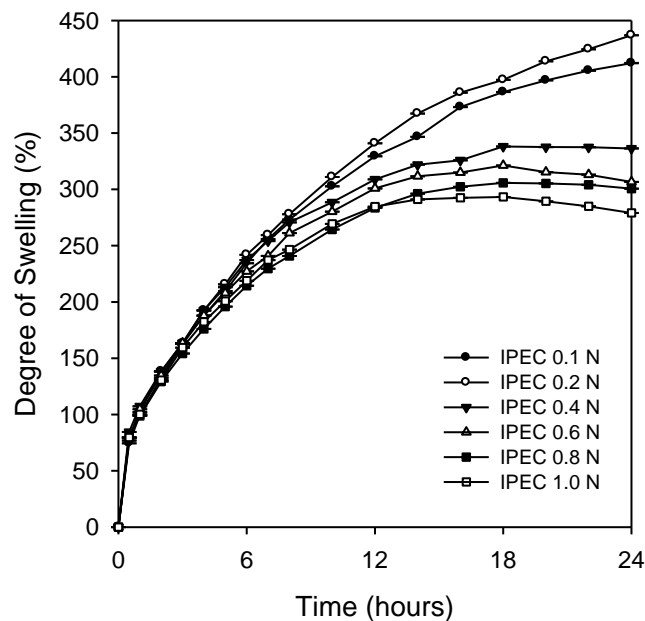


Figure 4.6c: Comparative degree of swelling for IPEC at different normalities of acetic acid.

4.3.7. *In vitro* drug release studies

Between the 2nd and 3rd hours, 96% of L-dopa had been released from methacrylate copolymer due to its solubility in 0.1N HCl (acidic media). This, however, confirms that methacrylate copolymer cannot be employed on its own for sustained release matrices. The deformation of NaCMC as it hydrated was clearly visible from the 3rd hour, though the rate of drug release was slightly slower from NaCMC matrix than from the IPEC hydrogel initially. However, with time, its rate of drug release increased while IPEC hydrogel continued to release at a more constant rate. The mechanisms of drug release from native NaCMC is envisaged to include swelling, diffusion and gradual leaching/dissolution of the NaCMC while drug release from the IPEC hydrogel is attributed to swelling and diffusion. By the twelfth hour, 80% of L-dopa had been released from NaCMC while that of the hydrogel released 64% of the same drug in a zero-order pattern as shown in Figure 4.7a. Furthermore, the drug release from IPECs synthesized with different normalities was undertaken in buffer pH values of 1.5 and 4.5 (Figure 4.7b and c). The matrices retained their three-dimensional networks in pH 1.5 while in pH 4.5 there was significant swelling and erosion indicating that IPEC may be pH-responsive. Initially, it was surface erosion but by the 16th hour bulk erosion occurred (Figure 4.7c) leading to non-linear profiles from the 16th hour. The susceptibility of IPEC matrices to bulk erosion increased as the normality of acetic acid utilized for synthesis increased.

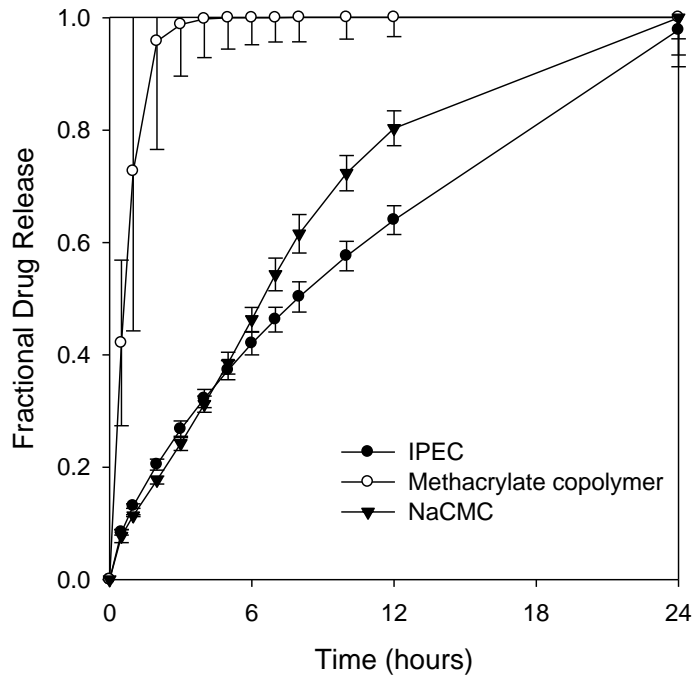


Figure 4.7a: Drug release profiles from the native polymers and the novel IPEC.

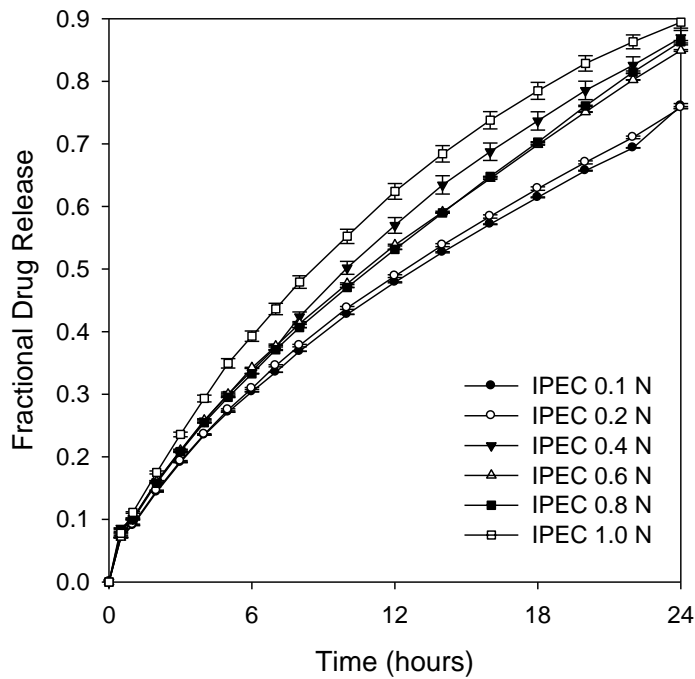


Figure 4.7b: Drug release profiles of IPECs of different normalities of acetic acid in buffer pH 1.5.

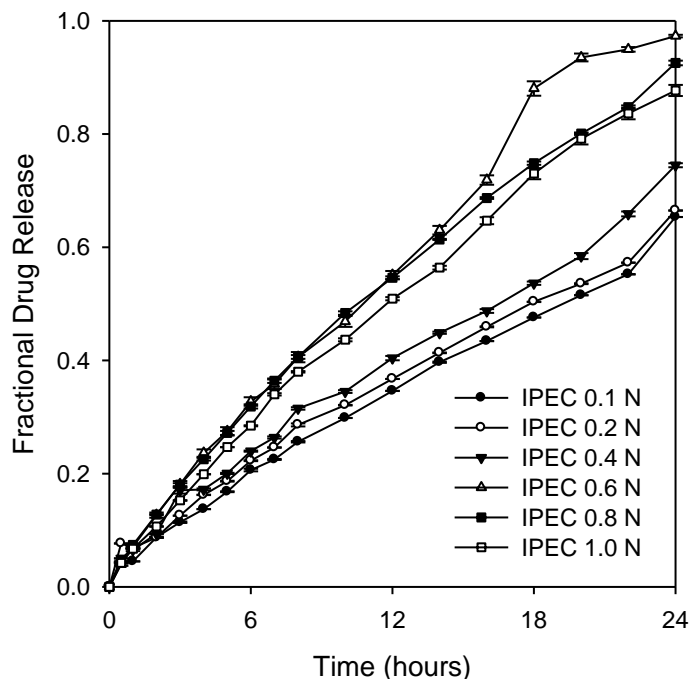


Figure 4.7c: Drug release profiles of IPECs of different normalities of acetic acid in buffer pH 4.5.

4.4. CONCLUDING REMARKS

The FTIR spectra confirmed the formation of IPEC which were also corroborated by thermal analyses (ADSC). The FTIR and ADSC analyses confirmed that the IPEC is a modified polymer with its own IR spectrum and thermal behavior different from those of the native polymers. The blending of methacrylate copolymer and NaCMC enhanced by the presence of ionic interactions and hydrogen bondings produced a hydrogel with enhanced drug delivery properties in comparison with the native polymers. The IPEC hydrogel retained its three dimensional network, had superior physicochemical properties; and exhibited a zero-order *in vitro* release kinetics of L-dopa over 24 hours. However, it undergoes bulk erosion and thus, prevention of bulk erosion by blending of a polysaccharide with IPEC in order to avoid burst release of L-dopa will be explored in the next Chapter.

CHAPTER FIVE

THE INFLUENCE OF ADDITION OF A POLYSACCHARIDE ON THE PHYSICOCHEMICAL CHARACTERISTICS OF THE INTERPOLYELECTROLYTE COMPLEX

5.1. INTRODUCTION

In Chapter four, it was shown that IPEC has the capability to delivery drugs over a prolonged period and at a constant rate. However, bulk erosion exhibited by IPEC from the 16th hour led to further investigations elaborated in this Chapter. It is envisaged that addition of a polysaccharide may prevent bulk erosion thereby hindering burst release and perhaps further improve the drug delivery properties of IPEC.

Polymer blending is a physicochemical process of mixing two or more polymers enhanced under mechanical or temperature field. When a chemical reaction is involved, the rates are influenced by blending characteristics, temperature gradients and diffusion of reagents and products (Prut and Zelenetskii, 2001). Polymer blending is one of the commonly employed methods for modification of polymers to improve their physicochemical characteristics. Synthesis and characterization of new polymers may be time consuming and all the desired properties may still not be achieved by synthesizing a polymer. However, blending of two polymers with their individual properties may result in optimum characteristics for the desired drug delivery system. In polymer blending, the polymer compositions can be manipulated and controlled in conformity to experimental requirements (Li et al., 2010). It is a cheap, convenient and less time consuming alternative to copolymerization and produces new materials with improved properties of the polymers utilized (Edlund and Albertsson, 2000).

Polymer blending has been employed to increase rate of degradation, control water content thereby manipulating permeability (Pitt et al., 1992; Edlund and Albertsson, 2000); control and extend drug release (Park et al., 1992; Kenawy et al., 2002); achieve zero order kinetics (Shen et al., 2000) moderate swelling (Lecomte et al., 2003), modification for protein delivery (Mi et al., 2003) and modulation of porosity (Thomas et al., 1997).

This study was undertaken to explore the possibilities of improving the drug delivery properties of an interpolyelectrolyte complex (IPEC) by the addition of a natural polysaccharide (forming interpolymeric blend). The physicochemical properties of the interpolymeric blend were assessed in comparison with IPEC. Thermal and structural analyses, swellability and erosion studies; and *in vitro* drug release studies were undertaken to determine the influence of the natural polysaccharide on IPEC.

5.2. EXPERIMENTAL SECTION

5.2.1. Materials

The materials employed in this study were those in Chapter 4, Section 4.2.1. However, the natural polysaccharide added to IPEC was locust bean from *Ceratonia siliqua* seeds (Sigma-Aldrich Inc, Steinheim, Germany).

5.2.2. Synthesis of interpolyelectrolyte complex

The synthesis of IPEC was undertaken as stated in Chapter 3, Section 3.2.3.1. Furthermore, the quantity (0.84g) of methacrylate copolymer utilized in this study was dissolved in different normalities of acetic acid - 0.1, 0.2, 0.4, 0.6, 0.8 and 1.0N. The interpolyelectrolyte complex was lyophilized for 48 hours and milled.

5.2.3. Formation of interpolymeric blend

The IPEC was synthesized as described above in the same quantities and different normalities of acetic acid. After the IPEC formation, 1.68g of locust bean was added to each IPEC with different normalities of acetic acid under continuous agitation for 15mins to form interpolymeric blend. The interpolymeric blend (IPB) was lyophilized for 48 hours and milled.

5.2.4. Structural elucidation of IPEC and interpolymeric blend

FTIR spectra of milled methacrylate copolymer, NaCMC, IPEC and IPB were obtained as described in Chapter 4, Section 4.2.4 to elucidate the interactions and structural modification of IPEC from IPB.

5.2.5. Evaluation of the polymeric thermal behavior of IPEC and interpolymeric blend

To compare the thermal properties of IPEC and IPB, differential scanning calorimetry (DSC 1 STAR^e system, Mettler Toledo, Schwerzenbach, Switzerland) and ADSC were undertaken as described in Chapter 4, Section 4.2.5.

5.2.6. Direct compression of IPEC and interpolymeric blend

L-dopa-loaded IPEC was directly compressed as described in Chapter 4, Section 4.2.6. The same process was applied to IPB thereby producing drug-loaded IPEC matrices and drug-loaded IPB matrices without excipients in order to assess their (IPEC and IPB) drug delivery properties unaided. A quantity of 100mg L-dopa per matrix was utilized. The matrices were utilized for swelling, erosion and *in vitro* drug release comparative studies.

5.2.7. Swellability and erosion studies of directly compressed matrices

The swelling test for the IPEC and IPB matrices was undertaken in pH 1.5 and 4.5. The swellability study in pH 1.5 was executed as stated in Chapter 4, Section 4.2.8. Increase in weights was determined gravimetrically at 2 hour intervals over 24 hours and swellability was obtained mathematically using Equation 4.1 (Chapter 4, Section 4.2.8). The ring mesh assembly was employed for swellability and erosion studies in pH 4.5 instead of mesh baskets to ensure the release of the eroded particles into the medium for more accurate determination of erosion and swelling. The ring mesh also ensured the samples were not handled. Swelling and erosion studies were carried out in a dissolution system (Erweka DT 700, Erweka GmbH, Heusenstamm, Germany) at $37\pm 0.5^{\circ}\text{C}$ and 50rpm over 8 hours. The matrices were weighed at 2 hour intervals and at the end of 8th hour; the samples were lyophilized to determine the final weight after erosion. Variation in weights was determined gravimetrically while the degrees of swelling and erosion were graphically represented.

5.2.8. *In vitro* drug release studies and data analysis

To obtain drug release profiles for IPEC and IPB matrices, dissolution testing was undertaken as stated in Chapter 4, Section 4.2.9. Thereafter, the drug release profiles of IPEC and IPB matrices were compared. The drug release profiles were analyzed with statistical standard deviation, dissolution efficiency, first order and zero order kinetics; Higuchi, Korsmeyer and Peppas equations.

5.2.9. Molecular modeling simulations

Molecular simulations were undertaken to elucidate the mechanisms and the energies behind the physicochemical characteristics of IPEC exhibited in Chapter 4 as well as understand the impact of locust bean on its physicochemical properties as will be explicated in this Chapter.

5.2.9.1. Static lattice atomistic simulations (SLAS)

All modeling procedures and calculations were performed using the softwares indicated in Chapter 3, Section 3.2.3.3. The methacrylate copolymer (E100) was drawn using ChemBio3D Ultra in its syndiotactic stereochemistry as a 3D model whereas the structures of CMC (4 saccharide units) and locust bean gum (LBG) were built from standard bond lengths and angles using sugar builder module on HyperChemTM 8.0.8. The models were energy-minimized using a progressive-convergence-strategy where initially the MM+ force field was used followed by energy-minimization using the Amber 3 (Assisted Model Building and Energy Refinements) force field. The conformer having the lowest energy was used to create the polymer-polymer and polymer-solvent complexes. A complex of one polymer molecule

with another was assembled by disposing the molecules in a parallel way, and the same procedure of energy-minimization was repeated to generate the final models: CMC-LBG, E100-LBG and CMC-E100-LBG. Full geometry optimization was carried out in vacuum employing the Polak–Ribiere conjugate gradient algorithm until an RMS gradient of 0.001kcal/mol was reached. For Molecular Mechanics calculations in vacuum, the force fields were utilized with a distance-dependent dielectric constant scaled by a factor of 1. The 1-4 scale factors used were electrostatic - 0.5 and van der Waals - 0.5 (Kumar et al., 2011).

5.2.9.2. Molecular dynamics simulation (MDS)

The polymer chains initially minimized by Molecular Mechanics were then minimized by molecular dynamics for 1.0ps (time step = 0.001ps) at 300K with the Nose–Hoover thermostat. For evaluation of the stability of a simulation and the extent of equilibration and for identification of the interesting low energy conformations, molecular dynamics calculations were averaged and saved as kinetic energy (EKIN), potential energy (EPOT), total energy (ETOT) and temperature (TEMP). Equilibrium was established before recording the measurements wherein the instantaneous potential and kinetic energy were monitored to determine when the system reaches equilibrium. Thereafter, the simulation was allowed to run for 1000 time-steps before taking measurements (Guo et al., 2003).

5.3. RESULTS AND DISCUSSION

5.3.1. Synthesis of IPEC and formation of interpolymeric blend

The stoichiometric ratio for a homogenous interaction between methacrylate copolymer and NaCMC is 0.5:1 respectively. Higher concentration of NaCMC is required to generate sodium acetate for the association of methacrylate copolymer and NaCMC. The association interactions are achieved by hydrogen bonding, hydrophilic interactions and ionic interactions enhanced in the presence of acetic acid. Incorporation of locust bean into IPEC did not alter the associations between methacrylate copolymer and NaCMC. The hydrophilic groups of locust bean associated themselves to the water holding bodies of IPEC. It may also be possible that some ionic interactions may have occurred between IPEC and Locust bean. The blend was light brown due to the color of locust bean. There was increase in viscosity on addition of locust bean and this is expected due to the nature of locust bean. However, the blending was done under ambient temperature and so locust bean did not swell excessively.

5.3.2. Structural analysis of IPEC and interpolymeric blend

The structural differences of IPEC and IPB in comparison to the native polymers are shown in Figure 5.1a while IPEC and IPB are compared in Figure 5.1b. As observed, the characteristic peaks of methacrylate copolymers at 2877.05, 1452.94, 1342.09, 1060.48,

961.33, 842.31, 747.27 cm^{-1} were absent in IPEC as well as in IPB. However, its characteristic distinct peak at 1722.46 cm^{-1} shifted to 1725.04 cm^{-1} in both IPEC and IPB while two other peaks, 1271.15 and 1239.97 shifted to 1266.47 and 1241.50 cm^{-1} respectively in both IPEC and IPB. However, the last two peaks were more pronounced in IPEC. Not much difference was seen between the spectra of IPEC and IPB apart from slight difference in shift of some peaks. Peak at frequency 1019.53 cm^{-1} of IPEC shifted to 1021.12 cm^{-1} in IPB and was more distinct. Broader peak of IPB at 1590.79 cm^{-1} as compared to IPEC may be due to the superimposing peak 1639.22 cm^{-1} of locust bean. The peak at frequency 1104.16 cm^{-1} of IPEC was not seen in IPB while peak 810.75 cm^{-1} of IPB was not seen in IPEC which is due to the fact that the peak is peculiar to locust bean. In summary, there was no distinct difference between IPEC and polymer blend observed from the spectra which may be an indication that the addition of locust bean to IPEC did not necessarily generate a chemical change.

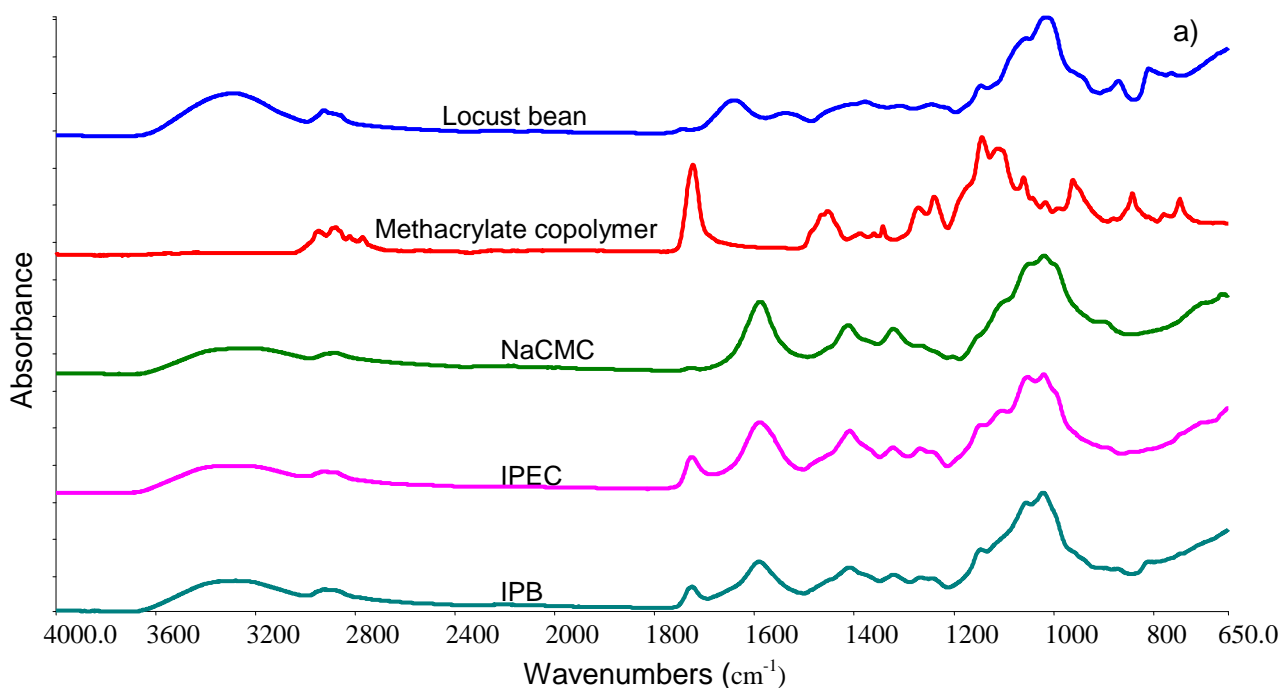


Figure 5.1a: FTIR spectra of native polymers – locust bean, methacrylate copolymer and NaCMC; IPEC and IPB.

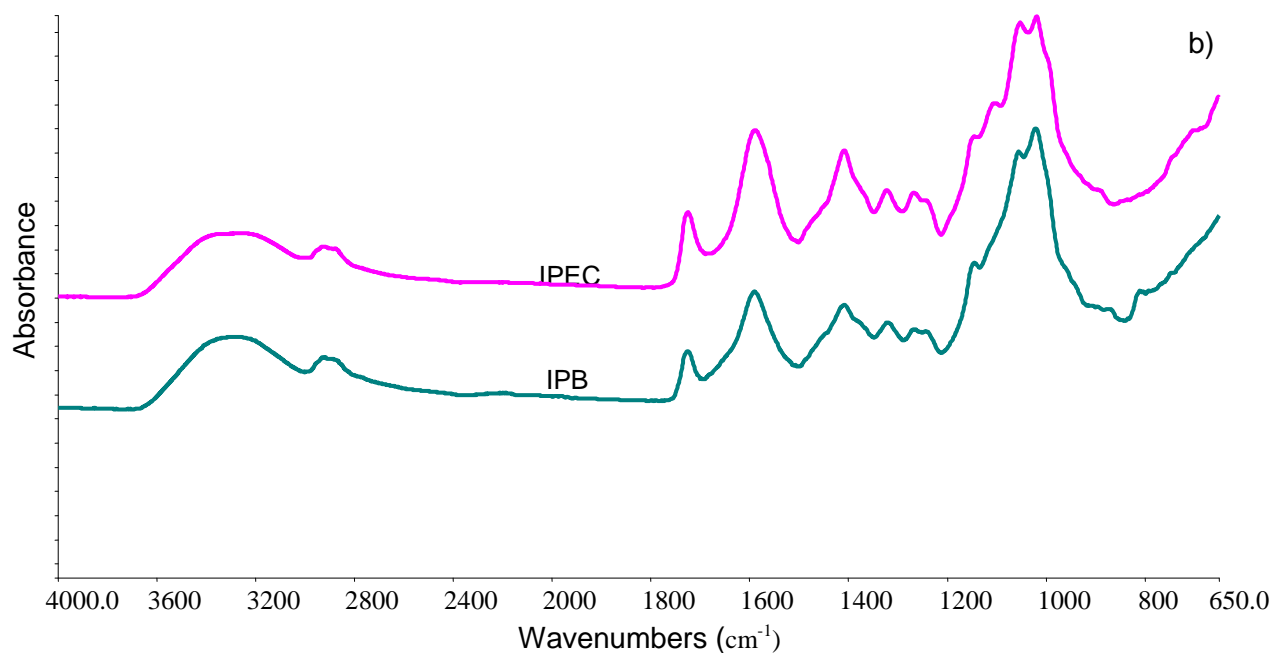


Figure 5.1b: Comparative spectra of interpolyelectrolyte complex and interpolymeric blend.

5.3.3. Polymeric thermal analysis of IPEC and interpolymeric blend

The thermograms of the three native polymers - methacrylate copolymer, NaCMC and locust bean - are shown in Figure 5.2a. The characteristic melting peak of methacrylate polymer was found at $\sim 58^{\circ}\text{C}$ while NaCMC and locust bean had broad endotherms at $\sim 110^{\circ}\text{C}$ and $\sim 90^{\circ}\text{C}$ respectively. As the temperature increased to 210°C , decomposition of the polymers occurred as shown by the upward movement of the thermograms. Comparing Figure 5.2b and 5.2c, there seem not to be much difference in the thermograms except perhaps in the depth of the endotherms. IPEC thermograms had shallow endotherms while those of IPB had deep endotherms. Furthermore, the presence of locust bean in the blend slightly lowered the temperature of the endotherms. For instance, the endotherm of IPEC 0.1N occurred at $\sim 85^{\circ}\text{C}$ while that of IPB 0.1N occurred at $\sim 80^{\circ}\text{C}$. The thermograms for IPEC and IPB were homogenous indicating the complete interactions and miscibility and thus each thermogram appeared as a thermogram for a single substance/material.

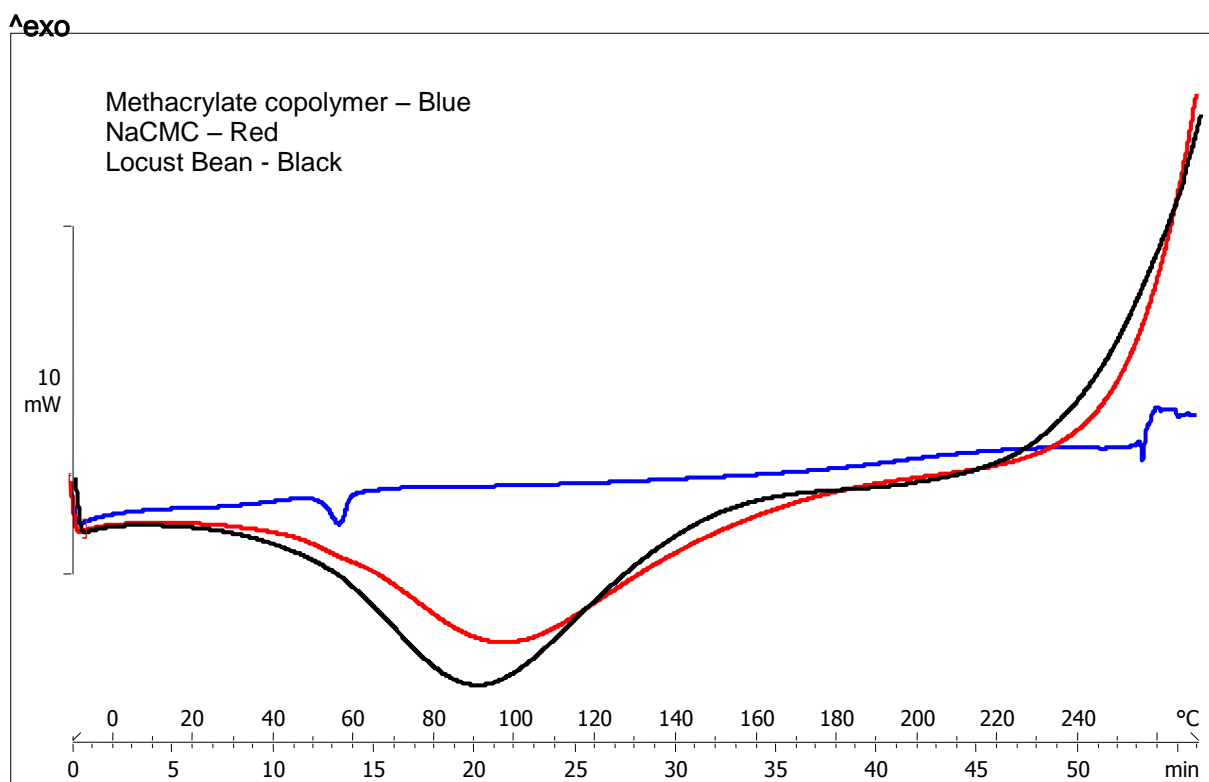


Figure 5.2a: Differential scanning calorimetric curves of native polymers – methacrylate copolymer, NaCMC and locust bean.

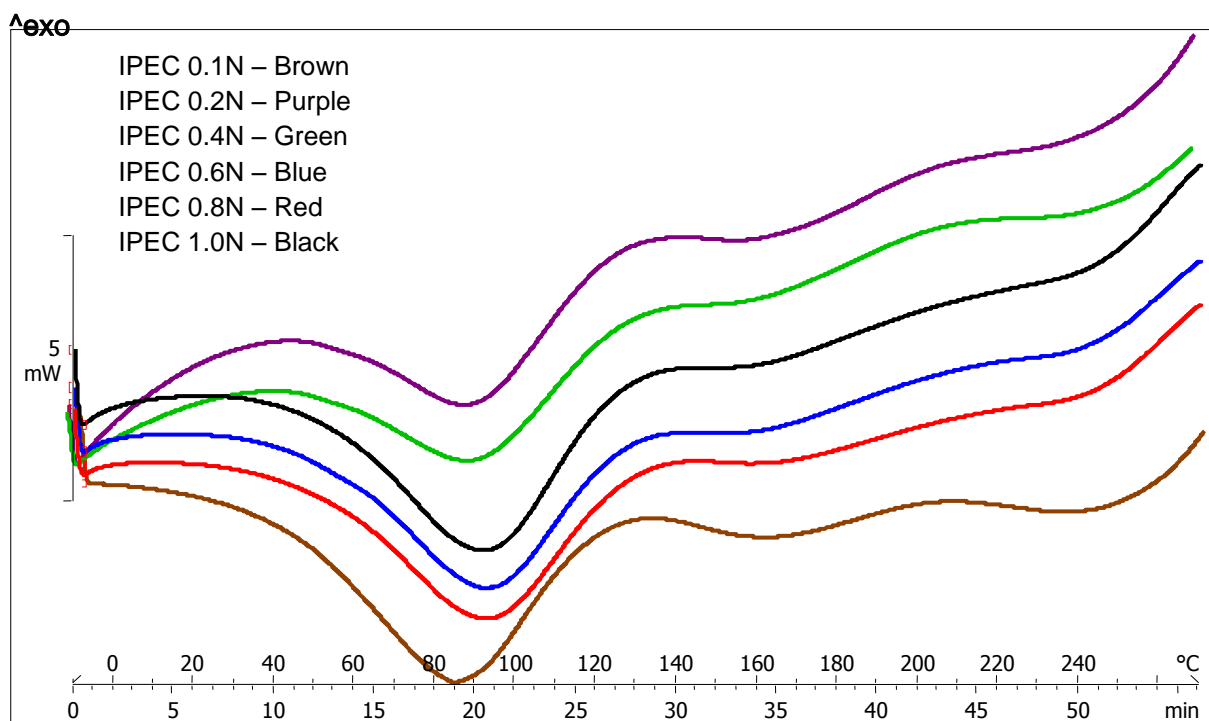


Figure 5.2b: Differential scanning calorimetric curves of IPEC synthesized at different normalities of acetic acid.

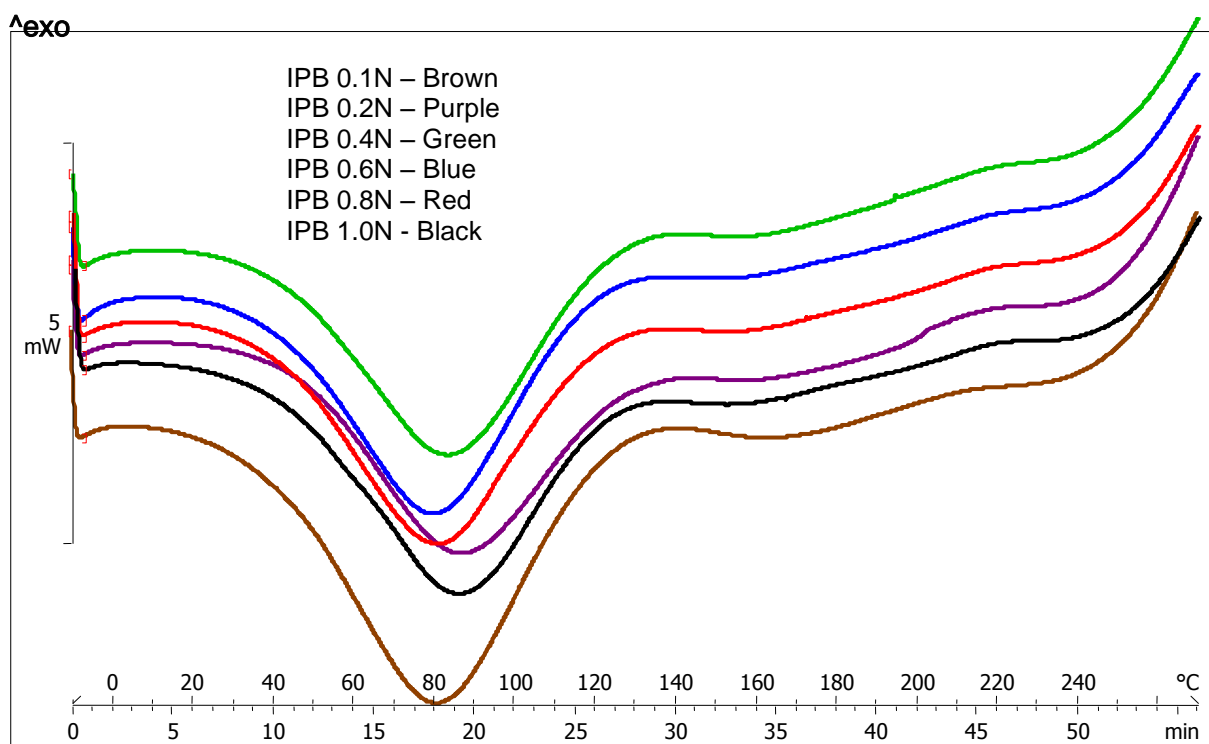


Figure 5.2c: Differential scanning calorimetric curves of interpolymeric blend synthesized with different normalities of acetic acid.

However, to further compare the thermal transitions of IPEC and IPB, ADSC was undertaken. The crystallization and melting endotherms were observed in both IPEC and IPB as shown in Figures 5.2d and 5.2e. However, while IPEC exhibited a sinusoidal modulation only, IPB exhibited a combination of sinusoidal and meander-type of modulation. As discussed in Chapter 4, Section 4.3.3, although NaCMC had combined modulations (Figure 5.2f). IPEC did not, possibly due to the fact that IPEC was a chemical modification behaving as one material with its own unique thermal properties. Introduction of locust bean into IPEC influenced the thermal behavior exhibited by IPB. Locust bean at -10 to 130°C (Figure 5.2h) exhibited a meander-type of modulation only and so IPB was exhibiting that aspect of locust bean. In the DSC thermogram, other than the deep endotherm, locust bean thermal transitions were not seen in IPB thermograms. However, ADSC elucidated the thermal transitions of IPEC and locust bean in IPB clarifying that the blend between IPEC and locust bean may be a physical miscible polymer blend.

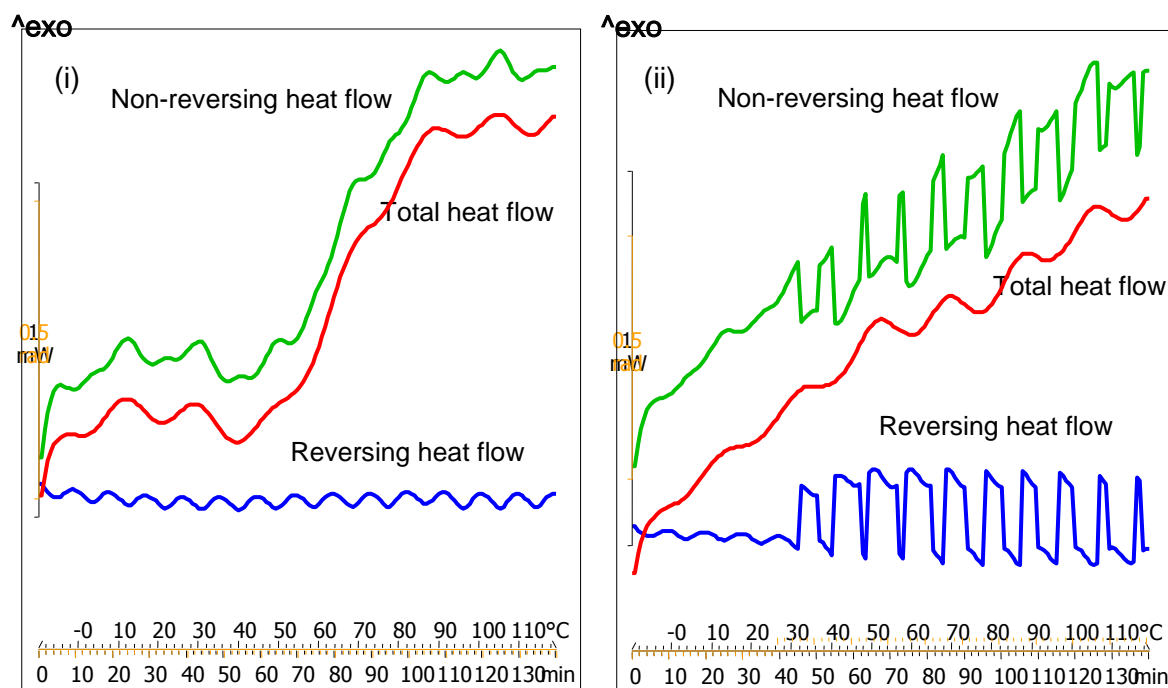


Figure 5.2d: Non-reversing, total and reversing heat flows derived from modulated DSC curves for: **i)** IPEC 0.4 N and; **ii)** IPB 0.4N at temperature range -10-130°C.

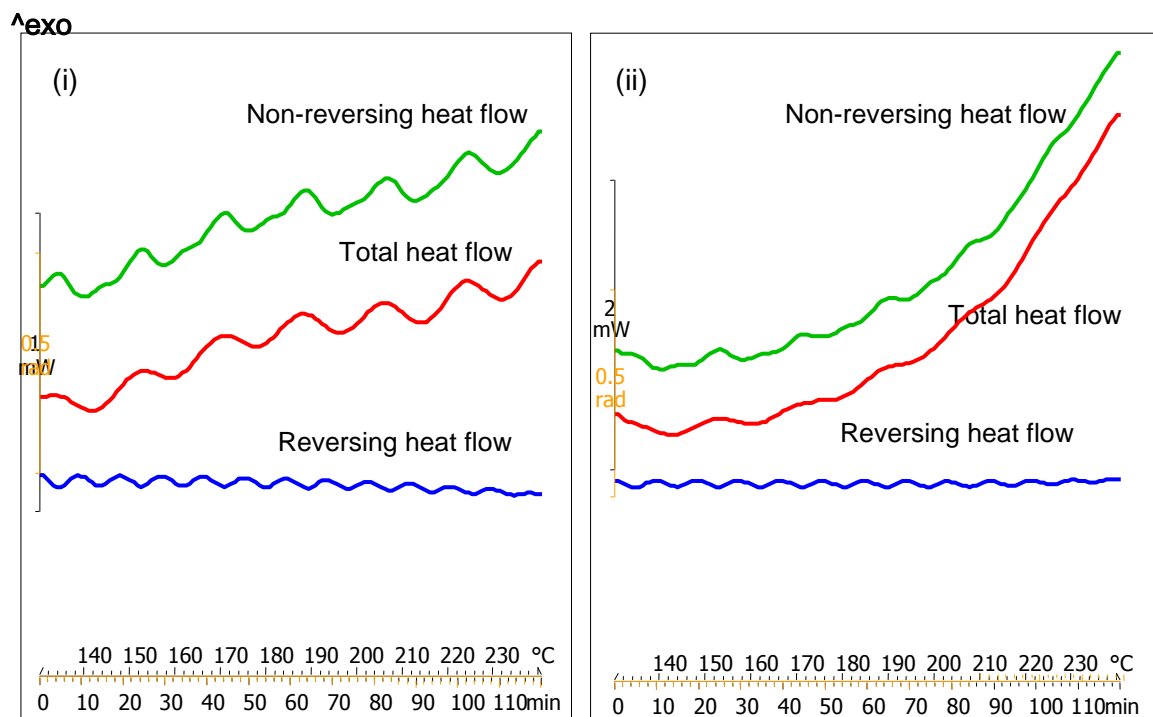


Figure 5.2e: Non-reversing, total and reversing heat flows derived from modulated DSC curves for: **i)** IPEC 0.4 N and; **ii)** IPB 0.4N at temperature range 130-250°C.

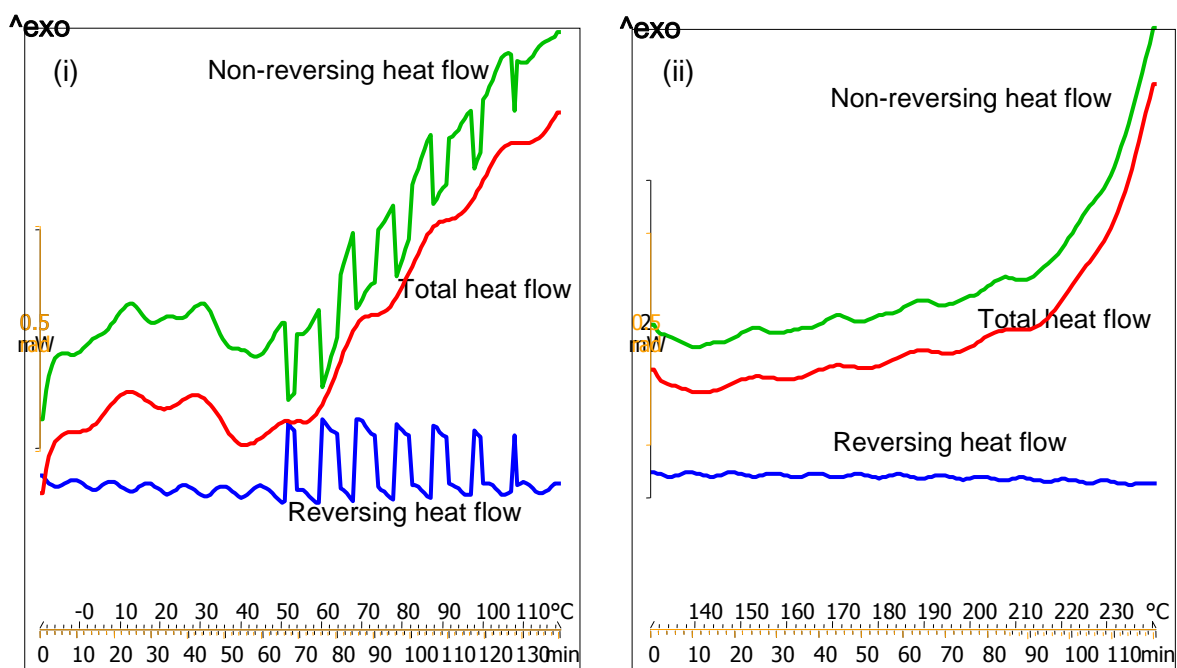


Figure 5.2f: Non-reversing, total and reversing heat flows derived from modulated DSC curves for NaCMC: **i)** temperature range -10 – 130°C and; **ii)** 130 – 250°C.

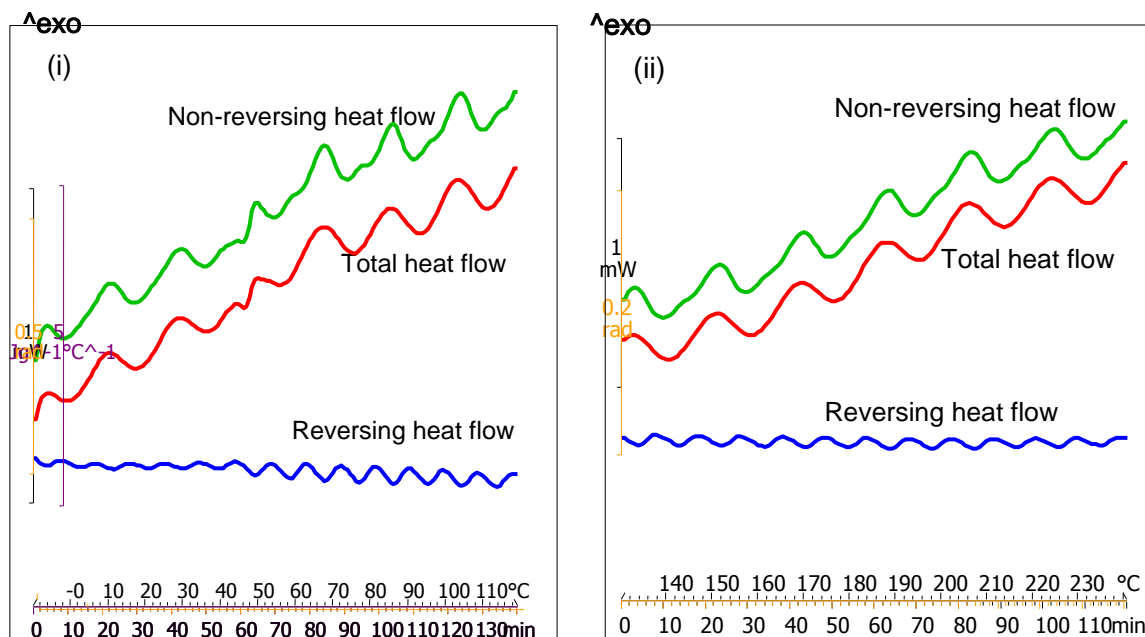


Figure 5.2g: Non-reversing, total and reversing heat flows derived from modulated DSC curves for methacrylate copolymer: **i)** temperature range -10 – 130°C and; **ii)** 130 – 250°C.

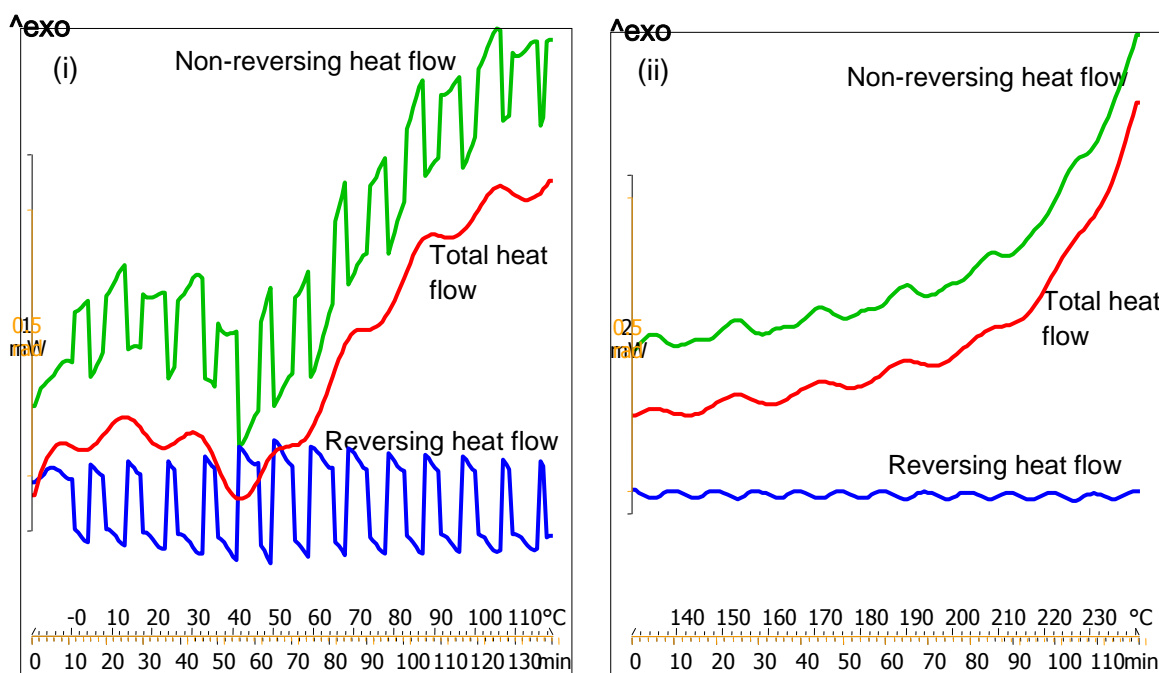


Figure 5.2h: Non-reversing, total and reversing heat flows derived from modulated DSC curves for locust bean: **i)** temperature range -10 – 130°C and; **ii)** 130 – 250°C.

5.3.4. Direct compression of drug-loaded IPEC and interpolymeric blend

The benefits of direct compression have been discussed in Chapter 4, Section 4.3.4. Both IPEC and IPB were directly compressible without any compression enhancing agents and were compatible with the model drug, L-dopa.

5.3.5. Swellability and erosion studies of IPEC and interpolymeric blend matrices

The degree of swelling of both IPEC and IPB (IPEC + locust bean) varied in the different media (Figure 5.3a – 5.3d). Swelling of IPEC in pH 4.5 was about twice its swelling in pH 1.5. Incorporation of locust bean into IPEC decreased the degree of swelling in both media. This is attributed to the fact that the hydrophilic groups of locust bean associated with the existing water bodies of IPEC thereby decreasing the water holding capacity of the hydrophilic pockets of IPEC. The degree of swelling is dependent on pH and the normality of acetic acid used to synthesize IPEC. In summary, as the normality of acetic acid increased from 0.1 to 1.0N, the swelling decreased in both media. In pH 1.5, IPEC and IPB matrices swelled but retained their three dimensional network (Figure 5.4a and 5.4b). However, in pH 4.5 as the matrix swelled, the polymer began to dissociate with evidence of surface erosion. However, with IPEC, rate of swelling exceeded rate of surface erosion. As swelling continued, bulk erosion occurred from the 16th hour as observed during dissolution studies, Chapter 4,

Section 4.3.7. However, in this phase of study, the swelling and erosion studies were set to end at the 8th hour in order to determine final weight after erosion.

In the presence of locust bean, the rate of surface erosion exhibited by IPB exceeded the rate of swelling, and bulk erosion did not occur at any point. This can be seen from Figure 5.3c-d and Table 5.1 which shows the final weight after lyophilization. IPB matrices eroded more than IPEC matrices in pH 4.5 for the different normalities of acetic acid.

Swellability study is undertaken due to its influence of drug release. As a polymer matrix hydrates and swells, the drug diffuses out into the medium. Generally, increase in rate of swelling increases the rate of drug release. This is achieved by the creation of pores by the ingress of solvent into the matrix through which the drug diffuses out after dissolving. Hence, the more the matrix is hydrated, the more the drug dissolves and diffuses out. However, IPEC and IPB matrices did not swell to their maximum in a few hours; they continued to swell throughout the 24 hours of study in pH 1.5 which is indicative that they have the potential to offer a controlled release delivery of drugs and hence reduce frequency of dosage.

The blocking of the pylorus of the stomach is not envisaged due to the inherent ability of IPEC to dissociate with time. The presence of food will increase the pH of the stomach and since IPEC responds to pH, it will begin to dissociate, experience surface erosion and as observed, undergo bulk erosion at some point. The IPB also will not block the pylorus as it degrades by surface erosion over time and so will not be retained permanently in the stomach.

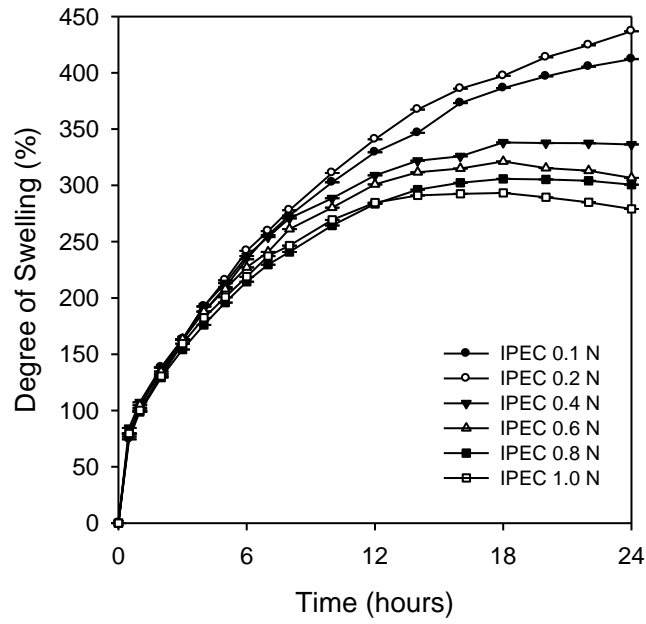


Figure 5.3a: The degree of swelling profiles of IPEC matrices in pH 1.5.

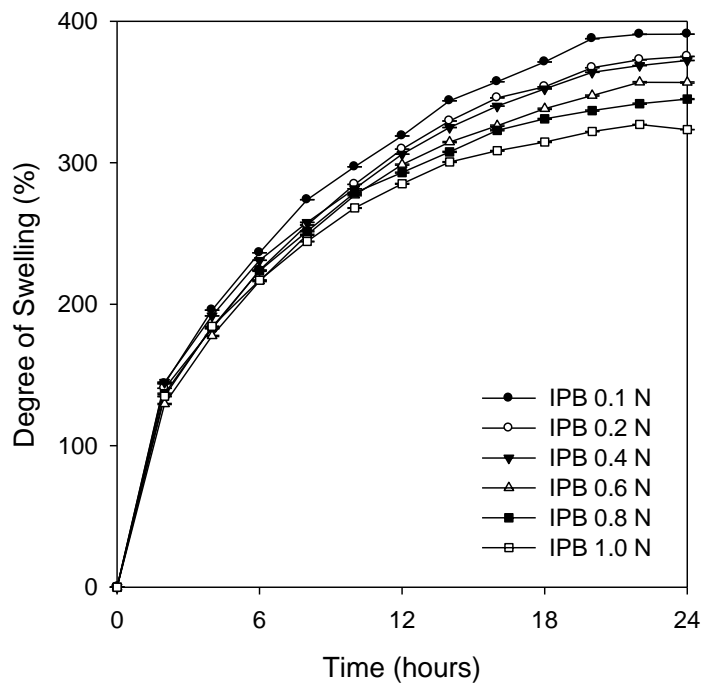


Figure 5.3b: The degree of swelling profiles of IPB matrices in pH 1.5.

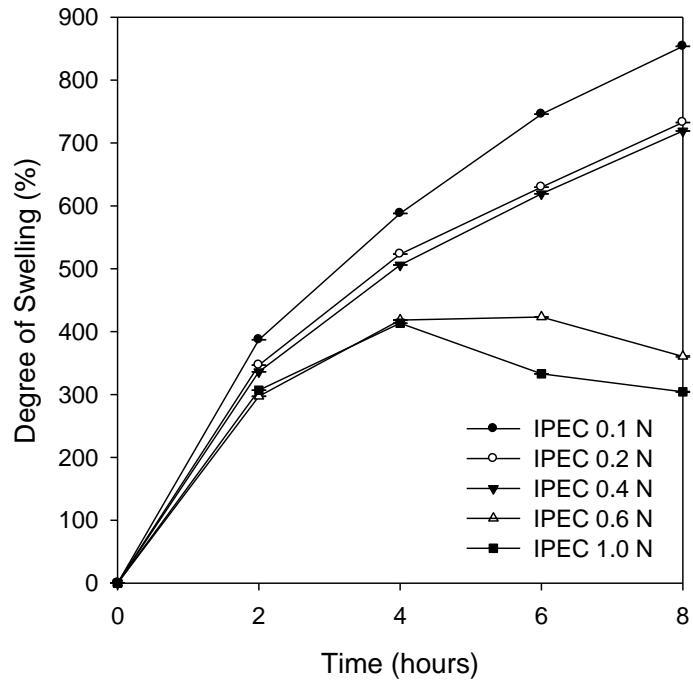


Figure 5.3c: The degree of swelling and erosion profiles of IPEC matrices in pH 4.5.

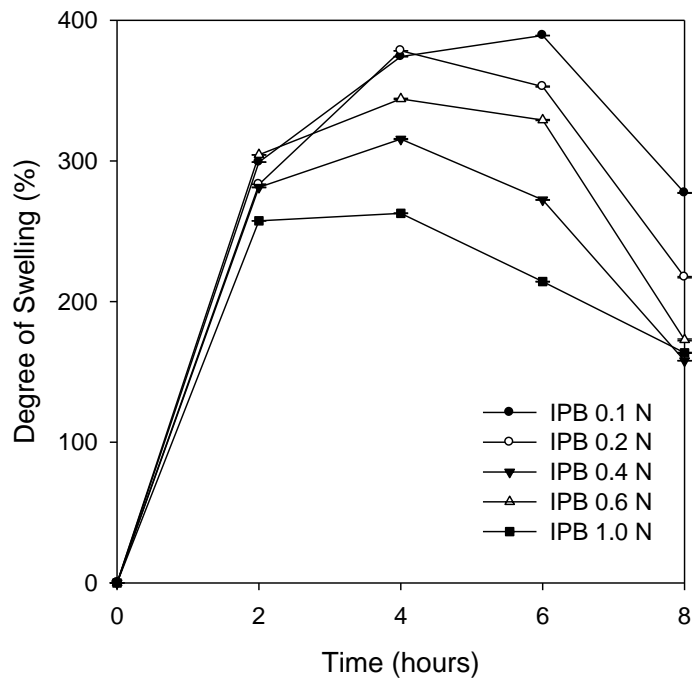


Figure 5.3d: The degree of swelling and erosion profiles of IPB matrices in pH 4.5.

Table 5.1: The degree of erosion (at the 8th hour) in pH 4.5 by gravimetric method.

Polymer composition	Normality of Acetic Acid (N)									
	0.1N		0.2N		0.4N		0.6N		1.0N	
	Initial	Final	Initial	Final	Initial	Final	Initial	Final	Initial	Final
IPEC (mg)	573.2	400.7	570.9	351.2	548.6	336.7	569.7	199.0	554.4	159.9
IPB (mg)	596.8	226.8	588.3	180.8	590.3	173.0	571.2	162.0	582.3	105.7

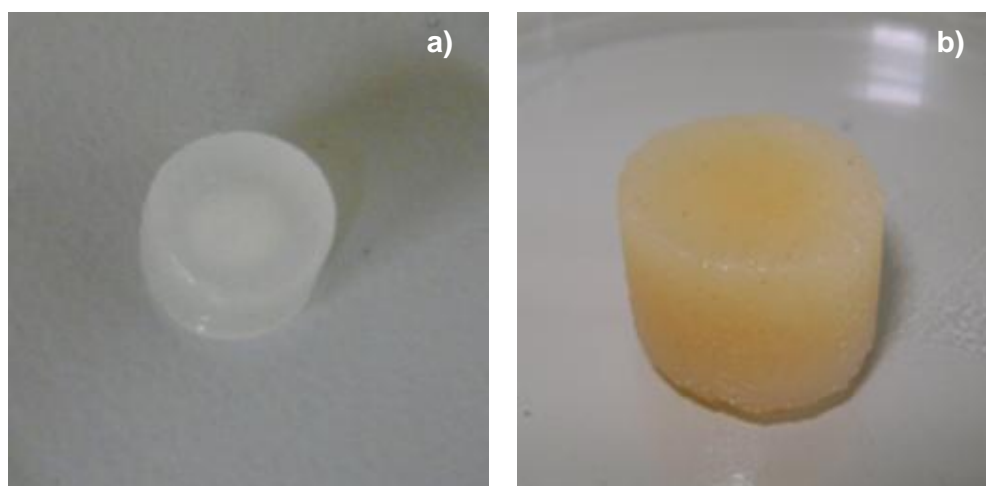


Figure 5.4: Digital images of swollen drug-loaded matrices in pH 1.5 after 24 hours a) IPEC matrix and; b) IPB matrix.

5.3.6. *In vitro* drug release studies and analyses of IPEC and interpolymeric blend matrices

Slight differences in drug release profiles (Figure 5.5a – 5.5d) were observed with the matrices prepared with IPEC and IPB synthesized with different normalities of acetic acid. Rate of release slightly increased as the normality increased. Both IPEC and IPB matrices released L-dopa over 24 hours thereby providing a controlled and prolonged delivery. The linearity of some of the profiles indicated the possible release of L-dopa at a constant rate thereby achieving a constant concentration of the drug over a prolonged period.

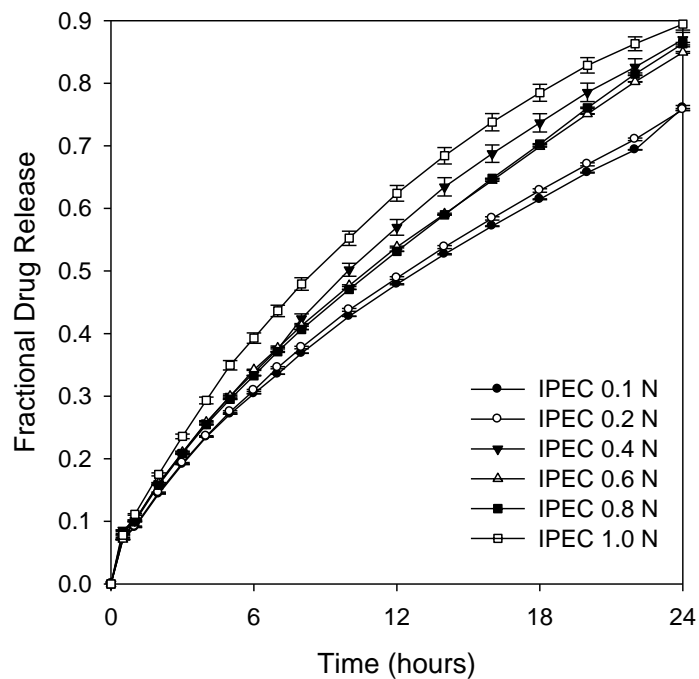


Figure 5.5a: Drug release profiles of IPEC formulations in pH 1.5.

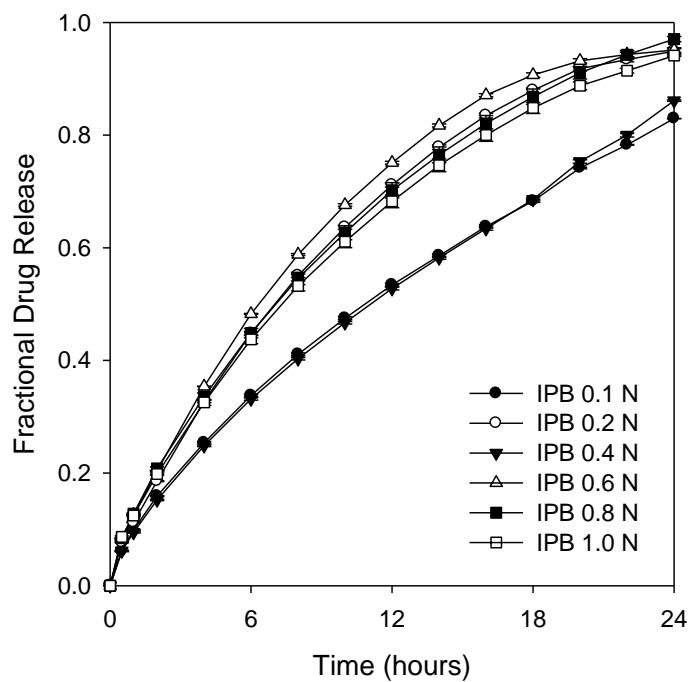


Figure 5.5b: Drug release profiles of IPB formulations in pH 1.5.

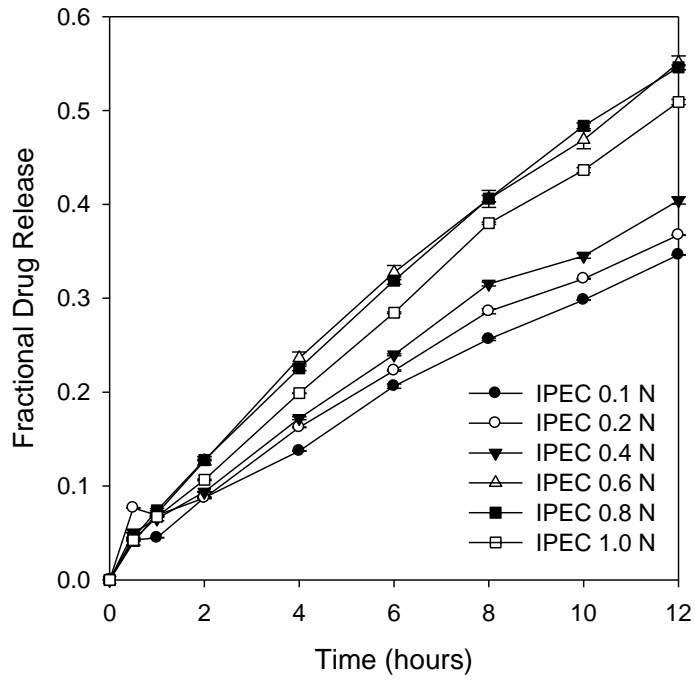


Figure 5.5c: Drug release profiles of IPEC formulations in pH 4.5.

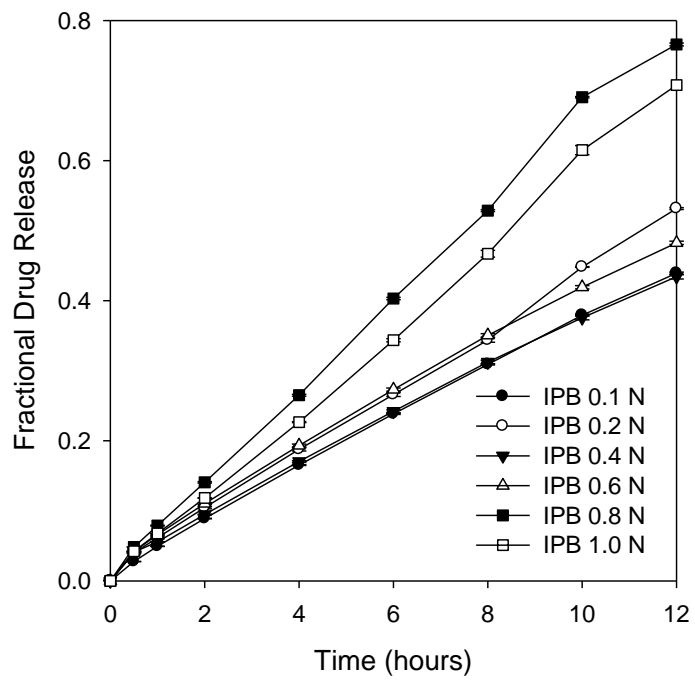


Figure 5.5d: Drug release profiles of IPB formulations in pH 4.5.

To analyze and compare the rates of drug release from IPEC and IPB, mathematical models were employed.

Dissolution Efficiency (DE) is referred to as the area under dissolution time curve within a time frame (t_1 - t_2) and is expressed as percentage of dissolution time curve at maximum dissolution y_{100} over the same time frame (Anderson et al., 1998). Dissolution Efficiency is obtained from Equation 5.1 below:

$$DE = \frac{\int_{t_1}^{t_2} y \cdot dt}{y_{100}(t_2 - t_1)} \times 100$$

Equation 5.1

Where y is the percentage dissolved at time t .

The integral of the numerator which is the area under the curve was calculated using the trapezoidal method:

$$AUC = \sum_{i=1}^{i=n} \frac{(t_i - t_{i-1})(y_{i-1} + y_i)}{2}$$

Equation 5.2

Dissolution efficiency can be employed to determine *in vitro* bioequivalence. The test and reference products can be said to be bioequivalent if the difference between their dissolution efficiencies is within appropriate limits and $\pm 10\%$ is usually used (Anderson et al., 1998). In this study, IPEC formulation was used as reference and it was found out that though IPB had slightly higher dissolution efficiencies (Table 5.2), IPEC and IPB formulations can be said to be bioequivalent and based on rate of drug release, they can be used interchangeably.

The drug release profiles were fitted into zero-order and first-order kinetics and the data are shown in Table 5.3. The zero-order model is simply expressed as:

$$f_t = K_0 t$$

Equation 5.3

Where f_t is the fraction of drug released in time t and K_0 is zero-order constant. The zero-order release constant and the regression squared were obtained by plotting fractional drug released versus time.

First-order model is expressed as:

$$\ln Q_t = \ln Q_0 - K_1 t$$

Equation 5.4

Where Q_t is the amount of drug release in time t , Q_0 is the initial amount of drug in the dissolution medium which is usually zero- and K_1 is the first-order constant. The first-order constant and regression squared were obtained by plotting the log of cumulative quantity remaining [$\log (Q_0 - Q_t)$] versus time.

The best fit model for IPEC and IPB formulations differed in the two dissolution media (Table 5.3). In pH 1.5, the best fit model between zero-order and first-order for IPEC and IPB formulations was first-order with exceptions of IPEC (EC 0.8N; $r^2 = 0.9786$) and IPB (ELC 0.4N; $r^2 = 0.9818$) whose best fit was zero-order. In pH 4.5, the best fit for most of IPEC formulations was first order while the best fit for 3 of IPB formulations was zero-order ($r^2 > 0.997$).

Furthermore, the drug release profiles were fitted into Higuchi and Korsmeyer-Peppas equations and the overall best fit model was obtained for the formulations. Higuchi equation based on Fick's law of diffusion is expressed as:

$$Q = K_H t^{1/2}$$

Equation 5.5

Where Q is amount of drug released per time t and K_H is Higuchi dissolution constant which is obtained by plotting cumulative percentage or fractional drug release versus square root of time (Merchant et al., 2006).

Korsmeyer-Peppas equation as expressed below was employed to evaluate the mechanism of drug release. The equation is used to explicate drug release pattern from polymeric systems when the mechanism of release is not well known or more than one release mechanism is entailed (Sriamornsak et al., 2007).

$$Q_t / Q_\infty = K t^n$$

Equation 5.6

Where Q_t / Q_∞ is the fractional drug release per time t , K is the constant indicating the structural and geometric characteristics of the tablet matrix and n is the release exponent. K and n were obtained in accordance to the equation below by plotting log of percentage drug released (< 60%) against log of time (Merchant et al., 2006).

$$\log[Q_t/Q_\infty] = \log K + n \log t$$

Equation 5.7

For a cylindrical matrix, the release mechanism is Fickian diffusion if $n = 0.45$; non-Fickian release or anomalous transport if $0.45 < n < 0.89$; Case II transport or zero-order release if $n = 0.89$ and Super Case II transport if greater than 0.89 (Merchant et al., 2006; Srimornsak et al., 2007). The values of the release exponent for the formulations are shown in Table 5.3.

The best fit model for most of the formulations was Korsmeyer-Peppas model except IPEC 0.4 and IPEC 1.0 which fitted first-order in pH 4.5; and IPB 0.2 ($r^2 = 0.9983$) and IPB 1.0 ($r^2 = 0.9981$) which fitted zero-order in pH 4.5. One formulation (IPB 0.1N) had n value of 0.89 indicating Case II transport or zero-order release while two formulations (IPB 0.8N and IPB 1.0N) had values of n greater than 0.89. However, the values of n for most of the formulations indicated that their mechanisms of release were anomalous. This is an indication that drug release for these formulations is a combination of mechanisms other than diffusion corroborating experimental observations during dissolution studies.

The release mechanism of IPEC and IPB in pH 1.5 was observed to be a diffusion controlled process which comprises hydration and swelling of matrix; and then dissolution and diffusion of the drug out of the matrix. However, in pH 4.5 the release mechanisms of IPEC matrices were surface and bulk erosion of matrix as well as diffusion-controlled mechanism while that of IPB was surface erosion of matrix and diffusion-controlled mechanism.

As discussed earlier, the degree of swelling was observed to be higher with IPEC formulations than with IPB formulations. However, that the DE of IPB formulations (Table 5.2) were slightly more than those of IPEC formulations indicated the role of other factors apart from swelling.

Table 5.2: Dissolution Efficiency of IPEC and IPB.

Drug Device	DE (%)
IPEC 0.1 N	59.37
IPEC 0.2 N	60.71
IPEC 0.4 N	59.01
IPEC 0.6 N	60.01
IPEC 0.8 N	59.07
IPEC 1.0 N	64.10
IPB 0.1 N	60.58
IPB 0.2 N	67.56
IPB 0.4 N	58.33
IPB 0.6 N	70.25
IPB 0.8 N	65.92
IPB 1.0 N	66.17

Table 5.3: Mathematical modeling of drug release profiles of IPEC and IPB.

Drug device ¹	Zero Order		First order		Higuchi		Korsmeyer-Peppas			Best Fit Model ²
	k_0	r^2	k_1	r^2	K_H	r^2	$K_{KP} (h^n)$	r^2	n	
IPEC 0.1 N (1.5)	0.0287	0.9688	-0.0233	0.9879	15.8654	0.9890	9.1453	0.9996	0.67	Korsmeyer-Peppas
IPEC 0.2 N (1.5)	0.0291	0.9665	-0.0238	0.9948	16.1475	0.9903	9.2406	0.9997	0.67	Korsmeyer-Peppas
IPEC 0.4 N (1.5)	0.0344	0.9687	-0.0356	0.9865	18.9809	0.9847	9.8901	0.9989	0.70	Korsmeyer-Peppas
IPEC 0.6 N (1.5)	0.0328	0.9724	-0.0320	0.9776	18.1128	0.9881	10.1321	0.9998	0.67	Korsmeyer-Peppas
IPEC 0.8 N (1.5)	0.0335	0.9786	-0.0338	0.9689	18.3049	0.9837	9.9289	1.0000	0.68	Korsmeyer-Peppas
IPEC 1.0 N (1.5)	0.0351	0.9487	-0.0398	0.9921	19.8822	0.9921	10.9623	0.9993	0.71	Korsmeyer-Peppas
IPB 0.1 N (1.5)	0.0331	0.9737	-0.0294	0.9887	17.6874	0.9909	9.9403	0.9998	0.68	Korsmeyer-Peppas
IPB 0.2 N (1.5)	0.0401	0.9365	-0.0540	0.9899	21.8141	0.9893	11.1250	0.9995	0.77	Korsmeyer-Peppas
IPB 0.4 N (1.5)	0.0341	0.9818	-0.0316	0.9696	18.0674	0.9857	9.4820	0.9999	0.69	Korsmeyer-Peppas
IPB 0.6 N (1.5)	0.0402	0.9155	-0.0570	0.9938	22.0765	0.9858	12.4366	0.9993	0.75	Korsmeyer-Peppas
IPB 0.8 N (1.5)	0.0397	0.9462	-0.0571	0.9604	21.5507	0.9941	12.8027	1.0000	0.70	Korsmeyer-Peppas
IPB 1.0 N (1.5)	0.0386	0.9452	-0.0485	0.9869	20.9589	0.9936	12.3396	0.9998	0.70	Korsmeyer-Peppas
IPEC 0.1 N (4.5)	0.0281	0.9904	-0.0147	0.9980	13.2243	0.9579	4.7087	0.9985	0.80	Korsmeyer-Peppas
IPEC 0.2 N (4.5)	0.0289	0.9777	-0.0152	0.9926	13.3739	0.9629	5.9786	0.9927	0.73	Korsmeyer-Peppas
IPEC 0.4 N (4.5)	0.0328	0.9865	-0.0178	0.9959	14.9610	0.9607	6.3900	0.9903	0.74	First order
IPEC 0.6 N (4.5)	0.0454	0.9898	-0.0281	0.9986	22.3562	0.9539	7.2444	0.9987	0.83	Korsmeyer-Peppas
IPEC 0.8 N (4.5)	0.0454	0.9924	-0.0282	0.9993	20.1442	0.9743	7.3519	0.9996	0.82	Korsmeyer-Peppas
IPEC 1.0 N (4.5)	0.0421	0.9946	-0.0252	0.9976	19.5963	0.9641	6.3533	0.9967	0.84	First order
IPB 0.1 N (4.5)	0.0365	0.9979	-0.0207	0.9986	17.6469	0.9555	4.8674	0.9999	0.89	Korsmeyer-Peppas
IPB 0.2 N (4.5)	0.0430	0.9983	-0.0262	0.9845	18.6198	0.9679	5.8803	0.9975	0.86	Zero order
IPB 0.4 N (4.5)	0.0356	0.9960	-0.0200	0.9990	16.4104	0.9678	5.4200	0.9995	0.84	Korsmeyer-Peppas
IPB 0.6 N (4.5)	0.0396	0.9949	-0.0232	0.9990	17.6911	0.9736	6.4240	0.9995	0.81	Korsmeyer-Peppas
IPB 0.8 N (4.5)	0.0650	0.9974	-0.0524	0.9705	24.5343	0.9733	7.6666	0.9986	0.92	Korsmeyer-Peppas
IPB 1.0 N (4.5)	0.0591	0.9981	-0.0437	0.9680	22.7318	0.9741	6.4938	0.9973	0.93	Zero order

¹ Insertions in parenthesis indicate the dissolution media used; 1.5 and 4.5 are indicative of buffers pH 1.5 and 4.5

² Best fit models were determined using correlation coefficient, r^2

5.3.7. Molecular modeling simulations

5.3.7.1. Elucidation of stabilization of IPEC using atomistic simulations

First, the inherent mechanism involved in the formation of the IPEC employing equations 3.5-3.8 (Chapter 3, Section 3.3.7.1.) and Table 5.4 will be discussed. The monomer length for the polymer chain depicting molecular structures of the polymers were determined on the basis of equivalent grid surface area covered by the polymers so that the inherent stereo-electronic factors at the interaction site can be perfectly optimized. The set of low-energy conformers that were in equilibrium with each other was identified and portrayed as the lowest energy conformational model.

Molecular modelling studies accounted for specific interactions between polymer segments and provided an estimate that the two polymers (E100 and CMC) form a stable combination as they fulfil the necessary condition for the favourable interaction of a mixture of two polymers by having a negative free energy of mixing (Tiller and Gorella, 1994). As evident from Equations 3.5-3.8 and Table 3.2, a potential and steric energy stabilization of -24.753kcal/mol was associated with the formation of the IPEC. This confirmed the favourable formation and stability of the IPEC in the unhydrated state. The energy computations/stabilization involved significant contribution from non-bonding interactions in the form of van der Waals forces ($\Delta E = -25.575\text{kcal/mol}$) and H-bonding ($\Delta E = -2.154\text{kcal/mol}$) and small but important contributions from bond stretching contributions ($\Delta E = -0.858\text{kcal/mol}$), bond angle contributions ($\Delta E = -1.096\text{kcal/mol}$), and torsional contributions ($\Delta E = -0.558\text{kcal/mol}$). These underlying chemical interactions may cause conformational changes responsible for physicochemical characteristics of the composites. The energy minimization seem inherent from rotation of saccharide and acrylate residues relieving strain due to steric interactions. However, this strain was further relieved by the inclusion of bond length and angle adjustment with respect to the degrees of freedom of the system which in turn may lead to the formation of H-bonds between CMC and E100, as displayed in Figure 5.6. In addition, the steric interactions may cause pendent aliphatic groups of E100 and hydroxyl and carboxyl groups of CMC to overcome torsional barriers presenting a larger accessible potential energy surface. This may lead to formation of an interconnected polymeric network structure providing the necessary physicochemical properties to the IPEC. The formation of a highly rigid structure instead of a continuous polymer structure may be due to this intercrosslinked network which led to the shredded nature of the novel material as shown in optical figure earlier in Chapter 4, Figure 4.1. A close look at Figure 5:6b reveals a highly crosslinked network structure where the H-bond lengths are in the range from 1.7678\AA to 2.8443\AA averaging 2.076\AA confirming strong hydrogen bonding interactions (Kumar et al., 2011).

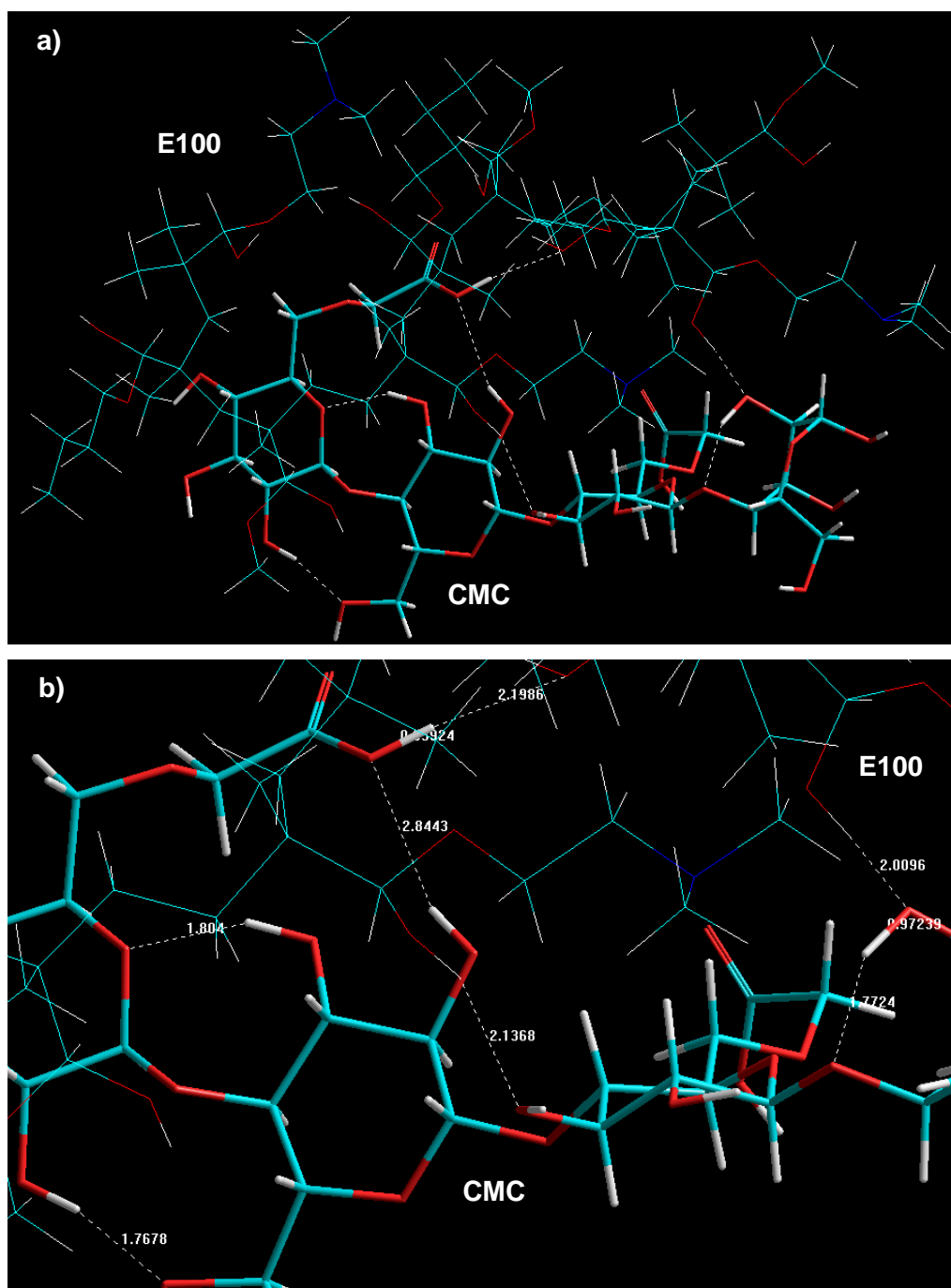


Figure 5.6: Visualization of geometrical preferences of **a)** CMC-E100 and; **b)** magnified view of CMC-E100 along with H-bond lengths after molecular simulation in vacuum. Color codes: C (cyan), O (red), N (blue) and H (white).

In addition, the molecular attributes (Table 5.4) also revealed the stabilized structural properties of the formed IPEC as follows:

1. The polarizability and refractivity values were lower than the respective summation values of the individual systems which may be due to induced dipoles in IPEC due to non-bonded attractive forces where the binding energy changes were further proportional to the polarizability of the substituents, which are in turn proportional to molar refractivity values. IPEC is hence highly stabilized as the structure with lower index of refraction is more stable (Ndesendo et al., 2011).
2. The volume of the polymer fractions as well as the solvent-accessible surface decreased during the reaction process. The surface-to-volume ratio (SVR) was calculated to be 0.400 which is significantly lower than the individual polymer systems. Lower SVR value in case of IPEC further confirms the higher stabilization as the lower the SVR, the more stable is the structure. The decrease in the molecular size may be related to the ordering of polysaccharide fraction, which usually accompanied with a lowering in steric energy (Tian et al., 2010).
3. Initial model building using a density derived from the average of the pure systems revealed that for the IPEC molecular system, a substantial increase in density was observed as compared to the average of the individual molecules involved, with the density going from 0.433 through 0.366 to 0.442 amu/Å³ for CMC, E100, and CMC-E100, respectively. This density increase is in agreement with the occurrence of specific interchain interactions leading to the perfect interactive miscibility between the polymer molecules (Abou-Rachid et al., 2008).

Table 5.4: Computational molecular attributes calculated for the simulated IPEC system in a molecular mechanics' force field setup performed using HyperChemTM 8.0.8 (Hypercube Inc., Gainesville, FL). See Equations 3.3, 3.4 and 3.8 for reference.

Molecular attributes	CMC	E100	IPEC (summation) ⁴
Energy (kcal mol ⁻¹) ¹	-9.605	100.577	66.219 (90.972)
$\Delta E_{\text{interaction}}$ ²	-	-	-24.753
Polarizability (Å ³)	63.88	138.59	198.01 (202.47)
Refractivity (Å ³)	154.83	343.89	470.96 (498.72)
Volume (Å ³)	1804.43	3474.27	4644.63 (5278.7)
Surface area (grid)	1002.06	1621.61	1858.52 (2623.67)
SVR ³	0.555	0.466	0.400 (0.497)
Mass (a.m.u.)	782.66	1271.83	2054.48 (2054.49)
Density (amu/Å ³)	0.433	0.366	0.442 (0.389)

¹ Minimized global energy for an optimized structure

² $\Delta E_{\text{interaction}} = E(\text{Host.Guest}) - E(\text{Host}) - E(\text{Guest})$

³ Surface-to-volume ratio

⁴ summation of individual values in parentheses wherever applicable

5.3.7.2. Elucidation of stabilization of IPEC using dynamic simulations

Molecular dynamic simulation was successfully used to further investigate the energy profile of interactions between the functional groups in the CMC and E100. Figure 5.7 represents the main energy attributes inherent to the formation and properties of IPEC. From Figure 5.7, it was observed that by 1000 time-steps, the potential (EPOT) and kinetic energy (EKIN) were fluctuating about equilibrium values. The atoms vibrate about fixed positions as a result of their thermal energy, and give rise to the graphs in Figure 5.7 depicting typical solid-type behaviour. In the case of CMC, EKIN and EPOT displayed equivalent values as evident from the energy overlap in Figure 5.7a. However, E100 displayed a significant difference among the constituent energies. The final total energy (ETOT) value in case of IPEC was stabilized by ~25kcal/mol further confirming the computational results (formation and conformation) obtained in Molecular Mechanics simulations (Table 5.5). The energy minimization is mainly due to potential energy changes which are evident from the EPOT_{IPEC} displaying a significant fluctuation owing to the interaction among the atoms of CMC and E100 which is also evident from oscillatory form of EKIN_{IPEC}. Furthermore, the total energy varied in direct proportionality to kinetic energy confirming the presence of a spring-mass system in IPEC which is in good corroboration with the resilience results obtained during experimental investigations. Interestingly, it was found that the potential energy decreased with an increase in the kinetic energy, obeying the well known behaviour of a high underdamping harmonic oscillator.

Table 5.5: Energy attributes calculated for the simulated IPEC system in a molecular dynamics setup performed using HyperChem™ 8.0.8 (Hypercube Inc., Gainesville, FL).

Molecule	Energy (kcal/mol)		
	EKIN	EPOT	ETOT
CMC	42.869	38.083	81.957
E100	85.777	222.858	308.636
IPEC	128.313	236.602	364.915 (-25.678) ¹

$$^1 \Delta E_{\text{Total(IPEC)}} = E_{\text{Total(IPEC)}} - (E_{\text{Total(CMC)}} + E_{\text{Total(E100)}})$$

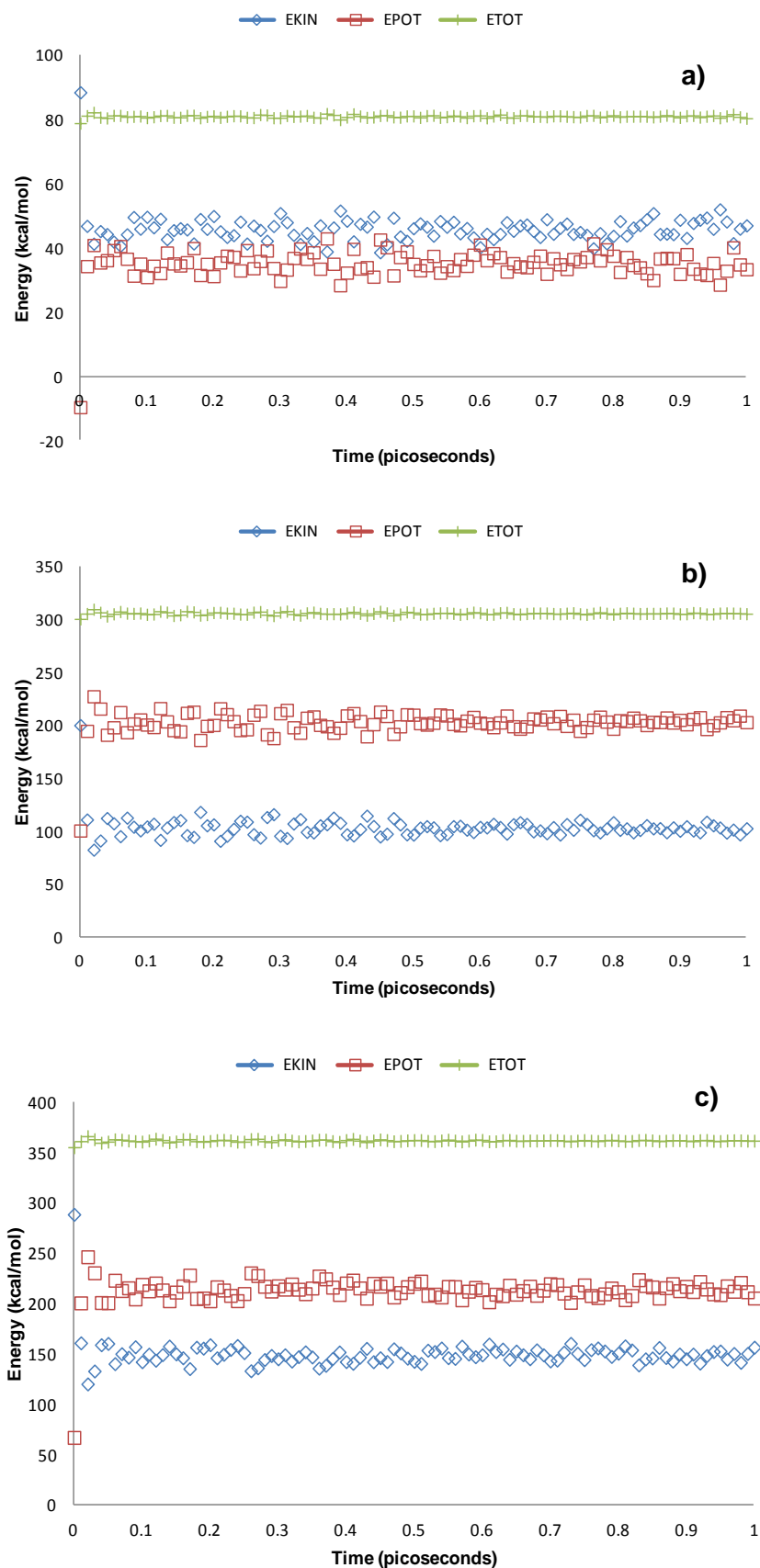


Figure 5.7: Kinetic energy (EMIN), potential energy (EPOT), total energy (ETOT) (kcal/mol), and temperature (Kelvin) varying with the time of **a)** CMC; **b)** E100 and; **c)** IPEC.

5.3.7.3. Molecular mechanics energy relationship analysis

Molecular mechanics energy relationship (MMER) has been explained in Chapter 3, Section 3.3.7. In the present static lattice atomistic simulations (SLAS) study, a set of three compounds were used to build the energy models for the polysaccharide-polyelectrolytic systems (IPB) (Figure 5.8 and 5.9). The synthesis and stability properties of the IPEC entities that may vary with the addition of a polysaccharide were studied using the static system. The global energy relationships for the various complexes derived after assisted model building and energy refinements are as follows:

$$E_{\text{CMC}} = -9.605 V_{\Sigma} = 3.024 V_b + 19.746 V_{\theta} + 32.574 V_{\varphi} + 8.459 V_{ij} - 1.759 V_{hb} - 71.649 V_{el} \dots (5.8)$$

$$E_{\text{E100}} = 100.577 V_{\Sigma} = 10.018 V_b + 45.058 V_{\theta} + 13.454 V_{\varphi} + 32.052 V_{ij} - 0.006 V_{hb} \dots (5.9)$$

$$E_{\text{LBG}} = -22.539 V_{\Sigma} = 4.04 V_b + 35.144 V_{\theta} + 45.613 V_{\varphi} + 14.835 V_{ij} - 2.435 V_{hb} - 119.737 V_{el} \dots (5.10)$$

$$E_{\text{CMC-E100}} = 66.219 V_{\Sigma} = 12.184 V_b + 63.708 V_{\theta} + 45.47 V_{\varphi} + 14.936 V_{ij} - 3.919 V_{hb} - 66.161 V_{el} \dots (5.11)$$

$$\Delta E = -24.753 \text{kcal/mol}$$

$$E_{\text{CMC-LBG}} = -87.263 V_{\Sigma} = 6.820 V_b + 55.229 V_{\theta} + 76.693 V_{\varphi} + 15.037 V_{ij} - 8.990 V_{hb} - 232.054 V_{el} \dots (5.12)$$

$$\Delta E = -55.119 \text{kcal/mol}$$

$$E_{\text{E100-LBG}} = 28.054 V_{\Sigma} = 12.970 V_b + 70.909 V_{\theta} + 62.175 V_{\varphi} + 22.328 V_{ij} - 3.920 V_{hb} - 136.41 V_{el} \dots (5.13)$$

$$\Delta E = -49.984 \text{kcal/mol}$$

$$E_{\text{CMC-E100-LBG}} = -19.775 V_{\Sigma} = 15.997 V_b + 93.049 V_{\theta} + 92.646 V_{\varphi} + 11.775 V_{ij} - 8.897 V_{hb} - 224.347 V_{el} (5.14)$$

$$\Delta E = -88.208 \text{kcal/mol}$$

In addition, the total potential energy deviation, ΔE_{total} , was calculated as the difference between the total potential energy of the complex system and the sum of the potential energies of isolated individual molecules, as follows:

$$\Delta E_{\text{Total(A/B)}} = E_{\text{Total(A/B)}} - (E_{\text{Total(A)}} + E_{\text{Total(B)}}) \dots (5.15)$$

The molecular stability can then be estimated by comparing the total potential energies of the isolated and complexed systems. If the total potential energy of complex is smaller than the sum of the potential energies of isolated individual molecules in the same conformation, the complexed form is more stable and its formation is favoured (Yu et al., 2008).

5.3.7.4. 3D-computational modeling for polymer-polymer complexes

The alteration in the performance of IPEC after addition of a polysaccharide, locust bean gum led to modeling of the IPB based on conformational analysis. It is hypothesized that these changes might have been brought upon by the presence of a “structurally defined macromolecular complex”. The measured differences in terms of swelling, erosion and drug release studies of the polymeric matrices may depend on confound geometry and the extent of network innervations and may require geometrically proportional networks for all simulations to systematically control and isolate the effects of a given parameter. Therefore, to carry out the static lattice atomistic simulations for the polymer-polymer complexes in vacuum, the three representative networks shown in Figure 5.8 and 5.9 were used for the measurements and randomly disposed CMC, LBG, and E100 around each other to form

interaction complexes viz. CMC/E100, CMC/LBG, E100/LBG, and CMC/E100/LBG to fully understand the effect of interaction of LBG.

It is evident from Equations 5.8-5.14, that the formation of CMC-E100, CMC-LBG, E100-LBG, and CMC-E100-LBG (in vacuum) was accompanied by energy stabilization of -24.753kcal/mol, -55.119kcal/mol, -49.984kcal/mol and -88.208kcal/mol, respectively. Molecular modeling studies can account for specific interactions between polymer segments and may provide an estimate of whether two polymers will form a compatible blend and a necessary condition for the miscibility of a mixture of two polymers is a negative free energy of mixing (Tiller and Gorella, 1994). This negative free energy of blending of IPEC (CMC-E100) with LBG confirms the results observed from thermal transitions (Section 5.3.3 and Figure 5.2c) where it was proposed that the blend may be miscible.

Table 5.6: Computational differential energy attributes calculated for the simulated IPEC/LBG system in a molecular mechanics' force field setup performed using HyperChem™ 8.0.8 (Hypercube Inc., Gainesville, FL).

Name	$\Delta E_{\text{Total}}^1$	ΔE_{Bond}	ΔE_{Angle}	$\Delta E_{\text{Dihedral}}$	ΔE_{Vdw}	$\Delta E_{\text{H-bond}}$	ΔE_{Elec}
CMC-E100	-24.753	-0.858	-1.096	-0.558	-25.575	-2.154	5.488
CMC-LBG	-55.119	-0.244	0.339	-1.494	-8.257	-4.796	-40.668
E100-LBG	-49.984	-1.088	-9.293	3.108	-24.559	-1.479	-16.673
CMC-E100-LBG	-88.208	-1.085	-6.899	1.005	-43.571	-4.697	-32.961

¹ ΔE calculated with in comparison to the energy values of the constituent molecules.

This confirms the compatibility of the polymers and stability of the hydrogel in unhydrated state. Furthermore, the energy data displays the involvement of both bonding and non-bonding interactions (Table 5.6). The formation of CMC-E100 has been described Chapter 3, Section 3.3.7 and here only the influence of addition of LBG is explained. The introduction of LBG provided additional interaction sites in the matrix system. CMC-LBG, stabilized by all energies except angle contributions, displayed -O...H...O...H...O- hydrogen bonding interactions. However, E100-LBG, stabilized by all constituent energies except torsional contributions, relied mainly on O-H...O-H bonding conformations. Interestingly, the addition of LBG to CMC-E100 formed a highly stabilized structure with constituent H-bonding interaction of all bi-polymeric complexes. A closer look at the tripolymeric matrix system conveys the ability of LBG to act as a linker between E100 and CMC with intermolecular hydrogen bondings occurring between E100 side chains and LBG oxygen atoms and between oxygen atoms belonging to the two polysaccharide polymers (NaCMC and LBG). LBG side chains are in an intermediate disposition between the E100 and CMC stretched arrangement moving away the polysaccharide symmetry to improve the intermolecular

interactions. In addition, some intramolecular hydrogen bonds are also maintained. These underlying chemical interactions may cause torsional and geometrical changes responsible for compactness and resilient characteristics of the composites. The energy minimizations were inherent from rotation of monosaccharide residues (LBG) producing strain due to steric interactions (angle in CMC-LBG and torsional in E100-LBG and tripolymer) which in turn are relieved by the inclusion of non-bonding adjustments. These steric adjustments lead to formation of H-bonds and hence a dense polymeric matrix showing reduced swelling at either pH values as described in the experimental section. This compactness may further lead to a centralized matrix hardness making the surface more vulnerable to aqueous media as compared to the core (Figure 5.9b). This may further lead to a two-dimensional surface erosion instead of three-dimensional bulk erosion as discussed in the experimental Section 5.3.5.

Although the polymeric complexes are stabilized by non-bonding interactions, the inherent bonding interaction in the form of slightly higher torsional energies in CMC-E100-LBG may induce degradation of the polymeric matrix in a quest to attain further energy stabilization on hydration. This makes the IPB complexes vulnerable to early release of drug due to diffusion of water molecules inside the torsional restraints. These observations are in line with the experimental results wherein slight increased release rates were observed from LBG-IPEC (Section 5.3.6 and Figure 5.5).

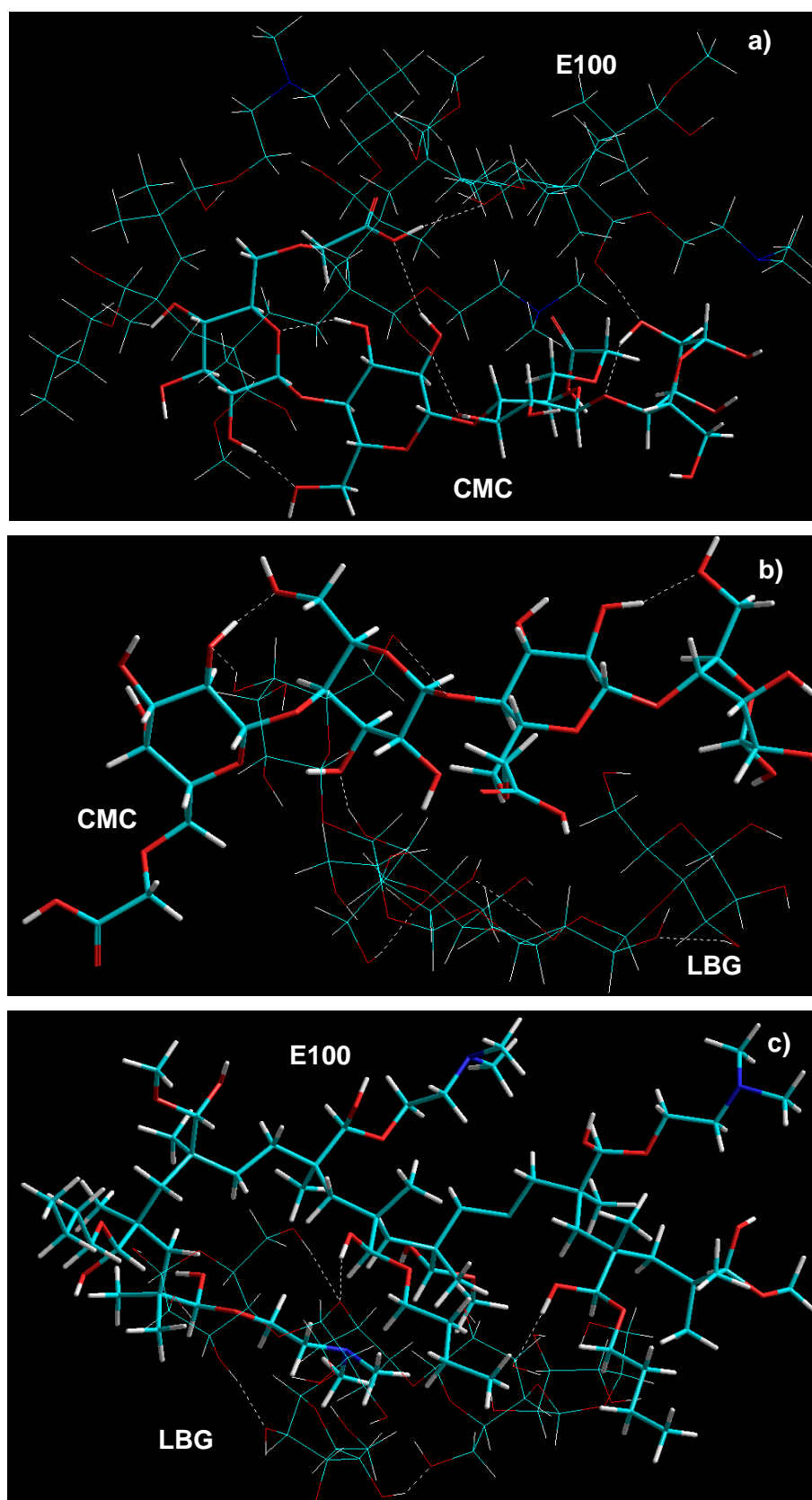


Figure 5.8: Visualization of geometrical preference of **a)** CMC in complexation with E100; **b)** CMC in complexation with LBG and; **c)** E100 in complexation with LBG, after Molecular Mechanics simulations. Color codes: C (cyan), O (red), N (blue) and H (white).

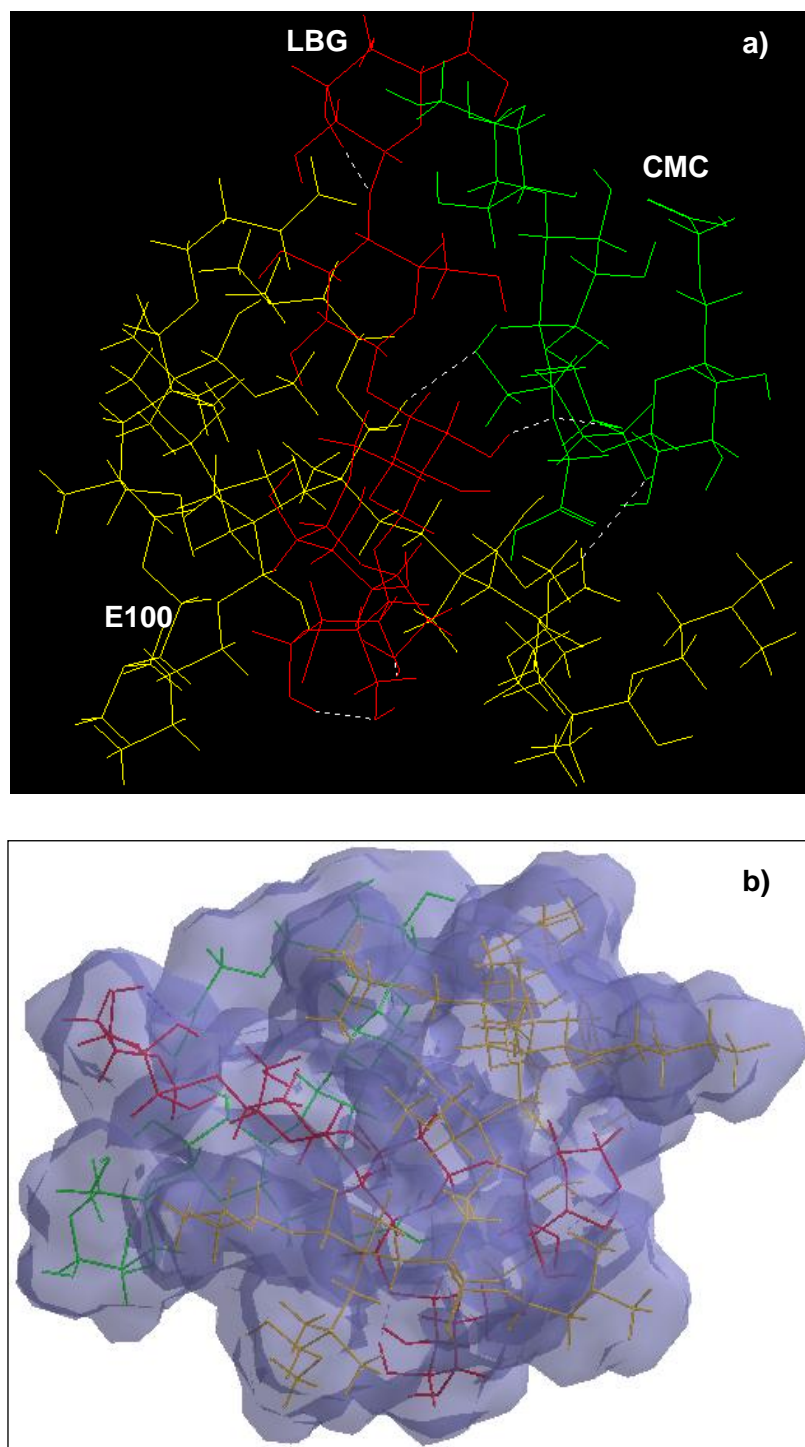


Figure 5.9: Visualization of geometrical preference of **a)** CMC-E100-LBG tripolymeric complex and; **b)** Connolly molecular electrostatic potential surfaces in translucent display mode showcasing the matrix compactness, after Molecular Mechanics simulations. Color codes: CMC (green), LBG (red), and E100 (yellow).

5.4. CONCLUDING REMARKS

Computational modeling methods were used for the prediction of preferred molecular conformations polymer-polymer complexes using force field minimizations and the modes of interaction were envisaged in relation to experimental results. The interactions between NaCMC and methacrylate copolymer were elucidated with MMER and MDS and the computational results revealed a highly crosslinked network structure based mainly on van der Waals forces and strong hydrogen bonding interactions. Furthermore, the computational results corroborated with the experimental and analytical results. For instance, the total energy elucidated by MDS confirmed the presence of spring-mass system in IPEC which corroborated with the physicomechanical results. Addition of locust bean to IPEC formed a highly stabilized structure leading to a centralized hardness making its surface more vulnerable to erosion than the core. Therefore, the introduction of locust bean modified the IPEC by reducing its excessive swelling and prevented its degradation by bulk erosion, but enhanced surface erosion. Furthermore, it slightly improved its dissolution efficiency and upgraded the linearity of the drug release profile close to 1 (0.99); thus producing a zero-order release. Hence, due to these attributes, IPB will be chosen over IPEC for formulation and characterization of a gastroretentive drug delivery system for the delivery of L-dopa in the next Chapter.

CHAPTER SIX

APPLICATION OF INTERPOLYMERIC BLEND IN FORMULATION OF TRIPLE-MECHANISM GASTRORETENTIVE DRUG DELIVERY SYSTEM

6.1. INTRODUCTION

Having chosen the interpolymeric blend to employ in developing a drug delivery device, the next stage of the research commenced with the development and characterization of a gastroretentive drug delivery system for the administration of narrow absorption window drugs such as L-dopa.

Initially, the traditional dosage forms were employed for practically all oral drugs. However, with time, they were noted to be more suitable for drugs that are absorbed all through the gastrointestinal tract (GIT) as it was observed that there are drugs such as levodopa, ciprofloxacin, furosemide, celiprolol hydrochloride and riboflavin that have specific sites of absorption within the GIT. Consequently, as the traditional dosage forms navigate the GIT, the absorption and bioavailability of these drugs are reduced which otherwise could be enhanced by some form of delay at their absorption sites (specifically the stomach and the upper small intestine). The site specificity for absorption is due to the low solubility of the drugs at the pH found in the lower GIT, enzymatic breakdown; drug degradation by microflora in the colon, chemical instability of the drug and binding of drug to the contents of the GIT (Rouge et al., 1996). Hence, pharmaceutical technologies that can ensure continuous and prolonged administration at these sites by increasing the gastric residence time in order to improve bioavailability is preferred to the traditional dosage forms.

Over the decades, efforts have been made to improve the absorption and bioavailability of drugs with specific sites of absorption by developing controlled release gastroretentive drug delivery systems (CR-GRDDS). Most drugs are absorbed at the proximal small intestine; hence CR-GRDDS are developed to retain such drugs in the stomach over prolonged period above the absorption window of these drugs to ensure absorption. CR-GRDDS for narrow absorption window drugs are able to improve the absorption and bioavailability of these drugs over a prolonged period, reduce frequency of dosing, targets drugs required at the stomach or proximal small intestine; reduce erratic concentrations of drugs and adverse effects; and enhance therapeutic efficacy (Hoffman et al., 2004; Arza et al., 2009).

Gastroretentive approaches employed include floating (Dave et al., 2004; Arza et al., 2009), concurrent administration of drugs (Hoffman et al., 2004), bioadhesion (Singh et al., 2006), swelling (Park and Kim, 2006), density of drug delivery system, superporous hydrogels and expandable gastroretentive dosage forms (Ahmed and Ayres, 2007).

Floating drug delivery systems are systems that are able to achieve buoyancy and float on gastric contents. A drug delivery system with density below the gastric content which has density of 1.004g/cm^3 (Bardonnet et al., 2006; Patel et al., 2009) will float on the gastric content and one way of achieving this is by incorporation of a gas-generating agent such as sodium bicarbonate (Dave et al., 2004). Another approach is the use of floatable polymers to formulate hydrodynamically balanced systems (HBS). The polymers which are mainly hydrocolloids float by the presence of entrapped air within the swelling-hydrated boundary layer formed by the hydrocolloids (Talukder and Fassihi, 2004). Other floating strategies include multiple unit system with incorporated air compartment (Iannuccelli et al., 1998); low density foam powder enabled floating microparticles (Streubel et al., 2002; Streubel et al., 2003) and microballoons (Jain et al., 2008). One of the drawbacks of floating drug delivery systems is that it requires the presence of fluid so as to float on gastric content. Also drugs that are unstable at gastric pH are not viable candidates to formulate as floating drug delivery systems (Arora et al., 2005).

High density systems are fabricated such that they sink to the antrum of the stomach where they are retained for a prolonged period for improved absorption of narrow absorption window drugs. The density determines the gastric residence of the system and its capability to withstand peristalsis (Chawla et al., 2003). The recommended density required for the system to be retained at the antrum of the stomach varies from 1.3 to 2.8g/mL (Chawla et al., 2003; Talukder and Fassihi, 2004; Bardonnet et al., 2006). High density systems can be achieved by incorporating inert diluents such as barium sulphate, zinc oxide, titanium dioxide and iron powder (Singh and Kim, 2000). Although a number of high density drug delivery systems have been developed over the decades, which proved encouraging in animal models, significant benefits were not observed in human and none have been commercialized (Rouge et al., 1998; Bardonnet et al., 2006).

Bioadhesion or mucoadhesion is the ability of a substance to adhere to a biological surface (mucus) for a prolonged period with resultant increase in absorption and subsequent bioavailability of the drug incorporated within. This gastroretentive mechanism, apart from prolonging gastric residence time of drug, can be employed for targeting and localization of drugs at specific sites (Deshmukh et al., 2009; Jain and Jangdey, 2009). For bioadhesive polymers to effectively adhere to the mucus of the GIT, the stomach for instance, they would undergo hydration, swelling and interaction or interpenetration with the mucus or epithelial surfaces (Singh et al., 2006; Mahalingam et al., 2009). The concept of bioadhesion has been utilized *in vitro* and *in vivo* in animal models. However, the successes have not been translated into humans; one of the challenges being the quick turnover of the mucus in humans (Davis, 2005).

A swelling system is a polymeric system that hydrates and swells beyond the size of the opening of the pylorus enabling it to be retained in the stomach. The degree of crosslinking within the polymeric network affects the swelling, mechanical strength and dissolution of the system (Chawla et al., 2003) which in turn determines the rates and patterns of drug release. Its controlled release properties can be enhanced by good mechanical properties to help withstand peristalsis and other forces within. The swelling properties of polymers allow them to be used as GRDDS providing sustained release of drugs over an extended period in the stomach (Park and Kim, 2006). The diameter of the pylorus in human is about 15mm implying that any single unit drug delivery system larger than this size can be retained in the stomach (Davis, 2005). After drug delivery, the system should exit the stomach through the intestine by degrading or reducing in size in order to pass through the pylorus and out of the GIT (Davis, 2005).

The model drug, levodopa remains the gold standard for the management of Parkinson's disease. However, its challenges have been poor absorption and bioavailability which are due to the fact that it has a specific site of absorption. The absorption of levodopa is undertaken by a facilitated transport mechanism specific for amino acids mainly located at the proximal small intestine (Muzzi et al., 2008). Hence prolonged gastric residence time will improve the absorption and subsequent bioavailability which may also improve the erratic concentrations in the plasma thereby enhancing therapeutic efficacy. Although other routes of administration have been explored for the delivery of levodopa such as duodenal administration (Nyholm et al., 2005a), transdermal route (Babita and Tiwary, 2005) and pulmonary route (Bartus et al., 2004), oral route is the most preferred due to cost, convenience and patient compliance.

This study was therefore undertaken to use interpolymeric blend to develop a triple-mechanism gastroretentive drug delivery system employing high density, swelling and bioadhesion to enhance the delivery of narrow absorption window drugs such as L-dopa at a constant rate over a prolonged period. To characterize and evaluate the drug delivery system, physicochemical and physicomachanical characterization techniques such as Fourier Transform Infra-Red (FTIR) spectroscopy, texture analyses, swellability testing, gastroadhesivity testing and *in vitro* drug release testing were employed. Furthermore, excipients/additives were utilized in this phase of study in order to assist in the formulation of a three-mechanism gastroretentive drug delivery system.

6.2. EXPERIMENTAL SECTION

6.2.1. Materials

Barium sulphate, potassium phosphate monobasic (KH_2PO_4), pullulan from *Aureobasidium pullulans* (Sigma-Aldrich Inc., Steinheim, Germany); sodium hydroxide (NaOH) (Rochelle Chemicals, Gauteng, South Africa); silica, (Saarchem, Krugersdorp, South Africa) and magnesium stearate (Merck Chemicals (PTY) LTD, Gauteng, South Africa). Other materials used are as stated in Chapter 4, Section 4.2.1 and Chapter 5, Section 5.2.1.

6.2.2. Synthesis of interpolymeric blend

The description of the process of synthesis of the IPB was undertaken in Chapter 5, Section 5.2.3. The interpolymeric blend F1 was further synthesized in 0.2, 0.4, 0.6, 0.8 and 1.0N acetic acid. The interpolymeric blend formed was lyophilized for 48 hours, milled and employed for direct compression. The ratios of the polymers within the interpolymeric blend are as shown in Table 6.1.

Table 6.1: Compositions of the polymers utilized for generation of interpolymeric blends.

Formulations (ratios)	Methacrylate copolymer (g)	Locust bean (g)	NaCMC (g)
F1 (0.5:1:1)	0.84	1.68	1.68
F2 (0.5:2:1)	0.6	2.4	1.2
F3 (1:0.5:2)	1.2	0.6	2.4

6.2.3. Structural elucidation of the interpolymeric blend

FTIR spectra were obtained for the native polymers and the interpolymeric blends as described in Chapter 4, Section 4.2.4 to elucidate the structural modification of the interpolymeric blend from the native polymers.

6.2.4. Direct compression of the interpolymeric blend into matrices

The interpolymeric blend (IPB) was directly compressed with additives and excipients as in Table 6.2 using a Carver Press (Model 3851-0, Carver Industries Inc., Wabash, IN, USA) at 3tonnes. Mixing of the components was undertaken in this sequence: Quantities of IPB were added and mixed in an alternate manner with other ingredients: silicon dioxide was mixed first with some quantity of IPB followed by L-dopa, then pullulan and barium sulphate while magnesium stearate was added last and mixed continuously for two minutes afterwards.

Table 6.2: Composition of a directly compressed matrix.

Components	Quantity per matrix (mg)
L-dopa	100
Polymeric blend (50%)	500
Pullulan (10%)	100
Magnesium Stearate (1%)	10.5
Silica (Silicon dioxide) (5%)	50.5
Barium Sulphate	234

6.2.5. Determination of the densities of matrices

The volume of each matrix was determined by obtaining the diameter and the thickness using 0-150mm electronic digital caliper (repeatability: 0.01mm) (Hangzhou United Bridge Tools Co Ltd, Zhejiang, China) while the weights were ascertained gravimetrically employing a weighing balance (taring range: 0-110g) (Denver Instrument Company, Colorado, USA). Hence, the density for each matrix was calculated having obtained the weights and volumes.

6.2.6. Evaluation of the physicomechanical strength of the matrices

The physicomechanical strength of the matrices was determined as described in Chapter 4, Section 4.2.7.

6.2.7. Gastroadhesivity testing of the matrices

Freshly excised stomach from a terminated pig was obtained from an abattoir and equilibrated in 0.1N HCl (pH of 1.2). The gastroadhesive strength was determined using the Texture Analyzer (TA.XT*plus*, Stable Microsystems, Surrey, UK) fitted with a cylindrical steel probe (10mm in diameter). The excised tissue was attached to the cylindrical probe while the matrix was mounted on the Texture Analyzer stage. The parameters settings are shown in Table 6.3. The data was captured through Texture Exponent Software (Version 3.2). The surface of the attached tissue was lubricated with 0.1N HCl and the probe on which it was attached was lowered to make contact with the matrix. The peak force and the work of adhesion were used to assess the gastroadhesivity of the matrices. The peak force is the maximum force required to detach the tissue from the matrices while the work of adhesion was determined from the Force-Distance profile.

Table 6.3: The parameter settings for the gastroadhesivity test of the matrices.

Parameters	Settings
Pre test speed	2 mm/sec
Test speed	0.5 mm/sec
Post test speed	10 mm/sec
Applied force ¹	1 N or 0.5N
Trigger type	Auto
Trigger force	0.05N
Contact time	5sec
Return distance	20mm

6.2.8. Degree of swelling of the matrices

The swelling of the matrices was undertaken as described in Chapter 4, Section 4.2.8.

6.2.9. *In vitro* drug release studies and data analysis

Drug release from the matrices was assessed as explained in Chapter 4, Section 4.2.9. *In vitro* drug release studies were also undertaken for F1 matrices formulated from IPB in varying normalities of acetic acid in buffer pH 1.5 (standard buffer KCl/HCl), pH 4.5 (0.025M $\text{KH}_2\text{PO}_4/\text{H}_2\text{PO}_4$) and pH 6.8 (standard buffer $\text{KH}_2\text{PO}_4/\text{NaOH}$) was employed to observe the physicochemical behavior (presence of swelling and/or erosion) of the matrices and not for drug release as the model drug levodopa is unstable at such pH levels. Drug release profiles were analyzed with mathematical models – first order and zero order kinetics; Higuchi, Korsmeyer and Peppas equations as described in Chapter 5, Section 5.3.6.

6.2.10. Static lattice atomistic simulations (SLAS)

All modeling procedures and calculations were performed using softwares as stated in Chapter 3, Section 3.2.3.3 to elucidate the interaction between pullulan, the adhesive and mucin (glycosylated mucopeptide analogue). The structure of pullulan (PLLN; 4 saccharide units) was built from standard bond lengths and angles using sugar builder module on HyperChem™ 8.0.8 while the structure of the mucopeptide analogue (MUC) was generated using the sequence editor module. The models were energy-minimized using a progressive-convergence-strategy where initially the MM+ force field was used followed by energy-minimization using the Amber 3 (Assisted Model Building and Energy Refinements) force field. The conformer having the lowest energy was used to create the polymer-polymer and polymer-solvent complexes. A complex of one polymer molecule with another was assembled by disposing the molecules in a parallel way, and the same procedure of energy-minimization was repeated to generate the final models: PLLN, MUC, and PLLN-MUC. Full geometry optimization was carried out in vacuum employing the Polak–Ribiere conjugate gradient algorithm until an RMS gradient of 0.001kcal/mol was reached. For molecular

mechanics calculations in vacuum, the force fields were utilized with a distance-dependent dielectric constant scaled by a factor of 1. The 1-4 scale factors used were electrostatic - 0.5 and van der Waals - 0.5 (Kumar et al., 2011).

6.3. RESULTS AND DISCUSSION

6.3.1. Synthesis of interpolymeric blend

The synthesis and computational modeling of IPEC has been discussed in Chapter 3, Section 3.3.7. Although locust bean is regarded as a neutral galactomannan polymer (Alves et al., 1999; Camacho et al., 2005; Sittikijyothin et al., 2005), it acted as a linker between E100 and CMC with intermolecular hydrogen bondings as discussed in Chapter 5, Section 5.3.7. The hydrophilic groups of locust bean associated themselves with the existing water molecules leading to a further increase in viscosity as the locust bean gum swelled. The water molecules held within the interpolymeric blend were sublimated during lyophilization resulting in dried porous wafer-like interpolymeric blend. However, the degree of porosity observed increased with increase in normality of acetic acid; though, after lyophilization, the wafer-like IPB was milled for further studies.

6.3.2. Structural elucidation of the interpolymeric blend

The spectra obtained of the native polymers (methacrylate copolymer and NaCMC) are shown in Figure 6.1a while the chemical structural transitions for various compositions of IPB are in Figures 6.1b – c. The characteristic peaks for methacrylate copolymer are found at 2821.42cm^{-1} , 2769.84 , 1725 , 1270.38cm^{-1} , 1239.56 , 1143.69 , 962.05 , 842.49 and 747.81cm^{-1} and those of NaCMC are found at 3210.04 , 1587.18 , 1411.77 , 1321.86 and 1019.59cm^{-1} . The blend between methacrylate copolymer and NaCMC was a chemical interaction as evidenced by the spectra obtained while incorporation of locust bean is envisaged to be a physical miscible interaction. The chemical interactions between methacrylate copolymer and NaCMC led to the disappearance or diminished characteristic peaks of methacrylate copolymer at the homogenous ratio (0.5:1) blend. This modification in the structure of methacrylate copolymer is envisaged to alter its solubility in acid thereby modifying its rate of drug release in acidic medium. The aliphatic aldehyde peaks of methacrylate copolymer at 2821.42 and 2769.84cm^{-1} had disappeared. In Figure 6.1b, the black spectrum is F3 which has a higher concentration of NaCMC, hence the characteristic peaks of NaCMC are more pronounced at 1587.18 , 1411.77 , 1321.86 and 1019.59cm^{-1} .

Furthermore, it is envisaged that the homogeneity of IPB resulted in an almost superimposed spectra (Figure 6.1c) with very slight differences in the degree of absorbance at the various frequencies or peaks with F1 in 1.0N acetic acid having the highest degree of absorbance at

peaks 1725, 1589, 1408, 1268.50 and 1019 cm^{-1} . This is indicative of the impact of varying the normality of acetic acid which may influence the behavior of IPB in terms of degree of swelling, matrix erosion and subsequent drug release.

Polymer modification in this case polymer-polymer interaction alters the properties of the native polymers to enhance the drug delivery properties. The IPB obtained is envisaged to improve drug release over a prolonged period at a fairly constant rate due to possible change in matrix behavior and performance of interpolyelectrolyte complex in dissolution media.

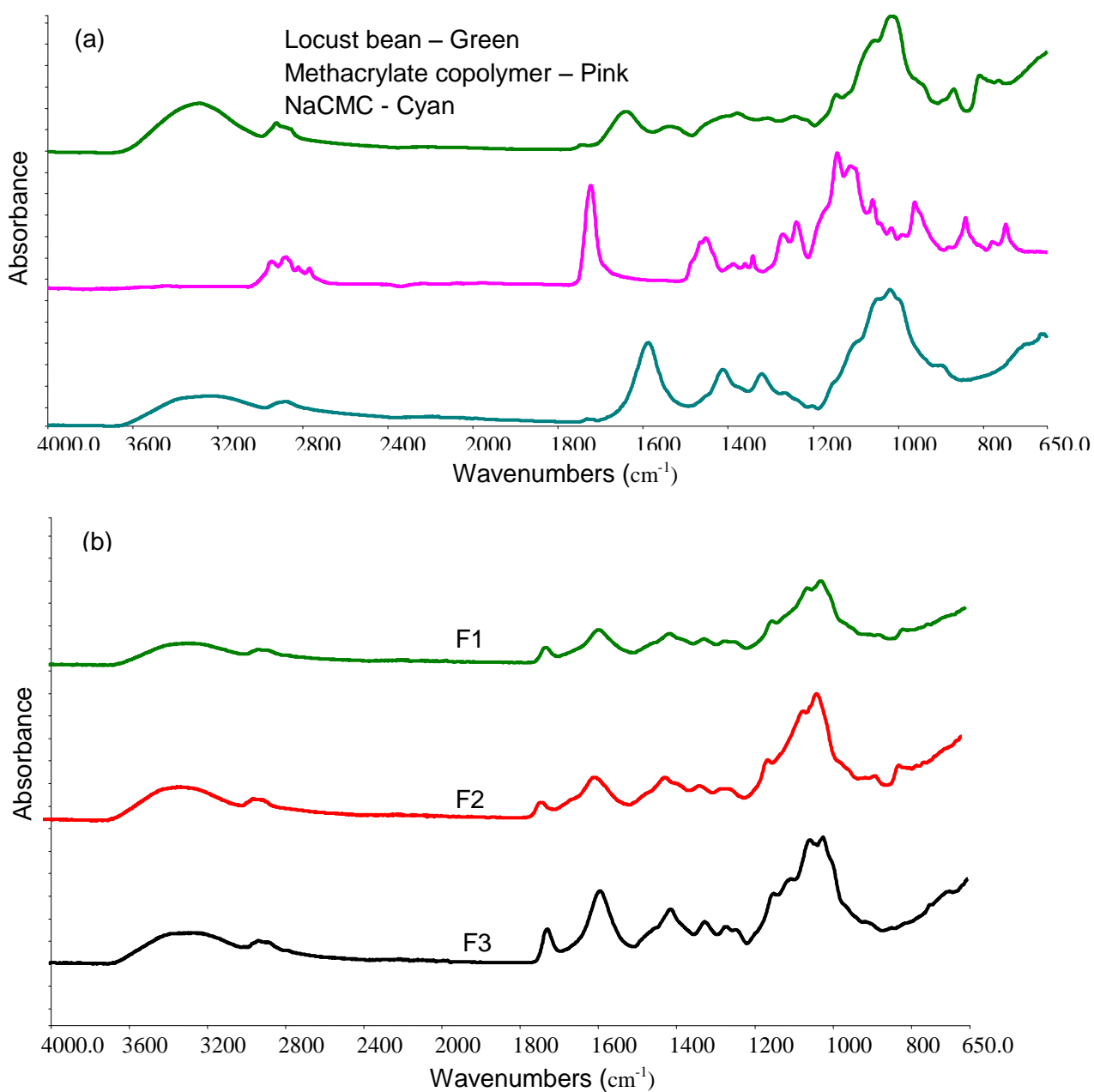


Figure 6.1: FTIR spectra for the interpolymeric blends; **a)** Native polymers-locust bean, methacrylate copolymer and NaCMC and; **b)** Formulations F1, F2 and F3.

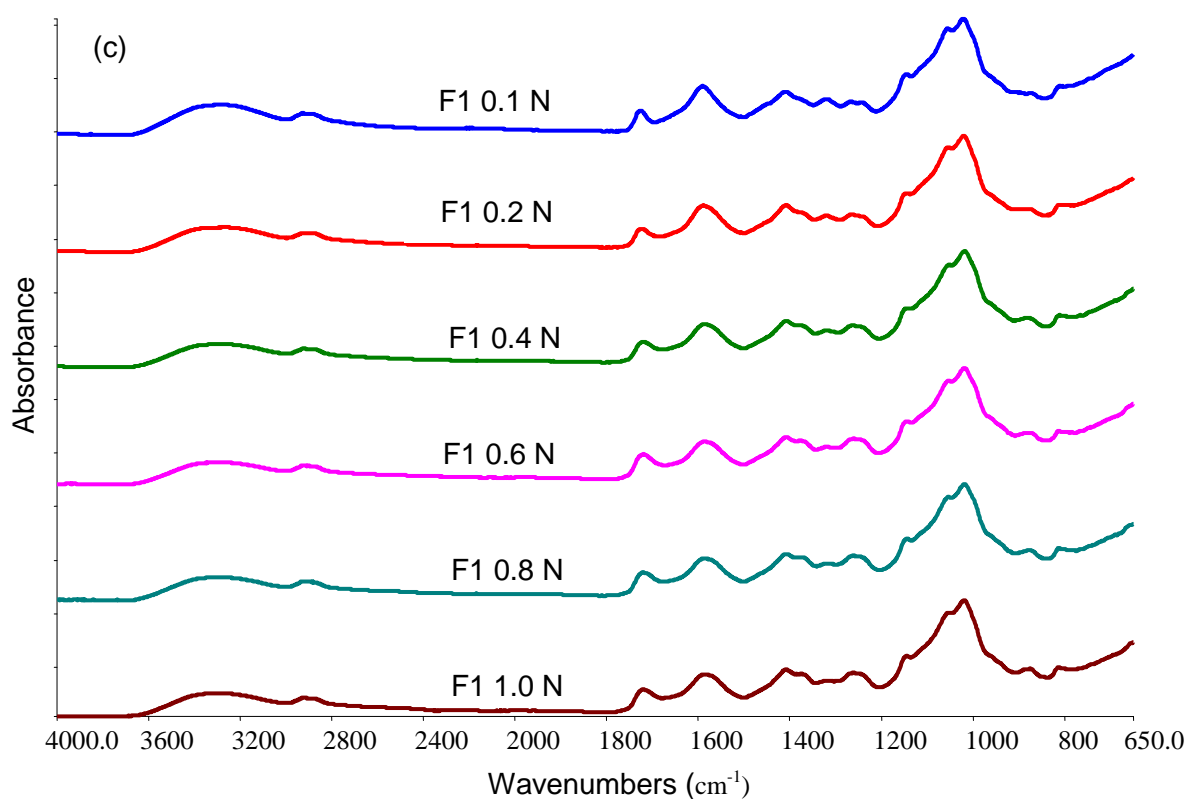


Figure 6.1c: FTIR spectra for Formulation F1 in varying normalities of acetic acid.

6.3.3. Direct compression of the interpolymeric blend into matrices

All compositions of IPB were directly compressible indicating that it would not require excipients to enhance compactness. Excipients included in this study were density enhancing agent – BaSO₄, glidant – silica, and lubricant – magnesium stearate to improve its flow properties, and pullulan - adhesive agent. The IPB showed excellent compactibility at 3 tonnes.

6.3.4. Densities of the matrices

The densities of the matrices from each formulation are shown in Table 6.4. The densities were between 1.43 and 1.51g/cm³. The densities obtained are indicative of the matrices' ability to sink down to the antrum of the stomach since they are significantly denser than the gastric content and fall within the density range (1.3-2.8g/cm³) for high density formulations. Although to ensure prolonged gastric residence time, a density above 2.4g/cm³ is advocated for high density delivery systems (Chawla et al., 2003; Bardonnnet et al., 2006), it is envisaged the IPB matrices may still provide prolonged gastric residence with densities less than recommended since they are employing three mechanisms of gastroretention- high density, swellability and gastroadhesivity.

From physiological studies, it can be stated that non-disintegrating single unit drug delivery systems would remain in the stomach in the fed phase and would be emptied with the housekeeping waves (Davis et al., 1986). Drug delivery systems are more prone to clear from the stomach at fasted state than fed state due to housekeeping waves. Hence, IPB matrix with a density of 1.4g/cm³ and non-disintegrating at the pH of the stomach when ingested will sink to the antrum of the stomach and can only be emptied during housekeeping waves. However, it is envisaged that its ability to swell beyond the size of the pylorus and its gastroadhesivity will enable it to be retained in the stomach beyond the period of the housekeeping waves.

Table 6.4: Densities of the IPB formulations.

Formulation	Density (mg/mm ³)
F1	1.50
F2	1.50
F3	1.51
F1 0.2N ¹	1.45
F1 0.4N	1.43
F1 0.6N	1.47
F1 0.8N	1.48
F1 1.0N	1.50

¹F1 0.4N means formulation F1 synthesized in 0.2N acetic acid etc.

6.3.5. Physicomechanical strength analyses of the matrices

Physicomechanical strength analyses were undertaken because the hardness and resilience are indications of the stability of the matrices and their ability to withstand pressure during compression and its capability to restore to its original dimensions after the compressional stress applied during textural analysis respectively. Matrix resilience also determines drug release kinetics. Matrix hardness and resilience indicate the degree of density and porosity of a matrix which affects the drug release profile from the matrix by affecting the rate of penetration of the dissolution medium into the matrix (Nur and Zhang, 2000).

Less hardness and resilience may indicate the presence of voids which collapse on application of stress. Porosity also determines the amount of deformation energy required; the harder the matrix, the less the energy absorbed or the more the deformation energy which also affect the matrix resilience. The inherent properties of the polymers utilized in formulation of matrices also determine the degree of hardness. Furthermore, in the course of this study, it was also observed that lyophilization can strengthen the physicomechanical properties of polymers causing native polymers which would not ordinarily retain three dimensional networks of matrices to do so.

The different formulations as shown in Table 6.5 indicated good hardness which ranged from 34.720 – 38.919N/mm; the deformation energy range from 1.2×10^{-2} – 1.4×10^{-2} Nm while percentage resilience was from 45.98 – 47.65%. Hence all the formulations had good physicomechanical strength and would be able to withstand pressures. Typical Force-Distance and Force-Time profiles obtained are shown in Figure 6.2.

Table 6.5: Texture profiling analysis of IPB formulations.

Formulation	Matrix Hardness (N/mm)	Deformation Energy $\times 10^{-2}$ (Nm)	Resilience (%)
F1	38.919	1.20	46.68
F2	37.070	1.20	47.65
F3	35.769	1.30	47.65
F1 0.2N	35.349	1.30	46.25
F1 0.4N	34.720	1.30	46.36
F1 0.6N	34.937	1.30	46.72
F1 0.8N	35.027	1.40	45.98
F1 1.0N	36.393	1.30	46.32

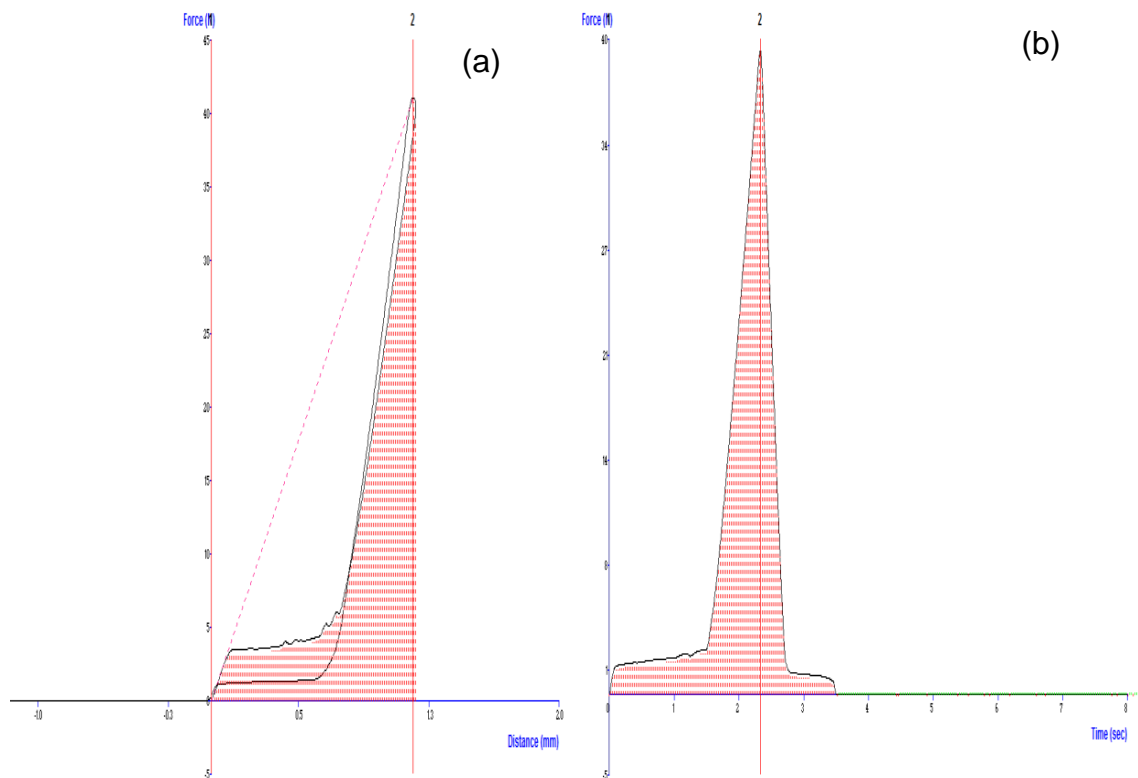


Figure 6.2: Typical Force-Distance and Force-Time profiles of the interpolymeric blends for determining: **a)** matrix hardness and deformation energy and; **b)** Matrix resilience.

6.3.6. Gastroadhesivity testing of the matrices

Figure 6.3 is a typical gastroadhesive Force-Distance profile. The IPB matrices from different quantities of polymers and normality of acetic acid were found to be gastroadhesive as shown in Figures 6.4 to 6.7. The interactions between the gastric mucosal surfaces and drug delivery systems formulated from bioadhesive polymers include covalent bonding, hydrogen bonding; electrostatic forces such as van der Waal forces, chain interlocking and hydrophobic interactions (Lee et al., 2000; Woodley, 2001; Thirawong et al., 2008) and these interactions are regulated by pH and ionic conditions. The degree of interaction between the polymers and mucus is also dependent on the mucus viscosity, degree of entanglement and water content (Lee et al., 2000).

As the applied force is increased from 0.5N to 1N, the peak adhesive force and work of adhesion increased. An increase in applied force would increase intimate contact by causing visco-elastic deformation at the interface between the mucus and the drug delivery system (Lee et al., 2000). Although the contact time employed was 5 seconds, the gastroadhesive results were commensurable and if contact time is increased, there will be subsequent increase in the interaction of the polymeric chains with the mucus which will lead to increase in gastroadhesion.

The peak adhesive force and work of adhesion were found to be higher when the IPB matrices adhered to the gastric epithelium. This may have been enhanced by the presence of a microbial adhesive agent, pullulan from *Aureobasidium pullulans* in the matrices. Microbial adhesions are postulated to have the capability to increase mucoadhesion to the epithelium (Vasir et al., 2003). It is envisaged that the incorporation of pullulan would overcome the challenge of quick mucus turnover thereby prolonging gastric residence time since it can adhere to the epithelial cells.

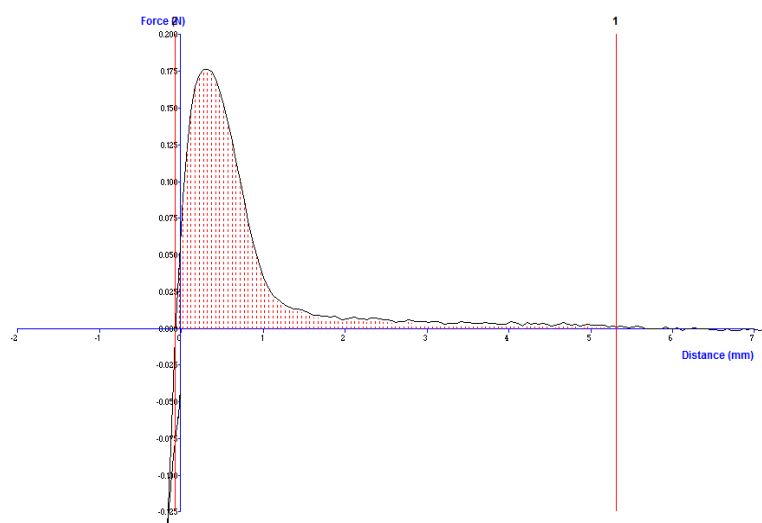


Figure 6.3: Typical gastroadhesive Force-Distance profile of the IPB.

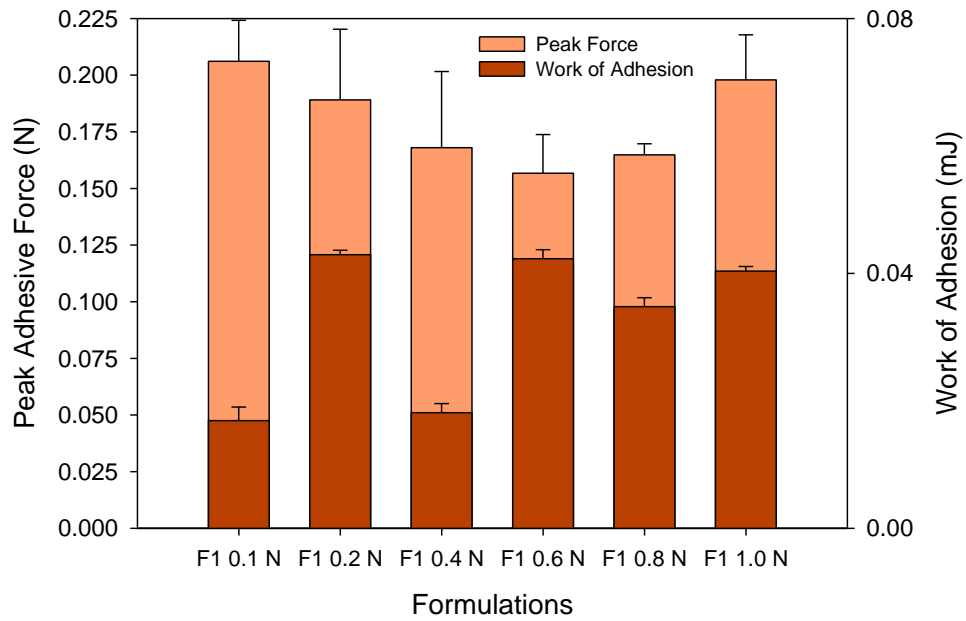


Figure 6.4: Gastroadhesive profiling of Formulation F1 in different normalities of acetic acid employing applied force of 1N.

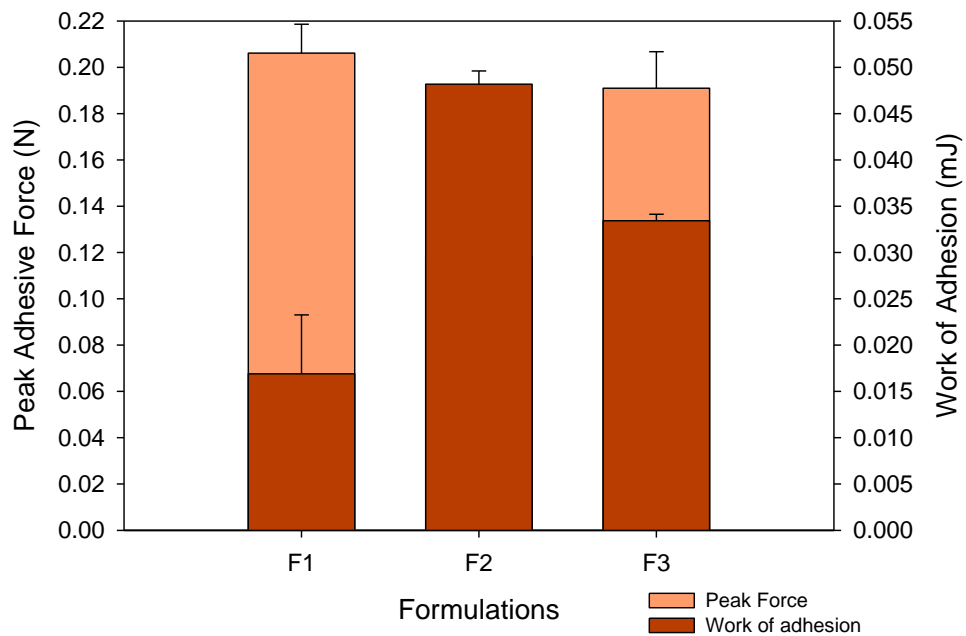


Figure 6.5: Gastroadhesive profiling of Formulations F1, F2, and F3 employing applied force of 1N.

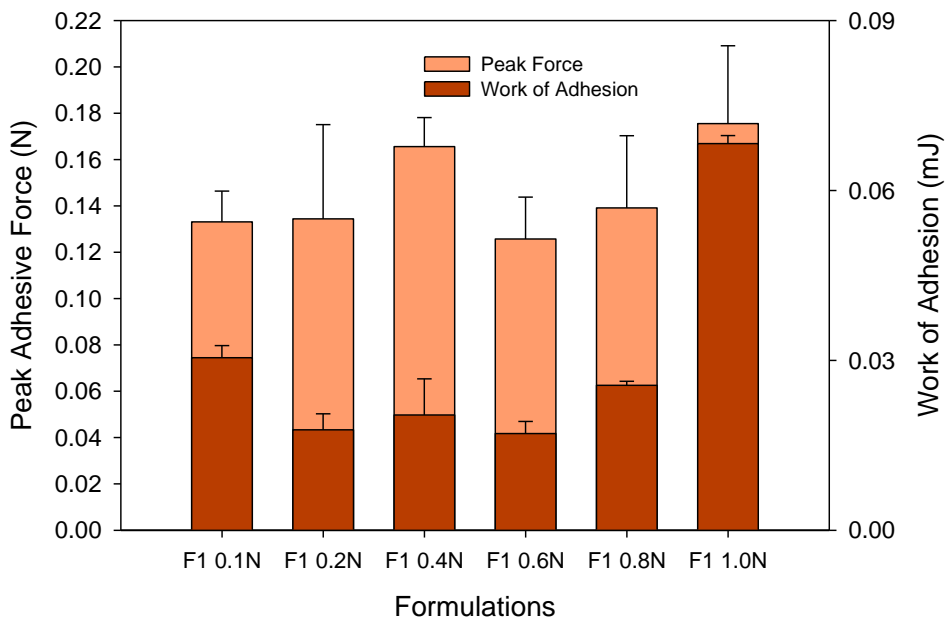


Figure 6.6: Gastroadhesive profiling for Formulation F1 in different normalities of acetic acid employing applied force of 0.5N.

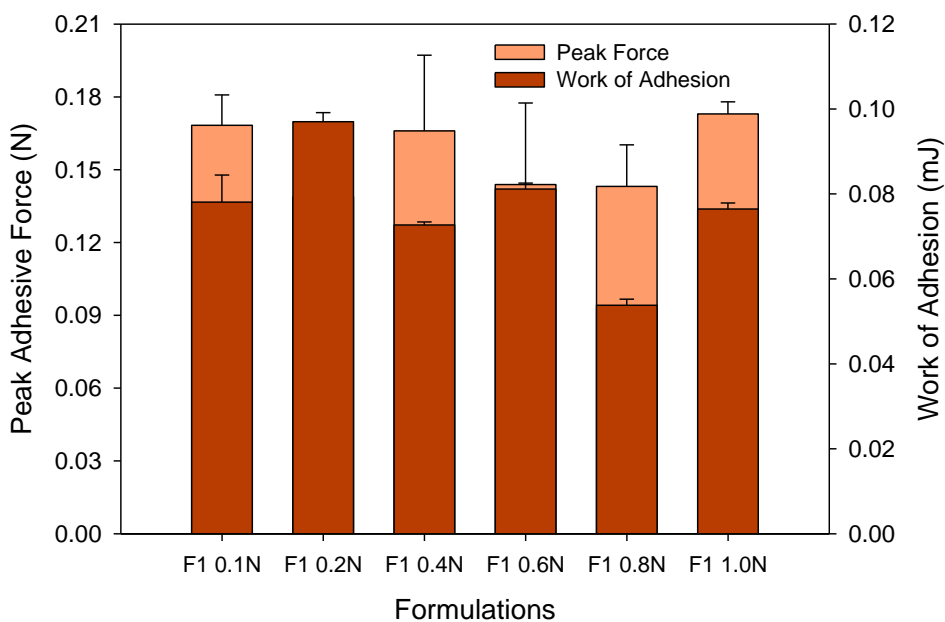


Figure 6.7: Epithelial adhesive profiling of Formulation F1 in different normalities of acetic acid employing applied force of 0.5N.

6.3.7. Degree of swelling of the matrices

The influence of swelling on drug release and the factors affecting it have been discussed in Chapter 4, Section 4.3.6. Matrices formulated with methacrylate copolymer alone dissolved in acidic medium while NaCMC alone swelled to 384% of its original size with loss of its three

dimensional network. However, the IPEC formed swelled much more than NaCMC as discussed in Chapter 4, Section 4.3.6. On addition of locust bean gum, its hydrophilic groups associated themselves to the available water holding capacity of the IPEC thereby reducing the degree of swelling below 300%. Table 6.6 exhibits the degree of swelling of the various formulations at 24th hour. However, F1 was chosen to determine the degree of swelling at time intervals over 24 hours and Figure 6.8 depicts the degree of swelling profile over 24 hours. Generally, it was observed that the degree of swelling decreased as the normality of acetic acid increased from 229% of 0.1N to 202% of 1.0N of acetic acid. Consequently, it is envisaged the rate of drug release from IPB will decrease as the normality of acetic acid increases.

Table 6.6: Degree of swelling of IPB matrices.

Formulation	Degree of Swelling (%)
F1	218.19
F2	211.63
F3	183.36
F1 0.1N	229.06
F1 0.2N	217.55
F1 0.4N	210.33
F1 0.6N	203.06
F1 0.8N	205.34
F1 1.0N	202.09

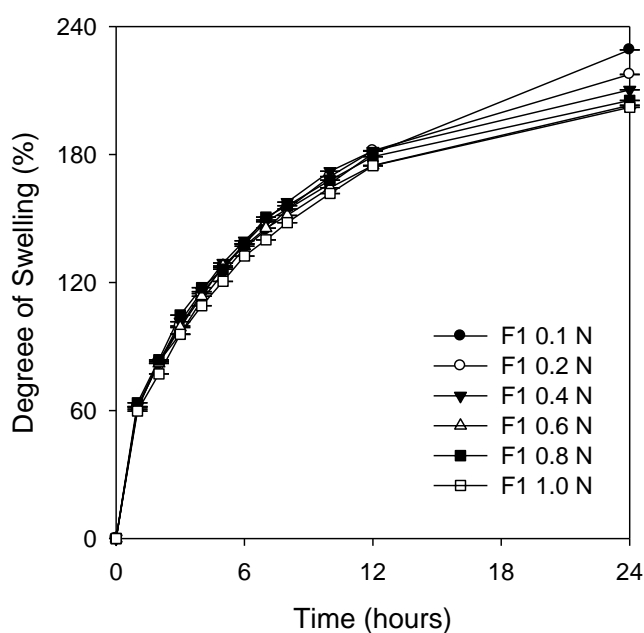


Figure 6.8: Degree of swelling for Formulation F1 in different normalities of acetic acid.

6.3.8. *In vitro* drug release studies and mathematical modeling

Drug release profiles were obtained and the three dimensional network of the matrices were retained over the 24 hour period of study. In Figures 6.9, the drug release profiles of formulations F1, F1 and F3 are shown. F2 which had the highest concentration of locust bean released the least by the 12th hour (68%). The mechanisms of release from the formulations were envisaged to be swelling, dissolution and diffusion of drug since the matrices retained their three dimensional network in 0.1N HCl and buffer pH 1.5.

The F1 matrices in dissolution media 0.1N HCl and buffer pH 1.5 (standard buffer KCl/HCl) generated the drug release profiles in Figures 6.10 and 6.11 respectively and still retained their three dimensional networks. Hence mechanisms of drug release involved in these media may be swelling of matrix, dissolution and then subsequent diffusion of the drug from the matrix.

Interestingly, as the pH is increased to 4.5, the matrices did swell with time but there was gradual surface erosion throughout the 24 hour period indicating the drug release pattern from IPB matrices may be pH dependent. Consequently, the drug release profiles at pH 4.5 as shown in Figure 6.12 differed from those obtained from pH 1.5 or 0.1N HCl. Surface erosion occurs when the rate of erosion is greater than the rate of hydration (rate of absorption of dissolution medium) of the matrix and occurs at constant velocity which leads to reproducible kinetics of erosion and drug release which is usually zero-order (Pillai and Panchagnula, 2001; Siepmann and Göpferich, 2001; Burkersroda et al., 2002; Faisant et al., 2002). Hence, the mechanism of drug release in pH 4.5 was principally surface erosion, swelling of matrix, dissolution and then subsequent diffusion of the drug from the matrix producing zero-order release profiles. Figure 6.13 shows digital images of F1 in pH 1.5 and 4.5.

It was observed the matrices did not completely erode at the 24th hour. However, the degree of erosion decreased as the normality of acetic acid increased which in turn affected the drug release profile as well as the fractional drug released at the 24th hour as shown in Figure 6.12. A zero-order drug release profile was obtained for F1 in 0.1N acetic acid which eroded to a greater extent than the other formulations indicating that erosion may have been its principal mechanism of release. This may be contrary to the erosion studies in Chapter 5, Table 5.1; however, there were no excipients/additives in the matrices employed in Chapter 5. Hence, it is envisaged that the presence of excipients in this study may have led to the matrices obtained from IPB synthesized with lower normality of acetic acid to erode more.

Although the dissolution was undertaken in pH 6.8, the focus was not on drug release but on the behavior of the IPB matrices at this pH. This is because the model drug used is unstable

at pH 6.8 and so fractional drug release was not obtained. However, it was observed that the matrices underwent surface erosion as well over 24 hours. Hence the novel interpolymeric blend synthesized may be explored for development of drug delivery device where a constant rate of delivery is required in other sites of the GIT.

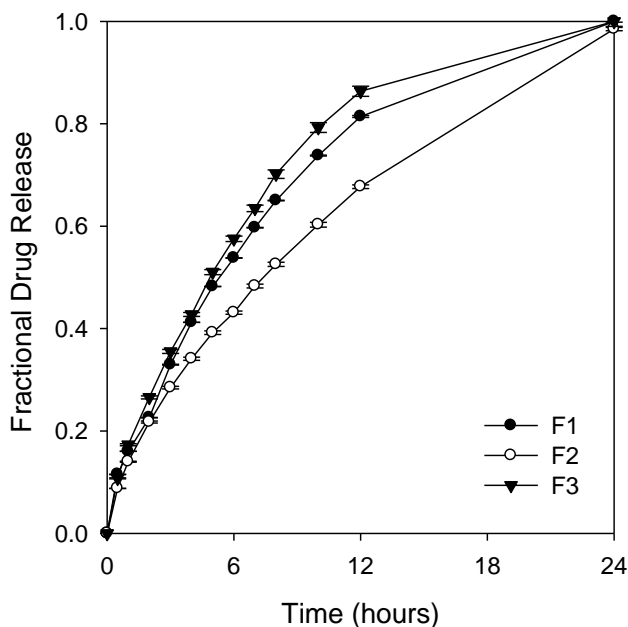


Figure 6.9: Drug release profiles for Formulations F1, F2 and F3 employing 0.1N HCl as dissolution medium.

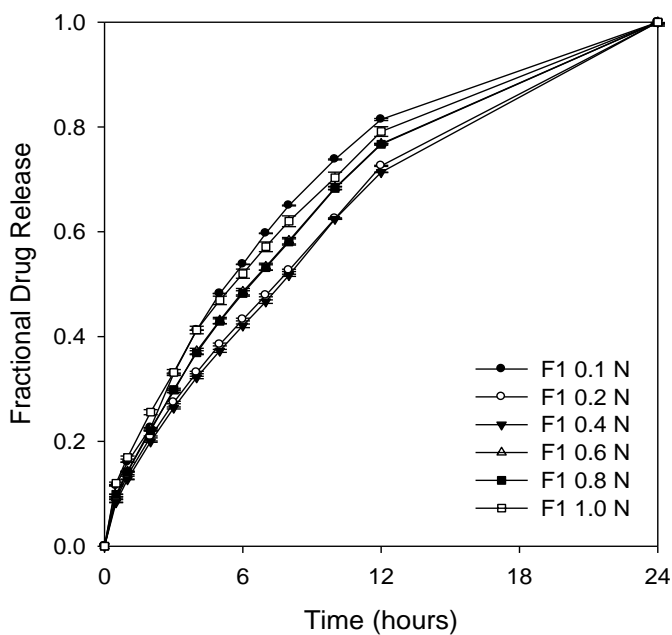


Figure 6.10: Drug release profiles for Formulation F1 in different normalities of acetic acid employing 0.1N HCl as dissolution medium.

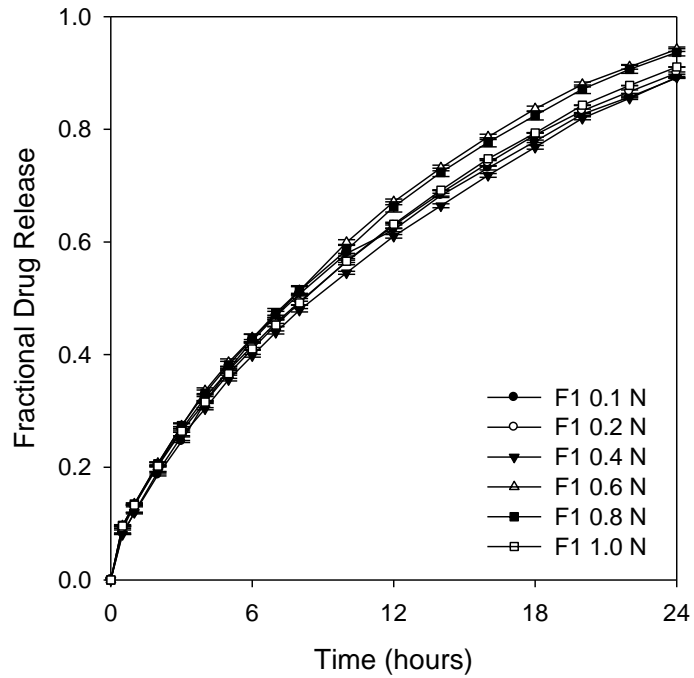


Figure 6.11: Drug release profiles for Formulation F1 in different normalities of acetic acid employing buffer pH 1.5 (standard buffer KCl/HCl) as dissolution medium.

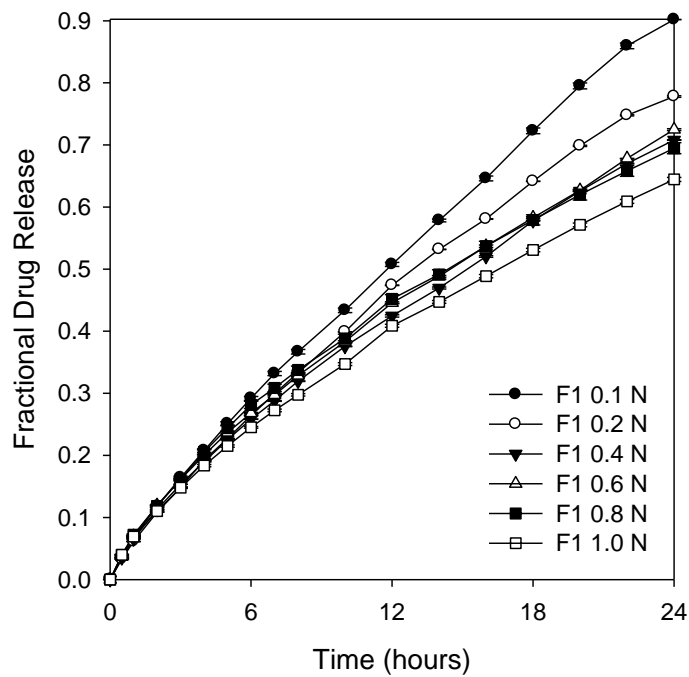


Figure 6.12: Drug release profiles for Formulation F1 in different normalities of acetic acid employing buffer pH 4.5 (0.025M $\text{KH}_2\text{PO}_4/\text{H}_2\text{PO}_4$) as dissolution medium.

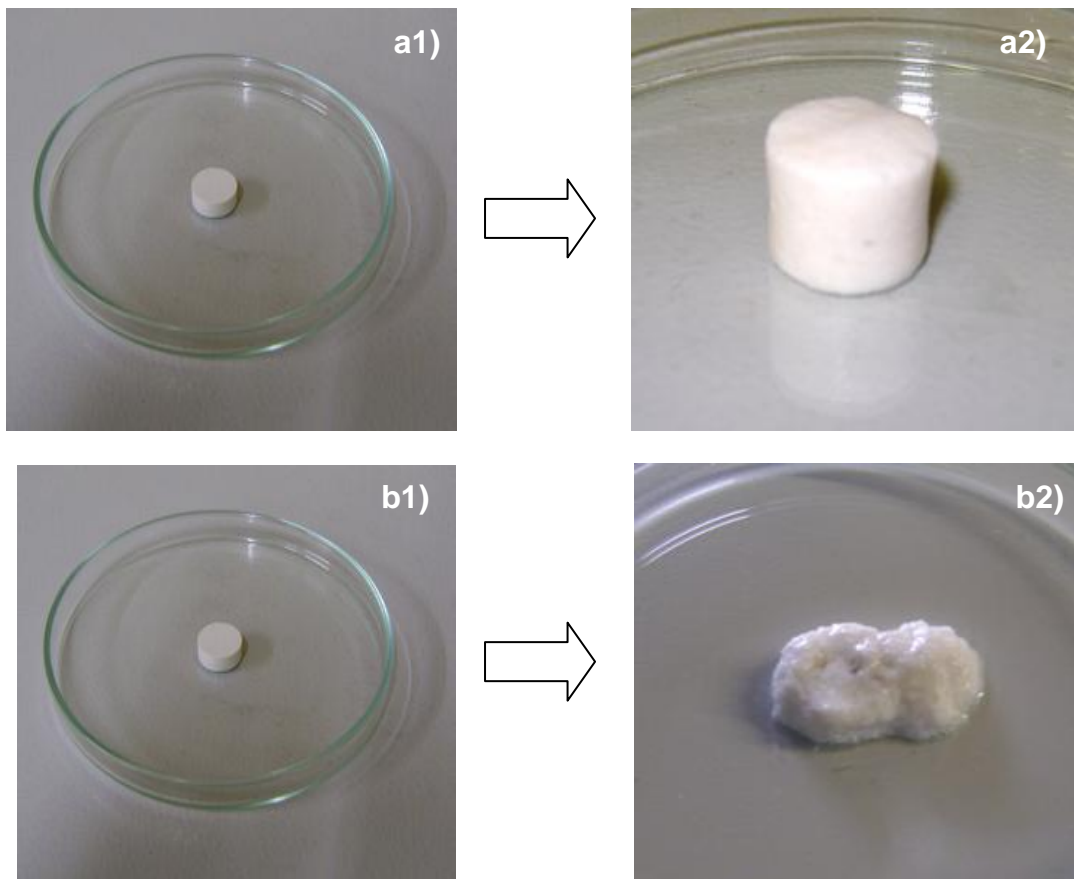


Figure 6.13: Digital images of F1 matrices in different pH media: **a)** matrix before and after *in vitro* drug release study in pH 1.5 and; **b)** matrix before and after *in vitro* drug release study in pH 4.5.

The result of the mathematical modeling is shown in Table 6.7 with most of the IPB formulations being fitted into Korsmeyer-Peppas model and all the values of release exponent n were anomalous transport and as discussed in Chapter 5, Section 5.3.6, the values are indication that the drug release patterns involved a combination of mechanisms as observed experimentally and explicated above.

Table 6.7: Mathematical modeling of drug release profiles of IPB formulations.

Drug device ¹	Zero Order		First Order		Higuchi		Korsmeyer-Peppas			Best-Fit Model ²
	k_0	r^2	K_1	r^2	K_H	r^2	$K_{KP} (h^{-n})$	r^2	n	
F1	6.6207	0.9644	-0.0581	0.9948	24.7393	0.9853	16.5501	0.9883	0.65	First order
F2	5.3556	0.9643	-0.0379	0.9983	20.0664	0.9905	13.8867	0.9997	0.64	Korsmeyer-Peppas
F3	7.0665	0.9634	-0.0691	0.9892	26.4468	0.9874	17.0805	0.9994	0.67	Korsmeyer-Peppas
F1 0.1N (HCl)	6.6207	0.9644	-0.0581	0.9948	24.7393	0.9853	16.5501	0.9883	0.65	First order
F1 0.2N (HCl)	5.6743	0.9810	-0.0426	0.9850	20.9499	0.9785	13.6584	0.9995	0.64	Korsmeyer-Peppas
F1 0.4N (HCl)	5.6414	0.9840	-0.0418	0.9863	20.7605	0.9750	12.9003	0.9995	0.66	Korsmeyer-Peppas
F1 0.6N (HCl)	6.1587	0.9741	-0.0495	0.9920	22.8820	0.9839	14.5211	0.9990	0.67	Korsmeyer-Peppas
F1 0.8N (HCl)	6.1349	0.9748	-0.0493	0.9914	22.7806	0.9835	14.7537	0.9973	0.66	Korsmeyer-Peppas
F1 1.0N (HCl)	6.2179	0.9594	-0.0521	0.9936	23.3766	0.9922	17.4703	0.9974	0.61	Korsmeyer-Peppas
F1 0.1N (1.5)	3.5204	0.9416	-0.0374	0.9937	19.5399	0.9946	12.3396	0.9963	0.67	Korsmeyer-Peppas
F1 0.2N (1.5)	3.5275	0.9497	-0.0386	0.9911	19.5139	0.9965	13.5457	0.9994	0.62	Korsmeyer-Peppas
F1 0.4N (1.5)	3.5094	0.9565	-0.0371	0.9881	19.3333	0.9953	12.3823	0.9994	0.65	Korsmeyer-Peppas
F1 0.6N (1.5)	3.7475	0.9500	-0.0474	0.9807	20.7090	0.9947	14.0056	0.9978	0.62	Korsmeyer-Peppas
F1 0.8N (1.5)	3.7072	0.9509	-0.0458	0.9807	20.4827	0.9953	14.0475	0.9977	0.62	Korsmeyer-Peppas
F1 1.0N (1.5)	3.5844	0.9550	-0.0403	0.9868	19.7611	0.9953	13.7784	0.9979	0.61	Korsmeyer-Peppas
F1 0.1N (4.5)	3.7339	0.9948	-0.0381	0.9452	19.8343	0.9624	6.5073	0.9993	0.83	Korsmeyer-Peppas
F1 0.2N (4.5)	3.2566	0.9896	-0.0266	0.9900	17.4162	0.9704	6.0007	0.9997	0.83	Korsmeyer-Peppas
F1 0.4N (4.5)	2.8601	0.9857	-0.0211	0.9943	15.3880	0.9783	6.4209	0.9986	0.77	Korsmeyer-Peppas
F1 0.6N (4.5)	2.8891	0.9829	-0.0217	0.9939	15.5919	0.9815	6.7983	0.9980	0.76	Korsmeyer-Peppas
F1 0.8N (4.5)	2.7972	0.9731	-0.0205	0.9989	15.2167	0.9874	7.0958	0.9982	0.74	First order
F1 1.0N (4.5)	2.5881	0.9809	-0.0205	0.9989	13.9935	0.9832	6.7280	0.9997	0.72	Korsmeyer-Peppas

¹ Insertions in parenthesis indicate the dissolution media used; HCl is hydrochloric acid while 1.5 and 4.5 are indicative of buffers pH 1.5 and 4.5; ² Best fit models were determined by correlation coefficient, r^2 .

6.3.9. Prediction of mucoadhesive potential of the GDDS

The global energy relationships for the various complexes derived after assisted model building and energy refinements are as follows:

$$E_{\text{PLLN}} = -8.370 V_{\Sigma} = 2.275 V_{\Sigma} + 19.829 V_{\theta} + 32.087 V_{\varphi} + 11.438 V_{ij} - 4.238 V_{hb} - 69.762 V_{el} \dots (6.1)$$

$$E_{\text{PDTR}} = -166.812 V_{\Sigma} = 5.474 V_{\Sigma} + 70.351 V_{\theta} + 55.173 V_{\varphi} - 29.066 V_{ij} - 7.096 V_{hb} - 261.649 V_{el} \dots (6.2)$$

$$E_{\text{PLLN-PDTR}} = -232.836 V_{\Sigma} = 7.997 V_{\Sigma} + 94.503 V_{\theta} + 92.414 V_{\varphi} - 32.182 V_{ij} - 10.993 V_{hb} - 384.576 V_{el} \dots (6.3)$$

$$\Delta E = -57.654 \text{kcal/mol}$$

The bioadhesive or mucoadhesive potential of the GDDS was elucidated as a measure of specific chemical interactions between pullulan (PLLN) and the glycosylated mucopeptide analogue after geometrical optimization using energy minimizations. Pullulan is known to be a mucoadhesive polymer and may impart bioadhesion to the drug delivery system (Vasir et al., 2003). The energy minimizations were found to be a collective phenomenon including non-bonding interactions in the form of van der Waals forces, H-bonding and electrostatic interactions (Equations 6.1-6.3). This contributed to a stress transduction requiring a large fraction of the surface to establish connectivity between chemically transformed regions. The binding energy of the PLLN with MUC was quite high with $\Delta E \sim 58 \text{kcal/mol}$ confirming the significant interactions among the molecular entities (Figure 6.14). A deeper inspection shows that the specificity of this complex arises due to $-\text{CO}\dots\text{NH}_2-$ and $-\text{CO}\dots\text{OH}-$ interactions of the PLLN and mucopeptide residue respectively (Figure 6.14c).

In addition, the molecular attributes in terms of surface-to-volume ratio (SVR) and final density corroborated with the experimental mucoadhesive findings with PLLN-MUC having lower SVR than that of either of the molecules individually (Table 6.8). The lower the SVR, the more stable is the structure. Furthermore, in the present case, initial models were built using a density derived from the average of that of the pure systems. For the polymer-mucopeptide system, a substantial increase in density was observed as compared to the average of the individual molecules involved, with the density going from 0.433 through 0.480 to 0.507 $\text{amu}/\text{\AA}^3$ for PLLN, MUC, and PLLN-MUC, respectively. This density increase is in agreement with the occurrence of specific interchain interactions leading to the mucoadhesivity of the GDDS (Abou-Rachid et al., 2008). Furthermore, a significant contribution was also provided by the strong H-bonding in PLLN-MUC with a bond lengths of $< 2\text{\AA}$ (data not shown). These interactions involving the non-bonded attractive forces may induce dipoles in the complex where the binding energy changes may be proportional to the polarizability of the substituents, which are in turn proportional to molar refractivity values where the structure with lower index of refraction is more stable (Table 6.8). Thus we conclude that the energy stabilization, low SVR, high density, lower polarizability, and lower

refractivity lead to highly efficient interactions between pullulan and mucosa. These results are in line with the previously reported observations by Murphy et al. (2011), where the mucoadhesivity of a polymer was defined in terms of the propensity of the molecules set up polar and hydrogen-bonding interactions (Murphy et al., 2011). The experimental mucoadhesion studies can be correlated to these *in silico* findings as we propose that pullulan may swell readily in contact with hydrated mucous membrane and become progressively rubbery due to uncoiling of polymer chains which may further result in increased mobility of the polymer chains producing a large adhesive surface for maximum contact with mucosa and flexibility to the polymer chains for interpenetration with mucosa (Kumar and Bhatia, 2010). In addition, some of the characteristics that might be responsible for increased hydrogel mucoadhesive properties include: high amount of hydrogen-bonding chemical groups (hydroxyls and carboxyls), anionic surface charges, high polymer molecular weight, high polymer chain flexibility and surface tensions that will induce spreading into the mucus layer (Kumar and Singh, 2010).

Table 6.8: Calculated molecular attributes of the complexes involving PLLN, MUC and PLLN-MUC.

Molecular Attributes	Molecular Complex(s)		
	PLLN	MUC	PLLN-MUC (Σ)
Minimised Energy (kcal mol ⁻¹)	-8.370	-166.812	- 232.836 (-175.182)
Polarizability (Å ³)	55.10	234.89	286.37 (289.99)
Refractivity (Å ³)	133.16	581.10	709.25 (714.26)
Volume (Å ³)	1537.50	5164.82	6200.90 (6702.32)
Mass (amu)	666.58	2479.62	3146.20 (3146.20)
Density (g/cm ³)	0.433	0.480	0.507 (0.469)
Surface area (grid) (Å ²)	848.62	2140.88	2384.89 (2989.5)
Surface-to-volume ratio (SVR)	0.552	0.414	0.385 (0.446)

Σ = summation of individual molecular attributes

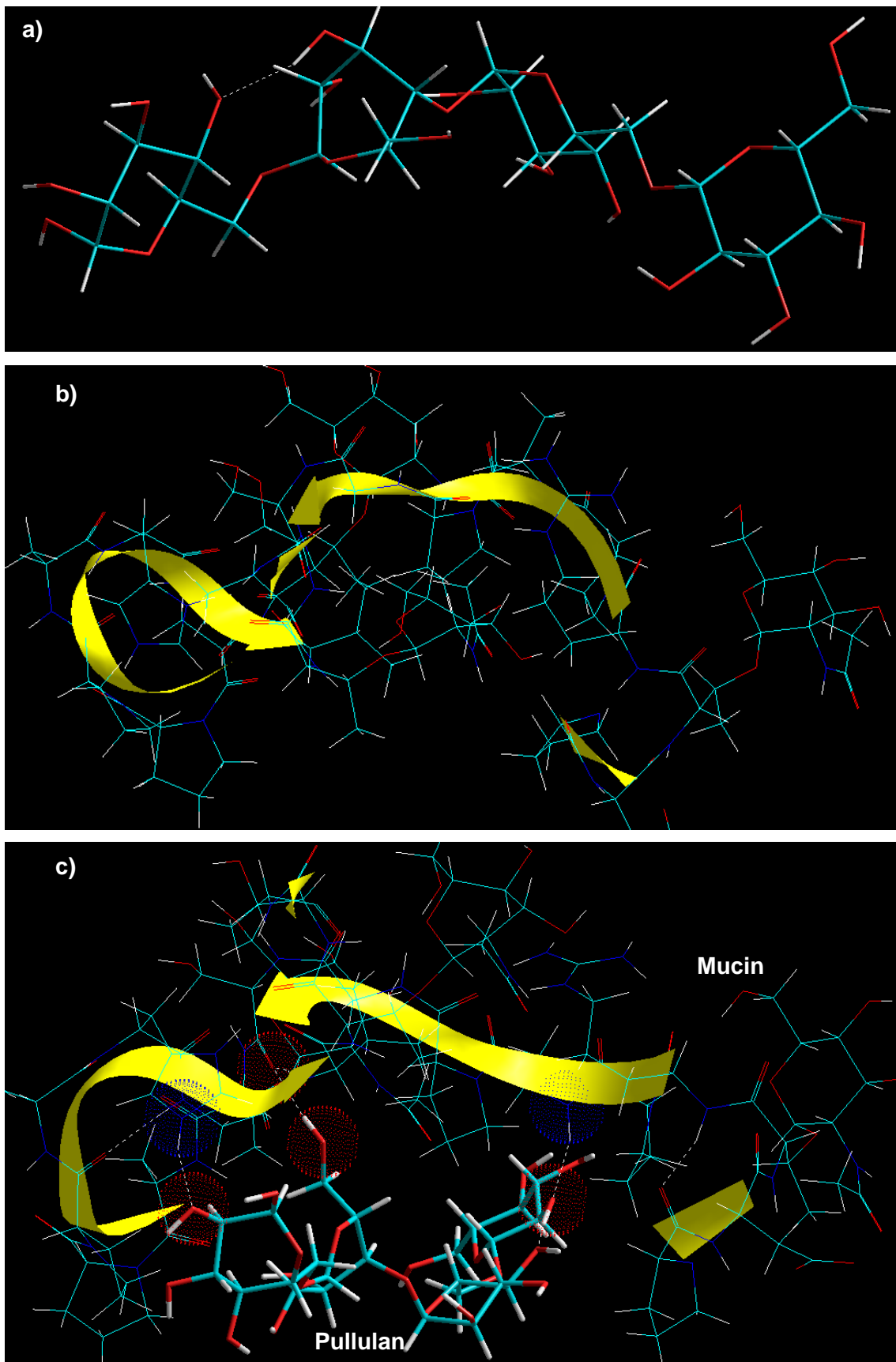


Figure 6.14: Visualization of energy minimized geometrical preference of **a)** Pullulan; **b)** glycosylated oromucoprotein and; **c)** Pullulan in complexation with mucin, after Molecular Mechanics simulations. Color codes: C (cyan), O (red), N (blue) and H (white).

6.4. CONCLUDING REMARKS

A triple-mechanism based gastroretentive drug delivery system has been developed with the potential for improving the absorption and bioavailability of narrow absorption drugs at a constant rate over prolonged period of time. It was dense, gastroadhesive and swelled. It is envisaged that the constant delivery of L-dopa as observed *in vitro* may ensure unfluctuating concentrations and sustained release in the plasma thereby providing optimal therapeutic effect. It was convenient to synthesize and it exhibited impressive drug delivery properties and pH responsiveness with zero-order release. Furthermore, it is anticipated that the three mechanisms – swelling, bioadhesion and high density - of gastroretention employed in this study will increase the gastric residence time of Narrow Absorption Window Drugs and improve their absorption. However, the experimental conditions which include the normality of acetic acid and quantities of polymers with regards to the responses such as bioadhesion, swelling, density and drug release need to be optimized. Hence, design of experiments and desirability function will be employed in the next Chapter to optimize the interpolymeric blend.

CHAPTER SEVEN

EMPLOYING DESIGN OF EXPERIMENTS AND DESIRABILITY FUNCTION FOR OPTIMIZATION OF THE GASTRORETENTIVE DRUG DELIVERY SYSTEM

7.1. INTRODUCTION

The process factors employed to influence the mechanisms of gastroretention include polymers, solvent and temperature. Polymers for instance, are required to generate bioadhesion and swelling responses; hence there is the need to assess how these process factors influence the responses and to determine the interaction between the factors. Consequently, a suitable method of analysis is required to assess the influence of the factors on the responses as well as obtain an optimum IPB with the desired characteristics for gastroretention and subsequent drug delivery.

Response surface methodology is a package of mathematical and statistical methods employed to improve or optimize a product or a process to achieve the desired responses (Myers, 2003; Liu et al., 2009). Response Surface Methodology assesses individual variables as well as the interactions of variables thereby overcoming the problem of assessing one variable while keeping the other variables constant. Response surface methodology (RSM) has been a useful tool in the development of drug delivery systems. Response Surface Methodology is classified into Box-Wilson Central Composite Designs and Box-Behnken designs.

The Box-Behnken design has been employed for optimization of drug delivery systems (Kramar, et al. 2003; Chopra et al., 2007; Solanki et al., 2007). The desirability function approach is usually employed to obtain the best possible process conditions for multiple response optimizations (Ficarra et al., 2002; Pizarro et al., 2006). The desirability function is also employed due to its broad versatility at transforming individual responses separately and incorporating all responses in an overall desirability function optimized globally in one measurement (Gupta et al., 2001; Sáiz-Abajo et al., 2005). Furthermore, it may require determining the optimum compromises between the responses.

A four factor two level Box-Behnken design was employed to optimize the interpolymeric blend for a gastroretentive drug delivery system. The independent variables were IPEC ratio, polymer quantity, solvent and temperature while the dependent variables were *in vitro* drug release, bioadhesion, swelling and density.

7.2. EXPERIMENTAL SECTION

7.2.1. Materials

Materials employed in this study are as stated in Chapter 4, Section 4.2.1, Chapter 5, Section 5.2.1 and Chapter 6, Section 6.2.1.

7.2.2. Generated composition

The design comprised of four factors (Table 7.1) which generated 27 runs on a Box-Behnken design (Table 7.2) with 4 response variables.

Table 7.1: The experimental variables employed in generating the formulation compositions.

Variables	Low value	Maximum value
Polymer 1(IPEC) ¹	1.8g	3.6g
Polymer 2 (L) ²	0.6g	2.4g
Solvent	0.1N	0.8 N
Temperature	25°C	70°C

¹ Polymer 1 is the interpolyelectrolyte complex of methacrylate polymer and carboxymethylcellulose.

² Polymer 2 is natural polysaccharide, locust bean gum

Table 7.2: The formulation compositions generated by Box-Behnken design (BBD).

Formulations	Variables			
	IPEC (g)	L (g)	SOLVENT (N)	TEMP (°C)
F1	1.8	1.5	0.10	47.5
F2	2.7	0.6	0.45	70.0
F3	2.7	2.4	0.45	25.0
F4	2.7	1.5	0.45	47.5
F5	3.6	1.5	0.45	70.0
F6	1.8	1.5	0.80	47.5
F7	3.6	1.5	0.80	47.5
F8	2.7	1.5	0.45	47.5
F9	3.6	1.5	0.45	25.0
F10	2.7	1.5	0.80	70.0
F11	2.7	2.4	0.10	47.5
F12	2.7	1.5	0.45	47.5
F13	2.7	0.6	0.80	47.5
F14	2.7	1.5	0.10	25.0
F15	2.7	0.6	0.45	25.0
F16	3.6	2.4	0.45	47.5
F17	2.7	1.5	0.10	70.0
F18	3.6	0.6	0.45	47.5
F19	1.8	1.5	0.45	25.0
F20	1.8	0.6	0.45	47.5
F21	1.8	2.4	0.45	47.5
F22	2.7	2.4	0.80	47.5
F23	2.7	1.5	0.80	25.0
F24	2.7	2.4	0.45	70.0
F25	3.6	1.5	0.10	47.5
F26	1.8	1.5	0.45	70.0
F27	2.7	0.6	0.10	47.5

7.2.3. Synthesis of the interpolymeric blends

Each blend composition generated by the Box Behnken design was synthesized by first milling methacrylate copolymer beads and the required quantity weighed and dissolved in 50mL of the solvent which is acetic acid at the stated temperature. Table 7.2 indicates the normalities of acetic acid for each composition. NaCMC was weighed as required for each blend and dissolved in 50mL at the stated temperature. A heating magnetic stirrer was employed with temperature stability of $\pm 1.0^{\circ}\text{C}$ and the beakers were sealed to minimize fluctuation in temperatures. The dissolved methacrylate copolymer was added to NaCMC solution under vigorous agitation to produce polymer 1 (IPEC). The figures under IPEC stand for the weights of methacrylate copolymer and NaCMC in the stoichiometric ratio of 1:2. When IPEC is synthesized, the designated quantity of polymer 2 (locust bean) is added. The period locust bean was added was dependent on the normality of acetic acid and temperature which sped up the rate of interaction. After the addition of locust bean, the polymeric blend was allowed to agitate for 15min and frozen at -70°C ; lyophilized for 48 hours and thereafter milled.

7.2.4. Direct compression of the polymeric blend into matrices

Each of the 27 polymeric blends was directly compressed with excipients as shown in Table 7.3 using a Carver Hydraulic Press (Carver Industries Inc., Wabash, IN, USA) at 3tonnes. Blending of the matrix constituents was undertaken in the sequence as stated in Chapter 6, Section 6.2.4.

Table 7.3: Composition of a directly compressed matrix employing BBD generated IPB.

Components	Quantity per matrix (mg)
L-dopa	100
Polymeric blend (50%)	500
Pullulan (10%)	100
Magnesium Stearate (0.5%)	5.5
Silica (Silicon dioxide) (5%)	50.5
Barium Sulphate	234

The evacuable pellet die (Specac Ltd, Orpington, Kent, England) employed was 13mm and directly compressed tablet matrices were obtained and assessed for density, gastroadhesivity, swelling and *in vitro* dissolution studies.

7.2.5. Determination of the densities of matrices

To obtain the densities of the matrices for each of the 27 formulations, the volume of each matrix was determined by acquiring the diameter and the thickness as described in Chapter

6, Section 6.2.5. Hence the density for each matrix was calculated having obtained the weights and volumes. Density was determined in triplicate for each of the formulations.

7.2.6. Adhesivity testing of the matrices

The adhesive strength of the formulations was assessed using a Texture Analyzer (TA.XT*plus*, Stable Microsystems, Surrey, UK). A seamless semi-permeable cellulose dialysis membrane (Spectra/Por[®]RC, MWCO:12-14,000, Dia:33mm, thickness:0.04064mm; Spectrum Labs, Rancho Dominguez, CA, USA) was fixed to a 10mm cylindrical probe (SMS P/10) which is attached to the Texture Analyzer (TA.XT*plus*, Stable Microsystems, Surrey, UK). Cellulose membrane was explored in this chapter as a substitute to mimic animal mucosa in evaluation of *in vitro* adhesivity since it is easily available. The parameters settings employed were as shown in Chapter 6, Table 6.4 and the data were captured through Texture Exponent Software (Version 3.2). The peak force (maximum force required to detach the membrane from the matrix) and the work of adhesion (determined from the force-distance profile) were used to determine the gastroadhesivity of the matrices and the test was undertaken in triplicates.

7.2.7. Swellability testing of matrices

Swelling was determined by assessing the physicommechanical strength of the matrices from Force-Distance profiles obtained using a Texture Analyzer (TA.XT*plus*, Stable Microsystems, Surrey, UK). The matrix hardness and deformation energy were performed with a 2mm flat-tipped steel probe for unhydrated and hydrated matrices. The matrices were hydrated by placing them in baskets, fixed to a dissolution apparatus and submerged in 900mL buffer pH 1.5; and allowed to run for two hours at 50rpm and 37°C. The data was captured through Texture Exponent Software (Version 3.2) and the settings employed are as shown in Chapter 6, Table 6.3.

7.2.8. *In vitro* drug release studies

In vitro drug release studies were undertaken using a USP apparatus II dissolution system (Erweka DT 700, Erweka GmbH, Heusenstamm, Germany) at 37±0.5°C and 50rpm in 900mL of buffer pH 1.5. Samples were withdrawn at intervals and replaced with the same volume of fresh medium to maintain sink conditions, and concentrations of L-dopa released per time were quantified spectrophotometrically at 280nm (LAMBDA 25 UV/Vis spectrophotometer, PerkinElmer, Massachusetts, USA). The studies were undertaken in triplicates for each of the 27 IPB.

7.3. RESULTS AND DISCUSSION

7.3.1. Observations for the generated experimental design

The densities for all formulations as shown in Table 7.4 were within the recommended density range from 1.3 – 2.8mg/mm³ for high density formulations which is indicative that the formulations are anticipated to sink down to the antrum of the stomach (Chawla et al., 2003; Talukder and Fassihi, 2004; Bardonnnet et al., 2006).

Table 7.4: Density data chart for the 27 formulations.

Formulation	Ave weight (mg)	Ave diameter (mm)	Radius sq (mm ²)	Ave thickness (mm)	Volume (mm ³)	Density (mg/mm ³)
F1	1002.80	12.93	41.77	5.10	669.18	1.50
F2	989.60	12.96	41.99	5.07	668.68	1.48
F3	994.30	12.98	42.12	5.13	679.13	1.46
F4	987.90	12.95	41.93	5.04	664.13	1.49
F5	994.27	13.02	42.36	5.21	693.62	1.43
F6	974.87	12.96	41.99	4.93	650.64	1.50
F7	991.43	12.97	42.06	5.08	671.47	1.48
F8	982.10	12.99	42.19	5.11	677.96	1.45
F9	995.10	13.01	42.29	5.21	692.11	1.44
F10	984.03	13.00	42.27	5.15	683.79	1.44
F11	1001.30	13.00	42.27	5.19	689.54	1.45
F12	992.90	12.96	42.01	5.07	669.46	1.48
F13	988.63	12.98	42.12	5.06	669.86	1.48
F14	1005.20	13.03	42.42	5.22	696.02	1.44
F15	990.30	12.98	42.10	5.12	677.01	1.46
F16	991.20	13.11	42.97	5.42	732.41	1.35
F17	1005.63	13.05	42.60	5.32	711.81	1.41
F18	987.93	13.11	42.95	5.38	726.19	1.36
F19	993.40	12.98	42.10	5.11	676.13	1.47
F20	983.47	13.06	42.64	5.23	700.93	1.40
F21	983.60	13.00	42.23	5.15	683.53	1.44
F22	985.77	13.01	42.29	5.16	686.35	1.44
F23	992.20	13.00	42.27	5.13	681.13	1.46
F24	993.80	13.01	42.34	5.23	695.93	1.43
F25	1003.93	13.10	42.90	5.40	727.70	1.38
F26	982.63	13.05	42.58	5.22	698.07	1.41
F27	999.57	13.06	42.66	5.29	708.88	1.41

The average force of adhesion for the formulations varied from 0.2671 to 0.7518N (Table 7.5). The wide range is indicative that the independent variables may have affected the bioadhesive behavior of the formulations even though the same quantity of pullulan, an

adhesive agent was added to all formulations. Formulation 26 has the lowest force of adhesion with the highest temperature (70°C) and had one of the lowest quantities of IPEC.

Table 7.5: Force of adhesion and work of adhesion data for the experimentally derived formulations.

Formulation	Ave Force (N)	Ave Distance (mm)	Ave Time (sec)	Ave AUC (N.sec)	Work of adhesion (J)
F1	0.5041	0.1803	5.3733	0.0233	0.0909
F2	0.5187	0.2617	5.2747	0.0250	0.1357
F3	0.4291	0.1493	5.3480	0.0167	0.0641
F4	0.5940	0.1850	5.2233	0.0217	0.1099
F5	0.6718	0.1737	5.2827	0.0277	0.1167
F6	0.4129	0.2207	5.2880	0.0187	0.0911
F7	0.6619	0.2430	5.1820	0.0320	0.1608
F8	0.4353	0.1940	5.2200	0.0197	0.0844
F9	0.3992	0.2403	5.2973	0.0190	0.0959
F10	0.3590	0.1573	5.2820	0.0140	0.0565
F11	0.3909	0.2113	5.2447	0.0180	0.0826
F12	0.7457	0.1973	5.1453	0.0267	0.1472
F13	0.7518	0.2420	5.1460	0.0290	0.1819
F14	0.3966	0.2587	5.1580	0.0150	0.1026
F15	0.5503	0.1077	5.6267	0.0283	0.0593
F16	0.4832	0.1070	5.5720	0.0253	0.0517
F17	0.4142	0.0823	5.6527	0.0207	0.0341
F18	0.5135	0.1233	5.5947	0.0290	0.0633
F19	0.4439	0.1570	5.4627	0.0203	0.0697
F20	0.4884	0.2030	5.3780	0.0263	0.0991
F21	0.3829	0.1513	5.4833	0.0183	0.0579
F22	0.3690	0.1140	5.5300	0.0180	0.0421
F23	0.5029	0.1447	5.4280	0.0220	0.0727
F24	0.3665	0.2080	5.3660	0.0170	0.0762
F25	0.3752	0.2030	5.4280	0.0187	0.0762
F26	0.2671	0.2270	5.3180	0.0120	0.0606
F27	0.5123	0.2270	5.3840	0.0287	0.1163

Swelling was assessed by determining the rigidity and deformation energy of the matrices at the 2nd hour (Table 7.6). The unhydrated matrices were rigid and could not be deformed at the forces applied. However, hydrating the matrices for two hours exhibited a significant change in rigidity and it can be inferred that the matrices swelled substantially leading to easy penetration of the probe and subsequent deformation. The mechanical strength of the swollen matrices is measured by the resistance to force. The less resistance exhibited or force required, the weaker the matrices due to hydration and subsequent increase in mobility of the polymer chains.

Table 7.6: Data depicting rigidity and deformation energy for unhydrated and hydrated matrices.

Formulation	Degree of Swelling			
	Unhydrated		Hydrated	
	Ave Rigidity (N/mm)	Ave Deform. Energy (J)	Ave Rigidity (N/mm)	Ave Deform. Energy (J)
F1	89.8445	0.0090	8.7925	0.0440
F2	87.2805	0.0090	4.5180	0.0415
F3	85.6745	0.0095	4.5135	0.0355
F4	82.8125	0.0100	4.5970	0.0575
F5	74.6320	0.0105	4.1625	0.0350
F6	79.4585	0.0095	4.2365	0.0585
F7	82.9040	0.0095	4.0775	0.0435
F8	87.1760	0.0090	4.1190	0.0500
F9	91.2020	0.0090	4.1415	0.0375
F10	75.4670	0.0100	4.1490	0.0370
F11	84.2135	0.0095	4.0810	0.0385
F12	84.1275	0.0090	4.2925	0.0540
F13	82.2665	0.0100	4.4135	0.0615
F14	85.1875	0.0095	4.4005	0.0475
F15	92.4185	0.0090	4.6585	0.0615
F16	61.8905	0.0115	4.0515	0.0290
F17	68.7035	0.0110	3.9315	0.0240
F18	65.4390	0.0115	4.1575	0.0235
F19	79.5645	0.0100	4.3770	0.0535
F20	69.9955	0.0115	4.3080	0.0370
F21	73.8110	0.0100	4.0800	0.0350
F22	75.3740	0.0105	4.2435	0.0345
F23	77.0655	0.0110	4.3705	0.0480
F24	76.0945	0.0100	4.0195	0.0280
F25	74.1130	0.0105	4.1715	0.0410
F26	68.7795	0.0110	3.9475	0.0285
F27	68.4800	0.0115	4.2760	0.0410

All formulations released over 80% of L-dopa over a period of 24 hours and the square regressions were above 0.9 with the lowest being F25 with a square regression of 0.9344. The regression values obtained as shown in Table 7.7 indicate the degree of fitness of the drug release profiles to zero-order kinetics. The formulations' drug release profiles are shown in Figures 7.1 to 7.4. All formulations exhibited the potential to release L-dopa with zero-order kinetics over a prolonged period.

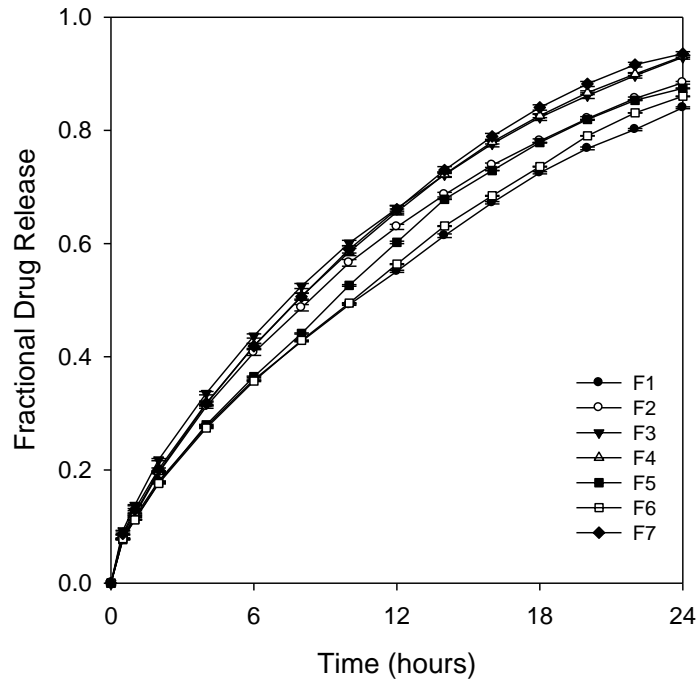


Figure 7.1: Drug release profiles of formulations F1 to F7.

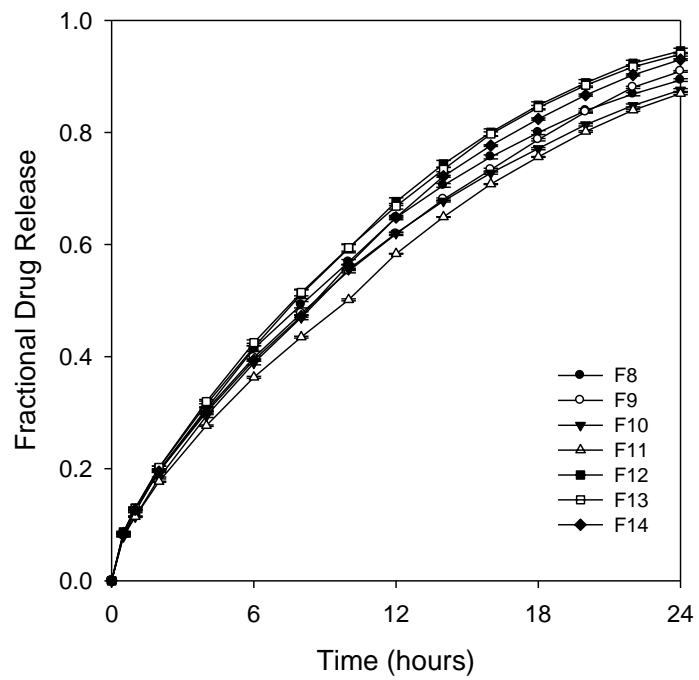


Figure 7.2: Drug release profiles of formulations F8 to F14.

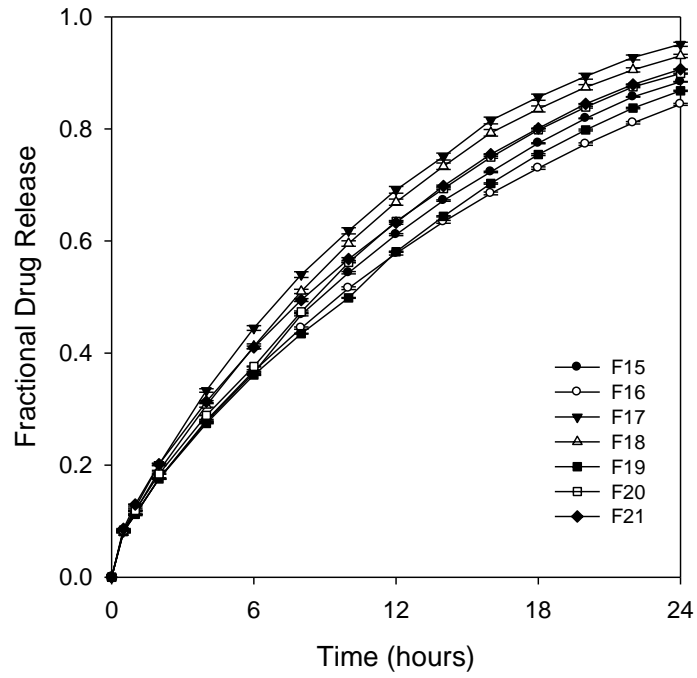


Figure 7.3: Drug release profiles of formulations F15 to F21.

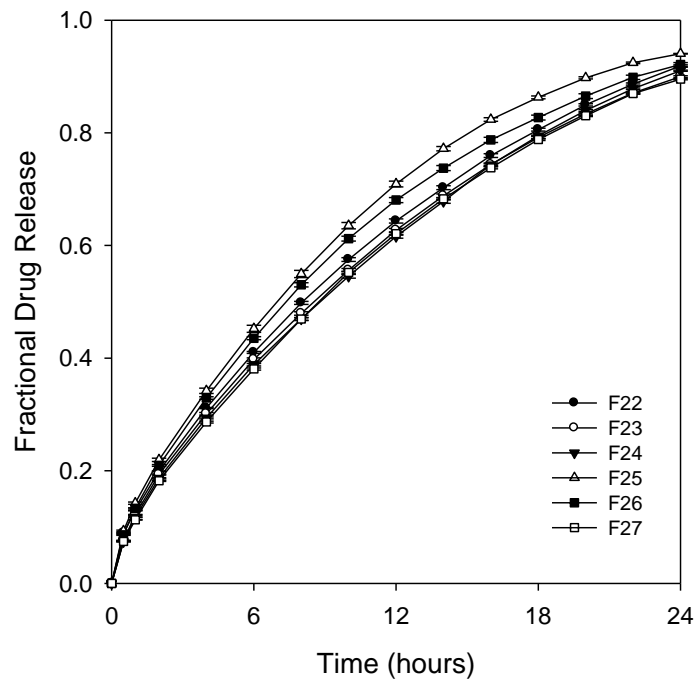


Figure 7.4: Drug release profiles of formulations F22 to F27.

Table 7.7: A cumulative data indicating the generated independent variables and the experimental values of dependent variables.

Formulations	Independent Variables				Dependent Variables			
	IPEC (g)	L (g)	SOLVENT (Normality)	TEMP (°C)	Density (mg/mm ³)	Dissolution - R ²	Bioadhesion - Ave Force (N)	Swelling (N/mm)
F1	1.8	1.5	0.10	47.5	1.50	0.9687	0.5041	8.7925
F2	2.7	0.6	0.45	70.0	1.48	0.9493	0.5187	4.5180
F3	2.7	2.4	0.45	25.0	1.46	0.9458	0.4291	4.5135
F4	2.7	1.5	0.45	47.5	1.49	0.9534	0.5940	4.5970
F5	3.6	1.5	0.45	70.0	1.43	0.9648	0.6718	4.1625
F6	1.8	1.5	0.80	47.5	1.50	0.9728	0.4129	4.2365
F7	3.6	1.5	0.80	47.5	1.48	0.9552	0.6619	4.0775
F8	2.7	1.5	0.45	47.5	1.45	0.9483	0.4353	4.1190
F9	3.6	1.5	0.45	25.0	1.44	0.9630	0.3992	4.1415
F10	2.7	1.5	0.80	70.0	1.44	0.9545	0.3590	4.1490
F11	2.7	2.4	0.10	47.5	1.45	0.9703	0.3909	4.0810
F12	2.7	1.5	0.45	47.5	1.48	0.9545	0.7457	4.2925
F13	2.7	0.6	0.80	47.5	1.48	0.9527	0.7518	4.4135
F14	2.7	1.5	0.10	25.0	1.44	0.9626	0.3966	4.4005
F15	2.7	0.6	0.45	25.0	1.46	0.9631	0.5503	4.6585
F16	3.6	2.4	0.45	47.5	1.35	0.9616	0.4832	4.0515
F17	2.7	1.5	0.10	70.0	1.41	0.9439	0.4142	3.9315
F18	3.6	0.6	0.45	47.5	1.36	0.9509	0.5135	4.1575
F19	1.8	1.5	0.45	25.0	1.47	0.9710	0.4439	4.3770
F20	1.8	0.6	0.45	47.5	1.40	0.9599	0.4884	4.3080
F21	1.8	2.4	0.45	47.5	1.44	0.9549	0.3829	4.0800
F22	2.7	2.4	0.80	47.5	1.44	0.9559	0.3690	4.2435
F23	2.7	1.5	0.80	25.0	1.46	0.9579	0.5029	4.3705
F24	2.7	2.4	0.45	70.0	1.43	0.9654	0.3665	4.0195
F25	3.6	1.5	0.10	47.5	1.38	0.9344	0.3752	4.1715
F26	1.8	1.5	0.45	70.0	1.41	0.9394	0.2671	3.9475
F27	2.7	0.6	0.10	47.5	1.41	0.9615	0.5123	4.2760

7.3.2. Analysis of the response surface design

The analysis of the response surface design was performed on the results using coded units; and linear, squared and two-way interactions terms were chosen to fit the model. The terms chosen to fit the models enabled the assessment of the effects of the individual factors as well as the interactions of the factors on the responses (dependent variables) as shown in Table 7.7. The confidence level employed was 95% which implies any p-value < 0.05 has a significant effect. The data was analyzed with regards to estimated regression coefficients, standard error of fits, and Pearson product moment correlation coefficient while residual plots (histogram, normal plot, residuals versus fits and residuals versus order) as well as surface plots were used to examine the goodness of the model fit.

7.3.2.1. Estimated regression coefficients and standard error of fits

The results were assessed to determine if the factors (IPEC, L, solvent and temperature) and their interactions had any significant effect on the outcomes of density, dissolution, bioadhesion and swelling. None of the factors had any significant effect on density though L had a notable effect with the p-value = 0.051. Furthermore, dissolution as it appeared, there was no significant effect of the factors or their interactions on dissolution. Meanwhile, temperature had a significant effect on bioadhesion with a p-value = 0.026 and interaction of IPEC and temperature also had significant effect with p-value = 0.025. The significant interaction effect of IPEC with temperature implies that the effect of IPEC on bioadhesion depends on temperature employed. However, the p-value of the interaction effect of IPEC with solvent on bioadhesion approached significance (0.052). In the case of swelling, interaction of EC and solvent had a significant effect with p-value of 0.033, while solvent had a notable effect with p-value = 0.052. The standard error of fits (SE Fit) provides insights into the variation in the estimated mean response for a given set of predicted values. The higher the standard error, the less precise is the estimated response. The SE Fit for the dependent variables are shown in Table 7.8. The smaller values of SE fit for density and dissolution indicate that the estimated mean responses did not vary so much from that of the predicted values whereas those of swelling and bioadhesion were higher and less precise estimations.

Table 7.8: Standard error of fits for the 27 formulations with respect to the responses.

Responses	SE Fit range	Large standard residuals
Density	0.020 – 0.026	Nil
Dissolution	0.006 – 0.008	3
Bioadhesion	0.510 – 0.670	2
Swelling	0.534 – 0.706	1

P-values for lack of fit were obtained to determine if any effect left out of the model was significant. Smaller p-values would imply that the linear model employed was not adequate to fit the response surface design and vice versa. The p-values for lack of fit for the responses are shown in Table 7.9. The higher values obtained indicated that the linear model employed adequately fitted the response surface design with respect to the terms included in the model.

Table 7.9: P-values for lack-of-fit with respect to responses.

Responses	Lack-of-Fit
Density	0.280
Dissolution	0.086
Bioadhesion	0.975
Swelling	0.056

7.3.2.2. Pearson product moment correlation coefficient

The degree of linear relationship between two variables is measured by Pearson product moment correlation coefficient. When correlation coefficient is negative, it is indicative that as one variable increases, the other decreases while its positivity is indicative that the two variables tend to increase together. A value of 0 indicates there is no correlation between the two variables. The correlation coefficient of the variables employed in this study is shown in Table 7.10.

Table 7.10: Correlations between the variables employed in the response surface design.

	IPEC	L	Solvent	Temp	Density	Dissolution	Bioadhesion
L	0.000						
Solvent	-0.000	0.000					
Temp	-0.000	0.000	0.000				
Density	-0.400	-0.028	0.270	-0.195			
Dissolution	-0.217	0.097	0.045	-0.272	0.329		
Bioadhesion	0.284	-0.428	0.218	-0.058	0.344	0.108	
Swelling	-0.315	-0.085	-0.263	-0.109	0.389	0.266	0.124

The value of 0 was observed amongst the independent variables which is understood as the correlations were between the independent variables and dependent responses. Negative correlation is observed between temperature and the responses (density, dissolution, bioadhesion and swelling) while correlation between IPEC and the responses showed negativity with density, dissolution and swelling; and positivity with bioadhesion. In the case of L and the responses, negative correlation is observed with density, bioadhesion and swelling while for solvent, positive correlation is observed for density, dissolution and bioadhesion. It is worthy to note that the responses correlated with each other in the positive direction which means for instance that as swelling increased, bioadhesion increased.

7.3.2.3. Residual plots

Residuals refer to the differences between the predicted values and the observed values. The plots are based on the theory that residuals are normally distributed. The normal probability plot is used to determine how closely the observed values follow a normal distribution. If all the residuals fall on a straight line, the residuals follow the normal distribution. In some instances, from the histogram and the normality probability plot, the normal distribution may not clearly be displayed and so goodness-of-fit test such as Anderson-Darling statistic which appeared on the plots (Figures 7.5a-d) can be used and this indicated whether the residuals actually follow normal distribution. The residuals do not follow a normal distribution if the p-value is lower than the chosen confidence level. From the residual plots and based on Anderson-Darling statistics, the residuals for density, dissolution and bioadhesion followed a normal distribution while those of swelling did not. The residuals for density were on or very close to the lines and so there were no outliers. However, there were a few outliers in the plots for dissolution (3 outliers), bioadhesion (2 outliers) and swelling (1 outlier).

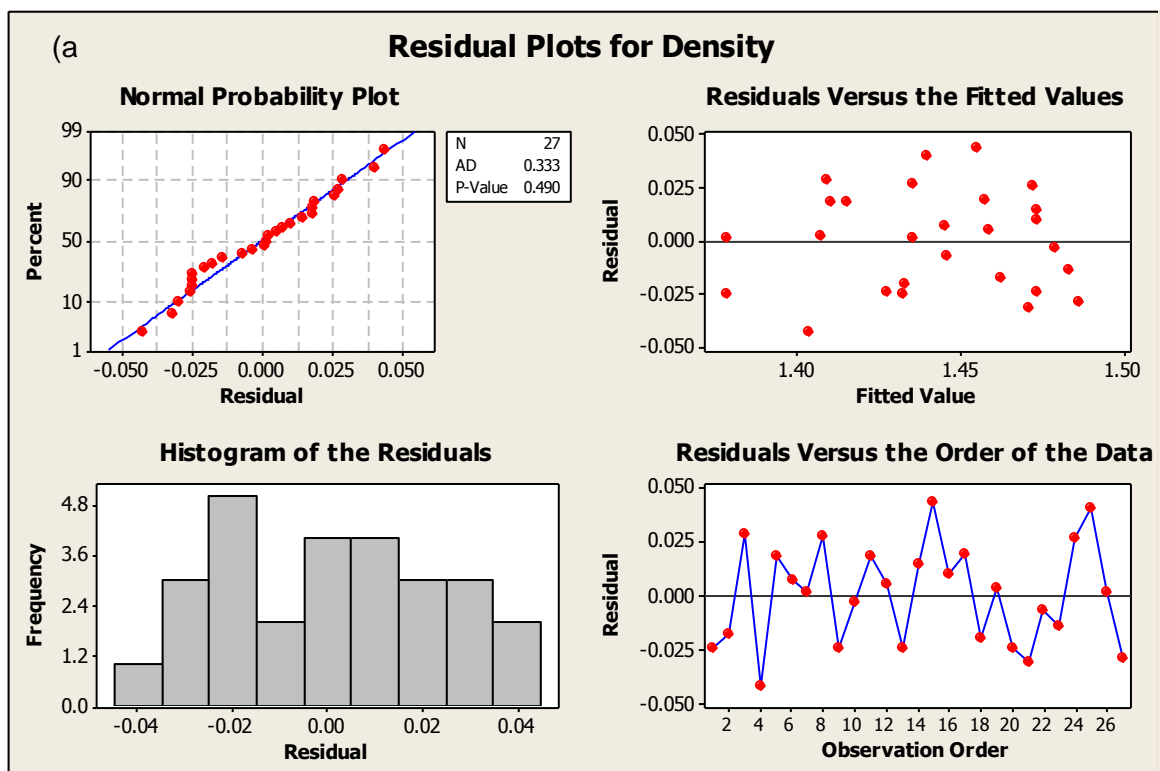


Figure 7.5a: Residual plots for density.

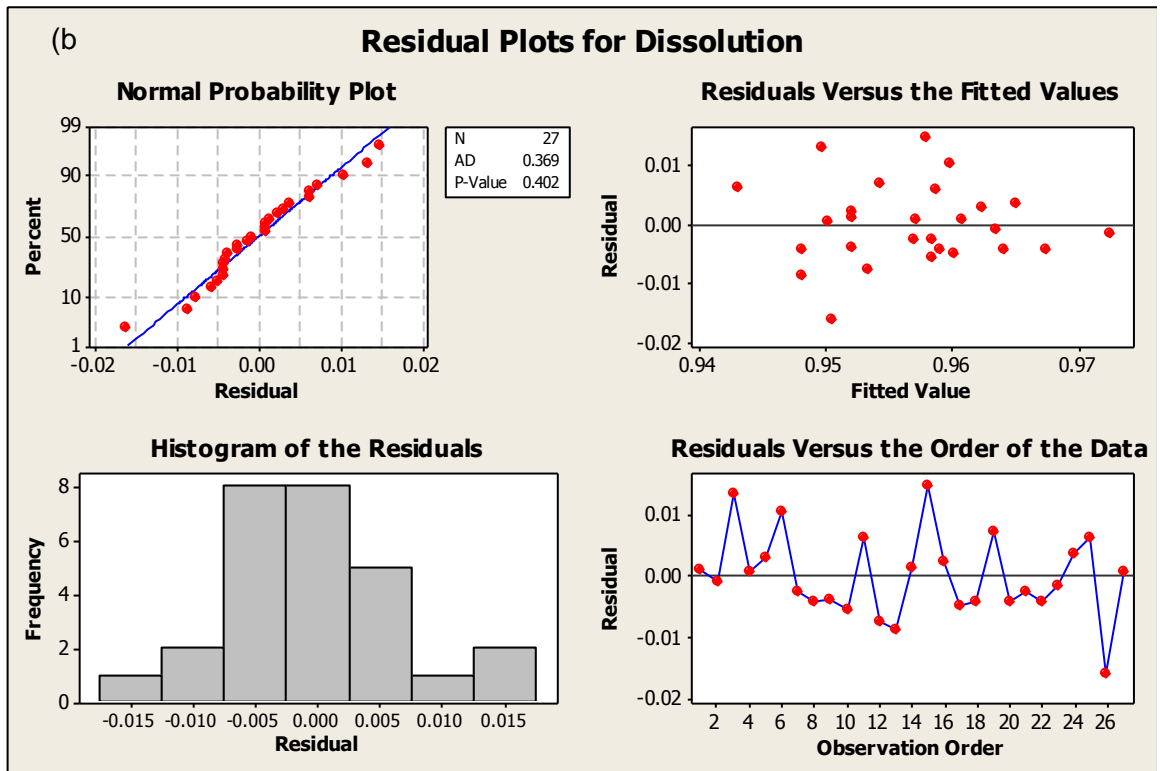


Figure 7.5b: Residual plots for dissolution.

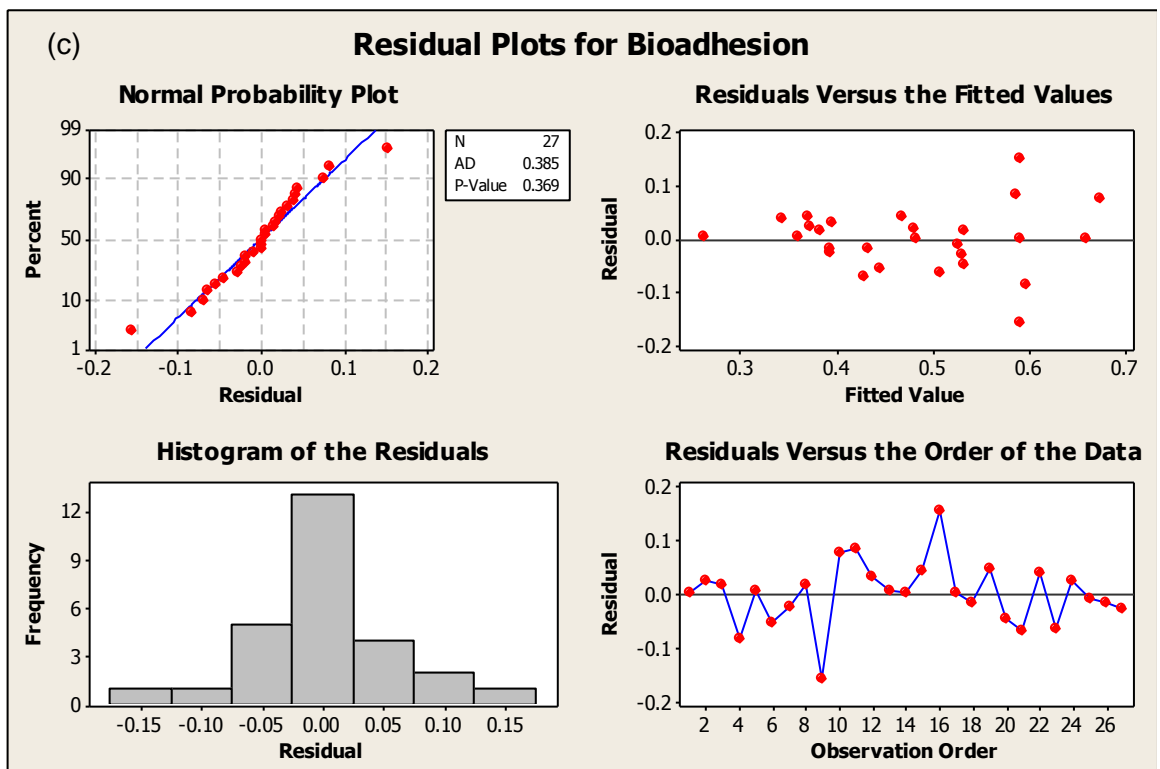


Figure 7.5c: Residual plots for bioadhesion.

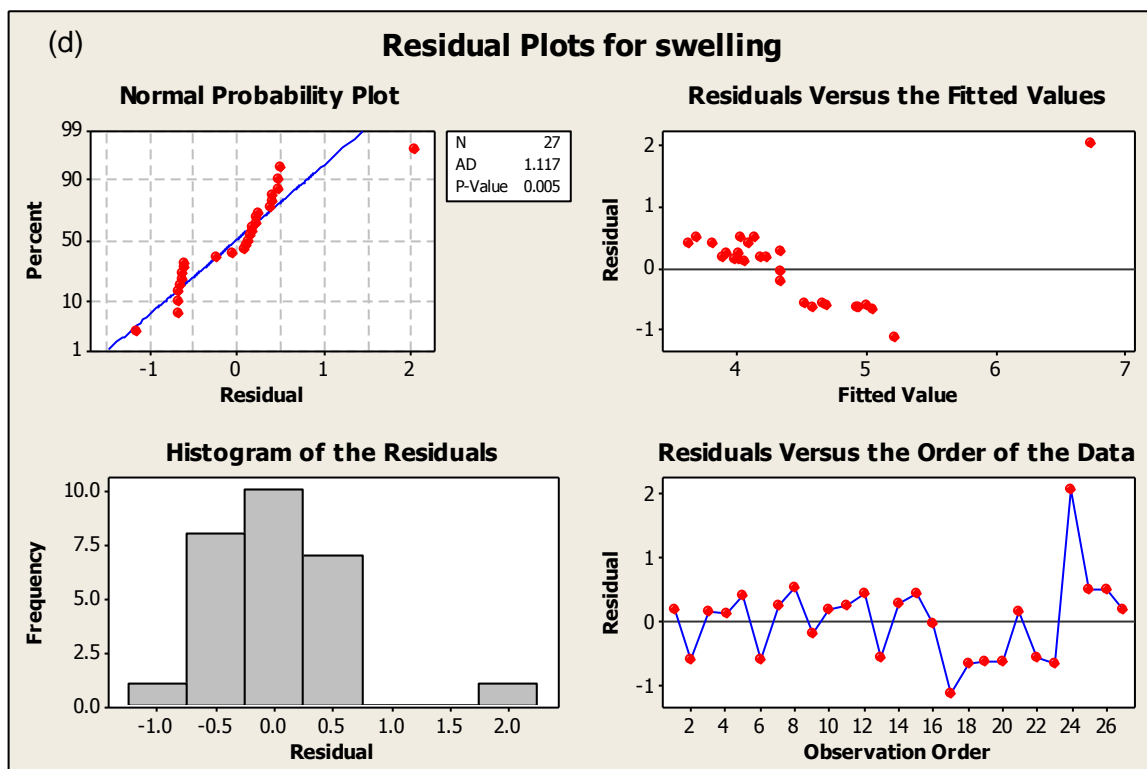


Figure 7.5d: Residual plots for swelling.

7.3.2.4. Surface plots

Surface plots (Figures 7.6a-d) elucidate the relationship between a response and two factors. However, if there are more than two factors, they are kept constant and are displayed in another plot. The surface plot of bioadhesion versus L and IPEC indicate that there is a maximum for bioadhesion of 0.7457N when L is 1.5g and IPEC is 2.7g as solvent and temperature are constant at 0.45N and 47.5°C respectively. The surface plot of swelling versus solvent and temperature shows that when the normality of acetic acid is as low as 0.1N and temperature is 25°C, swelling is highest at 8.7925N/mm. The surface plot of density versus solvent and temperature shows that density is highest (1.5mg/mm³) when the normality of the solvent is about 0.8N and the temperature is 47.5°C. The surface plot of dissolution versus temperature and IPEC shows that the rate of dissolution and subsequent concentration of drug released at the end of the study is highest when IPEC and temperature are low at 1.8g and 25°C respectively.

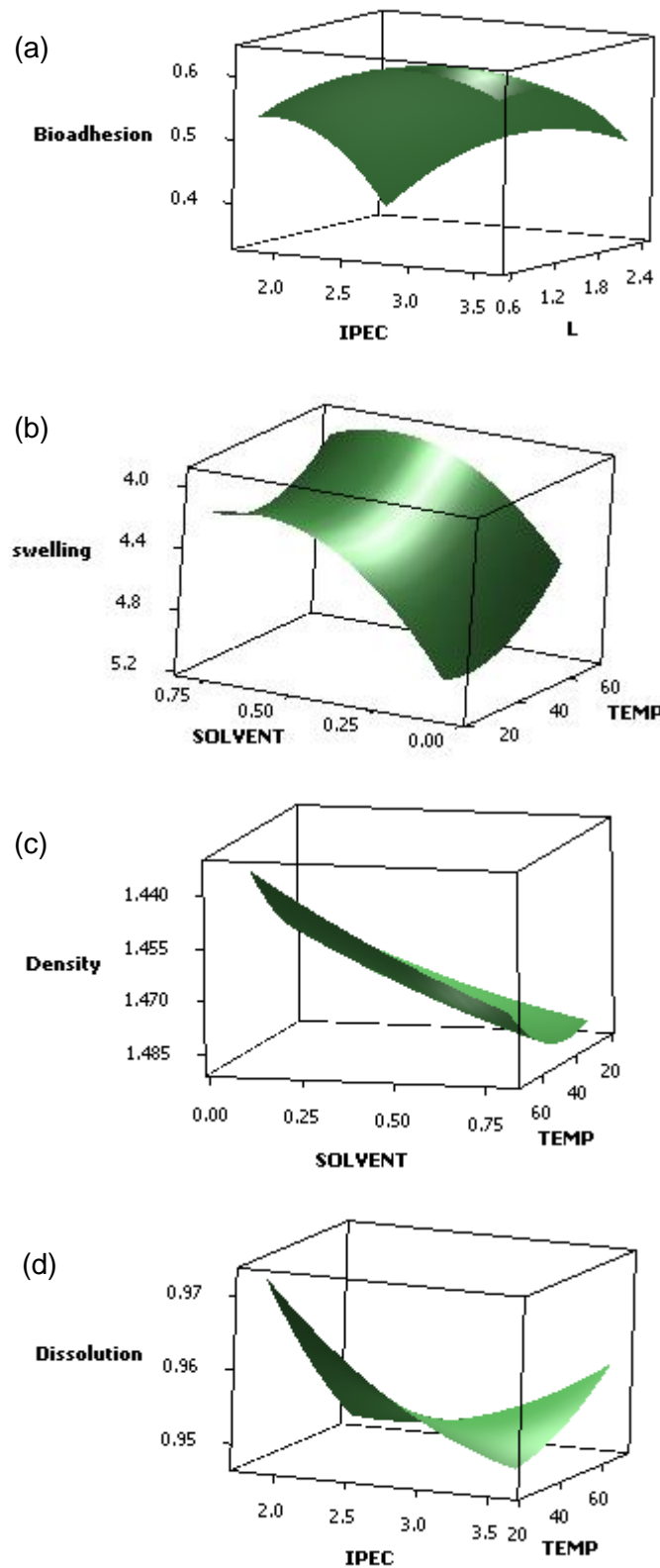


Figure 7.6: Surface plots of **a)** Bioadhesion versus locust bean and IPEC; **b)** Swelling versus solvent and temperature; **c)** Density versus temperature and solvent and; **d)** Dissolution versus temperature and IPEC.

7.3.2.5. Application of the desirability function for optimization

Desirability function was employed to obtain an optimal formulation for the four responses. The responses were transformed into the desirability set up and to achieve a desirability of 1, density was minimized while bioadhesion, swelling and dissolution were on target. The lower, target and upper values for the responses were input into the set up and the values for the independent variables – IPEC, L, solvent and temperature were generated for the composition of the optimized formulation as well as the predicted values for the responses expected to be obtained when the experimentals are undertaken. The output of optimization by desirability function is shown in Figure 7.7.

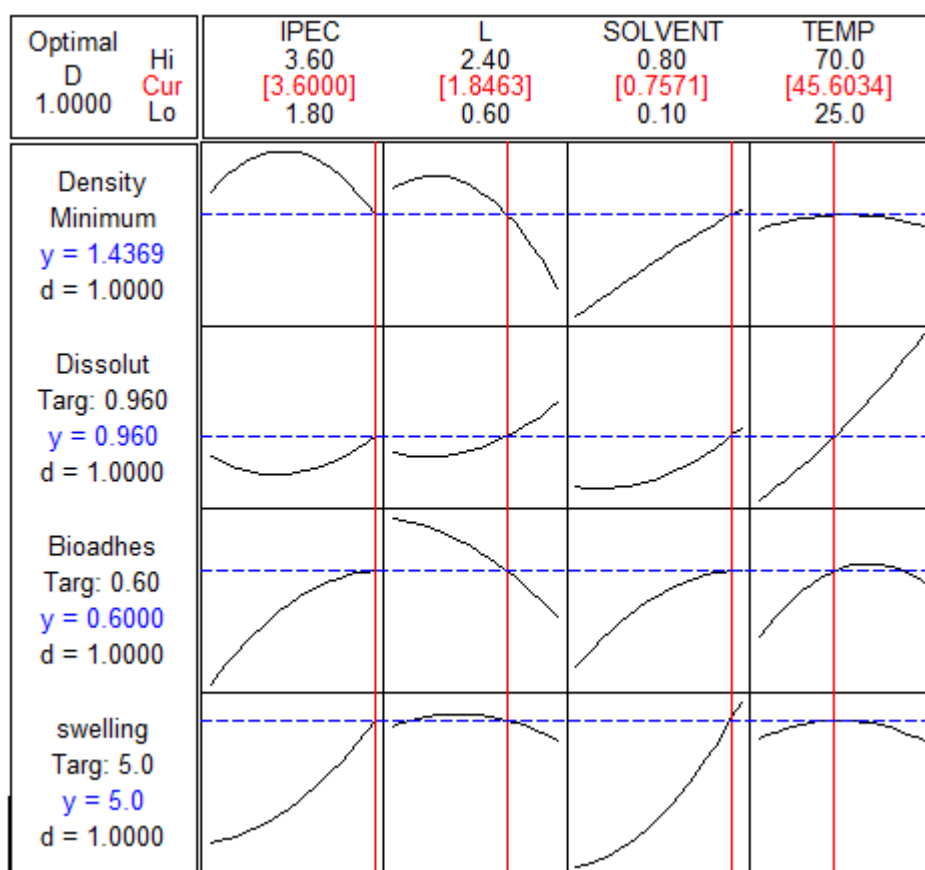


Figure 7.7: Output of optimization by desirability function showing the values for independent variables and predicted values for the responses.

7.4. CONCLUDING REMARKS

The Box-Behnken design and desirability function were adequate and effective in optimizing the interpolymeric blend. Analysis of the design portrayed the influence of the individual independent variables and their interactions on the responses. At the end, an optimal composition of interpolymeric blend was obtained. All the responses – dissolution, density, bioadhesion and swelling - had the desirability of 1. The values obtained for independent

variables will be utilized in development of the gastroretentive drug delivery system and characterization of the system will be undertaken to compare the predicted values and the observed values. However, before the predicted values will be tested, polymer-lipid nanoparticles which will be incorporated into the optimized interpolymeric blend will be fabricated and characterized in the next Chapter.

CHAPTER EIGHT

FABRICATION AND CHARACTERIZATION OF MULTI-CROSSLINKED POLYMER-LIPID NANOPARTICLES

8.1. INTRODUCTION

Despite the challenges posed by oral route on certain drugs such as narrow absorption window drugs and alternative routes being employed, the convenience of oral route behooves the quest to enhance peroral delivery of drugs. Poor or suboptimal therapeutic efficacy is usually obtained from drugs due to poor bioavailability which could be caused by biopharmaceutical, physiological or drugs' inherent factors. The two major factors affecting bioavailability are absorption and metabolism (Thomas et al., 2006), while other sub-factors relating to the two major factors are the physicochemical, biopharmaceutical and physiological factors such as solubility, permeability, particle size, chemical nature of the drug, enzymes, membrane transporters, effects of foods, gastrointestinal transit time, pH as well as type and process of formulation (Martinez and Amidon, 2002; Varma et al., 2004; Hurst et al., 2007). Technologies that have been employed to improve oral bioavailability include micronization (Thanos et al., 2003b; Rasenack and Müller, 2004), prodrugs (Chan et al., 1998; Gomez-Orellana, 2005; Baudy et al., 2009), salt formation (Gwak et al., 2005), absorption enhancement (Thanou et al., 2001), wetting (with wetting agent) and spray drying (Wong et al., 2006), solid dispersions (Leuner and Dressman, 2000; Vasconcelos et al., 2007), micellation (Sant et al., 2005), emulsification (Morishita et al., 1998; Dollo et al., 2003), micro- and nano-emulsification (Constantinides, 1995; Araya et al., 2005; Kuo et al., 2008; Yin et al., 2009), self-emulsification (Gershanik and Benita, 1996; Kang, et al. 2004), utilization of cyclodextrins (Reddy et al., 2004; Carrier et al., 2007), chemical modification (Song et al., 2002; Biron et al., 2008), sustained drug delivery, gastroretention and more recently, nanotechnology (Hu et al., 2004; Kesisoglou et al., 2007).

Nanotechnology is the study, fabrication, characterization and application of structures and materials at nanometer scale. Pharmaceutical nanotechnology employs mainly polymers to design, fabricate, characterize and apply nano-carriers for therapeutic purposes. While the field of engineering may describe nanoparticles as particles within 0.1 – 100nm, nano-drug carriers are less than 1 μ (Hans and Lowman, 2002; Sahoo and Labhasetwar, 2003), which is mainly due to the fact that they are fabricated with macromolecules-natural and synthetic polymers, lipids and proteins. Nanostructures that have been employed for drug delivery include polymeric nanoparticles, liposomes, dendrimers, nanoemulsions, solid lipid nanoparticles, nanocapsules and polymeric micelles (Gillies and Fréchet, 2005; Aliabadi and

Lavasanifar, 2006; Almeida and Souto, 2007; Jin and Ye, 2007; Bali et al., 2010; Drulis-Kawa and Dorotkiewicz-Jach, 2010; Kumari et al., 2010; Mora-Huertas et al., 2010).

Nanotechnology has been employed to improve bioavailability of some drugs where the difference when compared to the conventional system has been found to be significant. The *in vivo* studies of curcumin-loaded nanoparticles were found to have increased its bioavailability by at least 9-fold as compared to curcumin administered with piperine as an absorption enhancer (Shaikh et al., 2009). Other drugs with oral bioavailability enhanced by nanotechnology include cyclosporin-A (El-Shabouri, 2002), Amphotericin B (Italia et al., 2009), insulin (Pan et al., 2002; Sarmiento et al., 2007), HIV-1 protease inhibitors (Leroux, et al., 1996), Elcatonin (Kawashima et al., 2000), paclitaxel (Mu and Feng, 2003), Estradiol (Mittal et al., 2007), salmon calcitonin (Garcia-Fuentes et al., 2005), camptothecin (Yang et al., 1999) and mifepristone (He et al., 2007).

Nanostructures are fabricated utilizing a number/combination of technologies which include polymerization (De and Hoffman, 2001; Zhang et al., 2001), emulsion solvent evaporation (Desgouilles et al., 2003), salting out, emulsification-diffusion and nanoprecipitation (Zweers et al., 2003; Galindo-Rodríguez et al., 2005; Budhian et al., 2007); supercritical fluid technology (Byrappa et al., 2008; Varshosaz et al., 2009), coacervation and ionic gelation/crosslinking (Gan and Wang, 2007; Krauland and Alonso, 2007; Wang and Uludag, 2008). Crosslinking is a process of introducing bonds which may be chemical (covalent bonds) or physical (ionic bonds) between chains of the same material or different materials. It is basically an interaction that joins two molecular units thereby altering the material for characterization and improved functional properties.

The aim of this phase of study therefore, was to explore the feasibility of preparing L-dopa-loaded nanoparticles from a methacrylate copolymer/ methacrylate copolymer blend; and the various approaches of achieving sustained drug release from the nanoparticles. The method employed involved the application of miscible polymers in interaction with a phospholipid as the lipid component and a crosslinking agent with subsequent addition of a sequestrator as another crosslinking agent in a multi-crosslinking technology to fabricate polymer-lipid (*iPoly-X-Lipo*) nanoparticles. The nanoparticles were characterized by employing techniques such as computational modeling, size and surface analysis, FTIR spectroscopy, *in vitro* drug release studies and magnetic resonance imaging.

8.2. EXPERIMENTAL SECTION

8.2.1. Materials

Methacrylate copolymer (Eudragit E100) was purchased from Evonik Röhm GmbH & Co. KG (Evonik Röhm GmbH & Co. KG, Darmstadt, Germany), chitosan (food grade), (Wellable group, Fujian, China), sodium tripolyphosphate (TPP) (Sigma-Aldrich, Steinheim, Germany), lecithin from egg yolk (Lipoid E PC S, from Lipoid AG, Ludwigshafen, Germany), 3-(3,4-dihydroxyphenyl)-L-alanine (L-dopa), potassium phosphate monobasic (KH₂PO₄) (Sigma-Aldrich Inc., Steinheim, Germany), acetic acid glacial, hydrochloric acid (HCl) (Rochelle Chemicals, Gauteng, South Africa), potassium chloride (KCl) (Saarchem, Krugersdorp, South Africa), ortho-phosphoric acid (BDH Chemicals, Poole, England) and chloroform (Rochelle Chemicals, Gauteng, South Africa). All other reagents used were of analytical grade and were employed as purchased.

8.2.2. Nanofabrication of *iPoly-X-Lipo* nanoparticles

Weighed quantities of methacrylate copolymer and varying quantities of methacrylate copolymer with chitosan were dissolved in 10mL 0.2N HCl and 100mg of L-dopa was added into the polymeric solution. Lipoid E PC S (100mg) was dissolved in 1mL of chloroform and added to L-dopa-loaded polymeric solution under mechanical agitation for 10 minutes. Varying concentrations of TPP dissolved in 0.2N acetic acid were added under agitation for another 10mins, pre-frozen at -70°C for 24 hours and thereafter lyophilized for 48 hours. The different formulations of nanoparticles are shown in Table 8.1.

Table 8.1: Components and the respective quantities employed for nanoparticles formation.

Formulation	Eudragit (mg)	Chitosan (mg)	L-dopa (mg)	Lecithin (mL)	TPP (mg)
F1	150	150	100	1.00	250
F2	150	50	100	1.00	50
F3	100	100	100	1.00	50
F4	200	-	100	1.00	50
F5	50	50	100	1.00	100
F6	200	-	100	1.00	150
F7	100	100	100	1.00	150
F8	-	200	100	1.00	150
F9	-	200	100	1.00	-
F10	200	-	100	1.00	-
F11	100	100	100	1.00	-

8.2.3. Determination of pH and absorbance changes during fabrication

Initial pH values of the polymer solutions were obtained followed by changes in pH as materials were added in a stepwise manner in acidic media. Hence four pH values were obtained at the end of fabrication. pH determination was undertaken due to its influence on

the properties of polymeric materials/drug delivery systems such as zeta potential and drug release. The UV-Visible spectroscopic quantitation at 600nm was undertaken to elucidate the color changes/excitation which occurred at the different stages of nano-fabrication. The changes in absorbance from the polymer solution, on addition of lecithin and TPP afterwards were obtained. The absorbance changes were obtained in the absence of L-dopa so as to focus on the color changes during fabrication of nanoparticles without the pronounced absorbance impact of L-dopa.

8.2.4. Computational modeling of the fabrication of *iPoly-X-Lipo* nanoparticles

Computational modeling was performed to expound the interactions between the polymers and the crosslinking agents as well as the mechanism of the formation of nanoparticles. Models and graphics depicting the mechanisms of interactions were generated on ACD/I-Lab, V5.11 (Add-on) software (Advanced Chemistry Development Inc., Toronto, Canada, 2000). Interactions were interpreted by employing some general chemistry concepts and chemometric modeling concepts.

8.2.5. Size and surface charge analyses of the *iPoly-X-Lipo* nanoparticles

Nanoparticle size, size distribution profiles and zeta potential were generated using a ZetaSizer NanoZS instrument (Malvern Instruments, Malvern, Worcestershire, UK) equipped with non-invasive backscatter technology. The nanoparticles sizes and zeta potentials were profiled following the addition of lecithin, then after addition of TPP and finally after lyophilization.

8.2.6. Structural elucidation of the *iPoly-X-Lipo* nanoparticles

FTIR spectra over the range of 4000-650cm⁻¹ were obtained for the native polymers employed and the poly-lipo nanoparticles using a PerkinElmer Spectrometer (PerkinElmer Spectrum 100, Beaconsfield, United Kingdom) to elucidate the chemical structural transitions that occurred during nanofabrication.

8.2.7. Microscopical analysis of the L-dopa-loaded *iPoly-X-Lipo* nanoparticles

The surface morphology analyses of the *iPoly-X-Lipo* nanoparticles were undertaken by Digital Microscopy, Transmission Electron Microscopy (TEM) and Scanning Electron Microscopy (SEM). The digital microscopical images of the *iPoly-X-Lipo* nanoparticles after synthesis were obtained using an Olympus digital microscope; Olympus SZX-ILLD2-200 (Olympus Corporation, Tokyo, Japan). The nanosuspension was diluted tenfold with deionized water and drops were deposited on formvar coated nickel grids. They were allowed to dry in sealed petri dish and later viewed under TEM (JEOL-JEM 100S

Transmission Electron Microscope, Tokyo, Japan). Furthermore, lyophilized nanoparticles were thinly spread on a carbon tape, coated with gold-palladium and viewed under SEM (JEOL-JEM 840 scanning electron microscope, Tokyo, Japan) at a voltage of 15KeV and current of 6×10^{-10} Amp.

8.2.8. Determination of drug-loading and drug entrapment efficiency of the *iPoly-X-Lipo* nanoparticles

Percentage drug-loading efficiency was determined gravimetrically to assess the capacity of the nanoparticles with regards to the quantity of the loaded drug in the nanoparticles. The percentage drug-loading was calculated based on the weights of the incorporated drug and the nanoparticles employing Equation 8.1:

$$\text{Drug-loading (\%)} = \frac{\text{Quantity of drug in nanoparticles}}{\text{Quantity of nanoparticles}} \times 100$$

Equation 8.1

The drug entrapment efficiency was determined by dispersing the *iPoly-X-Lipo* nanoparticles in 0.1N HCl and the quantity of the drug in the medium was assessed spectrophotometrically at 280nm to obtain the quantity of drug in the poly-lipo nanoparticles with respect to the amount of drug used in the fabrication, employing equation 8.2:

$$\text{Drug Entrapment Efficiency (\%)} = \frac{\text{Actual Amount of drug}}{\text{Theoretical amount of drug}} \times 100$$

Equation 8.2

8.2.9. Direct compression of the *iPoly-X-Lipo* nanoparticles

8.2.9.1. Direct compression of the *iPoly-X-Lipo* nanoparticles

The lyophilized *iPoly-X-Lipo* nanoparticles were directly compressed without excipients in order to elucidate their drug release profiles unaided by excipients. The compression was undertaken using a Carver Hydraulic Press (Carver Industries Inc., Wabash, IN, USA) at 3tonnes.

8.2.9.2. Incorporation of *iPoly-X-Lipo* nanoparticles into an interpolymeric blend

The incorporation of *iPoly-X-Lipo* nanoparticles into an interpolymeric blend was undertaken by employing the IPB prepared in Chapter 5. The L-dopa-loaded *iPoly-X-Lipo* nanoparticles

were blended with the IPB (500mg per matrix) without adding any other excipients or additives. The nanoparticle-loaded interpolymeric blend was directly compressed employing Carver Hydraulic Press (Carver Industries Inc., Wabash, IN, USA) at 3tonnes. The composition of the nanoparticles utilized for incorporation into the interpolymeric blend is shown under Section 8.2.2, Table 8.1.

8.2.10. *In vitro* drug release studies

Drug release was assessed using USP apparatus II dissolution system (Erweka DT 700, Erweka GmbH, Heusenstamm, Germany). Temperature and stirring rate were $37\pm 0.5^{\circ}\text{C}$ and 50rpm respectively while the dissolution media were 900mL buffer pH 1.5 (standard buffer KCl/HCl) and pH 4.5 (0.025M $\text{KH}_2\text{PO}_4/\text{H}_2\text{PO}_4$). Samples were withdrawn at intervals and replaced with the same volume of fresh medium to maintain sink conditions. The amount of L-dopa released was quantified using UV spectrophotometer (LAMBDA 25 UV/Vis spectrophotometer, PerkinElmer, Massachusetts, USA) at 280nm. The drug release profiles were obtained from three (3) formulations of L-dopa-loaded nanoparticles:

8.2.10.1. Drug release studies of nanosuspension employing dialysis technique

Various quantities (depending on the varying composition) of L-dopa-loaded nanoparticles dispersed in 10mL of dissolution media; buffer pH 1.5 (standard buffer KCl/HCl) and pH 4.5 (0.025M $\text{KH}_2\text{PO}_4/\text{H}_2\text{PO}_4$) at separate periods were introduced into dialysis tubing (Dialysis tubing cellulose membrane, Ave flat width - 33mm, diameter – 21mm when full, M.W. 12,400, Sigma Aldrich, Steinheim, Germany). Both ends of the tubing were tightly sealed and placed in a dissolution vessel with 900mL of buffer and stainless ring-mesh assemblies were employed to keep the tubings in place to prevent erratic floatation due to unstable hydrodynamics above the paddle. Before incorporation of nanoparticles into the tubing, the dialysis tubing was immersed in deionized water for 3 hours to remove glycerol and sulfide from the tubing. The drug release studies were undertaken over 24 hours.

8.2.10.2. Drug release studies of the compressed matrices

The second and third drug release studies involved the matrices of the L-dopa-loaded nanoparticles alone and the L-dopa-loaded nanoparticles incorporated into the described IPB in pH 1.5 buffer (standard buffer KCl/HCl) and pH 4.5 (0.025M $\text{KH}_2\text{PO}_4/\text{H}_2\text{PO}_4$) over 24 hours. The apparatus and parameters employed for dissolution are as stated above.

8.2.11. Magnetic resonance imaging of mechanical behavior

A magnetic resonance system with digital MARAN-i System configured with a DRX2 HF Spectrometer console (Oxford Instruments Magnetic Resonance, Oxon, UK) equipped with a

compact 0.5 Tesla permanent magnet stabilized at 37°C and a dissolution flow through cell was employed for the viewing of the mechanical behaviors of the matrices. After duly configuring, optimizing the shims and probe tuning, the cone-like lower part of the cell was filled with glass beads to provide laminar flow at 16mL/min of the solvents employed. The matrices were placed in position each time within the cell which in turn was positioned in a magnetic bore of the system and magnetic resonance images were acquired hourly over 12 hours with MARAN-i version 1.0 software. The image was acquired after setting the frequency offset and testing gain employing RINMR version 5.7 under continuous solvent flow conditions. MARAN-i software comprises image acquisition software and image analysis software. The image acquisition parameters are depicted in Table 8.2.

Table 8.2: Image acquisition parameters applied during magnetic resonance imaging using MARAN-i.

Parameters	Value
Imaging protocol	FSHEF
Requested gain (%)	1.90
Signal strength	71.62
Average	2
Matrix size	128
Repetition time (ms)	1000.00
Spin Echo Tau (ms)	6.00
Image acquired after	60min
Total scans	64

8.2.12. Static lattice atomistic simulations

Molecular Mechanics computations in vacuum, which included the model building of the energy-minimized structures of multi-polymer-crosslinker complexes, were performed using the HyperChem™ 8.0.8 Molecular Modeling System (Hypercube Inc., Gainesville, Florida, USA) and ChemBio3D Ultra 11.0 (CambridgeSoft Corporation, Cambridge, UK) (Kumar, et al. 2011). The structures of methacrylate copolymer (E100-four monomer units), Phospholipid residues (PR) and TPP were generated as a 3D model from standard bond lengths and angles employing ChemBio3D Ultra whereas the structure of chitosan (CHT-ten glucosamine oligosaccharide units) was generated using sugar builder module on HyperChem 8.0.8. The generation of the overall steric energy associated with the energy-minimized structures was initially executed via energy-minimization using MM+ force field and the resulting structures were again energy-minimized using the Amber 3 (Assisted Model Building and Energy Refinements) force field. The conformer having the lowest energy was used to create the polymer-crosslinker complexes. A complex of one molecule with another was assembled by disposing them in a parallel fashion, and the same procedure of energy-minimization was repeated to generate the final models: CHT-TPP, CHT-PR, E100-PR and E100-PR-CHT. Full geometry optimizations were carried out in vacuum employing the

Polak–Ribiere conjugate gradient method until an RMS gradient of 0.001kcal/mol was reached. Force field options in the AMBER (with all hydrogen atoms explicitly included) and MM+ (extended to incorporate non-bonded cut-offs and restraints) methods were the HyperChem 8.0.8 defaults. For calculations of energy attributes, the force fields were utilized with a distance-dependent dielectric constant scaled by a factor of 1. The 1-4 scale factors used were electrostatic - 0.5 and van der Waals - 0.5 (Kumar et al., 2011).

8.3. RESULTS AND DISCUSSION

8.3.1. Modeling, changes in pH and absorbances of *iPoly-X-Lipo* nanoparticles during fabrication

Polymeric miscibility was observed between methacrylate copolymer and chitosan with no visible interactions. Hence, the enhancement of the individual properties of the polymers is envisaged to be through blending. Methacrylate copolymer is not as viscous as chitosan due to the fact that methacrylate copolymer has lesser molecular area and topology (structure). Hence, its chemical infrastructure will have more space for incoming entities while chitosan holds more molecular area with less internal spaces and so will require less TPP crosslinking as compared to methacrylate copolymer.

The similar molecular weight units (MW - methacrylate copolymer 968, chitosan 972) for both polymers were energetically minimized qualitatively (as no numerical values of energies were calculated by the software) using ACD software in molecular modeling based on three-dimensional (3D) structures of the polymeric units but depicted as dot models in Figure 8.1A-D:

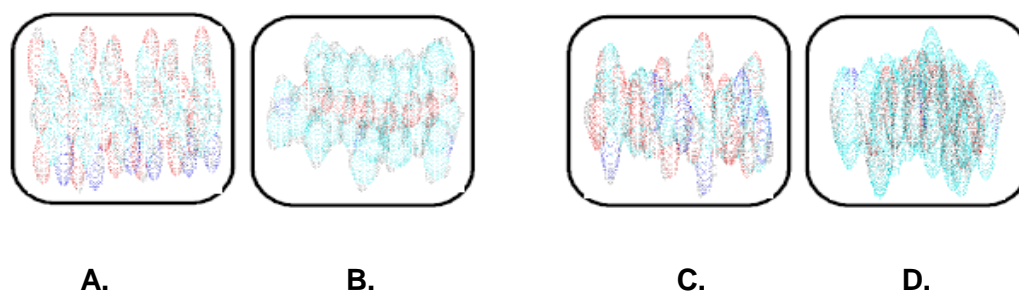


Figure 8.1: The molecular surface, topology and spaces of the polymers–chitosan and methacrylate copolymer for incoming ligands.

The models obtained were assessed for the maximum unit area of occupation within the given (universally equal) rounded squares defined as unit spaces for the static state of the polymeric units. e.g. (A) chitosan (equimolecular weighted units) at maximum unit area of occupation with highest surface area in the particular 2D dimension. (B) methacrylate

copolymer (equimolecular weighted units) at maximum unit area of occupation with highest surface area in 2D dimension of the model; the most area of occupancy state. (C) chitosan at maximum unit area of occupation with lowest surface area in 2D dimension of the model at static state; the least area of occupancy for the rounded square sizing unit, (D) methacrylate copolymer (equimolecular weighted units) at maximum unit area of occupation with lowest surface area in 2D dimension of the model in static state; the least area of occupancy state. Thus, it is presumed that the difference in edges and other 2D matrix areas in the unit space will be available to the incoming ligands or low molecular weight (LMW) entities. However, in 3D unit space, the difference in area will be nil but for the longer strands of the polymeric molecule, one dimension of the X, Y or Z will be comparatively inconsequential or least effective and at a larger scale, the structures may follow the 2D modeling for available spaces and facility for ligands/ LMW entities coming in. The 3D illustrations of maximum area of occupancy of chitosan and methacrylate copolymer as well as the fusion of the two polymers are shown in Figures 8.2 and 8.3:

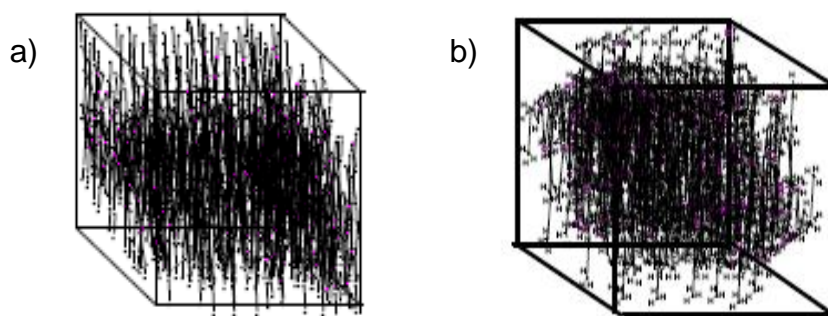


Figure 8.2: **a)** Space-fill/matrix occupation diagram showing maximum occupancy in unit area for chitosan and; **b)** Space-fill/matrix occupation diagram showing maximum occupancy in unit area for methacrylate copolymer.

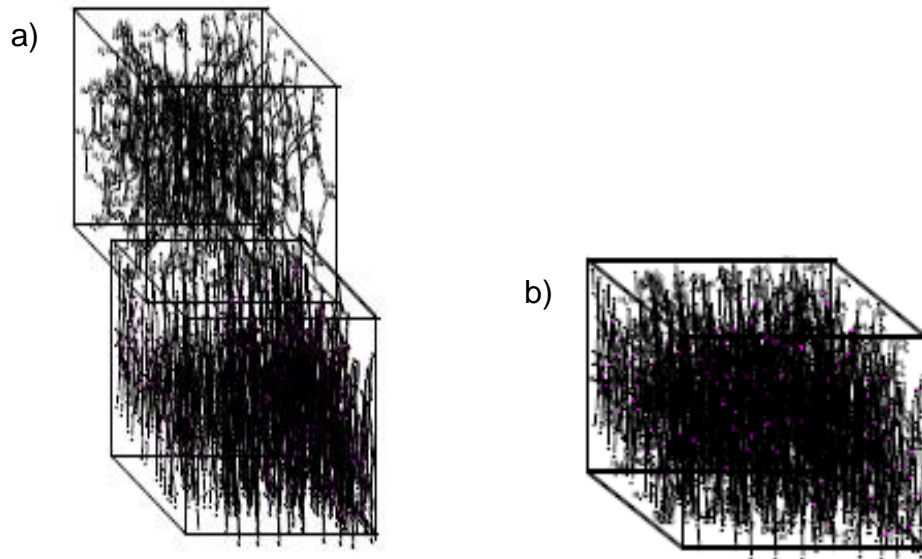


Figure 8.3: **a)** Space-fill/matrix occupation diagram showing maximum occupancy of methacrylate copolymer and chitosan before mixing or fusion in unit area for equal number of molecular weighted polymers (Both methacrylate copolymer and chitosan - approx mol weight $\sim 12K$ amu) and; **b)** Fused polymeric matrix containing methacrylate copolymer and chitosan (it may or may not have L-Dopa, lecithin, TPP or solvent - almost all filled in the space between chain).

The nanoparticle synthesis (with incoming entities - lecithin, L-dopa and TPP incorporated into the polymeric matrix) may follow either of seven patterns depending on the space, sizes of particles being formed initially and presence or absence of turbulence. These patterns are tree branching, nodal space fillings, cone array formations, mixed triangular formations, linear patterns, chaotic patterns and mixed patterns.

Figure 8.4 shows the octree, 2D and 3D representations of the tree branching pattern. The central cross-point (+) in Figure 8.4a denotes the progenitor point for the nanoparticle synthesis start-up which is followed by distribution to available spaces in an evolving 3D patterning-placement of emerging nanoparticles. The tree formation is dependent on the space available in the 3D matrix area following the branching pattern where the differentiations are outer and inner (back) space bound depending upon the accommodating space for the particles in all the directions.

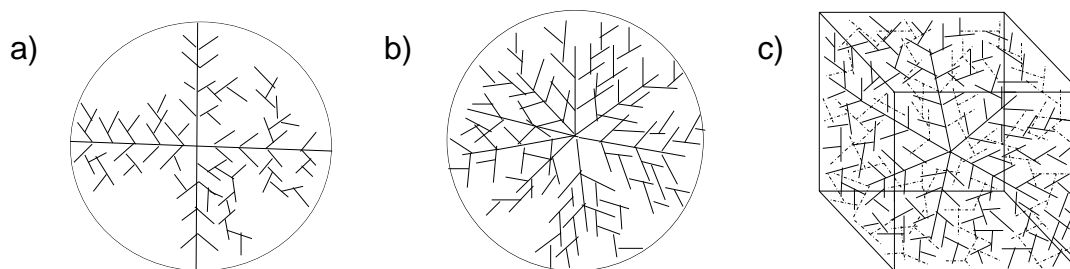


Figure 8.4: Tree branching pattern of nanoparticle formation: **a)** Octree representation; **b)** Two-dimensional depiction and; **c)** Three-dimensional representation.

Nodal space filling pattern (Figure 8.5) is dependent upon the space-fill in nodal points where the matrix accommodates the emerging nanoparticles while the node generation is dependent upon the changing coordinates of the matrix and their distance parameters (which could accommodate the incoming particles). The nanoparticle emergence in this fashion-order of patterning is dependent on the available space, size and distribution of the nanoparticles.

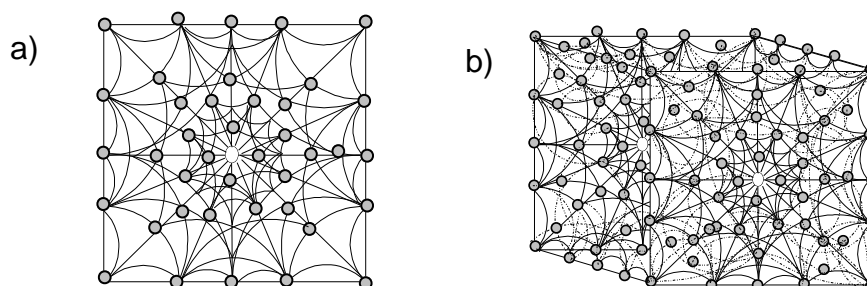


Figure 8.5: Nodal space fillings of nanoparticle formation: **a)** Two-dimensional and; **b)** Three-dimensional representation.

The progenitor area for cone-array pattern is a circle in the middle as shown in Figure 8.6. The formation of nanoparticles is patterned by cone formations where the single lines represent the initial line up and the merged lines depicting the cone formations onto which nanoparticles line up simultaneously as they are formed in the medium. The cone-arrays distributions within the matrix is dictated by the physicochemical properties of the polymeric matrix, the formation of the nanoparticles, their optimal formation, their crowding and ultimately the thinning density of the emerging nanoparticles which may be influenced by synthesis restrictions, raw materials and space limitations.

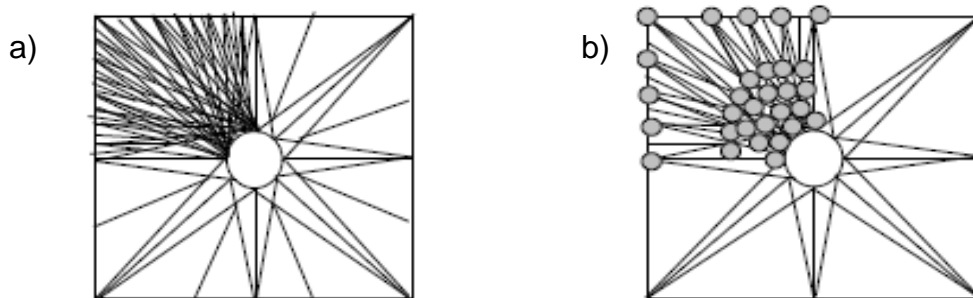


Figure 8.6: **a)** Two-dimensional depiction of cone-array formations and; **b)** Particle development, crowding and thinning of the density (space versus number of particles).

The particle formation in mixed triangle formations leads towards a triangular shape from the progenitor point and the end point tapering in 3D spaces trying to fill the unit matrix area in all plausible directions as shown in Figure 8.7. The triangles are formed due to the differentiation of the nanoparticles and changing shape of the matrix under applied force during experimental conditions from nanoparticles which are located along the triangular lines.

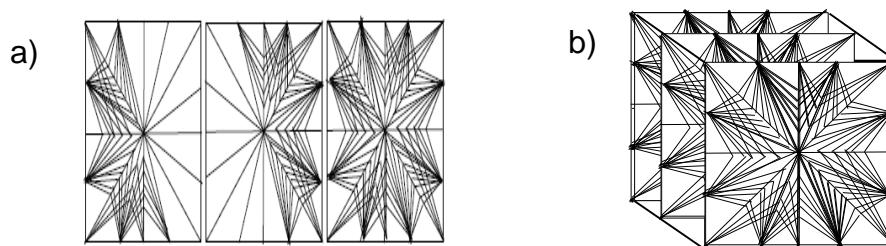


Figure 8.7: Frontal view of mixed triangle formations of nanoparticles: **a)** Two-dimensional slice representation and; **b)** Three-dimensional slice representation.

Figure 8.8 represents the linear pattern with progenesis also from the middle with formation of more lines of propagation while the nanoparticles are formed on the lines.

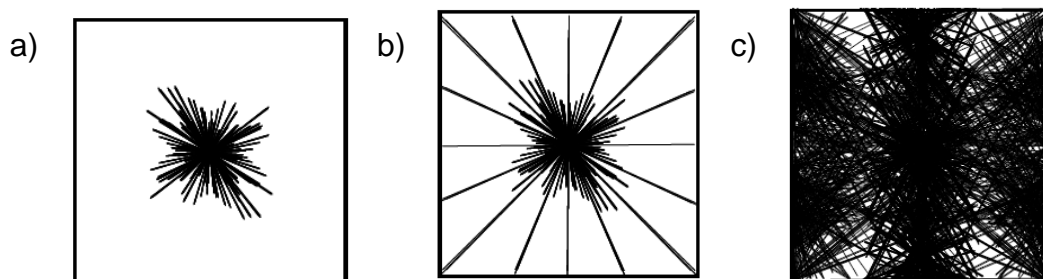


Figure 8.8: Linear pattern of nanoparticle formation: **a)** Progenesis and initial propagation; **b)** More lines of propagation and; **c)** Two-dimensional model of the matrix containing nanoparticles on the lines.

The chaotic pattern is dependent on the progenesis point and its location in a comparatively non-turbulent medium. The formation of nanoparticles may follow any design in the x, y, z, top or bottom arrangement of the matrix (Figure 8.9).

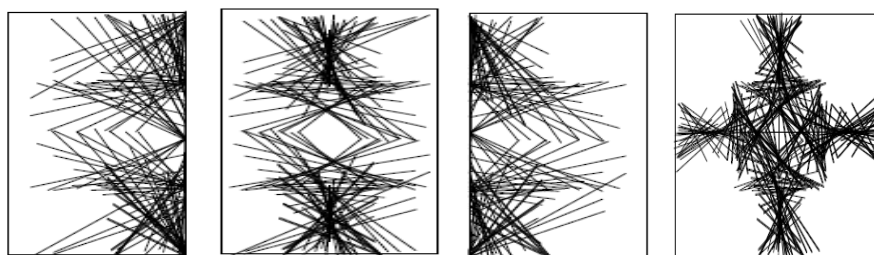


Figure 8.9: Two-dimensional chaotic pattern of nanoparticle formation

Mixed pattern in Figure 8.10 is based on randomization which can occur with a single progenitor or multiple progenitors. Multiple progenesis is initiated by the presence of turbulence in the medium.

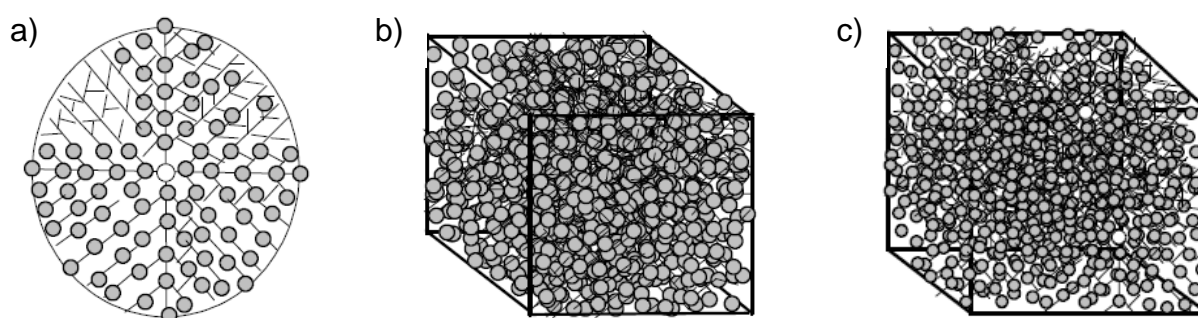


Figure 8.10: Mixed patterns of nanoparticle formation based on randomizations: **a)** Two-dimensional slice of a single progenitor random patterning; **b)** Three-dimensional model of single embedded progenitor in a chaotic-random mix state and; **c)** Three-dimensional model of the multiple progenitors in a chaotic-random mix state based on turbulence in the medium.

In summary, it is envisaged that the likely pattern of nanoparticle formation that could have occurred in the experimental conditions (agitation) employed for this study could be either mixed triangle formations or mixed patterns.

Lecithin is an anionic phospholipid and surfactant which physically crosslinks cationic methacrylate copolymer and methacrylate copolymer/chitosan polymeric solutions by electrostatic interactions to produce polymer-lipid (*iPoly-X-Lipo*) nanoparticles. Studies have confirmed the interactions between chitosan and phospholipids (lecithin) (Grant et al., 2005; Ho et al., 2005; Sonvico et al., 2006; Lim et al., 2008; Hafner et al., 2009; Zahedi et al., 2009), while the interaction between methacrylate copolymer and lecithin was observed in this study. The act of sequestration and crosslinking of TPP further binds the components in

a nanoparticulate complex. The addition of TPP increases the degree of crosslinking which is envisaged will influence rate of drug release from the *iPoly-X-Lipo* nanoparticles.

Increase in concentration of polymers and other ingredients increased the pH of nanosuspensions (Table 8.3). For methacrylate copolymer/chitosan blend, pH increased with addition of each component but the increase is slightly more pronounced when TPP is added. However, with methacrylate copolymer alone - B9 and B18, there was no change in pH from the addition of L-dopa to addition of lecithin.

White methacrylate copolymer nanoparticles and off-white methacrylate copolymer/chitosan nanoparticles were formed in the presence of lecithin and TPP. On addition of lecithin, a color change (colloidal dispersion) was observed indicating the presence of interactions between lecithin (phospholipid) and the polymeric solution. The color change could also be due to the formation of capsular wall and surfactant activity. Furthermore, the color change may be depicting energy perturbation. The oxygen excitation provides the color change – protons are absorbed and the rest of the visible spectrum wavelength are reflected back. The addition of TPP to chitosan or methacrylate copolymer/chitosan blend led to an increased intensity of the off-white color because of the oxygen related functions (excitable oxygen atoms, conjugated oxygen containing groups in higher degree are present in chitosan and TPP). The degree of absorbance of visible light increases as lecithin and TPP are added to polymeric solutions (Table 8.4) which is also an indication of color change and subsequent interactions between polymeric solution and the ionic agents (lecithin and TPP). However, it is observed that addition of TPP to methacrylate copolymer-lecithin blend led to a decrease in absorbance. This is due to the fact that chemical infrastructure of the methacrylate copolymer requires a greater quantity of TPP than utilized to achieve sufficient particulate complexation.

An increase in TPP generates drier and free flowing particles. This is attributed to increased quantity of TPP causing less room in the particles matrices for solvent and water molecules. From the modeling, the morphology of the nanoparticles formed is suggested to be nanocapsules, loosely filled hollow capsules or solid spherical particles.

Table 8.3: Comparative pH changes during nano-fabrication.

Formulation Code	Polymer Solution ¹	Addition of L-dopa	Polymer + L-Dopa + Lecithin	Polymer + L-dopa + Lecithin + TPP
F1	1.17	1.31	1.36	3.15
F2	1.17	1.34	1.40	1.73
F3	1.18	1.36	1.41	1.78
F4	1.13	1.28	1.28	1.68
F5	1.14	1.19	1.23	1.78
F6	1.13	1.28	1.28	2.37
F7	1.18	1.36	1.41	2.82

¹ pH of 0.2N HCL was 1.00

Table 8.4: Changes in absorbances during nano-fabrication.

Polymer composition	Polymer solution	Addition of lecithin	Addition of TPP
E100 ¹	0.0135	0.5681	0.4876
Chitosan	0.1382	3.3501	3.5597
E100 + Chitosan	0.0589	2.7885	3.1930

¹ E100 - methacrylate copolymer

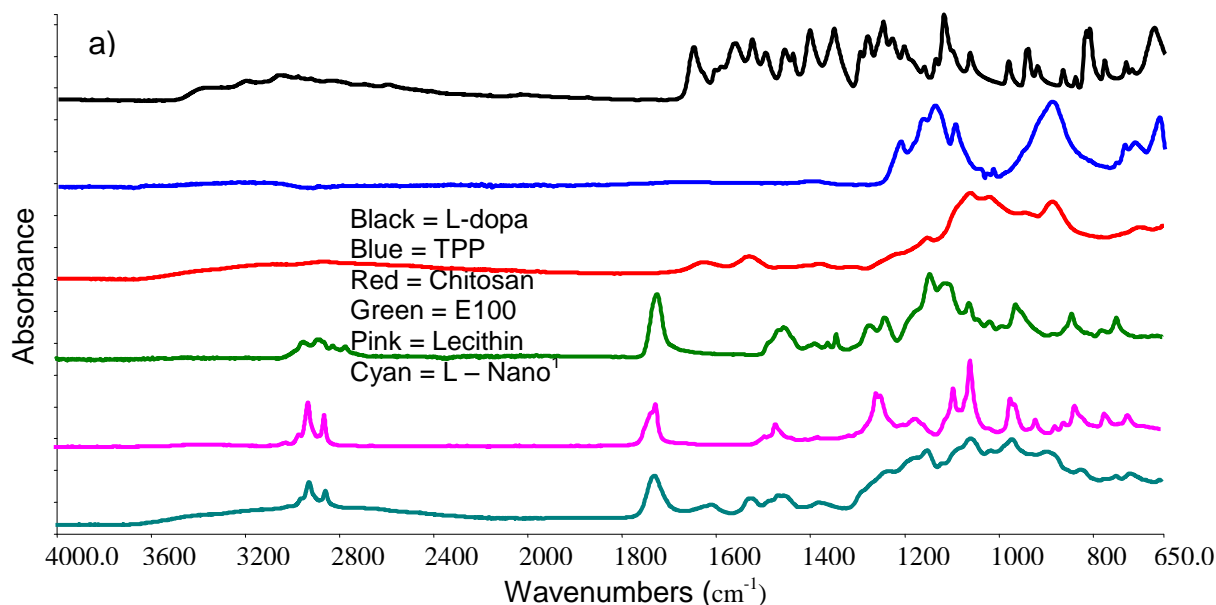
8.3.2. Size and surface charge analyses of *iPoly-X-Lipo* nanoparticles

The average particle sizes of the nanoparticles after the addition of lecithin ranged from 152nm for methacrylate copolymer only to 321nm for the methacrylate copolymer/chitosan blend while the zeta potential ranged from +15.8 to +43.3mV. As the quantity of chitosan increased, the particle size increased. Furthermore, as the degree of crosslinking increased by the addition of TPP, the particle size increased to average particle size of 424nm. The polydispersity index ranged from 0.19 to 0.61. Formulation of *iPoly-X-Lipo* nanoparticles as a nanosuspension may require an increased quantity of TPP to ensure free flowing nanoparticles. When administered as nanosuspension, it is envisaged that based on the mucoadhesive property of chitosan, the nanoparticles will adhere to the mucosal wall of the duodenum while L-dopa is released into the systemic circulation. Hence, obtaining size below 100nm may not primarily be the focus but rather free flowing particles to ensure effective packaging.

8.3.3. Structural elucidation of the *iPoly-X-Lipo* nanoparticles

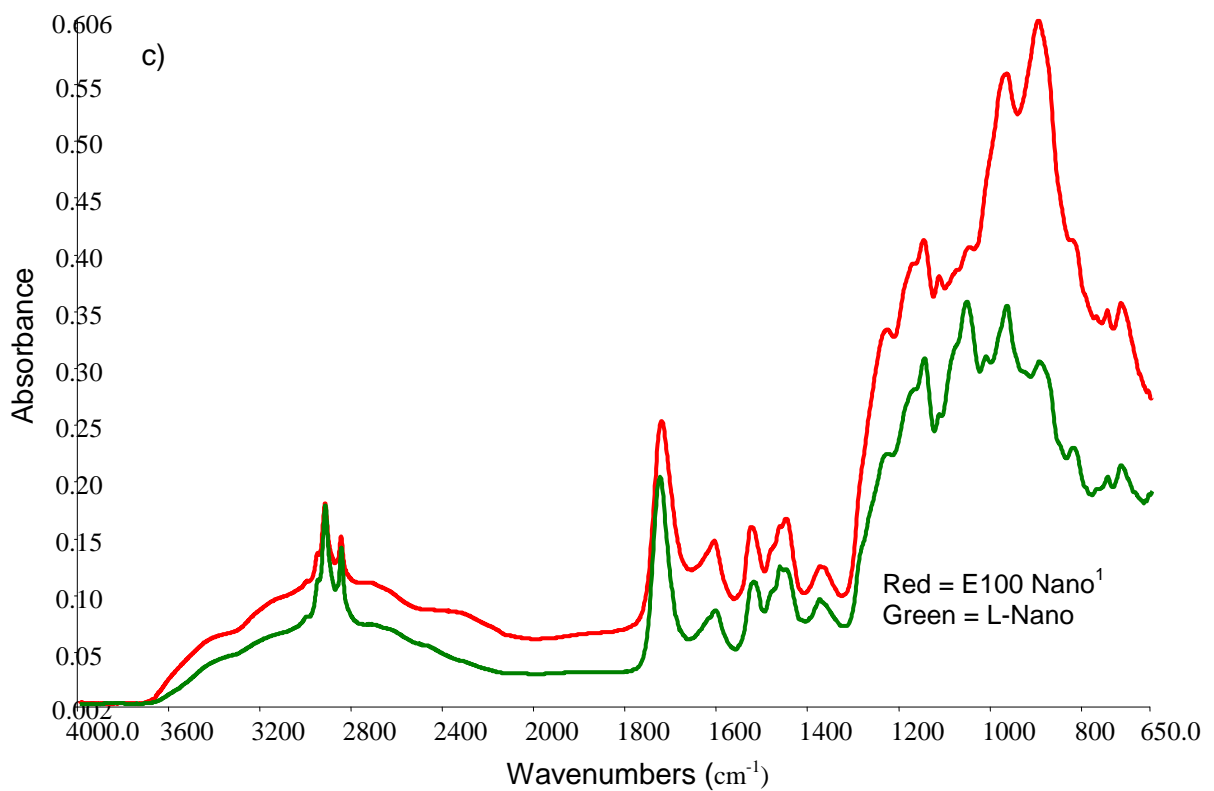
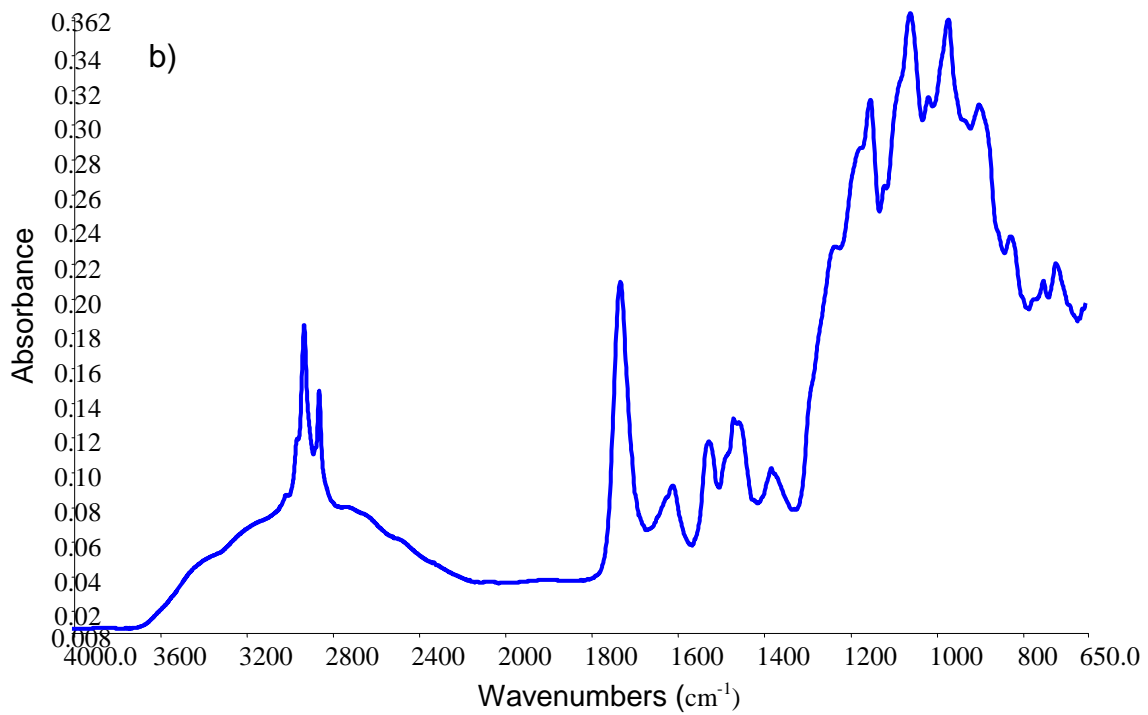
The spectra as shown in Figure 8.11 exhibited the chemical structural transitions that had occurred during nanofabrication by multi-crosslinking. In comparison with the spectra of the native polymers, the spectra of the nanoparticles showed absence of some peaks found in the native polymers such as at frequencies of 2769.74cm⁻¹ and 1268.73cm⁻¹ for methacrylate copolymer; 3357.51cm⁻¹, 1590.66cm⁻¹ and 1024.66cm⁻¹ for chitosan with emergence of new peaks after crosslinking at 1605cm⁻¹ which was found in methacrylate copolymer

nanoparticles as well as the blend (methacrylate copolymer/chitosan); 1519cm^{-1} in methacrylate copolymer which slightly shifted in the blend to $1518.75\text{-}1522.24\text{cm}^{-1}$ (envisaged to be determined by the degree of crosslinking in each nanoparticles formulation). Furthermore, the peaks in the native polymers which may be considered to still exist such as 2949.11cm^{-1} in methacrylate copolymer shifted to 2923.91cm^{-1} ; 1722.39cm^{-1} shifted to 1724.86cm^{-1} and 891.80cm^{-1} in chitosan shifted to 889.79cm^{-1} . The distinct aldehyde functional group (C=O) found in methacrylate copolymer at 1722.46cm^{-1} and in lecithin at 1722.16cm^{-1} was found in the nanoparticles at 1727.97cm^{-1} (Figures 8.11a and b). The disappearance of peaks and emergence of new peaks is attributed to the interactions between the ionic agents leading to a polymer-lipid-salt particulate complex. The differences between spectra of methacrylate copolymer nanoparticles and methacrylate copolymer/chitosan nanoparticles as shown in Figure 8.11c are found at the O-C bands (1056.09cm^{-1} and 1013.64cm^{-1}) and at 824.73cm^{-1} of methacrylate copolymer while the other peaks which are similar in both did not absorb at exactly the same place. Some peaks have a difference in absorbance frequencies of 1, 2 or 3cm^{-1} . No additional difference was found when benserazide was incorporated (Figure 8.11d) which may be an indication that the drugs – L-dopa and benserazide did not interact with other components or due to the small quantity of benserazide and its similarity in structure to levodopa; there was no observed distinct peak for it (benserazide).



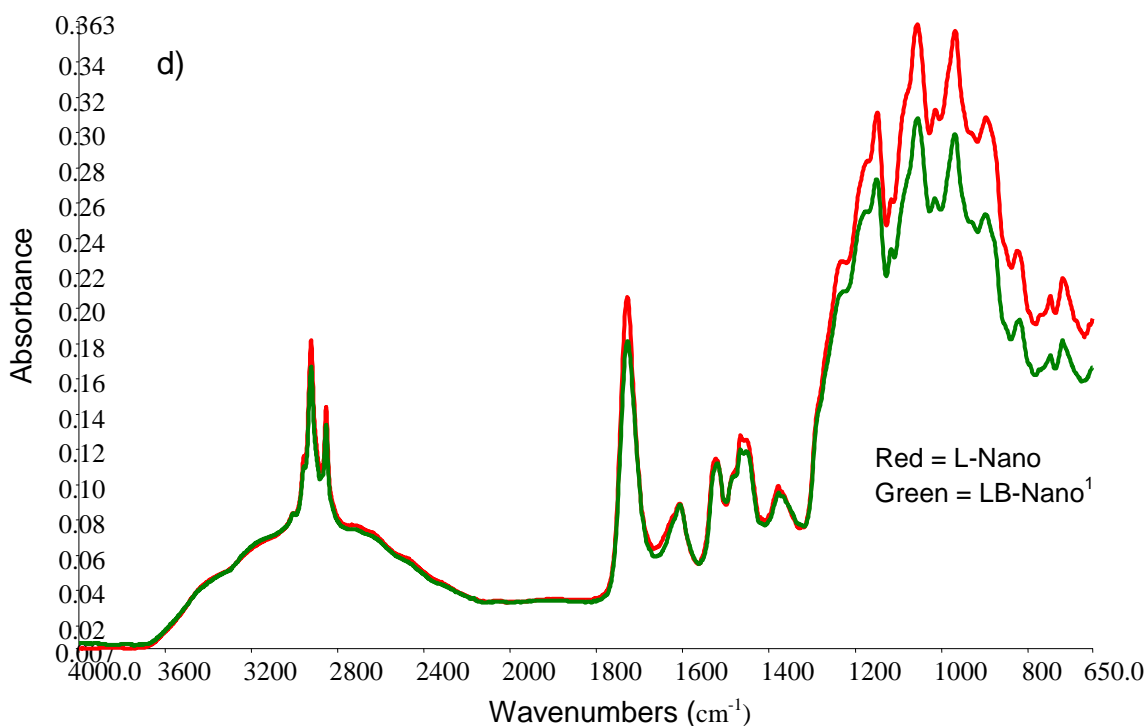
¹ L-dopa-loaded methacrylate copolymer/chitosan nanoparticles

Figure 8.11a: FTIR spectra of the various components employed for fabrication of nanoparticles as well as the fabricated L-dopa-loaded nanoparticles.



¹ L-dopa-loaded methacrylate copolymer nanoparticles

Figure 8.11: FTIR spectra of: **b)** L-dopa-loaded nanoparticles and; **c)** Methacrylate copolymer nanoparticles and methacrylate copolymer/chitosan nanoparticles.



¹ L-dopa/Benserazide-loaded nanoparticles

Figure 8.11d: FTIR spectra of L-dopa- and L-dopa/benserazide-loaded nanoparticles.

8.3.4. Surface morphology of the *iPoly-X-Lipo* nanoparticles

Spherically structured nanoparticles were observed as viewed under the digital microscope before lyophilization. Figure 8.12 shows digital images of methacrylate copolymer/chitosan crosslinked with lecithin only and multi-crosslinked methacrylate copolymer nanoparticles. The smaller sizes of methacrylate copolymer nanoparticles as compared to the polymeric blend with chitosan were further confirmed by the digital images.

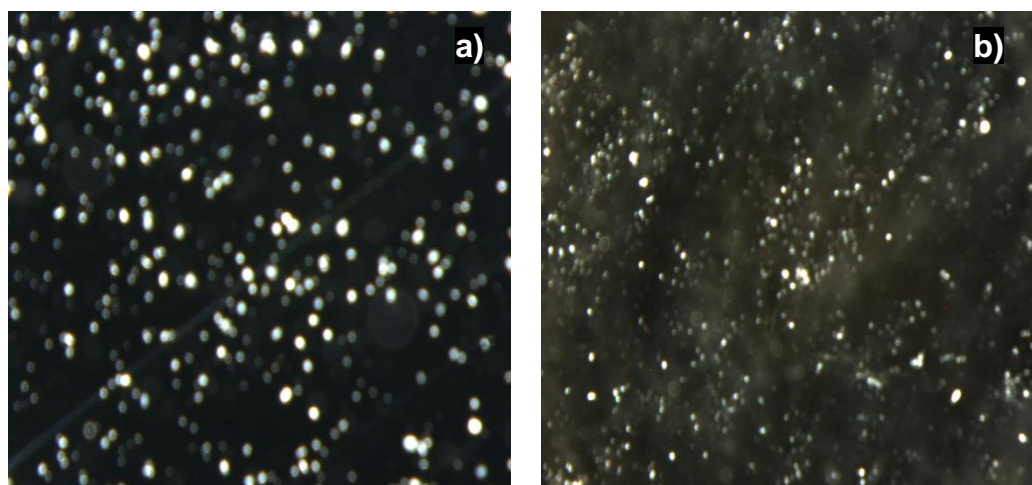


Figure 8.12: Digital images of: **a)** methacrylate copolymer/chitosan crosslinked with lecithin alone and; **b)** multi-crosslinked methacrylate copolymer nanoparticles (Mag x 32).

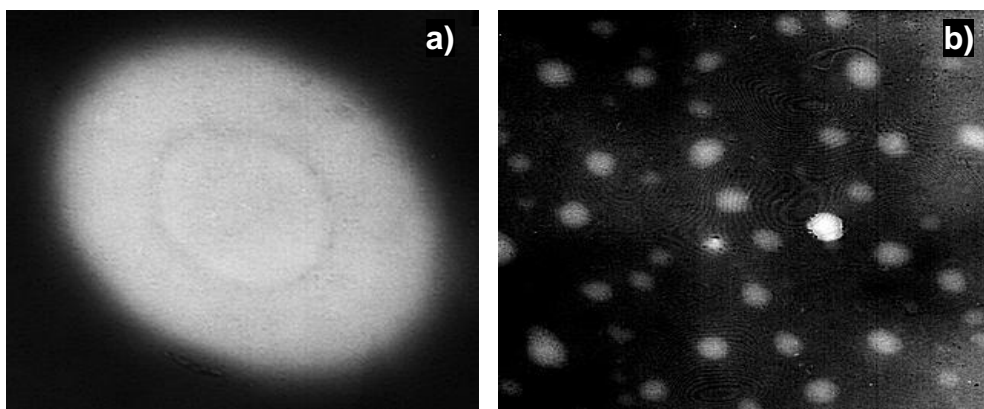


Figure 8.13: Transmission electron microscopic images of L-dopa-loaded methacrylate copolymer/chitosan *iPoly-X-Lipo* nanoparticles: **a)** Magnification x 20000 and; **b)** Magnification x 8000.

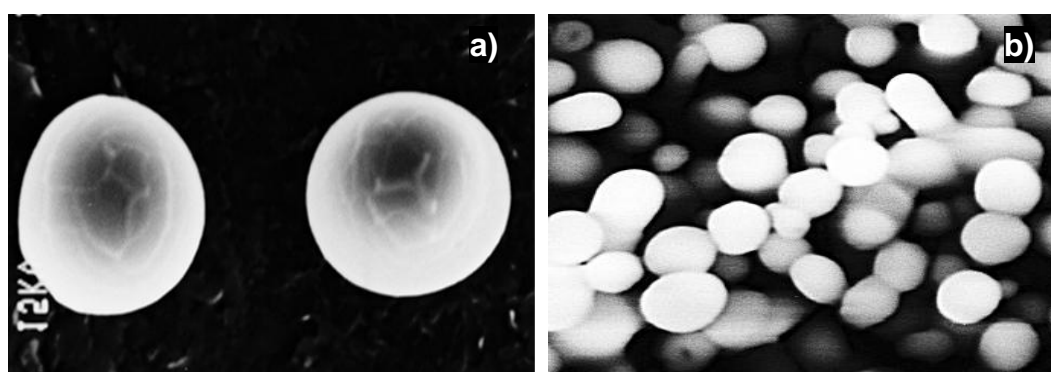


Figure 8.14: Scanning electron microscopic images of L-dopa-loaded methacrylate copolymer/chitosan *iPoly-X-Lipo* nanoparticles: **a)** Magnification x 15000 and; **b)** Magnification x 5500.

TEM confirmed the capsular wall of the L-dopa-loaded nanoparticles (Figure 8.13) while SEM displayed the hollow spherical nanocapsules (Figure 8.14).

8.3.5. Drug loading efficiency of *iPoly-X-Lipo* nanoparticles

The drug loading efficiency was found to be 93%. The *iPoly-X-Lipo* nanoparticles had high drug entrapment efficiency of 85% and though the fabrication was stepwise there was no washing, centrifuging or decanting. It is envisaged that drug incorporation into the nanoparticles is a combination of encapsulation and surface adsorption.

8.3.6. Direct compression of *iPoly-X-Lipo* nanoparticles into tablet matrices

All formulations of L-dopa-loaded nanoparticles were directly compressible. Direct compression is indeed a pharmaceutical technique employed for moisture-sensitive drugs such as L-dopa. Moisture being one of the major causes of instability of drugs is not utilized in direct compression unlike wet granulation. The compressibility of the nanoparticles

demonstrated the inherent compaction of the polymers which was not eliminated by the process of fabrication of the nanoparticles.

8.3.7. *In vitro* drug release studies

By the 5th hour, nanosuspensions had released more than 60% of L-dopa while all except F3 and F5 released more than 50% within two hours (Figure 8.15). Hence L-dopa-loaded nanosuspension can be employed for rapid relief of parkinsonian symptoms. The nanoparticles are anticipated to adhere to the mucosal walls by electrostatic interactions thereby improving the bioavailability of L-dopa. L-dopa release from nanosuspension into the two buffers utilized (pH 1.5 and 4.5) did not differ significantly as shown in Figures 8.15a and 8.15b. By the 24th hour, 86 – 94% of L-dopa was released. However, its release profiles in buffers differed upon incorporating the nanoparticles into an IPB (Figures 8.16a and b) due to the pH responsive nature of the IPB. As pH increased, the rate of release of L-dopa decreased. Furthermore, the fractional drug released by 24th hour from the IPB was less when compared to nanosuspension due to increased barrier and subsequent diffusion distance. While 78% drug release was the highest released in buffer pH 1.5 by one of the nanoparticulate compositions, 46% was the lowest released in buffer pH 4.5 at the 24th hour.

Comparing drug release profiles from the three formulations – nanosuspension, compressed nanoparticles and nanoparticles compressed within an interpolymeric blend, it was observed that incorporating methacrylate copolymer nanoparticles into an interpolymeric blend produced a sustained release of L-dopa as compared to direct compression of the nanoparticles alone (Figure 8.17a). As the buffer pH 1.5 percolates the compressed methacrylate copolymer nanoparticles, the particles are dispersed in the buffer such that 75% of L-dopa was released into the medium at the 1st hour. On the other hand, directly compressed L-dopa-loaded methacrylate copolymer/chitosan nanoparticles remained largely intact with swelling and slight erosion over 24 hours with release of L-dopa almost comparable to the release profile of the nanoparticles incorporated into an interpolymeric blend (Figure 8.17b).

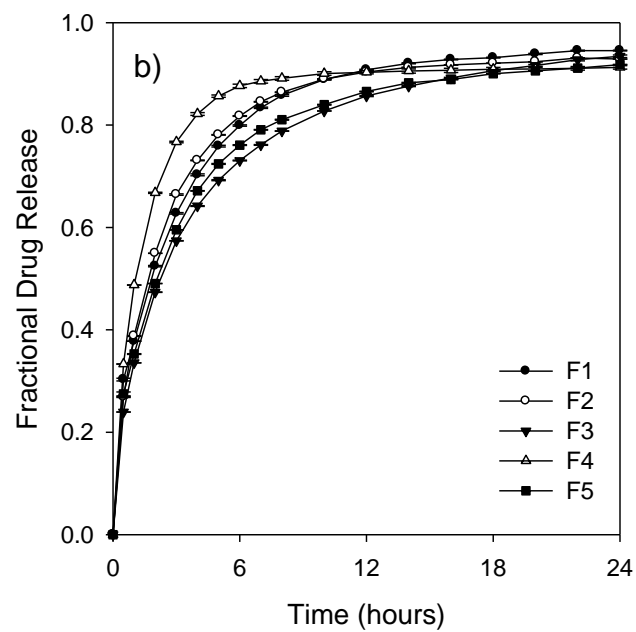
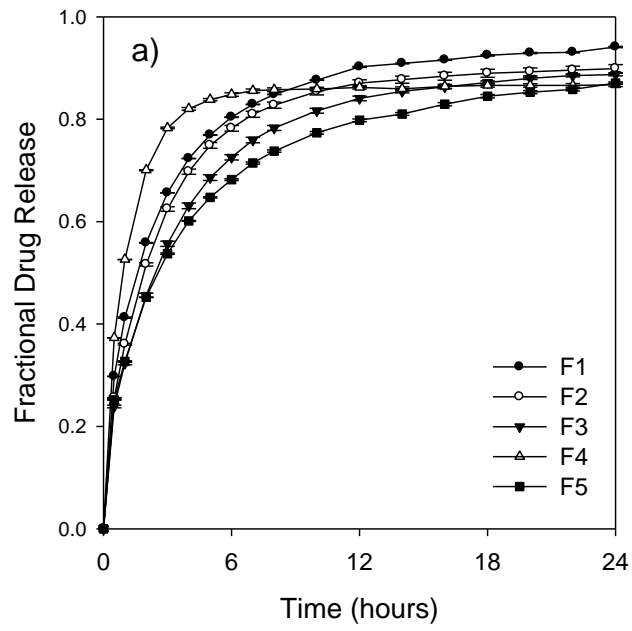


Figure 8.15: a) Drug release profiles of L-dopa-loaded nanoparticles employing dialysis technique in pH 1.5 buffer and; b) drug release profiles of L-dopa-loaded nanoparticles employing dialysis technique in pH 4.5 buffer.

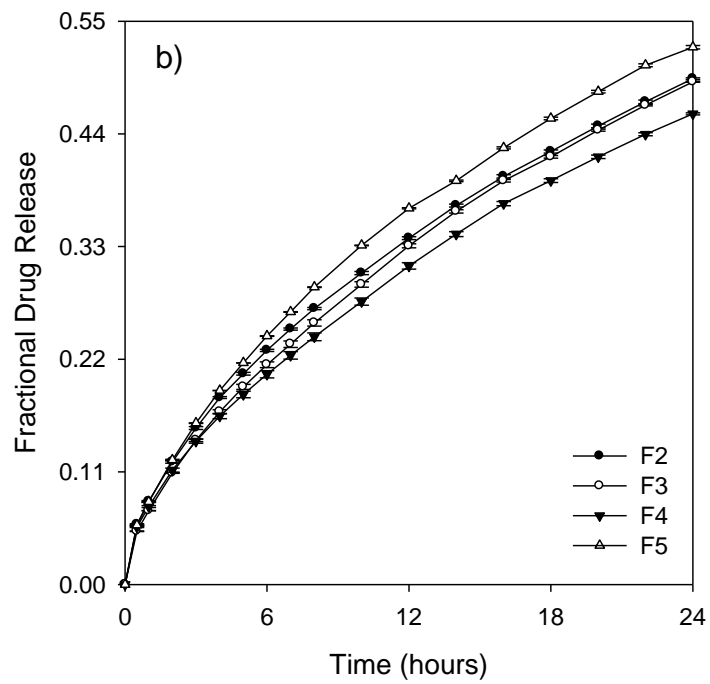
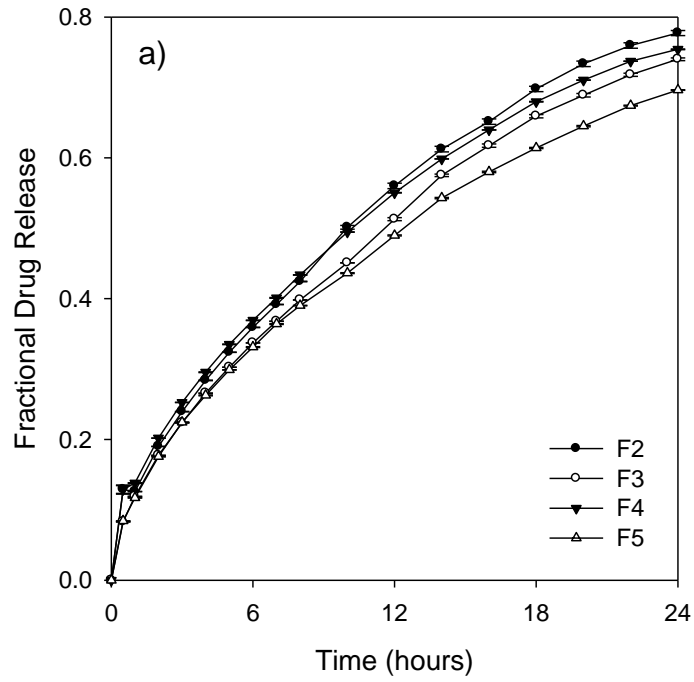


Figure 8.16: **a)** Drug release profiles of L-dopa-loaded nanoparticles incorporated into an interpolymeric blend in pH 1.5 buffer and; **b)** drug release profiles of L-dopa-loaded nanoparticles incorporated into an interpolymeric blend in pH 4.5 buffer.

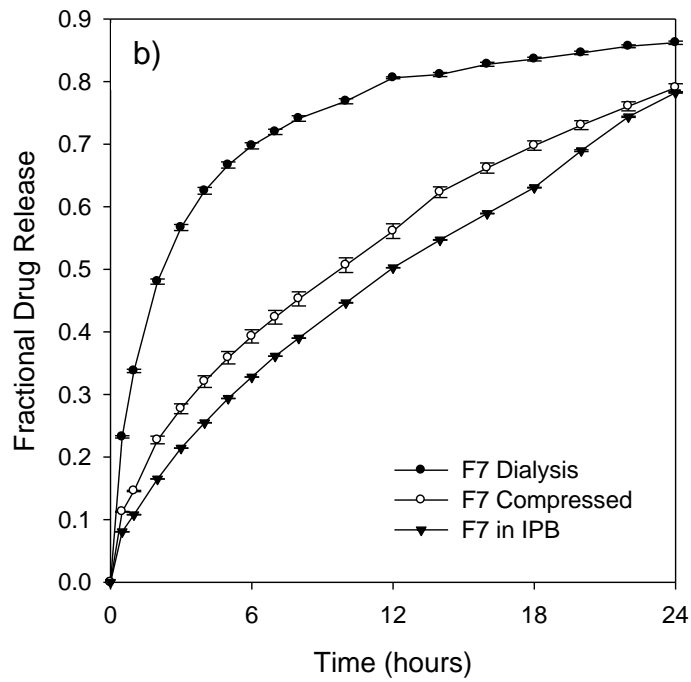
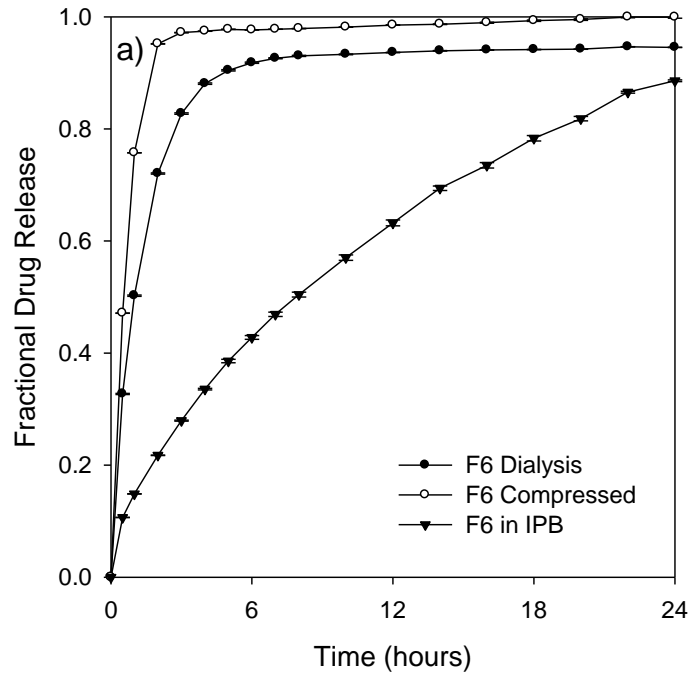


Figure 8.17: a) Comparative drug release profiles of the different formulations of levodopa-loaded methacrylate copolymer nanoparticles (F6) in pH 1.5 and; **b)** comparative drug release profiles of the different formulations of L-dopa-loaded methacrylate copolymer/chitosan nanoparticles (F7) in pH 1.5.

8.3.8. Improvement in mechanical strength afforded by polymeric nanoparticles

The IPB being pH responsive maintained its three-dimensional network in pH 1.5 but underwent surface erosion in higher pH values such as 4.5 as confirmed in Chapters 5 and 6. However, in the presence of incorporated nanoparticles, the three-dimensional network was maintained in both buffer media over the 24 hour drug release studies. The mechanical strength of the IPB was improved in pH 4.5 by the electrostatic interactions between the nanoparticles and the IPB. Studies have shown that nanoparticles can be employed to improve the mechanical strength of matrices (Park and Jana, 2003; Zhang et al., 2003; Rapoport et al., 2004; Gojny et al., 2005; Beun et al., 2007; Gomoll et al., 2008; Saha et al., 2008). These studies utilized inorganic nanoparticles to improve mechanical properties. However, in this study, polymeric nanoparticles improved the mechanical strength of a polymeric matrix preventing the polymeric matrix's erosional response at a higher pH.

Magnetic resonance imaging was employed to observe and confirm the mechanical behaviors that occurred during dissolution studies. Figure 8.18a exhibits the images obtained at pH 1.5 upon incorporating the nanoparticles into the IPB. Figure 8.18b shows IPB without nanoparticles at pH 4.5 while Figure 8.18c shows the mechanical behavior of the matrix upon incorporating the nanoparticles into the IPB at pH 4.5. The images shown were obtained at zero, 3rd, 6th, 9th and 12th hours. The grey part surrounding the matrix is the dissolution medium (buffer). The black part within the matrix is the non-hydrated and non-gelled part of the tablet. As the matrix hydrated, it swelled and gelled which is shown by the white part and its thickness increased over time until the matrix was fully hydrated and gelled. As shown, the matrix is a hydrogel which retains its three-dimensional network (shape) at pH 1.5. Figure 8.18b confirmed the gradual surface erosion that occurs at pH 4.5 without the nanoparticles. The matrix loses its shape at pH 4.5 as it hydrates, erodes and gels. Rapid erosion is not observed because the polymers employed to prepare the interpolymeric blend are three polymers with two forming the interpolyelectrolyte complex. It is typical for hydrogel matrices produced with high-molecular weight polymers not to exhibit rapid erosion as their helical chains form rigid interactions within the polymer molecules (Tajiri et al., 2010). Thus, usually it requires more than 24 hours for the interpolymeric blend to erode completely. However, when nanoparticles are added, at pH 4.5 the matrix retained its shape with less penetration of solvent into the matrix as the thickness of the white part is less when compared with images in Figure 8.18a and consequently less swelling. Hence, magnetic resonance imaging confirmed the mechanical influence of polymeric nanoparticles on polymeric matrices.

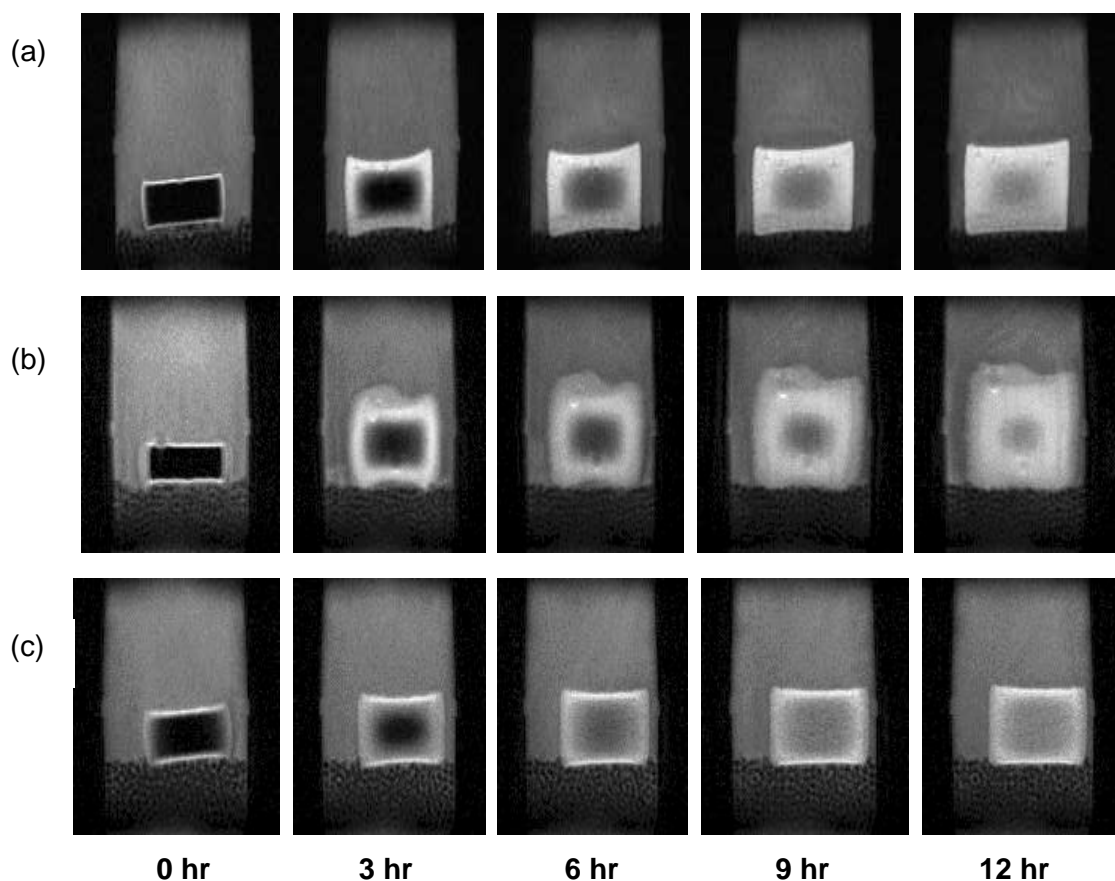


Figure 8.18: Magnetic resonance images of the mechanical behavioral changes of matrices at different pH values: **a)** Nanoparticles incorporated into interpolymeric blend at pH 1.5; **b)** Interpolymeric blend matrix without nanoparticles at pH 4.5 and; **c)** Nanoparticles incorporated into interpolymeric blend at pH 4.5 at 0, 3, 6, 9 and 12 hours.

8.3.9. Molecular mechanics assisted model building and energy refinements

A molecular mechanics conformational searching procedure was employed to acquire the data employed in the statistical mechanics analysis, and to obtain differential binding energies of a Polak–Ribiere algorithm and to potentially permit application to PR and TPP-mediated crosslinking of E100/CHT polymer composite assemblies. MM+ is a HyperChem modification and extension of Norman Allinger's Molecular Mechanics program MM2 (Warhurst et al., 2003), whereas AMBER, is a package of computer programs for applying molecular mechanics, normal mode analysis, molecular dynamics and free energy calculations to simulate the structural and energetic properties of molecules (Pearlman et al., 1995).

8.3.9.1. Molecular mechanics energy relationship (MMER) analysis

Molecular mechanics energy relationship (MMER), a method for analytico-mathematical representation of potential energy surfaces, was used to provide information about the

contributions of valence terms, non-covalent Coulombic terms, and non-covalent van der Waals interactions for the crosslinked-polymer morphologies. The MMER model for the potential/steric energy factors in various molecular complexes can be written as:

$$E_{\text{molecule/complex}} = V_{\Sigma} = V_b + V_{\theta} + V_{\varphi} + V_{ij} + V_{hb} + V_{el} \dots (8.3)$$

$$E_{\text{CHT}} = 35.555 V_{\Sigma} = 3.120 V_b + 18.035 V_{\theta} + 25.774 V_{\varphi} + 13.323 V_{ij} - 24.697 V_{el} \dots (8.4)$$

$$E_{\text{PR}} = 6.717 V_{\Sigma} = 0.145 V_b + 2.477 V_{\theta} + 4.743 V_{\varphi} - 0.484 V_{ij} - 0.163 V_{hb} \dots (8.5)$$

$$E_{\text{CHT-PR}} = 22.230 V_{\Sigma} = 12.683 V_b + 1.875 V_{\theta} + 27.680 V_{\varphi} + 7.176 V_{ij} - 0.596 V_{hb} - 26.757 V_{el} \dots (8.6)$$

$$[\Delta E_{\text{BINDING}} = -33.476 \text{kcal/mol}]$$

$$E_{\text{E100}} = 100.577 V_{\Sigma} = 10.018 V_b + 45.058 V_{\theta} + 13.454 V_{\varphi} + 32.052 V_{ij} - 0.0068 V_{hb} \dots (8.7)$$

$$E_{\text{E100-PR}} = 89.724 V_{\Sigma} = 10.579 V_b + 57.476 V_{\theta} + 39.343 V_{\varphi} - 16.028 V_{ij} - 1.647 V_{hb} \dots (8.8)$$

$$[\Delta E_{\text{BINDING}} = -24.287 \text{kcal/mol}]$$

$$E_{\text{E100-PR-CHT}} = 39.230 V_{\Sigma} = 13.645 V_b + 89.514 V_{\theta} + 91.042 V_{\varphi} - 122.797 V_{ij} - 2.847 V_{hb} - 29.327 V_{el} \dots (8.9)$$

$$[\Delta E_{\text{BINDING}} = -150.638 \text{kcal/mol}]$$

$$E_{\text{TTP}} = 199.744 V_{\Sigma} = 1.927 V_b + 93.088 V_{\theta} + 1.599 V_{\varphi} + 0.046 V_{ij} + 103.082 V_{el} \dots (8.10)$$

$$E_{\text{CHT-TTP}} = 901.408 V_{\Sigma} = 18.542 V_b + 514.621 V_{\theta} + 54.501 V_{\varphi} + 28.920 V_{ij} - 1.065 V_{hb} + 285.889 V_{el} \dots (8.11)$$

$$[\Delta E_{\text{BINDING}} = -132.867 \text{kcal/mol}]$$

where, V_{Σ} is related to total steric energy for an optimized structure, V_b corresponds to bond stretching contributions (reference values were assigned to all of a structure's bond lengths), V_{θ} denotes bond angle contributions (reference values were assigned to all of a structure's bond angles), V_{φ} represents torsional contribution arising from deviations from optimum dihedral angles, V_{ij} incorporates van der Waals interactions due to non-bonded interatomic distances, V_{hb} symbolizes hydrogen-bond energy function and V_{el} stands for electrostatic energy.

8.3.9.2. Energy-minimizations involving crosslinked-polymer morphologies

The energy changes brought about by crosslinking of methacrylate copolymer and chitosan with PR are given in equations 8.4-8.8 and the resulting geometrical minimizations are depicted in Figure 8.19. The total change in energy is calculated as the sum of an internal energy component, calculated from bond stretching, angle bending, and torsional rotation, and a non-bonded component calculated from Coulombic and Van der Waals interactions.

It is evident from Figure 8.19a that PR can crosslink CHT by forming hydrogen bonds between their functional groups such as $\text{PO}_4^- \dots \text{NH}$, $\text{NH} \dots \text{OH}^-$ and $\text{NH} \dots \text{NH}$ crosslinking. The $\Delta E_{\text{BINDING}} = -33.476 \text{kcal/mol}$ proved that CHT-PR forms a stable structure stabilized by all the three non-bonding interactions viz., van der Waals forces, hydrogen bonding and electrostatic interactions with London dispersion forces playing the major part (Eqns. 8.4-8.6). These interactions confirmed the previously reported interactions between chitosan and

phospholipids (lecithin) as discussed earlier (Grant et al., 2005; Ho et al., 2005; Sonvico et al., 2006; Lim et al., 2008; Hafner et al., 2009; Zahedi et al., 2009).

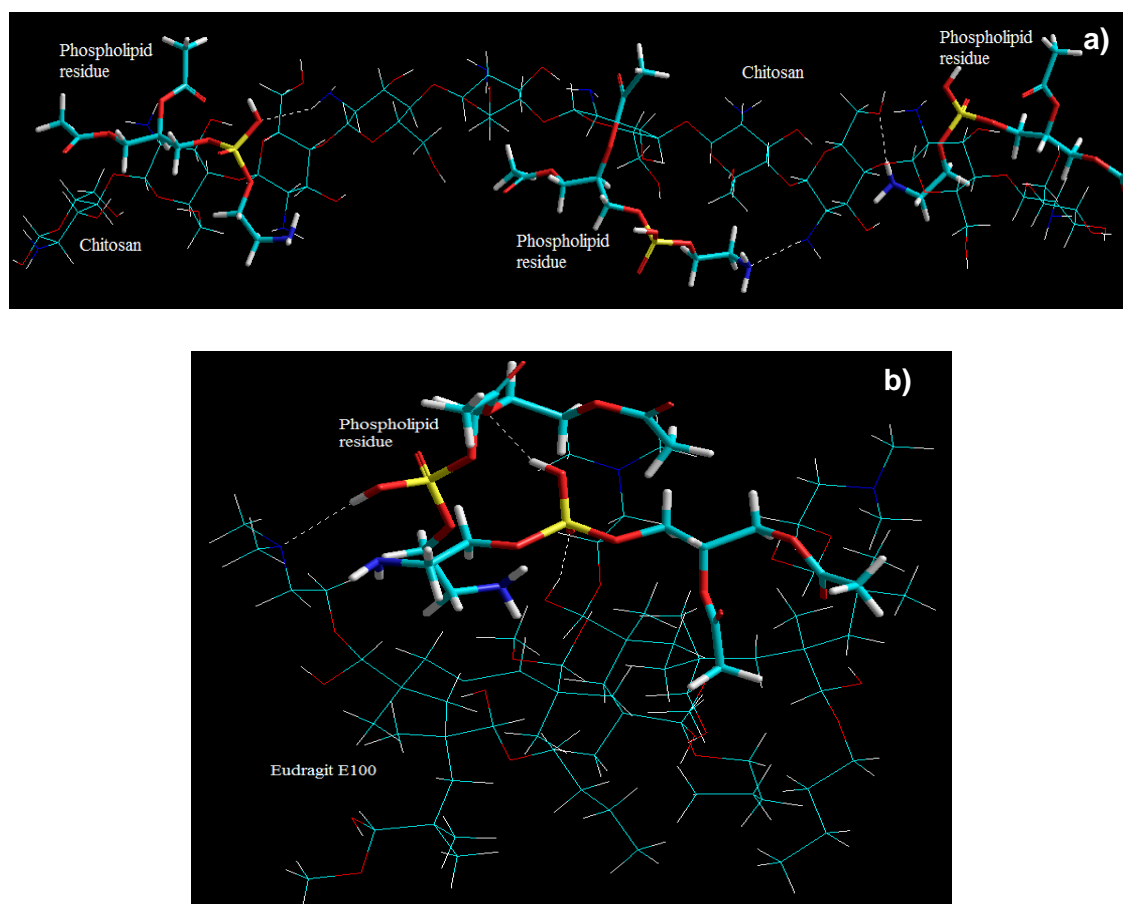


Figure 8.19: Visualization of geometrical preference of Phospholipid residues in complexation with: **a)** Chitosan and; **b)** Methacrylate copolymer (Eudragit E100) after molecular mechanics simulations. The atoms forming the hydrogen bonds are emphasized by dotted lines after recomputing the H bonds after energy minimizations. Color codes: C (cyan), O (red), N (blue), P (yellow) and H (white).

It is apparent from Figure 8.19b that methacrylate copolymer can also be crosslinked by PR, as postulated earlier in the paper, forming both intra- and inter-molecular bonding. Figure 8.19b depicts that the complexing of phosphate with an amine group proceeds via formation of both the hydrogen bond $\text{NH}\dots\text{O}=\text{P}$ and $\text{CO}\dots\text{O}=\text{P}$ and also the $\text{N}\delta^-\dots\text{p}\delta^+$ bond (Golovnya et al., 1973). The formation of a stabilized structure of E100-PR with $\Delta E_{\text{BINDING}} = -24.287\text{kcal/mol}$ also confirms the crosslinking action of TPP. The main difference between CHT-PR and E100-PR crosslinking is that there is no electrostatic interaction involved between E100 and PR. E100-PR is thus stabilized mainly by van der Waals hydrophobic interaction and negligibly by H-bonding (Equations. 8.7-8.8).

The above crosslinking reactions formed the basis of our postulation which states that the incorporation of lecithin might act as a bridge for interpolymeric crosslinking. To elucidate this concept, we modeled E100 and CHT together with PR (E100-PR-CHT), molecularly dispersed within the polymeric matrix (Figure 8.20). After global energy and geometry minimization, we observed that it is possible for PR to form an interpolymeric bridge between E100 and CHT as depicted in Figure 8.21c. Surprisingly, the $\Delta E_{\text{BINDING}}$ for the trimolecular complex was -150.638kcal/mol, which was ~5 times more stabilized than the individual polymer complex of E100-PR or CHT-PR (Equation 8.9).

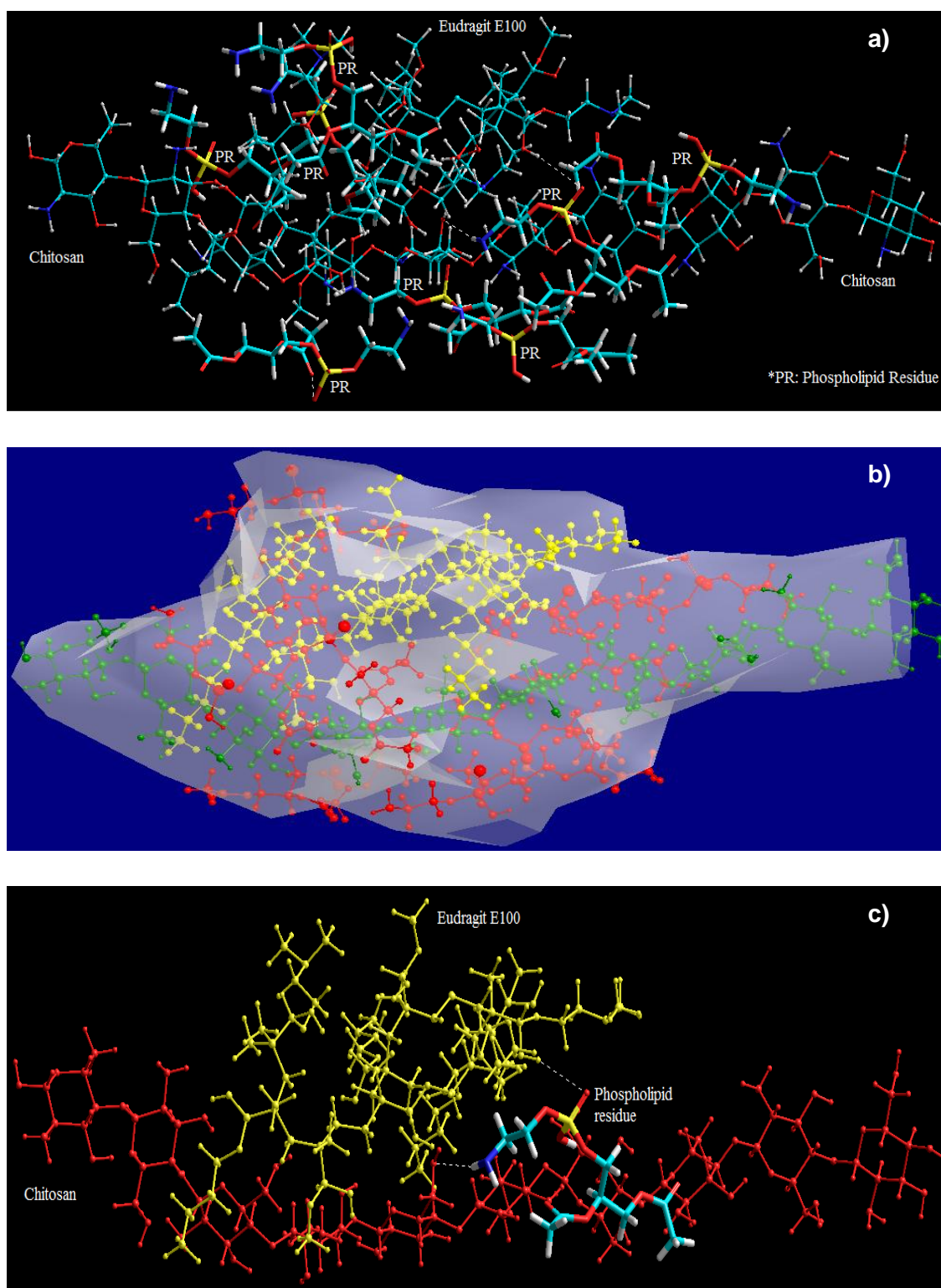


Figure 8.20: Visualization of geometrical preference of chitosan and methacrylate copolymer in complexation with Phospholipid residues (PR) after molecular mechanics simulations: **a)** E100-PR-CHT molecular complex in full geometry; **b)** Connolly molecular electrostatic potential surfaces in transparent display mode showcasing the nanoparticulate system and; **c)** A typical conformation showcasing the bridging of E100 and CHT by phospholipid residue. Color codes: C (cyan), O (red), N (blue), P (yellow) and H (white).

The final conformation model of E100-PR-CHT molecular network was generated for formable complex structures in relation to the co-operative ion-pair binding of the carbonyl (-CO), hydroxyl (-OH⁻), protonated amine (-NH₃⁺) groups of the polymers with the quaternary phosphonium ion (PO₄⁻) and protonated amine (-NH₃⁺) groups of the crosslinker (Figure 8.19a). The strong binding affinity in E100-PR-CHT was due to the hydrophobic interactions and charge distribution caused by the interacting moieties which act in co-operation with the short range van der Waal attractions and secondary interactions such as hydrogen bonding (Eqn. 8.9). Interestingly, the stabilized van der Waals energy demonstrated the importance of a structural backbone fit between the host and guest molecule. Figure 8.19b depicts the energy minimized van der Waals radii structure of E100-PR-CHT where, due to the flexibility of the polymer chains, the relevant segments of polymers arrange their configuration to form a remarkable structure fit between the various functional groups; the electrostatic, van der Waals and H-bond interactions being almost optimized.

Apart from these, the chitosan polymeric matrix in particular was further stabilized and crosslinked due to the addition of sodium tripolyphosphate (TPP) as shown in Figure 8.21 and Equations 8.10-8.11. The CHT-TPP molecular complex demonstrated a $\Delta E_{\text{BINDING}}$ of -132.867kcal/mol. The complex is mainly stabilized by non-bonding interactions in terms of London dispersion forces, H-H bonding and ion pair-ion pair electrostatic interactions (Eqns. 8.10-8.11). However, it is apparent in Figure 8.21 that direct linking of adjacent glucosamine units may have brought about the largest change in energy relative to the uncrosslinked state. The following possible crosslinks were formed: PO₄⁻ - OH crosslinking, PO₄⁻ - NH crosslinking, OH - PO₄⁻ - OH crosslinking, NH - PO₄⁻ - NH crosslinking and OH - PO₄⁻ - NH crosslinking.

Although the complex morphologies were finally stabilized by dominating non-bonding interactions, the chain interactions culminating from the crosslinking agents such as Lecithin (a phospholipid) and sodium tripolyphosphate (conjugate base of triphosphoric acid) may cause disturbance at high crosslink densities resulting in distortion of bond lengths, angles, and torsions from their equilibrium values eventually causing strained-unstable-rigid-framework (Figure 8.20b). In addition, the intermolecular crosslinking may initiate a significant axial stress due to buildup of the adjacent crosslinks. This provides a reasonable explanation for the experimentally observed controlled release behavior of the nanoparticle formulations due to formation of a dense polymeric matrix owing to this very crosslinking mechanism of PR and TPP.

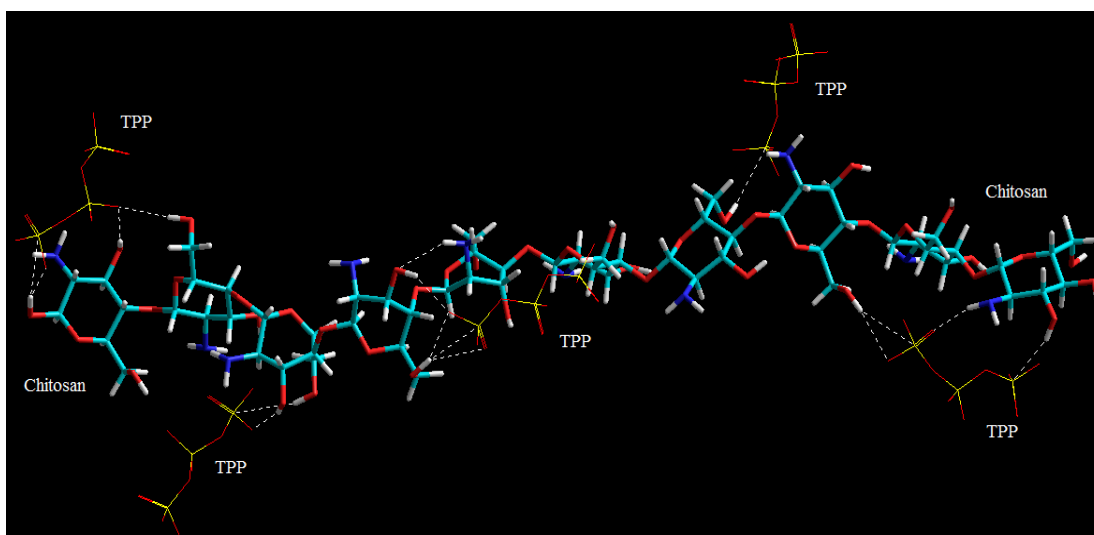


Figure 8.21: Visualization of geometrical preferences of TPP (stick rendering) in complexation with CHT (tube rendering) after molecular mechanics simulations. Color codes: C (cyan), O (red), N (blue), P (yellow) and H (white).

These modeling results are in corroboration with the observed experimental results where it was postulated that the color change after the addition of crosslinking agent may be due to energy perturbation. In addition, free flowing particles generated after the inclusion of TPP may be further attributed to less space in the particles matrices for solvent and water molecules due to the matrix stability and robustness displayed in energy minimized geometrical configurations. Furthermore, this matrix stability and robustness may induce a low degree of matrix loss, minimal swelling and limited distension resulting in a sustained and prolonged release of L-dopa from the nanoparticle formulations. The spectral analysis also corroborated with the mechanistic simulation in terms of disappearance of peaks and emergence of new peaks along with band shifting and broadening involved in coupling and complexation (FTIR structural variation analysis) which strengthens the experimental and computational correlation.

8.4. CONCLUDING REMARKS

This Chapter demonstrates the feasibility of fabricating of L-dopa-loaded nanoparticles. The obtained nanoparticles were hollow, capsular, nanoparticulate complex with 93% drug loading efficiency. The desired rate of drug release from methacrylate copolymer can be modulated by formulating L-dopa-loaded nanoparticles as a suspension, then directly compressing the nanoparticles into a tablet matrix or by loading the nanoparticles into a polymeric blended tablet matrix. Twenty-four hours of sustained release of L-dopa from

methacrylate copolymer nanoparticles was achieved by embedding the nanoparticles within an interpolymeric blended tablet matrix while sustained drug release from methacrylate copolymer/chitosan nanoparticles can be achieved by directly compressing the nanoparticles into a tablet matrix. This Chapter also elucidates the potentials of polymeric nanoparticles to enhance the mechanical strength of polymeric matrices. Furthermore, experimental and theoretical investigations on the effect of crosslinking on the release of L-dopa from the nanoparticles formulations were in excellent agreement. The experimentally observable drug release could be predicted by the computational method and the energy calculations allowed for a prediction of the interaction mechanisms. The developed delivery system may find applications in oral, sustained and localized drug delivery. The fabricated *iPoly-X-Lipo* nanoparticles will be incorporated into optimized IPB to formulate *PXLNET* in the next Chapter.

CHAPTER NINE

CHARACTERIZATION OF THE OPTIMIZED GASTRORETENTIVE LEVODOPA- LOADED POLYMER-X-LIPID NANO-ENABLED TABLET PLATFORM

9.1. INTRODUCTION

Having optimized the interpolymetric blend (Chapter 7) as well as fabricated and characterized L-dopa-loaded *iPoly-X-Lipo* nanoparticles (Chapter 8), further characterization of the gastroretentive nanoparticulate drug device is necessary in order to assess the predicted responses with experimental outcome and explore more drug delivery properties for oral administration of L-dopa.

The convenience of oral therapy will continue to propel voracious interests in oral drug delivery and new approaches to improve the bioavailability of narrow absorption window drugs. Factors that affect absorption and subsequent bioavailability of narrow absorption window drugs include physicochemical properties of drugs, physiological and biological factors as well as physicochemical properties of the drug delivery systems developed. Drug delivery systems are developed to overcome the limiting factors of absorption. While one drug delivery system may not be equipped to overcome all limiting factors, the system however, improves the bioavailability of the specific drug employed by overcoming some factors. While some drug delivery systems may appear to be 'one size fit all', some are tailored to be drug specific or site specific thereby enhancing therapeutic efficacy.

Some drug delivery systems employed to improve absorption and availability of drugs include the use of prodrugs (Buur and Bundgaard, 1987; Lokind and Lorenzen, 1996); lipid drug delivery systems (Neslihan and Benita 2004; Fatouros et al., 2007; Slabbert et al. 2011); polymeric micelles (Mathot et al., 2006; Kim et al., 2008); nano-drug delivery systems (Pandey et al., 2005; Mittal et al., 2010); micro-drug delivery systems (Lamprecht et al., 2004; Song et al., 2009); hydrogels (He et al., 2006; Josef et al., 2010; Singh and Chauhan, 2010); emulsions (Kang et al., 2004; Jang et al., 2006); solid dispersions (Barker et al., 2003; Joshi et al., 2004) and gastroretentive drug delivery systems (Klausner et al., 2003; Chavanpatil et al., 2006; Ali et al., 2007; Chen et al., 2010).

The mechanisms of gastroretention have been identified and explained in Chapter 6. Studies have shown one mechanism is usually not sufficient for prolonged gastroretention. For instance, *in vivo* analysis of chitosan mucoadhesive formulation by neutron activation-based gamma scintigraphy was found not to be reproducible and exhibited short duration of retention (Säkkinen et al., 2006). Prolonged gastric residence time of floating drug delivery systems is dependent on the filling of the stomach (Streubel et al., 2006). Hence researchers

are currently exploring the combination of gastroretention mechanisms to enhance gastroretention. The mechanism combinations that have been undertaken include bioadhesion and floating (Jiménez-Castellanos et al., 1994); floating, swelling and bioadhesion (Chavanpatil et al., 2006) and swelling and bioadhesion (Yin et al., 2007).

Hence, this study was undertaken to characterize the physicochemical properties of an optimized interpolymeric blend (IPB) as well as *PXLNET* gastroretentive drug delivery systems. While the IPB gastroretentive drug delivery system involved three mechanisms of gastroretention, *PXLNET* is a combination of nanotechnology and the three mechanisms of gastroretention technology.

Characterization of a drug delivery system is crucial to ascertain its physicochemical and physicomechanical stability as well as its biopharmaceutical suitability. This is needful in order to optimize the formulation and manufacturing processes to achieve the desired responses such as controlled the delivery rates, prolonged residence time and determination of potential therapeutic efficacy. The properties of materials employed in formulation of a drug delivery device significantly influence its performance *in vitro* and *in vivo*. Hence, techniques such as infra-red spectroscopy, thermal analysis, electron microscopy, gastro-adhesion studies, swelling and magnetic resonance imaging were employed to characterize the performance of the systems. Furthermore, the *in vitro* drug release profiles of the GDDS were compared with those of the conventional dosage forms.

9.2. EXPERIMENTAL SECTION

9.2.1. Materials

Materials used in this study are cumulative of materials used in Chapter 4, Section 4.2.1, Chapter 5, Section 5.2.1, Chapter 6, Section 6.2.1 and Chapter 8, Section 8.2.1.

9.2.2. Fabrication of *iPoly-X-Lipo* nanoparticles

Equal weights of methacrylate copolymer and chitosan as shown in Table 9.1 were dissolved in 10mL 0.2N HCl. Other materials in Table 9.1 were added and nanofabrication performed as described in Chapter 8, Section 8.2.2.

Table 9.1: Composition of L-dopa-loaded *iPoly-X-Lipo* nanoparticles.

Formulation Code	Eudragit (mg)	Chitosan (mg)	L-dopa (mg)	Benserazide (mg)	Lecithin (mL)	TPP (mg)
F5 ¹	50	50	100	25	1.00	100

¹ See Chapter 8, Table 8.1

9.2.3. Synthesis of interpolymeric blend

The quantities of polymers and experimental condition for synthesis of interpolymeric blend were based on the theoretical values for the optimized design given by the Box-Behnken design with desirability of 1.000 for the four dependent variables. The optimized values for the independent variables, IPEC (methacrylate copolymer and NaCMC), locust bean (L), solvent (acetic acid in normality) and temperature as well as the predicted values of the dependent variables are shown in Table 9.2.

Table 9.2: Optimized values for independent variables and predicted values for dependent variables.

IPEC (g)	L (g)	Solvent (N)	Temp (°C)	Dissolution (R ²)	Bioadhesion (N)	Swelling (N/mm)	Density (mg/mm ³)
3.6	1.8463	0.7571	45.6	0.96	0.6	5.0	1.4369

Methacrylate copolymer beads were milled; 1.2g was weighed and dissolved in 50mL 0.7571N acetic acid while 2.4g sodium carboxymethylcellulose (NaCMC) was dissolved in 50mL deionized water. The two polymer solutions were blended and stirred under vigorous agitation at 45.6±1°C for 30min. Thereafter, 1.8463g locust bean gum was added and stirred for fifteen minutes. The interpolymeric blend formed was frozen at -70°C for at least 24 hours, thereafter lyophilized for 48 hours, milled and employed for direct compression.

9.2.4. Structural elucidation of the interpolymeric blend and nanoparticles

FTIR spectra were obtained for the native polymers, optimized interpolymeric blend and nanoparticles with L-dopa and with or without benserazide using a PerkinElmer Spectrometer (PerkinElmer Spectrum 100, Beaconsfield, United Kingdom) over a range of 4000-650cm⁻¹ to elucidate the structural modification of the interpolymeric blend and nanoparticles from the native polymers.

9.2.5. Evaluation of thermal behavior of interpolymeric blend

DSC and ADSC (DSC 1 STAR[®] system, Mettler Toledo, Schwerzenbach, Switzerland) were employed to analyze the thermal behavior of optimized interpolymeric blend as described in Chapter 4, Section 4.2.5.

9.2.6. Direct compression of the interpolymeric blend and formation of *PXLNET*

The interpolymeric blend (IPB) was directly compressed with components as shown in Table 9.3 and described in Chapter 6, Section 6.2.4.

Table 9.3: Composition of a directly compressed matrix employing optimized IPB.

Components	Quantity per matrix (mg)
L-dopa	100
Benserazide/Carbidopa	25
Polymeric blend (50%)	500
Pullulan (10%)	100
Magnesium Stearate (1%)	10.5
Silica (Silicon dioxide) (5%)	50.5
Barium Sulphate	234

Formation of *PXLNET* was achieved by incorporating L-dopa-loaded nanoparticles into interpolymeric blend and blending with other components in Table 9.3 and thereafter, compressed. However, unlike the study in Chapter 8 where interpolymeric blend remained the same quantity even in addition of nanoparticles; in this phase of the study, interpolymeric blend was reduced with incorporation of nanoparticles to ensure that the tablet matrices were not more than 1000mg for easy administration to the pigs for *in vivo* investigations (Chapter 10) and therefore, ensure precise *in vitro* and *in vivo* correlation. Hence, 375.78mg of L-dopa-loaded nanoparticles and 224.22mg of interpolymeric blend were used to formulate *PXLNET*. Furthermore, excipients as shown in Table 9.3 were not added to the composition of the nano-enabled tablet matrices in Chapter 8 and since some of the excipients are needed for gastroretention, interpolymeric blend had to be reduced instead and the excipients utilized as stated in Table 9.3.

9.2.7. Determination of the densities of IPB and *PXLNET* matrices

The determination of densities of the matrices was undertaken as stated in Chapter 6, Section 6.2.5.

9.2.8. Gastroadhesivity testing of IPB and *PXLNET* matrices

The peak force and the work of adhesion were used to assess the gastroadhesivity of the matrices. The method employed is as stated in Chapter 6, Section 6.2.7 while the parameters employed are stated in Chapter 6, Table 6.3.

9.2.9. Physicomechanical characteristics and swellability of IPB and PXLNET matrices

Physicomechanical strengths of the matrices from Force-Distance profiles obtained using the Texture Analyzer (TA.XT*plus*, Stable Microsystems, Surrey, UK) was employed to determine swelling abilities of the matrices. Matrix rigidity, matrix resilience and deformation energy were performed for the unhydrated matrices while matrix rigidity and deformation energy were performed for hydrated matrices with a 2mm flat-tipped steel probe. The matrices were hydrated by placing them in baskets, fixed to a dissolution apparatus and submerged in 900mL buffer pH 1.5; and allowed to run at intervals of two hours at 50rpm and 37°C. Matrices were set to run at 2, 4, 6 and 8 hours and taken at the end of each time to perform the tests. The data was captured through Texture Exponent Software (Version 3.2) and the settings employed are as shown in Chapter 4, Table 4.1.

9.2.10. Surface morphological analysis of IPB matrices

The surface morphology of IPB matrices was undertaken by mounting the matrix samples on aluminum stubs with the aid of carbon paste. After drying, the matrix was sputter-coated with gold-palladium and then viewed under Quanta™ Scanning Electron Microscope (FEI Quanta 400 FEG (ESEM) FEI Company, Eindhoven, The Netherlands). The unhydrated and hydrated IPB matrices were viewed. The hydrated IPB matrix was left in the buffer pH 1.5 for 24 hours, frozen at -70°C for 24 hours and lyophilized for 48 hours before viewing under the Quanta™ Scanning Electron Microscope.

9.2.11. Surface area and porosity analyses of IPB matrices

The surface area and porosity analyses of IPB matrices were performed using a Porositometric Analyzer (ASAP 2020, Micromeritics, Norcross, GA, USA). First, the samples were cut into sizes capable of passing through the sample tubes (internal diameter = 9.53mm), weighed and inserted into the sample tubes for degassing. Glass filler rods were inserted into the sample tubes to aid reduction of degassing time by reducing the total free space volume. The degassing conditions were set up which comprised the evacuation and heating phases and the parameters employed are shown in Table 9.4. After degassing which took about 21 hours, the sample tube was transferred to the analysis port for determination of surface area, pore size and volume in accordance to BET and BJH analysis. The analysis lasted about 5 hours and the analysis conditions are shown in Table 9.5.

Table 9.4: Degassing parameters for evacuation and heating phases.

Parameters	Target/Rate
Evacuation phase	
Temperature ramp rate	10.0°C/min
Target temperature	30°
Evacuation rate	50.0mmHg/s
Unrestricted evacuation from	30.0mmHg
Vacuum set point	500µmHg
Evacuation Time	60min
Heating Phase	
Ramp rate	10.0°C/min
Hold temperature	40°C
Hold time	1320min
Hold pressure for evacuation and heating phases	100mmHg

Table 9.5: Parameter settings for analysis conditions.

Features	Settings
Preparations	
Fast Evacuation	No
Unrestricted evacuation from	5.0mmHg
Vacuum set point	10µmHg
Evacuation time	0.10hour
Dosing	
Use of first pressure fixed dose	No
Use of Maximum volume increment	No
Target tolerance	5.0% or 5.0mmHg
Low pressure dosing	No
Equilibrium	
Equilibrium time (P/Po = 1.0)	20secs
Minimum equilibrium delay at P/Po >= 0.995	600secs
Sample backfill	
Backfill at start of analysis	Yes
Backfill at end of analysis	Yes
Backfill gas	Nitrogen
Adsorptive properties	
Adsorptive	Nitrogen
Maximum manifold pressure	925.0mmHg
Non-ideality factor	0.0000620
Density conversion factor	0.0015468
Therm. Tran. Hard-sphere	0.3860nm
Molecular cross-sectional area	0.162nm ²

9.2.12. Comparative *in vitro* drug release studies and analytical method

USP apparatus II dissolution system (Erweka DT 700, Erweka GmbH, Heusenstamm, Germany) was employed to undertake the *in vitro* studies at 37 ± 0.5°C and 50rpm in 900mL of buffer pH 1.5 for IPB, *PXLNET* and the conventional products – Sinemet® CR, Sinemet® IR, Madopar® IR and Madopar® HBS. Samples were withdrawn at two-hour intervals for IPB, *PXLNET* and Madopar® HBS; at intervals of 0.17, 0.33, 0.5, 0.75, 1, 2, 4, 6, 10, 14, 18, 24 hours for Sinemet® IR and Madopar® IR and then 0.25, 0.5, 0.75, 1, 2, 4, 6, 10, 14, 18, 22, 24

hours for Sinemet[®] CR. The volumes withdrawn were replaced with the same volume of fresh medium to maintain sink conditions, and concentrations of L-dopa and benserazide/carbidopa released per time were quantified with Acquity[™] Ultra Performance Liquid Chromatography (UPLC, Waters[®], Manchester, UK). Methyl dopa was used as an internal standard and the gradient method was employed with mobile phase as water (A) and acetonitrile (B) running at 98% A, 0.50min at 95% A, 0.70min at 5% A and 95% A at 1.00min at a flow rate of 0.500mL/min. Run time for L-dopa/Benserazide was 1.00min and 1.20min for L-dopa/Carbidopa. The column used was Acquity UPLC[®] BEH shield RP18 1.7 μ m, 2.1 x100mm. The wavelength employed was 210nm, injection volume was 1.2 μ L and temperature was 25°C.

9.2.13. Elucidation of drug release mechanism

The drug release kinetics was elucidated by fitting L-dopa release from the controlled release formulations into zero order and first order while the drug release process was further characterized with Higuchi and Korsmeyers-Peppas equations, dissolution efficiency and similarity factor f_2 .

9.2.14. Magnetic resonance imaging of IPB matrices

The process of magnetic resonance imaging of IPB matrices is as described in Chapter 8, Section 8.2.11. L-dopa was assayed at 280nm using Varian Cary 50 Spectrophotometer (Varian, Inc., Mulgrave, Australia) which was coupled to the Magnetic Resonance System.

9.2.15. Stability of L-dopa/benserazide/carbidopa-loaded nanoparticles and matrices

The formulations were subjected to moisture, pH (1.5, 4.5 and 6.8) and temperature (25 and 37°C) to assess the stability of the L-dopa, benserazide and carbidopa.

9.3. RESULTS AND DISCUSSION

9.3.1. Fabrication of *iPoly-X-Lipo* nanoparticles

The fabrication and characterization of *iPoly-X-Lipo* nanoparticles have been substantially dealt with in Chapter 8.

9.3.2. Synthesis of interpolymeric blend

The synthesis and characterization of interpolymeric blend have been amply discussed in Chapters 4 and 5.

9.3.3. Structural elucidation of the interpolymeric blend and nanoparticles

Figures 9.1a and b show the spectra for IPB and *iPoly-X-Lipo* nanoparticles. The spectra for the native polymers have been elucidated in Chapters 4, 5 and 8. Peaks in the IPB spectrum were identified at 3330.02cm^{-1} with possible structural units as hydroxyl groups which are more characteristic of NaCMC part of the interpolyelectrolyte complex; 2880.95cm^{-1} with possible units as alkyl and carbonyl groups. This peak is different from the characteristic carbonyl groups of methacrylate copolymer at about the same peak indicating that some of the carbonyl groups may have been involved in the interaction with NaCMC. The characteristic carbonyl peak of methacrylate copolymer at 1722.46cm^{-1} shifted to 1719.54cm^{-1} and was diminished. Other carbonyl groups of IPB may be found at 1586.92cm^{-1} , 875.99cm^{-1} , and 1143.61cm^{-1} while the hydroxyl or amino groups may be found at 1407.48cm^{-1} , 1371.58cm^{-1} , 1258.98cm^{-1} , 1052.42cm^{-1} and 1017.84cm^{-1} . L-dopa-loaded *iPoly-X-Lipo* nanoparticles are a multi-component delivery system achieved by multi-crosslinking technology. The spectrum (Figure 9.1b) is distinctly different from spectra of the individual components (Chapter 8) with some peaks diminished, some no longer present and new peaks emerging. The mechanisms of interactions have also been discussed in Chapter 8. The *iPoly-X-Lipo* nanoparticles is a particulate complex which contain possible structural units such as alkyl groups, carbonyl groups and aliphatic ethers or alkoxy compounds which will explain the peaks from 2922.91 to 719.34cm^{-1} . The alkyl groups may be found at 2922.91cm^{-1} , 2853.09cm^{-1} and 1465.90cm^{-1} ; carbonyl groups may be found at 1727.46cm^{-1} , 1605.86cm^{-1} , 1150.66cm^{-1} , 1115.85cm^{-1} , 1055.41cm^{-1} and 1014.75cm^{-1} ; and the aliphatic ether or alkoxy compound may be found at 819.11cm^{-1} , 747.13cm^{-1} and 719.34cm^{-1} as well as a N-H II band at 1518.43cm^{-1} .

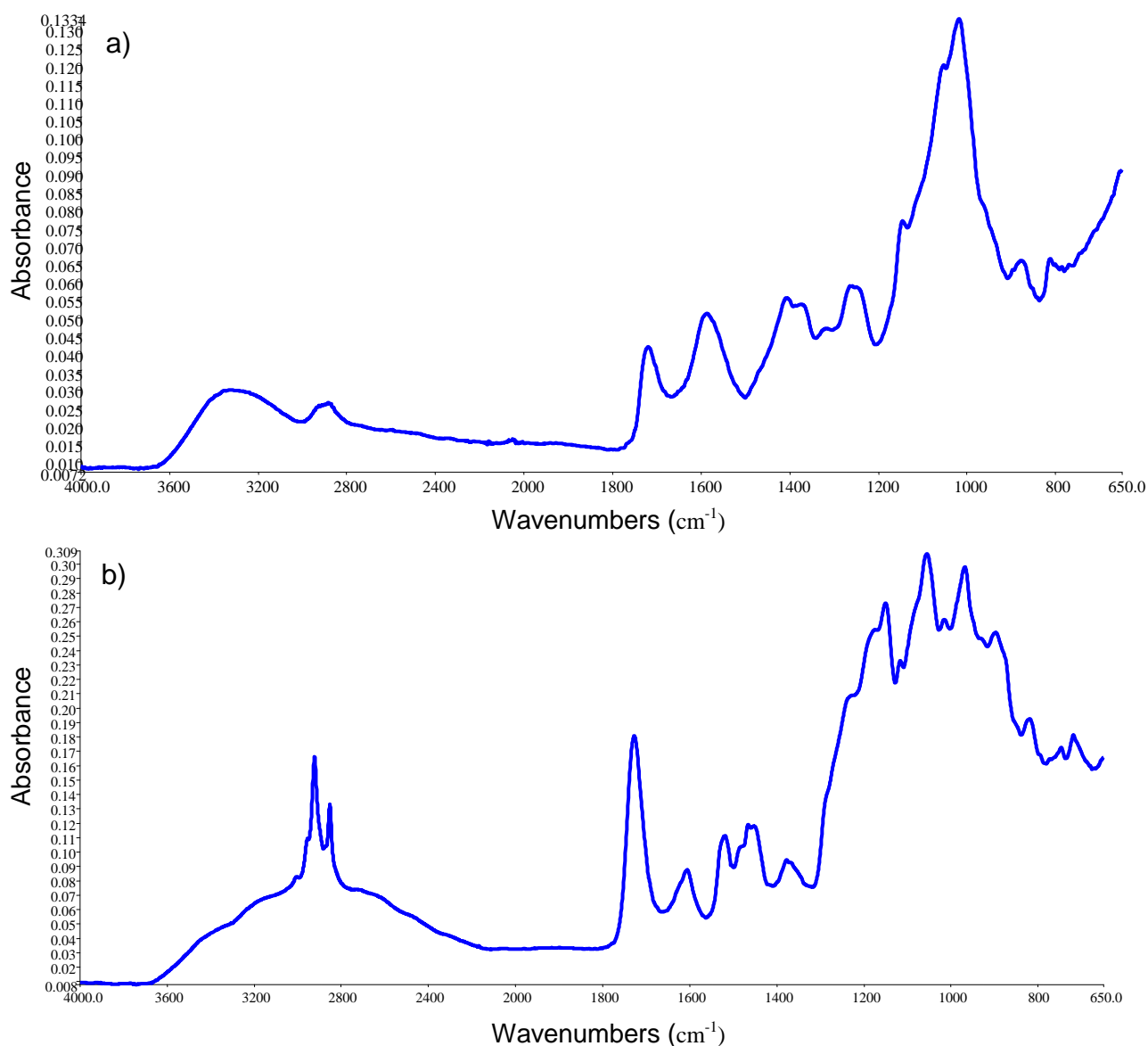


Figure 9.1: Infrared spectra of **a)** interpolymeric blend and; **b)** L-dopa-loaded *iPoly-X-Lipo* nanoparticles.

9.3.4. Analysis of thermal behavior of interpolymeric blend

The thermograms of NaCMC as shown in Figure 9.2a reveal an endotherm at $\sim 110^{\circ}\text{C}$. Such a broad endotherm seem distinct for polysaccharides though the temperature at which it occurs may differ from one polysaccharide to the other. Two exothermic peaks are observed after $\sim 300^{\circ}\text{C}$; one at $\sim 310^{\circ}\text{C}$ and another at $\sim 380^{\circ}\text{C}$ which occurred during the decomposition process of the polymer. As the scission of the glycosidic linkages occurred, the depolymerization took place and so the peak at $\sim 380^{\circ}\text{C}$ is due to the combustion of the degraded products (Biswal and Singh, 2004). Decomposition apparently is initiated before $\sim 300^{\circ}\text{C}$ because when the temperature was set between -10 to 270°C , the crucible was opened after the sample run and it was observed the polymer had turned black. However, the endotherm at 110°C did not clarify the transitions at this temperature which could include

glass transition, moisture evaporation or melting of some crystallites as NaCMC is known as a semi-crystallite polymer. Apart from the endotherm at $\sim 90^{\circ}\text{C}$ on the locust bean thermogram, no other distinct peak was observed as the temperature got to $\sim 450^{\circ}\text{C}$ (Figure 9.2b) except the endothermic curve which started at $\sim 200^{\circ}\text{C}$. However, it is envisaged that its decomposition process was initiated at a higher temperature in comparison to NaCMC. The depth of locust bean endotherm must have influenced the thermogram of the optimized interpolymetric blend, although unlike locust bean, the endotherm for optimized IPB occurred after 90°C . A difference between NaCMC and IPB was observed at the decomposition temperature range. While the exothermic peak of NaCMC at $\sim 310^{\circ}\text{C}$ was sharp and long, that of optimized IPB was broad and short and shifted to $\sim 335^{\circ}\text{C}$ and the combustion peak of the degraded products at $\sim 380^{\circ}\text{C}$ for NaCMC shifted to $\sim 390^{\circ}\text{C}$ in IPB and it was not as sharp (Figure 9.2c). This is indicative that modification occurred in IPB as the melting peak of methacrylate copolymer (Chapters 4 and 5) was not seen and there were differences in shape and shifts of endotherms and exotherms.

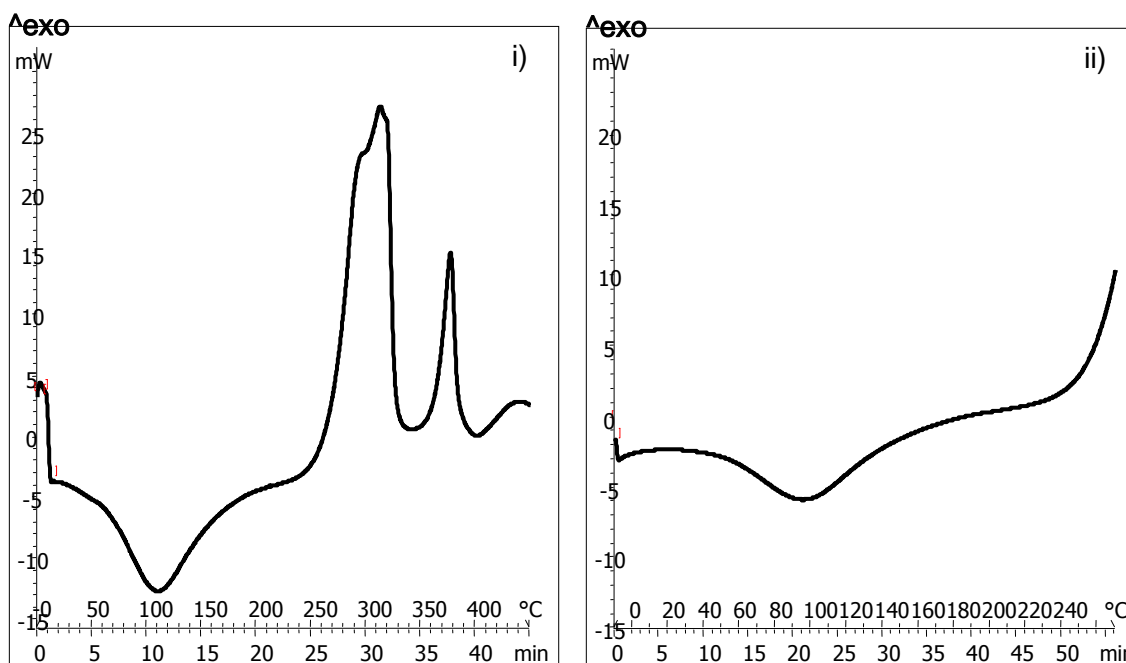


Figure 9.2a: Thermograms of sodium carboxymethylcellulose at temperature ranges: **i)** 0 to 450°C and; **ii)** -10 to 270°C .

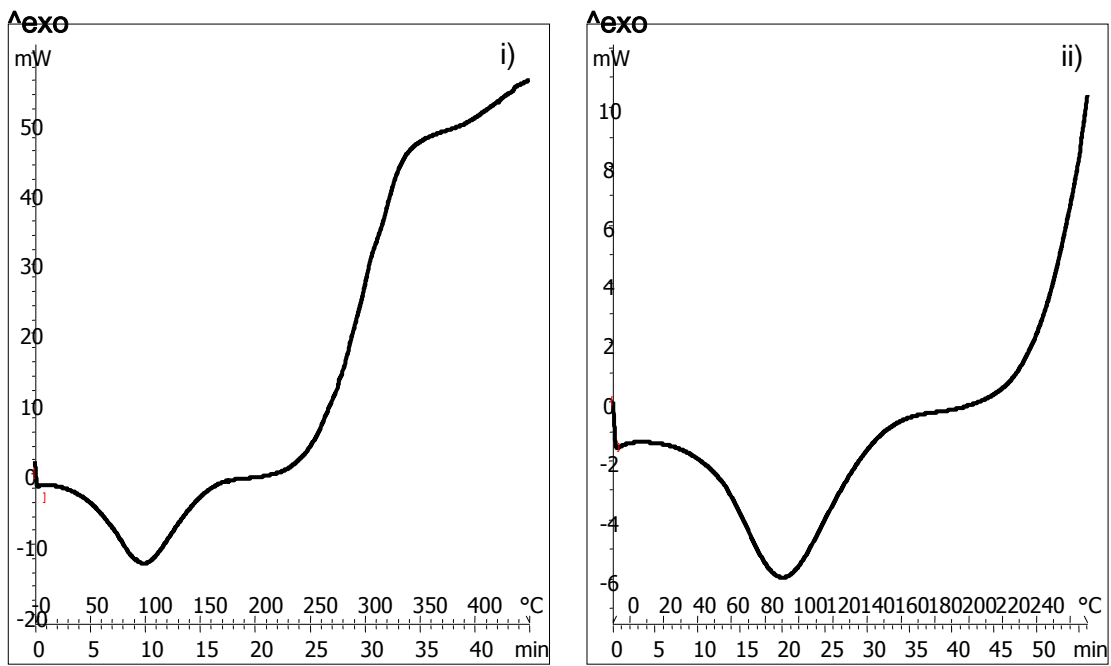


Figure 9.2b: Thermogram of locust bean at temperature ranges: **i)** 0 to 450°C and; **ii)** -10 to 270°C.

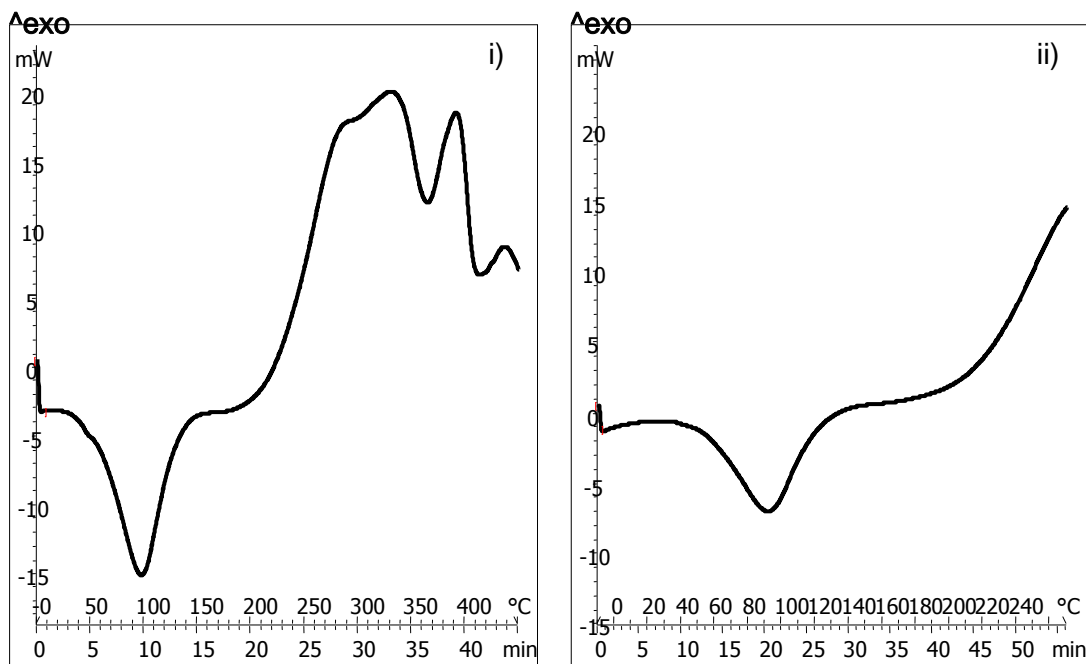


Figure 9.2c: Thermogram of optimized interpolymeric blend at temperature ranges: **i)** 0 to 450°C and; **ii)** -10 to 270°C.

ADSC revealed the semi-crystalline nature of the polysaccharides and their impact on the modified polymer IPB especially within the temperature range of -10 to 130°C. As discussed in Chapters 4 and 5, the optimized IPB with ADSC exhibited melting and crystallization at different temperatures which is typical of polymers. The ADSC curves from -10 to 250°C (Figure 9.2d) show an exponential increase of heat flow rate. Interestingly, the interpolymeric blend in Chapter 5 showed the meander-type modulation of locust bean thereby exhibiting sinusoidal and meander-type while the optimized exhibited only sinusoidal modulation. This may be due to low concentration of locust bean in the optimized interpolymeric blend. Furthermore, the degree of miscibility in the optimized interpolymeric blend may have been enhanced with increased temperature as dissolution of locust bean increases with increase in temperature.

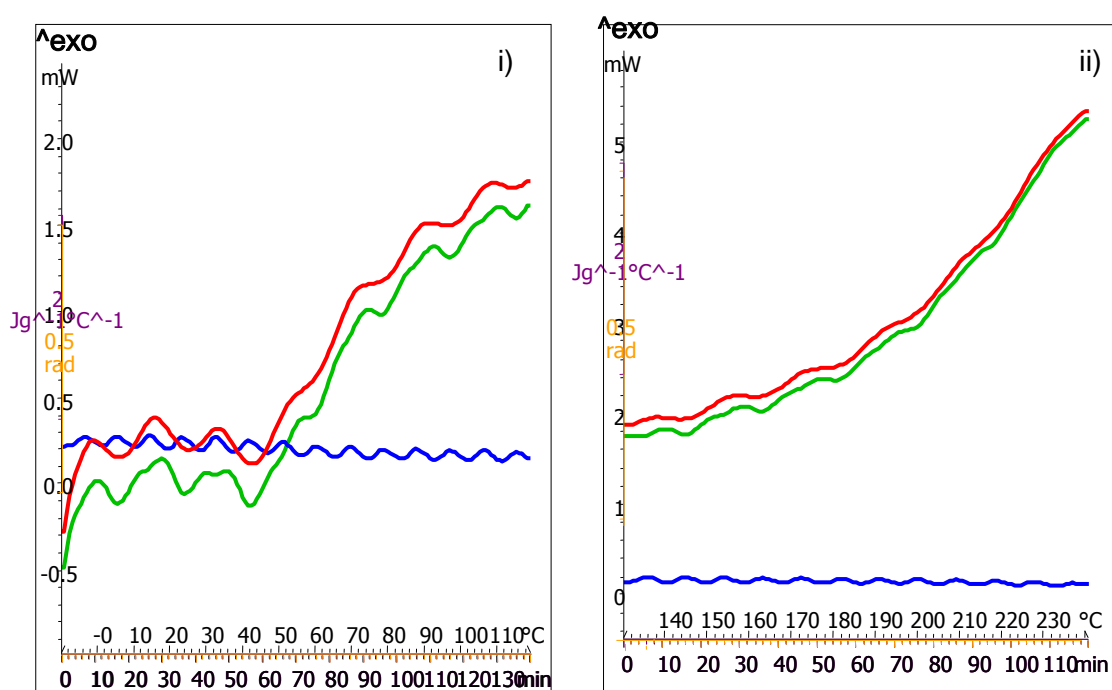


Figure 9.2d: Temperature modulated thermogram of optimized interpolymeric blend at temperatures: **i)** -10 to 130°C and; **ii)** 130 to 250°C.

9.3.5. Density of IPB and *PXLNET* matrices

The predicted value (1.4369mg/mm³) for density in Table 9.2 was for IPB matrices as it was interpolymeric blend that was optimized. The experimental value obtained as shown in Table 9.6 was close to the predicted value with a difference of 0.0269mg/mm³. Furthermore, the value falls within the range of recommended density for high density drug delivery systems. The recommended range for high density drug delivery systems is 1.3 to 2.8g/mm³ (Chawla et al., 2003; Talukder and Fassihi, 2004; Bardonnnet et al., 2006). This is indicative that IPB

and *PXLNET* matrices may sink to the antrum of the stomach to facilitate gastroretention leading to prolonged gastric residence time and availability of L-dopa for absorption.

Table 9.6: Density results for interpolymetric blend and nano-enabled tablet matrices.

Formulation	Ave wt (mg)	Ave dia (mm)	Radius sq (mm ²)	Ave thickness (mm)	Volume mm ³	Density mg/mm ³	Std Dev
IPB	1015.93	13.09	42.84	5.37	723.00	1.41	0.006342
<i>PXLNET</i>	994.67	13.06	42.66	4.76	638.71	1.56	0.008025

9.3.6. Gastroadhesivity of IPB and *PXLNET* matrices

Both IPB and *PXLNET* matrices were mucoadhesive as shown in Figure 9.3 by the force of adhesion and work of adhesion. However, the force of adhesion and work of adhesion for IPB matrices were found to be significantly more than *PXLNET*. In this study, the quantity of *iPoly-X-Lipo* nanoparticles loaded into IPB to produce *PXLNET* was more than the quantity of IPB into which they (nanoparticles) were incorporated. Both IPB and *PXLNET* matrices had pullulan which is a known adhesive agent. Furthermore, chitosan's excellent mucoadhesive properties have been studied (Lehr et al., 1992; He et al., 1998; Galovic et al., 2002; Dhawan et al., 2004). However, Sogias and co-workers in their study on the mucoadhesive nature of chitosan discovered that its interaction with mucin is suppressed by sodium chloride (Sogias et al., 2008). Hence, it is a possibility (which is worth investigating further) that sodium tripolyphosphate (TPP), a crosslinking agent which was used in fabrication of *iPoly-X-Lipo* (chitosan blend) nanoparticles, may have suppressed the interaction between chitosan and mucin. Furthermore, Majithiya and Murthy reported that increase in crosslinking time and volume of crosslinking agent reduced the mucoadhesive strength of chitosan (Majithiya and Murthy, 2005). Crosslinking reduces the number of functional groups required for interaction with mucin for excellent mucoadhesion. On the other hand, IPB is a combination of an interpolyelectrolyte complex (between methacrylate copolymer and sodium carboxymethyl cellulose) and a natural polysaccharide, locust bean. It may also be possible the mucoadhesive strength of sodium carboxymethyl cellulose have been reduced by the interactions. However, if so, the impact of the interaction was not as significant as that of chitosan. It is also worthy to note that contact time between mucin and the matrices was only 5secs which is indicative that mucoadhesion will increase as the contact time is increased. Therefore, IPB and *PXLNET* matrices have the potential to adhere to the mucus of the stomach thereby enabling retention and subsequent availability of L-dopa at the site of absorption.

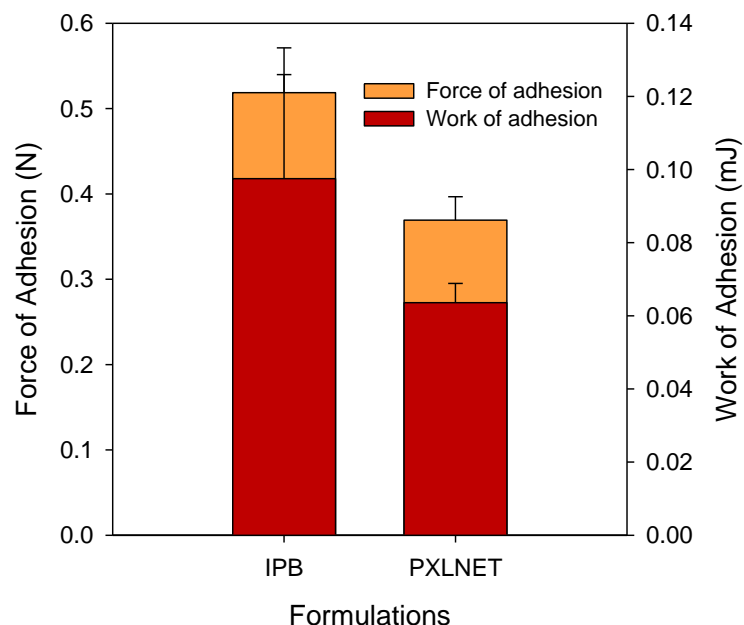


Figure 9.3: Gastro-adhesive profiling for the interpolymeric blend and *PXLNET* employing an applied force 0.5N.

9.3.7. Physicomechanical characteristics and swellability of IPB and *PXLNET* matrices

The unhydrated IPB and *PXLNET* matrices were found to be rigid and had close to 50% resilience which is an indication that they would withstand pressures and stress from date of manufacturing to consumption by patients. High force per distance as shown in Table 9.7a under matrix rigidity is an indication of the resistance offered by the matrices as the probe attempts to penetrate them which explicates that the matrices are robust in nature.

One of the drug release mechanisms for swellable polymers is swelling; hydration and subsequent swelling of matrix tablets leading to solubility of drug and consequent drug release by diffusion. Swelling process is made up of a transition from the glassy core of the polymer before hydration to rubbery phase as the matrix is in contact with a solvent and increases in volume (Colombo et al., 2000). The three stages of change in gel thickness during hydration are initial increase in the gel layer due to polymer swelling, maintenance of constant gel layer between swelling and dissolution front; and reduction in gel layer due to depletion of the glassy core (Li and Gu, 2007). The gel strength is determined by concentration, viscosity and the chemical structure of the rubbery polymer (Colombo et al., 2000). As the IPB and *PXLNET* matrices were hydrated, the resistance to force began to reduce over time. This is shown in Table 9.7b which reveals the drastic decrease of the force per distance and the decrease in the energy required for deformation as the matrices

hydrated over time. Figure 9.4 depicts the Force-Distance profiles at set time intervals - the area under the curve decreased as the matrices hydrated. As the matrices hydrated, gel formation occurred and as the IPB matrices hydrated over time, the gel strength decreased. The force per distance for IPB matrices continued to decrease over time while that of *PXLNET* appeared to be approaching constancy. This could be due to IPB matrices hydrating and retaining their shapes while *PXLNET* matrices were hydrating and eroding. Constant gel strength, as exhibited by *PXLNET* matrices, may occur when the rate of solvent penetration is retarded by gel layer thickness and polymer chain disentanglement is consistent (Yang et al., 1998).

Hence, swelling of the matrices may not only influence drug release but also prolongation of gastric residence time. As the matrices swell and increase in volume, the transit of the matrices from the stomach decreases. Gastroretention is enhanced if the matrix tablet swells and its diameter is more than that of the human pylorus ($\leq 15\text{mm}$) (Davis, 2005). The diameters and thicknesses of the IPB matrices were measured after 8 hours and were found to be 16mm and 9mm, respectively in pH 1.5 (measurement undertaken after lyophilization). This is an indication that the matrices may be retained in the stomach for a prolonged period. However, erosion occurs at pH 4.5; hence reduction in size is anticipated as the pH of the stomach increases in the presence of food and so undesirable blocking of the pylorus is not envisaged.

Table 9.7a: Textural data of unhydrated interpolymeric blend and *PXLNET* matrices.

Formulation	Ave matrix rigidity (N/mm)	Ave deformation energy (Nm)	Ave % resilience
IPB	75.047	0.0103	48.5366
PXLNET	84.933	0.0093	45.5975

Table 9.7b: Swellability results for IPB and *PXLNET* matrices employing Textural Analyzer.

Time (hours)	IPB		PXLNET	
	Ave. rigidity (N/mm)	Ave deformation energy (Nm)	Ave. rigidity (N/mm)	Ave deformation energy (Nm)
2.00	4.2095	0.0325	5.8220	0.0390
4.00	3.8265	0.0195	5.4000	0.0150
6.00	3.5880	0.0140	5.4090	0.0100
8.00	3.4400	0.0125	5.4425	0.0090

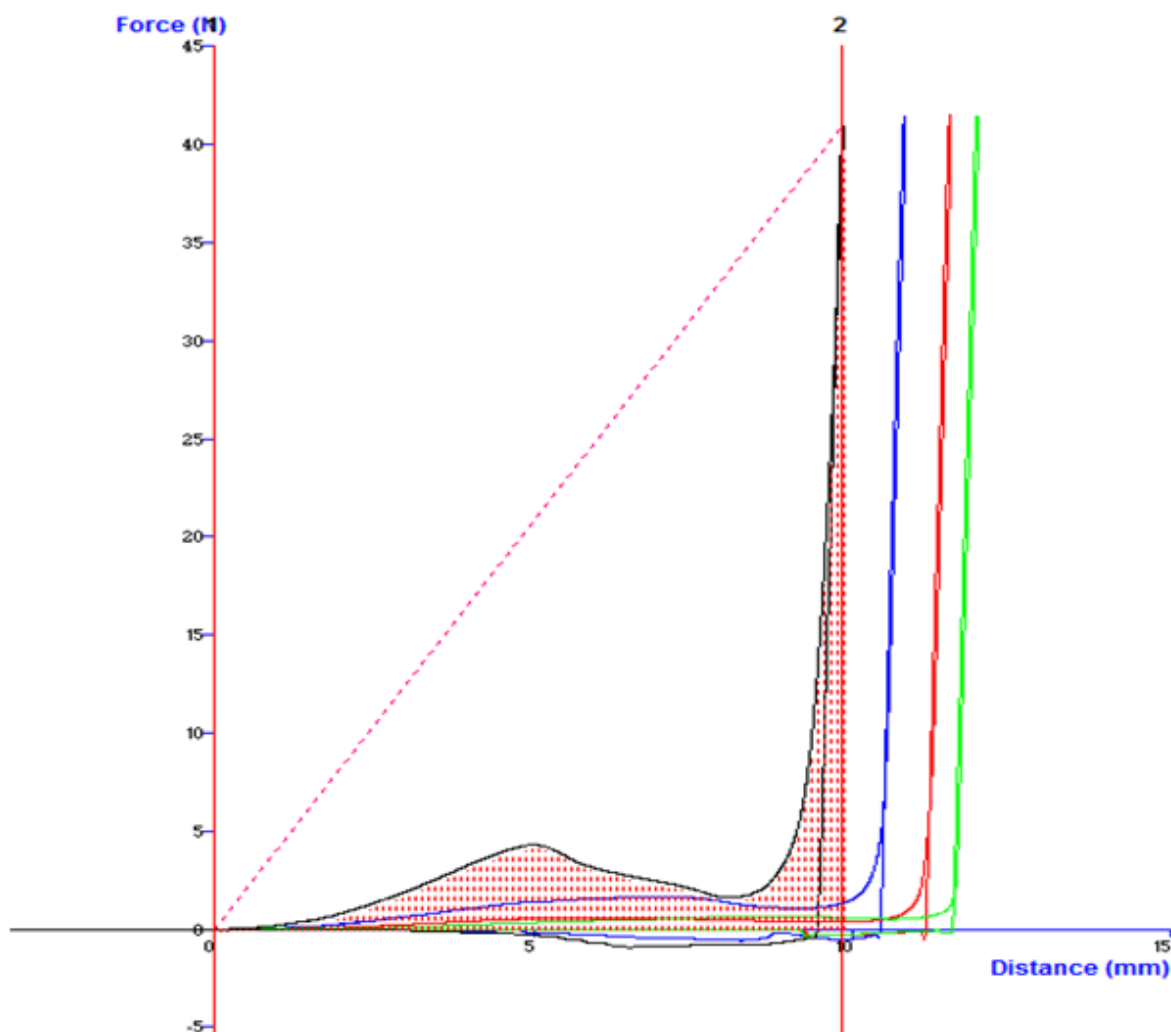


Figure 9.4: Textural profiling of IPB matrices at different time intervals (2nd, 4th, 6th and 8th hours).

9.3.8. Surface morphological analysis of IPB matrices

The microscopic images of the unhydrated and hydrated IPB polymer matrix is shown in Figures 9.5a, b and c. When the matrices are unhydrated, the pores are not visible. However, when hydrated, pores are visible having been created by solvent penetration and drug dissolution. As the drug dissolves, the spaces occupied by the drug granules are converted to pores (Siegel and Langer, 1990). It is envisaged that it was not only the dissolution of the drug that created the pores but also dissolution of other components such as pullulan. Figure 9.5c confirms that IPB matrices are porous swellable release systems. As the system continues to swell, changes in mobility of polymer chains and relaxations; and pore structures occur including changes in shape and size distribution (Korsmeyer et al., 1983). Indeed it is envisaged that among other mechanisms, the pores contribute to the diffusion-controlled mechanism of release of L-dopa from the matrices. Pores as shown in Figure 9.5c were randomly distributed and of various sizes and hence, the release of L-dopa

from the matrices may be attributed to drug dissolution and diffusion through the pores as well as swelling of the matrices.

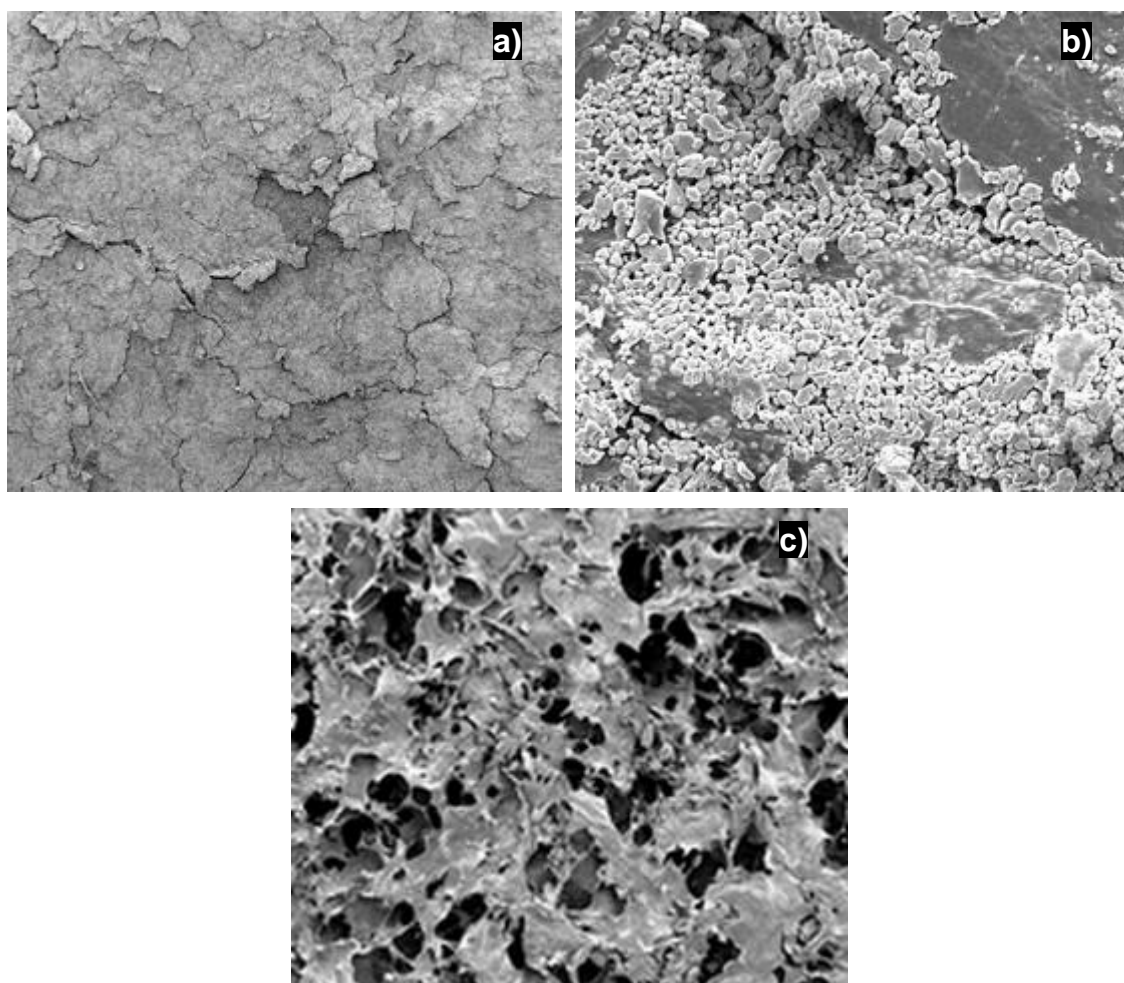


Figure 9.5: Surface morphology of the directly compressed IPB matrices **a)** Mag x 173; **b)** Mag x 10,178 showing the granules of the matrix components and crystals of L-dopa and; **c)** Surface morphology of hydrated and lyophilized IPB matrices showing the pores left after sublimation of water molecules during lyophilization (Mag x 168).

9.3.9. Surface area and porosity analyses

Surface area and pore size assessment is crucial in understanding disintegration, dissolution, adsorption and diffusion of drugs (Mehta et al., 2000). Pores influence matrix properties such as mechanical strength, bulk density, thermal conductivity, fluid flow and adsorption (Rouquerol et al., 1994). Figure 9.6 is a linear isothermic plot obtained which is characteristic of physisorption isotherm Type IV with its hysteresis loop (probably H2) associated with capillary condensation that usually occur in mesopores (Sing et al., 1985). The forced closure (Tensile strength effect) of adsorption and desorption isotherms occurred in the P/P₀ range of 0.30 to 0.35 due to a sudden drop in the volume adsorbed along the

desorption branch. Table 9.8 which gives a summary of the result obtained corroborates the linear isotherm plot indicating that IPB matrices are mainly mesoporous.

Although nitrogen adsorption is not the standard in studying macropores (Groen et al., 2003; Holland 2003), if gas adsorption technique is applied over a wide range of relative pressures (P/P_0), nitrogen adsorption isotherms would furnish information on size distributions in the micro, meso and macro size range (Groen et al., 2003). Hence, the pore size distribution (Figure 9.7a and b) obtained indicated that macropores as large as 237nm were measured giving an understanding that macropores were present but were less than 18% of the pore diameters. The pore area covered by the mesopores is depicted in Figure 9.7a. About 82% of the pore diameter ranges were mesopores. The pore size distribution was derived from the adsorption branch as pore distribution curve obtained from desorption branch may be unreliable if blocking effect or tensile strength effect occurs (TSE) (Sing et al., 1985). Figure 9.7b also indicates the presence of an average pore size of 1.9nm which should still be regarded as mesopores and not micropores. The absence of micropores is further confirmed by the t-plot which may not be used to determine micropore size but gives information on micropore volume. The micropore volume of IPB was negative ($-0.000673 \text{ cm}^3/\text{g}$) and consequently the micropore area could not be determined. Hence, IPB matrices are mainly mesoporous which is also an indication that one of the mechanisms of drug release from the IPB is diffusion.

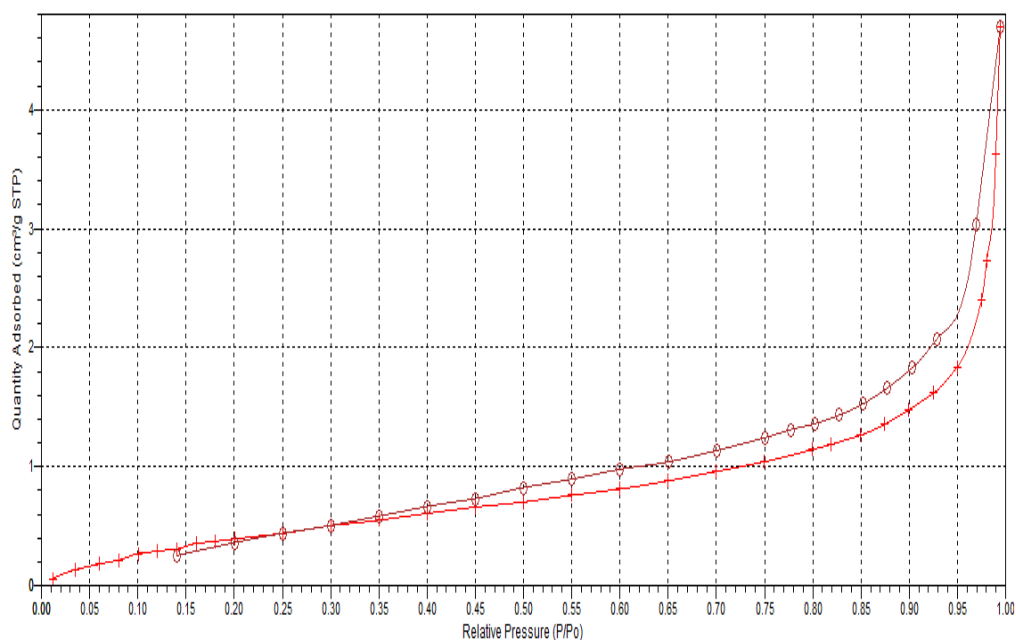


Figure 9.6: Linear Isothermic plot – Nitrogen adsorption (+ - red) and desorption (o – wine red) isotherms of interpolymeric blend.

Table 9.8: A summary of surface area and pore analyses of IPB matrices.

Surface area (m ² /g)				Pore volume (cm ³ /g)			Ave pore size (nm)		
SPSA	BET	BJH A	BJH D	SPAT	BJH A	BJH D	BET	BJH A	BJH D
1.3640	1.9548	1.880	2.2217	0.0037	0.0071	0.0070	7.5762	15.1976	12.6376

SPSA - Single point surface area at $P/P_0 = 0.200211845$; BJH A - BJH Adsorption cumulative surface area/volume of pores between 1.7 and 300nm; BJH D - BJH desorption cumulative surface area/volume of pores between 1.7 and 300nm; SPAT - Single point adsorption total pore volume of pores less than 78.9nm diameter at $P/P_0 = 0.9748$.

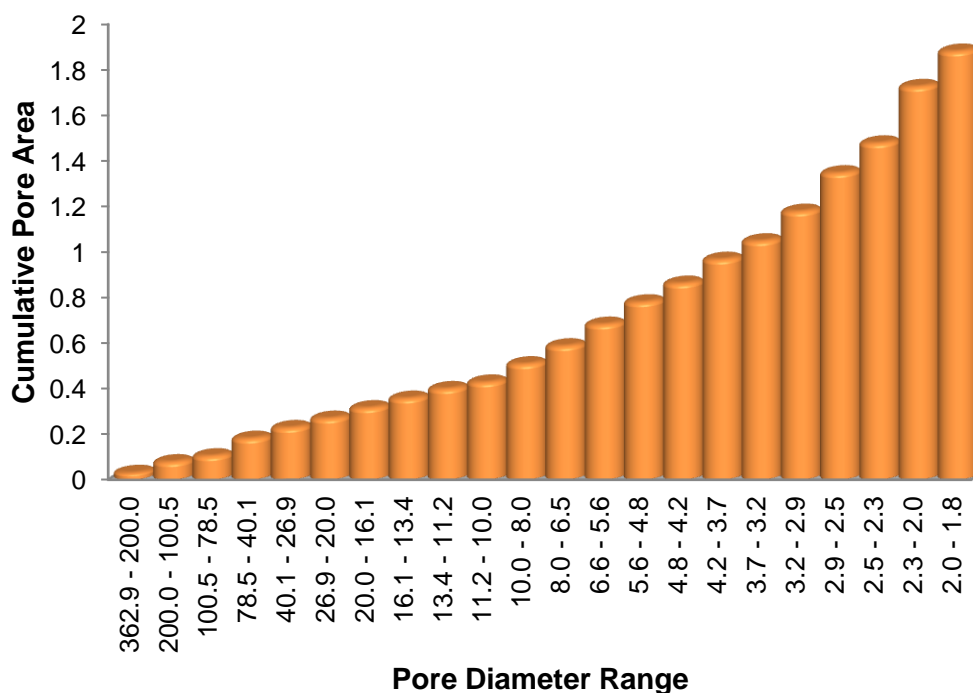


Figure 9.7a: Pore size distribution with respect to cumulative pore area of IPB matrix.

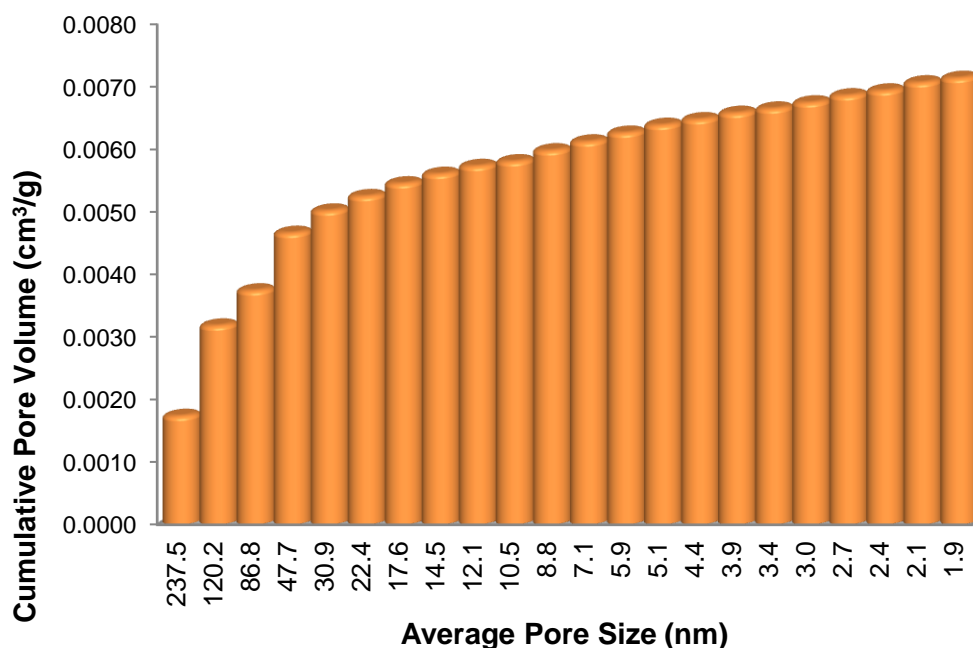


Figure 9.7b: Pore size distribution with respect to cumulative pore volume of IPB matrix.

9.3.10. Comparative *in vitro* drug release studies

In vitro drug release studies are critical in determining the rate and extent of drug absorption which in turn affects the therapeutic efficacy of a drug. Absorption of a drug is influenced by its release from the dosage form, its solubility and subsequent permeability into the systemic circulation amongst other factors (Hörter and Dressman, 2001). Rate of diffusion of a drug from a tablet matrix is mainly dependent on physicochemical properties of drug and polymer(s) (Li and Gu, 2007). However, the mechanisms of release are greatly influenced by the properties of the polymer(s) employed.

The influence of solubility of drug on rate of release is observed with respect to the drugs incorporated. As the aqueous solubility increased, the rate of drug released increased and vice versa. Figures 9.8a(i) and 9.8c(ii) show the rapid release of benserazide which is freely soluble in water in comparison with less soluble L-dopa. By the second hour, 73.3% of benserazide was released from Madopar[®] HBS while only 39.4% was released from IPB blend at the same time. This confirms the influence of the physicochemical properties of interpolymeric blend in slowing the rate of drug release despite the high aqueous solubility of benserazide. On the other hand, carbidopa though same amount as benserazide and a dopa decarboxylase inhibitor as well had profiles similar to levodopa as shown in Figure 9.8b (i and ii) and Figure 9.8d (i and ii). This is because carbidopa, like L-dopa, is a poorly soluble drug and so even though its quantity is one-fourth of levodopa its rate of release was

decreased due to its low rate of solubility in dissolution medium as well as the influence of the interpolymeric blend.

One of the properties of interpolymeric blend that may contribute to the controlled release of L-dopa and benserazide/carbidopa is its molecular weight. Studies have shown that high molecular weight decreases the rate of release (Castelli et al., 1996; Ramkisson-Ganorkar et al., 1999; Wu et al., 2005; Mittal et al., 2007) leading to a sustained and prolonged drug release. The polymers in Madopar[®] HBS are hydroxypropylmethylcellulose (HPMC) and gelatin (Sabale et al., 2010; Roche, 2010) while that of Sinemet[®] CR are hydroxypropylcellulose and HPMC (Merck Sharp & Dohme Corp., 2011). An interpolymeric blend is a blend of an interpolyelectrolyte complex (with merge of molecular weights of two polymers) and a polysaccharide. Hence it is envisaged that IPB has higher cumulative molecular weight which led to a more controlled release of the drug in comparison with the polymers employed in Madopar[®] HBS or Sinemet[®] CR.

In pH 1.5, Madopar[®] HBS capsules dissolved, the formulation gelled on hydration and remained floated throughout the study; not much swelling was observed and 100% of the L-dopa was released by the 16th hour. Its mechanism of drug release is by diffusion upon hydration (Erni and Held, 1987). Sinemet[®] CR matrices dissolved and eroded completely before the 4th hour releasing 100% of L-dopa drug thus confirming its release mechanism as stated by Dempski and co-workers (Dempski et al., 1989) The IPB matrices did not erode nor dissolve at pH 1.5 and released almost 90% of L-dopa by the 24th hour and thus the mechanism of release is mainly by swelling and diffusion. Furthermore, while Sinemet[®] CR eroded and dissolved in pH 1.5, IPB did not. Rather the matrices retained their three-dimensional network throughout the 24 hour period of study. IPB and Madopar[®] HBS are gastroretentive drug delivery system with different mechanisms of gastroretention. While Madopar[®] HBS is a floatable drug delivery system; interpolymeric blend is a triple mechanism (high density, swelling and gastro-adhesive) gastroretentive delivery system.

The drug release profiles of interpolymeric blend matrices, *PXLNET* matrices and the conventional dosage forms are shown in Figures 9.8a - f. L-dopa release from interpolymeric blend exhibited a more linear profile than Madopar[®] HBS and Sinemet[®] CR which may infer that interpolymeric blend may provide a constant quantity of L-dopa over a prolonged period. Figure 9.8e shows a comparative drug release profiles of the gastroretentive delivery systems – Madopar[®] HBS and IPB matrices while Figure 9.8f is a comparative drug release profiles of the three controlled release drug delivery systems – Madopar[®] HBS, Sinemet[®] CR and IPB matrices. Indeed interpolymeric blend is promising as an oral delivery system that

may improve the absorption and subsequent bioavailability of L-dopa/carbidopa or L-dopa/benserazide with constant therapeutic plasma concentrations.

It is worthy of note that the *PXLNET* release profiles obtained in this study differ from those of Chapter 8. In this study, *PXLNET* eroded precipitously at pH 1.5. It is proposed that this may be due to the presence of excipients (as excipients were not employed in Chapter 8) which may have hindered cohesion to occur between the nanoparticles. Furthermore, the quantity of IPB, which was substantially small, did not allow for a high degree of interactions between the nanoparticles and the IPB which would have retarded erosion and improved the mechanical strength of the matrices.

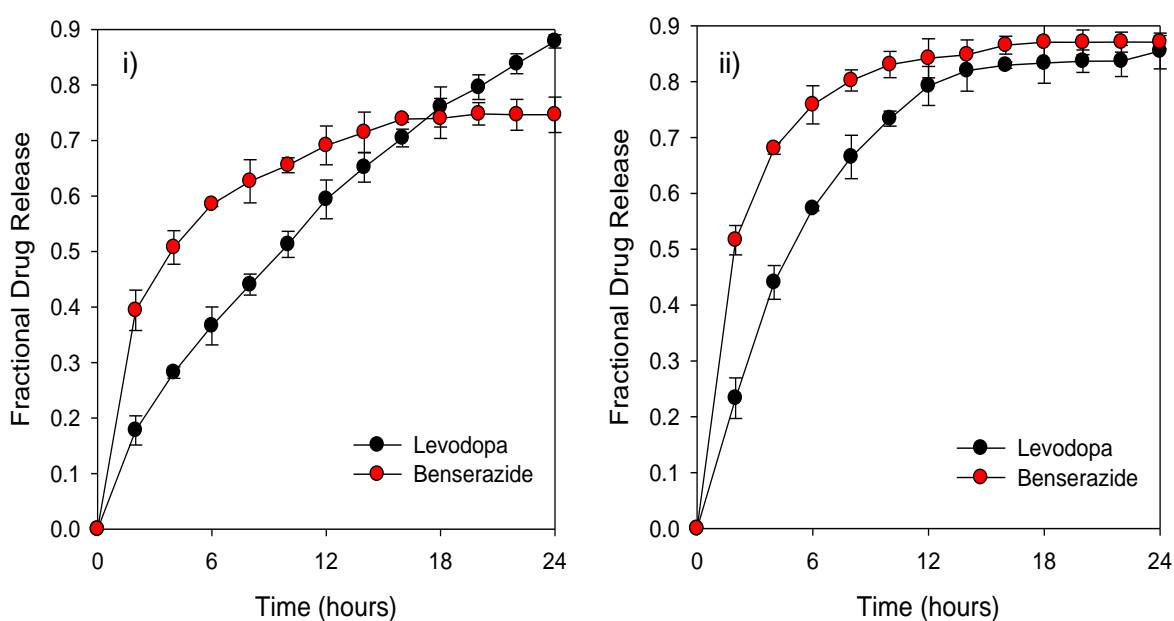


Figure 9.8a: Drug release profiles of: i) IPB matrices and; ii) *PXLNET* matrices with benserazide as the DOPA decarboxylase inhibitor.

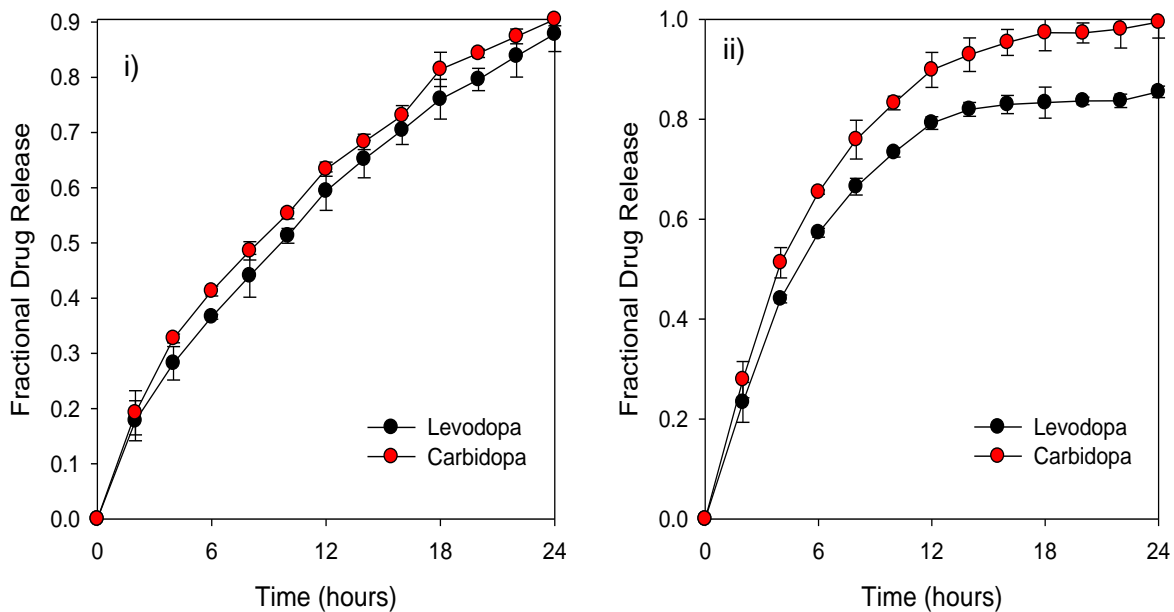


Figure 9.8b: Drug release profiles of: i) IPB matrices and; ii) PXLNET matrices with carbidopa as the DOPA decarboxylase inhibitor.

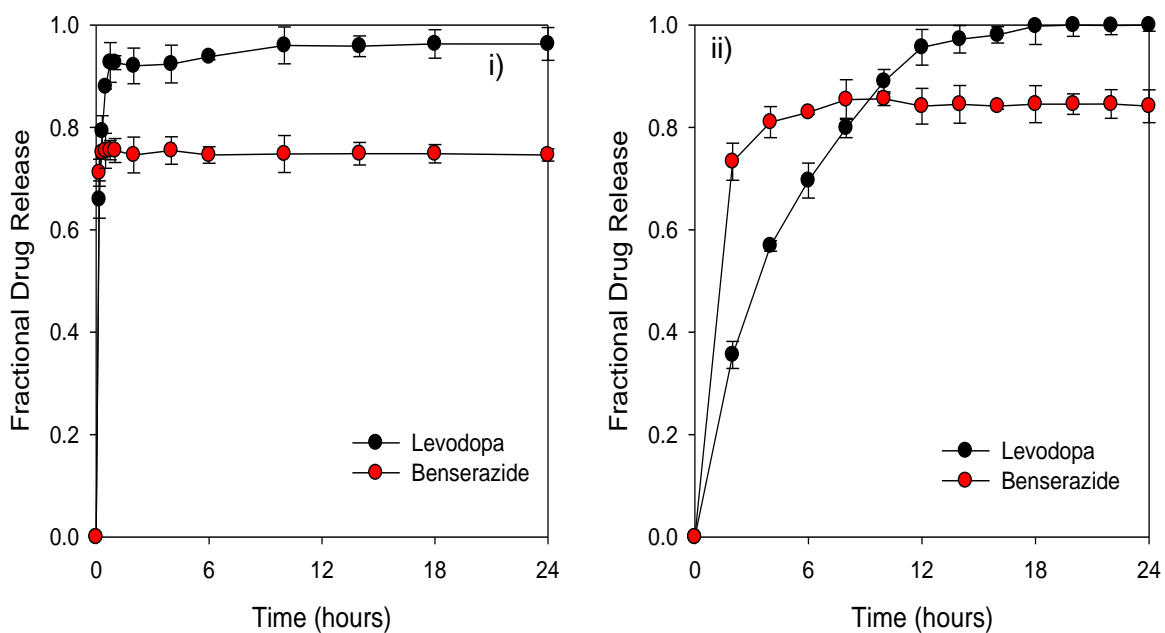


Figure 9.8c: Drug release profiles of: i) Madopar[®] IR and; ii) Madopar[®] HBS.

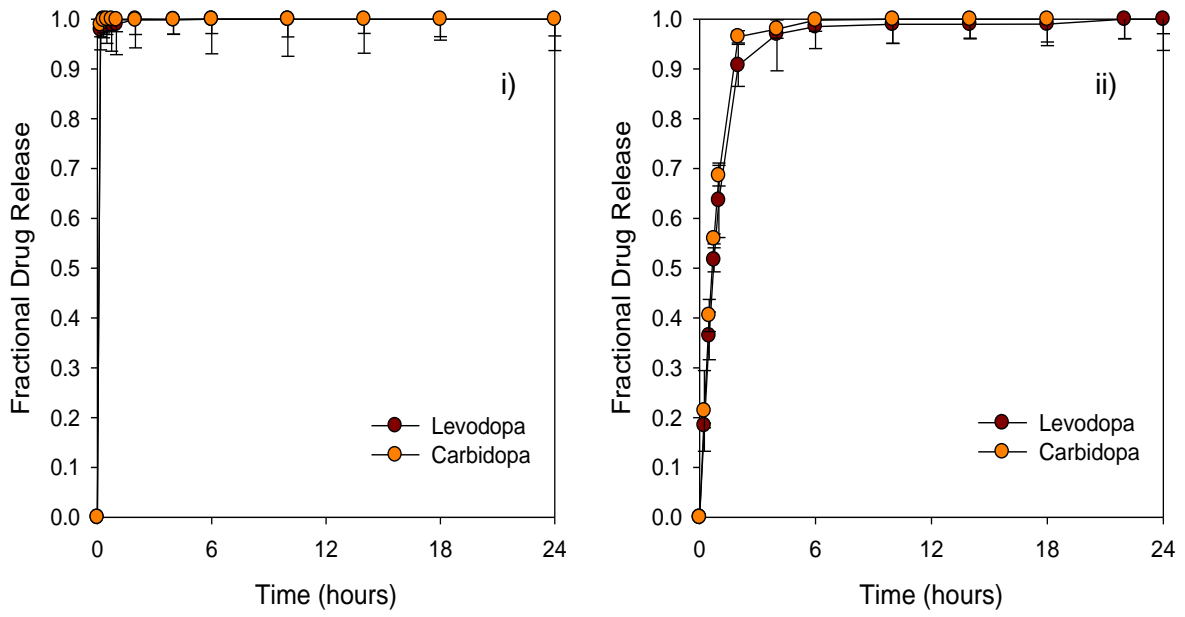


Figure 9.8d: Drug release profiles of: **i)** Sinemet[®] IR and; **ii)** Sinemet[®] CR.

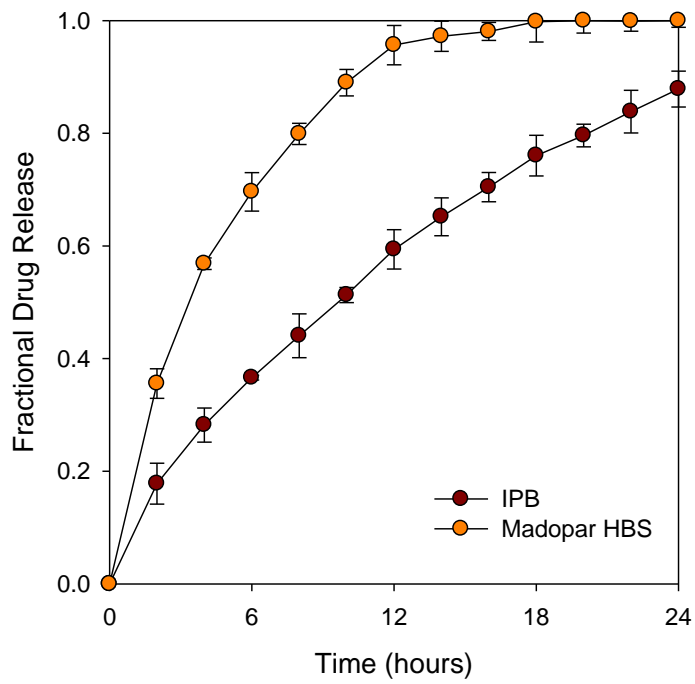


Figure 9.8e: Comparative drug release profiles of L-dopa from IPB matrices and Madopar[®] HBS capsules.

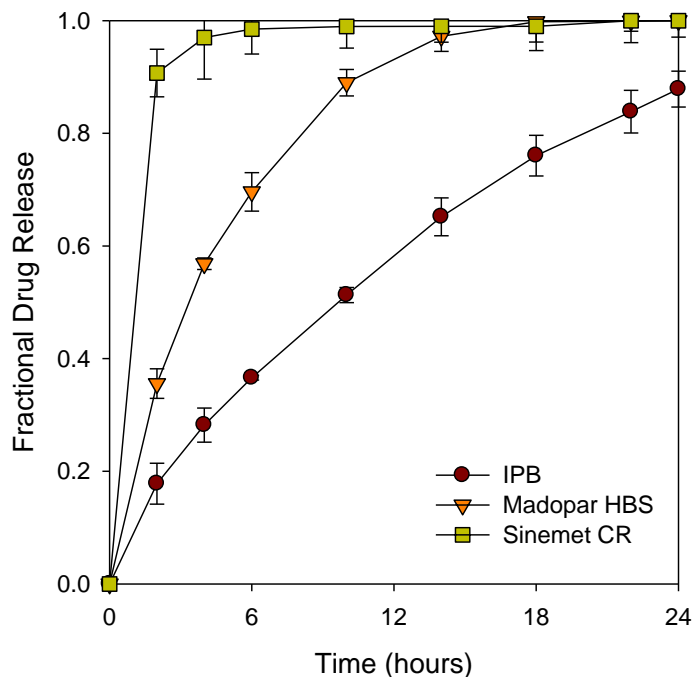


Figure 9.8f: Comparative drug release profiles of L-dopa from IPB matrices, Madopar[®] HBS capsules and Sinemet[®] CR.

The outcomes of the mathematical modeling are shown in Tables 9.9a and b. The modeling for zero and first order kinetics was done for the 12th and 24th hours and the drug delivery system that best fits into zero order is the IPB with correlation coefficients of 0.9718 at the 12th hour and 0.9611 at 24th hour. However, when the drug delivery systems were considered individually, the best fit model for Madopar[®] HBS was first order kinetics at the 12th hour ($r^2 = 0.9611$) while at the 24th hour, Higuchi model was its best fit with $r^2 = 0.8657$. The correlation coefficients of Sinemet[®] for zero and first order kinetics at 12th and 24th were < than 0.86. However, when the zero and first release kinetics were calculated at the 5th hour (not included in the table), it became clear that the best fit model was first order with $r^2 = 0.9946$. When that of the IPB blend was determined at the 12th hour or 24th, correlation coefficients for zero order and first order were > 0.96. However, the best fit model was Korsmeyer-Peppas model with $r^2 = 0.9994$ at the 24th hour. As discussed in Chapter 5, Section 5.3.6, n as shown in Table 9.9a is the release exponent and for cylindrical matrix, the release mechanism of IPB matrices is anomalous, which is an indication that drug release from the matrices is a combination of mechanisms. The best model for *PXLNET* was first order at 12th and 24th hours. Drug release kinetics were not determined for the immediate release formulations – Sinemet[®] IR and Madopar[®]. However, dissolution efficiency was determined for all formulations at 24th hour.

As stated in Chapter 5, the test and reference products can be said to be bioequivalent if the difference between their dissolution efficiencies is within appropriate limits ($\pm 10\%$) (Anderson et al., 1998). Hence, the immediate dosage forms (Sinemet[®] IR and Madopar[®]) are bioequivalent as the difference between their DE was within $\pm 10\%$. When Sinemet CR was used as reference and compared with Madopar[®] HBS, interpolymetric blend and *PXLNET*; bio-inequivalence was observed. However, when Madopar[®] HBS was used as reference product in comparison with interpolymetric blend and *PXLNET*; bioequivalence was found with *PXLNET* but not with interpolymetric blend. Since more than one comparison approach is widely accepted to determine bioequivalence (Polli et al., 1997); similarity factor f_2 was also employed.

The similarity factor f_2 is a model-independent method of comparing drug release profiles. It measures the similarity in the percent dissolution between two curves (Shah et al., 1998).

$$f_2 = 50 \cdot \log \left\{ \left[1 + \left(\frac{1}{n} \right) \sum_{t=1}^n (R_t - T_t)^2 \right]^{-0.5} \cdot 100 \right\}$$

Equation 9.1

Where n is the number of time points, R_t is the dissolution value of reference product at time t and T_t is the dissolution value for the test product at time t .

The comparison is usually between a reference product and the test product; between pre-change and post-change batches due to change in factors such as scale of manufacture, manufacture process, equipment or excipients and between different product strengths. Similarity factor f_2 is commonly used for dissolution profiles comparison perhaps mainly because it is recommended in FDA guidance documents (Center for Drug Evaluation and Research, 1997a; 1997b; Center for Drug Evaluation and Research, 2000). The dissolution profile of a test product is considered similar to that of a reference product if the f_2 value obtained of the two profiles is not less than 50. Sinemet[®] products were used as reference products in four cases out of six comparisons done (Table 9.10). In the other cases Madopar[®] HBS was used as reference product to compare with the drug delivery systems (IPB and *PXLNET*) in this study. None of the drug delivery systems were found to be bioequivalent.

Since f_2 is sensitive to measurements obtained after either the test or reference product has released 85% of the drug; it is recommended that f_2 should be calculated to not more than one sampling point after 85% drug release (Shah et al., 1998). Hence f_2 was recalculated at 85% drug release and once again, none of the comparative dissolution profiles were bioequivalent. Although with DE, Madopar[®] HBS and *PXLNET* were bioequivalent, with f_2 they were not because f_2 value should be not less than 50. However, it could be seen that

their f_2 value came close to 50 but not close enough. Furthermore since f_2 is the method of comparison approved by the regulatory bodies (Centre for Drug Evaluation and Research, 1997; Center for Drug Evaluation and Research, 1997; Center for Drug Evaluation and Research, 2000; Committee for Proprietary Medicinal Products (CPMP), 2000); it will be concluded that in this study that none of the drug delivery systems were found to be bioequivalent.

Table 9.9a: Comparative model dependent approaches for L-dopa from the various drug devices.

Drug device	Zero order ₁₂		Zero order ₂₄		First order ₁₂		First order ₂₄		Higuchi		Korsmeyer-Peppas			Best fit model ¹
	K_0	r^2	K_0	r^2	K_1	r^2	K_1	r^2	K_H	r^2	$K_{kp}(h^{-n})$	r^2	n	
IPB	4.6607	0.9718	3.4283	0.9611	-0.0299	0.9953	-0.0367	0.9876	20.7009	0.9980	11.1840	0.9994	0.67	Korsmeyer-Peppas
PXLNET	6.4326	0.9329	3.0021	0.7457	-0.0558	0.9968	-0.0312	0.8708	16.4915	0.8643	-	-	-	First order ₁₂
Madopar® HBS	7.4433	0.9126	3.3776	0.7204	-0.1116	0.9611	-0.1162	0.8498	17.6702	0.8657	-	-	-	First order ₁₂
SINEMET® CR	8.3737	0.5682	2.7174	0.4514	-0.2061	0.8509	-0.1056	0.6997	14.1401	0.6208	-	-	-	First order ₁₂

¹ Correlation coefficient r^2 was employed to determine best fit model

Table 9.9b: Dissolution Efficiency of the various devices.

Drug device	DE (%)
IPB	62.3
PXLNET	78.2
Madopar® HBS	83.3
SINEMET® CR	96.3
Madopar® IR	97.0
Sinemet® IR	100

Table 9.10: Similarity factor f_2 .

Comparing drug devices	Reference drug device	Similarity factor f_2 (24 th hour)	Similarity factor f_2 (85% drug release)
Madopar [®] HBS vs IPB	Madopar [®] HBS	27.61	25.14
Madopar [®] HBS vs <i>PXLNET</i>	Madopar [®] HBS	41.4	43.71
Sinemet [®] CR vs IPB	Sinemet [®] CR	16.05	7.47
Sinemet [®] CR vs <i>PXLNET</i>	Sinemet [®] CR	21.83	10.88
Madopar [®] HBS vs Sinemet [®] CR	Sinemet [®] CR	28.88	15.83
Madopar [®] IR vs Sinemet [®] IR	Sinemet [®] IR	45.14	32.03

9.3.11. Magnetic resonance imaging

Magnetic resonance imaging, a non-destructive and non-invasive method was employed to determine the mechanism of drug release in pH 1.5 and 4.5. Based on dissolution studies, it was observed that the matrices behaved as hydrogels in pH 1.5 thereby retaining its three-dimensional network while gradual surface erosion over time was observed in pH 4.5. These observations were confirmed by magnetic resonance images obtained as shown Figure 9.9a. Figure 9.9a (1) depicts images in pH 1.5 while 9.9a (2) show images in pH 4.5 at 0, 3rd, 6th, 9th and 12th hours.

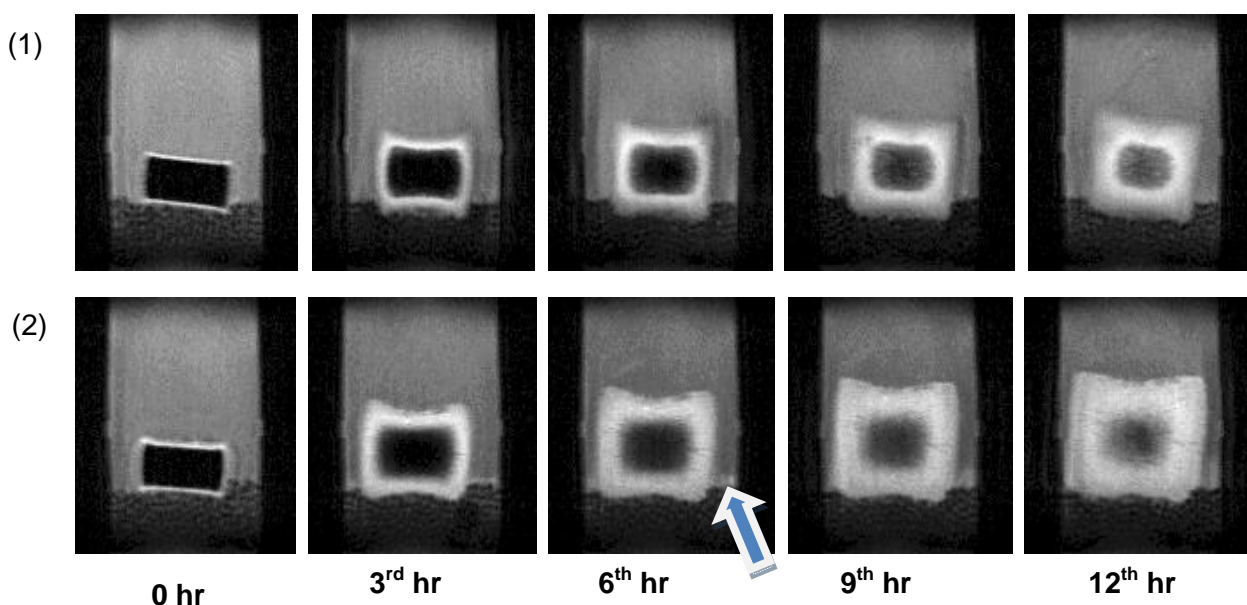


Figure 9.9a: MRI images of interpolymeric blend tablet matrices: **1)** at pH 1.5 and; **2)** at pH 4.5.

The grey portion around the matrix is the dissolution medium. The white part of the matrix is indicative of hydration and gelling while the black part is the dry core (unhydrated portion) of the matrix. Swelling was observed in both cases shown by the increase in the size of the matrix over time. As the rate of medium penetration increased, the rate of swelling increased. The evidence in Figure 9.9a (2) that the matrix was eroding is shown by the white section

around the matrix and at the base which represents eroded particles (shown by the arrow). The thickness of the white part relates to the concentration or degree of solvent penetration.

Figures 9.9b and c show the decrease in dry core area, the increase in hydrated and gelled area and representation of drug release over time in both media (pH 1.5 and 4.5). The values for the gelled and dry core areas were obtained using the MARAN-i-software (image analysis part of the software) . It showed that mechanism of solvent penetration influenced the release of L-dopa. Increase in rate of hydration increased the rate of release; for as the medium migrated into the matrix, L-dopa dissolved and diffused out. Water penetration and swelling of polymer is characteristic of diffusion-controlled mechanism of drug release (Richardson et al., 2005). While the dry core area profile of IPB matrix showed substantial hydration by the 12th hour at pH 1.5, there was still presence of dry core at 12th hour in pH 4.5 medium indicating that the rate of hydration is more in pH 1.5 than in pH 4.5. It is interesting to note that the highest white area was found in the gel area profile for pH 4.5. The white area is the high intensity area of the matrix due to the hydrogen bonds between the hydrophilic polymers and water (Tajiri et al., 2010). However, the white area is made up of the swollen front and eroded front making it appear that the polymer matrix swells more at pH 4.5. The rate of hydration and swelling and subsequently rate of L-dopa release was more in pH 1.5. Furthermore, the amount of drug release at pH 4.5 at 12th hour in comparison to that of pH 1.5 was less. The absorbance at the 12th hour in pH 4.5 medium was 0.6879 while that in pH 1.5 was 0.8013 which implies that the rate of drug release in pH 1.5 was higher than that of pH 4.5. The mechanisms of drug release in pH 4.5 were a combination of matrix erosion and diffusion controlled mechanisms.

In summary, in pH 1.5, the polymer matrix was able to resist erosion and hence, rate of L-dopa release was based on rate of hydration, swelling, dissolution and subsequent diffusion of L-dopa, which is shown by MRI as rate of increase in gel area; and subsequent dissolution and diffusion of L-dopa. In pH 4.5 the rate of release was by hydration and swelling, matrix erosion and dissolution and subsequent diffusion of L-dopa.

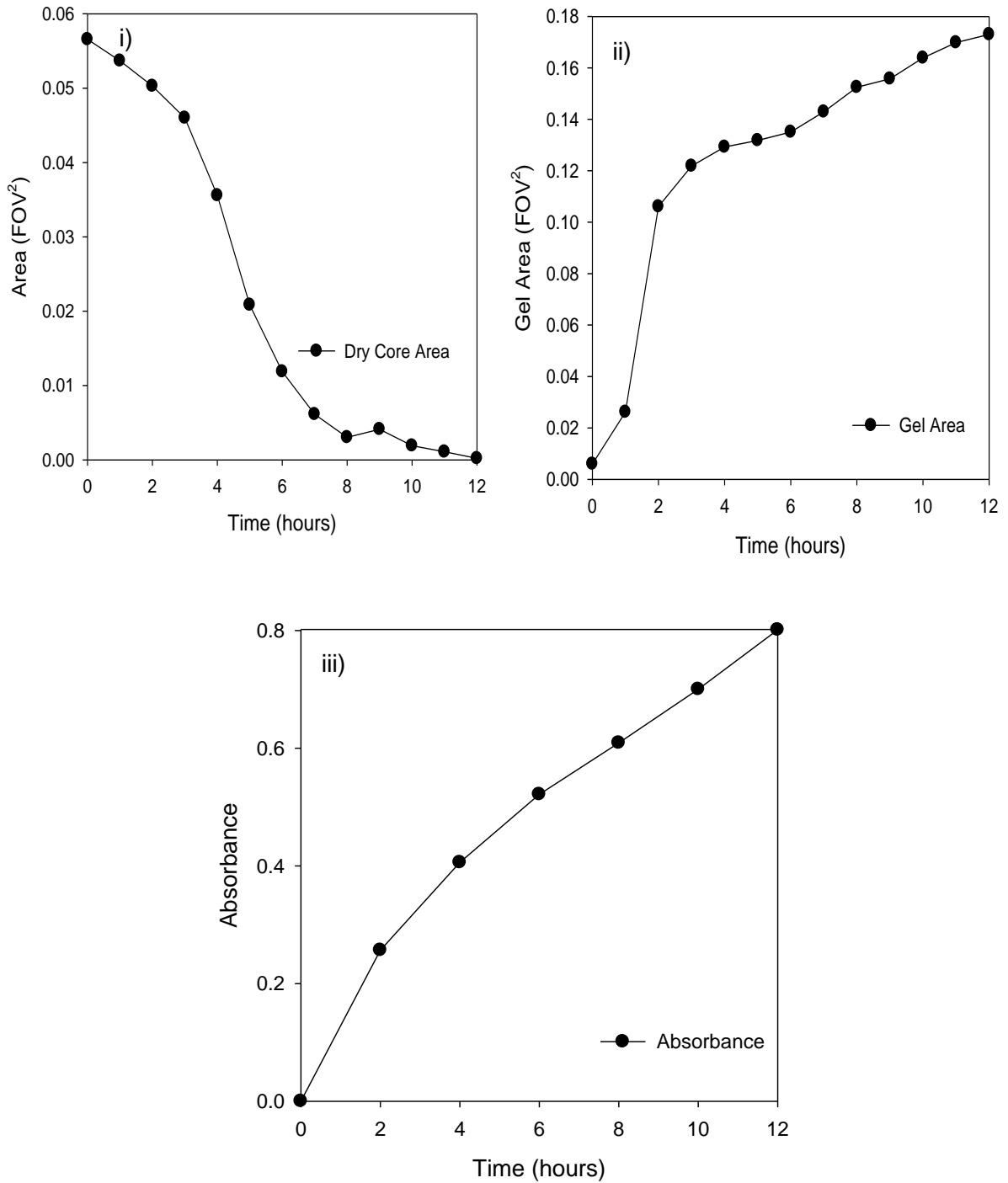


Figure 9.9b: Area analysis of MRI images as a function of time: **i)** the area of the dry core over time; **ii)** the hydrated and gelled area of the matrix over time at pH 1.5 and; **iii)** increase in absorbance over time which is indicative of rate of drug release over time at pH 1.5.

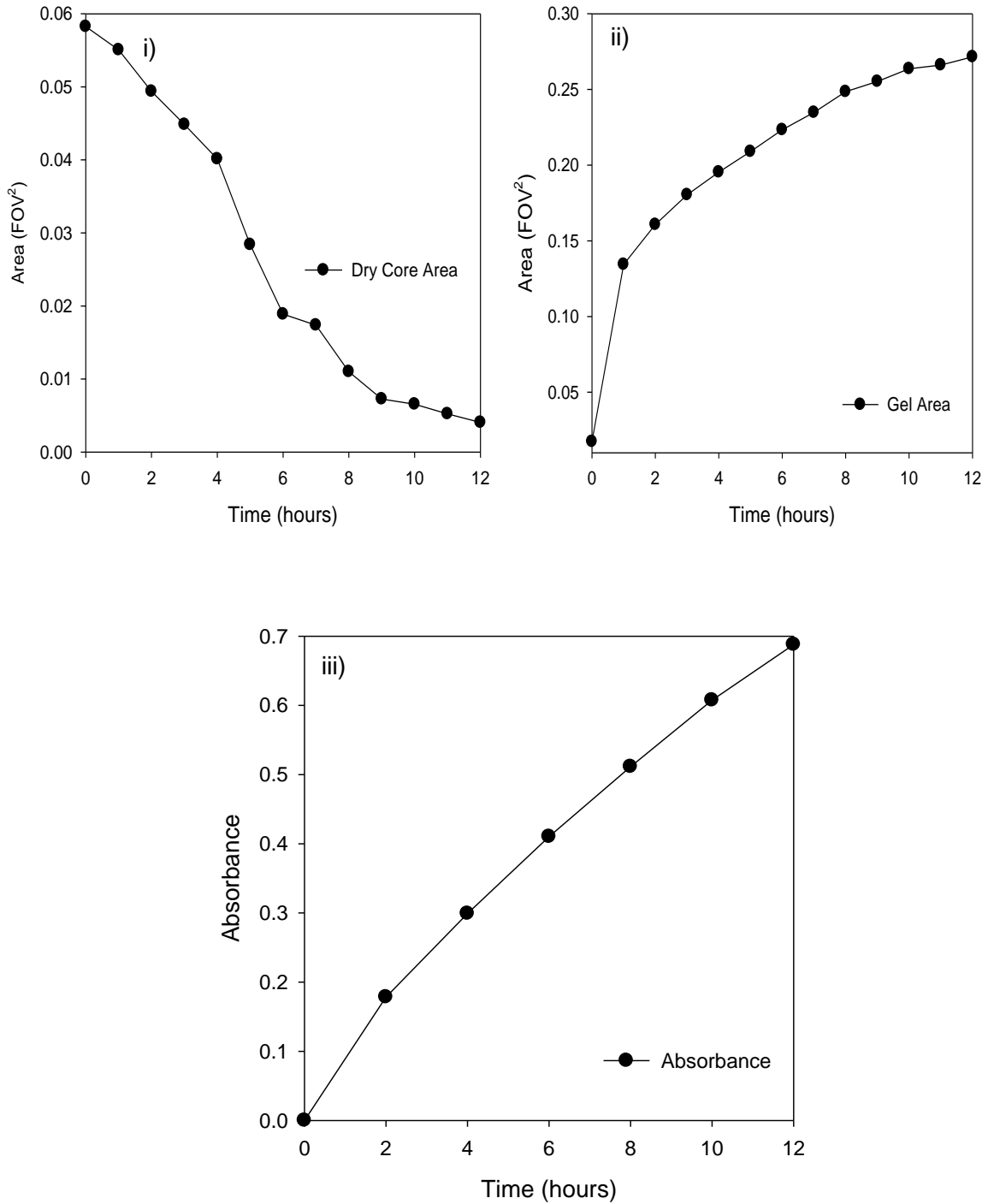


Figure 9.9c: Area analysis of MRI images as a function of time: **i)** the area of the dry core over time; **ii)** the hydrated and gelled area of the matrix over time at pH 1.5 and; **iii)** increase in absorbance over time which is indicative of rate of drug release over time at pH 1.5.

9.3.12. Stability of IPB, L-dopa-loaded nanoparticles and *PXLNET*

Studies have been undertaken on the stability of L-dopa, benserazide and carbidopa (Lennernäs et al., 1993; Pappert et al., 1996; 1997; Kankkunen et al., 2002). L-dopa and dopa decarboxylase inhibitors are unstable in the presence of moisture, oxygen, temperature and pH. The rate of oxidation of decarboxylase inhibitors is faster than that of L-dopa. While L-dopa can survive in pH 4.5, benserazide is oxidized. However, as the pH goes towards neutral (such as pH 6.8) L-dopa is oxidized and as the pH increases towards basicity, the rate of oxidation or degradation is fast. The color change moves from yellow to black as further oxidation takes place. At body temperature and pH 4.5, L-dopa is stable for over 24 hours while the oxidation of benserazide occurs. However, the drugs are stable in pH 1.5 and at ambient temperature. The lower the temperature, the more stable the drugs. The factors affecting instability are interwoven and the drugs cannot be stabilized independent of any factor. For instance, L-dopa in the presence a basic pH of 6.8 and ambient temperature of 25°C will be oxidized. To avoid oxidation, there should be low pH and low temperature. L-dopa-loaded nanoparticles had to be fabricated in acidic conditions to ensure stability during and after fabrication. It was found that in acidic medium (pH 1.2) and low temperature (4°C), no color change of the particles or medium was observed for 12 months. However, when the nanoparticles were lyophilized, exposure to moisture caused color changes as shown in Figure 9.10.

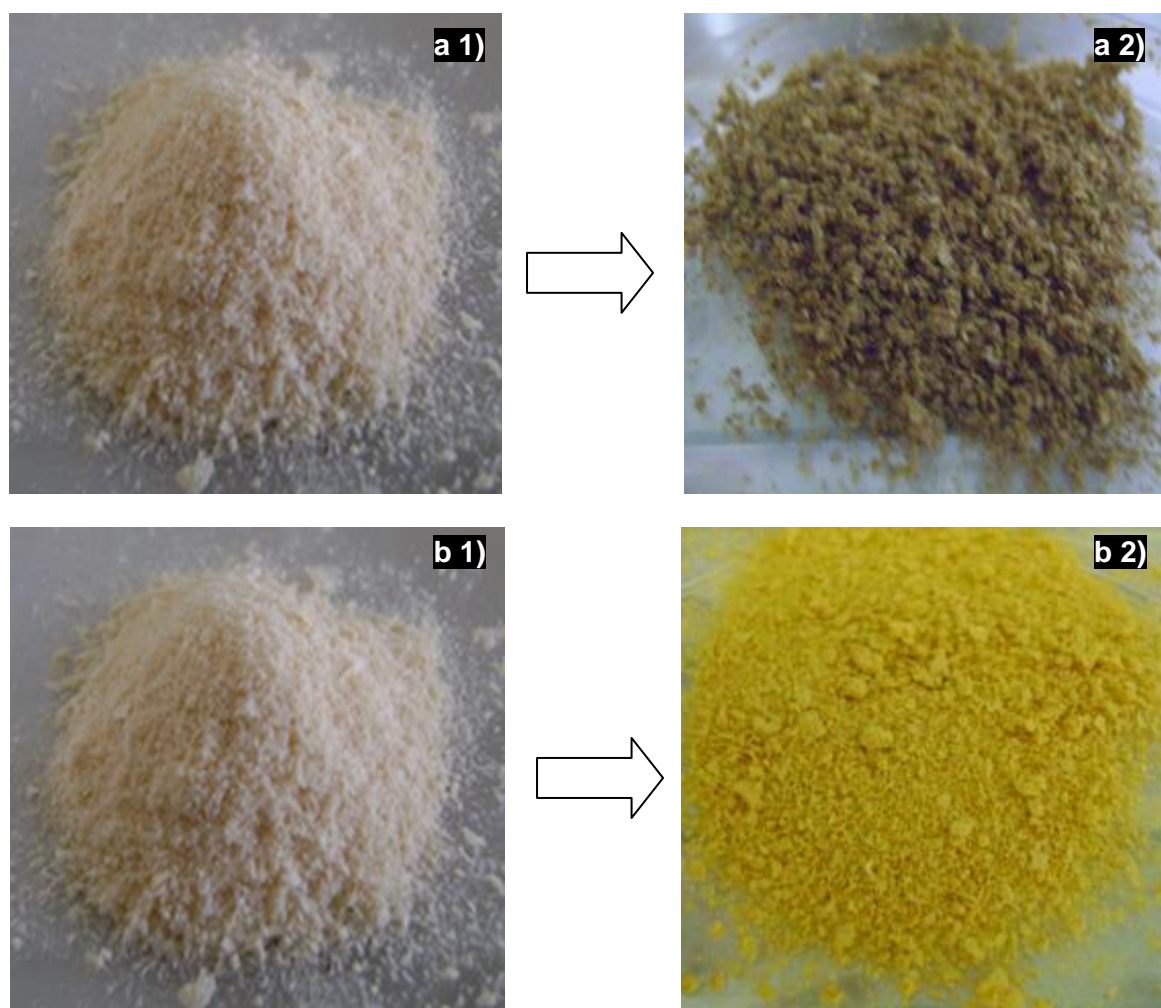


Figure 9.10: a) L-dopa-loaded nanoparticles changes to black color and; b) carbidopa-loaded nanoparticles change to yellow in the presence of moisture.

The L-dopa/benserazide/carbidopa-loaded nanoparticles and matrices are stored in air tight containers at low temperature. Furthermore, desiccants should be inserted into the packages to ensure dry drug formulations.

9.4. CONCLUDING REMARKS

The predicted values of density and dissolution for IPB matrices were comparable to the observed values while those of bioadhesion and swelling differed by 0.08N and 0.79N respectively. The morphological analysis and magnetic resonance imaging indicated IPB behaved as a porous swellable drug release system. *PXLNET* eroded which ensured the release of *iPoly-X-Lipo* nanoparticles and subsequent release of L-dopa. In comparisons to the conventional dosage forms, *PXLNET* and IPB matrices exhibited a more prolonged release than Sinemet[®] CR. Furthermore, IPB displayed constant delivery over a prolonged period than Madopar[®] HBS and was the best fit for zero-order release. Having obtained such

stirring *in vitro* results, *in vivo* studies will be undertaken of IPB and *PXLNET* in comparison with the conventional dosage forms to correlate *in vitro* and *in vivo* studies in the next Chapter.

CHAPTER TEN

IN VIVO INVESTIGATION AND ANALYSIS OF THE OPTIMIZED INTERPOLYMERIC BLEND/NANO-ENABLED THREE-MECHANISM GASTRORETENTIVE LEVODOPA DELIVERY SYSTEMS

10.1. INTRODUCTION

Although *in vitro* drug delivery studies are undertaken, the ultimate goal in developing and evaluating a drug delivery device is to achieve the desired drug delivery outcomes *in vivo*. Indeed despite attempts at simulating *in vivo* environment, they are still not the exact replicas of the functions and impacts of *in vivo* environment on drug delivery devices. Hence, after development and *in vitro* analyses, there is still the need to assess the device *in vivo* (within a living organism) before it is commercialized for administration to the end-user consumer. *In vivo* drug delivery studies are also important in order to obtain the pharmacodynamics and pharmacokinetics data of the drug delivery device.

The degree of absorption of a drug in the gastrointestinal tract is based on certain events which include drug release, drug in solution at absorptive sites, drug absorption into systemic circulation, liver and gut metabolism, decomposition and transit (Dressman and Reppas, 2000). Absorption and subsequent bioavailability of a drug is not only determined by the properties of the drug such as solubility which in turn is based on its crystallinity and lipophilicity but are also affected by the gastrointestinal environment which is determined by its pH, presence of food and certain substances such as surfactants in gastric juice or bile as well as enzymes. Other factors include viscosity of luminal contents, motility patterns and flow rate, secretions and co-administered fluids (Lipka and Amidon, 1999). Hence, oral drug delivery devices are developed to accommodate a number of these factors and at the same time ensure the absorption and subsequent bioavailability of the incorporated drug.

The optimized interpolymeric blend/nano-enabled L-dopa-loaded delivery systems have been developed to be gastroretentive and release L-dopa at a constant rate in order to maintain a constant concentration over a prolonged period. Hence, it was necessary to assess *in vivo*, the gastric residence time and drug release properties. In addition, since patients are the target consumers, it was also necessary to determine the degree of toxicity of the device.

The Large White pig model was chosen because of the close resemblance of its gastrointestinal tract to that of human and consequently, best suited for *in vivo* studies of oral drug delivery. The anatomy and physiology of each section of the pig's gastrointestinal tract is comparable to that of human (Davis et al., 2001; Rainsford et al., 2003). Consequently, the

choice of a pig model was deemed appropriate to assess the *in vivo* performance of L-dopa-loaded gastroretentive delivery system.

10.2. EXPERIMENTAL SECTION

10.2.1. Materials

Heparin sodium 1000 i.u/mL (Bodene (PTY) Limited as Intramed, Port Elizabeth, South Africa), normal saline (Adcock Ingram, Midrand, South Africa), two-lumen central venous catheterization set with ARROWgard Blue (Arrow International, Inc, Reading, PA, USA), CaCo 2 adhesion cells (Dept of pharmacology, Wits University, South Africa), CytoTox-Glo™ Kit (Promega Corporation, Madison, WI, USA) fetal bovine serum, penicillin and streptomycin, dulbecco's modified eagle's medium (DMEM) (Sigma-Aldrich Chemie, GmbH, Steinheim, Germany) acid washed alumina, TRIS buffer, phosphoric acid (Bio-Rad Laboratories, Hercules, CA, USA), Oasis HLB cartridges (3cc, Waters Corporation, milford, MA, USA), silicone Foley catheters (two way French size 10, Supra latex, Kempton park, Gauteng, South Africa), clinical speculum and veterinary laryngoscope; L-dopa, dopamine, methyl dopa, benserazide and carbidopa (Sigma-Aldrich Chemie, GmbH, Steinheim, Germany). Materials used for formulation of the tablet matrices in this study are cumulative of materials used in Chapter 4, Section 4.2.1, Chapter 5, Section 5.2.1, Chapter 6, Section 6.2.1 and Chapter 8, Section 8.2.1.

10.2.2. Methodology

10.2.2.1. *In vivo* animal ethics clearance

The animal ethics clearance (2009/01/05) for this study was obtained from the animal ethics screening committee of University of the Witwatersrand, Johannesburg, South Africa.

10.2.2.2. Arrival of pigs and habituation

Five Large White pigs (four females and a male) weighing 32.55 ± 4.38 kg were used for the study. The pigs were housed in cages with access to diet and water under a controlled temperature (20-24°C) and a 12hr light/dark cycle. Habituation was ensured before the pigs were subjected to surgery and dosing. Habituation was necessary for the pigs to get accustomed to their environment and the researchers. During the period of habituation, the pigs were visited a minimum of twice in a day and familiarization was encouraged with raisins and touch (Figure 10.1).



Figure 10.1: Images depicting habituation procedures.

10.2.2.3. Venous catheterization of the pigs for blood sampling

About ten days after arrival, surgery was undertaken under aseptic conditions to insert catheter in the internal jugular veins of the pigs for easy withdrawal of blood samples during dosing. Images of the surgical procedures are shown below (Figure 10.2):

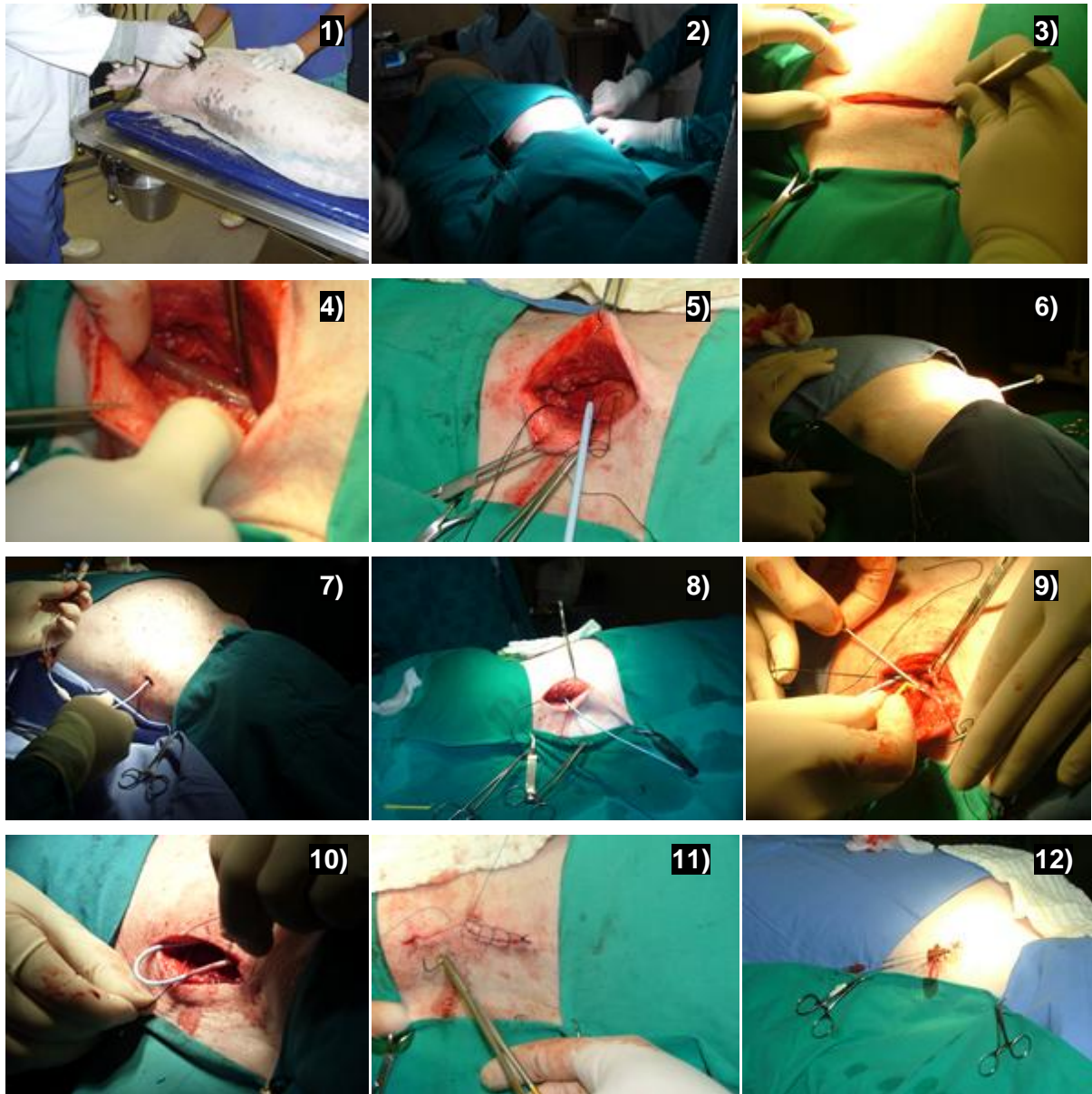


Figure 10.2: Surgical procedures for insertion of catheter into the jugular vein.

Briefly, each pig was anesthetized with ketamine (11mg/kg) and midazolam (0.3mg/kg) intramuscularly and maintained by intubation with 2% isoflurane in 100% oxygen. Analgesia was provided by intramuscular administration of buprenorphine (0.05mg/kg) and carprofen (4mg/kg). An incision was made on the lateral side of the neck to expose the jugular vein, which was isolated and a two-lumen central venous catheter was inserted into the lumen of the vein. The remaining of the catheter was tunneled subcutaneously with the help of a trocar to an exit point cranial to the dorsal aspect of the scapular. To avoid untimely removal of the catheter by the movements of the pig, the external sampling ports were sutured to the skin of the pig. The catheter was tested and cleaned by withdrawal of blood and flushing with heparinized saline (5000i.u./liter of 0.9% saline). The pigs were monitored after surgery to

ensure full recovery from anesthesia and allowed more than seven days to recover before the commencement of gastric dosing and sampling. However, daily flushing of the catheters was undertaken.

10.2.2.4. Flushing and bleeding

In order to keep the catheters open throughout the period of the study, the catheters had to be flushed twice a day with heparinized saline. Bleeding was also undertaken at intervals to ensure flow of blood through the catheters as well as to obtain blank plasma. Images of the daily flushing routine are shown below in Figure 10.3: First, gloves were worn and the hands were sprayed with antiseptic. Heparinized saline was withdrawn into syringes and the pig was distracted with food while the pots were sprayed with antiseptic and the catheter flushed with the withdrawn heparinized saline. The pots of the catheters had to be sprayed with antiseptic before and after flushing to avoid infections. Saline was heparinized to prevent blood clotting and blockage of catheters.

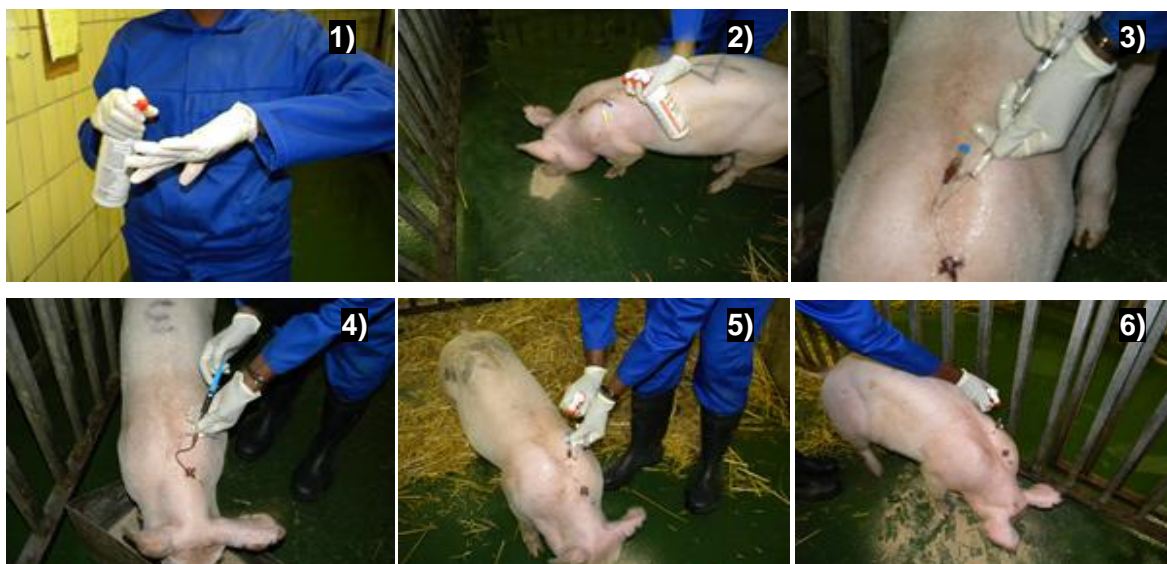


Figure 10.3: The daily flushing procedures to keep the catheter open and prevent infection.

10.2.2.5. Gastric dosing and blood sampling of the pigs

The pigs were fasted overnight before dosing. The formulations *PXLNET* and IPB matrices as well as Madopar[®] HBS were administered with intragastric tubes. However, before dosing, baseline blood sample was withdrawn for control analysis. The procedures for flushing and bleeding were utilized to withdraw the baseline blood samples and subsequent blood samples from the pigs after dosing. The procedures for gastric dosing are shown by the images in Figure 10.4:



Figure 10.4: Gastric dosing procedure for oral administration.

The pigs were anesthetized as described earlier and then each pig was raised in an upright position and with the help of an intragastric tube, the drug was administered through the tube and flushed down into the stomach with about 50mL of water. The pigs are taken back to their cages and monitored until they recover from anesthesia. As highlighted in Chapter 9, Section 9.2.6, the tablet matrices were not permitted to exceed 1000mg in order to ensure easy administration with an intragastric tube as well as the health of the pigs since their weights were $32.55 \pm 4.38\text{kg}$. The size of the intragastric tube used was limited to the weight range of the pigs. Hence, the composition of *PXLNET* was adjusted from what it was in Chapter 8 to that used in Chapter 9. The study was a crossover study with two days wash-out period where by the same pigs were employed for the different dosage forms. Blood samples were withdrawn from the chronically implanted venous catheters at specific time intervals (2, 4, 6, 8, 10, 12, 16, 20 and 24 hours) and collected in EDTA vacutainers (BD Vacutainers®, Franklin Lakes, NJ, USA) to avoid coagulation. The blood samples were centrifuged at 5000 rpm for 15mins to obtain plasma samples. Into 2mL of each plasma sample, 30uL of 10% sodium metabisulphite was added and the plasma samples were stored in -80°C freezer until period for analysis. A flow diagram below (Figure 10.5) explicates the crossover design and the dosage forms given.

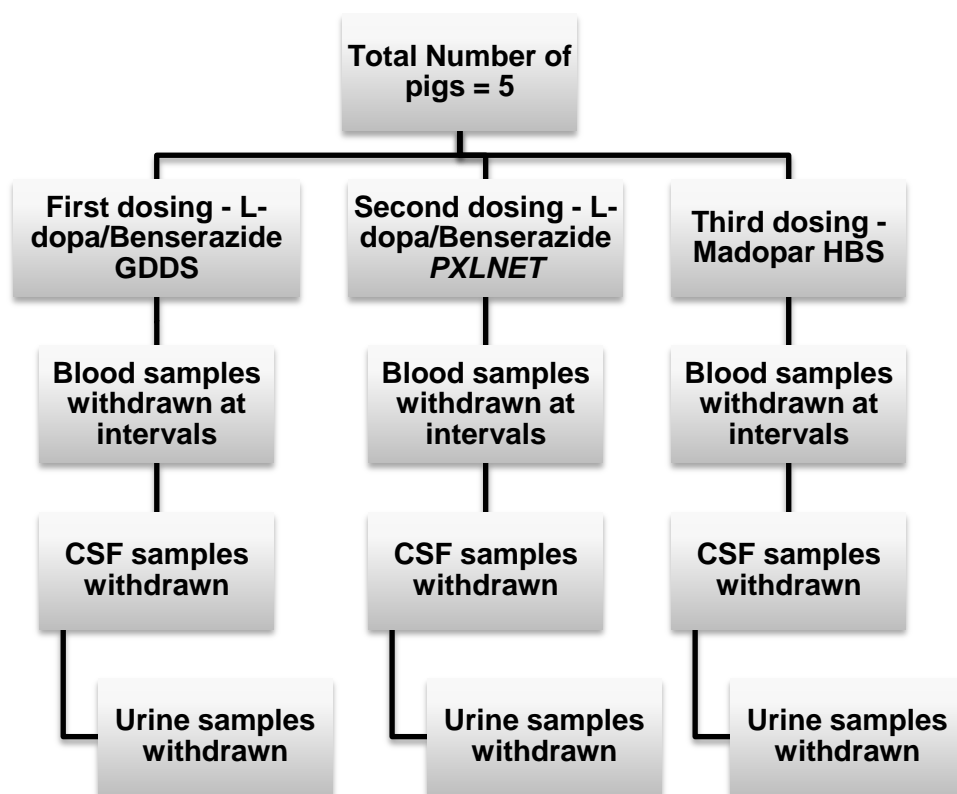


Figure 10.5: Flow diagram detailing *in vivo* animal studies for three drug delivery systems.

The formulations *PXLNET* and IPB matrices were prepared as described in Chapter 9, Section 9.2.6. As observed in Chapter 9, Sinemet® CR eroded completely and released 100% of L-dopa in less than 4 hours and was not comparable to Madopar® HBS, *PXLNET* and IPB formulation which exhibited more prolonged release over 24 hours. Furthermore, a study has shown the bioavailability of single dose Sinemet® CR was less than Sinemet® immediate release (Yeh et al., 1989) while multiple doses indicated relative bioavailability of Sinemet® CR was equivalent to that of Sinemet®, the immediate release dosage form (Cedarbaum et al., 1990). Consequently, in this *in vivo* study, Sinemet® CR was excluded. Madopar® HBS, a controlled release as well as a gastroretentive dosage form was employed for the comparative study with IPB and *PXLNET* GDDS.

10.2.2.6. Cerebrospinal fluid collection

Cerebrospinal fluid (CSF) was obtained from an anaesthetized pig by puncturing the cisterna magna. The cisterna magna can be accessed through the foramen magnum. The pig's neck was leaned off the table to flex the neck by an assistant. The caudal end of the occipital bone and the nuchal tubercles were palpated. A 20-gauge spinal needle was passed slightly caudal to this area at an angle approximately 60° towards the oral cavity to enter the foramen

magnum cranial to the body of the axis. CSF was withdrawn with a 2mL syringe and transferred into a collection tube containing 10% sodium metabisulphite. The CSF sample was then stored at -80°C until analysis. CSF was collected at the 2nd and 4th hour after post-dosing. CSF sampling was not carried out over the day because the pigs could only be anaesthetized for a limited number of times in a day and puncturing of the cisterna magna was invasive and so limited. The images of the procedure for withdrawal of CSF are shown below (Figure 10.6):

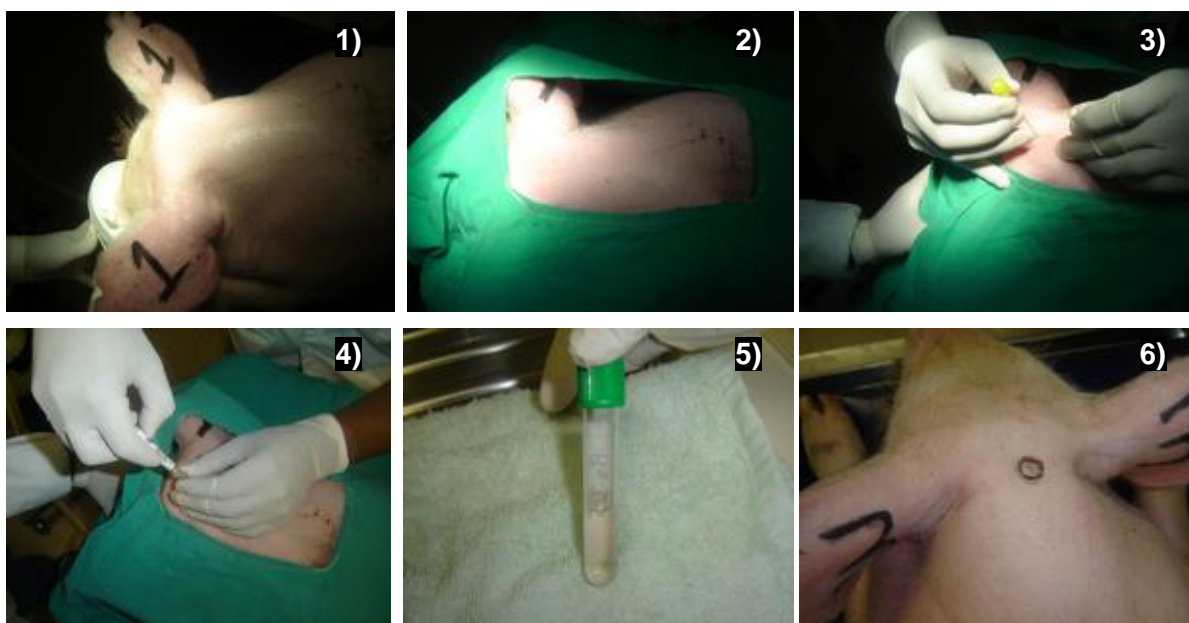


Figure 10.6: The process of withdrawing cerebrospinal fluid from a pig.

10.2.2.7. Urine collection

The pigs were anaesthetized and placed on their bellies. A lubricated speculum with a long blade was inserted into the urogenital opening to open the vaginal wall (Fig 10.7). To visualize the external urethral orifice, a veterinary laryngoscope with straight blade was inserted. The female urethral opening is located on the floor of the vagina; about a third or half the distance to the cervix. A Foley catheter French size 10 with a stylet was controlled with a blunt tip forceps and inserted into the bladder. As the catheter got into the bladder, the stylet was removed and urine was allowed to flow into the collection tube. Urine was collected at the 2nd and 4th hour after post-dosing. Urine sampling was limited due to the reasons stated in Section 10.2.2.6. This study adhered to the scope of approval by the animal ethics committee.

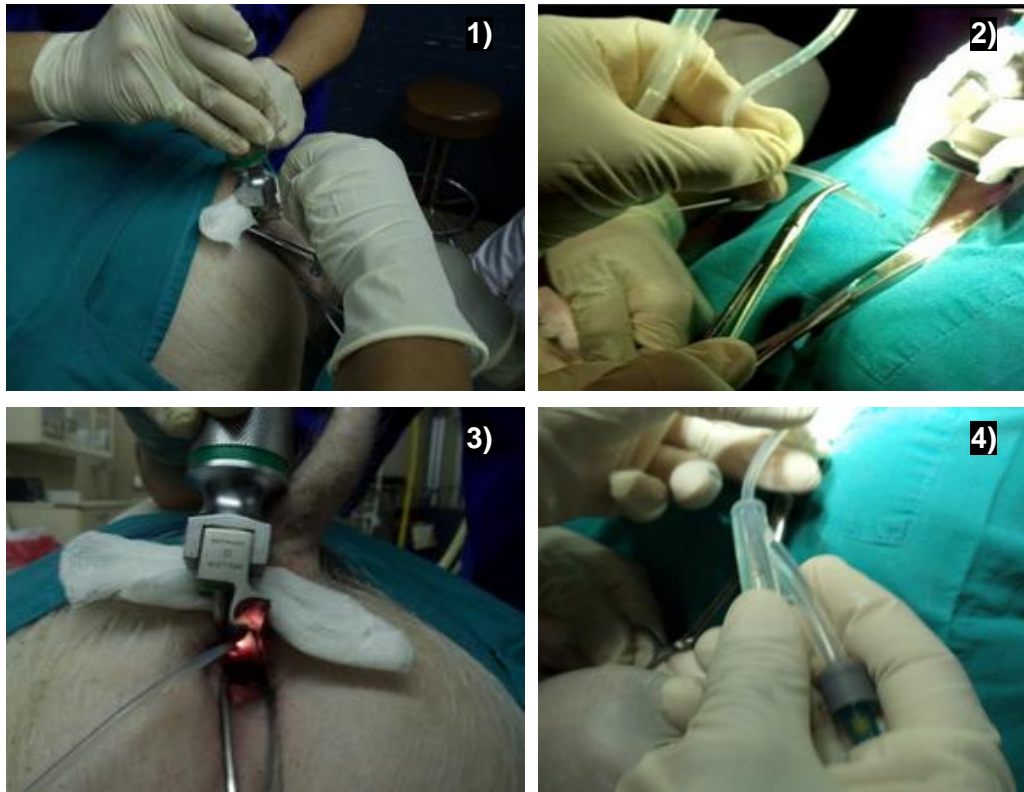


Figure 10.7: Process of bladder catheterization and urine sampling.

10.2.2.8. *In vivo* measurement of the GDDS and *PXLNET* residence times in a Large White pig model

Measurement of the gastric residence time of a drug delivery system at the application site is to provide information on the gastroretentive ability of the drug delivery system. X-ray imaging was employed as a non-invasive method of determining the residence time without affecting GIT motility. A radio-opaque marker, barium sulphate was incorporated into the GDDS and *PXLNET* formulations to determine the extent of gastroretention. Two of the large white pigs were fasted overnight and administered a radio-labeled GDDS and *PXLNET* on different occasions. The pigs were anaesthetized twice - first during drug administration and at the 7th hour post administration - to undergo X-ray imaging each time (Figure 10.8).



Figure 10.8: Images of a pig as it is prepared for X-ray imaging.

10.2.2.9. Histopathological evaluation

The stomach of a dosed and euthanized pig was cut open and the area the PXLNET was found was excised as well as the posterior and anterior section and fixed in neutral buffered formalin. The same sections were excised from the control pig (not dosed) and fixed in neutral buffered formalin as well in order to preserve the tissues as life-like a state as possible. The tissue samples were embedded on labeled cassettes and sectioned into blocks. An automated processor was used for fixation, dehydration and paraffin embedding. Routine histological methodology was undertaken which involved Mayer's hematoxylin and eosin staining procedure. Coverslipping was done to prevent the tissue from being scratched and to provide better optical quality during microscopic viewing. Descriptions of the microscopic features were made and a final microscopic diagnosis was reported.

10.2.2.10. Cytotoxicity testing

CaCo 2 adhesion cells were cultured in a 10mL cocktail media comprising 10% fetal bovine serum (5mL), 0.1% v/v of penicillin (100IU/mL) and streptomycin (100µg/mL) and dulbecco's modified eagle's medium (DMEM). The cells were maintained in a humidified atmospheric incubator (RS Biotech Galaxy, Irvine, UK) with 5% CO₂ at 37°C. The cells were cultured under aseptic conditions to avoid contamination and death. After growing the cells for two weeks, the medium was decanted and the adherent cells were rinsed with DMEM. Thereafter, the adherent cells were harvested by trypsinization (100µL trypsin was added and incubated for 5 minutes). The cells were washed with fresh medium (DMEM) to remove residual trypsin and re-suspended in fresh medium. The suspended cells (100 µL each) were placed in a 96 well plate as shown below and 10µL of samples (suspension of the samples were made – 10mg in 100µL) were added into each of the wells containing cells. The colored wells as shown in Figure 10.9 contain cells and samples tested. The figure also indicated the set up of the test. The 96 well plate was incubated for 24 hours.

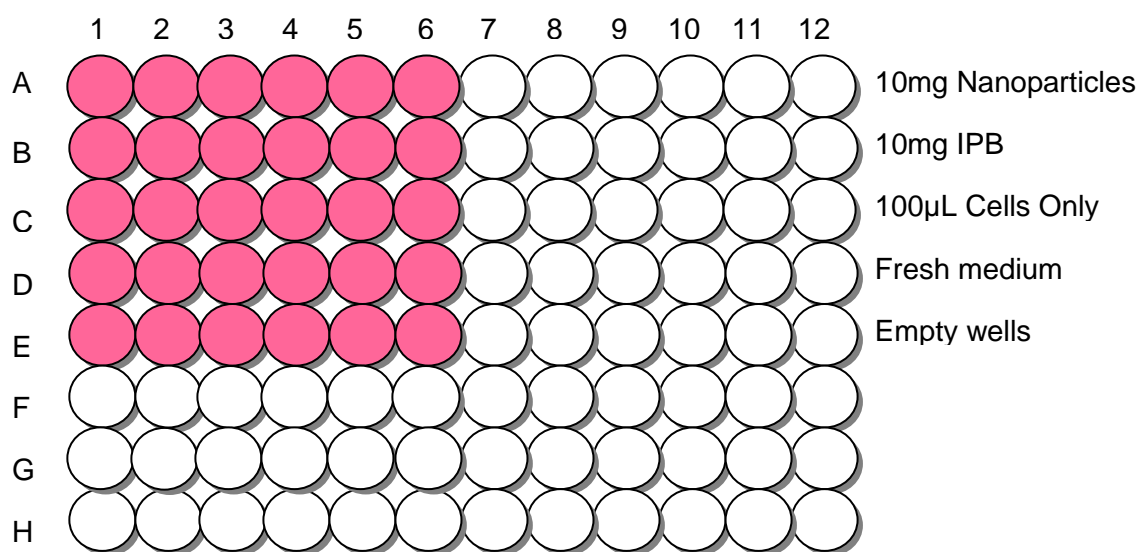


Figure 10.9: Schematic diagram of a 96-well plate depicting the arrangement of the samples, no-cell background and cells only.

After 24 hour incubation, the cytotoxicity assay was done by employing CytoTox-Glo™ Kit (Promega Corporation, Madison, WI, USA). CytoTox-Glo cytotoxicity assay is a homogenous luminescent assay which enables number of dead cells in a well to be counted. The assay has two steps: first is the addition of the luminogenic peptide substrate which enables the measurement of dead-cell protease activity released from cells that have lost membrane integrity while the second step requires the addition of the lysis reagent which delivers luminescent signal associated with the total numbers of cells (total cytotoxicity) in each well. The viability can be deduced by the subtraction of luminescent signal of experimental death from total luminescent signal. The number of dead cells was measured at each step after 15mins incubation at ambient temperature by a multilabel reader (PerkinElmer 2030 Victor™, Turku, Finland).

10.2.2.11. Ultra performance liquid chromatography for analysis of samples

10.2.2.11.1. Quantitative analyses of samples

Quantitative assays of samples were performed on Waters Acquity™ UPLC/MS/MS system (Waters Corporation, milford, MA, USA) of mass range 2000. The column used was Acquity UPLC® BEH shield RP18 1.7µm, 2.1 x100mm. Carbidopa was used as internal standard and a gradient method was employed using mobile phase - 2mmol/L ammonium acetate and 0.1% formic acid in water as solvent A and acetonitrile as solvent B. The ratio of the mobile phase gradient started at 30% A for 0.5min and increasing linearly to 100% B for 1 minute, returning to the original settings over the following 0.5 min at a flow rate of 0.3mL/min. The

injection volume was 10 μ L, run time was 2min and sample temperature was maintained at 4°C. The data was captured with Waters MassLynx™ software, version 4.0. Standards and analytes were detected using a triple quadrupole mass spectrometer fitted with electrospray ionization probe (ES+) and multiple reaction monitoring scan parameters [mass (m) –to-charge (z)] ratios (m/z) are as shown in Table 10.1.

Table 10.1: Multiple reaction monitoring parameters.

	Parent (m/z)	Daughter (m/z)
Dopamine	154.30	137.40
Levodopa	198.50	152.10
Methyldopa	212.90	165.90
Methyldopa	212.90	194.60
Carbidopa	226.40	181.1
Benserazide	258.70	139.10
Benserazide	294.70	258.70

10.2.2.11.2. Standard preparation

Stock solutions of L-dopa, dopamine, methyldopa, benserazide and carbidopa were prepared by dissolving 100mg of each drug in 100mL of 0.1N hydrochloric acid individually. From the stock solutions, a series of working standards was prepared in blank plasma to give 4000, 2000, 1000, 500, 250 and 125ng/mL each of L-dopa, dopamine, methyldopa and benserazide combined in each working standard while carbidopa added to the standards was 2000ng/mL to provide a standard curve required for quantitation. Extraction from plasma was undertaken before injection and standard curve was obtained from the peak ratio of drug/ internal standard versus the concentrations of standards. The curve type is linear with a weighting factor of 1/concentration.

10.2.2.11.3. Extraction of drugs and metabolites from plasma and CSF samples

Frozen plasma and CSF samples were thawed and 2mL of each sample was transferred into separate extraction tubes. A designated measuring spoon was used to add one level spoonful of alumina into each tube. Then, 2000 μ L of internal standard, carbidopa was added, followed by 1mL of TRIS buffer. The tubes were capped and agitated using a mechanical shaker for 5min. The tubes were centrifuged at 2500rpm for 2min. A disposable pipette was used to remove as much liquid as possible from each tube without disturbing the alumina. To wash the alumina, 1mL Milli-Q water was added to each tube; the tubes vortexed for 15secs and centrifuged for 2min at 2500rpm. Water was removed using disposable pipettes. The washing procedure was repeated and 200 μ L of 0.1% phosphoric acid was added to the tubes and vortexed for 30secs. The tubes were centrifuged for 2mins at 2500rpm and the

supernatant was transferred into appropriately labeled sample vials for subsequent injection into the column.

10.2.2.11.4. Extraction of drug and metabolites from urine

Solvent-phase extraction was employed to isolate metabolites from urine. Briefly, 2mL of methanol was used to condition each of the Oasis[®] HLB cartridges and 2mL of water was used to wash. Thereafter, 2mL of urine sample was loaded onto each cartridge, followed by 2mL of 5% methanol in water. The metabolites were then eluted with 500µL methanol and acetonitrile in the ratio of 1:1. The eluates were then transferred into appropriately labeled sample vials for subsequent injection into the column.

10.2.2.12. Pharmacokinetic modeling and analysis

PKSolver, an add-in program for Microsoft excel written in visual basic for application (VBA) for decoding problems in pharmacokinetic and pharmacodynamic data analysis was used to model and estimate the pharmacokinetic parameters. Analysis of variance (ANOVA) was used to determine the statistical significance of the differences between the data where possible.

10.3. RESULTS AND DISCUSSION

The pigs acclimatized to their new environment and got accustomed to the researcher and staff of central animal services. Venous catheterization was successful. The pigs healed as anticipated without infection and dosing commenced. There was successful blood sampling at time intervals as well as CSF withdrawals. Urine collection was not as successful in all pigs on all days of dosing and sampling. One of the pigs had a skewed urethra and three attempts on different days proved abortive. In another, the urogenital canal began to bleed during the process and urine was not sampled from the pig.

10.3.1. *In vivo* measurement of the IPB and PXLNET residence times in a Large White pig model

Two pigs were utilized for the *in vivo* gastroretentive study and the radiographic images were taken at the lateral and anterior-posterior positions as shown in the images below (Figure 10.10a and b). The radiographic imaging was only permitted to be taken only twice; immediately after dosing and at the 7th hour. This is due to the possible adverse effects of more than two administration of anesthesia per day on the pigs. The images in Figure 10.10a is the anterior-posterior position of the pig showing the presence of the device in the stomach immediately after dosing and at the 7th hour indicating that the IPB is able to be retained in

the stomach for at least 7 hours. The position of the IPB can be found within the red circles on the images. The radiographic images at the 7th hour showed that IPB retained its three-dimensional network. However, the presence of the IPB could not be seen in the second pig. It is envisaged that IPB could have been obscured by food as the pigs were allowed to eat after administration and recovery from anesthesia or it could have been emptied from the stomach which may be an indication of inter-subject variability.

However, as observed in Chapter 9, *PXLNET* lost its three-dimensional network due to erosion in the presence of fluid and may be showing as dispersed particles faintly seen in Figure 10.10c within the red circle. The reasons for *PXLNET*'s behavior have been discussed in Chapter 9, Section 9.3.10. Hence the *in vivo* radiographic image is corroborated by the *in vitro* observations. Furthermore, when a dosed pig was euthanized to harvest the stomach for histopathological testing 4-5 hours post-administration, *PXLNET* was found adhering to the wall of the stomach perhaps kept in place by the presence of food but it had lost its shape. This is indicative that *PXLNET* may be able to withstand peristalsis for at least 5 hours. In addition, the nanoparticles can be incorporated into more quantity of IPB to extend its gastric residence time.

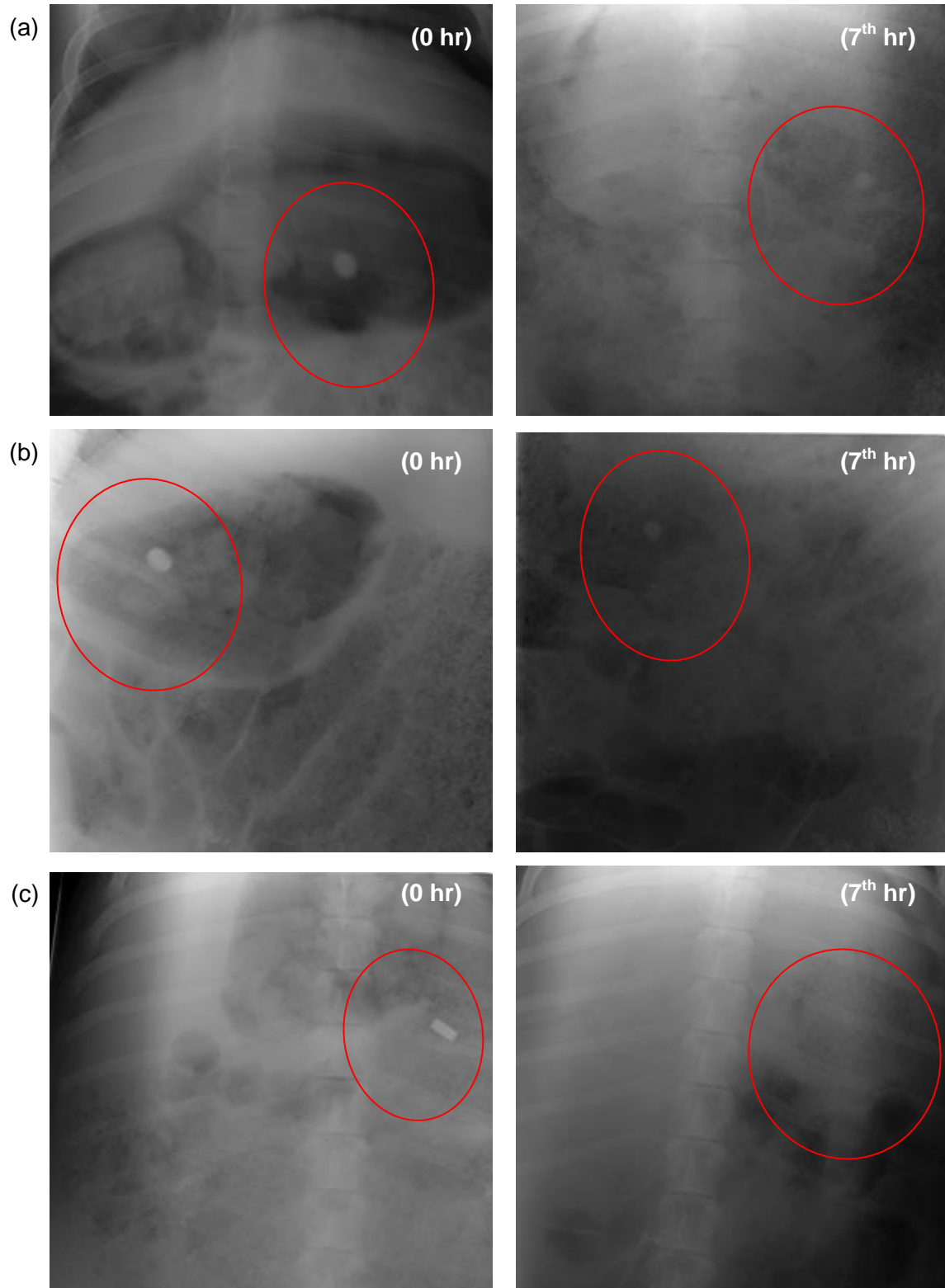


Figure 10.10: Radiographic images of **a)** GDDS with the pig in the anterior-posterior position **b)** GDDS with the pig in the lateral position and; **c)** PXLNET with the pig in the anterior-posterior position.

10.3.2. Histopathological findings

Histopathological findings for the dosed and control pigs are below and the histopathological images are shown in Figure 10.11.

10.3.2.1. Dosed pig

The mucosal epithelium was multifocally lost, likely due to autolytic changes of an early degree. The gastric glands appeared normal. Few normal appearing lymphoid follicles were visible in some sections, within the muscularis mucosa. The submucosa in few areas appeared mildly edematous. Very few lymphoplasmacytic aggregates were present in the lamina propria interstitium, mostly in one of the biopsy specimens from the pyloric area of the stomach wall.

10.3.2.2. Control pig

The stomach mucosal epithelium was multifocally lost, likely due to early autolytic changes. Where intact, the mucosal epithelium appeared normal with mucus accumulation together with intact desquamated epithelium cells on the surface. The underlying lamina propria multifocally showed mild lymphocytic infiltrates. These infiltrates extended to the muscularis mucosa, but not beyond. The gastric glands appeared within normal limits. Samples from both the fundus and pyloric portions of the stomach wall were available for examination. One section from the pylorus revealed moderate interstitial inflammation in which lymphocytes, plasma cells and eosinophils were all present in a mixed reaction. The submucosa appeared mildly edematous.

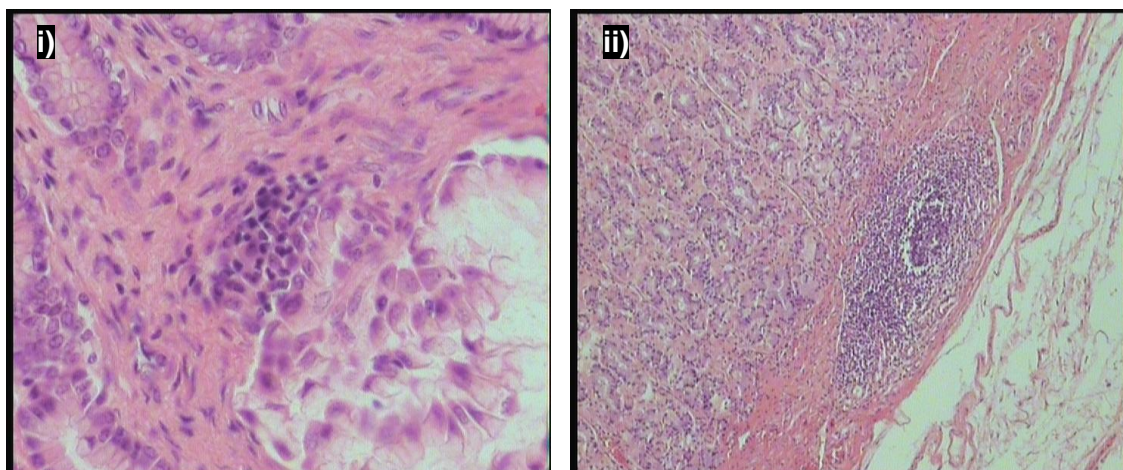


Figure 10.11a: Images from dosed pig's stomach showing **i)** Mild lymphocytic aggregate in lamina propria interstitium and; **ii)** Lymphoid follicle in deep lamina propria and sub-mucosal edema.

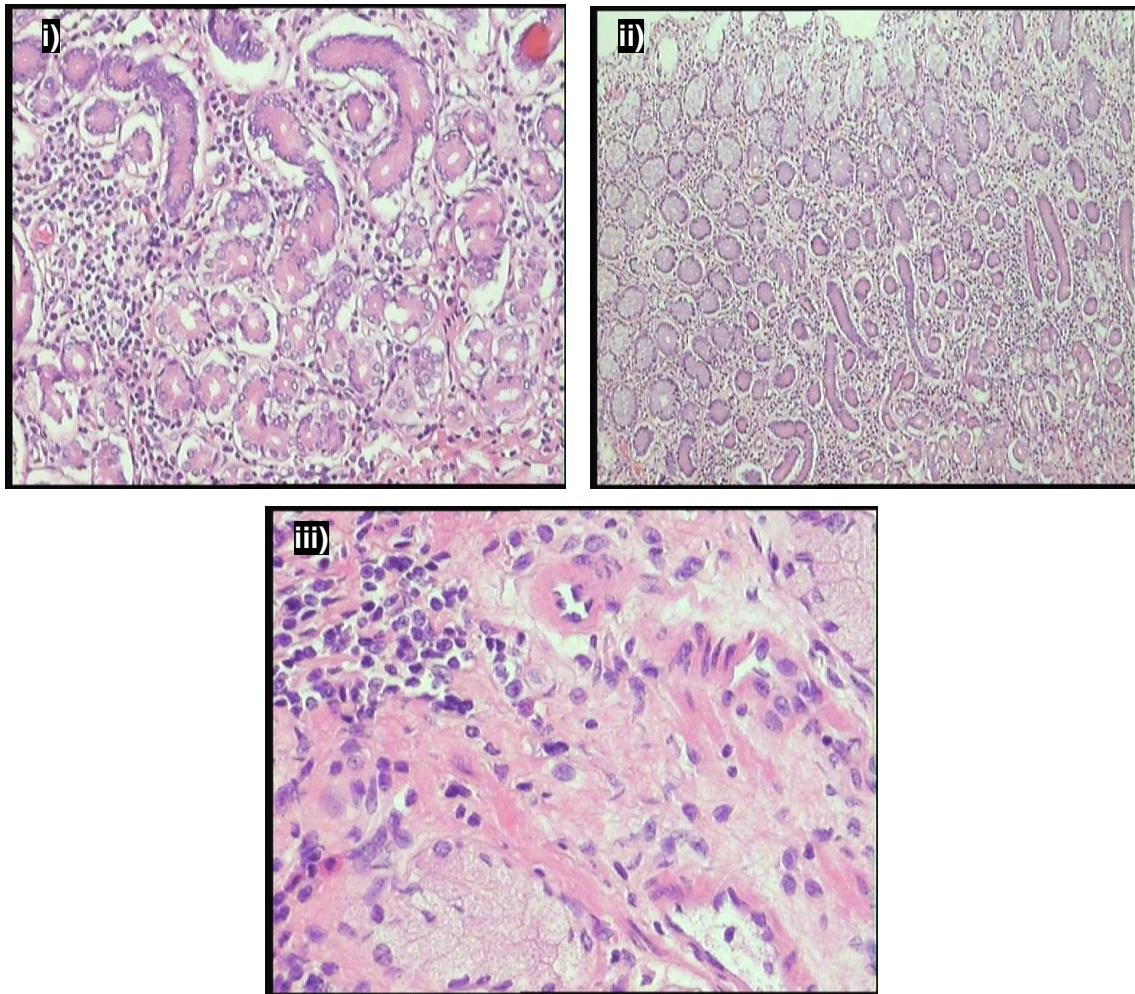


Figure 10.11b: Images from control tissue: **i)** Moderate lymphoplasmacytic interstitial lamina propria infiltration - higher magnification (x20); **ii)** Moderate lymphoplasmacytic interstitial lamina propria infiltration - Lower magnification (x10) and; **iii)** Mild lymphoplasmacytic interstitial aggregated in the lamina propria.

The control sample yielded more inflammatory changes in the stomach lamina propria than the dosed sample. Mild inflammation was however present in dosed and control pigs and changes can therefore not be related directly to the polymeric drug delivery system used in the dosed pig. Mild gastric inflammation is a non-specific lesion in many production animals and may be related to intestinal flora, intestinal pathogens and presence of worms.

10.3.3. Cytotoxicity testing

The results obtained from the cytotoxicity testing are shown in Table 10.2 depicting the percentage cytotoxicity for the samples. The luminescent signals observed for fresh medium and empty wells were used to correct those obtained for the samples and then the percentage cytotoxicity was calculated thereafter. The cytotoxicity data obtained indicate that the drug delivery devices are not cytotoxic. This is not unexpected as the polymer utilized

such as sodium carboxymethylcellulose (Vehige et al., 2003; Huang et al., 2005; Garrett et al., 2007) and chitosan (Ito et al., 2000; Khodagholi et al., 2010; Susan et al., 2011) have been found to be cytoprotective. While studies on the cytoprotective nature of locust bean could not be obtained, it is generally regarded as safe (GRAS). Figure 10.12 depicts confocal microscopical images of the cells viewed during culturing.

Table 10.2: Cytotoxicity step-wise data of *PXLNET* and IPB.

Samples	Well 1	Well 2	Well 3	Well 4	Well 5	Well 6
Measurement of dead cells (step 1)						
10mg Nanoparticles	684	744	716	732	656	576
10mg IPB	1474	1558	1428	1414	1466	1590
Measurement of total cytotoxicity (Step 2)						
10mg nanoparticles	778	772	834	924	832	868
10mg IPB	1676	1662	1576	1484	1628	1836
Signal from viable cells (Step 2 – step 1)						
10mg nanoparticles	94	28	118	192	176	292
10mg IPB	202	104	148	70	162	246
Percentage cytotoxicity						
10mg nanoparticles	5.18	2.19	6.57	14.46	13.06	15.78
10mg IPB	11.14	8.14	8.24	5.27	12.02	13.30

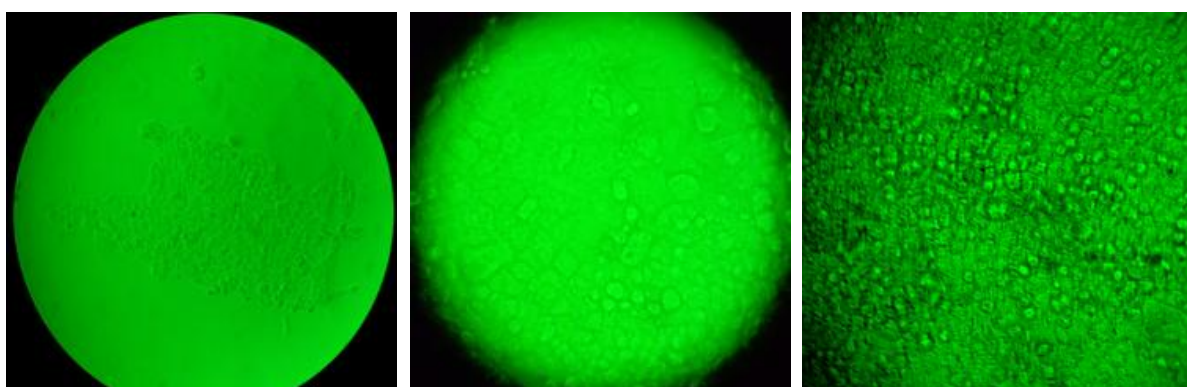


Figure 10.12: Microscopical images of CaCo 2 adhesion cells.

10.3.4. UPLC/MS/MS method validation: recovery, linearity and limit of detection

Catecholamines are in the submicroanalysis range – a few parts per billion in the plasma and also the fact they are to be extracted from complex biological systems such as plasma usually poses a challenge of obtaining high yields (Unceta et al., 2001). The lower the concentration, the more challenging it is to obtain high yields. However, efforts have been made to optimize the quantitation of L-dopa, benserazide and the metabolites. The recovery of the drugs was assessed by comparing the area under the curves and peak heights of the standards extracted from the plasma to those in aqueous solutions and of the same

concentrations. Percentage recovery ranged from 82-122% for Methyldopa, 89-125 % for dopamine and 81-114% for L-dopa at concentration ranges from 125-8000. Limit of detection is described as the concentration of the analyte that produces a signal equal to three times the standard deviation of the signal from the blank. Error limit of detection is calculated as 3 times the standard deviation obtained from the blank or as 3 times the height of the baseline of the blank. Limit of detection was 40.60ng/ml, 85.69ng/ml and 54.94ng/ml for Methyldopa, dopamine and L-dopa respectively. Specificity comes from the mass selectivity and multiple reaction monitoring transitions while linearity related to correlation coefficients ranging were 94-99% for Methyldopa, 86-97% for dopamine and 96-99% for L-dopa.

10.3.5. Pharmacokinetic data and analysis

Pharmacokinetics is crucial in order to assess the *in vivo* performance of a drug delivery system. Before a drug is orally absorbed, it has to be liberated first from its carrier. The factors that influence the oral absorption are broadly categorized as biological, physiochemical properties of drug as well as formulation factors. These factors influence the pharmacokinetic phase of drug administration and so determine the drug level in the systemic circulation, site of action and subsequently the therapeutic effect of the drug administered. The pigs fared well after administration of drug and recovery from anesthesia, though two pigs took a longer time to recover from the effect of anesthesia and puncturing of the cisterna magna. On visual observation, they did not seem to exhibit any side effects associated with administration of L-dopa. The L-dopa and metabolites plasma concentrations are presented Figures 10.13; 10.14 and 10.15 while CSF and urine concentrations are presented in Tables 10.3 and 10.4 respectively; and the pharmacokinetic parameters are presented in Table 10.5.

Benserazide was not detected in the samples. Benserazide as observed during the study and confirmed in literature is highly chemically unstable making its analytical quantitation challenging. It is rapidly metabolized to its main metabolite trihydroxybenzylhydrazine, a highly-potent decarboxylase inhibitor (Jorga et al., 1999). Jorga and co-workers also could not measure benserazide in some of the patients used in their study. They observed increase in benserazide levels in patients on 50mg (Jorga et al., 1999). In this study, 25mg of benserazide was used. Furthermore, Jorga and co-workers observed the metabolite trihydroxybenzylhydrazine was rapidly formed after the administration of benserazide and its concentration exceeded that of benserazide. Although benserazide is metabolized, the presence of its metabolite, trihydroxybenzylhydrazine ensured continued carboxylase inhibition leading to the presence of unchanged L-dopa in the urine and no significant difference in the level of dopamine plasma concentration.

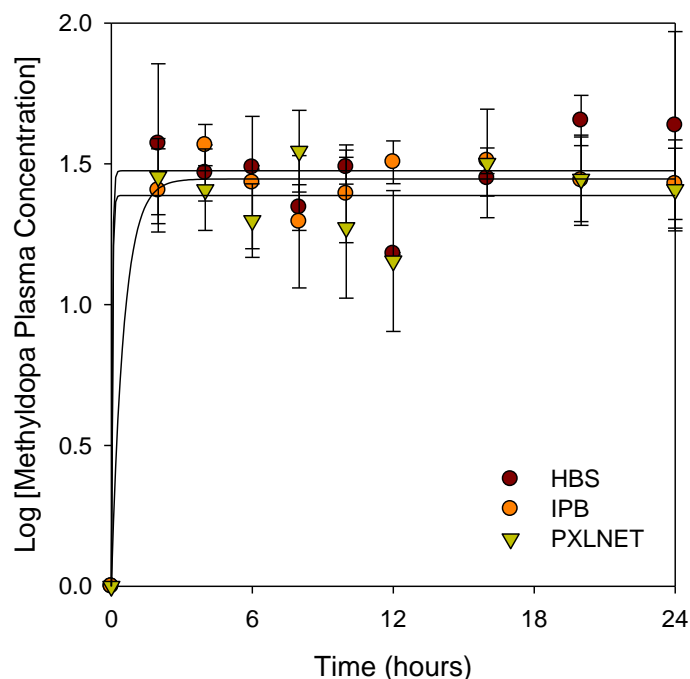


Figure 10.13: Mean methyldopa plasma concentration after administration of Madopar[®] HBS capsules, *PXLNET* and IPB matrices.

The plasma concentration of methyldopa was observed to fluctuate between 8-50ng/mL in the three formulations (Fig 10.13) and there was no marked increase over the period of sampling. Nutt and co-workers also observed that each dose of L-dopa probably made a small contribution to the plasma concentration of methyldopa (Nutt et al., 1987). They deduced that methyldopa fluctuations observed in the plasma concentrations may be due to redistribution within the tissues. Furthermore, the concentrations of methyldopa in the plasma in comparison to other large neutral amino acids suggest that it is not a major competitor of L-dopa for transport to the brain; and hence at the concentrations found during L-dopa dosing, it is not an important determinant of clinical response (Nutt et al., 1997). In addition, the fluctuations could be due to delay in gastric emptying by L-dopa or its metabolite. This will be further elucidated under the discussion on L-dopa pharmacokinetic curve.

In the absence of a carboxylase inhibitor, more than 90% of L-dopa is converted to dopamine (Khor and Hsu, 2007). In this study, dopamine was basically constant in all the formulations and confirms the effective carboxylase inhibition by benserazide and its active metabolite. A typical dopamine plasma concentration-time curve is shown Figure 10.14 which also indicated that mean endogenous dopamine obtained from blank samples was 91.6ng/mL. Dopamine was not detected in most of the CSF samples (Table 10.3). Olanow and co-workers also could not detect free dopamine in CSF (Olanow, et al., 1991). Furthermore, the

large presence of dopamine in the urine (Table 10.4) did not stem mainly from L-dopa dosing. The bulk of the urinary dopamine may be from renal production and uptake of dopamine; and decarboxylation of circulating dihydroxyphenylalanine (dopa) (Gill et al., 1991; Grossman et al., 1992) which is in turn from hydrolysis of tyrosine. However, the rationale for the large concentration of dopamine at the 4th hour for Madopar[®] HBS in comparison to *PXLNET* and IPB matrices is uncertain. It is known that urinary dopamine is increased by feeding (Mühlbauer and Osswald, 1992) and stress (Fibiger and Singer, 1984) amongst other factors.

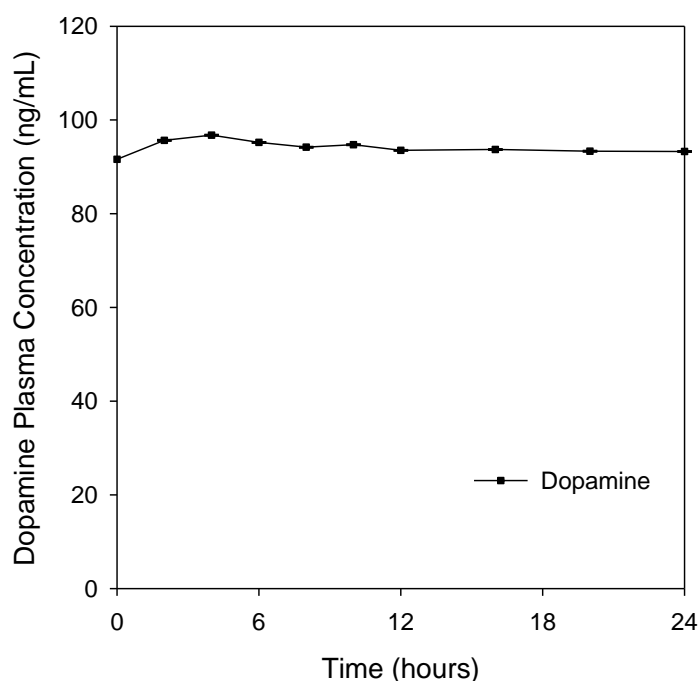


Figure 10.14: A typical mean dopamine plasma concentration observed for blank plasma samples (time t = 0hrs) and pigs dosed with formulations (from time t = 2hrs).

Table 10.3: Mean cerebrospinal fluid concentration after oral administration of Madopar[®] HBS capsules, *PXLNET* and IPB matrices.

Time (h)	Mean CSF concentration (ng/mL)								
	Madopar [®] HBS			<i>PXLNET</i>			IPB		
	M-D	D-M	L-D	M-D	D-M	L-D	M-D	D-M	L-D
2.00	36.47	-	88.69	35.63	83.01	70.48	3.27	-	71.96
4.00	28.31	-	224.12	27.86	82.94	87.79	30.44	-	97.15

M-D, methyl dopa; D-M, dopamine and L-D, L-dopa

Table 10.4: Mean urine concentration after oral administration of Madopar® HBS capsules, PXLNET and IPB matrices.

Time (h)	Mean urine concentration (ng/mL)								
	Madopar® HBS			PXLNET			IPB		
	M-D	D-M	L-D	M-D	D-M	L-D	M-D	D-M	L-D
2.00	604.6	5888	196.8	1532.7	4449	784.8	459.4	111.2	425.5
4.00	853.3	21938	755.1	-	-	-	1221.8	4571.1	1328

M-D, methyl dopa; D-M, dopamine and L-D, L-dopa

A comparative display of L-dopa concentration-time curves for the three formulations is shown in Figure 10.15. The pharmacokinetic curves and parameters obtained for each formulation is dependent on the rate of release of L-dopa from the formulation and biological factors such as health disposition of GIT, gastric emptying rate, rate of absorption, rate of metabolism, transporters, extent of distribution amongst other factors. These factors are expected to vary from pig to pig (inter-subject variation) and it is also possible to vary within a pig over time (intra-subject variation). Furthermore, a protein-loaded diet is known to decrease the oral absorption of L-dopa. This is due to competitive absorption in the presence of proteins as L-dopa uses the same transport system as large amino acids as discussed in Chapter 1. However, it is also been found that food effects vary with formulations (Khor and Hsu, 2007).

In addition, double peaks observed in the pharmacokinetic curves of Madopar HBS capsules and PXLNET matrices may be attributed to the effect of L-dopa on gastric emptying time. Studies have shown that L-dopa produces intermittent delays in gastric emptying time (Robertson et al., 1990; Waller et al., 1991; Robertson et al., 1992). In the studies undertaken by Robertson and co-workers, the double peaks were shown to correspond to the two distinct phases of gastric emptying separated by a period of negligible or no significant emptying. They employed paracetamol which is a biomarker for gastric emptying with radiolabeled diethylene triamine pentaacetic acid (⁹⁹Tc-DTPA) and gamma-camera imaging to explore the impact of L-dopa on gastric emptying (Waller et al., 1991). The mechanisms postulated by which L-dopa delays gastric emptying were stimulations of dopamine and osmoreceptors (Robertson et al., 1990). It is also envisaged that it could also be a metabolite that may be responsible for delayed gastric emptying (Robertson et al., 1990); however, whichever it is, affects both the absorption of L-dopa and its metabolite as this may also explicate the multiple peaks of methyl dopa as well. Although the mean pharmacokinetic curve of IPB matrices has a single peak, some of individual pigs had double peaks and this may also explain the mean T_{max} of IPB matrices being at the 4th hour. Furthermore, the variability of gastric emptying is high and apart from the presence of L-dopa is an outcome of a complex interaction between the structure and function of the stomach

and its nutrient content, which effects gastric emptying by meal volume and nutrient density. Gastric emptying is also affected by the physical and chemical properties of the meal, body movement, and position during emptying (Müller et al, 2006).

L-dopa was found in the urine unchanged. This is anticipated due to the presence of carboxylase inhibitor preventing its metabolism to dopamine. There was no urine data for *PXLNET* at the 4th hour as urine collection at that period proved abortive.

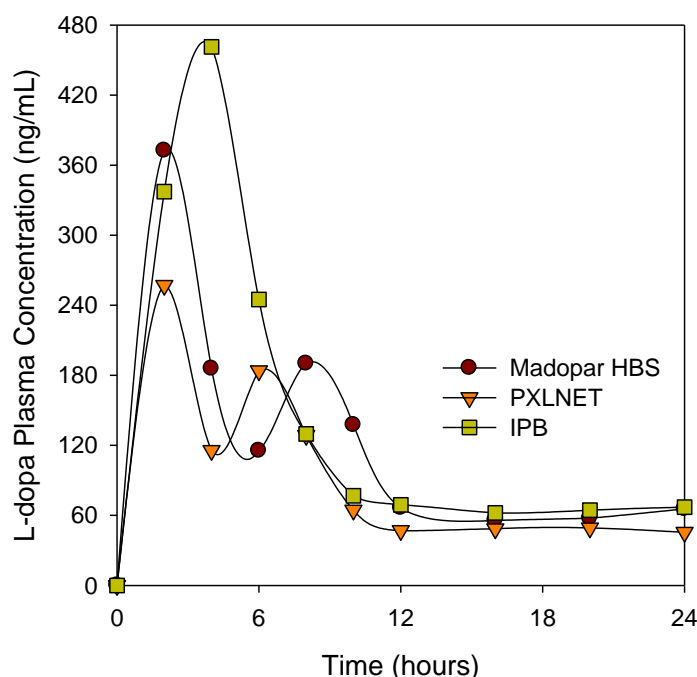


Figure 10.15: Comparative mean L-dopa pharmacokinetic curve of Madopar[®] HBS capsules, *PXLNET* and IPB matrices after single dose administration.

Table 10.5: L-dopa non-compartmental pharmacokinetic parameters following oral administration of Madopar[®] HBS capsules, *PXLNET* and IPB matrices.

Pharmacokinetic parameter	Madopar [®] HBS	<i>PXLNET</i>	IPB
T_{max} (h)	2	2	4
C_{max} (ng/mL)	372.37	257.02	461.28
AUC_{0-t} (ng/mL*h)	2816.47	2121.43	3347.45
AUC_{0-inf} (ng/mL*h)	3685.03	2722.42	4147.16
$AUMC_{0-inf}$ (ng/mL*(h) ²)	56590.17	40775.35	55147.93
MRT (h)	15.36	14.98	13.30
V_z/F [mg/(ng/mL)]	0.3598	0.4847	0.2874
Cl/F [mg/(ng/mL)/h]	0.0271	0.0367	0.0241

T_{max} , time for maximum concentration of drug; C_{max} maximum drug concentration; AUC_{0-t} area under the concentration-time curve; AUC_{0-inf} area under the concentration-time curve from time 0 to infinity; $AUMC_{0-inf}$ area under the first moment of concentration-time curve from time 0 to infinity; MRT, mean residence time; Cl/F is apparent clearance and V_z/F is apparent volume of distribution.

PKSolver, an add-in program for Microsoft excel with user-friendly interface, predefined menus and forms for easy recall (Zhang et al., 2010), was used for computation. It is a visual basic for application (VBA) program which can run a range of applications for PK/PD data analysis including non-compartmental and compartmental analyses; modelling of pharmacodynamic data; and also embedded are 20 frequently used pharmacokinetic functions that can be executed on an open spreadsheet. PKSolver was validated by comparing its results with those of WinNonlin (Pharsight, Mountain View, USA) and Scientist (Micromath, Saint Louis, USA) employing two sample data sets obtained from a published book (Zhang et al., 2010). The parameters generated with PKSolver were similar to those obtained from WinNonlin and Scientist (Zhang et al., 2010). In fact, the results were identical to Scientist in all parameters to two decimal points and to WinNonlin to one or two decimal points. Consequently, PKSolver is not only flexible and user-friendly but also robust and reliable.

Non-compartmental pharmacokinetic model was chosen to decode the parameters for L-dopa plasma concentration-time curve as it best describes the data obtained (Table 10.5). The IPB matrices are characterized by higher C_{max} , T_{max} , AUC_{0-t} , AUC_{0-inf} ; and less apparent volume of distribution and clearance in comparison to Madopar[®] HBS capsules and *PXLNET*. The mean T_{max} of 4 hours for IPB matrices is attributed to the variations in individual pigs attaining peak plasma concentrations at different times. However, its mean residence time was decoded to be less than those of Madopar[®] HBS capsules and *PXLNET*. On application of ANOVA, the pharmacokinetic curves of the three formulations were found not to be statistically different ($p = 0.49$) at significance level of 0.05. The C_{max} was also not statistically different ($p = 0.44$). Furthermore, when Madopar[®] HBS capsules was compared with either IPB or *PXLNET* there was no difference. However, statistical equivalence does not imply pharmaceutical equivalence or therapeutic equivalence. Furthermore, as observed in Chapter 9, Section 9.3.10, using Similarity factor f_2 , the *in vitro* drug release profiles of IPB and *PXLNET* matrices were not bioequivalent to that of Madopar[®] HBS capsules.

L-dopa is known to distribute widely into the body tissues while small amounts are found in the central nervous system. This is replicated and affirmed in this study by the large apparent volume of distribution observed with the three formulations. Furthermore, the large apparent volume of distribution may also clarify the low concentration of L-dopa in the plasma and appreciable concentration in urine when compared with plasma concentration. The volume of distribution when quantified per kilogram was 8.94, 15.09 and 11.20L/kg for IPB, *PXLNET* and Madopar[®] HBS respectively. *PXLNET* exhibited the largest volume of distribution. This is

expected with nanoparticles which are known to improve distribution and circulation time of drugs incorporated into them.

Based on the impracticality of continuous blood sampling throughout the day, from the observed values, the plasma concentrations for the times samples were not collected can be predicted. Figure 10.16 is a predicted pharmacokinetic curve for IPB matrices for 8 hours showing the possible concentration of L-dopa for the times samples were not collected. Obtaining predicted values is crucial in clinical situations as limited samples are collected after a dose to measure drug concentrations.

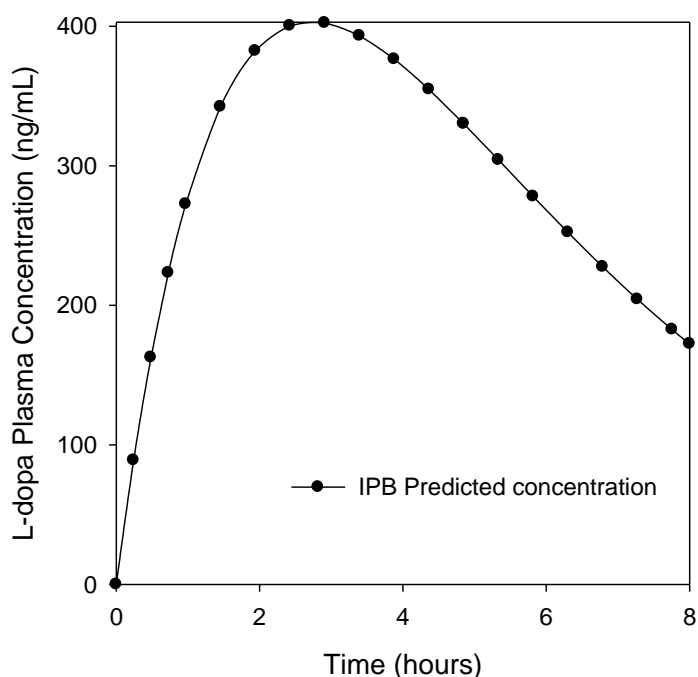


Figure 10.16: Predicted L-dopa plasma concentrations from 0.24 to 8 hours.

10.3.6. *In vitro* – *in vivo* correlation of dissolution and pharmacokinetic parameters

In vitro – *in vivo* correlation describes the relationship between *in vitro* and *in vivo* outcomes. Various parameters can be used to assess correlations – dissolution time points such as $T_{50\%}$, $T_{90\%}$, MDT, % released for *in vitro* parameters and AUC, C_{max} , MRT for *in vivo* parameters. Of the five correlation levels (levels A, B, C, multiple C and D), multiple-level C correlation was employed in this study. Multiple-level C correlation relates one or more pharmacokinetic parameters to the amount of drug dissolved (*in vitro*) at different time points of the dissolution profile and is an acceptable and useful *in vitro* – *in vivo* relationship (Emami 2006). In this study, a pharmacokinetic parameter, AUC was used to demonstrate a relationship with *in vitro* dissolution profile - drug released (%). An *in vivo* parameter (AUC) was profiled against an *in vitro* parameter (% drug released) at corresponding time intervals

and the coefficient correlation demonstrating the relationship was determined by linear regression. A linear regression multiple-level C IVIVC correlation models obtained for Madopar[®] HBS capsules, *PXLNET* and IPB matrices are shown in Figure 10.17. The correlation models had r^2 values of 0.936, 0.946 and 0.915 for Madopar[®] HBS capsules, *PXLNET* and IPB matrices respectively. Hence, the *in vitro* drug release studies of the formulations were efficient in predicting the respective *in vivo* release with greater than 90% accuracy.

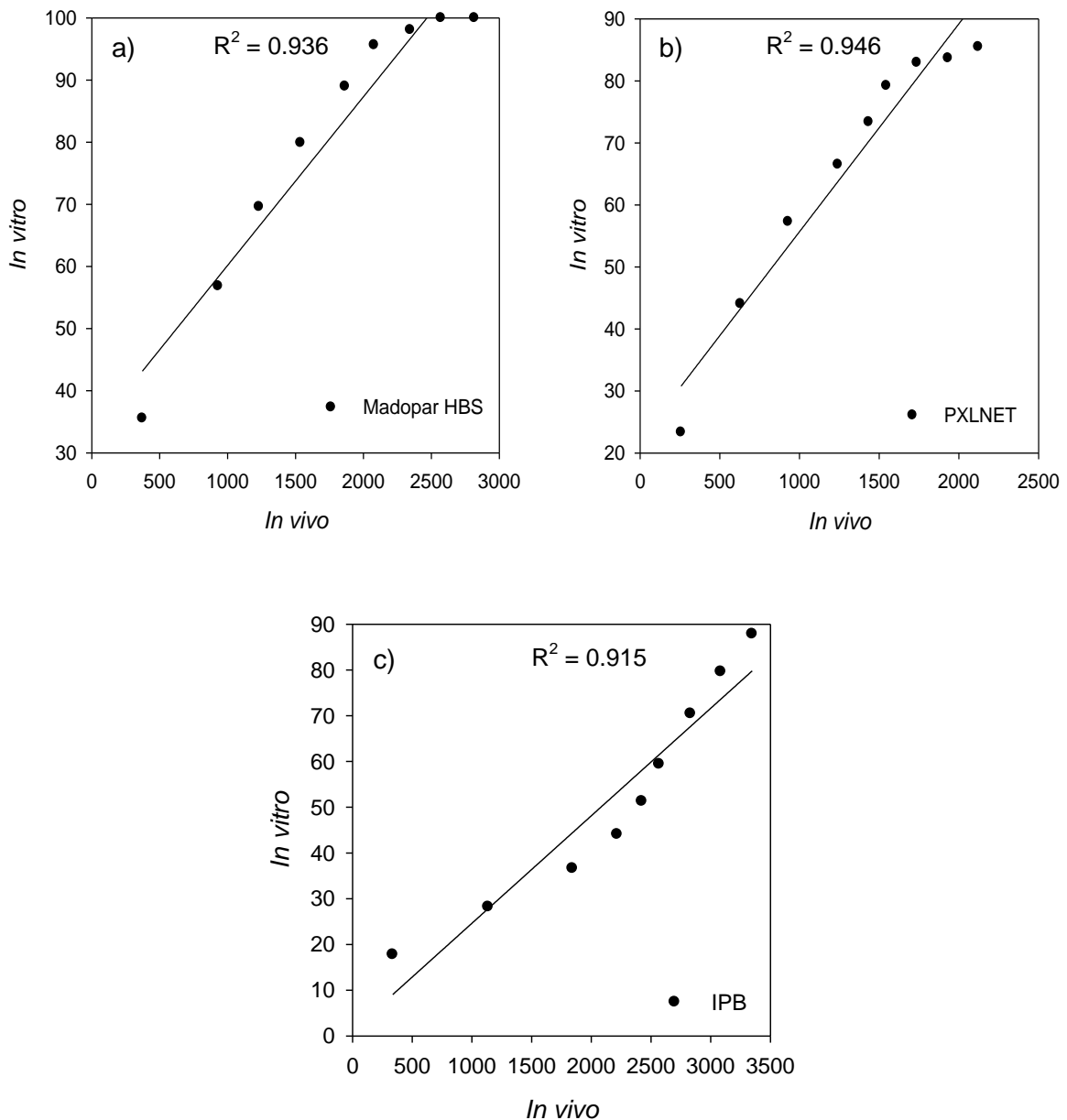


Figure 10.17: Linear regression multiple-level C IVIVC correlation models for a) Madopar[®] HBS capsules; b) *PXLNET* matrices and; c) IPB matrices.

10.4. CONCLUDING REMARKS

The IPB and *PXLNET* formulation has been proven *in vivo* to be gastroretentive and non-toxic to the tissues and cells. The pharmacokinetic parameters elucidated that L-dopa was liberated from the drug delivery systems, absorbed, widely distributed, metabolized and excreted both unchanged and as metabolites (such as methyl dopa). The *in vitro* and *in vivo* data of IPB and *PXLNET* matrices correlated strongly implying that quality gastroretentive drug delivery systems were developed which performs identically *in vitro* and *in vivo*. Therefore, IPB and *PXLNET* matrices designed and formulated, show promise as a gastroretentive drug delivery systems for delivery of L-dopa.

CHAPTER ELEVEN

CONCLUSIONS AND RECOMMENDATIONS

11.1. CONCLUSIONS

A novel interpolyelectrolyte complex was synthesized and characterized. Employing rheology to monitor the synthesis of interpolyelectrolyte complex (IPEC) in this research provided insights in the benefits of the interactions between two polymers with regards to the individual properties. Methacrylate copolymer is a low viscous polymer while NaCMC is an entangled polymer. However the complexation between the two polymers generated a three-dimensional network which had an increased elastic modulus exhibiting solid-like behavior having the potential for a controlled release delivery of drugs.

The characterization techniques employed to assess the drug delivery properties of IPEC confirmed the rheological characterization that IPEC can be employed for controlled release delivery of drugs. The *in vitro* drug release studies exhibited the ability of IPEC to sustain and prolong the release of L-dopa over 24 hours. It behaved like a hydrogel retaining its three-dimensional network in acidic medium and in summary, had improved properties in comparison to the native polymers. In addition, the incorporation of a natural polysaccharide into IPEC further improved its drug delivery properties by preventing bulk erosion and enhancing surface erosion which led to zero order release kinetics.

The interpolymeric blend prepared was successfully employed to develop a three-mechanism gastroretentive drug delivery system (GDDS) for administration of L-dopa. However, the IPB matrices so developed can be employed for other narrow absorption window drugs and poorly soluble drugs. Employing three mechanisms of gastroretention is envisaged to extend the gastric resident time thereby ensuring the availability of these drugs at their absorption sites over a prolonged period.

Fabrication of L-dopa-loaded nanoparticles was achieved in this research employing multi-crosslinking technology. The nanoparticles on analyses were found to be spherical hollow capsules with high drug entrapment efficiency. Furthermore, it was established in this study that polymeric nanoparticles are able to improve the mechanical strength of matrices. The molecular mechanics computations elucidated the interactions between the polymers and the crosslinking agents.

The Box-Behnken design and desirability function employed to optimize the interpolymeric blend were adequate and effective. The desirability of 1 was obtained for all the responses -

dissolution, density, bioadhesion and swelling. The values obtained for the independent variables were used to formulate the optimized GDDS.

The optimized GDDS (*PXLNET* and IPB) were formulated and characterized. The IPB matrices were found to be porous swellable drug release system. The magnetic resonance imaging explicated the mechanisms of drug release to be pH-dependent. The GDDS designed and developed in this study were found not to be bioequivalent with the conventional dosage forms. Furthermore, the GDDS fitted zero-order kinetics better than the conventional dosage forms.

The *in vivo* studies delineated that the IPB and *PXLNET* matrices to be gastroretentive and non-toxic. The pharmacokinetic parameters displayed the liberation from IPB and *PXLNET*, absorption, distribution, metabolism and excretion of L-dopa. Finally, there was strong *in vitro* and *in vivo* correlation qualifying the drug delivery systems (IPB and *PXLNET*) designed, developed and optimized in this study as congruous for delivery of L-dopa.

11.2. RECOMMENDATIONS

Due to its pH responsiveness, the novel interpolymetric blend synthesized may be explored for development of drug delivery devices where constant rate of delivery is required in other sites other than gastric. Interpolymetric blend also shows potential as a membrane for drug delivery and in fact other possible applications of interpolymetric blend in the field of drug delivery should be explored.

Chitosan has excellent mucoadhesive properties. However, in this study, there was decreased adhesion of *PXLNET* matrices in comparison to IPB matrices. It is envisaged the TPP used in fabrication of *iPoly-X-Lipo* (chitosan blend) nanoparticles may have suppressed the interaction between chitosan and mucin. This needs to be investigated further.

Animal studies may not be precisely predictive of human absorption, distribution and elimination. The best model for man is man and this is reiterated here. A pilot human study may be undertaken to assess the pharmacokinetics and pharmacodynamics of drug delivery systems, *PXLNET* and IPB matrices developed in this study. *PXLNET* should be prepared as described in Chapter 8 which could not be used for *in vivo* study due the constraints of administration to pigs and its pharmacokinetic curve obtained and compared to IPB matrices and conventional dosage forms.

REFERENCES

- Abdelbary, G.A., Tadros, M.I., 2008. Design and in vitro/in vivo evaluation of novel nicorandil extended release matrix tablets based on hydrophilic interpolymer complexes and a hydrophobic waxy polymer. *European Journal of Pharmaceutics and Biopharmaceutics*, 69, 1019-1028.
- Abdelrahim, K.A., Ramaswamy, H.S., 1995. High temperature/pressure rheology of carboxymethyl cellulose (CMC). *Food Research International*, 28, 285-290.
- Abou-Rachid, H., Lussier, L., Ringuette, S., Lafleur-Lambert, X., Jaidann, M., Brisson, J., 2008. On the correlation between miscibility and solubility properties of energetic plasticizers/polymer blends: modeling and simulation studies. *Propellants, Explosives, Pyrotechnics*, 33, 301-310.
- Adalja, S.B., Otaigbe, J.U., 2002. Creep and recovery behavior of novel organic-inorganic polymer hybrids. *Polymer Composites*, 23, 171-181.
- Adler, C.H., 2002. Relevance of motor complications in Parkinson's disease. *Neurology*, 58, S51-S56.
- Ahmed, I.S., Ayres, J.W., 2007. Bioavailability of riboflavin from a gastric retention formulation. *International Journal of Pharmaceutics*, 330, 146-154.
- Aitken, R.J., Creely, K.S., Tran, C.L., 2004. Nanoparticles: an occupational hygiene review. *Research Report*, 274, 1-102.
- Ali, J., Arora, S., Ahuja, A., Babbar, A.K., Sharma, R.K., Khar, R.K., Baboota, S., 2007. Formulation and development of hydrodynamically balanced system for metformin: In vitro and in vivo evaluation. *European Journal of Pharmaceutics and Biopharmaceutics*, 67, 196-201.
- Aliabadi, H.M., Lavasanifar, A., 2006. Polymeric micelles for drug delivery. *Expert Opinion on Drug Delivery*, 3, 139-162.
- Almeida, A.J., Souto, E., 2007. Solid lipid nanoparticles as a drug delivery system for peptides and proteins. *Advanced Drug Delivery Review*, 59, 478-490.
- Alves, M.M., Antonov, Y.A., Gonçalves, M.P., 1999. On the incompatibility of alkaline gelatin and locust bean gum in aqueous solution. *Food Hydrocolloids*, 13, 77-80.

- Ammar, H.O., Khalil, R.M., 1997. Preparation and Evaluation of Sustained-Release Solid Dispersions of Drugs with Eudragit Polymers. *Drug Development and Industrial Pharmacy*, 23, 1043.
- Anand, V., Kandarapu, R., Garg, S., 2007. Preparation and evaluation of taste-masked orally disintegrating tablets of prednisolone. *Asian Journal of Pharmaceutical Sciences*, 2, 227-238.
- Anderson, N.H., Bauer, M., Boussac, N., Khan-Malek, R., Munden, P., Sardaro, M., 1998. An evaluation of fit factors and dissolution efficiency for the comparison of in vitro dissolution profiles. *Journal Pharmaceutical and Biomedical Analysis*, 17, 811-822.
- Anseth, K.S., Bowman, C.N., Brannon-Peppas, L., 1996. Mechanical properties of hydrogels and their experimental determination. *Biomaterials*, 17, 1647-1657.
- Antonini, A., 2007. Continuous dopaminergic stimulation—from theory to clinical practice. *Parkinsonism and Related Disorders*, 13, S24-S28.
- Araya, H., Tomita, M., Hayashi, M., 2005. The novel formulation design of O/W microemulsion for improving the gastrointestinal absorption of poorly water soluble compounds. *International Journal of Pharmaceutics*, 305, 61-74.
- Arıca B, Kas H. S, Sargon M. F, Hıncal A. A, 1998. Physicochemical characteristics of L-dopa loaded chitosan microspheres for brain delivery. *AAPS PharmSci (Suppl 1)* S-32.
- Arıca, B., Kaş, H.S., Moghdam, A., Akalan, N., Hıncal, A.A., 2005. Carbidopa/levodopa-loaded biodegradable microspheres: in vivo evaluation on experimental Parkinsonism in rats. *Journal of Controlled Release*, 102, 689-697.
- Arora, S., Ali, J., Ahuja, A., Khar, R.K., Baboota, S., 2005. Floating drug delivery systems: A review. *AAPS PharmSciTech*, 06, E372-E390.
- Arza, R., Gonugunta, C., Veerareddy, P., 2009. Formulation and evaluation of swellable and floating gastroretentive ciprofloxacin hydrochloride tablets. *AAPS PharmSciTech*, 10, 220-226.
- Aubin, N., Curet, O., Deffois, A., Carter, C., 1998. Aspirin and salicylate protect against mptp-induced dopamine depletion in mice. *Journal of Neurochemistry*, 71, 1635-1642.
- Augsburger, L.L., Hoag, S.W., 2008. *Pharmaceutical dosage forms: units operations and mechanical properties*. 3rd Ed., Informa Healthcare, USA, 656 pages.

- Australian Department of Employment and Workplace Relations, 2005. Submission to inquiry into workplace exposure to toxic dusts and nanoparticles. http://www.aph.gov.au/senate/committee/clac_ctte/completed_inquiries/2004-07/toxic_dust/submissions/sub10.pdf Accessed 1 Feb, 2012.
- Babita, K., Tiwary, A.K., 2005. Transcutaneous delivery of levodopa: enhancement by fatty acid synthesis inhibition. *Molecular Pharmaceutics*, 2, 57-63.
- Babita, K., Rana, V., Tiwary, A.K., 2004. Epidermal lipids: thermotropic behavior and role in transcutaneous permeation of levodopa. *Drug Development Research*, 63, 190-199.
- Babita, K., Tiwary, A.K., 2005. Transcutaneous delivery of levodopa: enhancement by fatty acid synthesis inhibition. *Molecular Pharmaceutics*, 2, 57-63.
- Bali, V., Ali, M., Ali, J., 2010. Study of surfactant combinations and development of a novel nanoemulsion for minimizing variations in bioavailability of ezetimibe. *Colloids and Surfaces B: Biointerfaces*, 76, 410-420.
- Bardonnet, P.L., Faivre, V., Pugh, W.J., Piffaretti, J.C., Falson, F., 2006. Gastroretentive dosage forms: Overview and special case of *Helicobacter pylori*. *Journal of Controlled Release*, 111, 1-18.
- Barker, S.A., Yap, S.P., Yuen, K.H., McCoy, C.P., Murphy, J.R., Craig, D.Q.M., 2003. An investigation into the structure and bioavailability of α -tocopherol dispersions in Gelucire 44/14. *Journal of Controlled Release*, 91, 477-488.
- Barnes, H.A., 2000. A handbook of elementary rheology, The University of Wales Institute of Non-Newtonian Fluid Mechanics, UK, 200 pages.
- Barnes, H.A., Walters, K., 1985. The yield stress myth? *Rheologica Acta*, 24, 323-326.
- Baron, M.S., 2005. Movement disorders in the older patient: differential diagnosis and general management. *Cleveland Clinic Journal of Medicine*, 72, S38-S51.
- Barone, P., 2003. Clinical strategies to prevent and delay motor complications. *Neurology*, 61, S12-S16.
- Bartus, R.T., Emerich, D., Snodgrass-Belt, P., Fu, K., Salzberg-Brenhouse, H., Lafreniere, D., Novak, L., Lo, E., Cooper, T., Basile, A.S., 2004a. A pulmonary formulation of l-dopa enhances its effectiveness in a rat model of Parkinson's disease. *Journal of Pharmacology and Experimental Therapeutics*, 310, 828-835.

- Baudy, R.B., Butera, J.A., Abou-Gharbia, M., Chen, H., Harrison, B., Jain, U., Magolda, R., Sze, J.Y., Brandt, M.R., Cummons, T.A., Kowal, D., Pangalos, M.N., Zupan, B., Hoffmann, M., May, M., Mugford, C., Kennedy, J., Childers, W.E., 2009. Prodrugs of perzinfotel with improved oral bioavailability. *Journal of Medicinal Chemistry*, 52, 771-778.
- Benchabane, A., Bekkour, K., 2008a. Rheological properties of carboxymethyl cellulose (CMC) solutions. *Colloid and Polymer Science*, 286, 1173-1180.
- Benoit, J., Faisant, N., Venier-Julienne, M., Menei, P., 2000. Development of microspheres for neurological disorders: From basics to clinical applications. *Journal of Controlled Release*, 65, 285-296.
- Berger, J., Reist, M., Mayer, J.M., Felt, O., Gurny, R., 2004. Structure and interactions in chitosan hydrogels formed by complexation or aggregation for biomedical applications. *European Journal of Pharmaceutics and Biopharmaceutics*, 57, 35-52.
- Bettini, R., Acerbi, D., Caponetti, G., Musa, R., Magi, N., Colombo, P., Cocconi, D., Santi, P., Catellani, P.L., Ventura, P., 2002. Influence of layer position on in vitro and in vivo release of levodopa methyl ester and carbidopa from three-layer matrix tablets. *European Journal of Pharmaceutics and Biopharmaceutics*, 53, 227-232.
- Beun, S., Glorieux, T., Devaux, J., Vreven, J., Leloup, G., 2007. Characterization of nanofilled compared to universal and microfilled composites. *Dental Materials*, 23, 51-59.
- Bharath, S., Hsu, M., Kaur, D., Rajagopalan, S., Andersen, J.K., 2002. Glutathione, iron and Parkinson's disease. *Biochemical Pharmacology*, 64, 1037-1048.
- Birkmayer W, Hornykiewicz O, 1961. Der l-3,4-dioxyphenylalanin (=DOPA)-Effekt bei Parkinson-Akinese. *Wien Klin Wochenschr*, 73, 787-788.
- Biron, E., Chatterjee, J., Ovadia, O., Langenegger, D., Brueggen, J., Hoyer, D., Schmid, H., Jelinek, R., Gilon, C., Hoffman, A., Kessler, H., 2008. Improving oral bioavailability of peptides by multiple n-methylation: somatostatin analogues 13. *Angewandte Chemie International Edition*, 47, 2595-2599.
- Biswal, D.R., Singh, R.P., 2004. Characterization of carboxymethyl cellulose and polyacrylamide graft copolymer. *Carbohydrate Polymers*, 57, 379-387.

- Björklund, A., Dunnett, S.B., 2007. Dopamine neuron systems in the brain: an update. *Trends in Neurosciences*, 30, 194-202.
- Black, K.J., Carl, J.L., Hartlein, J.M., Warren, S.L., Hershey, T., Perlmutter, J.S., 2003. Rapid intravenous loading of levodopa for human research: clinical results. *Journal of Neuroscience Methods*, 127, 19-29.
- Bogdanov, M., Matson, W.R., Wang, L., Matson, T., Saunders-Pullman, R., Bressman, S.S., Beal, M.F., 2008. Metabolomic profiling to develop blood biomarkers for Parkinson's disease. *Brain*, 131, 389-396.
- Bokias, G., Mylonas, Y., Staikos, G., Bumbu, G.G., Vasile, C., 2001. Synthesis and aqueous solution properties of novel thermoresponsive graft copolymers based on a carboxymethylcellulose backbone. *Macromolecules*, 34, 4958-4964.
- Bonferoni, M.C., Rossi, S., Ferrari, F., Bertoni, M., Caramella, C., 1995. Influence of medium on dissolution-erosion behavior of Na carboxymethylcellulose and on visco-elastic properties of gels. *International Journal of Pharmaceutics*, 117, 41-48.
- Bridge, M.H., Williams, E., Lyons, M.E.G., Tipton, K.F., Linert, W., 2004. Electrochemical investigation into the redox activity of Fe(II)/Fe(III) in the presence of nicotine and possible relations to neurodegenerative diseases. *Biochimica et Biophysica Acta (BBA) - Molecular Basis of Disease*, 1690, 77-84.
- Brime, B., Ballesteros, M.P., Frutos, P., 2000. Preparation and in vitro characterization of gelatin microspheres containing Levodopa for nasal administration. *Journal of Microencapsulation*, 17, 777-784.
- Brocks, D.R., 1999. Anticholinergic drugs used in Parkinson's disease: An overlooked class of drugs from a pharmacokinetic perspective. *Journal of Pharmacy and Pharmaceutical Sciences*, 2, 39-46.
- Brotchie, J.M., Lee, J., Venderova, K., 2005. Levodopa-induced dyskinesia in Parkinson's disease. *Journal of Neural Transmission*, 112, 359-391.
- Bubeníková, S., Kalinovská, L., Theiszová, M., Danišovič, L., Bakoš, D., 2008. Biological tests of ofloxacin-releasing chitosan-based microspheres. *Journal of Controlled Release*, 132, e22-e23.

- Buchhammer, H., Mende, M., Oelmann, M., 2003. Formation of mono-sized polyelectrolyte complex dispersions: effects of polymer structure, concentration and mixing conditions. *Colloids and Surfaces A: Physicochemical and Engineering Aspects*, 218, 151-159.
- Budhian, A., Siegel, S.J., Winey, K.I., 2007. Haloperidol-loaded PLGA nanoparticles: Systematic study of particle size and drug content. *International Journal of Pharmaceutics*, 336, 367-375.
- Burkersroda, F.V., Schedl, L., Göpferich, A., 2002. Why degradable polymers undergo surface erosion or bulk erosion. *Biomaterials*, 23, 4221-4231.
- Buur, A., Bundgaard, H., 1987. Prodrugs of 5-fluorouracil. VIII. Improved rectal and oral delivery of 5-fluorouracil via various prodrugs. Structure-rectal absorption relationships. *International Journal of Pharmaceutics*, 36, 41-49.
- Byrappa, K., Ohara, S., Adschiri, T., 2008. Nanoparticles synthesis using supercritical fluid technology – towards biomedical applications. *Advanced Drug Delivery Review*, 60, 299-327.
- Calne, S.M., Kumar, A., 2003. Nursing Care of Patients with Late Stage Parkinson's disease. *Journal of Neuroscience Nursing*, 35, 242-251.
- Calvo, P., Gouritin, B., Chacun, H., Desmaële, D., D'Angelo, J., Noel, J., Georjgin, D., Fattal, E., Andreux, J.P., Couvreur, P., 2001. Long-circulating pegylated polycyanoacrylate nanoparticles as new drug carrier for brain delivery. *Pharmaceutical Research*, 18, 1157-1166.
- Camacho, M.M., Martínez-Navarrete, N., Chiralt, A., 2005. Rheological characterization of experimental dairy creams formulated with locust bean gum (LBG) and λ -carrageenan combinations. *International Dairy Journal*, 15, 243-248.
- Cancela, M.A., Álvarez, E., Maceiras, R., 2005. Effects of temperature and concentration on carboxymethylcellulose with sucrose rheology. *Journal of Food Engineering*, 71, 419-424.
- Carlsson, A., Lindqvist, M., Magnusson, T., 1957. 3,4-Dihydroxyphenylalanine and 5-hydroxytryptophan as reserpine antagonists. *Nature*, 180, 1200-1200.
- Carrier, R.L., Miller, L.A., Ahmed, I., 2007. The utility of cyclodextrins for enhancing oral bioavailability. *Journal of Controlled Release*, 123, 78-99.

- Castelli, F., Conti, B., Conte, U., Puglisi, G., 1996. Effect of molecular weight and storage times on tolmetin release from poly--lactide microspheres to lipid model membrane. A calorimetric study. *Journal of Controlled Release*, 40, 277-284.
- Cedarbaum, J., Silvestri, M., Clark, M., Toy, L., Harts, A., Green-Parsons, A., McDowell, F., 1990. Results of long-term treatment with controlled-release levodopa/carbidopa (Sinemet CR). *Journal of Neural Transmission: Parkinson's Disease and Dementia Section*, 2, 205-213.
- Center for Drug Evaluation and Research, 2000. Guidance for industry--waiver of *in vivo* bioavailability and bioequivalence studies for immediate-release solid oral dosage forms based on a biopharmaceutics classification system. FDA, Rockville, MD, USA. Accessed 6th March 2011.
- Center for Drug Evaluation and Research, 1997. Guidance for industry. extended release oral dosage forms: development, evaluation, and application of *in vitro/in vivo* correlations. FDA, Rockville, MD, USA. Accessed 6th March 2011.
- Centre for Drug Evaluation and Research, 1997. Guidance for industry: SUPAC-MR: modified release solid oral dosage forms; scale-up and post-approval changes: chemistry, manufacturing and controls, *in vitro* dissolution testing, and *in vivo* bioequivalence documentation. FDA, Rockville, MD, USA. Accessed 6th March 2011.
- Chan, O.H., Schmid, H.L., Stilgenbauer, L.A., Howson, W., Horwell, D.C., Stewart, B.H., 1998. Evaluation of a targeted prodrug strategy to enhance oral absorption of poorly water-soluble compounds. *Pharmaceutical Research*, 15, 1012-1018.
- Chavanpatil, M.D., Jain, P., Chaudhari, S., Shear, R., Vavia, P.R., 2006. Novel sustained release, swellable and bioadhesive gastroretentive drug delivery system for ofloxacin. *International Journal of Pharmaceutics*, 316, 86-92.
- Chawla, G., Gupta, P., Koradia, V., Bansal, A.K., July, 2003. Gastroretention: A means to address regional variability in intestinal drug absorption. *Pharmaceutical Technology*, 50-68.
- Chen, J.J., Trombetta, D.P., Fernandez, H.H., 2008a. Palliative management of Parkinson disease: Focus on nonmotor, distressing symptoms. *Journal of Pharmacy Practice*, 21, 262-272.

- Chen, E., Mahar Doan, K., Portelli, S., Coatney, R., Vaden, V., Shi, W., 2008b. Gastric pH and gastric residence time in fasted and fed conscious cynomolgus monkeys using the bravo® pH system. *Pharmaceutical Research*, 25, 123-134.
- Chen, R., Ho, H., Yu, C., Sheu, M., 2010. Development of swelling/floating gastroretentive drug delivery system based on a combination of hydroxyethylcellulose and sodium carboxymethyl cellulose for Losartan and its clinical relevance in healthy volunteers with CYP2C9 polymorphism. *European Journal of Pharmaceutical Sciences*, 39, 82-89.
- Choonara, Y.E., Pillay, V., Ndesendo, V.M.K., du Toit, L.C., Kumar, P., Khan, R.A., Murphy, C.S., Jarvis, D., 2011. Polymeric emulsion and crosslink-mediated synthesis of super-stable nanoparticles as sustained-release anti-tuberculosis drug carriers. *Colloids and Surfaces B: Biointerfaces*, 87, 243-254.
- Chopra, S., Motwani, S.K., Iqbal, Z., Talegaonkar, S., Ahmad, F.J., Khar, R.K., 2007. Optimization of polyherbal gels for vaginal drug delivery by Box-Behnken statistical design. *European Journal of Pharmaceutics and Biopharmaceutics*, 67, 120-131.
- Cohen S, Yoram S, Levy R, Shterman N, Melamed E, Atlas D, 1998. Pharmaceutical Composition of L-Dopa Ester. Patent US5840756.
<http://www.google.com/patents/US5840756> Accessed 10th October, 2010.
- Collister, K.A., Albenisi, B.C., 2005. Potential therapeutic targets in the NF- κ B pathway for Alzheimer's disease. *Drug News and Perspectives*, 18, 623-629.
- Colombo, P., Bettini, R., Santi, P., Peppas, N.A., 2000. Swellable matrices for controlled drug delivery: gel-layer behavior, mechanisms and optimal performance. *Pharmaceutical Science and Technology Today*, 3, 198-204.
- Committee for Proprietary Medicinal Products (CPMP), 2000. Note for guidance on the investigation of bioavailability and bioequivalence. EMEA, London, UK. Accessed 6th March 2011.
- Compton BJ, Solari NE, Flanagan MA., 1999. Oral Delivery Formulation WO/1999/030690.
<http://www.wipo.int/patentscope/search/en/WO1999030690> Accessed 10th October, 2010.
- Constantinides, P.P., 1995. Lipid Microemulsions for Improving Drug Dissolution and Oral Absorption: Physical and Biopharmaceutical Aspects. *Pharmaceutical Research*, 12, 1561-1572.

- Dapía, S., Tovar, C.A., Santos, V., Parajó, J.C., 2005. Rheological behavior of carboxymethylcellulose manufactured from TCF-bleached Milox pulps. *Food Hydrocolloids*, 19, 313-320.
- Dave, B.S., Amin, A.F., Patel, M.M., 2004. Gastroretentive drug delivery system for ranitidine hydrochloride: formulation and *in vitro* evaluation. *AAPS PharmSciTech*, 5, 77-82.
- Davis, S.S., Hardy, J.G., Fara, J.W., 1986. Transit of pharmaceutical dosage forms through the small intestine. *Gut*, 27, 886-892.
- Davis, S.S., Illum, L., Hinchcliffe, M., 2001. Gastrointestinal transit of dosage forms in the pig. *Journal of Pharmacy and Pharmacology*, 53, 33-39.
- Davis, S.S., Wilding, I.R., 2001. Oral drug absorption studies: the best model for man is man! *Drug Discovery Today*, 6, 127-130.
- Davis, S.S., 2005a. Formulation strategies for absorption windows. *Drug Discovery Today*, 10, 249-257.
- De, T.K., Hoffman, A.S., 2001. A reverse microemulsion polymerization method for preparation of bioadhesive polyacrylic acid nanoparticles for mucosal drug delivery: Loading and release of timolol maleate. *Artificial Cells, Blood Substitutes and Biotechnology*, 29, 31-46.
- Dempski, R.E., Scholtz, E.C., Oberholtzer, E.R., Yeh, K.C., 1989. Pharmaceutical design and development of a Sinemet controlled-release formulation. *Neurology*, 39, 20-24.
- Descombes, S., Bonnet, A.M., Gasser, U.E., Thalamas, C., Dingemans, J., Arnulf, I., Bareille, M.P., Agid, Y., Rascol, O., 2001. Dual-release formulation, a novel principle in L-dopa treatment of Parkinson's disease. *Neurology*, 56, 1239-1242.
- Desgouilles, S., Vauthier, C., Bazile, D., Vacus, J., Grossiord, J., Veillard, M., Couvreur, P., 2003. The Design of Nanoparticles Obtained by Solvent Evaporation: A Comprehensive Study. *Langmuir*, 19,
- Deshmukh, V., Jadhav, J., Sakarkar, D., 2009. Formulation and *in vitro* evaluation of theophylline anhydrous bioadhesive tablets. *Asian Journal of Pharmaceutics*, 3, 54-58.
- Dhawan, S., Singla, A., Sinha, V., 2004. Evaluation of mucoadhesive properties of chitosan microspheres prepared by different methods. *AAPS PharmSciTech*, 5, 122-128.

- Di Stefano, A., Sozio, P., Iannitelli, A., Cerasa, L.S., 2009. New drug delivery strategies for improved Parkinson's disease therapy. *Expert Opinion on Drug Delivery*, 6, 389-404.
- Di Stefano, A., Sozio, P., Iannitelli, A., Marianecchi, C., Santucci, E., Carafa, M., 2006. Maleic- and fumaric-diamides of (O,O-diacetyl)-L-Dopa-methylester as anti-Parkinson prodrugs in liposomal formulation. *Journal of Drug Targeting*, 14, 652-661.
- Dick, F.D., 2006. Parkinson's disease and pesticide exposures. *British Medical Bulletin*, 79-80, 219-231.
- Dick, S., Semple, S., Dick, F., Seaton, A., 2007. Occupational titles as risk factors for Parkinson's disease. *Occupational Medicine*, 57, 50-56.
- Djaldetti, R., Inzelberg, R., Giladi, N., Korczyn, A.D., Peretz-Aharon, Y., Rabey, M.J., Herishano, Y., Honigman, S., Badarny, S., Melamed, E., 2002. Oral solution of levodopa ethylester for treatment of response fluctuations in patients with advanced Parkinson's disease. *Movement Disorders*, 17, 297-302.
- Djaldetti, R., Melamed, E., 1996. Levodopa ethylester: A novel rescue therapy for response fluctuations in Parkinson's disease. *Annals of Neurology*, 39, 400-404.
- Dollo, G., Le Corre, P., Guérin, A., Chevanne, F., Burgot, J.L., Leverage, R., 2003. Spray-dried redispersible oil-in-water emulsion to improve oral bioavailability of poorly soluble drugs. *European Journal of Pharmaceutical Sciences*, 19, 273-280.
- Dressman, J.B., Reppas, C., 2000. In vitro–in vivo correlations for lipophilic, poorly water-soluble drugs. *European Journal of Pharmaceutical Sciences*, 11, S73-S80.
- Drulis-Kawa, Z., Dorotkiewicz-Jach, A., 2010. Liposomes as delivery systems for antibiotics. *International Journal of Pharmaceutics*, 387, 187-198.
- Durif, F., Vidailhet, M., Assal, F., Roche, C., Bonnet, A.M., Agid, Y., 1997. Low-dose clozapine improves dyskinesias in Parkinson's disease. *Neurology*, 48, 658-662.
- Edali, M., Esmail, M.N., Vatistas, G.H., 2001. Rheological properties of high concentrations of carboxymethyl cellulose solutions. *Journal of Applied Polymer Science*, 79, 1787-1801.
- Edlund, U., Albertsson, A.C., 2000. Microspheres from Poly (D,L-Lactide)/Poly(1,5-Dioxepan-2-One) Miscible Blends for Controlled Drug Delivery. *Journal of Bioactive and Compatible Polymers*, 15, 214-229.

- Ehringer, H., Hornykiewicz, O., 1998. Distribution of noradrenaline and dopamine (3-hydroxytyramine) in the human brain and their behavior in diseases of the extrapyramidal system. *Parkinsonism and Related Disorders*, 4, 53-57.
- Eisler, T., Eng, N., Plotkin, C., Calne, D.B., 1981. Absorption of levodopa after rectal administration. *Neurology*, 31, 215.
- Elliot, J., Ganz, A., 1974. Some rheological properties of sodium carboxymethylcellulose solutions and gels. *Rheologica Acta*, 13, 670-674.
- El-Shabouri, M.H., 2002. Positively charged nanoparticles for improving the oral bioavailability of cyclosporin-A. *International Journal of Pharmaceutics*, 249, 101-108.
- Emami, J., 2006. *In vitro-in vivo* correlation: from theory to applications. *Journal of Pharmacy and Pharmaceutical Sciences*, 9, 169-189.
- Erni, W., Held, K., 1987. The hydrodynamically balanced system: a novel principle of controlled drug release. *European Neurology*, 27, 21-27.
- Esposito, A., Sannino, A., Cozzolino, A., Quintiliano, S.N., Lamberti, M., Ambrosio, L., Nicolais, L., 2005. Response of intestinal cells and macrophages to an orally administered cellulose-PEG based polymer as a potential treatment for intractable edemas. *Biomaterials*, 26, 4101-4110.
- Fahn, S., 2008. The history of dopamine and levodopa in the treatment of Parkinson's disease. *Movement Disorders*, 23, S497-S508.
- Faisant, N., Siepmann, J., Benoit, J.P., 2002. PLGA-based microparticles: elucidation of mechanisms and a new, simple mathematical model quantifying drug release. *European Journal of Pharmaceutical Sciences*, 15, 355-366.
- Fatouros, D.G., Bergenstahl, B., Mullertz, A., 2007. Morphological observations on a lipid-based drug delivery system during *in vitro* digestion. *European Journal of Pharmaceutical Sciences*, 31, 85-94.
- FDA - CDER, 2000. Sinemet CR. FDA-Centre for Drug Evaluation and Research, http://www.accessdata.fda.gov/drugsatfda_docs/label/2008/019856s025lbl.pdf, Accessed 10th October 2010.
- Fibiger, W., Singer, G., 1984. Urinary dopamine in physical and mental effort. *European Journal of Applied Physiology and Occupational Physiology*, 52, 437-440.

- Ficarra, R., Cutroneo, P., Aturki, Z., Tommasini, S., Calabrò, M.L., Phan-Tan-Luu, R., Fanali, S., Ficarra, P., 2002. An experimental design methodology applied to the enantioseparation of a non-steroidal anti-inflammatory drug candidate. *Journal of Pharmaceutical and Biomedical Analysis*, 29, 989-997.
- Fix, J.A., Alexander, J., Cortese, M., Engle, K., Leppert, P., Repta, A.J., 1989. Short-chain alkyl esters of L-Dopa as prodrugs for rectal absorption. *Pharmaceutical Research*, 6, 501-505.
- Florjancic, U., Zupancic, A., Zumer, M., 2002. Rheological characterization of aqueous polysaccharide mixtures undergoing shear. *Chemical and Biochemical Engineering Quarterly*, 16, 105-118.
- Foda, N.H., El-laithy, H., Tadros, M.I., 2007. Implantable biodegradable sponges: Effect of interpolymer complex formation of chitosan with gelatin on the release behavior of tramadol hydrochloride. *Drug Development & Industrial Pharmacy*, 33, 7-17.
- Fotaki, N., Symillides, M., Reppas, C., 2005. Canine versus in vitro data for predicting input profiles of l-sulpiride after oral administration. *European Journal of Pharmaceutical Sciences*, 26, 324-333.
- Francis, M.F., Lavoie, L., Winnik, F.M., Leroux, J., 2003. Solubilization of cyclosporin A in dextran-g-polyethyleneglycolalkyl ether polymeric micelles. *European Journal of Pharmaceutics and Biopharmaceutics*, 56, 337-346.
- Galindo-Rodríguez, S.A., Puel, F., Briançon, S., Allémann, E., Doelker, E., Fessi, H., 2005. Comparative scale-up of three methods for producing ibuprofen-loaded nanoparticles. *European Journal of Pharmaceutical Sciences*, 25, 357-367.
- Galovic Rengel, R., Barisic, K., Pavelic, Z., Zanic Grubisic, T., Cepelak, I., Filipovic-Grcic, J., 2002. High efficiency entrapment of superoxide dismutase into mucoadhesive chitosan-coated liposomes. *European Journal of Pharmaceutical Sciences*, 15, 441-448.
- Gan, Q., Wang, T., 2007. Chitosan nanoparticle as protein delivery carrier—Systematic examination of fabrication conditions for efficient loading and release. *Colloids and Surfaces B: Biointerfaces*, 59, 24-34.
- Garber, C., 2007. The potential and the pitfalls of nanomedicine. Nanowerk LLC. <http://www.nanowerk.com/spotlight/spotid=1891.php> Accessed 10th October, 2010.

- Garcia-Fuentes, M., Torres, D., Alonso, M.J., 2005. New surface-modified lipid nanoparticles as delivery vehicles for salmon calcitonin. *International Journal of Pharmaceutics*, 296, 122-132.
- Garrett, Q., Simmons, P.A., Xu, S., Vehige, J., Zhao, Z., Ehrmann, K., Willcox, M., 2007. Carboxymethylcellulose binds to human corneal epithelial cells and is a modulator of corneal epithelial wound healing. *Investigative Ophthalmology & Visual Science*, 48, 1559-1567.
- Gasser, U.E., Crevoisier, C., Ouwerkerk, M., Lankhaar, G., Dingemans, J., 1998. Comparative single- and multiple-dose pharmacokinetics of levodopa and 3-O-methyldopa following a new dual-release and a conventional slow-release formulation of levodopa and benserazide in healthy subjects. *European Journal of Pharmaceutics and Biopharmaceutics*, 46, 223-228.
- Gershanik, T., Benita, S., 1996. Positively Charged Self-Emulsifying Oil Formulation for Improving Oral Bioavailability of Progesterone. *Pharmaceutical Development and Technology*, 1, 147-157.
- Ghannam, M.T., Esmail, M.N., 1997. Rheological properties of carboxymethyl cellulose. *Journal of Applied Polymer Science*, 64, 289-301.
- Ghosh, K., Shu, X.Z., Mou, R., Lombardi, J., Prestwich, G.D., Rafailovich, M.H., Clark, R.A.F., 2005. Rheological Characterization of in Situ Cross-Linkable Hyaluronan Hydrogels. *Biomacromolecules*, 6, 2857-2865.
- Gill, J., Grossman, E., Goldstein, D., 1991. High urinary dopa and low urinary dopamine-to-dopa ratio in salt-sensitive hypertension. *Hypertension*, 18, 614-621.
- Gillies, E.R., Fréchet, J.M.J., 2005. Dendrimers and dendritic polymers in drug delivery. *Drug Discovery Today*, 10, 35-43.
- Girault, J., Greengard, P., 2004. The neurobiology of dopamine signaling. *Archives of Neurology*, 61, 641-644.
- Goetz, C.G., 2011. The History of Parkinson's Disease: Early Clinical Descriptions and Neurological Therapies. *Cold Spring Harbor Perspectives in Medicine*, 1. doi: 10.1101/cshperspect.a008862.

- Gojny, F.H., Wichmann, M.H.G., Fiedler, B., Schulte, K., 2005. Influence of different carbon nanotubes on the mechanical properties of epoxy matrix composites – A comparative study. *Composites Science and Technology*, 65, 2300-2313.
- Golovnya, R.V., Zhuravleva, I.L., Zenin, S.V., Polyakov, V.A., Sergeev, G.B., 1973. Determination of thermodynamic characteristics of complexing of amines with alkyl and aryl phosphates by the NMR method. *Russian Chemical Bulletin*, 22, 2528-2530.
- Gomez-Orellana, I., 2005. Strategies to improve oral drug bioavailability. *Expert Opinion on Drug Delivery*, 2, 419-433.
- Gomoll, A.H., Fitz, W., Scott, R.D., Thornhill, T.S., Bellare, A., 2008. Nanoparticulate fillers improve the mechanical strength of bone cement. *Acta Orthopaedica*, 79, 421-427.
- Goole, J., Amighi, K., Vanderbist, F., 2008a. Evaluation and Floating Enhancement of Levodopa Sustained Release Floating Minitablets Coated with Insoluble Acrylic Polymer. *Drug Development and Industrial Pharmacy*, 34, 827-833.
- Goole, J., Deleuze, P., Vanderbist, F., Amighi, K., 2008b. New levodopa sustained-release floating minitables coated with insoluble acrylic polymer. *European Journal of Pharmaceutics and Biopharmaceutics*, 68, 310-318.
- Goole, J., Van Gansbeke, B., Pilcer, G., Deleuze, P., Blocklet, D., Goldman, S., Pandolfo, M., Vanderbist, F., Amighi, K., 2008c. Pharmacoscintigraphic and pharmacokinetic evaluation on healthy human volunteers of sustained-release floating minitables containing levodopa and carbidopa. *International Journal of Pharmaceutics*, 364, 54-63.
- Goole, J., Vanderbist, F., Amighi, K., 2007. Development and evaluation of new multiple-unit levodopa sustained-release floating dosage forms. *International Journal of Pharmaceutics*, 334, 35-41.
- Gordon, M., Markham, J., Hartlein, J.M., Koller, J.M., Loftin, S., Black, K.J., 2007. Intravenous levodopa administration in humans based on a two-compartment kinetic model. *Journal of Neuroscience Methods*, 159, 300-307.
- Grant, J., Blicher, M., Piquette-Miller, M., Allen, C., 2005. Hybrid films from blends of chitosan and egg phosphatidylcholine for localized delivery of paclitaxel. *Journal of Pharmaceutics Sciences*, 94, 1512-1527.

- Groen, J.C., Peffer, L.A.A., Pérez-Ramírez, J., 2003. Pore size determination in modified micro- and mesoporous materials. Pitfalls and limitations in gas adsorption data analysis. *Microporous and Mesoporous Materials*, 60, 1-17.
- Grossman, E., Goldstein, D.S., Hoffman, A., Wacks, I.R., Epstein, M., 1992. Effects of water immersion on sympathoadrenal and dopa-dopamine systems in humans. *American Journal of Physiology - Regulatory, Integrative and Comparative Physiology*, 262, R993-R999.
- Guo, W., Guo, Y., Gao, H., Zheng, Q., Zhong, W., 2003. Energy dissipation in gigahertz oscillators from multiwalled carbon nanotubes. *Physical Review Letters*, 91, 125501-4.
- Gupta, V.K., Assmus, M.W., Beckert, T.E., Price, J.C., 2001. A novel pH- and time-based multi-unit potential colonic drug delivery system. II. Optimization of multiple response variables. *International Journal of Pharmaceutics*, 213, 93-102.
- Gwak, H., Choi, J., Choi, H., 2005. Enhanced bioavailability of piroxicam via salt formation with ethanolamines. *International Journal of Pharmaceutics*, 297, 156-161.
- Hafner, A., Lovrić, J., Voinovich, D., Filipović-Grčić, J., 2009. Melatonin-loaded lecithin/chitosan nanoparticles: Physicochemical characterization and permeability through Caco-2 cell monolayers. *International Journal of Pharmaceutics*, 381, 205-213.
- Hameed, N., Guo, Q., 2008. Nanostructure and hydrogen bonding in interpolyelectrolyte complexes of poly(ϵ -caprolactone)-block-poly(2-vinyl pyridine) and poly(acrylic acid). *Polymer*, 49, 5268-5275.
- Han C, Hsu L, Hsu AF, 2006. Combination immediate release controlled release levodopa/carbidopa dosage forms. Patent US 7094427. http://patft.uspto.gov/netacgi/nph-Parser?Sect1=PTO1&Sect2=HITOFF&d=PALL&p=1&u=%2Fnetacgi%2FPTO%2Fsrc_hnum.htm&r=1&f=G&l=50&s1=7094427.PN.&OS=PN/7094427&RS=PN/709442
- Hans, M.L., Lowman, A.M., 2002. Biodegradable nanoparticles for drug delivery and targeting. *Current Opinion in Solid State and Materials Science*, 6, 319-327.
- Hauser, R.A., 2004. Levodopa/carbidopa/entacapone (Stalevo). *Neurology*, 62, S64-S71.
- He, H., Guan, J., Lee, J.L., 2006. An oral delivery device based on self-folding hydrogels. *Journal of Controlled Release*, 110, 339-346.

- He, P., Davis, S.S., Illum, L., 1998. In vitro evaluation of the mucoadhesive properties of chitosan microspheres. *International Journal of Pharmaceutics*, 166, 75-88.
- He, W., Horn, S.W., Hussain, M.D., 2007. Improved bioavailability of orally administered mifepristone from PLGA nanoparticles. *International Journal of Pharmaceutics*, 334, 173-178.
- Herrero-Vanrell, R., Refojo, M.F., 2001. Biodegradable microspheres for vitreoretinal drug delivery. *Advanced Drug Delivery Reviews*, 52, 5-16.
- Hickey, T., Kreutzer, D., Burgess, D.J., Moussy, F., 2002. Dexamethasone/PLGA microspheres for continuous delivery of an anti-inflammatory drug for implantable medical devices. *Biomaterials*, 23, 1649-1656.
- Ho, E.A., Vassileva, V., Allen, C., Piquette-Miller, M., 2005. In vitro and in vivo characterizations of a novel biocompatible polymer-lipid implant system for the sustained delivery of paclitaxel. *Journal of Controlled Release*, 104, 181-191.
- Hoare, T.R., Kohane, D.S., 2008. Hydrogels in drug delivery: Progress and challenges. *Polymer*, 49, 1993-2007.
- Hoffman, A., Stepensky, D., Lavy, E., Eyal, S., Klausner, E., Friedman, M., 2004b. Pharmacokinetic and pharmacodynamic aspects of gastroretentive dosage forms. *International Journal of Pharmaceutics*, 277, 141-153.
- Högl, B., Peralta, C., Wetter, T.C., Gershanik, O., Trenkwalder, C., 2001. Effect of sleep deprivation on motor performance in patients with Parkinson's disease. *Movement Disorders*, 16, 616-621.
- Holland, B., 2003. Determination of both mesopores and macropores in three-dimensional ordered porous materials by nitrogen adsorption. *Journal of Porous Materials*, 10, 17-22.
- Hörter, D., Dressman, J.B., 2001. Influence of physicochemical properties on dissolution of drugs in the gastrointestinal tract. *Advanced Drug Delivery Reviews*, 46, 75-87.
- Hsu AF, Han C-H, 2006. Oral disintegrating dosage forms. Patent WO/2006/073729. <http://www.wipo.int/patentscope/search/en/detail.jsf?docId=WO2006073729> Accessed 10th October, 2010.

- Hu, L., Tang, X., Cui, F., December 2004. Solid lipid nanoparticles (SLNs) to improve oral bioavailability of poorly soluble drugs. *Journal of Pharmacy and Pharmacology*, 56, 1527-1535.
- Huang, L.C., Jean, D., McDermott, A.M., 2005. Effect of preservative-free artificial tears on the antimicrobial activity of human β -defensin-2 and cathelicidin II-37 *in vitro*. *Eye & contact lens*, 31, 34-38.
- Hurst, S., Loi, C., Brodfuehrer, J., El-Kattan, A., 2007. Impact of physiological, physicochemical and biopharmaceutical factors in absorption and metabolism mechanisms on the drug oral bioavailability of rats and humans. *Expert Opinion on Drug Metabolism & Toxicology*, 3, 469-489.
- Hurtig, H.I., 1997. Problems with Current Pharmacologic Treatment of Parkinson's Disease. *Experimental Neurology*, 144, 10-16.
- Huwyler, J., Wu, D., Pardridge, W., 1996. Brain drug delivery of small molecules using immunoliposomes. *Proceedings of the National Academy of Sciences of the United States of America*, 93, 14164-14169.
- Iannuccelli V.[1], Coppi G., Bernabei M.T., Cameroni R., 1998. Air compartment multiple-unit system for prolonged gastric residence. Part I. Formulation study. *International Journal of Pharmaceutics*, 174, 47-54.
- Ishikiriyama, K., Wunderlich, B., 1997. Melting of poly(oxyethylene) analyzed by temperature-modulated calorimetry. *Macromolecules*, 30, 4126-4131.
- Italia, J., Yahya, M., Singh, D., Ravi Kumar, M., 2009. Biodegradable Nanoparticles Improve Oral Bioavailability of Amphotericin B and Show Reduced Nephrotoxicity Compared to Intravenous Fungizone®. *Pharmaceutical Research*, 26, 1324-1331.
- Italia, J.L., Bhatt, D.K., Bhardwaj, V., Tikoo, K., Kumar, M.N.V.R., 2007. PLGA nanoparticles for oral delivery of cyclosporine: Nephrotoxicity and pharmacokinetic studies in comparison to Sandimmune Neoral®. *Journal of Controlled Release*, 119, 197-206.
- Ito, M., Ban, A., Ishihara, M., 2000. Anti-ulcer effects of chitin and chitosan, healthy foods, in rats. *The Japanese Journal of Pharmacology*, 82, 218-225.
- Iyer, S.S., Morgan, J.C., Sethi, K.D., 2005. Absorption of orally disintegrating carbidopa-levodopa requires intact small bowel function. *Neurology*, 65, 1507.

- Jackson B, Bennet DJ, Bartus RT, Emerich DF, 2004. Pulmonary Delivery for Levodopa. http://appft.uspto.gov/netacgi/nph-Parser?Sect1=PTO1&Sect2=HITOFF&d=PG01&p=1&u=%2Fnethtml%2FPTO%2Fsrc_hnum.html&r=1&f=G&l=50&s1=%2220040018989%22.PG.NR.&OS=DN/20040018989&RS=DN/20040018989 Accessed 16th October 2010.
- Jain, S.K., Agrawal, G.P., Jain, N.K., 2008. Floating Microspheres as Drug Delivery System: Newer Approaches. *Current Drug Delivery*, 5, 220-223.
- Jain, S.K., Jangdey, M.S., 2009. Lectin conjugated gastroretentive multiparticulate delivery system of clarithromycin for the effective treatment of *Helicobacter pylori*. *Molecular Pharmaceutics*, 6, 295-304.
- Jang, D., Jeong, E.J., Lee, H., Kim, B., Lim, S., Kim, C., 2006. Improvement of bioavailability and photostability of amlodipine using redispersible dry emulsion. *European Journal of Pharmaceutical Sciences*, 28, 405-411.
- Jankovic, J., 2008. Parkinson's disease: clinical features and diagnosis. *Journal of Neurology, Neurosurgery and Psychiatry*, 79, 368-376.
- Jankovic, J., 2002. Levodopa strengths and weaknesses. *Neurology*, 58, S19-S32.
- Jiménez-Castellanos, M.R., Zia, H., Rhodes, C.T., 1994. Design and testing in vitro of a bioadhesive and floating drug delivery system for oral application. *International Journal of Pharmaceutics*, 105, 65-70.
- Jin, S., Ye, K., 2007. Nanoparticle-mediated drug delivery and gene therapy. *Biotechnology Progress*, 23, 32-41.
- Jivraj, M., Martini, L.G., Thomson, C.M., 2000. An overview of the different excipients useful for the direct compression of tablets. *Pharmaceutical Science and Technology Today*, 3, 58-63.
- Jorga, K.M., Larsen, J.P., Beiske, A., Schleimer, M., Fotteler, B., Schmitt, M., Moe, B., 1999. The effect of tolcapone on the pharmacokinetics of benserazide. *European Journal of Neurology*, 6, 211-219.
- Josef, E., Zilberman, M., Bianco-Peled, H., 2010. Composite alginate hydrogels: An innovative approach for the controlled release of hydrophobic drugs. *Acta Biomaterialia*, 6, 4642-4649.

- Joshi, H.N., Tejwani, R.W., Davidovich, M., Sahasrabudhe, V.P., Jemal, M., Bathala, M.S., Varia, S.A., Serajuddin, A.T.M., 2004. Bioavailability enhancement of a poorly water-soluble drug by solid dispersion in polyethylene glycol–polysorbate 80 mixture. *International Journal of Pharmaceutics*, 269, 251-258.
- Kabanov, A.V., Gendelman, H.E., 2007. Nanomedicine in the diagnosis and therapy of neurodegenerative disorders. *Progress in Polymer Science*, 32, 1054-1082.
- Kallioinen S, Kervinen L, Laaksonen M, Lintulaakso J, Niskanen M, Partanen M, Ritala M, Vahervuo K, Virkki, 2001. Levodopa/Carbidopa/Entacapone Pharmaceutical Preparation. Patent WO/2001/001984.
<http://www.wipo.int/patentscope/search/en/detail.jsf?docId=WO2001001984> Accessed 10th October, 2010.
- Kang, B.K., Lee, J.S., Chon, S.K., Jeong, S.Y., Yuk, S.H., Khang, G., Lee, H.B., Cho, S.H., 2004a. Development of self-microemulsifying drug delivery systems (SMEDDS) for oral bioavailability enhancement of simvastatin in beagle dogs. *International Journal of Pharmaceutics*, 274, 65-73.
- Kankkunen, T., Huupponen, I., Lahtinen, K., Sundell, M., Ekman, K., Kontturi, K., Hirvonen, J., 2002. Improved stability and release control of levodopa and metaraminol using ion-exchange fibers and transdermal iontophoresis. *European Journal of Pharmaceutical Sciences*, 16, 273-280.
- Kao, H.D., Traboulsi, A., Itoh, S., Dittert, L., Hussain, A., 2000. Enhancement of the systemic and CNS specific delivery of l-dopa by the nasal administration of its water soluble prodrugs. *Pharmaceutical Research*, 17, 978-984.
- Kawashima, Y., Yamamoto, H., Takeuchi, H., Kuno, Y., 2000. Mucoadhesive DL-lactide/glycolide copolymer nanospheres coated with chitosan to improve oral delivery of elcatonin. *Pharmaceutical Development and Technology*, 5, 77-85.
- Kempster, P.A., Hurwitz, B., Lees, A.J., 2007. A new look at James Parkinson's Essay on the Shaking Palsy. *Neurology*, 69, 482-485.
- Kenawy, E., Bowlin, G.L., Mansfield, K., Layman, J., Simpson, D.G., Sanders, E.H., Wnek, G.E., 2002. Release of tetracycline hydrochloride from electrospun poly(ethylene-co-vinylacetate), poly(lactic acid), and a blend. *Journal of Controlled Release*, 81, 57-64.
- Kesisoglou, F., Panmai, S., Wu, Y., 2007. Nanosizing — Oral formulation development and biopharmaceutical evaluation. *Advanced Drug Delivery Reviews*, 59, 631-644.

- Khodaghali, F., Eftekharzadeh, B., Maghsoudi, N., Rezaei, P., 2010. Chitosan prevents oxidative stress-induced amyloid β formation and cytotoxicity in NT2 neurons: involvement of transcription factors Nrf2 and NF- κ B. *Molecular and Cellular Biochemistry*, 337, 39-51.
- Khor, S., Hsu, A., 2007. The pharmacokinetics and pharmacodynamics of levodopa in the treatment of Parkinson's disease. *Current Clinical Pharmacology*, 2, 234-243.
- Kim, S.W., Bae, Y.H., Okano, T., 1992. Hydrogels: swelling, drug loading, and release. *Pharmaceutical Research*, 9, 283-290.
- Kim, S., Kim, J.Y., Huh, K.M., Acharya, G., Park, K., 2008. Hydrotropic polymer micelles containing acrylic acid moieties for oral delivery of paclitaxel. *Journal of Controlled Release*, 132, 222-229.
- Kim, T.K., Kang, W., Chun, I.K., Oh, S.Y., Lee, Y.H., Gwak, H.S., 2009. Pharmacokinetic evaluation and modeling of formulated levodopa intranasal delivery systems. *European Journal of Pharmaceutical Sciences*, 38, 525-532.
- Klausner, E.A., Eyal, S., Lavy, E., Friedman, M., Hoffman, A., 2003. Novel levodopa gastroretentive dosage form: in-vivo evaluation in dogs. *Journal of Controlled Release*, 88, 117-126.
- Koller, W., Guarnieri, M., Hubble, J., Rabinowicz, A.L., Silver, D., 2005. An open-label evaluation of the tolerability and safety of Stalevo® (carbidopa, levodopa and entacapone) in Parkinson's disease patients experiencing wearing-off. *Journal of Neural Transmission*, 112, 221-230.
- Koller, W.C., Hutton, J.T., Tolosa, E., Capilldeo, R., 1999. Immediate-release and controlled-release carbidopa/levodopa in PD: A 5-year randomized multicenter study. *Neurology*, 53, 1012-1019.
- Kopeček, J., 2007. Hydrogel biomaterials: A smart future? *Biomaterials*, 28, 5185-5192.
- Kopecek, J., Yang, J., 2007. Hydrogels as smart biomaterials. *Polymer International*, 56, 1078-1098.
- Kordower, J.H., Goetz, C.G., 1999. The first miracle in neurodegenerative disease: The discovery of oral levodopa. *Brain Research Bulletin*, 50, 377-378.

- Korsmeyer, R.W., Gurny, R., Doelker, E., Buri, P., Peppas, N.A., 1983. Mechanisms of solute release from porous hydrophilic polymers. *International Journal of Pharmaceutics*, 15, 25-35.
- Kostoff, R.N., Briggs, M.B., 2008. Literature-Related Discovery (LRD): Potential treatments for Parkinson's disease. *Technological Forecasting and Social Change*, 75, 226-238.
- Kramar, A., Turk, S., Vrecer, F., 2003. Statistical optimization of diclofenac sustained release pellets coated with polymethacrylic films. *International Journal of Pharmaceutics*, 256, 43-52.
- Krauland, A.H., Alonso, M.J., 2007. Chitosan/cyclodextrin nanoparticles as macromolecular drug delivery system. *International Journal of Pharmaceutics*, 340, 134-142.
- Kreuter, J., 2005. Application of nanoparticles for the delivery of drugs to the brain. *International Congress Series*, 1277, 85-94.
- Kulicke, W., Kull, A.H., Kull, W., Thielking, H., Engelhardt, J., Pannek, J., 1996. Characterization of aqueous carboxymethylcellulose solutions in terms of their molecular structure and its influence on rheological behavior. *Polymer*, 37, 2723-2731.
- Kumar, P., Bhatia, M., November/December 2010. Functionalization of Chitosan/Methylcellulose Interpenetrating Polymer Network Microspheres for Gastroretentive Application Using Central Composite Design. *PDA Journal of Pharmaceutical Science and Technology*, 64, 497-506.
- Kumar, P., Pillay, V., Choonara, Y.E., Modi, G., Naidoo, D., du Toit, L.C., 2011. In silico theoretical molecular modeling for Alzheimer's disease: the nicotine-curcumin paradigm in neuroprotection and neurotherapy. *International Journal of Molecular Sciences*, 12, 694-724.
- Kumar, P., Singh, I., 2010. Formulation and characterization of tramadol-loaded IPN microgels of alginate and gelatin: Optimization using response surface methodology. *Acta Pharmaceutica*, 60, 295-310.
- Kumari, A., Yadav, S.K., Yadav, S.C., 2010. Biodegradable polymeric nanoparticles based drug delivery systems. *Colloids and Surfaces B: Biointerfaces*, 75, 1-18.
- Kuo, F., Subramanian, B., Kotyla, T., Wilson, T.A., Yoganathan, S., Nicolosi, R.J., 2008. Nanoemulsions of an anti-oxidant synergy formulation containing gamma tocopherol

- have enhanced bioavailability and anti-inflammatory properties. *International Journal of Pharmaceutics*, 363, 206-213.
- Kushnir M, Heldman E, 2004. Apparatus for the Transdermal Treatment of Parkinson's Disease 6,746,688.
<http://patft.uspto.gov/netacgi/nph-Parser?Sect1=PTO1&Sect2=HITOFF&d=PALL&p=1&u=%2Fnetacgi/nph-num.htm&r=1&f=G&l=50&s1=6746688.PN.&OS=PN/6746688&RS=PN/6746688>
Accessed 16th October, 2010.
- Lamprecht, A., Yamamoto, H., Takeuchi, H., Kawashima, Y., 2004. pH-sensitive microsphere delivery increases oral bioavailability of calcitonin. *Journal of Controlled Release*, 98, 1-9.
- Langer, R., Peppas, N.A., 2003. Advances in biomaterials, drug delivery, and bionanotechnology. *American Institute of Chemical Engineers Journal*, 49, 2990-3006.
- Lecomte, F., Siepmann, J., Walther, M., MacRae, R.J., Bodmeier, R., 2003. Blends of enteric and GIT-insoluble polymers used for film coating: physicochemical characterization and drug release patterns. *Journal of Controlled Release*, 89, 457-471.
- Lee, C.H., Moturi, V., Lee, Y., 2009. Thixotropic property in pharmaceutical formulations. *Journal of Controlled Release*, 136, 88-98.
- Lee, J.W., Park, J.H., Robinson, J.R., 2000. Bioadhesive-based dosage forms: The next generation. *Journal of Pharmaceutical Sciences*, 89, 850-866.
- Lee, K.Y., Bouhadir, K.H., Mooney, D.J., 2004. Controlled degradation of hydrogels using multi-functional cross-linking molecules. *Biomaterials*, 25, 2461-2466.
- Lehr, C., Bouwstra, J.A., Schacht, E.H., Junginger, H.E., 1992. In vitro evaluation of mucoadhesive properties of chitosan and some other natural polymers. *International Journal of Pharmaceutics*, 78, 43-48.
- Lennernäs, H., Nilsson, D., Aquilonius, S., Ahrenstedt, O., Knutson, L., Paalzow, L., 1993. The effect of L-leucine on the absorption of levodopa, studied by regional jejunal perfusion in man. *British Journal of Clinical Pharmacology*, 35, 243-250.
- Leroux, J., Cozens, R.M., Roesel, J.L., Galli, B., Doelker, E., Gurny, R., 1996. pH-Sensitive Nanoparticles: An Effective Means to Improve the Oral Delivery of HIV-1 Protease Inhibitors in Dogs. *Pharmaceutical Research*, 13, 485-487.

- Leuner, C., Dressman, J., 2000. Improving drug solubility for oral delivery using solid dispersions. *European Journal of Pharmaceutics and Biopharmaceutics*, 50, 47-60.
- LeWitt, P.A., Nyholm, D., 2004. New developments in levodopa therapy. *Neurology*, 62, S9-S16.
- Li, H., Wu, B., Mu, C., Lin, W., 2011. Concomitant degradation in periodate oxidation of carboxymethyl cellulose. *Carbohydrate Polymers*, 84, 881-886.
- Li, H., Gu, X., 2007. Correlation between drug dissolution and polymer hydration: A study using texture analysis. *International Journal of Pharmaceutics*, 342, 18-25.
- Li, J., Barrow, D., Howell, H., Kalachandra, S., 2010. In vitro drug release study of methacrylate polymer blend system: effect of polymer blend composition, drug loading and solubilizing surfactants on drug release. *J. Mater. Sci. Mater. Med.*, 21, 583-588.
- Lim Soo, P., Cho, J., Grant, J., Ho, E., Piquette-Miller, M., Allen, C., 2008. Drug release mechanism of paclitaxel from a chitosan–lipid implant system: Effect of swelling, degradation and morphology. *European Journal of Pharmaceutics and Biopharmaceutics*, 69, 149-157.
- Lin, C., Ko, S., 1995. Effects of temperature and concentration on the steady shear properties of aqueous solutions of carbopol and CMC. *International Communications in Heat and Mass Transfer*, 22, 157-166.
- Linazasoro, G., 2008. Potential applications of nanotechnologies to Parkinson's disease therapy. *Parkinsonism & Related Disorders*, 14, 383-392.
- Lindner A., Sudo J.-i., Iwase H., Terui J., Kakuno K., Soyama, M., Takayama K., Nagai T., 1998. Transdermal absorption of L-dopa from hydrogel in rats. *European Journal of Pharmaceutical Sciences*, 7, 67-71.
- Lipatov, Y.S., Shumsky, V.F., Getmanchuk, I.P., Gorbatenko, A.N., 1982. Rheology of polymer blends. *Rheologica Acta*, 21, 270-279.
- Lipka, E., Amidon, G.L., 1999. Setting bioequivalence requirements for drug development based on preclinical data: optimizing oral drug delivery systems. *Journal of Controlled Release*, 62, 41-49.
- Liu, R.C.W., Morishima, Y., Winnik, F.M., 2001. A Rheological Evaluation of the Interactions in Water between a Cationic Cellulose Ether and Sodium Poly(2-acrylamido-2-methylpropanesulfonates). *Macromolecules*, 34, 9117-9124.

- Liu, Y., Zhang, P., Feng, N., Zhang, X., Wu, S., Zhao, J., 2009. Optimization and in situ intestinal absorption of self-microemulsifying drug delivery system of oridonin. *International Journal of Pharmaceutics*, 365, 136-142.
- Lokind, K.B., Lorenzen, F.H., 1996. Oral bioavailability of 17 β -estradiol and prodrugs tested in rats, pigs and dogs. *International Journal of Pharmaceutics*, 127, 155-164.
- Long Zhao, , Mitomo, H., Yosh, F., 2008. Synthesis of pH-sensitive and biodegradable cm-cellulose/chitosan polyampholytic hydrogels with electron beam irradiation. *Journal of Bioactive and Compatible Polymers*, 23, 319-333.
- Lu, Z., Chen, W., Hamman, J.H., October 2007. Chitosan-polycarbophil complexes in swellable matrix systems for controlled drug release. *Current Drug Delivery*, 4, 257-263.
- Lu, Z., Chen, W., Olivier, E., Hamman, J.H., 2008. Matrix polymeric excipients: comparing a novel interpolyelectrolyte complex with hydroxypropylmethylcellulose. *Drug Delivery*, 15, 87-96.
- Lum, Z.P., Tai, I.T., Krestow, M., Norton, J., Vacek, I., Sun, A.M., 1991. Prolonged reversal of diabetic state in NOD mice by xenografts of microencapsulated rat islets. *Diabetes*, 40, 1511-1516.
- Mahalingam, R., Jasti, B., Birudaraj, R., Stefanidis, D., Killion, R., Alfredson, T., Anne, P., Li, X., 2009. Evaluation of Polyethylene Oxide Compacts as Gastroretentive Delivery Systems. *AAPS PharmSciTech*, 10, 98-103.
- Majithiya, R.J., Murthy, R.S.R., 2005. Chitosan-Based Mucoadhesive Microspheres of Clarithromycin as A Delivery System for Antibiotic to Stomach. *Current Drug Delivery*, 2, 235-242.
- Mandel, S., Weinreb, O., Amit, T., Youdim, M.B.H., 2005. Mechanism of neuroprotective action of the anti-Parkinson drug rasagiline and its derivatives. *Brain Research Reviews*, 48, 379-387.
- Margetson, D.N., Jones, D.S., Andrew, G., McAllister, M.S., 2007. Physicochemical and drug release characteristics of quinine and polymers prepared by hot-melt extrusion *Processing Pharmaceutical Polymers*, Basel, Switzerland, 1-6.

- Martinez, M.N., Amidon, G.L., 2002. A mechanistic approach to understanding the factors affecting drug absorption: a review of fundamentals. *The Journal of Clinical Pharmacology*, 42, 620-643.
- Mathot, F., van Beijsterveldt, L., Pr at, V., Brewster, M., Ari n, A., 2006. Intestinal uptake and biodistribution of novel polymeric micelles after oral administration. *Journal of Controlled Release*, 111, 47-55.
- Mathur RS, Manan S, Mehta K., 2006. Carbidopa and L-dopa Dispersible Tablets WO/2006/035414.
<http://www.wipo.int/patentscope/search/en/detail.jsf?docId=WO2006035414> Accessed 10th October, 2010.
- Mehta, K.A., Kislalioglu, M.S., Phuapradit, W., Malick, A.W., Shah, N.H., 2000. Effect of formulation and process variables on porosity parameters and release rates from a multi unit erosion matrix of a poorly soluble drug. *Journal of Controlled Release*, 63, 201-211.
- Melamed, E., Offen, D., Shirvan, A., Ziv, I., 2000. Levodopa - an exotoxin or a therapeutic drug? *Journal of Neurology*, 247, II135-II139.
- Merchant, H., Shoaib, H., Tazeen, J., Yousuf, R., 2006. Once-daily tablet formulation and in vitro release evaluation of cefpodoxime using hydroxypropyl methylcellulose: A technical note. *AAPS PharmSciTech*, 7, E178-E183.
- Merck Sharp & Dohme Corp., 2011. Sinemet CR.,
http://www.merck.com/product/usa/pi_circulars/s/sinemet_cr/sinemet_cr_pi.pdf
Accessed 3rd October 2011.
- Mi, F., Shyu, S., Lin, Y., Wu, Y., Peng, C., Tsai, Y., 2003. Chitin/PLGA blend microspheres as a biodegradable drug delivery system: a new delivery system for protein. *Biomaterials*, 24, 5023-5036.
- Michailova, V., Titeva, S., Kotsilkova, R., Krusteva, E., Minkov, E., 1999. Influence of aqueous medium on visco-elastic properties of carboxymethylcellulose sodium, hydroxypropylmethylcellulose, and thermally pre-gelatinized starch gels. *Colloids and Surfaces A: Physicochemical and Engineering Aspects*, 149, 515-520.
- Mitrevej, A., Sinchaipanid, N., Rungvejhavuttivittaya, Y., Kositchaiyong, V., 2001. Multiunit controlled-release diclofenac sodium capsules using complex of chitosan with sodium alginate or pectin. *Pharmaceutical Development and Technology*, 6, 385-392.

- Mittal, G., Carswell, H., Brett, R., Currie, S., Kumar, M.N.V.R., 2011. Development and evaluation of polymer nanoparticles for oral delivery of estradiol to rat brain in a model of Alzheimer's pathology. *Journal of Controlled Release*, 150, 220-228.
- Mittal, G., Sahana, D.K., Bhardwaj, V., Ravi Kumar, M.N.V., 2007a. Estradiol loaded PLGA nanoparticles for oral administration: Effect of polymer molecular weight and copolymer composition on release behavior in vitro and in vivo. *Journal of Controlled Release*, 119, 77-85.
- Mora-Huertas, C.E., Fessi, H., Elaissari, A., 2010. Polymer-based nanocapsules for drug delivery. *International Journal of Pharmaceutics*, 385, 113-142.
- Morishita, M., Matsuzawa, A., Takayama, K., Isowa, K., Nagai, T., 1998. Improving insulin enteral absorption using water-in-oil-in-water emulsion. *International Journal of Pharmaceutics*, 172, 189-198.
- Morrison, R.A., Kripalani, K.J., Marino, A.M., Dean, A.V., Migdalof, B.H., Weinstein, S.H., Jain, N.B., Bathala, M.S., Singhvi, S.M., 1997. Intestinal absorption of captopril and two thioester analogs in rats and dogs. *Biopharmaceutics and Drug Disposition*, 18, 25-39.
- Moura, M.J., Figueiredo, M.M., Gil, M.H., 2007. Rheological study of genipin cross-linked chitosan hydrogels. *Biomacromolecules*, 8, 3823-3829.
- Mouradian, M.M., 2005. Should levodopa be infused into the duodenum? *Neurology*, 64, 182-183.
- Moustafin, R.I., Margulis, E.B., Sibgatullina, L.F., Kemenova, V.A., Van den Mooter, G., 2008. Comparative evaluation of interpolyelectrolyte complexes of chitosan with Eudragit® L100 and Eudragit® L100-55 as potential carriers for oral controlled drug delivery. *European Journal of Pharmaceutics and Biopharmaceutics*, 70, 215-225.
- Moustafine, R.I., Zaharov, I.M., Kemenova, V.A., 2006. Physicochemical characterization and drug release properties of Eudragit® E PO/Eudragit® L 100-55 interpolyelectrolyte complexes. *European Journal of Pharmaceutics and Biopharmaceutics*, 63, 26-36.
- Mu, L., Feng, S.S., 2003. A novel controlled release formulation for the anticancer drug paclitaxel (Taxol®): PLGA nanoparticles containing vitamin E TPGS. *Journal of Controlled Release*, 86, 33-48.

- Mühlbauer, B., Osswald, H., 1992. Feeding but not salt loading is the dominant factor controlling urinary dopamine excretion in conscious rats. *Naunyn-Schmiedeberg's Archives of Pharmacology*, 346, 469-471.
- Mukai S., Lipsitz L. A., 2002. Orthostatic hypotension. *Clinics in geriatric medicine*, 253-268.
- Müller, T., Erdmann, C., Bremen, D., Schmidt, W.E., Muhlack, S., Woitalla, D., Goetze, O., 2006. Impact of gastric emptying on levodopa pharmacokinetics in Parkinson disease patients. *Clinical Neuropharmacology*, 29, 61-67.
- Murphy, C., Pillay, V., Choonara, Y., du Toit, L., Ndesendo, V., Chirwa, N., Kumar, P., 2011. Optimization of a dual mechanism gastrofloatable and gastroadhesive delivery system for narrow absorption window drugs. *AAPS PharmSciTech*, 1-15. doi: 10.1208/s12249-011-9711-1.
- Mustafin, R., Protasova, A., Van den Mooter, G., Kemenova, V., 2006. Modification of chitosan by inclusion into interpolyelectrolyte complex with Eudragit L. *Pharmaceutical Chemistry Journal*, 40, 325-328.
- Mustafin, R.I., Van den Mooter, G., Kemenova, V.A., 2005. Eudragit E Modified by Inclusion Into an Interpolyelectrolyte Complex. *Pharmaceutical Chemistry Journal*, 39, 39-42.
- Muzzi, C., Bertocci, E., Terzuoli, L., Porcelli, B., Ciari, I., Pagani, R., Guerranti, R., 2008a. Simultaneous determination of serum concentrations of levodopa, dopamine, 3-O-methyldopa and α -methyldopa by HPLC. *Biomedicine & Pharmacotherapy*, 62, 253-258.
- Myers, W.R., 2003. Response Surface Methodology. *Encyclopedia of Biopharmaceutical Statistics: Second Edition*, Informa Healthcare, USA, pp. 858.
- Nakason, C., Kaewsakul, W., Kaesaman, A., 2012. Thermoplastic Natural Rubbers Based on Blending of Ethylene-Vinyl Acetate Copolymer with Different Types of Natural Rubber. *Journal of Elastomers and Plastics*, 44, 89-111.
- Nausieda, P.A., Pfeiffer, R.F., Tagliati, M., Kastenzholz, K.V., DeRoche, C., Slevin, J.T., 2005. A multicenter, open-label, sequential study comparing preferences for carbidopa-levodopa orally disintegrating tablets and conventional tablets in subjects with Parkinson's disease. *Clinical Therapeutics*, 27, 58-63.
- Ndesendo, V.M.K., Pillay, V., Choonara, Y.E., Du Toit, L.C., Meyer, L.C.R., Buchmann, E., Kumar, P., Khan, R.A., 2011. In vivo evaluation of the release of zidovudine and

- polystyrene sulfonate from a dual intravaginal bioadhesive polymeric device in the pig model. *Journal of Pharmaceutical Sciences*, 100, 1416-1435.
- Nel, A., Xia, T., Madler, L., Li, N., 2006. Toxic potential of materials at the nanolevel. *Science*, 311, 622-627.
- Neslihan G.R., Benita, S., 2004. Self-emulsifying drug delivery systems (SEDDS) for improved oral delivery of lipophilic drugs. *Biomedicine & Pharmacotherapy*, 58, 173-182.
- Ngwuluka, N., Pillay, V., Du Toit, L.C., Ndesendo, V., Choonara, Y., Modi, G., Naidoo, D., 2010. Levodopa delivery systems: advancements in delivery of the gold standard. *Expert Opinion on Drug Delivery*, 7, 203-224.
- Nilsson, D., Nyholm, D., Aquilonius, S.M., 2001. Duodenal levodopa infusion in Parkinson's disease long-term experience. *Acta Neurologica Scandinavica*, 104, 343-348.
- Nimesh, S., Manchanda, R., Kumar, R., Saxena, A., Chaudhary, P., Yadav, V., Mozumdar, S., Chandra, R., 2006. Preparation, characterization and in vitro drug release studies of novel polymeric nanoparticles. *International Journal of Pharmaceutics*, 323, 146-152.
- Nur, A., Zhang, J., 2000. Captopril floating and/or bioadhesive tablets: design and release kinetics. *Drug Development and Industrial Pharmacy*, 26, 965-969.
- Nurkeeva, Z.S., Mun, G.A., Khutoryanskiy, V.V., 2003. Interpolymer Complexes of Water-Soluble Nonionic Polysaccharides with Polycarboxylic Acids and Their Applications. *Macromolecular Bioscience*, 3, 283-295.
- Nutt, J.G., Carter, J.H., Lea, E.S., Woodward, W.R., 1997. Motor fluctuations during continuous levodopa infusions in patients with Parkinson's disease. *Movement Disorders*, 12, 285-292.
- Nutt, J.G., Obeso, J.A., Stocchi, F., 2000. Continuous dopamine-receptor stimulation in advanced Parkinson's disease. *Trends in Neurosciences*, 23, S109-S115.
- Nutt, J.G., Woodward, W.R., Gancher, S.T., Merrick, D., 1987. 3-O-Methyldopa and the response to levodopa in Parkinson's disease. *Annals of Neurology*, 21, 584-588.
- Nyholm, D., Nilsson Remahl, A.I.M., Dizdar, N., Constantinescu, R., Holmberg, B., Jansson, R., Aquilonius, S.-., Askmark, H., 2005a. Duodenal levodopa infusion monotherapy vs oral polypharmacy in advanced Parkinson disease. *Neurology*, 64, 216-223.

- Nyholm, D., Jansson, R., Willows, T., Remahl, I.N., 2005b. Long-term 24-hour duodenal infusion of levodopa: Outcome and dose requirements. *Neurology*, 65, 1506-1507.
- O'Brien, S., Wang, Y., Vervaet, C., Remon, J.P., 2009a. Starch phosphates prepared by reactive extrusion as a sustained release agent. *Carbohydrate Polymers*, 76, 557-566.
- Obering, C.D., Chen, J.J., Swope, D.M., 2006. Update on apomorphine for the rapid treatment of hypomobility ("off") episodes in Parkinson's disease. *Pharmacotherapy*, 26, 840-852.
- Okazaki, I., Wunderlich, B., 1997. Reversible melting in polymer crystals detected by temperature-modulated differential scanning calorimetry. *Macromolecules*, 30, 1758-1764.
- Okereke, C.S., 2002. Role of integrative pharmacokinetic and pharmacodynamic optimization strategy in the management of Parkinson's disease patients experiencing motor fluctuations with levodopa. *Journal of Pharmacy and Pharmaceutical Sciences*, 5, 146-161.
- Olanow, C.W., Obeso, J.A., Stocchi, F., 2006. Continuous dopamine-receptor treatment of Parkinson's disease: scientific rationale and clinical implications. *The Lancet Neurology*, 5, 677-687.
- Olanow, C.W., 2004. The scientific basis for the current treatment of Parkinson's disease. *Annual Review of Medicine*, 55, 41-60.
- Olanow, C.W., Gauger, L.L., Cedarbaum, J.M., 1991. Temporal relationships between plasma and cerebrospinal fluid pharmacokinetics of levodopa and clinical effect in Parkinson's disease. *Annals of Neurology*, 29, 556-559.
- Olanow, C.W., Stocchi, F., 2004. COMT inhibitors in Parkinson's disease: Can they prevent and/or reverse levodopa-induced motor complications? *Neurology*, 62, S72-S81.
- Palhagen, S., Heinonen, E., Hagglund, J., Kaugesaar, T., Maki-Ikola, O., Palm, R., the Swedish Parkinson Study Group, 2006. Selegiline slows the progression of the symptoms of Parkinson disease. *Neurology*, 66, 1200-1206.
- Pan, Y., Li, Y., Zhao, H., Zheng, J., Xu, H., Wei, G., Hao, J., Cui, F., 2002. Bioadhesive polysaccharide in protein delivery system: chitosan nanoparticles improve the intestinal absorption of insulin in vivo. *International Journal of Pharmaceutics*, 249, 139-147.

- Pandey, R., Ahmad, Z., Sharma, S., Khuller, G.K., 2005. Nano-encapsulation of azole antifungals: Potential applications to improve oral drug delivery. *International Journal of Pharmaceutics*, 301, 268-276.
- Pappert, E.J., Buhrfiend, C., Lipton, J.W., Carvey, P.M., Stebbins, G.T., Goetz, C.G., 1996. Levodopa stability in solution: Time course, environmental effects, and practical recommendations for clinical use. *Movement Disorders*, 11, 24-26.
- Pappert, E.J., Lipton, J.W., Goetz, C.G., Ling, Z.D., Stebbins, G.T., Carvey, P.M., 1997. The stability of carbidopa in solution. *Movement Disorders*, 12, 608-610.
- Pardridge, W.M., 2005. Tyrosine hydroxylase replacement in experimental Parkinson's disease with Transvascular Gene Therapy. *NeuroRX*, 2, 129-138.
- Pardridge, W.M., 1999. Vector-mediated drug delivery to the brain. *Advanced Drug Delivery Reviews*, 36, 299-321.
- Park, H., Kim, D., 2006. Swelling and mechanical properties of glycol chitosan/poly(vinyl alcohol) IPN-type superporous hydrogels. *Journal of Biomedical Materials Research Part A*, 78A, 662-667.
- Park, J.H., Jana, S.C., 2003. The relationship between nano- and micro-structures and mechanical properties in PMMA–epoxy–nanoclay composites. *Polymer*, 44, 2091-2100.
- Park, T.G., Cohen, S., Langer, R., 1992. Poly (L-lactic acid)/Pluronic blends: characterization of phase separation behavior, degradation, and morphology and use as protein-releasing matrixes. *Macromolecules*, 25, 116-122.
- Parkinson Study Group, 2006. A randomized controlled trial of etilevodopa in patients with Parkinson disease who have motor fluctuations. *Archives of Neurology*, 63, 210-216.
- Parkinson, J., 2002. An essay on the shaking palsy. *Journal of Neuropsychiatry and Clinical Neurosciences*, 14, 223-236.
- Patel, G.M., Patel, H.R., Patel, M., Patel, J.K., 2009. Floating drug delivery system: An innovative approach to prolong gastric retention. *Pharminfo.net*, 5, <http://www.pharminfo.net/reviews/floating-drug-delivery-system-innovative-approach-prolong-gastric-retention>. Accessed 16th June, 2009.
- Paulson, S.K., Vaughn, M.B., Jessen, S.M., Lawal, Y., Gresk, C.J., Yan, B., Maziasz, T.J., Cook, C.S., Karim, A., 2001. Pharmacokinetics of celecoxib after oral administration in

dogs and humans: effect of food and site of absorption. *Journal of Pharmacology and Experimental Therapeutics*, 297, 638-645.

Pearlman, D.A., Case, D.A., Caldwell, J.W., Ross, W.S., Cheatham, T.E., DeBolt, S., Ferguson, D., Seibel, G., Kollman, P., 1995. AMBER, a package of computer programs for applying molecular mechanics, normal mode analysis, molecular dynamics and free energy calculations to simulate the structural and energetic properties of molecules. *Computer Physics Communications*, 91, 1-41.

Pénczes, T., Csóka, I., Erős, I., 2004. Rheological analysis of the structural properties effecting the percutaneous absorption and stability in pharmaceutical organogels. *Rheologica Acta*, 43, 457-463.

Peppas, N.A., 2004. Intelligent therapeutics: Biomimetic systems and nanotechnology in drug delivery. *Advanced Drug Delivery Reviews*, 56, 1529-1531.

Pergushov, D., Remizova, E., Zezin, A., Kabanov, V., 2006. Interpolyelectrolyte complex formation is possible in low-polarity organic media. *Doklady Physical Chemistry*, 406, 38-42.

Périer, C., Marin, C., Jimenez, A., Bonastre, M., Tolosa, E. and Hirsch, E. C., 2003. Effect of subthalamic nucleus or entopeduncular nucleus lesion on levodopa-induced neurochemical changes within the basal ganglia and on levodopa-induced motor alterations in 6-hydroxydopamine-lesioned rats. *Journal of Neurochemistry*, 86, 1328-1337.

Pfeiffer, R.F., 2005. A promising new technology for Parkinson's disease. *Neurology*, 65, S6-S10.

Piccini, P., Brooks, D.J., Korpela, K., Pavese, N., Karlsson, M., Gordin, A., 2000. The catechol-O-methyltransferase (COMT) inhibitor entacapone enhances the pharmacokinetic and clinical response to Sinemet CR in Parkinson's disease. *Journal of Neurology, Neurosurgery & Psychiatry*, 68, 589-594.

Pillai, O., Panchagnula, R., 2001. Polymers in drug delivery. *Current Opinion in Chemical Biology*, 5, 447-451.

Pinto Reis, C., Neufeld, R.J., Ribeiro, António J., Veiga, F., 2006. Nanoencapsulation I. Methods for preparation of drug-loaded polymeric nanoparticles. *Nanomedicine: Nanotechnology, Biology and Medicine*, 2, 8-21.

- Pitt, G.G., Cha, Y., Shah, S.S., Zhu, K.J., 1992. Blends of PVA and PGLA: control of the permeability and degradability of hydrogels by blending. *Journal of Controlled Release*, 19, 189-199.
- Pizarro, C., González-Sáiz, J.M., Pérez-del-Notario, N., 2006. Multiple response optimization based on desirability functions of a microwave-assisted extraction method for the simultaneous determination of chloroanisoles and chlorophenols in oak barrel sawdust. *Journal of Chromatography A*, 1132, 8-14.
- Poewe, W., 2004. The role of COMT inhibition in the treatment of Parkinson's disease. *Neurology*, 62, S31-S38.
- Polli, J.E., Rekhi, G.S., Augsburger, L.L., Shah, V.P., 1997. Methods to compare dissolution profiles and a rationale for wide dissolution specifications for metoprolol tartrate tablets. *Journal of Pharmaceutical Sciences*, 86, 690-700.
- Prado, H.J., Matulewicz, M.C., Bonelli, P., Cukierman, A.L., 2008. Basic butylated methacrylate copolymer/kappa-carrageenan interpolyelectrolyte complex: Preparation, characterization and drug release behavior. *European Journal of Pharmaceutics and Biopharmaceutics*, 70, 171-178.
- Prado, H.J., Matulewicz, M.C., Bonelli, P.R., Cukierman, A.L., 2009. Preparation and characterization of a novel starch-based interpolyelectrolyte complex as matrix for controlled drug release. *Carbohydrate Research*, 344, 1325-1331.
- Prut, E.,V., Zelenetskii, A.,N., 2001. Chemical modification and blending of polymers in an extruder reactor. *Russian Chemical Reviews*, 70, 65-79.
- Qiu, Y., Park, K., 2001. Environment-sensitive hydrogels for drug delivery. *Advanced Drug Delivery Reviews*, 53, 321-339.
- Rainsford, K.D., Stetsko, P.I., Sirko, S.P., Debski, S., 2003. Gastrointestinal mucosal injury following repeated daily oral administration of conventional formulations of indometacin and other non-steroidal anti-inflammatory drugs to pigs: a model for human gastrointestinal disease. *Journal of Pharmacy and Pharmacology*, 55, 661-668.
- Ramkisson-Ganorkar, C., Liu, F., Baudys, M., Kim, S.W., 1999. Modulating insulin-release profile from pH/thermosensitive polymeric beads through polymer molecular weight. *Journal of Controlled Release*, 59, 287-298.

- Rapoport, L., Nepomnyashchy, O., Verdyan, A., Popovitz-Biro, R., Volovik, Y., Ittah, B., Tenne, R., 2004. Polymer Nanocomposites with Fullerene-like Solid Lubricant. *Advanced Engineering Materials*, 6, 44-48.
- Rasenack, N., Müller, B.W., 2004. Micron-Size Drug Particles: Common and Novel Micronization Techniques. *Pharmaceutical Development & Technology*, 9, 1-13.
- Reddy, M., Rehana, T., Ramakrishna, S., Chowdary, K., Diwan, P., 2004. β -cyclodextrin complexes of celecoxib: Molecular-modeling, characterization, and dissolution studies. *The AAPS Journal*, 6, 68-76.
- Rekas, A., Lo, V., Gadd, G.E., Cappai, R., Yun, S.I., 2009. PAMAM Dendrimers as Potential Agents against Fibrillation of α -Synuclein, a Parkinson's Disease-Related Protein. *Macromolecular Bioscience*, 9, 230-238.
- Remenar J, Almarsson O, Meehan AJ, Zhang Z, 2005. Pharmaceutical Compositions and Method of using L-dopa and Carbidopa Patent WO/2005/099678. <http://www.wipo.int/patentscope/search/en/detail.jsf?docId=WO2005099678> Accessed 16th October, 2010
- Repta, A.J., 1987. Rectally Absorbable Form of Levodopa Patent 4, 663, 349. http://patft.uspto.gov/netacgi/nph-Parser?Sect1=PTO1&Sect2=HITOFF&d=PALL&p=1&u=%2Fnetacgi%2FPTO%2Fsrc_hnum.htm&r=1&f=G&l=50&s1=4663349.PN.&OS=PN/4663349&RS=PN/4663349 Accessed 16th October, 2010
- Richardson, J.C., Bowtell, R.W., Mäder, K., Melia, C.D., 2005. Pharmaceutical applications of magnetic resonance imaging (MRI). *Advanced Drug Delivery Reviews*, 57, 1191-1209.
- Robertson, D., Renwick, A., Wood, N., Cross, N., Macklin, B., Fleming, J., Waller, D., George, C., 1990. The influence of levodopa on gastric emptying in man. *British Journal of Clinical Pharmacology*, 29, 47-53.
- Robertson, D.R.C., Renwick, A.G., Macklin, B., Jones, S., Waller, D.G., George, C.F., Fleming, J.S., 1992. The influence of levodopa on gastric emptying in healthy elderly volunteers. *European Journal of Clinical Pharmacology*, 42, 409-412.
- Robeson, L.M., 2007. *Polymer Blends: A Comprehensive Review*, Illustrated Ed., Hanser Verlag, Germany, 459 pages.

Roche, 2010. Madopar® Datasheet.

<http://www.medsafe.govt.nz/profs/datasheet/m/Madoparcapdisptab.pdf> Accessed 3rd September, 2011.

Rodríguez, R., Alvarez-Lorenzo, C., Concheiro, A., 2001. Rheological Evaluation of the Interactions between Cationic Celluloses and Carbopol 974P in Water. *Biomacromolecules*, 2, 886-893.

Rouge, N., Buri, P., Doelker, E., 1996. Drug absorption sites in the gastrointestinal tract and dosage forms for site-specific delivery. *International Journal Pharmacology*, 136, 117-139.

Rouge, N., Allémann, E., Gex-Fabry, M., Balant, L., Cole, E.T., Buri, P., Doelker, E., 1998. Comparative pharmacokinetic study of a floating multiple-unit capsule, a high-density multiple-unit capsule and an immediate-release tablet containing 25 mg atenolol. *Pharmaceutica Acta Helvetiae.*, 73, 81-87.

Rouquerol, J., Avnir, D., Fairbridge, C., Everett, D., Haynes, J., Pernicone, N., Ramsay, J., Sing, K., Unger, K., 1994. Recommendations for the characterization of porous solids (Technical Report). *Pure and Applied Chemistry*, 66, 1739-1758.

Rubin A.A, 2000. Improvement in the treatment of Parkinson's disease and related disorders by novel formulations of the combination carbidopa-L-dopa. Patent WO/2000/015197. <http://www.wipo.int/patentscope/search/en/detail.jsf?docId=WO2000015197> Accessed 16th October, 2010.

Rudraraju, V.S., Wyandt, C.M., 2005. Rheological characterization of Microcrystalline Cellulose/Sodium carboxymethylcellulose hydrogels using a controlled stress rheometer: part I. *International Journal of Pharmaceutics*, 292, 53-61.

S., Sajesh., Sharma, C.P., 2006. Interpolymer complex microparticles based on polymethacrylic acid-chitosan for oral insulin delivery. *Journal of Applied Polymer Sciences*, 99, 506-512. d

Sabel, B., Dominiak, P., Hauser, W., Doring, M., Freese, A., 1990. Levodopa delivery from controlled-release polymer matrix: delivery of more than 600 days in vitro and 225 days of elevated plasma levels after subcutaneous implantation in rats. *Journal of Pharmacology and Experimental Therapeutics*, 255, 914-922.

Sabale, V., Sakarkar, S., Pund, S., Sabale, P., 2010. Formulation and evaluation of floating dosage forms: An overview. *Systematic Reviews in Pharmacy*, 1, 33-39.

- Sagar, K.A., Smyth, M.R., 2000. Bioavailability studies of oral dosage forms containing levodopa and carbidopa using column-switching chromatography followed by electrochemical detection. *Analyst*, 125, 439-445.
- Saha, M.C., Kabir, M.E., Jeelani, S., 2008. Enhancement in thermal and mechanical properties of polyurethane foam infused with nanoparticles. *Materials Science and Engineering: A*, 479, 213-222.
- Sahoo, S.K., Labhasetwar, V., 2003a. Nanotech approaches to drug delivery and imaging. *Drug Discovery Today*, 8, 1112-1120.
- Sáiz-Abajo, M.J., González-Sáiz, J.M., Pizarro, C., 2005. Multi-objective optimization strategy based on desirability functions used for chromatographic separation and quantification of proline and organic acids in vinegar. *Analytica Chimica Acta*, 528, 63-76.
- Säkkinen, M., Marvola, J., Kanerva, H., Lindevall, K., Ahonen, A., Marvola, M., 2006. Are chitosan formulations mucoadhesive in the human small intestine?: An evaluation based on gamma scintigraphy. *International Journal of Pharmaceutics*, 307, 285-291.
- Sandoval, K.E., Witt, K.A., 2008. Blood-brain barrier tight junction permeability and ischemic stroke. *Neurobiology of Disease*, 32, 200-219.
- Sant, V.P., Smith, D., Leroux, J., 2005. Enhancement of oral bioavailability of poorly water-soluble drugs by poly(ethylene glycol)-block-poly(alkyl acrylate-co-methacrylic acid) self-assemblies. *Journal of Controlled Release*, 104, 289-300.
- Santoveña, A., Alvarez-Lorenzo, C., Llabrés, M., Concheiro, A., Fariña, J.B., 2009. hGH release from directly compressed hGH-PLGA biodegradable implantable tablets: Influence of physicomechanical factors. *European Polymer Journal*, 45, 2830-2838.
- Sarmiento, B., Ribeiro, A., Veiga, F., Ferreira, D., Neufeld, R., 2007. Oral Bioavailability of Insulin Contained in Polysaccharide Nanoparticles. *Biomacromolecules*, 8, 3054-3060.
- Sauer, B.B., Kampert, W.G., Neal Blanchard, E., Threefoot, S.A., Hsiao, B.S., 2000. Temperature modulated DSC studies of melting and recrystallization in polymers exhibiting multiple endotherms. *Polymer*, 41, 1099-1108.
- Schapira, A.H.V., 2005. Present and future drug treatment for Parkinson's disease. *Journal of Neurology, Neurosurgery and Psychiatry*, 76, 1472-1478.
- Schapira, A.H.V., 2006. Etiology of Parkinson's disease. *Neurology*, 66, S10-S23.

- Schrag, A., Jonathan, M.S., 2006. Epidemiological, clinical, and genetic characteristics of early-onset parkinsonism. *Lancet Neurology*, 5, 355-363.
- Seeberger, L.C., Hauser, R.A., 2007. Optimizing bioavailability in the treatment of Parkinson's disease. *Neuropharmacology*, 53, 791-800.
- Shah, V.P., Tsong, Y., Sathe, P., Liu, J., 1998. In Vitro Dissolution Profile Comparison—Statistics and Analysis of the Similarity Factor, f2. *Pharmaceutical Research*, 15, 889-896.
- Shaikh, J., Ankola, D.D., Beniwal, V., Singh, D., Kumar, M.N.V.R., 2009. Nanoparticle encapsulation improves oral bioavailability of curcumin by at least 9-fold when compared to curcumin administered with piperine as absorption enhancer. *European Journal of Pharmaceutical Sciences*, 37, 223-230.
- Shen, Y., Sun, W., Zhu, K.J., Shen, Z., 2000. Regulation of biodegradability and drug release behavior of aliphatic polyesters by blending. *Journal of Biomedical Materials Research*, 50, 528-535.
- Shishu, Bhatti, A., Singh, T., 2007. Preparation of tablets rapidly disintegrating in saliva containing bitter taste-masked granules by compression method. *Indian Journal of Pharmaceutical Sciences*, 69, 80-84.
- Siegel, R.A., Langer, R., 1990. Mechanistic studies of macromolecular drug release from macroporous polymers. II. Models for the slow kinetics of drug release. *Journal of Controlled Release*, 14, 153-167.
- Siepmann, J., Göpferich, A., 2001. Mathematical modeling of bioerodible, polymeric drug delivery systems. *Advanced Drug Delivery Reviews*, 48, 229-247.
- Sing, K., Everett, D., Haul, R., Moscou, L., Pierotti, R., Rouquerol, J., Siemieniowska, T., 1985. Reporting physisorption data for gas/solid systems. *Pure and Applied Chemistry*, 57, 603–619.
- Singh, B., Chauhan, N., 2010. Dietary fiber psyllium based hydrogels for use in insulin delivery. *International Journal of Diabetes Mellitus*, 2, 32-37.
- Singh, B., Chakkal, S., Ahuja, N., 2006. Formulation and optimization of controlled release mucoadhesive tablets of atenolol using response surface methodology. *AAPS PharmSciTech*, 7, E19-E28.

- Singh, B.N., Kim, K.H., 2000. Floating drug delivery systems: an approach to oral controlled drug delivery via gastric retention. *Journal of Controlled Release*, 63, 235-259.
- Singh, N., Pillay, V., Choonara, Y.E., 2007. Advances in the treatment of Parkinson's disease. *Progress in Neurobiology*, 81, 29-44.
- Sittikijyothin, W., Torres, D., Gonçalves, M.P., 2005. Modeling the rheological behavior of galactomannan aqueous solutions. *Carbohydrate Polymers*, 59, 339-350.
- Slabbert, C., du Plessis, L.H., Kotzé, A.F., 2011. Evaluation of the physical properties and stability of two lipid drug delivery systems containing mefloquine. *International Journal of Pharmaceutics*, 409, 209-215.
- Smith, L.A, Jackson, M.J., Al-barghouthy, G., Rose, S., Kuoppamaki, M., Olanow, W., Jenner, P., 2004. Multiple small doses of levodopa plus entacapone produce continuous dopaminergic stimulation and reduce dyskinesia induction in MPTP-treated drug-naïve primates. *Movement Disorders*, 20, 9, 306-314.
- Sogias, I.A., Williams, A.C., Khutoryanskiy, V.V., 2008. Why is Chitosan Mucoadhesive? *Biomacromolecules*, 9, 1837-1842.
- Solanki, A., Parikh, J., Parikh, R., 2007. Formulation and optimization of piroxicam proniosomes by 3-factor, 3-level Box-Behnken design. *AAPS PharmSciTech*, 8, 43-49.
- Somani, P.M., 2008. Parkinson's disease. *Latest Reviews*, 6, 3048.
- Song, Y., Clizbe, L., Bhakta, C., Teng, W., Li, W., Wong, P., Huang, B., Sinha, U., Park, G., Reed, A., Scarborough, R.M., Zhu, B., 2002. Substituted acrylamides as factor Xa inhibitors: improving bioavailability by P1 modification. *Bioorganic and Medicinal Chemistry Letters*, 12, 2043-2046.
- Song, Y., Lee, J., Lee, H.G., 2009. α -Tocopherol-loaded Ca-pectinate microcapsules: Optimization, in vitro release, and bioavailability. *Colloids and Surfaces B: Biointerfaces*, 73, 394-398.
- Sonvico, F., Cagnani, A., Rossi, A., Motta, S., Di Bari, M.T., Cavatorta, F., Alonso, M.J., Deriu, A., Colombo, P., 2006. Formation of self-organized nanoparticles by lecithin/chitosan ionic interaction. *International Journal of Pharmaceutics*, 324, 67-73.
- Soppimath, K.S., Aminabhavi, T.M., Kulkarni, A.R., Rudzinski, W.E., 2001. Biodegradable polymeric nanoparticles as drug delivery devices. *Journal of Controlled Release*, 70, 1-20.

- Sriamornsak, P., Thirawong, N., Weerapol, Y., Nunthanid, J., Sungthongjeen, S., 2007. Swelling and erosion of pectin matrix tablets and their impact on drug release behavior. *European Journal of Pharmaceutics and Biopharmaceutics*, 67, 211-219.
- Stacy, M., 2000. Pharmacotherapy for Advanced Parkinson's Disease. *Pharmacotherapy*, 20, 8S-16S.
- Stocchi, F., Barbato, L., Bramante, L., Nordera, G., Vacca, L., Ruggieri, S., 1996. Fluctuating parkinsonism: a pilot study of single afternoon dose of levodopa methyl ester. *Journal of Neurology*, 243, 377-380.
- Stocchi, F., Barbato, L., Nordera, G., Bolner, A., Caraceni, T., 2004. Entacapone improves the pharmacokinetic and therapeutic response of controlled release levodopa/carbidopa in Parkinson's patients. *Journal of Neural Transmission*, 111, 173-180.
- Stocchi, F., 2003. Prevention and treatment of motor fluctuations. *Parkinsonism and Related Disorders*, 9, 73-81.
- Stocchi, F., Tagliati, M., Olanow, C.W., 2008. Treatment of levodopa-induced motor complications. *Movement Disorders*, 23, S599-S612.
- Streubel A., Siepmann J., Bodmeier R.[1], 2002. Floating microparticles based on low density foam powder. *International Journal of Pharmaceutics*, 241, 279-292.
- Streubel, A., Siepmann, J., Bodmeier, R., 2006. Drug delivery to the upper small intestine window using gastroretentive technologies. *Current Opinion in Pharmacology*, 6, 501-508.
- Streubel, A., Siepmann, J., Bodmeier, R., 2003. Multiple unit gastroretentive drug delivery systems: a new preparation method for low density microparticles. *Journal of Microencapsulation*, 20, 329-347.
- Susan, M., Baldea, I., Senila, S., Macovei, V., Dreve, S., Ion, R.M., Cosgarea, R., 2011. Photodamaging effects of porphyrins and chitosan on primary human keratinocytes and carcinoma cell cultures. *International Journal of Dermatology*, 50, 280-286.
- Tajiri, T., Morita, S., Sakamoto, R., Suzuki, M., Yamanashi, S., Ozaki, Y., Kitamura, S., 2010a. Release mechanisms of acetaminophen from polyethylene oxide/polyethylene glycol matrix tablets utilizing magnetic resonance imaging. *International Journal of Pharmaceutics*, 395, 147-153.

- Talukder, R., Fassihi, R., 2004. Gastroretentive Delivery Systems: A Mini Review. *Drug Development & Industrial Pharmacy*, 30, 1019-1028.
- Tapia, C., Escobar, Z., Costa, E., Sapag-Hagar, J., Valenzuela, F., Basualto, C., Nella Gai, M., Yazdani-Pedram, M., 2004. Comparative studies on polyelectrolyte complexes and mixtures of chitosan–alginate and chitosan–carrageenan as prolonged diltiazem clorhydrate release systems. *European Journal of Pharmaceutics and Biopharmaceutics*, 57, 65-75.
- Taylor, K.S.M., Counsell, C., 2006. Is it Parkinson's disease, and if not, what is it? *Practical Neurology*, 6, 154-165.
- Thanos, C.G., Liu, Z., Goddard, M., Reineke, J., Bailey, N., Cross, M., Burrill, R., Mathiowitz, E., 2003a. Enhancing the oral bioavailability of the poorly soluble drug dicumarol with a bioadhesive polymer. *Journal of Pharmaceutical Sciences*, 92, 1677-1689.
- Thanos, C.G., Liu, Z., Reineke, J., Edwards, E., Mathiowitz, E., 2003b. Improving relative bioavailability of dicumarol by reducing particle size and adding the adhesive poly(fumaric-co-sebacic) anhydride. *Pharmaceutical Research*, 20, 1093-1100.
- Thanou, M., Verhoef, J.C., Junginger, H.E., 2001. Oral drug absorption enhancement by chitosan and its derivatives. *Advanced Drug Delivery Reviews*, 52, 117-126.
- Thanvi, B.R., Lo, T.C.N., 2004. Long term motor complications of levodopa: clinical features, mechanisms, and management strategies. *Postgraduate Medical Journal*, 80, 452-458.
- Thirawong, N., Kennedy, R.A., Sriamornsak, P., 2008. Viscometric study of pectin–mucin interaction and its mucoadhesive bond strength. *Carbohydrate Polymers*, 71, 170-179.
- Thomas, P.A., Padmaja, T., Kulkarni, M.G., 1997. Polyanhydride blend microspheres: novel carriers for the controlled release of macromolecular drugs. *Journal of Controlled Release*, 43, 273-281.
- Thomas, V.H., Bhattachar, S., Hitchingham, L., Zocharski, P., Naath, M., Surendran, N., Stoner, C.L., El-Kattan, A., August 2006. The road map to oral bioavailability: an industrial perspective. *Expert Opinion on Drug Metabolism and Toxicology*, 2, 591-608.
- Tian, Y., Li, Y., Xu, X., Jin, Z., Jiao, A., Wang, J., Yu, B., 2010. A novel size-exclusion high performance liquid chromatography (SE-HPLC) method for measuring degree of amylose retrogradation in rice starch. *Food Chemistry*, 118, 445-448.

- Tiller, A.R., Gorella, B., 1994. Estimation of polymer compatibility from molecular mechanics calculations. *Polymer*, 35, 3251-3259.
- Tintner, R., Jankovic, J., 2002. Treatment options for Parkinson's disease. *Current Opinion in Neurology*, 15, 467-476.
- Tyler, C.M., Federoff, H.J., March 2006. CNS Gene Therapy and a Nexus of Complexity: Systems and Biology at a Crossroads. *Cell Transplantation*, 15, 267-273.
- Umezawa, F., Eto, Y., 1988. Liposome targeting to mouse brain: Mannose as a recognition marker. *Biochemical and Biophysical Research Communications*, 153, 1038-1044.
- Unceta, N., Rodriguez, E., de Balugera, Z.G., Sampedro, C., Goicolea, M.A., Barrondo, S., Sallés, J., Barrio, R.J., 2001. Determination of catecholamines and their metabolites in human plasma using liquid chromatography with coulometric multi-electrode cell-design detection. *Analytica Chimica Acta*, 444, 211-221.
- Van Eerdenbrugh, B., Froyen, L., Martens, J.A., Bleton, N., Augustijns, P., Brewster, M., Van den Mooter, G., 2007. Characterization of physico-chemical properties and pharmaceutical performance of sucrose co-freeze-dried solid nanoparticulate powders of the anti-HIV agent loviride prepared by media milling. *International Journal of Pharmaceutics*, 338, 198-206.
- Van Tomme, S.R., De Geest, B.G., Braeckmans, K., De Smedt, S.C., Siepmann, F., Siepmann, J., van Nostrum, C.F., Hennink, W.E., 2005. Mobility of model proteins in hydrogels composed of oppositely charged dextran microspheres studied by protein release and fluorescence recovery after photobleaching. *Journal of Controlled Release*, 110, 67-78.
- Varma M.V.S., Kaushal A.M., Garg A. Garg S. 2004, Factors affecting mechanism and kinetics of drug release from matrix-based oral controlled drug delivery systems, *American Journal of Drug Delivery*, 2, 43-57.
- Varshosaz, J., Hassanzadeh, F., Mahmoudzadeh, M., Sadeghi, A., 2009. Preparation of cefuroxime axetil nanoparticles by rapid expansion of supercritical fluid technology. *Powder Technology*, 189, 97-102.
- Vasconcelos, T., Sarmiento, B., Costa, P., 2007. Solid dispersions as strategy to improve oral bioavailability of poor water soluble drugs. *Drug Discovery Today*, 12, 1068-1075.

- Vasile, C., Bumbu, G.G., Petronela Dumitriu, R., Staikos, G., 2004. Comparative study of the behavior of carboxymethyl cellulose-g-poly(N-isopropylacrylamide) copolymers and their equivalent physical blends. *European Polymer Journal*, 40, 1209-1215.
- Vasir, J.K., Tambwekar, K., Garg, S., 2003. Bioadhesive microspheres as a controlled drug delivery system. *International Journal of Pharmaceutics*, 255, 13-32.
- Veazey, C., Ozlem Erden Aki, S., Cook, K.F., Lai, E.C., Kunik, M.E., 2005. Prevalence and treatment of depression in Parkinson's disease. *Journal of Neuropsychiatry and Clinical Neurosciences*, 17, 310-323.
- Vehige, J.G., Simmons, P.A., Anger, C., Graham, R., Tran, L., Brady, N., 2003. Cytoprotective properties of carboxymethyl cellulose (CMC) when used prior to wearing contact lenses treated with cationic disinfecting agents. *Eye & contact lens*, 29, 177-180.
- Verdonck, E., Schaap, K., Thomas, L.C., 1999. A discussion of the principles and applications of Modulated Temperature DSC (MTDSC). *International Journal of Pharmaceutics*, 192, 3-20.
- Verhagen Metman, L., 2002. Recognition and treatment of response fluctuations in Parkinson's disease: Review article. *Amino Acids*, 23, 141-145.
- Waller, D., Roseveare, C., Renwick, A., Macklin, B., George, C., 1991. Gastric emptying in healthy volunteers after multiple doses of levodopa. *British Journal of Clinical Pharmacology*, 32, 691-695.
- Wang, G., Uludag, H., 2008. Recent developments in nanoparticle-based drug delivery and targeting systems with emphasis on protein-based nanoparticles. *Expert Opinion on Drug Delivery*, 5, 499-515.
- Warhurst, D., Craig, J., Adagu, I., Meyer, D., Lee, S., 2003. The relationship of physico-chemical properties and structure to the differential antiplasmodial activity of the cinchona alkaloids. *Malaria Journal*, 2, 26.
- Waterman, K.C., 2007. A critical review of gastric retentive controlled drug delivery. *Pharmaceutical Development and Technology*, 12, 1-10.
- Wei, L., Cai, C., Lin, J., Chen, T., 2009. Dual-drug delivery system based on hydrogel/micelle composites. *Biomaterials*, 30, 2606-2613.

- Yang, S., Zhu, J., Lu, Y., Liang, B., Yang, C., 1999. Body distribution of camptothecin solid lipid nanoparticles after oral administration. *Pharmaceutical Research*, 16, 751-757.
- Yang, X., Zhu, W., 2007. Viscosity properties of sodium carboxymethylcellulose solutions. *Cellulose*, 14, 409-417.
- Yaşar, F., Toğrul, H., Arslan, N., 2007. Flow properties of cellulose and carboxymethyl cellulose from orange peel. *Journal of Food Engineering*, 81, 187-199.
- Yeh, K., August, T., Bush, D., Lasseter, K., Musson, D., Schwartz, S., Smith, M., Titus, D., 1989. Pharmacokinetics and bioavailability of Sinemet CR: a summary of human studies. *Neurology*, 39, 25-38.
- Yih, T.C., Al-Fandi, M., 2006. Engineered nanoparticles as precise drug delivery systems. *Journal of Cellular Biochemistry*, 97, 1184-1190.
- Yin, L., Fei, L., Cui, F., Tang, C., Yin, C., 2007. Superporous hydrogels containing poly(acrylic acid-co-acrylamide)/O-carboxymethyl chitosan interpenetrating polymer networks. *Biomaterials*, 28, 1258-1266.
- Yin, Y., Cui, F., Mu, C., Choi, M., Kim, J.S., Chung, S., Shim, C., Kim, D., 2009. Docetaxel microemulsion for enhanced oral bioavailability: Preparation and in vitro and in vivo evaluation. *Journal of Controlled Release*, 140, 86-94.
- Yu, B.Y., Chung, J.W., Kwak, S., 2008. Reduced migration from flexible poly(vinyl chloride) of a plasticizer containing β -cyclodextrin derivative. *Environmental Science and Technology*, 42, 7522-7527.
- Yu, S., Mi, F., Wu, Y., Peng, C., Shyu, S., Huang, R., 2005. Antibacterial activity of chitosan-alginate sponges incorporating silver sulfadiazine: Effect of ladder-loop transition of interpolyelectrolyte complex and ionic crosslinking on the antibiotic release. *Journal of Applied Polymer Science*, 98, 538-549.
- Zahedi, P., De Souza, R., Piquette-Miller, M., Allen, C., 2009. Chitosan-phospholipid blend for sustained and localized delivery of docetaxel to the peritoneal cavity. *International Journal of Pharmaceutics*, 377, 76-84.
- Zhang, L., Chen, G., Hu, Q., Fang, Y., 2001. Separation and determination of levodopa and carbidopa in composite tablets by capillary zone electrophoresis with amperometric detection. *Analytica Chimica Acta*, 431, 287-292.

- Zhang, L., Huang, S., 2000. Viscosity properties of homogeneous polyelectrolyte complex solutions from sodium carboxymethyl cellulose and poly(acrylamide-co-dimethyldiallylammonium chloride). *Polymer International*, 49, 528-532.
- Zhang, M.Q., Rong, M.Z., Zhang, H.B., Friedrich, K., 2003. Mechanical properties of low nano-silica filled high density polyethylene composites. *Polymer Engineering and Science*, 43, 490-500.
- Zhang, Q., Shen, Z., Nagai, T., 2001. Prolonged hypoglycemic effect of insulin-loaded polybutylcyanoacrylate nanoparticles after pulmonary administration to normal rats. *International Journal of Pharmaceutics*, 218, 75-80.
- Zhang, Y., Huo, M., Zhou, J., Xie, S., 2010. PKSolver: An add-in program for pharmacokinetic and pharmacodynamic data analysis in Microsoft Excel. *Computer Methods and Programs in Biomedicine*, 99, 306-314.
- Zhao, Q., Qian, J., An, Q., Gao, C., Gui, Z., Jin, H., 2009a. Synthesis and characterization of soluble chitosan/sodium carboxymethyl cellulose polyelectrolyte complexes and the pervaporation dehydration of their homogeneous membranes. *Journal of Membrane Science*, 333, 68-78.
- Zhao, Q., Qian, J., An, Q., Gui, Z., Jin, H., Yin, M., 2009b. Pervaporation dehydration of isopropanol using homogeneous polyelectrolyte complex membranes of poly(diallyldimethylammonium chloride)/sodium carboxymethyl cellulose. *Journal of Membrane Science*, 329, 175-182.
- Zweers, M.L.T., Grijpma, D.W., Engbers, G.H.M., Feijen, J., 2003. The preparation of monodisperse biodegradable polyester nanoparticles with a controlled size. *Journal of Biomedical Materials Research Part B: Applied Biomaterials*, 66B, 559-566.

APPENDIX A: Research Publications

1. Levodopa Delivery Systems: Advancements in Delivery of the Gold Standard. Ndidi C. Ngwuluka, Viness Pillay, Girish Modi, Dinesh Naidoo, Yahya E. Choonara and Lisa C. du Toit. *Expert Opinion on Drug Delivery*, 7(2): 203-224, 2010.

Review

Expert Opinion

1. Introduction
2. Immediate release oral drug delivery systems for the administration of levodopa
3. Conventional controlled release formulations for levodopa administration
4. Administration of levodopa as a liquid formulation
5. Dispersible tablets for delivery of levodopa
6. Oral disintegrating levodopa tablets
7. Dual-release formulations for the delivery of levodopa
8. Delivery of levodopa by infusions
9. Biodegradable microspheres as a drug delivery system for levodopa
10. Gastroretentive dosage forms as drug delivery systems for levodopa
11. Long-term implantable levodopa controlled release matrix
12. Pulmonary delivery of levodopa
13. Nasal delivery of levodopa
14. Transdermal delivery systems for levodopa
15. Prodrugs as a delivery vehicle for levodopa
16. Delivery of levodopa by means of the rectal route
17. Expert opinion

Levodopa delivery systems: advancements in delivery of the gold standard

Ndidi Ngwuluka, Viness Pillay[†], Lisa C Du Toit, Valence Ndesendo, Yahya Choonara, Girish Modi & Dinesh Naidoo

[†] *University of the Witwatersrand, Department of Pharmacy and Pharmacology, 7 York Road, Parktown, 2193, Johannesburg, South Africa*

Importance of the field: Despite the fact that Parkinson's disease (PD) was discovered almost 200 years ago, its treatment and management remain immense challenges because progressive loss of dopaminergic nigral neurons, motor complications experienced by the patients as the disease progresses and drawbacks of pharmacotherapeutic management still persist. Various therapeutic agents have been used in the management of PD, including levodopa (L-DOPA), selegiline, amantadine, bromocriptine, entacapone, pramipexole dihydrochloride and more recently istradefylline and rasagiline. Of all agents, L-DOPA although the oldest, remains the most effective. L-DOPA is easier to administer, better tolerated, less expensive and is required by almost all PD patients. However, L-DOPA's efficacy in advanced PD is significantly reduced due to metabolism, subsequent low bioavailability and irregular fluctuations in its plasma levels. Significant strides have been made to improve the delivery of L-DOPA in order to enhance its bioavailability and reduce plasma fluctuations as well as motor complications experienced by patients purportedly resulting from pulsatile stimulation of the striatal dopamine receptors.

Areas covered in this review: Drug delivery systems that have been instituted for the delivery of L-DOPA include immediate release formulations, liquid formulations, dispersible tablets, controlled release formulations, dual-release formulations, microspheres, infusion and transdermal delivery, among others. In this review, the L-DOPA-loaded drug delivery systems developed over the past three decades are elaborated.

What the reader will gain: The ultimate aim was to assess critically the attempts made thus far directed at improving L-DOPA absorption, bioavailability and maintenance of constant plasma concentrations, including the drug delivery technologies implicated.

Take home message: This review highlights the fact that neuropharmaceutics is at a precipice, which is expected to spur investigators to take that leap to enable the generation of innovative delivery systems for the effective management of PD.

Keywords: bioavailability, conventional dosage forms, drug delivery systems, levodopa, microspheres, motor complications, nanotechnology, neuropharmaceutics, Parkinson's disease, pulmonary delivery, transdermal delivery

Expert Opin. Drug Deliv. (2010) 7(2):203-224

2. Fabrication, modeling and characterization of multi-crosslinked Eudragit E100/Eudragit E100 polymer blended nanoparticles for oral drug delivery, Ndidi C. Ngwuluka, Viness Pillay, Girish Modi, Dinesh Naidoo, Yahya E. Choonara and Lisa C. du Toit. *International Journal of Molecular Sciences*, 12, 6194-6225, 2011.

Int. J. Mol. Sci. 2011, 12, 1-x manuscripts; doi:10.3390/ijms120x000x

OPEN ACCESS

International Journal of
Molecular Sciences
ISSN 1422-0067
www.mdpi.com/journal/ijms

Article

Fabrication, Modeling and Characterization of Multi-Crosslinked Methacrylate Copolymeric Nanoparticles for Oral Drug Delivery

Ndidi C. Ngwuluka ¹, Viness Pillay ^{1*}, Yahya E. Choonara ¹, Girish Modi ², Dinesh Naidoo ³, Lisa C. du Toit ¹, Pradeep Kumar ¹, Valence M.K. Ndesendo ¹ and Riaz A. Khan ⁴

¹ Department of Pharmacy and Pharmacology, University of the Witwatersrand, 7 York Road, Parktown, 2193, Johannesburg, South Africa

* Author to whom correspondence should be addressed; E-Mail: viness.pillay@wits.ac.za;
Tel.: +27-11-717-2274; Fax: +27-86-553-4733.

Received: 15 March 2011; in revised form: 30 July 2011 / Accepted: 4 August 2011 / Published:

Abstract: Nanotechnology remains the field to explore in the quest to enhance therapeutic efficacies of existing drugs. Fabrication of a methacrylate copolymer-lipid nanoparticulate (MCN) system was explored in this study for oral drug delivery of levodopa. The nanoparticles were fabricated employing multicrosslinking technology and characterized for particle size, zeta potential, morphology, structural modification, drug entrapment efficiency and *in vitro* drug release. Chemometric Computational (CC) modeling was conducted to deduce the mechanism of nanoparticle synthesis as well as to corroborate the experimental findings. The CC modeling deduced that the nanoparticles synthesis may have followed the mixed triangular formations or the mixed patterns. They were found to be hollow nanocapsules with a size ranging from 152 nm to 321 nm and a zeta potential range of 15.8–43.3 mV. The nanoparticles were directly compressible and it was found that the desired rate of drug release could be achieved by formulating the nanoparticles as a nanosuspension, and then directly compressing them into tablet matrices or incorporating the nanoparticles directly into polymer tablet matrices. However, sustained release of MCNs was achieved only when it was incorporated into a polymer matrix. The experimental results were well corroborated by the CC modeling. The developed technology may be potentially useful for the fabrication of multi-crosslinked polymer blend nanoparticles for oral drug delivery.

APPENDIX B: Research presentations

1. Presentation at the School of Therapeutic Sciences research day, University of Witwatersrand, South Africa, August, 12, 2009.

Enhancing the drug delivery properties of a carbohydrate polymer by lyophilization

Ndidi C. Ngwuluka¹, Viness Pillay^{1*}, Girish Modi², Yahya E. Choonara¹ and Lisa C. du Toit¹

¹University of the Witwatersrand, Department of Pharmacy and Pharmacology, 7 York Road, Parktown, 2193, Johannesburg, South Africa.

²University of the Witwatersrand, Department of Neurology, 7 York Road, Parktown, 2193, Johannesburg, South Africa.

Purpose:

To improve the mechanical strength and drug release profile of a carbohydrate polymer by lyophilization.

Method:

A carbohydrate polymer was dispersed in distilled water under agitation and thereafter lyophilized. The lyophilized polymer was milled and some characterizations as well as swellability analyses and *in vitro* drug release studies were undertaken in comparison with the native polymer.

Result:

The lyophilized polymer was directly compressible but the native polymer was not. The lyophilized polymer retained its shape during swelling analyses attaining a swelling of 273% at t_{24} while the native polymer disintegrated in contact with the medium. Drug release profile of the native polymer exhibited an erratic pattern of drug release and the lyophilized polymer showed a more sustained linear drug release. The crystallization temperature of the native polymer was 292°C and that of the lyophilized polymer could not be ascertained. However, FTIR spectra of the lyophilized polymer distinctly differed from the native polymer at 1537.90 cm^{-1} , which is an indication of the change in the structure of the polymer after lyophilization that enhanced its drug delivery properties.

Conclusion:

Lyophilization is a simple and durable process that can be employed to improve the compressibility, mechanical strength and drug release profiles of polymers.

2. Presentation at the British Pharmaceutical Conference, Manchester, United Kingdom, September, 6 – 9, 2009.



Ndidi C. Ngwuluka¹, Viness Pillay^{1*}, Girish Modi², Yahya E. Choonara¹, Lisa C. du Toit¹ and Dinesh Naidoo³

¹University of the Witwatersrand, Department of Pharmacy and Pharmacology, 7 York Road, Parktown, 2193, Johannesburg, South Africa.

²University of the Witwatersrand, Department of Neurology, 7 York Road, Parktown, 2193, Johannesburg, South Africa.

³University of the Witwatersrand Department of Neurosurgery, 7 York Road, Parktown, 2193, Johannesburg, South Africa.

*Corresponding Author: viness.pillay@wits.ac.za

Title

Characterization of prolamine-based polymeric nanocomposites

Objectives:

To determine the influence of varying prolamine-blended polymeric compositions on the particle size and molecular structural transitions during nanocomposite formation. Fourier Transform Infra-Red (FTIR) spectroscopy was used to assess the extent of interactions between the prolamine-polymeric blended structure to form nanocomposite particles while Temperature Modulated Differential Scanning Calorimeter (TMDSC) elucidated the thermal properties and provided insight into the molecular dynamics of the prolamine-blended polymeric nanocomposites.

Methods

Prolamine-based polymeric blends were prepared in 50%_v acetic acid in ratios of 1:1, 2:1, 1:2, 4:1, 1:4, 3:4 and 4.3 of prolamine:polymer. The blends were prepared comprising Tween 80 (1mL) prior to the addition of 0.25%_w of an aqueous sequestrator under agitation. The nanoparticulate suspensions were centrifuged (2750rpm) and thereafter lyophilized. The size and zeta potential of the nanocomposites were measured using a ZetaSizer NanoZS. FTIR spectra were obtained for the native polymers and the prolamine-based nanocomposites using a PerkinElmer spectrometer over the wavenumber range of 4000-650cm⁻¹ while the thermal behavior was evaluated with a TMDSC.

Results and Discussion

The average particle size obtained was in the range of 146-527nm while the zeta potential value was between +1.23 to -8.11mV. As the concentration of prolamine increased, the particle size increased due to agglomeration. However, at a ratio of 1:1, the average particle size was 206nm which was indicative of miscibility between the prolamine and polymer components. FTIR analysis of the native polymers indicated the presence of weak bands due to less bond vibration. The absorption bands were strengthened by blending with the presence of newly formed unsaturated bonds at 1735.59cm⁻¹, 1639.79cm⁻¹, 944.5cm⁻¹, and 887.97cm⁻¹. The FTIR spectra of the prolamine-based polymeric blends distinctly differed from the native polymer at 1735.59cm⁻¹, 1639.79cm⁻¹, 1349.42cm⁻¹, 1149.84cm⁻¹, 1064.31cm⁻¹ and 944.65cm⁻¹ which may influence drug delivery due to the presence of unsaturated bonds for potential polymer-drug interaction. The crystallization temperatures of the native polymers were increased to the range of 237–242°C by blending. The close crystallization temperature range of the blends collaborated with the FTIR spectra indicating that the varying compositions of the blends did not significantly alter the spectra obtained; rather they varied slightly in the degree of peak absorbance.

Conclusion

The FTIR spectra of the prolamine-based polymeric blends distinctly differed from the native polymers. This indicated the presence of interaction between the prolamine-polymeric blend during nanocomposites formation. The higher crystallization temperature range also supported the interactive mechanism of the prolamine-polymeric blend for nanocomposites formation.

3. Presentation at 2nd postgraduate cross faculty symposium, University of Witwatersrand, South Africa, October, 19 – 22, 2009.

Comparative Textural and Drug Release Profiling of a Native Polymer and its Lyophilized Form

Ndidi C. Ngwuluka¹, Viness Pillay^{1*}, Girish Modi², Dinesh Naidoo³, Yahya E. Choonara¹ and Lisa C. du Toit¹

¹University of the Witwatersrand, Department of Pharmacy and Pharmacology, 7 York Road, Parktown, 2193, Johannesburg, South Africa.

²University of the Witwatersrand, Department of Neurology, 7 York Road, Parktown, 2193, Johannesburg, South Africa.

³University of the Witwatersrand, Department of Neurosurgery, 7 York Road, Parktown, 2193, Johannesburg, South Africa.

Purpose:

To compare the mechanical strength and drug release kinetics of a native polymer and its lyophilized form employed in formulation of direct compressible matrices.

Method:

A carbohydrate polymer was dispersed in distilled water under agitation, lyophilized and milled. The milled lyophilized polymer and native polymer were separately mixed with a drug and excipients and directly compressed. The physicochemical properties were determined with a Texture Analyzer (TA.XTplus, Stable Microsystems, UK). *In vitro* drug release studies were also performed in 0.1N HCl at 37°C and stirring rate of 50rpm employing USP apparatus II dissolution system (Erweka DT 700).

Result:

The native polymer compressed directly but was highly friable compared to the lyophilized polymer. The matrix rigidity values were 7.328N/mm and 34.850N/mm for the native polymer and its lyophilized form, respectively. The deformation energy values were 0.030Nm and 0.012Nm while the matrix resilience values were 34.5% and 46.95% for the native polymer and its lyophilized form, respectively. The native polymer possesses poor physicochemical strength, which was improved by lyophilization. Drug release profiles of the native polymer demonstrated an erratic pattern of release with 64% of the model drug, levodopa, released in half an hour while a sustained linear drug release of 13% in half an hour was observed with the lyophilized form.

Conclusion:

The physicochemical strength of a polymer can be improved by lyophilization which imparts rigidity furnishing drug delivery systems that are fit to withstand various forms of stresses as well as enhancing the controlled drug delivery properties of the polymer.

4. Presentation at American Association of Pharmaceutical Scientists, Los Angeles Convention Center, Los Angeles, USA, November, 8 -12, 2009.

Synthesis and Characterization of a Novel Hydrogel Formulation for Oral Drug Delivery
Ndidi C. Ngwuluka¹, Viness Pillay^{1*}, Girish Modi², Yahya E. Choonara¹, Lisa C. du Toit¹
and Dinesh Naidoo³

¹University of the Witwatersrand, Department of Pharmacy and Pharmacology, 7 York Road, Parktown, 2193, Johannesburg, South Africa.

²University of the Witwatersrand, Department of Neurology, 7 York Road, Parktown, 2193, Johannesburg, South Africa.

³University of the Witwatersrand Department of Neurosurgery, 7 York Road, Parktown, 2193, Johannesburg, South Africa.

*Corresponding Author: viness.pillay@wits.ac.za

Purpose:

To explore an approach in advancing the challenges of rapid drug release from polymethacrylate matrices and the poor mechanical strength of cellulosic derivatives by inter-polymeric blending of the two polymers as a novel hydrogel to provide robust matrices with zero-order drug release kinetics.

Methods:

A solution of a polymethacrylate was obtained by dissolving in 0.1N acetic acid and a cellulose derivative was dissolved in distilled water. A blend of the polymethacrylate and the cellulose derivative was prepared at a homogenous ratio of 0.5:1 under vigorous agitation and thereafter lyophilized. The newly synthesized hydrogel was analyzed by FTIR spectra obtained for the native polymers and the hydrogel over a range of 4000-650cm⁻¹. Digital microscopy (Olympus SZX-ILLD2-200) was also undertaken to examine the outward character of the hydrogel. Swellability analysis was undertaken in 0.1N HCl placed in a shaker bath (Orbital Shaker incubator), while *in vitro* drug release studies were also performed in 0.1N HCl at 37°C and stirring rate of 50rpm employing USP apparatus II dissolution system (Erweka DT 700).

Results:

Digital images of the synthesized hydrogel revealed white irregularly shaped particles. The FTIR spectra of the hydrogel after washing in distilled water indicated the presence of aliphatic OH- assigned at 3500-3100cm⁻¹, 2850-2000cm⁻¹, 1210-900cm⁻¹ and 1510-1405cm⁻¹ that were obtained by the reduction of aliphatic CHO- from the polymethacrylate assigned between 4000-3125cm⁻¹, 3000-2835cm⁻¹, 2775-2690cm⁻¹ and 1745-1720cm⁻¹. However the aliphatic OH- in the washed hydrogel after synthesis was sublimated during lyophilization. In terms of swellability when compared to the cellulosic derivative a higher degree of linear symmetrical swelling at t_{24hours} (465%) was noted whereas the cellulosic derivative had no distinct geometry. The symmetrical swelling of the hydrogel contributed to the zero-order release of the model drug levodopa from the inter-polymeric hydrogel blend.

Conclusions:

Inter-polymeric blending of the native polymers produced a hydrogel with improved properties. The hydrogel retained its three dimensional network, had robust physicomechanical strength and exhibited zero-order release of model drug levodopa over 24 hours.

5. Presentation at American Association of Pharmaceutical Scientists, New Orleans Ernest N. Morial Convention Center, New Orleans, Louisiana, USA, November, 13 – 18, 2010.

Physicochemical characterization of nanoparticles prepared from a basic ester of poly (acrylic) acid for sustained levodopa delivery

Ndidi C. Ngwuluka¹, Viness Pillay^{1*}, Girish Modi², Dinesh Naidoo³, Yahya E. Choonara¹ and Lisa C. du Toit¹

¹University of the Witwatersrand, Department of Pharmacy and Pharmacology, 7 York Road, Parktown, 2193, Johannesburg, South Africa.

²University of the Witwatersrand, Department of Neurology, 7 York Road, Parktown, 2193, Johannesburg, South Africa.

³University of the Witwatersrand Department of Neurosurgery, 7 York Road, Parktown, 2193, Johannesburg, South Africa.

*Corresponding Author: viness.pillay@wits.ac.za

Purpose:

To prepare and characterize nanoparticles employing a basic ester of poly(acrylic) acid and to explore various approaches of achieving sustained drug release from the nanoparticles.

Methods:

A solution of a basic ester of poly(acrylic) acid was prepared in 0.2N HCl and the model drug, levodopa was added under agitation. A lipid surfactant (1mL) was incorporated. Thereafter, a sequestering solution obtained in 0.2N acetic acid was added which produced nanoparticles that were lyophilized into a free-flowing powder. The average particle size and zeta potential were measured using a ZetaSizer NanoZS while the surface morphology was ascertained via transmission electron microscopy (TEM). Comparative drug release studies were undertaken employing three formulation approaches namely: a nanosuspension, levodopa-loaded nanoparticles directly compressed into tablet matrices and levodopa-loaded nanoparticles incorporated into a polymeric blend and directly compressed into tablet matrices. Drug release studies were undertaken using a dialysis technique for the nanosuspension and USP dissolution apparatus II was employed for the latter two formulation approaches. The quantity of levodopa released was determined by UV spectrophotometry.

Results:

Nanoparticles that were obtained appeared as white spherical particles as confirmed by TEM with an average particle size of 223nm (RSD=2.9%) and zeta potential of 35.1mV (RSD=5.97%). At t_5 hours, 90% of levodopa was released from the nanosuspension while 97.2% was released from the directly compressed nanoparticle tablet matrices as the nanoparticles were completely dispersed in the dissolution medium. However, only 28% of levodopa was released from the polymeric blended tablet matrix by t_5 hours and 88.5% by t_{24} hours providing a zero-order release of levodopa.

Conclusion:

The desired rate of release can be modulated by formulating levodopa-loaded nanoparticles as a suspension, directly compressing the nanoparticles into a tablet matrix or by loading the nanoparticles into a polymeric blended tablet matrix. However, sustained delivery of levodopa was achieved by embedding the nanoparticles within a polymeric blended tablet matrix.

6. Presentation at American Association of Pharmaceutical Scientists, New Orleans Ernest N. Morial Convention Center, New Orleans, Louisiana, USA, November, 13 – 18, 2010.

Computational modeling and drug release characteristics of a pH-responsive interpolyelectrolyte complex

Ndidi C. Ngwuluka¹, Viness Pillay^{1*}, Girish Modi², Dinesh Naidoo³, Yahya E. Choonara¹, Lisa C. du Toit¹, Riaz Khan⁴ and Pradeep Kumar¹

¹University of the Witwatersrand, Department of Pharmacy and Pharmacology, 7 York Road, Parktown, 2193, Johannesburg, South Africa.

²University of the Witwatersrand, Department of Neurology, 7 York Road, Parktown, 2193, Johannesburg, South Africa.

³University of the Witwatersrand Department of Neurosurgery, 7 York Road, Parktown, 2193, Johannesburg, South Africa.

⁴Manav Rachna International University, Aravali Hills, Faridabad, India.

*Corresponding Author: viness.pillay@wits.ac.za

Purpose:

To employ computational modeling to proffer an insight into the interaction between an acrylate copolymer and a cellulose derivative as well as to explicate the mechanisms of formation of an interpolyelectrolyte complex (IPEC) and to ascertain levodopa release from the compressed IPEC tablet matrices.

Methods:

An acrylate copolymer was milled and dissolved in acetic acid and a cellulose polymer derivative was solubilized in deionized water. The two solutions were blended in a ratio of 0.5:1 respectively under agitation at ambient temperature until homogenous white strands were obtained resulting in the IPEC. The IPEC was then lyophilized, milled, loaded with the model drug, levodopa, and directly compressed into tablet matrices (13x5mm). A computational model was developed to depict the mechanistic complexation of the polymers employing a hybrid computer simulation/polymeric-interaction modeling approach (ACD/I-Lab, V5.11 Add-on software). Drug release studies were undertaken in pH 1.5 and 4.5 at 50rpm and maintained at 37±0.5°C over 24 hours using USP apparatus II and drug content was analyzed by UV spectrophotometry.

Results:

Computational modeling revealed that the polymeric interactions were strong ionic associations, hydrogen bondings and hydrophilic interactions. As the acrylate copolymer was dissolved in acetic acid, the polymer interacted with acetate ions to stabilize the ammonium cations of the acrylate copolymer with the release of hydrogen ions from acetic acid. Some of the acetate ions served as counter ions for the cations released from the cellulose polymer derivative generating a salt required for threshold crosslinking at a ratio of 0.5:1. Mechanisms of drug release at pH 1.5 were swelling and subsequent diffusion as the matrices retained their three-dimensional network over 24 hours. In pH 4.5, the mechanisms of drug release were significant swelling, diffusion and surface erosion up to the 16th hour. Surface erosion ensued by bulk erosion were envisaged to have occurred due to the dissociation of the IPEC at pH 4.5.

Conclusion:

Interactions between the acrylate copolymer and the cellulose polymer derivative were computationally modeled and the mechanisms of levodopa release from the IPEC tablet matrices were found to be pH dependent.

7. Presentation at Controlled Release Society Meeting, National Harbor, Maryland, USA, July, 30th - 3rd August 2011.

A Triple-Mechanism Gastroretentive System for Zero-Order Delivery of Levodopa

Ndidi C. Ngwuluka^{1*}, Viness Pillay¹, Girish Modi², Dinesh Naidoo³, Yahya E. Choonara¹ and Lisa C. du Toit¹

¹Department of Pharmacy and Pharmacology, ²Department of Neurology ³ Department of Neurosurgery
University of the Witwatersrand, 7 York Road, Parktown, 2193, Johannesburg, South Africa.

*Corresponding Author: viness.pillay@wits.ac.za

ABSTRACT SUMMARY

A novel controlled oral gastroretentive drug delivery system was developed by employing three mechanisms of gastroretention to enhance the benefits and overcome the setbacks of gastroretentive systems for levodopa delivery. Polymer blend was synthesized, formulated and characterized. The system was directly compressible with good mechanical properties; exhibiting pH and density dependence with impressive gastro-adhesion and gastroretentive behaviours.

INTRODUCTION

Levodopa (L-dopa) remains the most effective and widely used anti-parkinsonian agent and is eventually required by all PD patients. However, conventional oral immediate release and controlled release formulations of levodopa have been challenged by poor bioavailability and plasma fluctuations which are due to the fact that levodopa has a specific site of absorption in the proximal region of the small intestine. Therefore, the development of an oral formulation with prolonged gastric residence time may improve the absorption and subsequent bioavailability of L-dopa with constant therapeutic plasma concentrations.

This study was undertaken to overcome the setbacks of various mechanisms of gastroretention by employing three mechanisms – high density, swelling and bioadhesion - to enhance the delivery of levodopa. A polymeric gastroretentive drug delivery system was formulated by employing techniques such as Fourier Transform Infra-Red (FTIR) spectroscopy, texture analyses, gastroadhesivity testing and *in vitro* drug release testing.

EXPERIMENTAL METHODS

A polymer blend was prepared by first synthesizing an interpolyelectrolyte complex (IPEC) of a polymethacrylate and a cellulose derivative, NaCMC in a stoichiometric ratio of 0.5:1. Polymethacrylate (0.84g) was dissolved in 50mL of 0.1N acetic acid while NaCMC (1.88g) was

dissolved in water before blending under vigorous agitation. A natural polysaccharide, locust bean was added on completion of synthesis of IPEC and subsequently lyophilized. The polymer blend was milled and mixed with some excipients which included barium sulphate, silica, magnesium stearate and levodopa; and compressed directly to produce a gastroretentive drug delivery system (GDDS).

The structural modification of the polymer blend from the native polymers was elucidated over a range of 4000-850cm⁻¹ using a PerkinElmer spectrometer. The density was assessed by determining the volumes, thicknesses and weights using a 0-150mm electronic digital calliper and a gravimetric method. Gastro-adhesivity was assessed with a freshly excised pig's stomach equilibrated in 0.1N HCl using a texture analyzer to determine force and work of adhesion. Matrix hardness, deformation and resilience were assessed with a texture analyzer.

The degree of swelling was obtained by placing the weighed tablets in wire baskets, submerged in 100mL 0.1N HCl and placed in a shaker bath (at 37°C. Increase in mass was gravimetrically assessed at intervals over 24 hours. Furthermore, *in vitro* drug release studies were performed in USP Apparatus II at 37 ± 0.5°C and 50rpm while the dissolution media comprised 900mL of buffers at pH 1.5 and 4.5. Furthermore comparative drug release studies with conventional dosage forms were undertaken.

RESULTS AND DISCUSSION

The blend between the polymethacrylate and NaCMC in the FTIR spectra (Figure 1) was a chemical interaction while the addition of the natural polysaccharide was a physical interaction. The carbonyl peak at 1725 cm⁻¹ of polymethacrylate was diminished indicative that some carbonyl groups may have been involved in the interaction. The structural modification altered the properties of the native polymers to enhance drug delivery properties of the polymer blend.

APPENDIX C: ADSC Scans

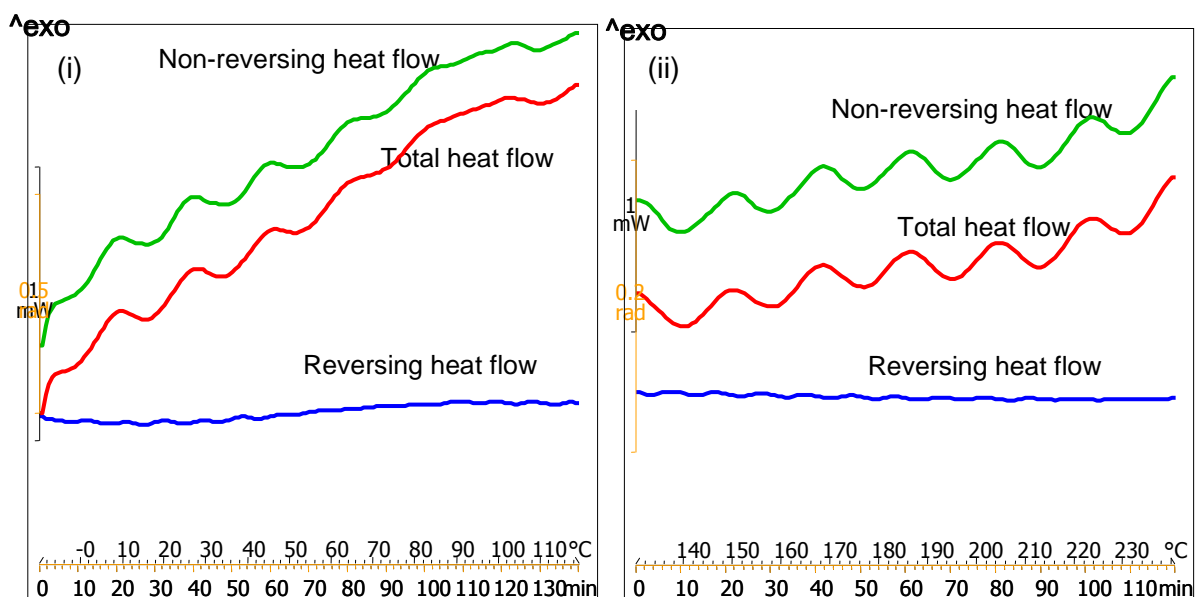


Figure 4.8e: Non-reversing, total and reversing heat flows derived from ADSC scans for EC 0.2 N: **i)** temperature range -10 – 130°C and; **ii)** 130 – 250°C.

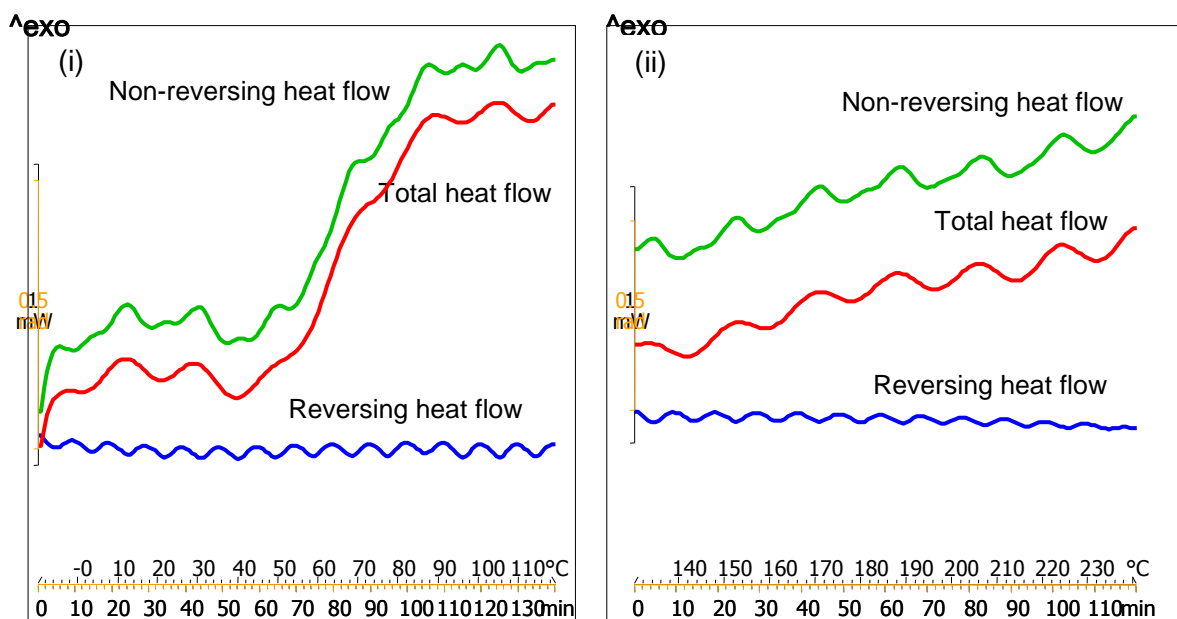


Figure 4.8f: Non-reversing, total and reversing heat flows derived from ADSC scans for EC 0.4 N: **i)** temperature range -10 – 130°C and **ii)** 130 – 250°C.

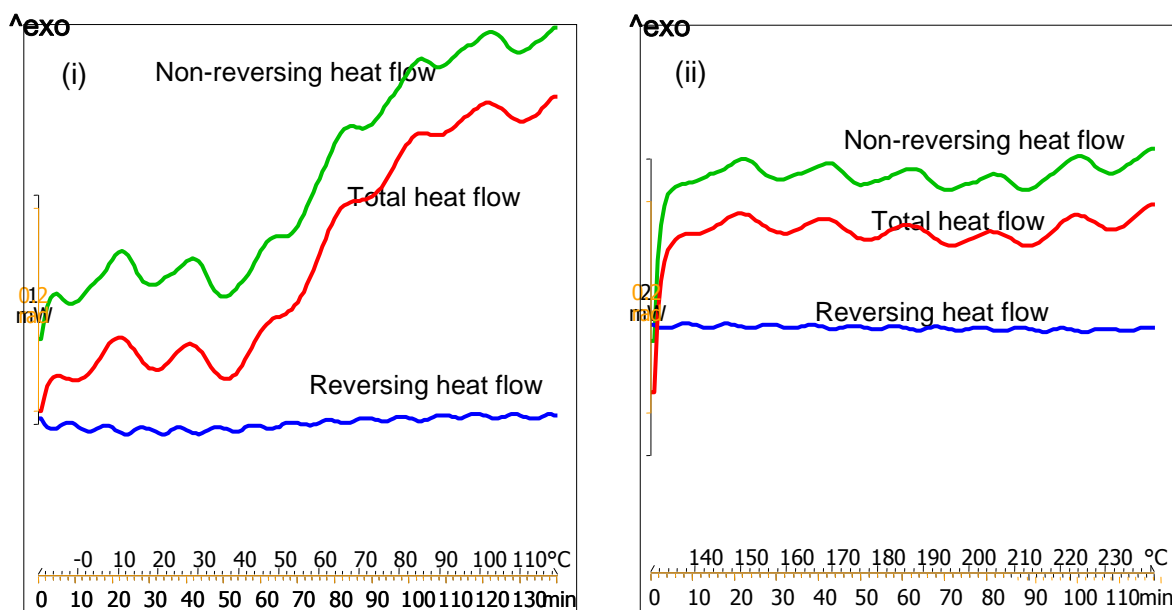


Figure 4.8g: Non-reversing, total and reversing heat flows derived from ADSC scans for EC 0.6 N: **i)** temperature range -10 – 130°C and; **ii)** 130 – 250°C.

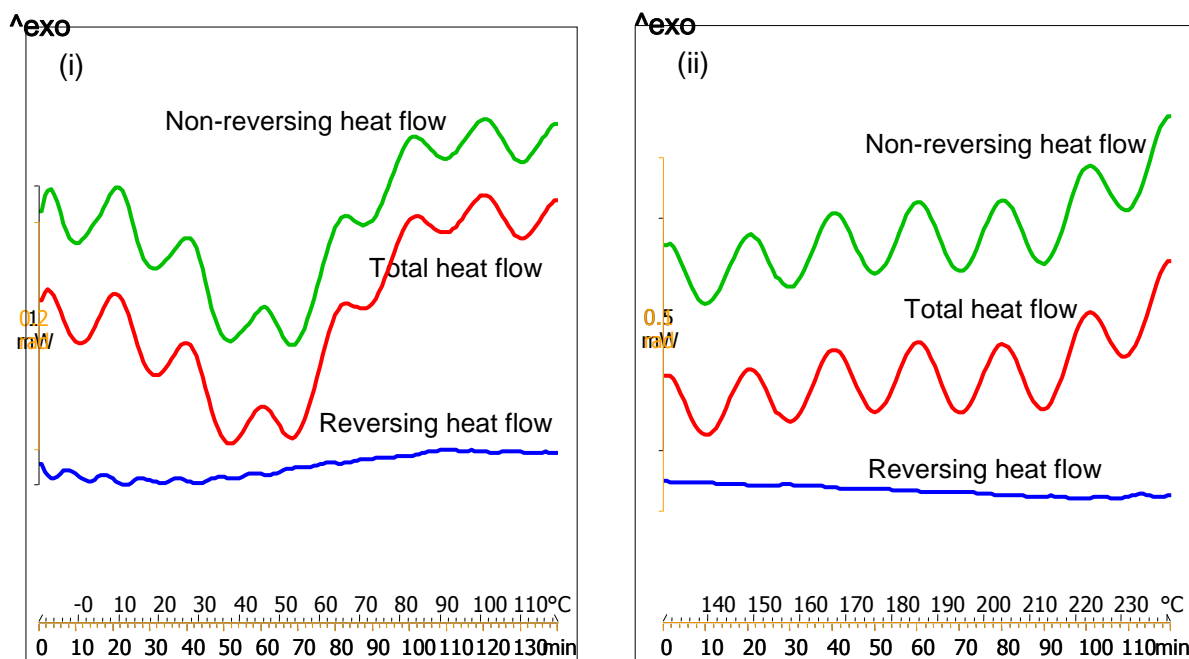


Figure 4.8h: Non-reversing, total and reversing heat flows derived from ADSC scans for EC 0.8 N: **i)** temperature range -10 – 130°C and; **ii)** 130 – 250°C.

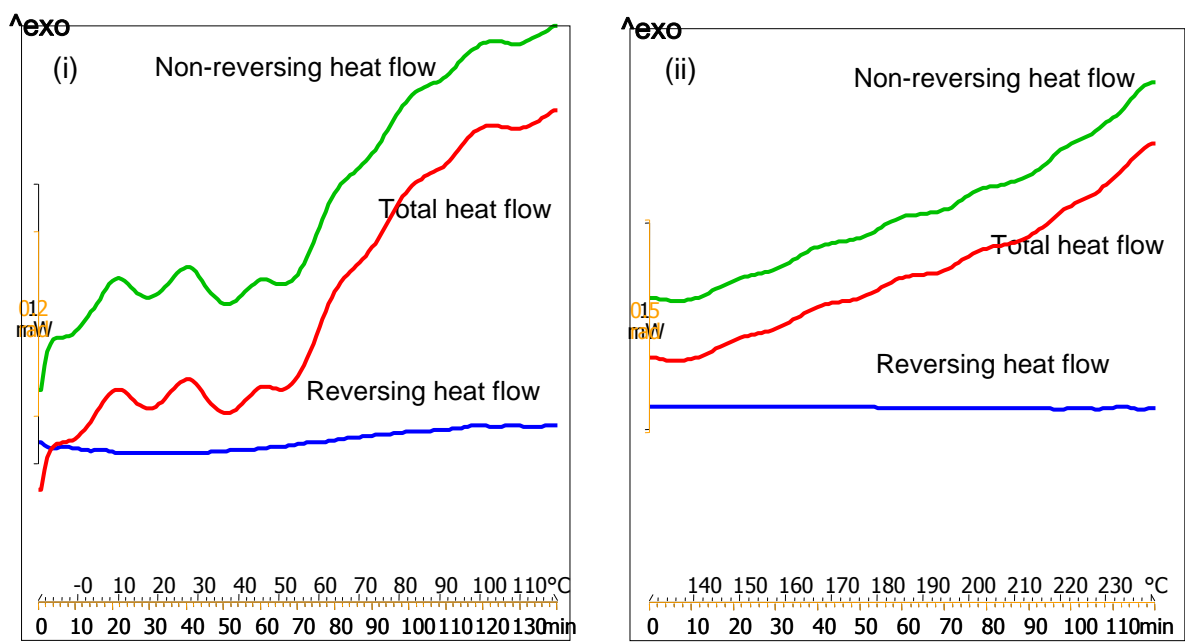


Figure 4.8i: Non-reversing, total and reversing heat flows derived from ADSC scans for EC 1.0 N: **i)** temperature range -10 – 130°C and; **ii)** 130 – 250°C.

APPENDIX D: Animal ethics approval

UNIVERSITY OF THE WITWATERSRAND, JOHANNESBURG

STRICTLY CONFIDENTIAL

ANIMAL ETHICS SCREENING COMMITTEE (AESC)

CLEARANCE CERTIFICATE NO. 2009/01/05

APPLICANT: Prof V Pillay
SCHOOL: Pharmacy and Pharmacology
DEPARTMENT:
LOCATION:

PROJECT TITLE: In vivo assessment of novel biocompatible polymeric drug delivery systems in pigs

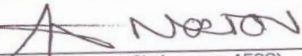
Number and Species

40 pigs

Approval was given for the use of animals for the project described above at an AESC meeting held on 27.01.2009. This approval remains valid until 27.01.2011

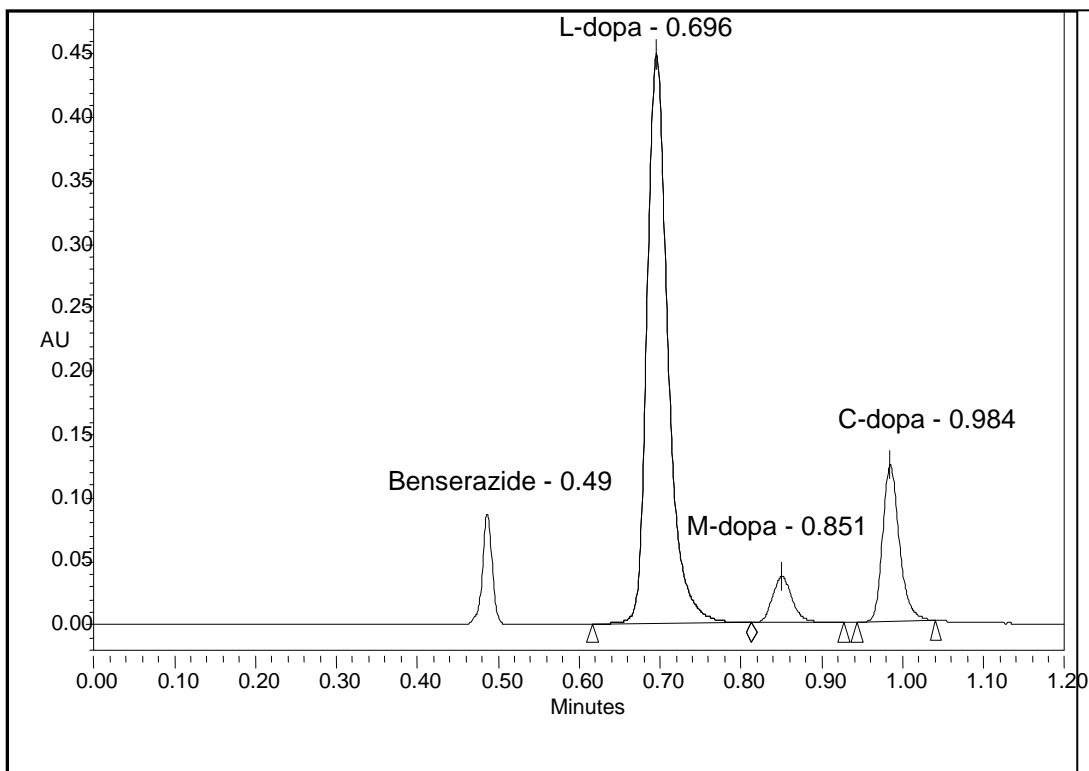
The use of these animals is subject to AESC guidelines for the use and care of animals, is limited to the procedures described in the application form and to the following additional conditions:

- a) Clinical monitoring of the animals for the first 24 hours after drug dosing to ensure that no unwanted side-effects occur. This monitoring should be performed by the investigators as guided by the CAS veterinarian.
- b) A written report should be submitted to the AESC on the clinical safety of the drug combinations observed in one animal per drug combination before proceeding to further animals in each drug combination group.
- c) A letter addressed to the chairperson of AESC should be provided to indicate the exact pharmacological combinations being studied and the route of delivery of these combinations. Obviously this should be provided when the appropriate combinations are known.
- d) The protocol should be revised with the inclusion of a detailed description of the procedure that will be employed for intraduodenal infusion and the person qualified to do this.
- e) The protocol should be revised with a justification and rationale for the use of 2 calcium channel blockers employed together as implied by the present protocol.
- f) Discussion should occur with the CAS veterinarian regarding the precise procedures required for the collection of blood and CSF samples.

Signed: 
(Chairperson, AESC)

Date: 06/02/2009

APPENDIX E: UPLC/PDA chromatogram for *in vitro* drug release



UPLC/MS/MS chromatogram for *in vivo* drug release

